



**ADSORPTION OF SELECTED POLLUTANTS FROM
AQUEOUS SOLUTIONS ONTO MODIFIED CARBON
NANOTUBES**

by

OLUWASEUN AKINWOLE OYETADE

Submitted in fulfillment of the academic requirements for the degree of
Doctor of Philosophy in the School of Chemistry and Physics,
University of KwaZulu-Natal, Durban

December 2015

Abstract

The significance of wastewater remediation before its discharge into the aquatic environment cannot be overemphasized. Adsorption has been proven to be effective for the removal of toxic pollutants from industrial effluents and/or wastewater, due to its simplicity in operation and the possibility of regenerating sorbents for reuse. This concept was exploited to achieve the effective removal of toxic contaminants from simulated wastewater. Carbon nanotubes, a fascinating member of the carbon family, possessing unique physical and chemical properties, have been reported as superior adsorbents for wastewater remediation purposes. Their large specific surface areas and porosity, hollow and layered structures, and great mechanical and thermal stability, makes them good candidates as sorbents for wastewater treatment and contamination control.

This thesis interrogates the efficacy of carbon-structured nanomaterials containing multiwalled carbon nanotubes (MWCNTs) as the backbone, for the removal of divalent metal ions and organic contaminants from aqueous solutions. In this work, a novel adsorbent was successfully synthesized by incorporating a nitrogen-donor ligand (4-phenyl-2, 2':6', 2''-terpyridine) onto MWCNTs to afford nitrogen-functionalized MWCNTs (MWCNT-ttpy). The effectiveness of this sorbent towards the removal of divalent metal ions (Pb^{2+} , Cd^{2+} , Zn^{2+} , Hg^{2+} and Cu^{2+}), and organic contaminants (bisphenol A and ibuprofen) from aqueous solutions was investigated. The adsorption uptake of these pollutants onto MWCNT-ttpy was compared with that of acid-functionalized MWCNTs (MWCNT-COOH) to determine the sorbent with best removal efficiencies. Further, magnetic nanocomposites containing cobalt ferrite nanoparticles and MWCNT-COOH were synthesized in varying ratios to investigate their effectiveness for the removal of rhodamine B from aqueous solutions. All nanomaterials synthesized were characterized by means of TEM, SEM, TGA, BET, FTIR and Raman spectroscopy before application.

Batch adsorption experiments were conducted to determine the effects of pH, contact time, adsorbent dose, initial adsorbate concentration and temperature for each sorption process in order to evaluate the best experimental conditions necessary for pollutant removal. The experimental data were fitted into the pseudo-first order, pseudo-second order, intraparticle diffusion and Elovich models to determine the dynamics and rate-determining step of the adsorption processes. The mechanism of the process was investigated by fitting the experimental data into various two- and three-parameter isotherms.

The application of MWCNT-ttpy for the removal of both heavy metal ions and organic pollutants demonstrated much enhanced uptakes than MWCNT-COOH. The incorporation of nitrogen onto MWCNT-COOH significantly improved the affinity towards the removal of metal ions, forming strong electrostatic and coordination interactions between the active sites on the adsorbent and metal ion cations. Increasing hydrophobicity of MWCNT-ttpy over MWCNT-COOH accounted for the enhanced removal of bisphenol A and ibuprofen, since their uptake is primarily decided on by the hydrophobic nature of sorbates. Further, the application of both MWCNT-COOH and magnetic carbon nanotube-cobalt ferrites nanocomposites showed good removal efficiencies for rhodamine B from aqueous solution, with the best uptake achieved by using MWCNT-COOH. However, the magnetic nanocomposites give an advantage of separation under magnetic influence, hence, limiting inconveniences encountered during separation. The kinetics of adsorption were mostly described by the pseudo-second order and the Elovich models, while the equilibrium data were best described by the Langmuir and the Sips isotherm models.

The thermodynamic parameters of adsorption, namely, the change in Gibbs energy (ΔG°), change in enthalpy (ΔH°) and change in entropy (ΔS°) were estimated for each adsorption process. The adsorption of all adsorbates were endothermic in nature except in the case of ibuprofen and Cd^{2+} which exhibited an exothermic process. All adsorption processes described in this study were spontaneous, implying the feasibility of the sorbents for the removal of targeted pollutants from wastewater.

Desorption studies aimed at regenerating the adsorbents for reuse were successful. High recovery efficiencies between 60-95% were achieved by using eluents such as 0.1 mol dm^{-3} HCl for metal ions, and ethanol and acetone/acetic acid for organic contaminants. This process averts the production of secondary pollutants, supporting the reutilization of both the adsorbents and the adsorbates. Thus, all adsorbents used in this study were efficiently regenerated by using simple conventional chemicals and can be reused for the removal of targeted pollutants from aqueous solutions.

The competitive adsorption of Pb^{2+} , Cd^{2+} , Zn^{2+} and Cu^{2+} and the binary adsorption of bisphenol A and ibuprofen onto MWCNT-ttpy was also investigated in both single-solute and multi-component adsorption systems. The sorption of metal ions onto MWCNT-ttpy was in the sequence $\text{Cd} > \text{Pb} > \text{Cu} > \text{Zn}$ and $\text{Pb} > \text{Cu} > \text{Cd} > \text{Zn}$ in single-solute and multicomponent systems, respectively, while the removal of ibuprofen was higher than that of bisphenol A in a typical binary adsorption system. For the first time, the competitive sorption of organic contaminants (bisphenol A and ibuprofen) in the presence of metal ions (Cd^{2+} and Pb^{2+}) onto nitrogen-functionalized MWCNT was investigated. The

study revealed a cooperative mechanism of adsorption between metal ions and organic pollutants in a multicomponent system. Thus, the novel adsorbent proved effective for the removal of metal ions, bisphenol A and ibuprofen in both single-solute and multicomponent adsorption systems.

MWCNT-ttpy also proved remarkably effective for removing three heavy metal ions, Pb^{2+} , Cu^{2+} and Zn^{2+} , in three different real-life water samples, obtained from the Umgeni River. Removal efficiencies greater than 95% were achieved for all three metal ions.

The modification of MWCNTs to afford both nitrogen-functionalized MWCNTs and cobalt-ferrite/MWCNT nanocomposites was successful. These sorbents exhibited excellent pollutant removal abilities, attributed to improved textural characteristics of the nanomaterials synthesized. The application of these sorbents for wastewater and industrial effluent remediation should be further explored for prudent management of water resources.

Preface

The experimental work described in this thesis was performed by the author in the School of Chemistry and Physics, University of KwaZulu-Natal, Durban, from March 2013 to August 2015, under the supervision of Professor S. B. Jonnalagadda, Professor B. S. Martincigh and Professor V. O. Nyamori.

These studies represent the original work of the author and have not otherwise been submitted in any form for any degree or diploma to any tertiary institution. Where use has been made of the work of others, it has been duly acknowledged in the text.

Declaration 1 - Plagiarism

I, Oluwaseun Akinwole Oyetade, declare that

1. The research reported in this thesis, except where otherwise indicated is my original research.
2. This thesis has not been submitted for any degree or examination at any other University.
3. This thesis does not contain other person's data, pictures, graphs or other information, unless specifically acknowledged as being sourced from other persons.
4. This thesis does not contain other person's writing, unless specifically acknowledged as being sourced from other researchers. Where other written sources have been quoted, then:
 - a. Their words have been re-written but, the general information attributed to them has been referenced.
 - b. Where their exact words have been used, then their writing has been placed in italics and inside quotation marks, and referenced.
5. This thesis does not contain text, graphics or tables copied and pasted from the Internet, unless specifically acknowledged, and the source being detailed in the thesis and in the references sections.

Signed

.....

Declaration 2 - Publications

DETAILS OF CONTRIBUTION TO PUBLICATIONS that form part and/or include research presented in this thesis (include publications, submitted, *in press* and published and give details of the contributions of each author to the experimental work and writing of each publication).

Publication

Publication 1

Oluwaseun A. Oyetade, Vincent O. Nyamori, Bice S. Martincigh and Sreekantha B. Jonnalagadda. Effectiveness of carbon nanotube–cobalt ferrite nanocomposites for the adsorption of rhodamine B from aqueous solutions. *RSC Adv.*, 2015, **5**, 22724-22739.

I prepared the nanomaterials and tested their efficiency towards the removal of rhodamine B from aqueous solutions. The initial draft of the manuscript was also written by me. The work was supervised by Professor B. Martincigh, Professor S. Jonnalagadda and Professor V. Nyamori. Significant corrections through reading, correction and editing of the manuscript were also done by my supervisors. This work has been presented in Chapter 10.

Publication 2

Oluwaseun A. Oyetade, Vincent O. Nyamori, Bice S. Martincigh and Sreekantha B. Jonnalagadda. Nitrogen-functionalised carbon nanotubes as a novel adsorbent for the removal of Cu(II) from aqueous solution. *RSC Adv.*, 2016, **6**, 2731-2745.

I planned, executed and wrote the initial draft manuscript under the supervision of Professor B. Martincigh, Professor S. Jonnalagadda and Professor V. Nyamori. Significant corrections through reading, correction and editing of the manuscript were also done by my supervisors. This work has been presented in Chapter 4.

Manuscript 1

Oluwaseun A. Oyetade, Vincent O. Nyamori, Bice S. Martincigh and Sreekantha B. Jonnalagadda. Perfluoroalkyl compounds: Occurrence, fate and their adsorption mechanism onto carbon nanotubes (unpublished work).

I planned, executed and wrote the initial draft manuscript under the supervision of Professor B. Martincigh, Professor S. Jonnalagadda and Professor V. Nyamori. This work has been presented in Chapter 3.

Manuscript 2

Oluwaseun A. Oyetade, Vincent O. Nyamori, Bice S. Martincigh and Sreekantha B. Jonnalagadda. Adsorption of Pb^{2+} and Zn^{2+} from aqueous solution onto nitrogen-functionalized multiwalled carbon nanotubes (unpublished work).

I planned, executed and wrote the initial draft manuscript under the supervision of Professor B. Martincigh, Professor S. Jonnalagadda and Professor V. Nyamori. This work has been presented in Chapter 5.

Manuscript 3

Oluwaseun A. Oyetade, Vincent O. Nyamori, Bice S. Martincigh and Sreekantha B. Jonnalagadda. Removal of Cd^{2+} and Hg^{2+} onto nitrogen-functionalized carbon nanotubes from aqueous solutions: kinetics and equilibrium (unpublished work).

I planned, executed and wrote the initial draft manuscript under the supervision of Professor B. Martincigh, Professor S. Jonnalagadda and Professor V. Nyamori. This work has been presented in Chapter 6.

Manuscript 4

Oluwaseun A. Oyetade, Vincent O. Nyamori, Bice S. Martincigh and Sreekantha B. Jonnalagadda. Adsorption of Pb^{2+} , Zn^{2+} , Cd^{2+} and Cu^{2+} onto nitrogen-functionalized multiwalled carbon nanotubes: Single- and multi-metal competitive adsorption study (unpublished work).

I planned, executed and wrote the initial draft manuscript under the supervision of Professor B. Martincigh, Professor S. Jonnalagadda and Professor V. Nyamori. This work has been presented in Chapter 7.

Manuscript 5

Oluwaseun A. Oyetade, Vincent O. Nyamori, Bice S. Martincigh and Sreekantha B. Jonnalagadda. Kinetics, isotherm and thermodynamic studies of the removal of bisphenol A and ibuprofen from aqueous solution by using nitrogen-functionalized multiwalled carbon nanotubes (unpublished work).

I planned, executed and wrote the initial draft manuscript under the supervision of Professor B. Martincigh, Professor S. Jonnalagadda and Professor V. Nyamori. This work has been presented in Chapter 8.

Manuscript 6

Oluwaseun A. Oyetade, Vincent O. Nyamori, Bice S. Martincigh and Sreekantha B. Jonnalagadda. Co-adsorption of bisphenol A and ibuprofen onto functionalized multiwalled carbon nanotubes: Influence of metal ions in solution (unpublished work).

I planned, executed and wrote the initial draft manuscript under the supervision of Professor B. Martincigh, Professor S. Jonnalagadda and Professor V. Nyamori. This work has been presented in Chapter 9.

Signed:

.....

Conference contributions

1. Poster Presentation

Oluwaseun A. Oyetade, Vincent O. Nyamori, Bice S. Martincigh and Sreekantha B. Jonnalagadda. Effectiveness of carbon nanotube–cobalt ferrite nanocomposites for the adsorption of rhodamine B from aqueous solutions. Presented at the 5th International IUPAC Conference on Green Chemistry, Durban, South Africa, on 17th August – 21st August 2014.

2. Poster Presentation

Oluwaseun A. Oyetade, Vincent O. Nyamori, Bice S. Martincigh and Sreekantha B. Jonnalagadda. Effectiveness of carbon nanotube–cobalt ferrite nanocomposites for the adsorption of rhodamine B from aqueous solutions. Presented at the 2nd International Symposium and Workshop of the Global Green Chemistry Centres (G₂C₂), CapeTown, South Africa, on 24th August – 26th August 2014.

3. Oral Presentation

Oluwaseun A. Oyetade, Vincent O. Nyamori, Bice S. Martincigh and Sreekantha B. Jonnalagadda. Effectiveness of carbon nanotube–cobalt ferrite nanocomposites for the adsorption of rhodamine B from aqueous solutions. Presented on 27th October 2014 at the College of Agriculture, Engineering and Science Research Day 2014, UKZN, Westville Campus.

4. Poster Presentation

Oluwaseun A. Oyetade, Vincent O. Nyamori, Bice S. Martincigh and Sreekantha B. Jonnalagadda. Terpyridyl-functionalised carbon nanotubes as a novel adsorbent for the removal of Cu(II) from aqueous solution. Presented at the 12th International Conference on Materials Chemistry, York, United Kingdom, on 20th July – 23rd July 2015.

5. Oral Presentation

Oluwaseun A. Oyetade, Vincent O. Nyamori, Bice S. Martincigh and Sreekantha B. Jonnalagadda. Nitrogen-functionalized carbon nanotubes for the removal of bisphenol A and ibuprofen from aqueous solution by using nitrogen-functionalized multiwalled carbon nanotubes. Presented at the 42nd National Convention of the South African Chemical Institute, Durban, South Africa, 29th November – 4th December 2015.

Acknowledgements

I will like to thank my supervisors and mentors: Professor S. B. Jonnalagadda, Professor B. S. Martincigh and Professor V. O. Nyamori, for their patience, financial, moral and academic guidance throughout the period of this programme. So much has been learnt from you and will serve to make me a better researcher in future.

I would also like to extend my appreciation to the School of Chemistry and Physics, University of KwaZulu-Natal and her staff for providing a well-equipped environment wherein this research was carried out. My appreciation goes to the technical staff (Anita Naidoo, Neal Broomhead, Unathi Bongoza, Greg Moodley and Brian Ndlovu) for their guidance.

Many thanks to my colleagues and friends in the Physical and Nano-chemistry unit, with whom we have spent these years together. Your friendship and guidance have enormously contributed to the success of this work, and for this, I am grateful and glad to have met you all. Of notable mention is the contribution from Dr. B. O. Owaga, Dr. C. M. A. Iwegbue and Dr. I. A. A. Hamza for your words of wisdom and encouragement.

To my wonderful parents, Rev & Mrs A.O. Oyetade, for keeping faith in me, for supporting me financially, morally and emotionally and for your words of encouragement, I am most grateful. I would also like to appreciate my siblings, Dupe, Titi and Anu, for their continued support.

Finally, unto Almighty God all praise and glory return to, for his immense protection and divine guidance during the period of this study. To this end, "I will sing praises to thee, and not be silent. O Lord my God, I will give thanks unto thee forever" (Psalm 30:12).

Table of Contents

Abstract	ii
Preface.....	v
Declaration 1 - Plagiarism.....	vi
Declaration 2 - Publications	vii
Conference contributions	x
Acknowledgements	xi
Table of Contents	xii
Chapter 1	1
Introduction	1
1.1. Statement of the problem	2
1.2. Aim and objectives of the study	4
1.3. Thesis overview.....	5
References	8
Chapter 2	10
Background information and literature review	10
2.1. Metal pollutants in water.....	10
2.1.1. Lead.....	11
2.1.2. Cadmium	11
2.1.3. Mercury	12
2.1.4. Copper	12
2.1.5. Zinc.....	13
2.2. Organic pollutants in water	13
2.2.1. Bisphenol A.....	14
2.2.2. Ibuprofen	15
2.3. Organic dyes in water.....	15
2.3.1. Rhodamine B.....	16
2.4. Technologies for wastewater remediation.....	16
2.4.1. Advanced oxidation processes	17
2.4.2. Membrane separation	18
2.4.3. Ion-exchange	18
2.4.4. Aerobic and anaerobic treatment.....	19
2.5. Adsorption.....	19
2.5.1. Types of adsorption.....	20
2.5.1.1. Physical adsorption (physisorption)	20
2.5.1.2. Chemical adsorption (chemisorption)	20
2.6. Adsorption kinetics	21
2.6.1. Pseudo-first order model	22

2.6.2.	Pseudo-second order model.....	22
2.6.3.	Intraparticle diffusion model.....	22
2.6.4.	Elovich model	23
2.7.	Adsorption isotherms	23
2.7.1.	Langmuir isotherm.....	23
2.7.2.	Freundlich isotherm.....	24
2.7.3.	Temkin isotherm	25
2.7.4.	Dubinin-Radushkevich isotherm.....	25
2.7.5.	Sips isotherm.....	26
2.7.6.	Toth isotherm	26
2.7.7.	Khan isotherm	27
2.7.8.	Redlich-Peterson isotherm	27
2.8.	Thermodynamic parameters of adsorption.....	27
2.9.	Adsorbents.....	29
2.10.	Carbon nanotubes.....	29
2.10.1.	Functionalization of CNTs	30
2.10.2.	CNT/ferrite composites	33
2.11.	Desorption.....	36
2.12.	Characterization/analytical techniques.....	36
2.12.1.	Nuclear magnetic resonance spectrometry.....	37
2.12.2.	Mass spectrometry.....	37
2.12.3.	Fourier transform infrared spectrophotometry	37
2.12.4.	Raman spectroscopy.....	38
2.12.5.	Thermogravimetric analysis	38
2.12.6.	Imaging and microscopic techniques	38
2.12.7.	Brunauer, Emmet and Teller analysis	39
2.12.8.	Elemental analysis.....	39
2.12.9.	Inductively coupled plasma-optical emission spectroscopy.....	39
2.12.10.	Cold vapour atomic absorption spectrophotometry	40
2.12.11.	High performance liquid chromatography	40
2.12.12.	Boehm titration.....	40
2.12.13.	Point of zero charge.....	41
	References.....	42
	Chapter 3	58
	Perfluoroalkyl compounds: Occurrence, fate and their adsorption mechanism onto carbon nanotubes.....	58
	Abstract	59
3.1.	Introduction	60
3.2.	Occurrence of PFAAs in the environment	64
3.2.1.	PFAA in aqueous solution.....	64

3.3.	Adsorption.....	66
3.3.1.	Activated carbon	67
3.3.2.	Sludge.....	68
3.3.3.	Resins	68
3.3.4.	Zeolite.....	69
3.4.	Carbon nanotubes.....	70
3.4.1.	Functionalization of carbon nanotubes.....	71
3.4.2.	Covalent functionalization of CNTs.....	71
3.4.3.	Non-covalent functionalization of CNTs	73
3.5.	PFC adsorption onto carbon nanotubes.....	73
3.5.1.	Effect of solution pH.....	74
3.5.2.	Adsorption kinetics	74
3.5.3.	Adsorption Isotherms	76
3.6.	Adsorption mechanisms of PFAAs	79
3.7.	Conclusion.....	81
	References	83
	Chapter 4	92
	Nitrogen-functionalised carbon nanotubes as a novel adsorbent for the removal of Cu(II) from aqueous solution.....	92
	Abstract	93
4.1.	Introduction	94
4.2.	Experimental	96
4.2.1.	Materials.....	96
4.2.2.	Characterization	96
4.2.2.1.	Determination of point of zero charge (pH_{PZC})	97
4.2.2.2.	Boehm titration.....	97
4.2.3.	Procedure for the synthesis of 4'-(4-hydroxyphenyl)-2,2':6',2''-terpyridine	98
	(HO-Phttpy)	98
4.2.4.	Preparation of MWCNT-COOH	98
4.2.5.	Preparation of MWCNT-COCl	99
4.2.6.	Preparation of MWCNT-COOtpty	99
4.2.7.	Functionalization of MWCNT-tpty	99
4.2.8.	Adsorbate preparation	99
4.2.9.	Sorption experiments.....	99
4.2.9.1.	Kinetics, isotherm and thermodynamic studies.....	100
4.2.9.2.	Desorption experiments.....	101
4.2.10.	Data analysis	102
4.3.	Results and discussion.....	102

4.3.1.	Synthesis of 4'-(4-hydroxyphenyl)-2,2':6',2"-terpyridine (HO-Phttpty).....	102
4.3.2.	Synthesis of MWCNT-ttpty	103
4.3.3.	Characterization of adsorbents	104
4.4.	Batch adsorption processes	109
4.4.1.	Effect of pH.....	109
4.4.2.	Effect of contact time	110
4.4.3.	Kinetics studies	111
4.4.4.	Effect of adsorbent dose	113
4.4.5.	Effect of initial adsorbate concentration.....	114
4.4.6.	Effect of temperature.....	114
4.4.7.	Adsorption isotherms	115
4.4.8.	Thermodynamic parameters of adsorption.....	118
4.4.9.	Desorption studies	119
4.5.	Conclusions	120
	References	121
	Chapter 5	125
	Adsorption of Pb ²⁺ and Zn ²⁺ from aqueous solution onto functionalized multiwalled carbon nanotubes.....	125
	Abstract	126
5.1.	Introduction	127
5.2.	Experimental	128
5.2.1.	Materials and chemicals	128
5.2.2.	Preparation of adsorbents	129
5.2.3.	Metal analysis procedure.....	129
5.2.3.1.	Equipment	129
5.2.3.2.	Preparation of adsorbate solution	129
5.2.4.	Adsorption experiments	130
5.2.5.	Desorption studies	132
5.2.6.	Data analysis	132
5.3.	Results and Discussion.....	133
5.3.1.	Characterization of adsorbents	133
5.3.2.	Batch adsorption experiments	133
5.3.2.1.	Effect of pH.....	133
5.3.2.2.	Effect of contact time	135
5.3.2.3.	Effect of adsorbent dose	138
5.3.2.4.	Effect of temperature.....	139
5.3.2.5.	Isotherm studies.....	141
5.3.2.6.	Thermodynamic studies	145
5.3.2.7.	Desorption	146

5.4. Conclusions	147
References	148
Chapter 6	153
Removal of Cd ²⁺ and Hg ²⁺ onto nitrogen-functionalized carbon nanotube from aqueous solutions	153
Abstract	154
6.1. Introduction	155
6.2. Experimental	157
6.2.1. Materials and chemicals	157
6.2.2. Adsorbent preparation	157
6.2.2.1. Preparation of oxidized MWCNTs (MWCNT-COOH)	157
6.2.2.2. Synthesis of 4'-(4-hydroxyphenyl)-2,2':6',2''-terpyridine (HO-Phttpy)	158
6.2.2.3. Preparation of nitrogen-functionalized MWCNTs (MWCNT-tpty)	158
6.2.3. Metal analysis procedure	159
6.2.3.1. Equipment	159
6.2.3.2. Preparation of adsorbate solution	159
6.2.3.3. Calibration of spectrophotometers	159
6.2.4. Batch adsorption studies	159
6.2.4.1. Kinetics, isotherm and thermodynamic studies	160
6.2.5. Desorption experiments	162
6.2.6. Data analysis	163
6.3. Results and discussion	163
6.3.1. Characterization of adsorbents	163
6.3.2. Batch adsorption experiments	163
6.3.2.1. Effect of pH	164
6.3.2.2. Effect of contact time	166
6.3.2.3. Effect of adsorbent dose	169
6.3.2.4. Effect of initial metal ion concentration	170
6.3.2.5. Effect of temperature	171
6.3.2.6. Isotherm studies	172
6.3.2.7. Thermodynamic parameters of adsorption	176
6.3.3. Desorption studies	177
6.4. Conclusions	178
References	179
Chapter 7	185
Adsorption of Pb ²⁺ , Zn ²⁺ , Cd ²⁺ and Cu ²⁺ onto nitrogen-functionalized multiwalled carbon nanotubes: Single- and multi- component adsorption study	185
Abstract	186
7.1. Introduction	187

7.2.	Experimental	188
7.2.1.	Materials and chemicals	188
7.2.2.	Adsorbent preparation	188
7.2.2.1.	Preparation of MWCNT-COOH	188
7.2.2.2.	Synthesis of 4'-(4-hydroxyphenyl)-2,2':6',2"-terpyridine (HO-Phttpy)	189
7.2.2.3.	Preparation of MWCNT-ttpty	189
7.2.3.	Metal analysis procedure.....	190
7.2.3.1.	Equipment	190
7.2.3.2.	Preparation of adsorbate solution	190
7.2.3.3.	Calibration of ICP-OES spectrometer.....	190
7.2.4.	Batch adsorption studies.....	190
7.2.4.1.	Isotherms	192
7.2.4.2.	Data analysis	192
7.2.4.3.	Distribution coefficient.....	192
7.2.5.	Analysis of real water samples	192
7.3.	Results and discussion.....	193
7.3.1.	Adsorption of metal ions in single-solute systems	193
7.3.2.	Adsorption of metal ions in multicomponent systems	194
7.3.2.1.	Effect of pH.....	194
7.3.2.2.	Effect of equal initial metal ion concentration	195
7.3.2.3.	Effect of varying metal ion concentration	197
7.3.3.	Adsorption isotherms	201
7.3.4.	Analysis of real samples.....	202
7.4.	Conclusions	203
	References	204
	Chapter 8	207
	Kinetics, isotherm and thermodynamic studies for the removal of bisphenol A and ibuprofen from aqueous solution by using nitrogen-functionalized multiwalled carbon nanotubes.....	207
	Abstract	208
8.1.	Introduction	209
8.2.	Experimental	211
8.2.1.	Materials and chemicals	211
8.2.2.	Synthesis and characterization of adsorbents	211
8.2.3.	Instrumentation.....	211
8.2.3.1.	Chromatographic conditions	212
8.2.4.	Sorbate preparation.....	212
8.2.5.	Sorption Experiments and detection of BPA and IBP.....	212
8.2.6.	Desorption studies	214

8.2.7.	Data analysis	214
8.3.	Results and discussion.....	215
8.3.1.	Effect of pH.....	215
8.3.2.	Effect of time.....	216
8.3.2.1	Kinetic studies	217
8.3.3.	Effect of adsorbent dose.....	219
8.3.4.	Effect of temperature.....	220
8.3.5.	Isotherm studies.....	221
8.3.6.	Thermodynamic studies	225
8.3.7.	Desorption studies	226
8.4.	Conclusions	227
	References	228
	Chapter 9	233
	Co-adsorption of bisphenol A and ibuprofen onto functionalized multiwalled carbon nanotubes: Influence of metal ions in solution	233
	Abstract	234
9.1.	Introduction	235
9.2.	Experimental	236
9.2.1.	Materials and chemicals	236
9.2.2.	Synthesis and characterization of adsorbents	237
9.2.3.	Analysis of adsorbates.....	237
9.2.3.1.	Instrumentation.....	237
9.2.3.2.	Preparation of standard stock solutions.....	238
9.2.3.3.	Chromatographic conditions for the quantification of BPA and IBP.....	238
9.2.3.4.	ICP-OES conditions for quantification of metal ions.....	238
9.2.4.	Batch adsorption studies.....	239
9.2.4.1.	Isotherms	240
9.2.4.2.	Data analysis	240
9.2.4.3.	Distribution coefficients.....	241
9.3.	Results and discussion.....	241
9.3.1.	Adsorption of BPA and IBP in single adsorption systems.....	241
9.3.2.	Adsorption in binary systems	242
9.3.2.1.	Effect of pH.....	242
9.3.2.2.	Effect of equal initial concentration	244
9.3.2.3.	Effect of varying adsorbate concentration.....	245
9.3.3.	Competitive adsorption isotherms.....	250
9.4.	Conclusions	251
	References	253

Chapter 10.....	257
Effectiveness of carbon nanotube/cobalt ferrite nanocomposites for the adsorption of rhodamine B from aqueous solutions.....	257
Abstract	258
10.1. Introduction.....	259
10.2. Experimental	260
10.2.1. Chemicals	260
10.2.2. Preparation of cobalt ferrite nanoparticles	261
10.2.3. Preparation of functionalized multiwalled carbon nanotubes	261
10.2.4. Preparation of composite samples (MWCNT-COOH-CoFe ₂ O ₄).....	261
10.2.5. Characterization of adsorbents	262
10.2.5.1. Determination of point of zero charge (pH _{PZC})	262
10.2.6. Adsorbate preparation	262
10.2.7. Batch adsorption procedure.....	263
10.2.7.1. Kinetics studies	263
10.2.7.2. Adsorption isotherms	264
10.2.7.3. Desorption experiments.....	265
10.2.8. Data Analysis	265
10.3. Results and discussion.....	266
10.3.1. Characterization of adsorbents	266
10.3.2. Batch adsorption experiments	270
10.3.2.1. Effect of pH.....	270
10.3.2.2. Effect of contact time	272
10.3.2.3. Adsorption kinetics	273
10.3.2.4. Effect of adsorbent dose.....	274
10.3.2.5. Effect of initial RhB concentration	275
10.3.2.6. Effect of temperature.....	276
10.3.2.7. Adsorption isotherms	278
10.3.2.8. Thermodynamic parameters of adsorption.....	286
10.3.3. Desorption Studies	289
10.4. Conclusions	289
References.....	291
Chapter 11	295
General conclusions and recommendations	295
Appendix I.....	300
Data for Copper(II).....	300
Appendix II	309
Data for Lead(II) and Zinc(II)	309
Appendix III.....	321

Data for cadmium(II) and mercury(II)	321
Appendix IV	334
Data for competitive adsorption of divalent metal ions	334
Appendix V	341
Data for Bisphenol (BPA) and Ibuprofen (IBP).....	341
Appendix VI.....	356
Data for competitive adsorption of bisphenol A and ibuprofen	356
Appendix VII	361
Data for Rhodamine B (RhB).....	361

Chapter 1

Introduction

Water is a substance upon which all known forms of life depend.^{1,2} It covers about 71% of the earth's surface, with the largest portion contained in seas and oceans.^{3,4} The availability of fresh water to man for domestic purposes is in short supply, resulting in water scarcity across the world. In 2010, a study conducted by the Consulting Engineers SA, envisages that South Africa would suffer major water scarcity by 2025 (Fig 1.1).⁵ Physical factors, such as increasing urbanization, population and infrastructure, were highlighted as the main reasons behind this impending problem. The complexities associated with water scarcity therefore require prudent management for the continued survival of man and animals.

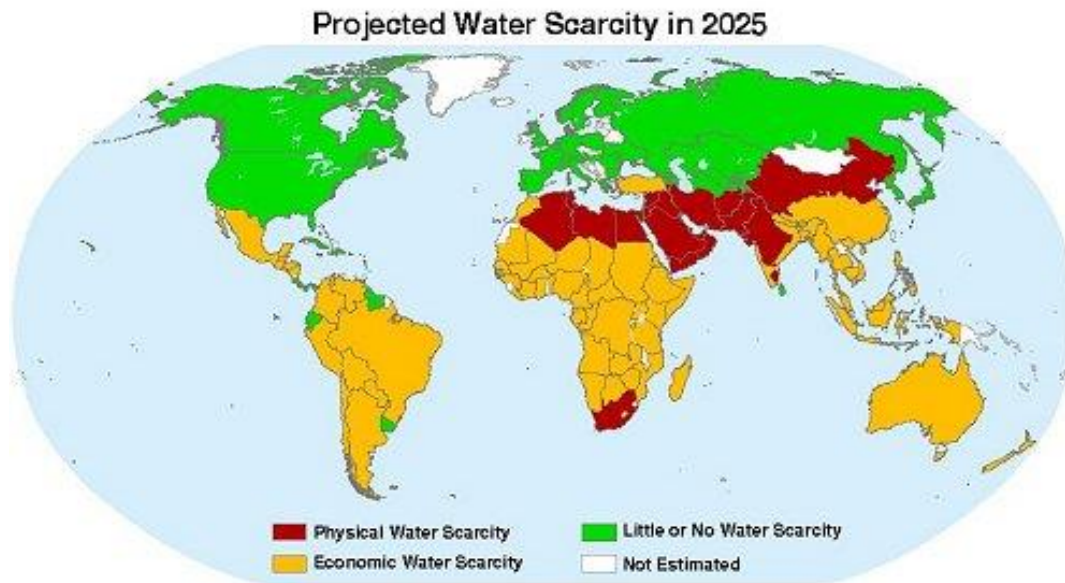


Fig. 1.1: Projected water scarcity in the world by 2025.⁵

Anthropogenic activities involving the introduction of chemical, physical, microbial and radioactive substances into aqueous media are responsible for increased pollution, hence, exacerbating the scarcity of clean water.⁶ Wastewaters containing several toxic pollutants are regularly generated by industries, and are taken through little or no further treatment before their disposal into the environment. Unfortunately, most pollutants are water-soluble and eventually end up in groundwater, rivers, streams and oceans through various natural processes. Water pollution therefore limits the availability of clean water, posing serious environmental and health challenges to its dependants and can lead to death and the spread

of diseases. It is estimated that water pollution accounts for more than 14000 deaths daily.^{7,8} To avert this problem, a crucial need exists for the remediation of wastewater produced by industries in order to alleviate water scarcity and generate freshwater to cater for human needs.

This study sought to develop nanomaterials containing carbon nanotubes (CNTs) as adsorbents for the purification of contaminated water. To achieve this, functional groups were anchored onto the side/walls of CNTs to increase the activity of tubes towards the removal of heavy metal ions and organic contaminants from aqueous solutions. Magnetic nanocomposites were also developed for the removal of dyes from aqueous solution. This chapter describes the problem, and the aim and objectives of this work.

1.1 Statement of the problem

Increased industrialization and urbanization have been highlighted as two primary sources of water pollution and mortification of the environment.⁹ The discharge of waste products from industries containing several toxic contaminants into the environment, exposes man, biotic and abiotic organisms to various health complications.¹⁰ Industrial applications such as mining, electroplating, fertilizer and pesticide production, battery manufacturing and agricultural spills produce effluents containing high amounts of heavy metal ions such as lead, zinc, cadmium, mercury and copper.¹¹

Heavy metals are usually referred to as metallic elements with atomic numbers greater than 20 and densities above 5 g cm^{-3} .¹² These substances are water-soluble, stable, persistent in the environment and non-degradable under natural processes.¹³ Due to these factors, they are easily transported by natural means and remain for long periods of time in the environment. Accumulation of these substances in humans may result in reproductive disorders, cancer, liver, muscle and bone diseases, and in extreme cases lead to death.^{11,13} Some metals such as copper and zinc are essential to both plants and animals, however, they are considered toxic when their amounts exceed the threshold limit.¹⁴

Similarly, the ingestion of organic compounds such as bisphenol A (BPA) and ibuprofen (IBP) result in changes in neurological, developmental and reproductive organs, and may lead to diseases such as cancer, birth defects and brain damage.¹⁵ Although IBP is a pharmaceutical product and one of the most commonly used medicines in the world,¹⁶ indiscriminate ingestion may result in infertility and several reproductive disorders in man.¹⁷ In addition, textile manufacturing, printing and painting industries generate coloured effluents, which off-sets biological activities when released into aqueous media.¹⁸ A

literature review providing insights into the fate and effects of heavy metals and organic pollutants is provided in Chapter 2.

It is therefore necessary to develop a simple, effective and efficient technique for the removal of pollutants from effluents/wastewater before their discharge into the natural environment. In recent times, various techniques such as ion-exchange, chemical precipitation, coagulation, osmosis, membrane separation and adsorption, amongst many others, have been investigated in order to achieve purification. These methods will be discussed in Chapter 2, together with the advantages and disadvantages associated with each method.

Of these methods, adsorption is considered best and for the removal of toxic pollutants from wastewater.¹⁰ The technique is simple, obtaining good removal efficiencies for high and low adsorbate concentration, and most importantly offers the possibility of adsorbent regeneration for reuse. However, the development of sorbents with multiple functional groups to enhance faster or dual removal of pollutants is still a challenge. Regeneration of adsorbents often poses a significant problem, as recovered sorbents lose their efficiencies, resulting in low uptake of pollutants. Since, effluents usually contain multiple pollutants in them, there is therefore an urgent need to develop sorbents containing multiple functional groups which will aid the simultaneous removal of pollutants from wastewater. It is also imperative to develop sorbents with high adsorption capacities and retain their efficiencies after regeneration.

Carbon nanotubes (CNTs), a member of the fullerene structural family, were discovered by Iijima in 1991.¹⁹ These carbon nanostructured materials were observed to possess tubular structures, possessing remarkable mechanical, thermal and optical properties.²⁰ CNTs may be classified into single-walled carbon nanotubes (SWCNTs) or multiwalled carbon nanotubes (MWCNTs), depending on the number of concentric graphene sheets rolled to form them.²⁰ The growing interest in the use of CNTs in environmental sciences, especially as superior adsorbents for inorganic and/or organic pollutant removal, stems from the fact that they possess high surface areas and porosity, and can be easily tuned to contain expected functional groups. Acidic functionalization of CNTs introduces oxygen-containing groups which increases their dispersability in aqueous media. These groups can serve as active sites for the removal of pollutants such as metal ions from aqueous solution. To increase the activity of CNTs, new functional groups such as $-NR$, $-F$, $-Cl$ and $-SR$, can also be incorporated onto the walls/sides of the tubes through wet chemistry. Additionally, composites involving CNTs and other nanomaterials can be formed to produce a synergy between the involved nanomaterials. For instance, magnetic carbon nanotubes can be developed by forming composites with ferrites so as to have increased magnetism, surface area, porosity and active sites.

In spite of increasing number of studies on the removal of pollutants by using CNTs, to the best of my knowledge, no known study has been investigated on the functionalization of CNTs by the use of the nitrogen-donor ligand, 4'-(4-hydroxyphenyl)-2,2':6',2''-terpyridine. This concept will introduce nitrogen-containing functional groups onto the CNT walls to achieve increased removal of organic and/or inorganic pollutants from aqueous solutions. Also, magnetic carbon nanotubes were synthesized in varying doping ratios of CNTs with cobalt ferrite nanoparticles, so as to produce an adsorbent which can be easily removed from solution *via* an external magnetic field. This concept was adopted to produce magnetic MWCNTs for the removal of the dye, rhodamine B (RhB), from aqueous solutions.

1.2. Aim and objectives of the study

The aim of this research was to develop functionalized carbon nanomaterials or nanocomposites for the removal of metal ions, bisphenol A, ibuprofen and rhodamine B from contaminated water. This was achieved through the following objectives:

- i. To functionalize commercially obtained pristine-MWCNTs with a mixture of concentrated nitric and sulphuric acids.
- ii. To synthesize the ligand, 4'-(4-hydroxyphenyl)-2,2':6',2''-terpyridine, and characterize it by using nuclear magnetic resonance and mass spectrometry, melting point measurements and Fourier transform infrared (FTIR) spectrophotometry.
- iii. To synthesize nitrogen-functionalized MWCNTs by using the ligand, 4'-(4-hydroxyphenyl)-2,2':6',2''-terpyridine.
- iv. To prepare composites of varying doping ratios of acid-functionalized MWCNTs with cobalt ferrite nanoparticles.
- v. To characterize all adsorbents by using techniques such as transmission and scanning electron microscopy, thermogravimetric analysis (TGA), Brunauer, Emmett and Teller (BET) surface area, FTIR and Raman spectroscopy, Boehm titration and elemental analysis.
- vi. To carry out batch adsorption processes investigating the influence of pH, contact time, adsorbent dose, initial adsorbate concentration and temperature on the adsorption of Pb^{2+} , Zn^{2+} , Cu^{2+} , Cd^{2+} , Hg^{2+} , BPA, IBP from aqueous solution using acid-modified and nitrogen-functionalized MWCNTs.
- vii. To perform batch adsorption processes investigating the effects of pH, contact time, adsorbent dose, initial RhB concentration and temperature on the adsorption of RhB from aqueous solution by using cobalt ferrite nanoparticles, acid-functionalized MWCNTs, 29%, 50% and 75% cobalt ferrite-MWCNTs nanocomposites.

- viii. To fit the equilibrium adsorption data into two- and three-parameter isotherm models, such as the Langmuir, Freundlich, Temkin, Sips, Toth, Khan, Redlich-Peterson and Dubinin-Radushkevich models.
- ix. To investigate the mechanisms or dynamics of each adsorption process from kinetics models such as the pseudo-first order, pseudo-second order, intraparticle diffusion and Elovich models.
- x. To compute the thermodynamic parameters of adsorption, such as change in Gibbs energy (ΔG°), change in entropy, (ΔS°) and change in enthalpy (ΔH°) of the sorption process.
- xi. To investigate the competitive adsorption involved in the sorption of metal ions such as Pb^{2+} , Zn^{2+} , Cu^{2+} and Cd^{2+} .
- xii. To evaluate the competitive adsorption involved in the sorption of BPA and IBP.
- xiii. To investigate the simultaneous sorption of BPA, IBP and metal ions such as Pb^{2+} and Cd^{2+} .
- xiv. To perform desorption studies on each adsorbent to evaluate the possibility of regenerating the adsorbents and the recovering the adsorbates for reuse.

1.3. Thesis overview

This thesis contains eleven chapters, which are briefly described below. The novel aspect of this work include the synthesis of nitrogen-functionalized multiwalled carbon nanotubes using 4'-(4-hydroxyphenyl)-2,2':6',2''-terpyridine as a modifier and its application for the removal of heavy metal ions such as Pb^{2+} , Cu^{2+} , Cd^{2+} , Zn^{2+} and Hg^{2+} from aqueous solutions and the preparation of composites containing carbon nanotubes and cobalt ferrite nanoparticles for the removal of rhodamine B from aqueous solution. Isotherm and kinetics studies was also investigated to understand the mechanism of each adsorption process.

This thesis is written in manuscript format and consists of a series of stand-alone chapters. Hence, the style of each chapter will be unique to the format where the manuscript has been published or in preparation to be submitted. The thesis, however, should be coherent with the objectives as listed previously.

Chapter 1 includes a brief introduction on water pollution and the impending problems that arise from the drought of water. It further highlights the need for the remediation of wastewater before they are discharged into the aquatic environment. A statement of the problem, and the aim and objectives of the study are presented in the chapter.

Chapter 2 presents a background information and a literature review on the topic of the study. The fate, sources and effects of targeted pollutants (i.e. Pb, Cu, Cd, Zn, Hg, BPA, IBP and RhB) are described. An overview of the methods used for wastewater remediation, and a review on the use of carbon nanotubes as adsorbents for water treatment purposes is given.

Chapter 3 is a literature review on the removal of perfluorinated compounds from aqueous solutions. The nitrogen-functionalized CNTs were originally designed for the simultaneous removal of perfluorinated compounds (PFCs) and heavy metal ions from aqueous solutions. However, because of the breakdown of the high performance liquid chromatography-mass spectrometry (HPLC-MS), the detection and quantification of PFCs could not be carried out. Hence, the material synthesized was tested on heavy metal ions and the organic pollutants, bisphenol A and ibuprofen, for which analysis equipment was available. This chapter therefore presents a review on intended future work by applying synthesized nitrogen-functionalized CNTs for the removal of perfluorinated compounds (PFCs) in aqueous solution. The occurrence, fate, effects and adsorption mechanism of perfluorinated compounds onto carbon nanotubes are presented in this chapter.

Chapter 4 presents a detailed study of the preparation of acid- and nitrogen-functionalized multiwalled carbon nanotubes. Characterization of the adsorbents and their application for the removal of Cu^{2+} from aqueous solutions is described. The kinetics and isotherms of the processes were equally provided.

Chapter 5 describes the adsorption process involved for the removal of Pb^{2+} and Zn^{2+} from aqueous solutions onto acid- and nitrogen-functionalized multiwalled carbon nanotubes. The kinetics, isotherm and thermodynamics of the adsorption process are also presented in the chapter.

Chapter 6 discusses the behaviour of acid- and nitrogen-functionalized multiwalled carbon nanotubes for the adsorption of Cd^{2+} and Hg^{2+} .

Chapter 7 reports on the competitive adsorption of Pb^{2+} , Cu^{2+} , Cd^{2+} , and Zn^{2+} from aqueous solutions onto nitrogen-functionalized multiwalled carbon nanotubes.

Chapter 8 gives a detailed investigation into the removal of bisphenol A and ibuprofen from aqueous solution by adsorption onto acid- and nitrogen-functionalized multiwalled carbon nanotubes.

Chapter 9 investigates the binary adsorption of bisphenol A and ibuprofen from aqueous solution. The influence of Pb^{2+} or Cd^{2+} as examples of heavy metals on the adsorption of bisphenol A and ibuprofen is also presented in this chapter.

Chapter 10 discusses the preparation of cobalt-ferrite-multiwalled carbon nanotube nanocomposites and their application for the removal of the dye, rhodamine B, from aqueous solutions. This chapter has already been published in a peer-reviewed article (RSC Adv., 2015, **5**, 22724-22739).

Chapter 11 provides some general conclusions arising from the work conducted in this study and also suggests plausible avenues for future research.

References

- (1) World Health Organization (WHO). Guidelines for Drinking-water Quality, Geneva. 2011.
- (2) World Health Organization (WHO). Guidelines for Drinking-water Quality, Geneva. 2008.
- (3) Greenlee, L. F.; Lawler, D. F.; Freeman, B. D.; Marrot, B.; Moulin, P. Reverse osmosis desalination: water sources, technology, and today's challenges. *Water Res.* 2009, *43*, 2317-2348.
- (4) <http://en.wikipedia.org/wiki/Water>. Accessed on 27th March 2015.
- (5) <http://www.rainharvest.co.za/2010/03/warning-on-water-demand-in-south-africa/>. Accessed on 27th March 2015.
- (6) <http://www.eoearth.org/view/article/156920/>. Accessed on 27th March 2015
- (7) Hamza, I. A. A. Preparation and evaluation of a sugarcane bagasse multi-walled carbon nanotube composite for the adsorption of heavy metals from aqueous solutions. *PhD Thesis* 2013, *University of KwaZulu-Natal, Durban, South Africa*.
- (8) Daniel, M. H. B.; Montebelo, A. A.; Bernardes, M. C.; Ometto, J. P. H. B.; de Camargo, P. B.; Krusche, A. V.; Ballester, M. V.; Victoria, R. L.; Martinelli, L. A. Effects of urban sewage on dissolved oxygen, dissolved inorganic and organic carbon, and electrical conductivity of small streams along a gradient of urbanization in the Piracicaba river basin. *Water, Air, Soil Pollut.* 2002, *136*, 189-206.
- (9) Senthilkumaar, S.; Bharathi, S.; Nithyanandhi, D.; Subburam, V. Biosorption of toxic heavy metals from aqueous solutions. *Bioresour. Technol.* 2000, *75*, 163-165.
- (10) Hamza, I. A. A.; Martincigh, B. S.; Ngila, J. C.; Nyamori, V. O. Adsorption studies of aqueous Pb(II) onto a sugarcane bagasse/multi-walled carbon nanotube composite. *Phys. Chem. Earth* 2013, *66*, 157-166.
- (11) Melichova, Z.; Hromada, L. Adsorption of Pb²⁺ and Cu²⁺ ions from aqueous solutions on natural bentonite. *Pol. J. Environ. Stud.* 2013, *22*, 457-464.
- (12) Duffus, J. H. "Heavy metals"- A meaningless term? *Pure Appl. Chem.* 2002, *74*, 793-807.
- (13) Li, Y.-H.; Wang, S.; Wei, J.; Zhang, X.; Xu, C.; Luan, Z.; Wu, D.; Wei, B. Lead adsorption on carbon nanotubes. *Chem. Phys. Lett.* 2002, *357*, 263-266.
- (14) Appenroth, K.-J.: Definition of "heavy metals" and their role in biological systems. In *Soil Heavy Metals, Soil Biol.*, 2010; Vol. 19; pp 19-29.
- (15) Dehghani, M. H.; Mahvi, A. H.; Rastkari, N.; Saeedi, R.; Nazmara, S.; Irvani, E. Adsorption of bisphenol A (BPA) from aqueous solutions by

- carbon nanotubes: kinetic and equilibrium studies. *Desalin. Water Treat.* 2014, 1-9.
- (16) Cho, H.-H.; Huang, H.; Schwab, K. Effects of solution chemistry on the adsorption of ibuprofen and triclosan onto carbon nanotubes. *Langmuir* 2011, 27, 12960.
- (17) Jung, C.; Park, J.; Lim, K. H.; Park, S.; Heo, J.; Her, N.; Oh, J.; Yun, S.; Yoon, Y. Adsorption of selected endocrine disrupting compounds and pharmaceuticals on activated biochars. *J. Hazard. Mater.* 2013, 263, 702-710.
- (18) Namasivayam, C.; Muniyasamy, N.; Gayatri, K.; Rani, M.; Ranganathan, K. Removal of dyes from aqueous solutions by cellulosic waste orange peel. *Bioresour. Technol.* 1996, 57, 37-43.
- (19) Iijima, S. Helical microtubules of graphitic carbon. *Nature* 1991, 354, 56-58.
- (20) Ombaka, L. M.; Ndungu, P.; Nyamori, V. O. Usage of carbon nanotubes as platinum and nickel catalyst support in dehydrogenation reactions. *Catal. Today* 2013, 217, 65-75.

Chapter 2

Background information and literature review

In this study, a novel adsorbent was synthesized by incorporating 4'-(4-hydroxyphenyl)-2,2':6',2''-terpyridine onto acid-functionalized MWCNTs to afford nitrogen-functionalized MWCNTs. This adsorbent was applied for the removal of heavy metal ions, bisphenol A and ibuprofen from aqueous solutions, and its adsorption efficiency compared with acid-functionalized MWCNTs. Further, the removal of rhodamine B from aqueous solution was investigated by using nanocomposites containing varying ratios of MWCNTs and cobalt ferrite nanoparticles. This chapter provides in-depth information on the sources, fate and health effects associated with the exposure of heavy metals (lead, zinc, copper, cadmium and mercury), organic contaminants (bisphenol A and ibuprofen) and rhodamine B dye to man, aquatic life and the environment. The remediation of wastewater by using various techniques is explored, with particular interest on adsorption. The adsorption kinetics, isotherms and thermodynamics studies of carbon-based nanomaterials to the highlighted pollutants was further reviewed. Desorption of adsorbents for the purpose of regeneration and adsorbate recovery for possible reuse was also investigated

2.1. Metal pollutants in water

The pollution of aqueous media by heavy metal ions is one of the major environmental concerns of contemporary society.^{1,2} In 2007, metals were listed as priority hazardous substances by the Agency for Toxic Substances and Disease Control (ATSDR).^{3,4} This is due to their persistence, bioaccumulation and non-biodegradable nature in the environment.^{5,6} Although, the exposure of metals to man, aquatic life and animals has been well-documented, efforts to reduce their intrusion into water streams are still yielding very few results,¹ especially in developing countries such as South Africa. The contamination of natural water (rivers, lakes, oceans and seas) with metal ions has been accelerated by the frequent discharge of effluents generated from industries.⁷⁻⁹ Some metals (cadmium, chromium, lead and mercury) are considered toxic even at low concentrations,^{2,7,10} while other micronutrients such as iron, copper and zinc are essential at low concentrations,^{11,12} but may become harmful with increased exposure. In this study, the effects and sources of five metal ions (lead, cadmium, mercury, copper and zinc) were reviewed, due to the high toxicity associated with lead, cadmium and mercury and the health complications accompanying increased exposure to copper and zinc by man.

2.1.1. Lead

Lead (Pb) is ranked as the second most toxic substance in the 2013 priority list of hazardous compounds,^{3,13} due to the high level of toxicity associated with its intake. The maximum acceptable concentrations of lead in water (0.01-0.1 mg dm⁻³),^{14,15} soil (0.09 mg kg⁻¹)¹³ and air (0.003 mg m⁻³)¹³ were established by various environmental agencies in order to enact laws against its incessant disposal into the environment. Unfortunately, its addition as a priority contaminant has not limited its usage in construction, radioactive shields, petrochemical industries, water pipe lining, metal plating, battery and textile manufacturing. Evidence of lead is regularly reported in various samples, such as water,^{16,17} soil,¹⁸ air,¹⁹ electrical equipments,²⁰ and food,²¹ amongst many others. The principal point source of lead is *via* the discharge of untreated effluents into water streams, hence, accumulating in run-offs and intruding into other media such as the soil, sediments and air. Lead ingestion and accumulation can result in several diseases such as damage to the kidney, liver, central nervous system, bones, cancer, mental dysfunction, intelligence inhibitors and in extreme cases, may eventually result in death.²²⁻²⁴

The speciation of Pb is controlled by the pH of the aqueous solution. Pb exists as divalent ions in acidic conditions, however, lead hydroxides, such as [Pb(OH)₂], [Pb(OH)]⁺, [Pb(OH)₃]⁻, [Pb₃(OH)₄]²⁺, [Pb₂(OH)]³⁺, [Pb₄(OH)₄]⁴⁺ and [Pb₆(OH)₈]⁴⁺, may be formed in basic conditions.^{25,26}

2.1.2. Cadmium

Cadmium (Cd) is a soft, rare, malleable, bluish-white metal, which may be found naturally on the earth's crust and occurs in combination with zinc, lead or copper ores.^{27,28} Cadmium, classified as the seventh most toxic substance,³ gains wide application in industries for batteries and alloy manufacturing, refining, mining, electroplating, smelting and paint pigment, plastics, fertilizer and pesticide production.^{29,30} As a consequence of its toxic classification, the use of cadmium and its compounds in industries is gradually declining. However, high concentrations of cadmium have been reported in water, soil, landfill, food, and other media.³¹ Although cadmium can be released into the atmosphere through natural activities such as volcanic eruptions, weathering and erosion, anthropogenic activities such as tobacco smoking, mining, fossil fuel burning, incineration of municipal wastes, recycling activities, batteries and phosphate fertilizer manufacturing are the major routes through which cadmium is released into the environs.²⁸ Contamination of aqueous solutions is largely attributed to the release of industrial and agricultural effluents into receiving waters.³² Due to its solubility in water, mobility and non-biodegradable nature,³² excessive ingestion results in its accumulation in the human body, with a half-life of more than ten years,²⁹ thereby resulting in several acute and chronic health issues. Health complications

such as renal dysfunction, anaemia, lung and kidney damage, dizziness, *itai-itai* disease,[‡] numbness, amidst many cardiovascular diseases can occur.^{28,33} As a result of these effects, the US EPA recommends a permissible limit of 5 $\mu\text{g dm}^{-3}$ in drinking water,^{13,30,33} in order to abate consequences associated with cadmium intake.

Cadmium exists in various soluble forms in water, largely as the divalent cation (Cd^{2+}), however, it can also exist in other forms such as ¹as $[\text{Cd}(\text{OH})]^+$, $[\text{Cd}(\text{OH})_2]$, $[\text{Cd}_2(\text{OH})]^{3+}$, $[\text{Cd}(\text{OH})_3]^-$ and $[\text{Cd}(\text{OH})_4]^{2-}$ under alkaline conditions.^{25,26}

2.1.3. Mercury

Mercury (Hg) is a heavy, rare, silvery-white liquid metal, and exists naturally in its sulfide form (cinnabar). Mercury, ranked as the third most toxic substance,³ due to high toxicity associated with its intake, is used in refining, rubber processing, fertilizer, paper and pulp production, pharmaceuticals, consumer batteries, insecticides, disinfectants, electrical appliances and as a catalyst in industries.³⁴ The intrusion of mercury into the aquatic environment is largely attributed to effluent discharge from chlor-alkali plants and fossil fuel combustion, and add up to wastewater generated from water treatment plants and industries.^{35,36} Ingestion of mercury into the human body results in severe health problems such as lung and brain dysfunction, birth defects, disruption of the central nervous system, allergic reactions such as skin rashes, headaches, vomiting, diarrhoea, and may lead to death on increased exposure.^{37,38} As a result of these effects, the maximum permissible limit established by environmental agencies in drinking water is 0.003 mg dm^{-3} .^{13,38,39} Efforts must be taken to drastically control and reduce the increase of mercury in the aquatic environment. Mercury exists in various soluble forms in water, largely as the divalent cation (Hg^{2+}), however, it can also exist in other forms such as $[\text{Hg}(\text{OH})]^+$, $[\text{Hg}(\text{OH})_2]$, $[\text{Hg}(\text{OH})_3]^-$ and $[\text{Hg}(\text{OH})_4]^{2-}$ under alkaline conditions.^{26,40}

2.1.4. Copper

Copper (Cu) is a trace essential element needed by all living organisms for lipid metabolism and the proper functioning of the heart and blood vessels.^{12,41,42} Copper deficiency in humans is rare,⁴³ but results in fatigue, anaemia and reduced white blood cells when insufficient, especially in children. In spite of this, excessive amounts may also lead to respiratory disorders, kidney, lung and liver failure, nausea, bleeding, gastrointestinal complications, Wilson's disease and may also result in death if ingested in high amount.^{12,42,44} Due to the great thermal strength, corrosion resistance and electrical properties possessed by copper, it is usually applied as an insulating material for alloy

[‡]Name given to Cd poisoning which occurred in Jinzu River basin, Toyama

formation and for architectural purposes such as building materials and construction of vehicles. Other applications include chemical manufacturing, mining, metal cleaning, electroplating and fertilizer applications^{12,45} amongst many others. Hence, its usage is considered very important in our society.

Waste discharges from industries contribute significantly to high concentrations of copper ions found in aqueous solutions, hence, resulting in its accumulation in natural water. The recommended acceptable limit of copper in drinking water is 1.5 mg dm^{-3} as suggested by the World Health Organization (WHO).^{12,45} However, higher concentrations are detected in environmental samples such as groundwater, sediments, soils and landfills owing to increased industrialization.⁴⁶

Copper exists as free divalent ions in water, however, hydroxide complexes such as $[\text{Cu}(\text{OH})]^+$, $[\text{Cu}(\text{OH})_2]$, $[\text{Cu}(\text{OH})_3]^-$, $[\text{Cu}(\text{OH})_4]^{2-}$, $[\text{Cu}_2(\text{OH})]^+$, $[\text{Cu}_3(\text{OH})_4]^{2+}$ and $[\text{Cu}_2(\text{OH})_2]^{2+}$ may be formed depending on the pH of the solution.^{25,26}

2.1.5. Zinc

Zinc is an essential micronutrient needed for the development of the immune system, cell growth and fertility in man.⁴⁷ Its deficiency in the body results in irritations such as vomiting, loss of appetite, diarrhoea, growth retardation and susceptibility to disease exposure. The intake of zinc is required in trace amounts at a maximum acceptable limit of 5 mg dm^{-3} .^{48,49} Higher concentrations in the body may lead to health effects such as respiratory difficulty, skin irritations, gastrointestinal distress and cancer amongst many others.⁴⁷ Anthropogenic activities, primarily through the discharge of wastewater generated from mining, smelter slags, and metallurgical industries, accounts for the route *via* which zinc is introduced into the environment.⁴⁹ Evidence of zinc has been reported in air, water, soil and landfills with highest concentrations near point sources. The formation of zinc hydroxides occur in water at $\text{pH} > 7$ to form different species such as $[\text{Zn}(\text{OH})]^+$, $[\text{Zn}(\text{OH})_2]$, $[\text{Zn}(\text{OH})_3]^-$, $[\text{Zn}(\text{OH})_4]^{2-}$, $[\text{Zn}_2(\text{OH})]^{3+}$ and $[\text{Zn}_4(\text{OH})_4]^{4+}$.^{25,26,48,50}

2.2. Organic pollutants in water

In recent times, increasing detection of organic pollutants in water sources presents environmentalists with concerns over their sources and effects, and strategies to mitigate such contamination. Organic pollution arises primarily when wastes (liquid or solid) produced from industries, water treatment plants, sewage, farming and urban run-offs are discharged directly without treatment into water streams.⁵¹⁻⁵³ Several emerging organic

pollutants such as endocrine disrupting chemicals (EDC),⁵⁴ pharmaceuticals (PPCP),⁵⁵ halogenated compounds,^{56,57} and polyaromatic hydrocarbons (PAHs),⁵⁸ amongst many others, have been detected in water sources owing to various anthropogenic activities. Organic pollutants are toxic chemicals which persist in the environment for long periods of time and bioaccumulate in the food chain.^{52,53} The presence of these contaminants in water poses significant risks to its dependants (man, wildlife, aquatic life) and prevents use for domestic purposes.

In this section, bisphenol A (BPA) and ibuprofen (IBP) as examples of EDCs and PPCPs respectively, are discussed as emerging contaminants introduced into aqueous solution. Their sources, effects and fate in water bodies are also further reviewed.

2.2.1. Bisphenol A

Bisphenol A is an organic compound used in plastic industries for the manufacture of plastics, flame retardants, household electrical equipment and consumer goods. The molecular structure of BPA (4,4'-(propane-2,2-diyl)diphenol), has the chemical formula $C_{15}H_{16}O_2$ as shown in Fig 2.1. BPA has been listed as an endocrine disruptor (EDC)^{59,60} based on its ability to mimic hormones, hence resulting in reproductive, hormonal and neurological changes in humans and aquatic wildlife.⁵⁹⁻⁶¹ Erler *et al.* reported that both children and adults are exposed to BPA on a daily basis in the United States of America⁶² through intake from plastic containers, dental seals and microwaved food products.⁶³ The contamination of water sources with this pollutant is due to the incessant disposal of BPA-containing products or industrial effluents into water streams, hence, exposing living organisms to its accumulation.^{61,64,65} The intake of this pollutant into the body interferes with the transport and secretion of naturally occurring hormones, hence resulting into heart and respiratory diseases, male sterility, diabetes, cancer and brain dormancy amongst many others.⁶³⁻⁶⁵

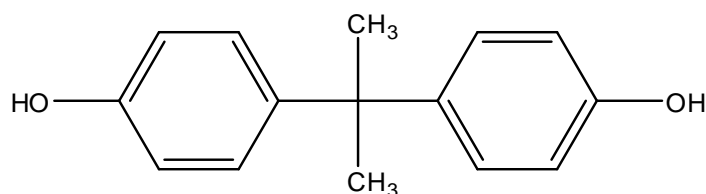


Fig. 2.1: Structure of bisphenol A (BPA) [molar mass: $228.29 \text{ g mol}^{-1}$; density: 1.20 g cm^{-3} ; boiling point: $220 \text{ }^\circ\text{C}$; melting point: $158 \text{ }^\circ\text{C}$; solubility in water: $120\text{-}300 \text{ mg dm}^{-3}$ ($21 \text{ }^\circ\text{C}$); acid dissociation constant (pK_a): $9.6\text{-}10.2$].⁵¹

2.2.2. Ibuprofen

Ibuprofen is a nonsteroidal anti-inflammatory (NSAID) drug used to relieve pain and fever.⁶⁶⁻⁶⁸ It is one of the commonest medicines in the world;^{66,67} hence, its importance is a requisite in modern society. The molecular structure of IBP (2-(4-isobutylphenyl)propanoic acid, with the chemical formula $C_{13}H_{18}O_2$, is shown in Fig 2.2. The release of IBP into the aquatic environment is principally from wastes discharged from humans, veterinary, industrial and agricultural applications, wastewater treatment plants and septic tanks.⁶⁶⁻⁶⁹ The presence of IBP in water presents environmental agencies with the challenge of developing strategies for controlling the discharge of wastes generated by using pharmaceutical products. Although, the maximum concentration limits of IBP are not yet established, there is a growing concern on its toxicity to aquatic life and humans due to its increasing discharge in water.⁶⁶ Indiscriminate intake of IBP in humans is perceived to result in long-term health diseases which might give rise to complications such as hormonal and renal dysfunction, gastrointestinal bleeding and liver and heart failures if adequate disposal routes are not taken.^{68,70,71}

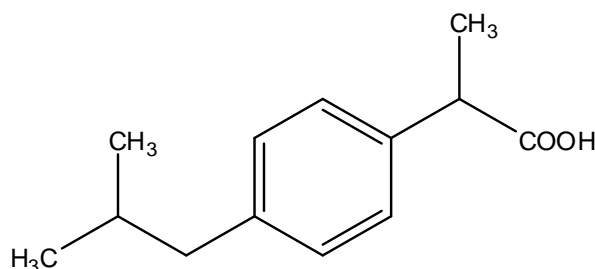


Fig. 2.2: Structure of ibuprofen (IBP) [molar mass: 206.3 g mol^{-1} ; acid dissociation constant (pK_a): 4.91; water solubility: 21 mg dm^{-3} ; density: 1.03 g cm^{-1} ; melting point: $76 \text{ }^\circ\text{C}$; boiling point: $157 \text{ }^\circ\text{C}$].⁶⁹

2.3. Organic dyes in water

Dyes are organic compounds which have wide application in textile manufacturing, paper and pulp production and paint, plastic, dyeing, cosmetic, tannery and pharmaceutical industries.⁷²⁻⁷⁴ The widespread use of these compounds presents environmental challenges, such as the disposal of coloured effluents generated from these industries. Unfortunately, effluents produced are mostly discharged into various aquatic media, hence generating a high intensity of colour in them.⁷⁴⁻⁷⁶ Dyes are toxic due to their biodegradable nature, and can therefore persist for long periods of time in the environment.⁷⁷ The presence of dyes in aqueous solutions prevents the transmission of light into water, inhibiting photosynthesis, and affecting dependants of such water resources for domestic purposes.^{72,75} Dyes are

considered carcinogenic to human health and can result in other severe ailments such as damage to the kidney, liver, brain and central nervous system.⁷⁵ In the next section, the sources and health hazards associated with the intake of rhodamine B (RhB) are reviewed. Rhodamine B was used in this work as an example of a typical dye discharged into the environment.

2.3.1. Rhodamine B

Rhodamine B is a water-soluble cationic dye containing a positive ion, either as the hydrochloride salt or the zinc chloride complex in its structure.⁷⁵ The molecular structure of RhB is shown in Fig 2.3 and it has a chemical formula of $C_{28}H_{31}N_2O_3Cl$. It is primarily used in textile industries for production of cotton, leather, silk and wool.⁷⁸ The release of RhB-contaminated wastewater generated from industries produces coloured cations in solution and hinders its use for other domestic purposes.⁷⁵ RhB is a toxic substance; stable to photo- and biological degradation and its intake can result in skin irritations, restlessness, dermatitis, gastrointestinal diseases, respiratory complications and cancer in humans.^{78,79}

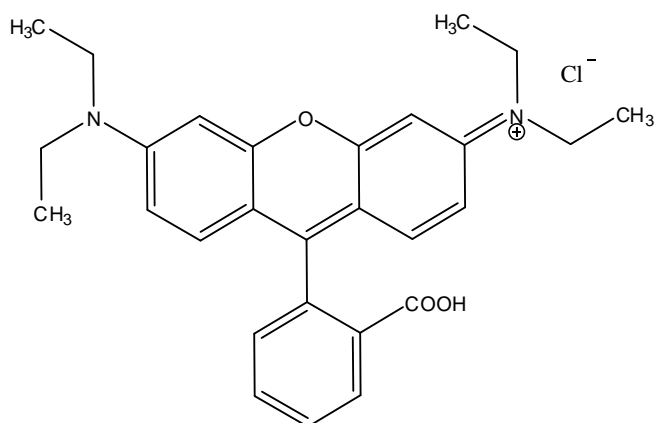


Fig. 2.3: Structure of rhodamine B (RhB) [molar mass: 479.02 g mol⁻¹; acid dissociation constant (pK_a): 3.71; solubility in water: 15 g dm⁻³; density: 1.31 g cm⁻¹ (20 °C); melting point: 210-211 °C].⁸⁰

2.4. Technologies for wastewater remediation

As a result of the stated consequences, the presence of these recalcitrant pollutants in aqueous media continues to be of serious environmental concern, generating discussion towards the effective remediation of wastewater before disposal into the receiving environment. An urgent need exists for developing effective strategies for pollutant removal since most water treatment plants are not designed for the effective removal of some of these pollutants.

In recent times, various chemical, physical and biological techniques have been proposed to achieve degradation/removal of contaminants from wastewater. The following section examines the effectiveness, problems and advantages associated with some of these techniques.

2.4.1. Advanced oxidation processes

This is one of the most commonly used methods for the degradation of the discussed pollutants from wastewater. Advanced oxidation processes (AOPs) involve the generation of highly reactive hydroxyl radicals by using chemical methods, aimed at the degradation of organic and/or inorganic pollutants in wastewater.^{81,82} The hydroxyl radical produced reacts unselectively with contaminants to initiate pollutant conversion into less harmful substances.⁸³ Oxidative processes could be photo-catalytic, photo-oxidation, ozone-based (ozonation), photo-Fenton, or chemical precipitation, depending on the substrate producing the radical.^{82,84} Table 2.1 presents some common AOPs used in the remediation of wastewater.

Table 2.1: Common AOPs used in wastewater treatment⁸²

Photochemical processes	Non-photochemical processes
UV oxidation	Ozonation
UV/H ₂ O ₂	Fenton
UV/O ₃	Ultrasound
Photo-Fenton	Ultrasound/H ₂ O ₂
Photo-catalysis	Wet-oxidation, e.g. precipitation
Microwave	Electron-beam irradiation
Sono-chemical	Pulsed-plasma
Vacuum-UV	Electrochemical oxidation

Metal ions can be oxidized through abiotic processes and further precipitated as hydroxides as illustrated in Eq. 2.1. For instance, Kosolapov *et al.* reported the oxidation of ferrous iron (Fe²⁺) in solution into ferric iron (Fe³⁺), and subsequent conversion of Fe³⁺ into insoluble hydroxides in water.⁸³



Similarly, degradation of EDCs such as BPA and IBP can be achieved through oxidative processes. Rosenfeldt *et al.* reported the degradation of BPA by using radiation photolysis and UV/H₂O₂ processes, obtaining effective pollutant conversion in each case.⁸⁵ Also, Al

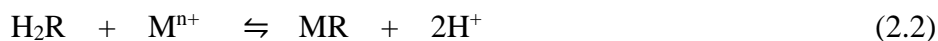
Hamedi *et al.* investigated the photo-oxidation of RhB from wastewater by using UV/H₂O₂ light.⁸⁶ The simplicity of these processes justifies their increasing application for the treatment of wastewater, however, disadvantages such as activation of chemical agent by UV light, sludge generation, high energy generation, short half-life of ozone, formation of toxic by-products and high set-up costs, restricts their usage for wastewater remediation.⁷⁵

2.4.2. Membrane separation

This technique adopts the use of a semipermeable membrane for the removal of contaminants (bacteria, organics and inorganics) by passing the liquid at high pressure, to obtain the purified permeate and the concentrated mixed liquor at the feed side.^{25,87} Examples of membrane processes used for water remediation are reverse osmosis (RO), electrodialysis, microfiltration (MF), ultrafiltration (UF) and nanofiltration (NF).^{88,89} RO is considered best suited for effluent remediation to achieve water reuse, hence reducing the total water consumption.⁸⁹ Urgan-Demirtas *et al.* reported the use of RO, MF, UF, and NF for mercury removal from wastewater generated from an oil refinery.⁹⁰ Although, low mercury levels were achieved after treatment, limitations such as membrane narrowing and pore blockage, low permeate quality, fouling and high operating conditions, were highlighted as drawbacks for these processes.⁹⁰ In a study by Jian *et al.*, poly (vinylidene fluoride) membranes were also applied for the removal of both polar and non-polar compounds from wastewater.⁹¹ Although, membrane separation is cost-effective, its application for effluent remediation is constrained by short membrane half-life, fouling, low selectivity, liquid viscosity and concentration polarization.^{87,90}

2.4.3. Ion-exchange

This process involves the exchange of charged ions in solution with ions on the surface of a solid. The use of synthetic resins is usually applied for the removal of both organic and inorganic contaminants from wastewater. A decrease in sludge production and metal ion concentration of Cr(III) was reported by Tiravanti *et al.*⁹² and Rengaraj *et al.*⁹³ by using ion-exchangers. Metal ions are usually removed by using a cationic exchanger *via* the replacement of hydrogen or sodium atoms on the resin with cations (pollutants) as illustrated in Eq. 2.2.²⁵



where R is the resin, and M is the metal ion.

Similarly, anions such as sulfates replace hydroxide or chloride ions in anionic resins as demonstrated in Eq. 2.3.²⁵



Although, ion-exchange processes have been applied for the removal of dyes from wastewater, their application is not considered effective based on the fact that exchangers cannot remove a wide range of dyes.⁷⁶ Ion-exchangers are easily recyclable, hence can be reused, however, their application is limited due to high cost and inability to remove pollutants at high concentration ranges.^{25,75,76}

2.4.4. Aerobic and anaerobic treatment

This process involves the use of bacteria or microorganisms for the biological degradation of contaminants in wastewater. Aerobic treatment adopts the use of free/molecular oxygen by using microorganisms (aerobes), in the presence of air for the conversion of contaminants into biomass, carbon dioxide and water.⁹⁴ On the other hand, anaerobic treatments adopt the use of microorganisms (anaerobes), in the absence of air/oxygen for the biological degradation of pollutants to generate methane and carbon dioxide.⁹⁴ Chipasa, in his study, investigated the removal of heavy metal ions (Cd, Cu, Pb and Zn) by using anaerobic sludge samples.⁹⁵ Unfortunately, the metal ion content in samples was observed to increase on a dry weight basis due to microbial degradation of organic and inorganic compounds in sludges.⁹⁵ However, a considerable decrease in metal ion concentration was reported by da Silva Oliveira *et al.* with an anaerobic sludge.⁹⁶ The degradation of organic contaminants such as BPA, estrone, 17 β -estradiol, alkylphenols, phthalates amongst many, have also been carried out by using biological treatments.⁹⁷⁻¹⁰⁰ In spite of its convenience, several limitations such as high set-up cost, sludge generation, regeneration of activated sludge, breakdown to some harmful compounds such as hydrogen sulfide and inability to completely metabolize some pollutants (dyes) under aerobic conditions restricts its use for large-scale purposes.^{75,76,101}

2.5. Adsorption

Adsorption is a phenomenon which describes the accumulation of substances (molecules, ions or atoms) from a liquid/gas solute onto the surface of a solid. The solid upon which the solute accumulates is referred to as the *adsorbent* and the substance (solute) which is being removed is the *adsorbate*. This concept has gained application since the eighteenth century for the purification of air containing toxic gases such as H₂S.¹⁰² For instance, a filter made of fiberglass cloth was constructed by Shiratori *et al.* to remove toxic gases such as ammonia and acetaldehyde from air.¹⁰³ Hence, the application of adsorption for pollutant removal is well-documented by various authors.

Additionally, this concept can be applied for water reclamation and wastewater treatment purposes. In fact, it is considered as an ideal, superior and effective method for the treatment of contaminated wastewater,¹⁰² due to the fact that its operation is simple, cost-effective, time-saving, and high pollutant removal can be achieved at high and low adsorbate concentrations. Sorbents are also easily handled and may be regenerated for reuse.^{22,102}

2.5.1. Types of adsorption

Adsorption is primarily described based on the attractive/binding forces which hold the adsorbate molecule onto the surface of an adsorbent. Adsorption is a surface phenomenon and the solid-liquid interaction may be held either by van der Waals (weak) or strong binding forces; hence, adsorption is classified into two types, namely:

- i. physical adsorption (physisorption), or
- ii. chemical adsorption (chemisorption).

2.5.1.1. Physical adsorption (physisorption)

This process is characterised by weak Van der Waals forces existing between the adsorbed molecule and the adsorbent. Physisorption is typified by low heats of adsorption (ΔH°) in the order of 2.1-20.9 kJ mol⁻¹.^{104,105} This therefore implies that physical adsorption can be easily reversible when heated, since the heat of adsorption is in magnitude similar to the heat of condensation.¹⁰⁶

2.5.1.2. Chemical adsorption (chemisorption)

Chemisorption is characterised by strong chemical forces existing between the adsorbed molecule and the adsorbent. The attraction of adsorbate molecules onto the adsorbent is selective, since adsorption is site-specific. Chemical adsorption, therefore, depends largely on the chemical properties of the adsorbent and adsorbate, so as to permit the formation of a chemical bond *via* the sharing (covalent bonding) or transfer of electrons (ionic bonding). Higher heats of adsorption (ΔH°) in the magnitude of 80-200 kJ mol⁻¹ are noticed for chemisorption.^{104,105} Table 2.2 offers a clear distinction between physisorption and chemisorption.

Table 2.2: Differences between physisorption and chemisorption^{25,107}

Physisorption	Chemisorption
The forces of attraction are weak.	The forces of attraction are strong.
The process is observed at low temperatures/heat of adsorption.	The process is typified by high temperatures/heat of adsorption.
Formation of multi-molecular layers are possible.	Monomolecular layer is formed.
The process is reversible.	The process is irreversible.
It is non-specific.	It is highly specific.
Activation energy is usually equal to zero.	Activation energy is usually small.

It is worthy to note that adsorption processes are affected by the solution pH, adsorbate temperature, initial adsorbate concentration, contact time, ionic strength and amount or nature of the adsorbent.^{22,105} Hence, the kinetics, isotherms and thermodynamics of adsorption were studied and the most significant aspects are described in 2.6, 2.7 and 2.8, respectively, in order to understand the dynamics, mechanism and feasibility of the adsorption process.

2.6. Adsorption kinetics

The rate-determining step of adsorption is usually determined by the adsorption kinetics. The uptake of adsorbates as a function of time helps in establishing the equilibration time and the rate at which sorption of contaminants occur in solution.¹⁰⁸ This information aids in designing treatment plants for the reclamation of wastewater on a large-scale. The dynamics/mechanism of adsorption is usually investigated by fitting the experimental data obtained for adsorption into kinetic models. Commonly used kinetic models for describing solid-liquid adsorption systems are the: pseudo-first order, pseudo-second order, intraparticle diffusion and Elovich models. The adsorption process is usually controlled by one or more of the following mechanisms:

- i. diffusion of solute from the bulk solution to the external surface of the adsorbent,
- ii. solute transfer from the bulk solution to the boundary film which surrounds the adsorbent surface (film diffusion),
- iii. solute diffusion through the internal pores of the adsorbent (intraparticle diffusion);
and
- iv. interaction between adsorbate molecules and active sites of the adsorbent to enhance the formation of bonds between the adsorbate and adsorbent.

In order to minimise error distribution associated with kinetic models in linear forms, Lin *et al.* proposed non-linear forms of models to obtain accurate fitting of data into models.¹⁰⁹ Hence, the experimental data obtained in this study were fitted into the stated models by using non-linear least squares (NLLS) analysis to determine the model which best describes the kinetics of the adsorption process.

2.6.1. Pseudo-first order model

The pseudo-first order model was first presented by Lagergren,¹¹⁰ and later reviewed by Ho and McKay,¹¹¹⁻¹¹³ to describe solid-liquid systems. The equation is expressed as shown in the following equations.

$$q_t = q_{eq}(1 - e^{-k_1 t}) \quad (2.4)$$

$$\ln(q_{eq} - q_t) = \ln q_{eq} - k_1 t \quad (2.5)$$

where q_t and q_{eq} are the quantities of adsorbate adsorbed at any time t and at equilibrium, respectively (mg g^{-1}); and k_1 , is the pseudo-first order rate constant (min^{-1}). A plot of $\ln(q_{eq} - q_t)$ against t gives a straight line, from which k_1 and q_{eq} can be calculated from the slope and intercept, respectively.

2.6.2. Pseudo-second order model

The pseudo-second order model is expressed in both non-linear and linear forms as illustrated in Eqs. 2.6 and 2.7, respectively.^{108,109,112}

$$q_t = \frac{k_2 q_{eq}^2 t}{1 + k_2 q_{eq} t} \quad (2.6)$$

$$\frac{t}{q_t} = \frac{1}{k_2 q_{eq}^2} + \left(\frac{1}{q_{eq}}\right) t \quad (2.7)$$

where k_2 is the pseudo-second order rate constant ($\text{g mg}^{-1} \text{min}^{-1}$). A plot of $\frac{t}{q_t}$ vs t should give a straight line wherein q_{eq} and k_2 can be calculated from the slope and intercept, respectively.

2.6.3. Intraparticle diffusion model

The intraparticle diffusion model was described by Weber and Morris in order to explain the diffusion of adsorbates through adsorbent pores and may be estimated as given in Eq. 2.8.^{114,115}

$$q_t = k_{id} \sqrt{t} + l \quad (2.8)$$

where k_{id} is the intraparticle diffusion rate constant ($\text{mg g}^{-1} \text{min}^{-0.5}$) and l , is a constant related to the boundary layer thickness (mg g^{-1}). A plot of q_t vs \sqrt{t} should give a straight line where the slope and intercept correspond to the value of k_{id} and l , respectively. It is generally assumed that if the linear plot passes through the origin, the mechanism of the adsorption

process is controlled only by intraparticle diffusion.^{2,116} However, if the linear plot does not pass through the origin, the rate-determining step is multi-step, hence, controlled by two or more processes.^{2,116}

2.6.4 Elovich model

Chien and Clayton proposed a modified model to describe the sorption of solutes on highly heterogeneous sorbents, which could not be described adequately by the first-order kinetic equation.^{2,117} The application of the model was first used to investigate phosphate release and sorption of soils in 1980.¹¹⁷ Its use is currently adapted for the modelling of experimental data obtained for aqueous solutions.^{22,45,118} The Elovich model is expressed as illustrated in Eq. (2.9):¹¹⁷

$$q_t = \frac{1}{\beta} \ln(\alpha\beta) + \frac{1}{\beta} \ln t \quad (2.9)$$

where α ($\text{mg g}^{-1} \text{min}^{-1}$) is the adsorption rate constant; β (g mg^{-1}) is the desorption rate constant. A plot of q_t vs $\ln(t)$ should give a straight line wherein $\frac{1}{\beta}$ and $\frac{1}{\beta} \ln(\alpha\beta)$ correspond to the slope and intercept, respectively.

2.7. Adsorption isotherms

Isotherms describe the equilibrium relationship between the concentration of solute on the adsorbent (solid phase) and in the liquid phase. A plot of the amount of the solute on the adsorbent (q_{eq}) versus the equilibrium concentration of solute in solution (C_{eq}), produces a curve to understand the mechanism of the adsorption process. Isotherms provide information on the amount of adsorbent needed to remove a unit mass of solute per gram of adsorbent, hence, the ability of the adsorbent to remove the pollutant can be estimated. Isotherm models consisting of various two- and three-parameter models have been designed to enable the prediction of procedures for contaminant removal in a large-scale scenario.

In this study, eight isotherm models involving two-parameters (Langmuir,¹¹⁹ Freundlich,¹²⁰ Temkin,¹²¹ and Dubinin-Radushkevich¹²²) and three-parameter (Sips,¹²³ Toth,¹²⁴ Khan,¹²⁵ and Redlich-Peterson¹²⁶) were tested for the description of the adsorption processes.

2.7.1. Langmuir isotherm

The Langmuir isotherm is one of the commonest models used for describing the adsorption of solutes in solution onto a solid substance. This isotherm assumes that adsorption takes place on a finite number of adsorption sites with the formation of monolayer coverage of adsorbates on adsorbents.¹¹⁹ This implies that the adsorption sites are equivalent (i.e.

homogeneous) having uniform energies and each site can hold an adsorbate molecule without interaction with adjacent molecules.^{127,128} The Langmuir isotherm is represented as given in Eq. (2.10):

$$q_{eq} = \frac{q_m C_{eq} b}{1 + b C_{eq}} \quad (2.10)$$

where q_{eq} is the amount adsorbed per unit mass of adsorbent at equilibrium (mg g^{-1}); C_{eq} is the equilibrium concentration of adsorbate in solution (mg dm^{-3}); q_m is the maximum monolayer adsorption capacity (mg g^{-1}); and b is the Langmuir isotherm constant ($\text{dm}^3 \text{mg}^{-1}$). A linear form of equation 2.10 can be rewritten as given in Eq. (2.11).¹²⁸

$$\frac{C_{eq}}{q_{eq}} = \frac{1}{q_{max} b} + \frac{C_{eq}}{q_{max}} \quad (2.11)$$

Hence, a plot of $\frac{C_{eq}}{q_{eq}}$ against C_{eq} should give a straight line wherein the slope and intercept correspond to $\frac{1}{q_{max} b}$ and $\frac{1}{q_{max}}$, respectively. The values of b and q_{max} are related to the binding energy of adsorption and the capacity of the adsorbent to remove a unit mass of pollutant per mass of sorbent, respectively.

A dimensionless constant known as the separation factor or equilibrium constant, R_L , expresses the essential characteristics of the Langmuir isotherm and is defined as represented by equation (2.12):¹²⁹

$$R_L = \frac{1}{1 + b C_i} \quad (2.12)$$

where b is the Langmuir isotherm constant ($\text{dm}^3 \text{mg}^{-1}$) and C_i is the initial concentration of adsorbate (mg dm^{-3}). Adsorption is assumed to be favourable if $0 < R_L < 1$, unfavourable if $R_L > 1$, irreversible if $R_L = 0$ and linear if $R_L = 1$.^{22,128,130}

2.7.2. Freundlich isotherm

The Freundlich isotherm is an empirical model which assumes that adsorption occurs on heterogeneous surfaces of an adsorbent. Hence, the isotherm describes adsorption for both monolayer and multilayer adsorption. The exponential equation is only applied in the low to intermediate adsorbate concentration ranges.¹⁰⁴ The Freundlich isotherm is defined as given in Eq. (2.13):¹²⁰

$$q_{eq} = K_F C_{eq}^{1/n} \quad (2.13)$$

where K_F and n represent the Freundlich isotherm constant (mg g^{-1}) and the adsorption intensity, respectively. A linear form of equation (2.13) can be written as given in Eq. (2.14):¹²⁸

$$\log(q_{eq}) = \log(K_F) + \frac{1}{n}\log(C_{eq}) \quad (2.14)$$

A plot of $\log(q_{eq})$ against $\log(C_{eq})$ should give a straight line and the values of K_F and $\frac{1}{n}$ corresponding to the intercept and slope, respectively. Adsorption is favourable when the value of n lies between 1 and 10.^{45,128} Additionally, the surface of the adsorbent is assumed to become more heterogeneous as the value of n approaches zero.¹³¹

2.7.3. Temkin isotherm

The Temkin isotherm assumes that the heat of adsorption decreases linearly with an increase in the coverage of the adsorbent surface due to sorbent-sorbate interactions. It is most appropriate for the prediction of gas phase equilibrium; however, its application in solid-liquid systems has been reported.^{22,127,131} The Temkin equation is represented by Eq. (2.15):¹²¹

$$q_{eq} = \frac{RT}{b_T} \ln(A_T C_{eq}) \quad (2.15)$$

where b_T is the Temkin isotherm constant related to the heat of adsorption (J mol^{-1}), A_T is the Temkin isotherm equilibrium binding constant ($\text{dm}^3 \text{g}^{-1}$), R is the universal gas constant ($8.314 \text{ J K}^{-1} \text{ mol}^{-1}$) and T is the absolute temperature in Kelvin. The linear form of the Temkin equation can be written as given in Eq. (2.16):¹²⁷

$$q_{eq} = \frac{RT}{b_T} \ln A_T + \frac{RT}{b_T} \ln C_{eq} \quad (2.16)$$

Equation 2.16 can be further represented as given in Eq. (2.17):¹²⁷

$$q_{eq} = \alpha + \beta \ln C_{eq} \quad (2.17)$$

where $\alpha = \frac{RT}{b_T} \ln A_T$ and $\beta = \frac{RT}{b_T}$, hence, the values of α and β can be calculated from the intercept and slope of the line, respectively.

2.7.4. Dubinin-Radushkevich isotherm

The Dubinin-Radushkevich (D-R) isotherm is an empirical model used for the adsorption of vapours onto microporous adsorbents through the pore filling mechanism.^{122,131} It is used to explain the adsorption mechanism onto heterogeneous surfaces¹³¹ with an assumption that sorption is multilayer and involves the van der Waals interactions, hence, it can be applied for physical adsorption processes.¹³² The porosity of adsorbents and the free energy of adsorption can be evaluated by using the D-R model.¹³¹ Equations (2.18) and (2.19) represent the D-R model in its non-linear and linear forms, respectively.¹³³

$$q_{eq} = q_m \exp\left(-B_D \left[RT \ln\left(1 + \frac{1}{c_{eq}}\right)\right]^2\right) \quad (2.18)$$

$$\ln q_{eq} = \ln q_m - B_D \varepsilon^2 \quad (2.19)$$

where q_{eq} is the amount of solute adsorbed at equilibrium (mg g^{-1}), q_m is the maximum adsorption capacity (mg g^{-1}), B_D is the D-R constant related to free energy ($\text{mol}^2 \text{kJ}^{-2}$) and ε is the Polanyi potential (J mol^{-1}) and correlated as illustrated in Eq. (2.20):¹³¹

$$\varepsilon = RT \ln\left(1 + \frac{1}{c_{eq}}\right) \quad (2.20)$$

Hence, if β is substituted for B_D in Eq. (2.18), it can be rewritten as

$$q_{eq} = q_m e^{-\beta \varepsilon^2} \quad (2.21)$$

The values of q_m and B_D can be calculated from the intercept and slope of the straight line obtained by plotting $\ln q_{eq}$ versus ε^2 , while the mean free energy (E) can be calculated from Eq. (2.22):¹³¹

$$E = \frac{1}{\sqrt{2B_D}} \quad (2.22)$$

2.7.5. Sips isotherm

The Sips isotherm is a combination of the Langmuir and Freundlich isotherms for describing heterogeneous systems.¹³¹ It is used to describe conditions where the Langmuir and Freundlich isotherms do not describe the equilibrium data well. It predicts the Freundlich isotherm at low adsorbate concentration, and the monolayer adsorption is predicted at high adsorbate concentrations.¹³¹ It is worthy of note that the equation parameters are influenced by conditions such as the pH, temperature and concentration of adsorbate solution.^{25,131} The Sips equation is defined in its non-linear form as illustrated in Eq. (2.23):¹²³

$$q_{eq} = \frac{b q_m c_{eq}^{1/n}}{1 + b c_{eq}^{1/n}} \quad (2.23)$$

where q_m is the maximum monolayer capacity (mg g^{-1}), b is the Sips equilibrium constant ($\text{dm}^3 \text{mg}^{-1}$), and n is the adsorption intensity. The adsorption process is Langmuir when $n = 1$ and Freundlich when $n > 1$.¹³⁴

2.7.6. Toth isotherm

The Toth isotherm is an empirical equation designed to improve the fit of the data for the Langmuir and Freundlich isotherms. It also describes data appropriately obtained for both

low and high adsorbate concentrations, and hence, may be used in explaining heterogeneous systems.¹³¹ The Toth equation is expressed as represented in Eq. (2.24):¹²⁴

$$q_{eq} = \frac{q_m C_{eq}}{\left(\frac{1}{K_T} + C_{eq}^{n_T}\right)^{1/n_T}} \quad (2.24)$$

where K_T is the Toth isotherm constant (mg g^{-1}); n_T , is the dissociation constant (Toth model constant). The value of n_T describes the heterogeneity of the adsorption process.

2.7.7. Khan isotherm

The Khan isotherm was developed as a general model for describing multi-component systems in aqueous solutions.¹²⁵ It is expressed as illustrated in Eq. (2.25):¹²⁵

$$q_{eq} = \frac{q_m b_K C_{eq}}{(1 + b_K C_{eq})^{a_K}} \quad (2.25)$$

where a_k and b_k , are the Khan isotherm exponent and constant, respectively.

2.7.8. Redlich-Peterson isotherm

The Redlich-Peterson (R-P) isotherm is a three-parameter empirical equation, designed to explain adsorption systems over a wide concentration range.¹³¹ This isotherm can be used to explain both homogeneous and heterogeneous surfaces, hence it incorporates both the Langmuir and Freundlich isotherm features, similar to the Sips isotherm.^{104,131} The R-P model is represented as given in Eq. (2.26):¹²⁶

$$q_{eq} = \frac{K_{RP} C_{eq}}{1 + \alpha_{RP} C_{eq}^g} \quad (2.26)$$

where K_{RP} ($\text{dm}^3 \text{g}^{-1}$) and α_{RP} ($\text{dm}^3 \text{mg}^{-1}$) are the R-P isotherm constants and g is the R-P isotherm exponent, which lies between 0 and 1.

2.8. Thermodynamic parameters of adsorption

The concept of thermodynamics is important to understand the energy changes, feasibility and mechanism of adsorption. Additionally, to achieve maximum efficiency, the adsorbate temperature is usually varied over a particular range, in order to provide sufficient information into the binding forces responsible for adsorption. An increase in adsorbate temperature may lead to an increase in adsorbate uptake *via* any of these processes:

- i. Reduction of the electrostatic repulsion between the adsorbate and adsorbent surface;
- ii. Increasing mobility of sorbate ions/molecules to active sites, and

- iii. Activation of the active sites responsible for adsorption, resulting in the creation of adsorption sites.¹³⁵

Consequently, an increase in adsorbate temperature may also lead to weak binding interactions between adsorbates and adsorbents; hence, a decrease in adsorption is observed. Sharma and Kaur associated a decreased sorbate uptake with increasing temperature to the ‘swelling effect’ produced in the internal surface of the adsorbent, thereby resulting in the formation of weak binding forces between dye molecules and adsorbent surface.¹³⁵ Hence, increasing adsorbate temperature may enhance adsorption removal or in some cases may lead to a decrease in physical adsorptive forces and result in low removal of adsorbates.

Thermodynamic parameters such as the change in entropy, (ΔS°), change in enthalpy, (ΔH°) and change in Gibbs energy, (ΔG°), were calculated to examine the spontaneity of the adsorption process over a temperature range. The change in Gibbs energy (ΔG°) is calculated as presented in Eq. (2.27):

$$\Delta G^\circ = -RT \ln K \quad (2.27)$$

where R is the universal gas constant ($8.314 \text{ J K}^{-1} \text{ mol}^{-1}$), T is the absolute temperature in Kelvin and K is the equilibrium constant, obtained from the product of the Langmuir constant, b ($\text{dm}^3 \text{ mg}^{-1}$) and the Langmuir monolayer adsorption capacity, q_m (mg g^{-1}), hence the value of K is calculated in $\text{dm}^3 \text{ g}^{-1}$.^{136,137} As proposed by Milonjic *et al.*, the value of K must be corrected to be dimensionless, since adsorption is carried out in aqueous solution and for ΔG° to be obtained in J mol^{-1} .¹³⁷ The value of K must therefore be multiplied by 1000, since $1 \text{ dm}^3 = 1000 \text{ cm}^3$ or g (density of solution = 1 g cm^{-3}). Hence, Eqn (2.27) may be rewritten as given in Eq. (2.28):²⁵

$$\Delta G^\circ = -RT \ln (1000K) \quad (2.28)$$

The change in enthalpy, (ΔH°) and the change in entropy, (ΔS°) can be calculated by using the Van't Hoff equation given in Eq. (2.29):¹³⁸

$$\ln K = -\frac{\Delta H^\circ}{RT} + \frac{\Delta S^\circ}{R} \quad (2.29)$$

A plot of $\ln K$ against $1/T$ should be linear, and the values of ΔH° and ΔS° obtained from the slope and intercept of the plot, respectively. This only holds true over a small temperature range to assume ΔH° and ΔS° fits the equation.

The values obtained for ΔH° may be used to determine the nature of an adsorption process. Positive ΔH° values indicate an endothermic process and an exothermic nature of adsorption is signified by negative ΔH° values.¹³⁹ The degree of disorderliness in the system and the adsorbate molecule affinity to the adsorbent may also be estimated by the value of ΔS° .¹³⁵

A positive ΔS° value indicates a high level of disorderliness leading to increased affinity of the adsorbate molecule for the adsorbent and *vice versa* for a negative ΔS° .¹³⁹ The spontaneity and feasibility of the process is usually estimated from ΔG° values. A negative ΔG° signifies a spontaneous process and a positive value is indicative of a non-spontaneous process.¹³⁸

2.9. Adsorbents

Adsorbents are solid materials which have affinities for attracting substances in solution (pollutants) onto their surface. The attraction of pollutants may proceed *via* electrostatic, ion-exchange, hydrophobic, hydrogen or π - π interactions to the active sites on the adsorbents. The affinity for easy interaction largely depends on the chemical properties, porosity and surface area of the adsorbent. In recent times, the application of porous shaped carbon nanomaterials has generated increasing interest for wastewater remediation, due to the large surface areas possessed by these materials.

In this study, carbon nanotubes (CNTs) were used as the adsorbent for the removal of metal ions (Pb, Cu, Zn, Cd, Hg) and organic (BPA, IBP) pollutants from wastewater. The affinity of CNTs towards the removal of these pollutants was enhanced through functionalization. This process aided the introduction of functional groups to CNT walls, hence, determining the type of interaction involved in the removal of adsorbates from solution. The application of CNT composites was also explored for effective removal of RhB from wastewater. The succeeding sections discuss the properties of the sorbents used in this study, while reviewing previous work, with a view to determining the efficacy of these sorbents for the targeted pollutants.

2.10. Carbon nanotubes

Carbon nanotubes are members of the fullerene family which were discovered by Iijima in 1991,¹⁴⁰ possessing extraordinary physical, mechanical, chemical, electrical and optical properties and thermal stability.¹⁴¹ These materials are composed of finite graphene sheets, arranged in an helical manner to consist of needle-like shaped tubes, ranging from one to hundred nanometres in diameter.¹⁴⁰ The geometric arrangement of carbon atoms determines the structure, properties and chirality of CNTs (Fig 2.4).¹⁴² CNTs may also be classified as single-walled CNTs (SWCNTs), double-walled CNTs (DWCNTs) or multiwalled CNTs (MWCNTs), depending on the number of concentric graphene sheets rolled to form them.¹⁴³

SWCNTs, having a simple geometry contain one concentric cylinder, while MWCNTs may contain more than two cylinder in their structure.¹⁴²

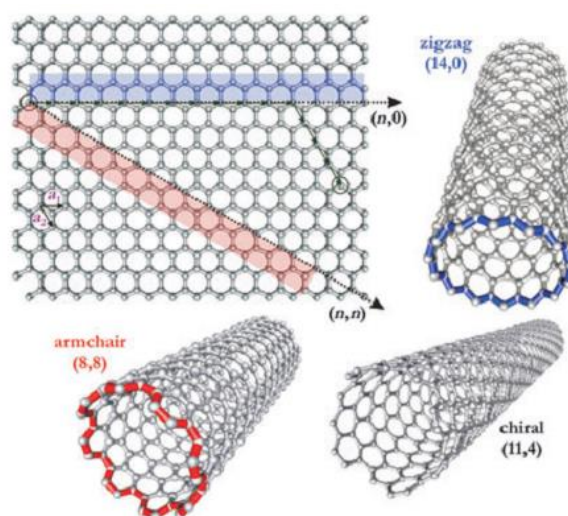


Fig. 2.4: Geometric arrangement of carbon atoms to give three types of CNT based on chirality.¹⁴²

Of the three versatile methods (laser ablation,¹⁴⁴ arc-discharge¹⁴⁵ and chemical vapour deposition (CVD)¹⁴⁶) used for CNT synthesis, CVD is commonly applied owing to its suitability for mass production, diameter control and vertically aligned tubes formed *via* this method.¹⁴¹ CNTs find great application for the manufacture of semi-conductors,¹⁴⁷ energy devices,¹⁴⁸ catalysts and catalyst supports,¹⁴⁹ sensors,¹⁵⁰ medicinal purposes¹⁵¹ and recently as sorbents for pollutant recovery.²² The sensitivity of CNTs must, however, be enhanced through functionalization in order to introduce functional groups which will initiate pollutant removal from aqueous solutions. Hence, various functionalization strategies are discussed in the following section, to review methods available for CNT modification.

2.10.1. Functionalization of CNTs

CNTs usually possess high level of impurities either as amorphous carbon and/or residual metal nanoparticles derived from the catalyst used in their synthesis. These tubes have closed ends which make them unreactive and inert to chemical reactions. Consequently, after synthesis, they are first purified and thereafter functionalized. Purification can be achieved by washing/refluxing CNTs in 6 mol dm^{-3} HCl or HNO_3 acid to reduce the inherent metal nanoparticles in them. To improve their reactivity, functionalization is usually carried out *via* both covalent and non-covalent processes, in order to introduce new functional groups to their open ends. Chapter 3 explores these two functionalization strategies and examine their ability towards removal of perfluorinated compounds from aqueous solutions.

Nevertheless, solution chemistry can be applied through covalent functionalization to attach functional groups onto CNT walls to further increase their reactivity for other applications. Multiple functional groups such as carboxyl and amino groups were attached to MWCNTs by Zhao and his co-workers.¹⁵² In their study, 1,4-benzenediamine was used as a modifier after acidic functionalization was done. The properties of the functionalized MWCNTs were verified through various characterization techniques, and revealed the successful introduction of nitrogen and oxygen atoms, hence, a significant amount of carboxyl and amino functional groups were evident on the surface of the tubes.¹⁵² Additionally, successful immobilization of 8-hydroxyquinoline on MWCNT (8-HQ-MWCNT) was reported by Kosa *et al.*¹⁵³ The modified CNTs were tested for metal ion removal and an improved efficiency was reported for 8-HQ-MWCNT.¹⁵³ Amine-functionalized MWCNTs were synthesized by Wang *et al.* by the chemical reaction of the corresponding primary and secondary amines (cis-myrtanylamine, 2,4-dinitroaniline, 2,6-dinitroaniline, N-decyl-2,4,6-trinitroaniline and N-(3-morpholinopropyl)-2,4,6-trinitroaniline) with acylated MWCNTs.¹⁵⁴ The nanotubes produced were suggested to possess properties which could make them effective for drug delivery and biosensor applications.¹⁵⁴ Addition reactions involving diazonium salts and 1,3-dipolar cycloaddition reaction of azomethine ylides with MWCNTs were carried out through a microwave-induced method by Brunetti *et al.*, in order to introduce multiple functional groups to the walls of tubes. The synthesized tubes had higher reactivity and were also proposed for biomedical applications.¹⁵⁵ In a similar vein, diol-functionalized MWCNTs were synthesized by Jing *et al.*¹⁵⁶ through the selective grafting of polycaprolactone diol on acylated MWCNTs. This process significantly improved MWCNT dispersion, resulting in increased mechanical properties and thermal stability, hence, increasing their application for many other purposes.¹⁵⁶ To increase dispersion in organic solvents and the mechanical properties of MWCNTs, Hill *et al.* also applied poly(styrene-*co-p*-(4-(4'-vinylphenyl)-3-oxabutanol) as a modifier with MWCNTs for esterification reactions.¹⁵⁷

Hence, increased reactivity can be achieved through functionalization of MWCNTs with organic molecules to suit specific purposes for further usage in many other fields. The application of CNTs for pollutant removal is of interest to environmentalists due to the increased surface area and porosity possessed by these materials. The ease with which new functional groups can be attached to CNT walls considerably increases the number of active sites, hence increasing the sorption activity between the adsorbent and pollutant. Functionalization of MWCNTs by using various chemical agents is therefore becoming an alternative means for achieving suitable adsorbents for wastewater remediation.

Reports have demonstrated that CNTs (both pristine and functionalized) possess good potential for the removal of organic and/or inorganic contaminants from aqueous solution. The efficiency of CNTs has been investigated for the removal of toxic metal ions such as Pb^{2+} ,^{105,158} Cu^{2+} ,¹⁵⁹ Cd^{2+} ,^{30,160} Zn^{2+} ,⁵⁰ Mn^{2+} ,¹⁵⁹ and Hg^{2+} ,³⁶ amongst many others, from wastewater. Metal ions may bind to oxygen- and/or nitrogen- functional groups present in CNTs *via* chelation, ion-exchange or electrostatic interactions. Organic pollutants such as polyaromatic hydrocarbons,¹⁶¹ 17 α -ethinyl estradiol,^{64,162} trihalomethane,¹⁶³ 2,4,6-trichlorophenol,¹⁶⁴ dioxin,¹⁶⁵ phenol,¹⁶⁶ aniline,¹⁶⁶ BPA¹⁶⁷ and IBP¹⁶⁸ have also shown good sorption ability onto CNTs. The removal of organic pollutants from aqueous solutions has been accounted to hydrophobic or π - π interactions between the adsorbent and adsorbates.^{53,161} Hence, the more hydrophobic an adsorbate is, the better its removal onto CNTs. However, increased removal of contaminants has been reported for functionalized tubes over pristine CNTs, due to the increase in active sites on the sorbents. The uptake of contaminants from aqueous solution depends on the pH, adsorbent dose, initial adsorbate concentration, contact time and temperature of the adsorbate solution. Optimum adsorption conditions reported in literature were therefore compared for the sorption of Pb^{2+} , Cu^{2+} , Cd^{2+} , Hg^{2+} and Zn^{2+} onto pristine and functionalized CNTs in Table 2.3. Increased removal of these metal ions was noticed for functionalized CNTs than pristine CNTs (Table 2.3). This was accounted to enhancement of electrostatic interactions between metal cations and nitrogen/oxygen functional groups incorporated onto CNT walls. Further, Table 2.4 compares the optimum conditions achieved for the removal of BPA and IBP onto pristine and functionalized CNTs. From previously published reports, the adsorption of organic contaminants was noticed to be more effective by using pristine MWCNTs/SWCNTs than functionalized tubes (Table 2.4). Functionalization of CNTs reduces their hydrophobic nature, hence increasing their dispersion in aqueous media. Increased sorption which was observed with pristine tubes could be as a result of improved hydrophobic interaction between organic molecules in solution and the surface of CNTs.

Hence, in this study, nitrogen-functionalized tubes were synthesized while incorporating a ligand containing π - π bonds onto CNTs surface with the purpose of improving metal ion chelation and organic sorption simultaneously. Chapters 4 to 9 present the single and competitive removal of metal ions (Pb^{2+} , Cu^{2+} , Cd^{2+} , Hg^{2+} and Zn^{2+}) and organic (BPA and IBP) pollutants from aqueous solutions by using both oxygen- and nitrogen-functionalized MWCNTs. The optimum experimental conditions were determined and their efficiencies for pollutant removal compared to determine the adsorbent with the best sorption uptake for each process.

2.10.2. CNT/ferrite composites

Ferrites are ceramic ferromagnetic compounds composed of iron oxides (α -Fe₂O₃) with one or more metallic element.¹⁶⁹ They are usually non-conductive, possessing excellent magnetic and optical properties, great thermal and corrosion resistance and non-expensive.¹⁶⁹ Ferrites are spinel-shaped, with a general formula of AB₂O₄, where A and B are metal cations, including iron. Magnetite (Fe₃O₄) is the commonest, most magnetic mineral of the oxides of iron, and its properties have been investigated for various applications by environmental, chemical and biological scientists.¹⁷⁰

Nanocomposites containing ferrites and CNTs can be fabricated to optimise their potential applications.¹⁷¹ The properties of both nanomaterials can be harnessed to obtain composites with high surface area and porosity, strong magnetic properties and may contain multiple functional groups available for interaction. Nano-sized magnetic composites are potential adsorbents which should be effective for wastewater remediation, since they offer an advantage of easy separation of the sorbents under an external magnetic field.¹⁷² The activity of these composites can also be enhanced since new functional groups can be incorporated into them, hence increasing the number of active sites and promoting pollutant removal. Thus, CNT-ferrite nanocomposites should serve as good alternatives for wastewater remediation. This was evident from Table 2.4, where an increased sorption of RhB was observed compared to its removal by pristine CNTs. The effectiveness of CNTs to RhB removal was largely improved by using composite materials.

Although much work has been conducted on the wastewater remediation by using magnetite as adsorbents, the application of other ferrites such as cobalt ferrite has not been investigated. In this study, cobalt ferrites (CoFe₂O₄), MWCNTs and CNT-CoFe₂O₄ nanocomposites were synthesized and their effectiveness for the removal of RhB from aqueous solutions investigated. Chapter 10 also discusses the effect of increasing percentage of CNTs in the composites for RhB removal.

Table 2.3: Adsorption conditions for the removal of Pb²⁺, Cd²⁺, Hg²⁺, Cu²⁺ and Zn²⁺ onto CNTs

Modifying agent(s)	Species	pH	Time/min	Adsorbent dose/mg	[M ⁿ⁺]/mg dm ⁻³	T/°C	Isotherm	Kinetics	q _m /mg g ⁻¹	Ref.
Pristine	Pb ²⁺	9	240	50	2–20	NA	F	NA	2.960	159
HNO ₃	Pb ²⁺	9	240	50	2–20	NA	F	NA	2.960	159
HNO ₃	Pb ²⁺	9	240	50	2–20	NA	F	NA	3.110	159
HNO ₃	Pb ²⁺	3	360	50	2–14	25	L, F	NA	1.660	173
HNO ₃	Pb ²⁺	5	360	50	2–14	25	L, F	NA	17.44	173
Pristine	Pb ²⁺	5	360	50	2–14	25	L, F	NA	1.000	173
Ethylenediamine	Pb ²⁺	6.2	90	1	5–100	25	L	PSO	40.12	105
Diethylenetriamine	Pb ²⁺	6.2	90	1	5–100	25	L	PSO	54.27	105
8-hydroxyquinoline	Pb ²⁺	7	10	250	0.5	25	NA	NA	0.076	153
Pristine	Cu ²⁺	9	240	50	2–20	NA	F	NA	3.490	159
HNO ₃	Cu ²⁺	9	240	50	2–20	NA	F	NA	3.720	159
HNO ₃	Cu ²⁺	9	240	50	2–20	NA	F	NA	3.690	159
CNT/SiO ₂	Cu ²⁺	6.2	180	20	10–500	25	L	PSO	66.58	174
HNO ₃ /H ₂ SO ₄	Cu ²⁺	4	300	50	1–20	25	L, F	PSO	29.69	175
HNO ₃	Cu ²⁺	8	120	50	2–50	25	L	PSO	24.70	176
HNO ₃	Zn ²⁺	8	120	50	2–50	25	L	PSO	14.70	176
HNO ₃	Zn ²⁺	7	NA	50	101–1200	25	L, F	PSO	74.62	177
NaOCl	Zn ²⁺	7	60	50	10–80	25	L	NA	32.68	50
8-hydroxyquinoline	Zn ²⁺	7	10	250	0.5	25	NA	NA	0.075	153
Pristine	Cd ²⁺	5.5	240	50	9.50	25	NA	NA	1.10	30
Pristine	Cd ²⁺	6.0	4	100	67.5	25	L	BAT	9.33	160
H ₂ O ₂	Cd ²⁺	5.5	240	50	9.50	25	NA	NA	2.60	30
KMnO ₄	Cd ²⁺	5.5	240	50	9.50	25	NA	NA	5.10	30
HNO ₃	Cd ²⁺	5.5	240	50	9.50	25	NA	NA	11.00	30

N-doped CNT	Cd ²⁺	6.0	4	100	67.5	25	L	BAT	15.63	160
Thiol-SWCNT	Hg ²⁺	5.0	60	2.5	80	25	L,F	PFO	131.	37
Thiol-MWCNT	Hg ²⁺	6.0	60	40	5-100	25	L	PSO	84.66	36

*NA: Not available, L: Langmuir, F: Freundlich, PSO: pseudo-second order, PFO: pseudo-first order, BAT: Bohart-Adam-Thomas

Table 2.4: Adsorption conditions for the removal of BPA, IBP and RhB onto CNTs

Modifying agent(s)	Species	pH	Time/min	Adsorbent dose/mg	[M ⁿ⁺]/mg dm ⁻³	T/°C	Isotherm	Kinetics	q _m /mg g ⁻¹	Ref.
SWCNT	BPA	9	60	50	2-50	20	S, L	PSO	71	65
SWCNT	BPA	8.2	240	15	0.23	25	L, F	NA	13.39	64
Pristine	BPA	9	60	50	2-50	20	S, L	PSO	111	65
Pristine	BPA	6	1440	25	10	7	L	PSO	60.98	178
SOCl ₂ /NH ₄ OH	BPA	6	1440	25	10	7	L	NA	69.96	178
HNO ₃ /H ₂ SO ₄	BPA	NA	10080	125	0.1 - 40	NA	L, PMM	NA	1.25	162
SWCNT	IBP	7	8640	2	0.05 - 2	23	PMM	NA	232	168
Pristine	IBP	7	8640	2	0.05 - 2	23	PMM	NA	81	168
HNO ₃	IBP	7	8640	2	0.05 - 2	23	PMM	NA	19	168
Pristine	RhB	7	30	100	10	NA	L, T	PSO	3.533	79
MWCNT/Fe ₂ O ₄	RhB	6	80	3	15	25	L	PSO	11.44	179
MWCNT/Fe ₂ O ₄	RhB	NA	450	NA	NA	NA	L	PFO	11.02	180

*NA: Not available, L: Langmuir, F: Freundlich, PMM: Polanyi Mane model, T: Temkin, PSO: pseudo-second order, PFO: pseudo-first order

2.11. Desorption

Desorption is the process whereby a substance is removed from the surface of an adsorbent. The disposal of spent adsorbents generates secondary pollutants which result in another environmental problem. The removal of adsorbates from the sorbent's surface therefore becomes an important step in wastewater remediation. This step is economical since it permits the regeneration of the adsorbent for reuse in another adsorption cycle and the recovery of adsorbates. Desorption is achieved by the alteration of solution pH, displacement of the active compound, ion-exchange and solute concentration decrease and in some cases by thermal processes.

Thermal and chemical methods are the most prominent methods used for adsorbent recovery.¹⁸¹ In recent times, various chemical agents such as HCl,¹⁵ HNO₃,¹⁵ EDTA,¹⁸² NaOH,¹⁸³ H₂SO₄,¹⁸² NaCl,¹⁸² NH₄Cl,¹⁸⁴ NH₄NO₃¹⁸⁴ and ethanol,^{72,185} amongst many others, have been employed for the possible desorption of the adsorbate from the surface of adsorbent. The choice of agent used for desorption depends largely on the chemical properties of the adsorbates. Acidic solutions such as HCl, HNO₃ and H₂SO₄ desorb metal ions through electrostatic/ion-exchange interactions, while solvents such as acetone, ethanol may desorb organic contaminants *via* extraction. Good desorption efficiencies have been reported by these authors, demonstrating that adsorbents can be regenerated for reuse.

The desorption efficiency was calculated by using Eq. (2.30):

$$\% \text{ desorption} = \frac{\text{amount of adsorbate desorbed}}{\text{amount of adsorbate adsorbed}} \times 100 \quad (2.30)$$

2.12. Characterization/analytical techniques

A number of techniques were applied for the characterization of the adsorbents and ligand synthesized in this study. This was done to understand the physical, chemical and surface properties of the adsorbents and to elucidate/confirm the structure of the synthesized ligand. The influence of CNT functionalization was also investigated by using various techniques to understand the interactions/mechanisms involved in the solid-liquid phase. Similarly, various analytical techniques were applied for the detection and quantification of analytes in aqueous solution. The subsequent sections consider the principles which underlie these techniques and their application depending on their suitability to obtain the required information.

2.12.1. Nuclear magnetic resonance spectrometry

Nuclear magnetic resonance (NMR) spectrometry is a non-destructive technique generally used to predict the structure of an organic compound. NMR spectroscopy measures the energy absorbed or emitted at a specific resonance frequency by the nuclei of a sample, hence enabling the monitoring of the nuclei magnetic properties within a molecule.¹⁸⁶ The resonance frequency of a sample depends on the strength of the magnetic field. The physical, chemical, electronic and structural properties of a molecule can be determined based on the chemical shifts (resonance frequency) of the sample. Proton NMR (¹H NMR) and carbon NMR (¹³C NMR) employ the monitoring of the carbon-hydrogen framework in an organic compound, hence accounting for protons and carbons present within the molecule of the sample.

2.12.2. Mass spectrometry

Mass spectrometry is used to determine the molecular mass of compounds, to detect fragmented species and possible sites of fragmentation and identify analytes based on their mass-to-charge (m/z) ratio.¹⁸⁶ This technique employs the bombardment of the atoms in a molecule with electrons to obtain highly energetic positively and negatively charged ions (molecular ion).¹⁸⁷ The molecular ion is fragmented and separated based on the m/z ratio of the fragments and these are detected in proportion to their abundance.¹⁸⁷ A plot of relative abundance *versus* the m/z ratio generates a spectrum, from which information regarding the nature and structure of the molecule can be obtained.¹⁸⁷ The molecular mass of the compound represents the molecular ion, which appears at the highest value of m/z ratio.

2.12.3. Fourier transform infrared spectrophotometry

This technique involves the direct radiation of infrared (IR) light onto an adsorbent, from which some of the light beam is either absorbed or transmitted through the sample.¹⁸⁶ A absorption peak, analogous to the frequency of vibration between the bonds of the atoms within the sorbent, and the bonds between the molecules in the sorbent is obtained and represented on an IR spectrum. The spectrum represents the light output (absorbance/transmittance) as a function of frequency. FTIR is a non-destructive qualitative technique, used to identify the surface functional groups which are responsible for sorbate-sorbent interactions in wastewater.¹⁸⁸ In this study, all sorbents were embedded into KBr pellets to obtain a translucent disc, which was then subjected to IR radiation. The simplicity of this technique makes it an acceptable and widely used method for confirmation or identification of functional groups which have been attached to the CNT structure.

2.12.4. Raman spectroscopy

This is a non-destructive technique which offers specific information on the structure, purity (defects) and crystallinity of an adsorbent. It employs the monitoring of scattered photons generated after the sorbent is radiated with monochromatic light, to study the vibrational and rotational modes in the sample.¹⁸⁸ The measurement of the intensity of scattered light as a function of its frequency produces the Raman spectrum, from which the photon frequency of the sample can be obtained.¹⁸⁹ The purity and crystalline arrangement of CNTs are evaluated based on ratio of the intensity of the D (I_D) and G (I_G) bands. The D band (defect/disorder) depends on the scattering of photons from a defective site in the sp^2 carbon structure of the CNTs.¹⁹⁰ The band is observed at $\approx 1300\text{--}1350\text{ cm}^{-1}$, depending on the source and defects on the sidewalls of CNTs.¹⁸⁸ The G-band (graphitic), observed at $\approx 1500\text{--}1600\text{ cm}^{-1}$, is related to in-plane vibrations of the C-C bond in the graphene sheets.^{188,191} The crystallinity and purity of the CNTs therefore increases with a lower value of the I_D/I_G ratio and an increase in defective sites is associated with higher I_D/I_G values.

2.12.5. Thermogravimetric analysis

The thermal stability, purity, amount of volatile components and quality of the adsorbents can be evaluated by using thermogravimetric analysis (TGA). This technique employs the monitoring of the change in mass of a sample (Δm) as a function of temperature whilst the sample is being subjected to heating. A plot of the weight percentage against temperature produces the TGA curve, from which information such as decomposition temperature (maximum temperature where decomposition occurs), ash content (mass of sample remaining after decomposition) and initiation temperature (temperature where decomposition begins) is obtained.¹⁸⁸ The amount of residual metal nanoparticles, amorphous carbon and carbonaceous impurities can also be estimated from the TGA curve, hence providing indications on the purity of CNTs.

2.12.6. Imaging and microscopic techniques

Of key importance in confirming the tubular structure (shape), morphology, and size distribution of CNTs, is the application of microscopic techniques such as scanning electron microscopy (SEM), transmission electron microscopy (TEM) and high resolution transmission electron microscopy (HRTEM). These techniques adopt the production of images by focusing a beam of electrons on the sample to induce interactions between CNT atoms and electrons,¹⁸⁸ hence, generating information on the surface morphology and quality of adsorbents. TEM and HRTEM employ high energy electrons to obtain images of higher magnification. Nanotube

outer and inner diameters, effect of functionalization and lattice fringes can be observed from images produced at high magnification.¹⁸⁸ Microscopic techniques are therefore used in studying the structural integrity of nanotubes and monitoring changes associated with defects on CNT side-walls

2.12.7. Brunauer, Emmet and Teller analysis

The Brunauer, Emmet and Teller (BET) method is employed to obtain the specific surface area (SSA) of adsorbents through gas adsorption experiments. Typically the sample is evacuated to remove all adsorbed materials and nitrogen at 77 K is used to obtain the adsorption data, which is fitted into the BET equation to obtain q_m values. The BET method is based on the evaluation of the monolayer adsorption capacity of adsorbents by fitting gas adsorption data to the BET equation, to obtain the SSA of a material. This is an important parameter because it gives information on the number or amount of active sites present on the adsorbent. The pore size distribution of the CNTs can also be obtained by using the Barrett-Joyner-Halenda (BJH) theory.

2.12.8. Elemental analysis

Elemental analysis gives information on the percentage composition of elements such as carbon, oxygen and nitrogen contained in the adsorbents. This technique, often referred to as CHNX, employs the complete combustion of a sample in oxygen to convert organic and inorganic substances into combustible gaseous products such as carbon dioxide, water and nitric acid.¹⁹³ As a result of these, the percentage composition of carbon, oxygen and nitrogen is obtained from the masses of the combustible products.¹⁹³ CHN analysis provides quantitative information into the purity and chemical/empirical formula of the unknown sample.

2.12.9. Inductively coupled plasma-optical emission spectroscopy

Inductively coupled plasma-optical emission spectroscopy (ICP-OES) is an analytical technique used for the detection of metal ion concentrations in aqueous samples. The technique adopts the use of a plasma (10000 K) to produce excited atoms/ions that emit radiation at wavelengths characteristic to each element. The concentration of the metal in the sample is determined as a function of the intensity of light emitted by the element. The sensitivity and sample throughput makes this technique a preferred choice rather than other spectrophotometric methods such as atomic absorption spectrophotometry for the determination of metals in aqueous solutions.¹⁹⁴

2.12.10. Cold vapour atomic absorption spectrophotometry

As is the case with ICP-OES, atomic absorption spectrometry¹⁹⁵ is a technique employed for the determination of elements in solution. The technique, however, atomises the sample (i.e. converts to ground-state free atoms) by using either a flame or a graphite atomizer, to produce radiation at specific wavelengths. The concentration of an element is estimated from the amount of light energy absorbed which is proportional to the number of atoms in solution.

Since free mercury atoms can exist at room temperature, a technique which requires the atomization of samples without a flame is therefore needed for this element. The cold vapour atomic absorption spectrophotometry (CV-AAS) is a sensitive technique used for the determination of total mercury concentrations in aqueous samples.¹⁹⁶ The technique employs the reduction of mercury to its elemental form by reacting the sample with a strong reducing agent such as stannous chloride (SnCl_2) or sodium borohydride (NaBH_4) in a closed system. Volatile free mercury is driven from a closed vessel by introducing an inert gas (argon) into the sample. Atoms are then produced after irradiation by the light source and the concentration of mercury estimated from the amount of light energy absorbed by free atoms.

2.12.11. High performance liquid chromatography

High performance liquid chromatography (HPLC) is an analytical technique, used for the separation, identification and quantification of non-volatile organic components from an aqueous mixture. It involves the injection of a small volume of sample into a column packed with porous materials (stationary phase), and the individual components are driven by a liquid (mobile phase) at high pressure conditions. The separated components are then transferred to a detector (e.g. UV-vis absorbance detector), from which the amount (concentration) of components can be quantitatively estimated from an output (chromatogram). Separation of analytes depends on the chemical interaction of the sample with the mobile and stationary phases. Hence, the chemical properties of the components determine the stationary and mobile phases to be used for elution.

2.12.12. Boehm titration

The Boehm titration was developed by Hans Peter Boehm in 1991 to quantify the amount of oxygen functional groups present on carbon-based nanomaterials.^{197,198} Quantitative information on the amount of acidic (lactone, carboxyl and phenol) and basic groups present on the nanomaterial is estimated by means of an acid-base titration.¹⁹⁹ In this method, a strong acid (HCl) and base (NaOH) is made to react with bases and acids in the sample, respectively.

Typically, a particular amount of material is weighed separately into solutions of 0.05 mol dm^{-3} of NaOH, NaHCO₃, Na₂CO₃ and HCl and then agitated on a shaker for a period of time. The solid material is then separated from the solutions and aliquots of the filtrates are back-titrated against standardized NaOH/HCl solution.²⁰⁰ It is assumed that NaOH will neutralize carboxylic, lactonic and phenolic groups by accepting protons from the Bronsted acids, Na₂CO₃ is assumed to neutralize both the lactonic and carboxylic groups, while NaHCO₃ will only neutralize the carboxylic groups.^{199,201} The amount of basic sites on the carbon nanomaterial is estimated from the quantity of HCl required. This method is often used to complement results obtained from FTIR, in order to explain the functional groups present on carbon nanomaterials.

2.12.13. Point of zero charge

The point of zero charge (pzc) is the pH at which the electrical charge density of an adsorbent is equal to zero. In adsorption studies, this concept provides information to the ability of an adsorbent to either remove a cation or an anion from a solution. In this method, an adsorbent is weighed into plastic vials containing a solution of high ionic strength (NaCl/KCl) and their pH varied within 1-10. The suspensions are then agitated for a period of time and the filtrates are collected after agitation. The pH value of the filtrate is obtained and a plot of $\text{pH}_{\text{initial}} - \text{pH}_{\text{final}}$ vs. $\text{pH}_{\text{initial}}$ will be obtained. The point of intersection of the curves will give pH_{PZC} of the adsorbent.²⁰² Hence, the surface of the adsorbent is negative/anionic when the pH of the solution is greater than the pH_{PZC} of the adsorbent, hence, facilitating cationic removal. Whereas, the adsorbent's surface is positive if the solution pH is less than the pH_{PZC} of the adsorbent, enhancing anionic exchange.

References

- (1) Abdel Salam, M.; Al-Zhrani, G.; Kosa, S. A. Removal of heavy metal ions from aqueous solution by multi-walled carbon nanotubes modified with 8-hydroxyquinoline: Kinetic study. *J. Ind. Eng. Chem.* 2014, 20, 572-580.
- (2) Liu, D.; Li, Z.; Li, W.; Zhong, Z.; Xu, J.; Ren, J.; Ma, Z. Adsorption behavior of heavy metal ions from aqueous solution by soy protein hollow microspheres. *Ind. Eng. Chem. Res.* 2013, 52, 11036-11044.
- (3) Agency for Toxic Substances and Disease Registry (ATSDR). CERCLA Priority List of Hazardous Substances. 2007.
- (4) Srivastava, S. Sorption of divalent metal ions from aqueous solution by oxidized carbon nanotubes and nanocages: A review. *Adv. Mat. Lett.* 2013, 4, 2-8.
- (5) Feng, Y.; Gong, J.-L.; Zeng, G.-M.; Niu, Q.-Y.; Zhang, H.-Y.; Niu, C.-G.; Deng, J.-H.; Yan, M. Adsorption of Cd(II) and Zn(II) from aqueous solutions using magnetic hydroxyapatite nanoparticles as adsorbents. *Chem. Eng. J.* 2010, 162, 487-494.
- (6) Lai, Y.-L.; Thirumavalavan, M.; Lee, J.-F. Effective adsorption of heavy metal ions (Cu^{2+} , Pb^{2+} , Zn^{2+}) from aqueous solution by immobilization of adsorbents on Ca-alginate beads. *Toxicol. Environ. Chem.* 2010, 92, 697-705.
- (7) Senthilkumar, S.; Bharathi, S.; Nithyanandhi, D.; Subburam, V. Biosorption of toxic heavy metals from aqueous solutions. *Bioresour. Technol.* 2000, 75, 163-165.
- (8) Rao, G.; Lu, C.; Su, F. Sorption of divalent metal ions from aqueous solution by carbon nanotubes: A review. *Sep. Purif. Technol.* 2007, 58, 224-231.
- (9) Mubarak, N. M.; Sahu, J. N.; Abdullah, E. C.; Jayakumar, N. S. Removal of heavy metals from wastewater using carbon nanotubes. *Sep. Purif. Rev.* 2013, 43, 311-338.
- (10) Bao, W.-W.; Zou, H.-F.; Gan, S.-C.; Xu, X.-C.; Ji, G.-J.; Zheng, K.-Y. Adsorption of heavy metal ions from aqueous solutions by zeolite based on oil shale ash: Kinetic and equilibrium studies. *Chem. Res. Chin. Univ.* 2013, 29, 126-131.
- (11) Iwegbue, C. M. A. Heavy metal composition of livers and kidneys of cattle from southern Nigeria *Vet. Arhiv.* 2008, 78, 401-410.
- (12) Ahamed, A. J.; Begum, A. S. Adsorption of copper from aqueous solution using low cost adsorbent. *Arch. Appl. Sci. Res.* 2012, 4, 1532-1539.
- (13) http://www.atsdr.cdc.gov/SPL/resources/ATSDR_2013_SPL_Detailed_Data_Table.pdf. Accessed on 28th March 2015.

- (14) <http://water.epa.gov/drink/index.cfm>. Accessed on 28th March 2015.
- (15) Naiya, T. K.; Bhattacharya, A. K.; Das, S. K. Adsorption of Cd(II) and Pb(II) from aqueous solutions on activated alumina. *J. Colloid Interface Sci.* 2009, 333, 14-26.
- (16) Chen, J.; Xiao, S.; Wu, X.; Fang, K.; Liu, W. Determination of lead in water samples by graphite furnace atomic absorption spectrometry after cloud point extraction. *Talanta* 2005, 67, 992-996.
- (17) Chen, J.; Teo, K. C. Determination of cadmium, copper, lead and zinc in water samples by flame atomic absorption spectrometry after cloud point extraction. *Anal. Chim. Acta* 2001, 450, 215-222.
- (18) Mahan, K. I.; Foderaro, T. A.; Garza, T. L.; Martinez, R. M.; Maroney, G. A.; Trivisonno, M. R.; Willging, E. M. Microwave digestion techniques in the sequential extraction of calcium, iron, chromium, manganese, lead, and zinc in sediments. *Anal. Chem.* 1987, 59, 938-945.
- (19) Awang, N.; Jamaluddin, F. Determination of lead, cations, and anions concentration in indoor and outdoor air at the primary schools in Kuala Lumpur. *J. Environ. Public Health* 2014, 2014, 408275-408277.
- (20) Ogundiran, M. B.; Oyetade, O. A.; Babayemi, J. O.; Osibanjo, O. Potential environmental hazards of non-rechargeable electric torch wastes in Nigeria. *Int. J. Environ. Waste Manag.* 2014, 13, 115-130.
- (21) Behbahani, M.; Hassanlou, P. G.; Amini, M. M.; Moazami, H. R.; Abandansari, H. S.; Bagheri, A.; Zadeh, S. H. Selective solid-phase extraction and trace monitoring of lead ions in food and water samples using new lead-imprinted polymer nanoparticles. *Food Anal. Methods* 2014, 8, 558-568.
- (22) Hamza, I. A. A.; Martincigh, B. S.; Ngila, J. C.; Nyamori, V. O. Adsorption studies of aqueous Pb(II) onto a sugarcane bagasse/multi-walled carbon nanotube composite. *Phys. Chem. Earth* 2013, 66, 157-166.
- (23) Yang, B.; Gong, Q.; Zhao, L.; Sun, H.; Ren, N.; Qin, J.; Xu, J.; Yang, H. Preconcentration and determination of lead and cadmium in water samples with a MnO₂ coated carbon nanotubes by using ETAAS. *Desalination* 2011, 278, 65-69.
- (24) Yan, H. L.; Shuguang, W.; Jinquan, W.; Xianfeng, Z.; Cailu, X.; Zhaokun, L.; Dehai, W.; Bingqing, W. Lead adsorption on carbon nanotubes. *Chem. Phys. Lett.* 2002, 357, 263-266.
- (25) Hamza, I. A. A. Preparation and evaluation of a sugarcane bagasse multi-walled carbon nanotube composite for the adsorption of heavy metals from aqueous

- solutions. *PhD Thesis* 2013, *University of KwaZulu-Natal, Durban, South Africa*.
- (26) Smith, R. M.; Martell, A. E. *Critical Stability Constants* 1976, 6, Plenum Press, New York.
 - (27) Bernard, A. Cadmium & its adverse effects on human health. *Indian J. Med. Res.* 2008, 128, 557-564.
 - (28) Llewellyn, T. O. Cadmium. <http://pubs.usgs.gov/usbmic/ic-9380/cadmium.pdf> Accessed on 28th March 2015.
 - (29) Wu, S.; Zhang, K.; Wang, X.; Jia, Y.; Sun, B.; Luo, T.; Meng, F.; Jin, Z.; Lin, D.; Shen, W.; Kong, L.; Liu, J. Enhanced adsorption of cadmium ions by 3D sulfonated reduced graphene oxide. *Chem. Eng. J.* 2015, 262, 1292-1302.
 - (30) Li, Y.-H.; Wang, S.; Luan, Z.; Ding, J.; Xu, C.; Wu, D. Adsorption of cadmium(II) from aqueous solution by surface oxidized carbon nanotubes. *Carbon* 2003, 41, 1057-1062.
 - (31) Sun, J.; Yang, Z.; Lee, H.; Wang, L. Simultaneous speciation and determination of arsenic, chromium and cadmium in water samples by high performance liquid chromatography with inductively coupled plasma mass spectrometry. *Anal. Meth.* 2015, 7, 2653-2658.
 - (32) Chen, T.; Zhou, Z.; Han, R.; Meng, R.; Wang, H.; Lu, W. Adsorption of cadmium by biochar derived from municipal sewage sludge: Impact factors and adsorption mechanism. *Chemosphere* 2015, 134, 286-293.
 - (33) Liang, J.; Liu, J.; Yuan, X.; Dong, H.; Zeng, G.; Wu, H.; Wang, H.; Liu, J.; Hua, S.; Zhang, S.; Yu, Z.; He, X.; He, Y. Facile synthesis of alumina-decorated multi-walled carbon nanotubes for simultaneous adsorption of cadmium ion and trichloroethylene. *Chem. Eng. J.* 2015, 273, 101-110.
 - (34) Wahby, A.; Abdelouahab-Reddam, Z.; El Mail, R.; Stitou, M.; Silvestre-Albero, J.; Sepúlveda-Escribano, A.; Rodríguez-Reinoso, F. Mercury removal from aqueous solution by adsorption on activated carbons prepared from olive stones. *Adsorption* 2011, 17, 603-609.
 - (35) Di Natale, F.; Erto, A.; Lancia, A.; Musmarra, D. Mercury adsorption on granular activated carbon in aqueous solutions containing nitrates and chlorides. *J. Hazard. Mater.* 2011, 192, 1842-1850.
 - (36) Hadavifar, M.; Bahramifar, N.; Younesi, H.; Li, Q. Adsorption of mercury ions from synthetic and real wastewater aqueous solution by functionalized multi-walled carbon nanotube with both amino and thiolated groups. *Chem. Eng. J.* 2014, 237, 217-228.

- (37) Bandaru, N. M.; Reta, N.; Dalal, H.; Ellis, A. V.; Shapter, J.; Voelcker, N. H. Enhanced adsorption of mercury ions on thiol derivatized single wall carbon nanotubes. *J. Hazard. Mater.* 2013, *261*, 534-541.
- (38) Wajima, T.; Sugawara, K. Adsorption behaviors of mercury from aqueous solution using sulfur-impregnated adsorbent developed from coal. *Fuel Proc. Technol.* 2011, *92*, 1322-1327.
- (39) Lv, J.; Luo, L.; Zhang, J.; Christie, P.; Zhang, S. Adsorption of mercury on lignin: combined surface complexation modeling and X-ray absorption spectroscopy studies. *Environ. Pollut.* 2012, *162*, 255-261.
- (40) Boszke, L.; Glosinska, G.; Siepak, J. Some aspects of speciation of mercury in water environment. *Pol. J. Environ. Stud.* 2002, *11*, 285-298.
- (41) Yu, B.; Zhang, Y.; Shukla, A.; Shukla, S. S.; Dorris, K. L. The removal of heavy metal from aqueous solutions by sawdust adsorption — removal of copper. *J. Hazard. Mater.* 2000, *B80*, 33-42.
- (42) Popuri, S. R.; Frederick, R.; Chang, C.-Y.; Fang, S.-S.; Wang, C.-C.; Lee, L.-C. Removal of copper(II) ions from aqueous solutions onto chitosan/carbon nanotubes composite sorbent. *Desalin. Water Treat.* 2013, *52*, 691-701.
- (43) Williams, D. In *Tilte* 1983.
- (44) Goyal, M.; Rattan, V. K.; Aggarwal, D.; Bansal, R. C. Removal of copper from aqueous solutions by adsorption on activated carbons. *Colloids Surf. A Physicochem. Eng. Asp.* 2001, *190*, 229-238.
- (45) Tong, K. S.; Kassim, M. J.; Azraa, A. Adsorption of copper ion from its aqueous solution by a novel biosorbent *Uncaria gambir*: Equilibrium, kinetics, and thermodynamic studies. *Chem. Eng. J.* 2011, *170*, 145-153.
- (46) Lim, T. T.; Chu, J. Assessment of the use of spent copper slag for land reclamation. *Waste Manage. Res.* 2006, *24*, 67-73.
- (47) Nriagu, J. Zinc Toxicity in Humans. *School of Public Health, University of Michigan* 2007.
- (48) Sen, T. K.; Gomez, D. Adsorption of zinc (Zn^{2+}) from aqueous solution on natural bentonite. *Desalination* 2011, *267*, 286-294.
- (49) Mohan, D.; Singh, K. P. Single-and multi-component adsorption of cadmium and zinc using activated carbon derived from bagasse—an agricultural waste. *Water Res.* 2002, *36*, 2304-2318.
- (50) Lu, C.; Chiu, H. Adsorption of zinc(II) from water with purified carbon nanotubes. *Chem. Eng. Sci.* 2006, *61*, 1138-1145.

- (51) Zheng, S.; Sun, Z.; Park, Y.; Ayoko, G. A.; Frost, R. L. Removal of bisphenol A by Ca-montmorillonite modified with selected surfactants. *Chem. Eng. J.* 2013, 234, 416-422.
- (52) Ahrens, L. Polyfluoroalkyl compounds in the aquatic environment: A review of their occurrence and fate. *J. Environ. Monit.* 2011, 13, 20-31.
- (53) Hall, S.; Tang, R.; Baeyens, J.; Dewil, R. Removing polycyclic aromatic hydrocarbons from water by adsorption on silicagel. *Polycycl. Aromat. Comp.* 2009, 29, 160-183.
- (54) Staples, C. A.; Dorn, P. B.; Klecka, G. M.; Sondra, T. O.; Branson, D. R.; Harris, L. R. Bisphenol A concentrations in receiving waters near US manufacturing and processing facilities. *Chemosphere* 2000, 40, 521-525.
- (55) Nikolaou, A.; Meric, S.; Fatta, D. Occurrence patterns of pharmaceuticals in water and wastewater environments. *Anal. Bioanal. Chem.* 2007, 387, 1225-1234.
- (56) Potter, D. W.; Pawliszyn, J. Rapid determination of polyaromatic hydrocarbons and polychlorinated biphenyls in water using solid-phase microextraction and GC/MS. *Environ. Sci. Technol.* 1994, 28, 298-305.
- (57) Kim, J.-W.; Tue, N. M.; Isobe, T.; Misaki, K.; Takahashi, S.; Viet, P. H.; Tanabe, S. Contamination by perfluorinated compounds in water near waste recycling and disposal sites in Vietnam. *Environ. Monit. Assess.* 2013, 185, 2909-2919.
- (58) Nirmaier, H.-P.; Fischer, E.; Meyer, A.; Henze, G. Determination of polycyclic aromatic hydrocarbons in water samples using high-performance liquid chromatography with amperometric detection. *J. Chromatogr. A* 1996, 730, 169-175.
- (59) Tsai, W.-T.; Lai, C.-W.; Su, T.-Y. Adsorption of bisphenol-A from aqueous solution onto minerals and carbon adsorbents. *J. Hazard. Mater.* 2006, B134, 169-175.
- (60) Xu, J.; Wang, L.; Zhu, Y. Decontamination of bisphenol A from aqueous solution by graphene adsorption. *Langmuir* 2012, 28, 8418-8425.
- (61) Zhou, Y.; Lu, P.; Lu, J. Application of natural biosorbent and modified peat for bisphenol A removal from aqueous solutions. *Carbohydr. Polym.* 2012, 88, 502-508.
- (62) Kabbashi, N. A.; Elwathig, M.; AbuSam, A.; Bt Jamil, I. N. Kinetic study on Hg(II) removal by CNT. *Prog. Nanotech. Nanomater.* 2015, 4, 1-6.
- (63) Erler, C.; Novak, J. Bisphenol A exposure: human risk and health policy. *J. Pediatr. Nurs.* 2010, 25, 400-407.

- (64) Joseph, L.; Heo, J.; Park, Y.-G.; Flora, J. R. V.; Yoon, Y. Adsorption of bisphenol A and 17 α -ethinyl estradiol on single walled carbon nanotubes from seawater and brackish water. *Desalination* 2011, 281, 68-74.
- (65) Dehghani, M. H.; Mahvi, A. H.; Rastkari, N.; Saeedi, R.; Nazmara, S.; Irvani, E. Adsorption of bisphenol A (BPA) from aqueous solutions by carbon nanotubes: Kinetic and equilibrium studies. *Desalin. Water Treat.* 2014, 54, 84-92.
- (66) Mestre, A. S.; Pires, J.; Nogueira, J. M. F.; Carvalho, A. P. Activated carbons for the adsorption of ibuprofen. *Carbon* 2007, 45, 1979-1988.
- (67) Estevez, E.; Hernandez-Moreno, J. M.; Fernandez-Vera, J. R.; Palacios-Diaz, M. P. Ibuprofen adsorption in four agricultural volcanic soils. *Sci. Total Environ.* 2014, 468-469, 406-414.
- (68) Paul, S. C.; Githinji, L. J. M.; Ankumah, R. O.; Willian, K. R.; Pritchett, G. Sorption behavior of ibuprofen and naproxen in simulated domestic wastewater. *Water, Air, Soil Pollut.* 2013, 225, 1821-1830.
- (69) Behera, S. K.; Oh, S. Y.; Park, H. S. Sorptive removal of ibuprofen from water using selected soil minerals and activated carbon. *Int. J. Environ. Sci. Technol.* 2012, 9, 85-94.
- (70) Jung, C.; Park, J.; Lim, K. H.; Park, S.; Heo, J.; Her, N.; Oh, J.; Yun, S.; Yoon, Y. Adsorption of selected endocrine disrupting compounds and pharmaceuticals on activated biochars. *J. Hazard. Mater.* 2013, 263, 702-710.
- (71) Amdany, R.; Chimuka, L.; Cukrowska, E. Determination of naproxen, ibuprofen and triclosan in wastewater using the polar organic chemical integrative sampler (POCIS): A laboratory calibration and field application. *Water SA* 2014, 40, 407-413.
- (72) Gong, J.-L.; Wang, B.; Zeng, G.-M.; Yang, C.-P.; Niu, C.-G.; Niu, Q.-Y.; Zhoua, W.-J.; Liang, Y. Removal of cationic dyes from aqueous solution using magnetic multi-wall carbon nanotube nanocomposite as adsorbent. *J. Hazard. Mater.* 2009, 164, 1517-1522.
- (73) Madrakian, T.; Afkhami, A.; Mahmood-Kashani, H.; Ahmad, M. Adsorption of some cationic and anionic dyes on magnetite nanoparticles-modified activated carbon from aqueous solutions: equilibrium and kinetics study. *Iran Chem. Soc.* 2013, 10, 481-189.
- (74) Guclu, G. Removal of basic dyes from aqueous solution by dimethyl terephthalate distillation residue. *Desalination* 2010, 259, 53-58.

- (75) Salleh, M. A.; Mahmoud, D. K.; Abdul Karim, W. A.; Idris, A. Cationic and anionic dye adsorption by agricultural solid wastes: A comprehensive review. *Desalination* 2011, 280, 1-13.
- (76) Robinson, T.; McMullan, G.; Marchant, R.; Nigam, P. Remediation of dyes in textile effluent: A critical review on current treatment technologies with a proposed alternative. *Bioresour. Technol.* 2001, 77, 247-255.
- (77) Iyim, T. B.; Acar, I.; Ozgumus, S. Removal of basic dyes from aqueous solutions with sulfonated phenol-formaldehyde resin. *J. Appl. Polym. Sci.* 2008, 109, 2774-2780.
- (78) Khan, T. A.; Dahiya, S.; Ali, I. Use of kaolinite as adsorbent: Equilibrium, dynamics and thermodynamic studies on the adsorption of rhodamine B from aqueous solution. *Appl. Clay Sci.* 2012, 69, 58-66.
- (79) Kumar, S.; Bhanjana, G.; Jangra, K.; Dilbaghi, N.; Umar, A. Utilization of carbon nanotubes for the removal of rhodamine B dye from aqueous solutions. *J. Nanosci. Nanotechnol.* 2014, 14, 4331-4336.
- (80) Merouani, S.; Hamdaoui, O.; Saoudi, F.; Chiha, M. Sonochemical degradation of rhodamine B in aqueous phase: effects of additives. *Chem. Eng. J.* 2010, 158, 550-557.
- (81) Vogelpohl, A. I.; Kim, S. M. Advanced oxidation processes (AOPs) in wastewater treatment. *J. Ind. Eng. Chem.* 2004, 10, 33-40.
- (82) Gültekin, I.; Ince, N. H. Synthetic endocrine disruptors in the environment and water remediation by advanced oxidation processes. *J. Environ. Manage.* 2007, 85, 816-832.
- (83) Kosolapov, D.; Kuschik, P.; Vainshtein, M.; Vatsourina, A.; Wiessner, A.; Kästner, M.; Müller, R. Microbial processes of heavy metal removal from carbon-deficient effluents in constructed wetlands. *Eng. Life Sci.* 2004, 4, 403-411.
- (84) Pignatello, J. J.; Oliveros, E.; MacKay, A. Advanced oxidation processes for organic contaminant destruction based on the Fenton reaction and related chemistry. *Crit. Rev. Env. Sci. Technol.* 2006, 36, 1-84.
- (85) Rosenfeldt, E. J.; Linden, K. G. Degradation of endocrine disrupting chemicals bisphenol A, ethinyl estradiol, and estradiol during UV photolysis and advanced oxidation processes. *Environ. Sci. Technol.* 2004, 38, 5476-5483.
- (86) Al Hamedi, F.; Rauf, M.; Ashraf, S. Degradation studies of rhodamine B in the presence of UV/H₂O₂. *Desalination* 2009, 239, 159-166.

- (87) Visvanathan, C.; Aim, R. B.; Parameshwaran, K. Membrane separation bioreactors for wastewater treatment. *Crit. Rev. Env. Sci. Technol.* 2000, *30*, 1-48.
- (88) Greenlee, L. F.; Lawler, D. F.; Freeman, B. D.; Marrot, B.; Moulin, P. Reverse osmosis desalination: water sources, technology, and today's challenges. *Water Res.* 2009, *43*, 2317-2348.
- (89) Vourch, M.; Balannec, B.; Chaufer, B.; Dorange, G. Treatment of dairy industry wastewater by reverse osmosis for water reuse. *Desalination* 2008, *219*, 190-202.
- (90) Urgun-Demirtas, M.; Benda, P. L.; Gillenwater, P. S.; Negri, M. C.; Xiong, H.; Snyder, S. W. Achieving very low mercury levels in refinery wastewater by membrane filtration. *J. Hazard. Mater.* 2012, *215-216*, 98-107.
- (91) Jian, K.; Pintauro, P. N.; Ponangi, R. Separation of dilute organic/water mixtures with asymmetric poly (vinylidene fluoride) membranes. *J. Membr. Sci.* 1996, *117*, 117-133.
- (92) Tiravanti, G.; Petruzzelli, D.; Passino, R. Pretreatment of tannery wastewaters by an ion exchange process for Cr(III) removal and recovery. *Water Sci. Technol.* 1997, *36*, 197-207.
- (93) Rengaraj, S.; Joo, C. K.; Kim, Y.; Yi, J. Kinetics of removal of chromium from water and electronic process wastewater by ion exchange resins: 1200H, 1500H and IRN97H. *J. Hazard. Mater.* 2003, *102*, 257-275.
- (94) Mittal, A. Biological wastewater treatment. *Water Today* 2011, *1*, 32-44.
- (95) Chipasa, K. B. Accumulation and fate of selected heavy metals in a biological wastewater treatment system. *Waste Manage.* 2003, *23*, 135-143.
- (96) da Silva Oliveira, A.; Bocio, A.; Trevilato, T.; Takayanagui, A.; Domingo, J.; Segura-Muñoz, S. Heavy metals in untreated/treated urban effluent and sludge from a biological wastewater treatment plant. *Env. Sci. Pollut. Res.* 2007, *14*, 483-489.
- (97) Mohapatra, D.; Brar, S.; Tyagi, R.; Surampalli, R. Physico-chemical pre-treatment and biotransformation of wastewater and wastewater sludge—fate of bisphenol A. *Chemosphere* 2010, *78*, 923-941.
- (98) Sánchez-Avila, J.; Bonet, J.; Velasco, G.; Lacorte, S. Determination and occurrence of phthalates, alkylphenols, bisphenol A, PBDEs, PCBs and PAHs in an industrial sewage grid discharging to a municipal wastewater treatment plant. *Sci. Total Environ.* 2009, *407*, 4157-4167.

- (99) Servos, M.; Bennie, D.; Burnison, B.; Jurkovic, A.; McInnis, R.; Neheli, T.; Schnell, A.; Seto, P.; Smyth, S.; Ternes, T. Distribution of estrogens, 17 β -estradiol and estrone, in Canadian municipal wastewater treatment plants. *Sci. Total Environ.* 2005, *336*, 155-170.
- (100) Behnisch, P. A.; Fujii, K.; Shiozaki, K.; Kawakami, I.; Sakai, S. Estrogenic and dioxin-like potency in each step of a controlled landfill leachate treatment plant in Japan. *Chemosphere* 2001, *43*, 977-984.
- (101) Belgiorno, V.; Rizzo, L.; Fatta, D.; Della Rocca, C.; Lofrano, G.; Nikolaou, A.; Naddeo, V.; Meric, S. Review on endocrine disrupting-emerging compounds in urban wastewater: occurrence and removal by photocatalysis and ultrasonic irradiation for wastewater reuse. *Desalination* 2007, *215*, 166-176.
- (102) Ruthven, D.: *Principles of adsorption and adsorption processes*; John Wiley & Sons: Canada, 1984.
- (103) Shiratori, S.; Inami, Y.; Kikuchi, M. Removal of toxic gas by hybrid chemical filter fabricated by the sequential adsorption of polymers. *Thin Solid Films* 2001, *393*, 243-248.
- (104) Liu, Y.; Liu, Y.-J. Biosorption isotherms, kinetics and thermodynamics. *Sep. Purif. Technol.* 2008, *61*, 229-242.
- (105) Vuković, G. D.; Marinković, A. D.; Škapin, S. D.; Ristić, M. Đ.; Aleksić, R.; Perić-Grujić, A. A.; Uskoković, P. S. Removal of lead from water by amino modified multi-walled carbon nanotubes. *Chem. Eng. J.* 2011, *173*, 855-865.
- (106) Sharma, K. K.; Sharma, L. K. A textbook of physical chemistry, India. *Vikas Publishing House PVT Ltd.* 2004.
- (107) <https://www.classle.net/book/types-adsorption>. Accessed on 6th April 2015.
- (108) Ho, Y. S.; Wang, C. C. Pseudo-isotherms for the sorption of cadmium ion onto tree fern. *Process Biochem.* 2004, *39*, 759-763.
- (109) Lin, J.; Wang, L. Comparison between linear and non-linear forms of pseudo-first-order and pseudo-second-order adsorption kinetic models for the removal of methylene blue by activated carbon. *Front. Environ. Sci. Eng.* 2009, *3*, 320-324.
- (110) Lagergren, S. Zur theorie der sogenannten adsorption geloster stoffe, Kungliga Svenska Vetenskapsakademiens. *Handlingar* 1898, *24*, 1-39.
- (111) Ho, Y.-S. Citation review of Lagergren kinetic rate equation on adsorption reactions. *Scientometrics* 2004, *59*, 171-177.
- (112) Ho, Y. S.; McKay, G. Kinetic models for the sorption of dye from aqueous solution by wood. *Process Saf. Environ. Prot.* 1998, *76*, 183-191.

- (113) Ho, Y.-S.; McKay, G. Sorption of dye from aqueous solution by peat. *Chem. Eng. J.* 1998, *70*, 115-124.
- (114) Weber, W. J.; Morris, J. C. Kinetics of adsorption on carbon from solution. *J. Sanit. Engng. Div. Am. Soc. Civ. Engrs.* 1963, *89*, 31-60.
- (115) Demirbas, E.; Kobya, M.; Senturk, E.; Ozkan, T. Adsorption kinetics for the removal of chromium(VI) from aqueous solutions on the activated carbons prepared from agricultural wastes. *Water SA* 2004, *30*, 533-539.
- (116) Muntean, S. G.; Radulescu-Grad, M. E.; Sfarloaga, P. Dye adsorbed on copolymer, possible specific sorbent for metal ions removal. *RSC Adv.* 2014, *4*, 27354-27362.
- (117) Chien, S. H.; Clayton, W. R. Application of Elovich equation to the kinetics of phosphate release and sorption in soils. *Soil Sci. Soc. Am. J.* 1980, *44*, 265-268.
- (118) Guedidi, H.; Reinert, L.; Soneda, Y.; Bellakhal, N.; Duclaux, L. Adsorption of ibuprofen from aqueous solution on chemically surface-modified activated carbon cloths. *Arabian J. Chem.* 2014, In Press.
- (119) Langmuir, I. The adsorption of gases on plane surfaces of glass, mica and platinum. *J. Am. Chem. Soc.* 1918, *40*, 1361-1402.
- (120) Freundlich, H. Adsorption in solids. *Z. Phys. Chem.* 1906, *57*, 385-470.
- (121) Temkin, M. I.; Pyzhev, V. Kinetics of ammonia synthesis on promoted iron catalysts. *Acta Phys. Chim.* 1940, *12*, 327-356.
- (122) Dubinin, M. M.; Radushkevich, L. V. The equation of the characteristic curve of activated charcoal. *Proc. Acad. Sci, U.S.S.R, Phys. Chem. Sect.* 1947, *55*, 327-329.
- (123) Sips, R. Combined form of Langmuir and Freundlich equations. *J. Chem. Phys.* 1948, *16*, 490-495.
- (124) Toth, J. State equations of the solid-gas interface layers. *Acta Chim. Acad. Sci. Hung.* 1971, *69*, 311-328.
- (125) Khan, A. R.; Al-Waheab, I. R.; Al-Haddad, A. A generalized equation for adsorption isotherms for multi-component organic pollutants in dilute aqueous solution. *Environ. Technol.* 1996, *17*, 13-23.
- (126) Redlich, O.; Peterson, D. L. A useful adsorption isotherm. *J. Phys. Chem.* 1959, *63*, 1024.
- (127) Dada, A.; Olalekan, A.; Olatunya, A.; Dada, O. Langmuir, Freundlich, Temkin and Dubinin–Radushkevich isotherms studies of equilibrium sorption of Zn²⁺ unto phosphoric acid modified rice husk. *J. Appl. Chem.* 2012, *3*, 38-45.

- (128) Bhattacharya, A.; Naiya, T.; Mandal, S.; Das, S. Adsorption, kinetics and equilibrium studies on removal of Cr(VI) from aqueous solutions using different low-cost adsorbents. *Chem. Eng. J.* 2008, *137*, 529-541.
- (129) Weber, T. W.; Chakravorti, R. K. Pore and solid diffusion models for fixed-bed adsorbents. *AIChE J.* 1974, *20*, 228-238.
- (130) Soon-An, O.; Chye-Eng, S.; Poh-Eng, L. Kinetics of adsorption of Cu(II) and Cd(II) from aqueous solution on rice husk and modified rice husk. *Electronic J. Environ. Agric. Food Chem.* 2007, *6*, 764-1774.
- (131) Foo, K. Y.; Hameed, B. H. Insights into the modeling of adsorption isotherm systems. *Chem. Eng. J.* 2010, *156*, 2-10.
- (132) Hutson, N. D.; Yang, R. T. Theoretical basis for the Dubinin-Radushkevitch (DR) adsorption isotherm equation. *Adsorption* 1997, *3*, 189-195.
- (133) Laus, R.; Costa, T. G.; Szpoganicz, B.; Fávere, V. T. Adsorption and desorption of Cu(II), Cd(II) and Pb(II) ions using chitosan crosslinked with epichlorohydrin-triphosphate as the adsorbent. *J. Hazard. Mater.* 2010, *183*, 233-241.
- (134) Maurya, N. S.; Mittal, A. K. Biosorptive color removal: applicability of equilibrium isotherm models. *Pract. Period Hazard. Toxic. Radioact. Waste Manag.* 2009, *14*, 25-36.
- (135) Sharma, P.; Kaur, H. Sugarcane bagasse for the removal of erythrosin B and methylene blue from aqueous waste. *Appl. Water Sci.* 2011, *1*, 135-145.
- (136) Al Othman, Z. A.; Hashem, A.; Habila, M. A. Kinetic, equilibrium and thermodynamic studies of cadmium(II) adsorption by modified agricultural wastes. *Molecules* 2011, *16*, 10443-10456.
- (137) Milonjić, S. K. A consideration of the correct calculation of thermodynamic parameters of adsorption. *J. Serb. Chem. Soc.* 2007, *72*, 1363-1367.
- (138) Moradi, O. The removal of ions by functionalized carbon nanotube: Equilibrium, isotherms and thermodynamic studies. *Chem. Biochem. Eng. Q.* 2011, *25*, 229-240.
- (139) Demarchi, C. A.; Campos, M.; Rodrigues, C. A. Adsorption of textile dye Reactive Red 120 by the chitosan-Fe(III)-crosslinked: Batch and fixed-bed studies. *J. Environ. Chem. Eng.* 2013, *1*, 1350-1358.
- (140) Iijima, S. Helical microtubules of graphitic carbon. *Nature* 1991, *354*, 56-58.
- (141) O'Connell, M. J.: *Carbon nanotubes: Properties and applications*; CRC press: United States, 2006.

- (142) Balasubramanian, K.; Burghard, M. Chemically functionalized carbon nanotubes. *Small* 2005, *1*, 180-192.
- (143) Ombaka, L. M.; Ndungu, P.; Nyamori, V. O. Usage of carbon nanotubes as platinum and nickel catalyst support in dehydrogenation reactions. *Catal. Today* 2013, *217*, 65-75.
- (144) Thess, A.; Lee, R.; Nikolaev, P.; Dai, H.; Petit, P.; Robert, J.; Xu, C.; Lee, Y. H.; Kim, S. G.; Rinzler, A. G. Crystalline ropes of metallic carbon nanotubes. *Science* 1996, *273*, 483-487.
- (145) Journet, C.; Maser, W.; Bernier, P.; Loiseau, A.; de La Chapelle, M. L.; Lefrant, D. I. S.; Deniard, P.; Lee, R.; Fischer, J. Large-scale production of single-walled carbon nanotubes by the electric-arc technique. *Nature* 1997, *388*, 756-758.
- (146) Cassell, A. M.; Raymakers, J. A.; Kong, J.; Dai, H. Large scale CVD synthesis of single-walled carbon nanotubes. *J. Phys. Chem. B* 1999, *103*, 6484-6492.
- (147) Appenzeller, J.; Lin, Y.-M.; Knoch, J.; Avouris, P. Band-to-band tunneling in carbon nanotube field-effect transistors. *Phys. Rev. Lett.* 2004, *93*, 196805.
- (148) Keru, G.; Ndungu, P. G.; Nyamori, V. O. A review on carbon nanotube/polymer composites for organic solar cells. *Int. J. Energy Res.* 2014, *38*, 1635-1653.
- (149) Ombaka, L. M.; Ndungu, P. G.; Nyamori, V. O. Pyrrolic nitrogen-doped carbon nanotubes: Physicochemical properties, interactions with Pd and their role in the selective hydrogenation of nitrobenzophenone. *RSC Adv.* 2014, *5*, 109-122.
- (150) Ueda, T.; Katsuki, S.; Takahashi, K.; Narges, H.; Ikegami, T.; Mitsugi, F. Fabrication and characterization of carbon nanotube based high sensitive gas sensors operable at room temperature. *Diam. Relat. Mater.* 2008, *17*, 1586-1589.
- (151) Zhang, Y.; Bai, Y.; Yan, B. Functionalized carbon nanotubes for potential medicinal applications. *Drug Discov. Today* 2010, *15*, 428-435.
- (152) Zhao, Z.; Yang, Z.; Huc, Y.; Li, J.; Fan, X. Multiple functionalization of multi-walled carbon nanotubes with carboxyl and amino groups. *Appl. Surf. Sci.* 2013, *276*, 476-481.
- (153) Kosa, S. A.; Al-Zhrani, G.; Abdel Salam, M. Removal of heavy metals from aqueous solutions by multi-walled carbon nanotubes modified with 8-hydroxyquinoline. *Chem. Eng. J.* 2012, *181-182*, 159-168.
- (154) Wang, Y.; Iqbal, Z.; Malhotra, S. V. Functionalization of carbon nanotubes with amines and enzymes. *Chem. Phys. Lett.* 2005, *402*, 96-101.
- (155) Brunetti, F. G.; Herrero, M. A.; Munoz, J. D. M.; Diaz-Ortiz, A.; Alfonsi, J.; Meneghetti, M.; Prato, M.; Vázquez, E. Microwave-induced multiple

- functionalization of carbon nanotubes. *J. Amer. Chem. Soc.* 2008, *130*, 8094-8100.
- (156) Jing, Q.; Law, J. Y.; Tan, L. P.; Silberschmidt, V. V.; Li, L.; Dong, Z. Preparation, characterization and properties of polycaprolactone diol-functionalized multi-walled carbon nanotube/thermoplastic polyurethane composite. *Composites Part A* 2015, *70*, 8-15.
- (157) Hill, D. E.; Lin, Y.; Rao, A. M.; Allard, L. M.; Sun, Y.-P. Functionalization of carbon nanotubes with polystyrene. *Macromolecules* 2002, *35*, 9466-9471.
- (158) Bayazit, Ş. S.; İnci, İ. Adsorption of Pb(II) ions from aqueous solutions by carbon nanotubes oxidized different methods. *J. Ind. Eng. Chem.* 2013, *19*, 2064-2071.
- (159) Stafiej, A.; Pyrzynska, K. Adsorption of heavy metal ions with carbon nanotubes. *Sep. Purif. Technol.* 2007, *58*, 49-52.
- (160) Perez-Aguilar, N. V.; Muñoz-Sandoval, E.; Diaz-Flores, P. E.; Rangel-Mendez, J. R. Adsorption of cadmium and lead onto oxidized nitrogen-doped multiwall carbon nanotubes in aqueous solution: equilibrium and kinetics. *J. Nanopart. Res.* 2010, *12*, 467-480.
- (161) Yang, K.; Zhu, L.; Xing, B. Adsorption of polycyclic aromatic hydrocarbons by carbon nanomaterials. *Environ. Sci. Technol.* 2006, *40*, 1855-1861.
- (162) Pan, B.; Lin, D.; Mashayekhi, H.; Xing, B. Adsorption and hysteresis of bisphenol A and 17 α -ethinyl estradiol on carbon nanomaterials. *Environ. Sci. Technol.* 2008, *42*, 5480-5485.
- (163) Lu, C.; Chung, Y.-L.; Chang, K.-F. Adsorption of trihalomethane from water with carbon nanotubes. *Water Res.* 2005, *39*, 1183-1189.
- (164) Chen, G.-C.; Shan, X.-Q.; Wang, Y.-S.; Wen, B.; Pei, Z.-G.; Xie, Y.-N.; Liu, T.; Pignatello, J. J. Adsorption of 2,4,6-trichlorophenol by multi-walled carbon nanotubes as affected by Cu(II). *Water Res.* 2009, *43*, 2409-2418.
- (165) Long, R. Q.; Yang, R. T. Carbon nanotubes as superior sorbent for dioxin removal. *J. Am. Chem. Soc.* 2001, *123*, 2058-2059.
- (166) Yang, K.; Wu, W.; Jing, Q.; Zhu, L. Aqueous adsorption of aniline, phenol, and their substitutes by multi-walled carbon nanotubes. *Environ. Sci. Technol.* 2008, *42*, 7931-7936.
- (167) Zhang, L.; Lv, J.; Xu, T.; Yang, L.; Jiang, X.; Li, Q. High efficiency removal and recovery of an endocrine disrupting compound—bisphenol AF from wastewaters. *Sep. Purif. Technol.* 2013, *116*, 145-153.

- (168) Cho, H.-H.; Huang, H.; Schwab, K. Effects of solution chemistry on the adsorption of ibuprofen and triclosan onto carbon nanotubes. *Langmuir* 2011, 27, 12960.
- (169) Sugimoto, M. The past, present, and future of ferrites. *J. Am. Ceram. Soc.* 1999, 82, 269-280.
- (170) Blaney, L. Magnetite (Fe₃O₄): Properties, Synthesis, and Applications. <http://preserve.lehigh.edu/cas-lehighreview-vol-15/5> 2007, 15.
- (171) Zhang, Q.; Zhu, M.; Zhang, Q.; Li, Y.; Wang, H. Synthesis and characterization of carbon nanotubes decorated with manganese–zinc ferrite nanospheres. *Mater. Chem. Phys.* 2009, 116, 658-662.
- (172) Wang, L.; Li, J.; Wang, Y.; Zhao, L.; Jiang, Q. Adsorption capability for Congo red on nanocrystalline MFe₂O₄(M= Mn, Fe, Co, Ni) spinel ferrites. *Chem. Eng. J.* 2010, 181-182, 72-79.
- (173) Li, Y.-H.; Wang, S.; Wei, J.; Zhang, X.; Xu, C.; Luan, Z.; Wu, D.; Wei, B. Lead adsorption on carbon nanotubes. *Chem. Phys. Lett.* 2002, 357, 263-266.
- (174) Yang, W.; Ding, P.; Zhou, L.; Yu, J.; Chen, X.; Jiao, F. Preparation of diamine modified mesoporous silica on multi-walled carbon nanotubes for the adsorption of heavy metals in aqueous solution. *Appl. Surf. Sci.* 2013, 282, 38-45.
- (175) Wang, J.; Li, Z.; Li, S.; Qi, W.; Liu, P.; Liu, F.; Ye, Y.; Wu, L.; Wang, L.; Wu, W. Adsorption of Cu(II) on oxidized multi-walled carbon nanotubes in the presence of hydroxylated and carboxylated fullerenes. *PloS one* 2013, 8, e72475.
- (176) Pyrzynska, K.; Stafiej, A. Sorption behavior of Cu(II), Pb(II), and Zn(II) onto carbon nanotubes. *Solvent Extr. Ion Exch.* 2012, 30, 41-53.
- (177) Tofighy, M. A.; Mohammadi, T. Adsorption of divalent heavy metal ions from water using carbon nanotube sheets. *J. Hazard. Mater.* 2011, 185, 140-147.
- (178) Kuo, C.-Y. Comparison with as-grown and microwave modified carbon nanotubes to removal aqueous bisphenol A. *Desalination* 2009, 249, 976-982.
- (179) Kerkez, K.; Bayazit, S. S. Magnetite decorated multi-walled carbon nanotubes for removal of toxic dyes from aqueous solutions. *J. Nanopart. Res.* 2014, 16, 2431-2441.
- (180) Wang, B.; Gong, J.-l.; Yang, C.-P.; Zeng, G.-M.; Zhou, W.-J. Removal of rhodamine B from aqueous solution by magnetic multi-wall carbon nanotubes. *J. Environ. Sci. (China)* 2008, 11, 012.
- (181) Chiang, P.; Chang, E.; Wu, J. Comparison of chemical and thermal regeneration of aromatic compounds on exhausted activated carbon. *Water Sci. Technol.* 1997, 35, 279-285.

- (182) Stirk, W.; van Staden, J. Desorption of cadmium and the reuse of brown seaweed derived products as biosorbents. *Bot. Mar. J.* 2002, *45*, 9-16.
- (183) Jain, R.; Sikarwar, S. Adsorption and desorption studies of Congo red using low-cost adsorbent: activated de-oiled mustard. *Desalin. Water Treat.* 2013, *52*, 7400-7411.
- (184) Krishnamurti, G.; Huang, P.; Kozak, L. Desorption kinetics of cadmium from soils using M ammonium nitrate and M ammonium chloride. *Commun. Soil Sci. Plant Anal.* 1999, *30*, 2785-2800.
- (185) Chern, J.-M.; Wu, C.-Y. Desorption of dye from activated carbon beds: Effects of temperature, pH, and alcohol. *Water Res.* 2001, *35*, 4159-4165.
- (186) Kemp, W. Organic spectroscopy. *Edinburgh* 1991, *Palgrave Macmillian*.
- (187) de Hoffmann, E.; Stroobant, V. Mass spectrometry: Principles and applications, Brussels. *John, Wiley and Sons Ltd* 2007.
- (188) Herrero-Latorre, C.; Álvarez-Méndez, J.; Barciela-García, J.; García-Martín, S.; Peña-Crecente, R. M. Characterization of carbon nanotubes and analytical methods for their determination in environmental and biological samples: A review. *Anal. Chim. Acta* 2015, *853*, 77-94.
- (189) Dresselhaus, M. S.; Dresselhaus, G.; Saito, R.; Jorio, A. Raman spectroscopy of carbon nanotubes. *Phys. Rep.* 2005, *409*, 47-99.
- (190) Costa, S.; Borowial-Palen, E.; Kruszynska, M.; Bachmatiuk, A.; Kalenczuk, R. J. Characterization of carbon nanotubes by Raman spectroscopy. *Mater. Sci-Poland* 2008, *26*, 433-441.
- (191) Bokobza, L. Raman spectroscopic characterization of multiwall carbon nanotubes and of composites. *Express Polym. Lett.* 2012, *6*, 601-608.
- (192) Hozumi, K. Some recent approaches to micro- and ultramicro- elemental organic analysis *Anal. Sci.* 1993, *9*, 167-177.
- (193) Tyler, G.; Jobin Yvon, S. ICP-OES, ICP-MS and AAS Techniques Compared. *ICP Optical Emission Spectroscopy. Technical Note* 1995, *5*.
- (194) Plum, L. M.; Rink, L.; Haase, H. The essential toxin: Impact of zinc on human health. *Int. J. Environ. Res. Public Health* 2010, *7*, 1342-1365.
- (195) Silva, F.; de Alcântara, I.; Roldan, P.; Padilha, C.; de Araújo, A.; Valente, J.; Florentino, A.; Padilha, P. Determination of Hg in water by CVAAS using 2-aminothiazole modified silica. *Eclética Química* 2005, *30*, 47-55.
- (196) Boehm, H. P. Surface oxides on carbon and their analysis: A critical assessment. *Carbon* 2002, *40*, 145-149.

- (197) Boehm, H. Some aspects of the surface chemistry of carbon blacks and other carbons. *Carbon* 1994, 32, 759-769.
- (198) Kalijadis, A. M.; Vukčević, M. M.; Jovanović, Z. M.; Laušević, Z. V.; Laušević, M. D. Characterization of surface oxygen groups on different carbon materials by the Boehm method and temperature programmed desorption. *J. Serb. Chem. Soc.* 2011, 76, 757-768.
- (199) Goertzen, S. L.; Thériault, K. D.; Oickle, A. M.; Tarasuk, A. C.; Andreas, H. A. Standardization of the Boehm titration. Part I. CO₂ expulsion and endpoint determination. *Carbon* 2010, 48, 1252-1261.
- (200) Fidel, R. B.; Laird, D. A.; Thompson, M. L. Evaluation of modified boehm titration methods for use with biochars. *J. Environ. Qual.* 2013, 42, 1771-1778.
- (201) Khan, T. A.; Nazir, M.; Khan, E. A. Adsorptive removal of rhodamine B from textile wastewater using water chestnut (*Trapa natans L.*) peel: Adsorption dynamics and kinetic studies. *Toxicol. Environ. Chem.* 2013, 95, 919-931.
- (202) Cardenas-Peña, A. M.; Ibanez, J. G.; Vasquez-Medrano, R. Determination of the point of zero charge for electrocoagulation precipitates from an iron anode. *Int. J. Electrochem. Sci.* 2012, 7, 6142-6153.

Chapter 3

Perfluoroalkyl compounds: Occurrence, fate and their adsorption mechanism onto carbon nanotubes

Oluwaseun A. Oyetade, Vincent O. Nyamori, Bice S. Martincigh* and Sreekantha B. Jonnalagadda

School of Chemistry and Physics, University of KwaZulu-Natal, Westville Campus, Private Bag X54001, Durban 4000, South Africa

*Corresponding author: Tel: +27 31 2601394; Fax: +27 31 2603091; E-mail: martinci@ukzn.ac.za

Abstract

The presence of perfluoroalkyl acids (PFAAs) in aquatic environment is a cause of concern, due to increased toxicity associated with their intake by man. The release of these pollutants to receiving water bodies is primarily *via* the discharge of untreated wastewater and industrial effluents. These activities necessitates the remediation of wastewater containing these compounds before discharge. In this review, the occurrence and fate of PFAAs in water streams was revised, with an aim of providing in-depth information to the harmful effects caused by the exposure of these pollutants to both man and its environs. Adsorption, as a viable technique was studied for the removal of PFAAs from wastewater and its mechanisms towards their removal onto carbon nanotubes (CNTs) were explored. Further, various functionalization strategies were assessed to investigate the increased efficiency of CNTs to PFAA removal. The adsorption capacities of CNTs were then compared with that of other conventional adsorbents.

The sorption of PFAAs onto CNTs demonstrated good removal efficiencies and was found to attain equilibrium faster than conventional adsorbents. This was attributed to inherent properties of CNTs such as large surface area/porosity and the ease with which new functional groups are introduced to the walls of tubes. Adsorption mechanism of PFAA was primarily enhanced through electrostatic interactions; however, other processes such as hydrogen, hydrophobic and ion-exchange have also been reported. This review aims at providing information on the occurrence, fate and interactions involved for the removal of PFAA from aqueous solution by using CNTs.

Keywords: Perfluoroalkyl acids, carbon nanotubes, adsorption, wastewater, mechanism, functionalization

3.1. Introduction

The release of perfluorinated compounds (PFCs) into the environment is of major interest to the scientific community due to their toxicity, persistence and global distribution (Deng *et al.*, 2013; Valsecchi *et al.*, 2013). These compounds comprise a wide group of chemicals which are used as surface coatings for carpets, textiles and cooking utensils owing to their great thermal and chemical stability (De Voogt and Saez, 2006; Zhao *et al.*, 2014). They bio-accumulate in wildlife and humans and are persistent in the environment due to strong C-F forces between them (Domingo *et al.*, 2012; Kim *et al.*, 2013; Zhao *et al.*, 2014).

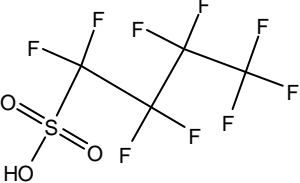
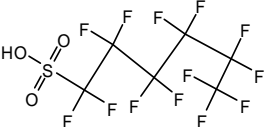
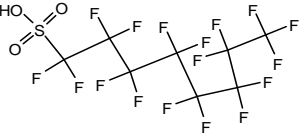
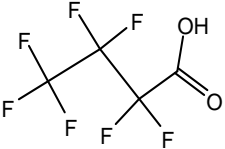
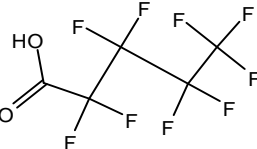
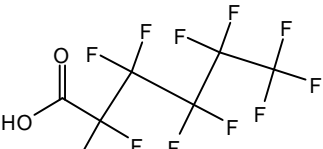
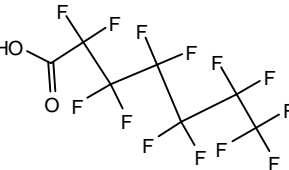
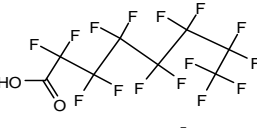
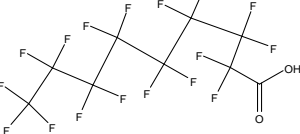
PFCs are a broad group of anthropogenic chemicals with each hydrogen atom on the linear alkyl chain replaced by a fluorine atom. The structure is made up of a hydrophobic perfluorinated tail of varying carbon lengths (C₄ to C₁₆) and a hydrophilic functional group head, thus, making them amphiphilic in nature (Du *et al.*, 2014). PFCs can be divided into two subgroups, namely: perfluorinated alkyl substances (PFAS) and perfluoroalkyl acids (PFAA). PFAS are neutral volatile fluorinated compounds, which bind to polymers through acrylate or urethane linkages and used in the production of textiles, papers, carpets and other impregnation agents (Domingo *et al.*, 2012). Examples of such compounds include fluorotelomer alcohols (FTOHs), perfluoroalkylsulfonamides (FASAs) and sulfonamidoethanols (FASEs). PFAAs are ionic compounds containing carboxylic or sulfonic functional groups in a linear perfluoroalkyl chain (Ahrens, 2011). They are persistent in the environment and bio-accumulate in tissues resulting in health complications in man and wildlife. The commonest examples of PFAAs are perfluorooctanoic acid (PFOA) and perfluorooctane sulfonic acid (PFOS). The inclusion of PFOS to Annex B of the Stockholm Convention on Persistent Organic Pollutants (POPs) in 2009, and the proposed elimination of PFOA by the United States of America Environmental Protection Agency (USEPA), has not limited its continued application in consumer products (Domingo *et al.*, 2012; Jogsten *et al.*, 2012). The use of PFOS and other related compounds, which may degrade into fluorinated compounds, is still on the increase especially in developing countries (Domingo *et al.*, 2012; Müller *et al.*, 2012). Table 3.1 lists some common examples of PFAAs, which are generally used in industries for consumer products. It is worthy of note that PFAS degrade into PFAAs through biotic and abiotic processes (Lau *et al.*, 2007; Ahrens, 2011), hence, the occurrence and fate of PFAAs in the environment becomes of utmost importance.

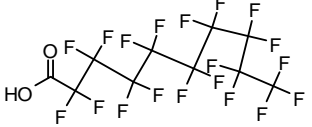
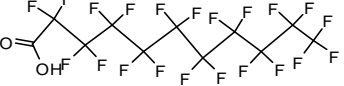
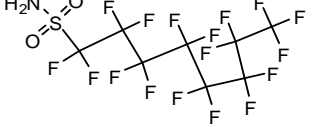
The removal of PFAAs from the environment through simple, effective and efficient technologies becomes imperative, since exposure to these contaminants introduces man and its environment to various necrotic diseases (Deng *et al.*, 2013; Du *et al.*, 2014; Yu *et al.*, 2014).

Adsorption has been considered an effective technology for their removal from wastewater, due to its simplicity, cost-effectiveness, high efficiency, high sorption and possibility of regeneration of adsorbents for the process of reuse (Ochoa-Herrera and Sierra-Alvarez, 2008; Deng *et al.*, 2013; Du *et al.*, 2014). The development of effective adsorbents with fast sorption ability for PFAA removal is therefore of utmost importance. This review therefore aims at providing an insight into the occurrence of PFAAs in aqueous solution, with a view to assessing the options for removal by using carbon nanotubes as adsorbents. The review also discusses mechanisms for PFAA removal; providing answers to the following questions:

- Are carbon nanotubes effective for PFAA removal from wastewater?
- In what ways do the properties of carbon nanotubes provide better sorption ability for the removal of PFAAs?
- Do carbon nanotubes exhibit improved adsorption capacities for PFAAs than other adsorbents after functionalization?
- What mechanisms determine the removal of PFAAs onto CNTs from aqueous solution?

Table 3.1: Common PFAAs used for industrial and commercial applications

Compound	Acronym	Structure	Molar mass/g mol ⁻¹	Chemical formula
Perfluorobutyl sulfonic acid	PFBS		299.21	C ₄ HF ₉ SO ₃
Perfluorohexane sulfonic acid	PFHxS		399.21	C ₆ HF ₁₃ SO ₃
Perfluorooctane sulfonic acid	PFOS		499.23	C ₈ HF ₁₇ SO ₃
Perfluorobutanoic acid	PFBA		214.04	C ₄ HF ₇ O ₂
Perfluoropentanoic acid	PFPeA		264.05	C ₅ HF ₉ O ₂
Perfluorohexanoic acid	PFHxA		314.05	C ₆ HF ₁₁ O ₂
Perfluoroheptanoic acid	PFHpA		364.06	C ₇ HF ₁₃ O ₂
Perfluorooctanoic acid	PFOA		414.07	C ₈ HF ₁₅ O ₂
Perfluorononanoic acid	PFNA		464.08	C ₉ HF ₁₇ O ₂

Perfluorodecanoic acid	PFDA		514.09	$C_{10}HF_{19}O_2$
Perfluoroundecanoic acid	PFUnA		564.09	$C_{11}HF_{21}O_2$
Perfluorooctane sulfonamide	PFOSA		499.14	$C_8H_2F_{17}SO_2N$

3.2. Occurrence of PFAAs in the environment

There are increasing numbers of reports providing evidence of PFAAs and related compounds in various environmental media such as in water (Hansen *et al.*, 2002), the marine environment (Giesy and Kurunthachalam, 2001; Naile *et al.*, 2013), soils (Davis *et al.*, 2007; Naile *et al.*, 2013), sediments (Higgins and Luthy, 2006; Naile *et al.*, 2013), landfills and indoor and outdoor air (Martin *et al.*, 2002; Naile *et al.*, 2013). Effects such as developmental, hormonal and neurological changes, dysfunction of the liver and kidney and cardiovascular damage (Jogsten *et al.*, 2012) are some of the suspected consequences of the intake of PFAAs by humans. In recent times, PFAAs such as PFOS, PFOA and PFHxS have been detected in maternal umbilical cords and serum at delivery sites in Korea. Lee *et al.*, (2013) reported concentrations levels between 0.67 and 3.44 ng ml⁻¹ in umbilical cord and between 1.35 and 10.77 ng ml⁻¹ in maternal serum. These results suggests that exposure of pregnant women to these contaminants may further introduce the foetus to some birth complications such as decrease in weight, birth length and ponderal index. Similar studies in Vietnam (Rylander *et al.*, 2009), Canada (Monroy *et al.*, 2008), South Africa (Hanssen *et al.*, 2010), Japan and Korea (Harada *et al.*, 2010) reported similar concentration levels in pregnant women. PFAAs have also been detected in waste recycling sites (Kim *et al.*, 2013), popcorn packaging (Martinez-Moral and Tena, 2012), blood (Lindh *et al.*, 2012), marine shellfish (Munschy *et al.*, 2013), house dusts (Xu *et al.*, 2013), industrial discharges (Dauchy *et al.*, 2012) and foodstuffs (Domingo *et al.*, 2012) to name but a few. In fact Domingo *et al.*, (2012) observed that food processing and packaging may be one of many routes through which PFAAs enter into the human body. It is, however, obvious that the phase-out of PFOS which started in 2001 has not abated the usage of PFAAs in various manufacturing processes, hence resulting in their detection in various environmental media. Unfortunately, water bodies are the major recipients of the discharge of untreated effluents from industries, and hence the need to review the occurrence of PFAAs in various aqueous solutions.

3.2.1. PFAA in aqueous solution

Wastewaters are frequently discharged into the aqueous environment with little or no treatment, therefore resulting in the accumulation of contaminants in the environment. Industrial or municipal wastewater treatment plants (WWTP) are considered the major point source by which PFAAs are introduced into the environment (Ahrens). Most PFAA congeners are water-soluble, which makes the aquatic environment a possible sink for their disposal. The relationship between discharges from a fluoropolymer manufacturing plant and the contamination of raw water resources was investigated by Dauchy *et al.*, (2012). Ten different PFAAs were detected with a total concentration in the range of 0.4 µg dm⁻³ to 41.4 µg dm⁻³ in water samples collected around the vicinity of a manufacturing plant. An estimate of 4.5 and 10 tonnes of PFNA and

PFHxA, respectively were reported to be discharged into water resources each year (Dauchy *et al.*, 2012). Predominant PFAAs were PFNA, PFOS, PFOA and PFHxA, which were found prevalent in groundwater. Although, reported concentrations were significantly low, increased discharge of polluted wastewaters will expose both man and animals to several health complications. The presence of PFAAs in aqueous solution (e.g. groundwater) was attributed to the possible degradation of fluorotelomers used for the production of fluorinated copolymers and the infiltration of products into the soil discharged from a nearby manufacturing industry (Dauchy *et al.*, 2012). Evidence of PFOS in concentrations less than 4 ng dm⁻³ was also found in tap waters obtained in Japan, close to a sewage treatment plant. Higher concentrations were reported in water supplied from a waterworks station closer to the treatment plant, wherein heavy contamination (303-404 ng dm⁻³) of PFOS was reported (Harada *et al.*, 2003). In the United States of America, Moody and Field, (1999) detected high concentrations of C₆-C₈ PFAAs in groundwater with total concentrations between 124 and 7090 ng dm⁻³ at a naval base and air-force station close to a fire-fighting station. The dominant contaminants were the C₈ precursors which accounted for about 83% to 93% of the total concentration. The presence of these contaminants in groundwater was attributed to the close proximity of the sample sites to a fire-fighting station even after 7 to 10 years of inactivity. An average of about 3 to 8 years is the half-life of most PFAAs in the environment (Lee *et al.*, 2013). A similar study conducted by Arias *et al.* (2015), associated the high concentrations in groundwater to the persistence of these contaminants in the environment for long periods of time, and thereby intruding into various water resources. The presence of PFCs in groundwater is therefore a major challenge, as humans and animals who consume these contaminants are exposed to several health effects.

The presence of PFAAs and their precursors have also been reported in larger water bodies such as rivers, oceans and lakes. Kim *et al.*, (2013) reported the presence of seventeen different PFAAs in various aqueous media, such as rivers, municipal wastewater discharge points, creeks and ponds near a disposal and recycling site in Vietnam. The most abundant contaminants were PFOS, PFOA, PFNA and PFUnA in concentration levels of 0.5 to 20 ng dm⁻³. Results obtained from this study suggest that the contamination of aqueous bodies was associated with recycling activities of waste electrical and electronic equipment (WEEE), including household appliances such as televisions and computers. This study confirms that PFAAs are used in electrical and electronic equipment, and discharge of spent-equipment could leach contaminants into aqueous media. Furthermore, concentrations of 88 and 77 ng dm⁻³ were found for PFHpA and PFHxA in collected leachates, indicating the possible leaching of contaminants from electrical and electronic equipment into other media. Zhou *et al.*, (2012) detected sixteen PFAAs from surface water obtained from the Baiyangdian Lake in North China. Concentrations of PFAAs were

obtained in the range of 0.1 to 56.8 ng dm⁻³ with PFOA, PFOS and PFBA identified as the predominant species. Reported concentrations were higher than those obtained from Lake Ontario, Lake Erie, Lake Chaplain and Lake Shinhwa (Rostkowski *et al.*, 2006; Sinclair *et al.*, 2006). The contamination of Lake Baiyangdian was associated with the in-flow from the Pinghe and Fuhe Rivers, which receive discharged effluents from paper, textile, leather, insecticide and pesticide manufacturing industries (Zhou *et al.*, 2012). Water samples collected from Lake Tangxun in China showed significant high values of PFAAs in the range of 3660 and 4770 ng dm⁻³ (Zhou *et al.*, 2012). PFBS and PFBA were the most predominant in these samples. Increasing concentrations of PFAAs were attributed to the discharge from a fluorochemical industry close to the sampling point. The occurrence of PFAAs was also reported by Zhang *et al.*, (2012) in concentrations of about 30.98 ng dm⁻³ in water samples collected from Dianchi Lake in China. PFOA was the dominant contaminant in a concentration range of 3.41 to 35.44 ng dm⁻³ in water samples. Also, PFOS and PFOA were the most abundant contaminants in water samples collected from the Yellow Sea by Naile *et al.*, (2013) in China. The presence of these pollutants in rivers, lakes and oceans presents harmful effects to aquatic life such as crabs, gastropods, bivalves and fish, due to the bioaccumulation of PFAAs in the tissue of animals. Eighteen PFCs containing carboxylates, sulfonates and sulfonamides were detected in wastewater and sludge samples collected from two different wastewater treatment plants in Greece (Arvaniti *et al.*, 2012). These results obtained by Arvaniti *et al.*, (2012) showed the presence of PFAAs in collected wastewater and sludge samples. Concentrations of 75.7 and 76.0 ng dm⁻³ were reported in raw and treated wastewater for PFTrDA and PFPeA, respectively, with higher values reported in effluents than in influents.

Results from these studies demonstrate that PFAAs are extensively intruding into aqueous bodies primarily through discharges from manufacturing industries. Efforts must be taken in order to explore technologies which will effectively treat PFAA-contaminated wastewater before its discharge into aquatic environment.

3.3. Adsorption

Treatment of organic contaminants in wastewater treatment facilities continues to be a major hurdle since conventional treatment strategies are not efficient for their removal. Technologies such as biological treatment (Zhang *et al.*, 2015), coagulation/flocculation (Altmann *et al.*, 2015), membrane separation (Ahmad *et al.*, 2012; Madsen *et al.*, 2015), photocatalysis (Pare *et al.*, 2011; Rueda-Márquez *et al.*, 2015), advanced oxidation (Jonnalagadda and Shezi, 2009; Dachipally and Jonnalagadda, 2011; Rueda-Márquez *et al.*, 2015), electrochemical destruction

(Jonnalagadda and Nadupalli, 2004; Brillas and Martínez-Huitle, 2015) and ion exchange (Wang *et al.*, 2015) have been applied for the removal of organic pollutants. In fact, new technologies are currently being developed to optimize the removal of organic pollutants from wastewater and industrial effluents (Ma *et al.*, 2012). Adsorption has been considered one of the most attractive processes for removal because adsorbents are generally easy to handle, can be regenerated by suitable desorption processes, are highly effective, are economical and can be used without large apparatus (Yu *et al.*, 2009; Deng *et al.*, 2013; Du *et al.*, 2014; Oyetade *et al.*, 2015). This process has been applied for PFC removal by using adsorbents such as activated carbon (Ochoa-Herrera and Sierra-Alvarez, 2008; Yu *et al.*, 2009; Yao *et al.*, 2014), clay (Zhao *et al.*, 2014), resin (Yu *et al.*, 2009), chars (Chen *et al.*, 2011), soil (Milinovic *et al.*, 2015), sediment (Ahrens *et al.*, 2011), rice husk (Deng *et al.*, 2012), alumina (Arvaniti *et al.*, 2015), zeolite (Ochoa-Herrera and Sierra-Alvarez, 2008) and activated sludge (Ochoa-Herrera and Sierra-Alvarez, 2008). The behaviour of some of these conventional adsorbents to PFAA removal is further explored.

3.3.1. Activated carbon

Activated carbon (AC) is one of the commonest adsorbents used for the treatment of contaminated water, because of the high surface area and porosity possessed by this material (Du *et al.*, 2014). It consists of graphitic units composed of layers of fused hexagons held together by weak van der Waals forces. It can be made from numerous varieties of raw materials such as coal, wood, cotton, peat or coconut shells, which are composed of high percentages of carbon. Adsorption of organic pollutants such as dyes (Namasivayam and Kavitha, 2002), polyaromatic hydrocarbons (PAHs) (Walters and Luthy, 1984), phenol (Khan *et al.*, 1997), dioxins (Maes *et al.*, 2005) and polychlorinated biphenyls (PCBs) (McDonough *et al.*, 2008) have been explored by various forms of ACs especially powdered activated carbon (PAC) and granulated activated carbons (GAC). The application of ACs for PFAA adsorption has exhibited significant improvement towards understanding the processes involved in removal. Yu *et al.*, (2009) reported an adsorption capacity of 519.19 and 1209 mg g⁻¹ for the removal of PFOS and PFOA, respectively, from aqueous solution by using PAC. Also, Punyapalakul *et al.*, (2013) reported good sorption uptakes of 434.8 and 714.3 mg g⁻¹ for the removal of PFOA and PFOS respectively by using PAC. Adsorption capacities of 22.1 and 22.7 mg g⁻¹ were also obtained for the sorption of PFOS and PFOA, respectively, by Yao *et al.*, (2014) by using GAC. Removal efficiencies between the ranges of 90% to 99% have been reported for the sorption of PFOS and PFOA by using PAC and GAC (Qiu *et al.*, 2005; Fujii *et al.*, 2007; Yao *et al.*, 2014). These results indicate that the sorption of PFOA and PFOS onto activated carbon has thus far proved effective; however, the regeneration of these adsorbents for the process of reutilization

remains a major problem. Adsorbent reuse is almost impossible since spent-AC is not easily regenerated by using simple conventional solvents; hence, disposal of secondary pollutants into the environment is inevitable. Also, reports have shown that a high equilibration time is required for the sorption of PFOS and PFOA onto ACs. An equilibration time of 168 h and 12 h was reported by Yu *et al.*, (2009) for the removal of PFOS/PFOA by using GAC and PAC respectively. This implies that the sorption of PFOA and PFOS onto ACs require long periods of time. These limitations significantly restrict its use for the removal of PFCs from aqueous solution; hence the need to develop more efficient adsorbents for removal continues to grow.

3.3.2. Sludge

The application of sludge for PFAA removal has also been explored due to its availability, low-cost, and its ability to remove hydrophobic contaminants from wastewater. Anaerobic granular sludge and anaerobic digested sewage sludge (ADS) (Madsen *et al.*, 2015) were used as adsorbents for the removal of PFOS from aqueous solution in a study by Ochoa-Herrera and Sierra-Alvarez, (2008). Their results showed that the type/characteristics of sludge used significantly influenced the extent of removal of PFOS, since higher removal efficiencies were obtained for granulated sludge than ADS. A similar observation was reported by Kwadijk *et al.*, (2013) involving the sorption of PFOS onto sediments. The sorption of PFOS onto sediments was greatly influenced by the organic content of the adsorbents. Milinovic *et al.*, (2015) reported an increase in the sorption of PFOS with increasing organic content in soils. Higher adsorption capacities were reported for PFOS sorption than for PFOA and PFBS, due to increased hydrophobic interactions between PFOS molecules and organic matter contained in soil. Hence, the adsorption of PFAAs onto adsorbents such as soils, sediments and sludge is greatly influenced by the organic matter content rather than the mineral surface of the adsorbents (Higgins and Luthy, 2006; Ochoa-Herrera and Sierra-Alvarez, 2008; Kwadijk *et al.*, 2013; Zareitalabad *et al.*, 2013; Milinovic *et al.*, 2015).

3.3.3. Resins

These are porous polymeric materials, designed to trap volatiles and semi-volatiles from air/liquid/solid matrices for the purpose of remediation. Anionic-exchange and non-ionic resins have been applied as sorbents for PFAA removal owing to properties such as good surface area and ease in regeneration of the adsorbents. Deng *et al.*, (2010) investigated the behaviour of anion-exchange resins for PFOS removal. Reports indicated that adsorption of PFOS was influenced by the polymer matrix, the porosity and functional groups on the adsorbent. The adsorption capacity was highest for polyacrylic resins, followed by porous and gel-type polystyrene resins for the removal of PFOS. This behaviour was explained by Yu *et al.*, (2009)

wherein inferences were made that PFC molecules could not easily diffuse into the pores of gel-type resins, hence, explaining the trend in adsorption. The sorption rate was also largely influenced by this factor as polyacrylic resins attained equilibrium faster (48 h) than the macroporous or gel-type ones (168 h) (Deng *et al.*, 2010; Yao *et al.*, 2014). Similarly, anion-exchange resins were reported to have better sorption uptake to PFOA than non-ionic resins in a study by Chularueangakorn *et al.*, (2013) and Du *et al.*, (2015). Amine-functionalized resins have also been shown to adsorb better than un-functionalized resins, owing to increased functional groups contained in the adsorbents (Du *et al.*, 2015). Adsorption of ionic PFCs onto resins is therefore largely influenced by the porosity, functional groups and polymer matrix of the adsorbent.

3.3.4. Zeolite

These are porous aluminosilicate minerals joined together by the sharing of oxygen atoms. Zeolites are explored as alternative adsorbents for wastewater purification of organic and inorganic pollutants due to their abundance, cost, high surface area and high-cation exchange properties (Wang and Peng, 2010). Their chemistries can be modified such that they contain functional groups which permit the removal of organic compounds such as PFAAs. Ochoa-Herrera and Sierra-Alvarez, (2008) reported that the extent of PFOS adsorption onto zeolites was affected by the increase in the aluminium content of the adsorbents. Sorption of PFOS was significantly enhanced with an increase in siliceous materials of the adsorbents; hence, adsorption was reported to be favoured through hydrophobic interactions, since sorption was highest for more hydrophobic zeolites. Punyapalakul *et al.*, (2013) reported a higher sorption uptake for the removal of PFOS and PFOA by using PAC rather than zeolites. This trend was attributed to the higher surface area exhibited by PAC and poor accessibility of the adsorbates to the internal surface area of zeolites.

Limitations such as the regeneration of adsorbents, slow sorption velocity and difficulty in modifying the surfaces of adsorbents, amongst many others, are some of the major drawbacks experienced with conventional sorbents (Deng *et al.*, 2013). To overcome these problems, efforts have been tailored towards the removal of PFAAs *via* nanostructured nanomaterials. Adsorption depends on the porosity, surface area and the ease with which modification can be achieved to incorporate functional groups which might aid removal. Carbon-based nanomaterials such as carbon nanotubes (CNTs) possess moderately high surface areas/porosity and are currently generating interest for organic pollutant removal such as PFAAs. Their properties, structure, modification strategies and behaviour to PFAA removal is further investigated to understand the sorption mechanisms involved for removal.

3.4. Carbon nanotubes

Much interest has been developed in the synthesis and application of CNTs since their discovery (Oyetade *et al.*, 2015). CNTs are tubular-shaped macromolecules with diameters ranging between 1 and 100 nm and can be grown up to 20 cm in length (Balasubramanian and Burghard, 2005). They are allotropes of carbon consisting of one or more layers of graphene arranged in a tubular form (Fig 1) (Balasubramanian and Burghard, 2005; Ombaka *et al.*, 2014; Herrero-Latorre *et al.*, 2015). They possess extraordinary abilities such as great electrical, structural and mechanical properties, which makes them useful for many applications (Kanoun *et al.*, 2014). CNTs may be classified as single-walled or multiwalled depending on the number of concentric graphene sheets contained in the tube. Single-walled carbon nanotubes (SWCNTs), double-walled carbon nanotubes (DWCNTs) and multiwalled carbon nanotube (MWCNT) depending on the number of graphene sheets contained in them (Herrero-Latorre *et al.*, 2015). SWCNTs possess diameters ranging between 0.4 and 3 nm, while MWCNTs have diameters reaching 100 nm (Balasubramanian and Burghard, 2005; Ombaka *et al.*, 2014). The demand for these materials is growing due to their increasing usage in many fields such as nanotechnology (Cambré *et al.*, 2015), electronics (Kanoun *et al.*, 2014; Keru *et al.*, 2014), optics (Cambré *et al.*, 2015), medicine (McCarthy *et al.*, 1999) and environmental sciences (Hamza *et al.*, 2013; Oyetade *et al.*, 2015). CNTs can be synthesized through chemical vapour deposition (CVD) (Bamoharram *et al.*, 2011; Jenkins *et al.*, 2014), laser ablation (Yuge *et al.*, 2014) and electric-arc discharge (Arora and Sharma, 2014) methods. Of these methods, CVD is largely employed due to the ease in scale-up and diameter reproducibility.

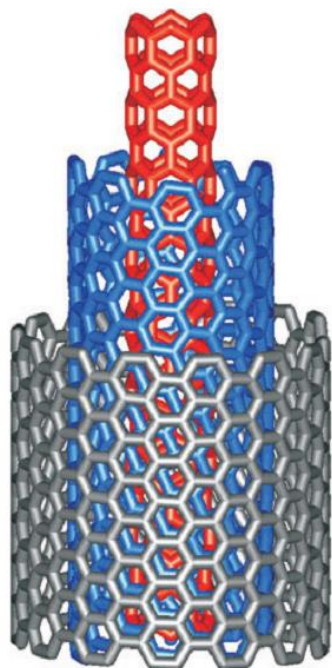


Fig. 3.1: Structure of carbon nanotubes rolled into a cylindrical shape (Balasubramanian and Burghard, 2005).

3.4.1. Functionalization of carbon nanotubes

Due to strong intrinsic van der Waals attractive forces between CNTs, they have high hydrophobicity and inert surfaces, which limits their chemical reactivity and dispersion in aqueous or organic solvents. Various strategies are employed to introduce substituents such as carboxyl and hydroxyl groups to allow further chemical modification and improve dispersability in aqueous and organic media (Zhang *et al.*, 2009), in order to increase their application for other purposes. Functionalization of CNTs is usually employed through covalent and non-covalent strategies to attach functional groups which aid interactions with other molecules. Through these processes, CNT agglomeration can be reduced, such that dispersability in both organic and aqueous solution is enhanced. Also, to reduce residual metal nanoparticles and amorphous carbon in pristine CNTs, purification processes involving sonication of CNTs in acidic media are usually employed through dissolution (Datsyuk *et al.*).

3.4.2. Covalent functionalization of CNTs

Incorporation of hydrophilic substituents, such as carboxyl, carboxylic and hydroxyl groups, onto the exterior sidewalls of tubes has been carried out by using various chemical processes. Covalent functionalization of MWCNTs was carried out by Wepasnick *et al.*, (2011) by using

various chemical agents such as HNO_3 , KMnO_4 , $\text{HNO}_3/\text{H}_2\text{SO}_4$, H_2O_2 , O_3 and $(\text{NH}_4)_2\text{S}_2\text{O}_8$ to study the surface chemistry of MWCNTs after functionalization by means of different characterization techniques. In their report, they observed that the distribution of oxygen-containing species were insensitive to the reaction conditions, but changed with oxidant used. Aggressive oxidants (HNO_3 and KMnO_4) produced higher carboxyl groups than oxidants such as O_3 , H_2O_2 and $(\text{NH}_4)_2\text{S}_2\text{O}_8$, which had higher fractions of hydroxyl and carbonyl groups. Fig 2 showed micrographs obtained from the study which revealed the presence of amorphous carbon (indicated by arrows) on the pristine MWCNTs (Fig 3.2a), while functionalized MWCNTs revealed a decrease in amorphous carbon with a high level of defects on the side walls of tubes (indicated with circles) in Figs 2 (b-d). Dispersion in aqueous solution was also enhanced as a result of the functionalization of MWCNTs.

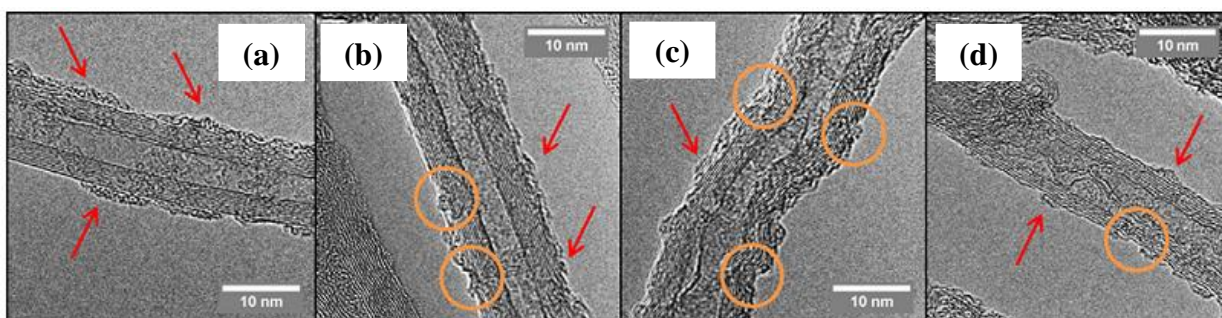


Fig 3.2: TEM images of (a) pristine MWCNT, (b) H_2O_2 treated MWCNTs, (c) $\text{H}_2\text{SO}_4/\text{HNO}_3$ treated MWCNTs and (d) KMnO_4 treated MWCNT (Amorphous carbon is indicated with arrows and sidewall defects highlighted with circles) (Wepasnick *et al.*, 2011).

The structural integrity of MWCNTs was investigated by Datsyuk *et al.*, (2008) by using acidic (nitric acid, piranha solution) and basic (ammonium hydroxide/hydrogen peroxide mixture) chemical agents to investigate the influence of oxidation on the surface of tubes. MWCNTs were initially purified with hydrochloric acid to reduce the residual metal nanoparticles, followed by oxidative treatment. Reported results indicated that acidic treatment of MWCNTs resulted in major alteration, introducing defects onto the surfaces of tubes. Aggressive oxidations lead to the shortening of long strands of tubes, with a large population of disordered sites and introducing new functional groups such as carboxyl and hydroxyl groups to the walls of the tubes. Basic oxidation treatments, however, produced no visible change in the morphology of CNTs accompanied with the complete removal of amorphous carbon from the surface of tubes. Dispersion tests revealed better dispersability in aqueous solution after various acidic treatments. This was attributed to the presence of large amounts of oxygen-containing functional groups at the defective sites which resulted in better dispersion of CNTs in aqueous

solution (Zhang *et al.*, 2009). The chemical agent used for oxidation significantly influenced the amount of oxygen-containing functional groups on CNTs (Datsyuk *et al.*, 2008). These results were consistent with the study by Santangelo *et al.*, (2012), wherein oxygen-containing functional groups (carboxyl, carbonyl, lactonic, quinone and phenolic) were attached to the defective sites of the walls, hence, reducing the hydrophobic state of pristine-MWCNTs and also increasing their wettability in solvents.

3.4.3. Non-covalent functionalization of CNTs

Non-covalent functionalization involves the immobilization of macromolecules to the hydrophobic ends of CNTs *via* either van der Waals forces, π - π bonds, or electrostatic interactions (Zhao *et al.*, 2012). This method of functionalization is usually employed for obtaining polymer-CNT matrices (Zhao *et al.*, 2012; Keru *et al.*, 2014) and the endohedral functionalization of CNTs (Ombaka *et al.*). Although, the structure of CNTs is not altered in this process, alignment of CNTs within the matrix becomes a problem such that conductivity is hindered and also it influences the activity of CNT-conducting polymers (Zhao *et al.*, 2012). These limitations were controlled by Shang *et al.*, (2011) wherein they synthesized nanocomposites from MWCNTs and polyurethane with the aid of an ionic liquid. Properties such as the mechanical strength and conductivity of MWCNTs were retained in the nanocomposite. Limitations associated with the alignment and dispersion of CNTs in polymer matrix were also averted by using this process. Carrion *et al.*, (2010) also effectively synthesized well-dispersed SWCNT-polymers by using an ionic liquid (1-octyl, 3-methylimidazolium tetrafluoroborate) and obtained polymers with increased thermal stability, thereby increasing the tribological performance of SWCNTs. Yue *et al.*, (2007) synthesized SWCNT/poly (methyl-methacrylate) (PMMA) nanocomposites by means of *in-situ* polymerization in supercritical CO₂. Composite growth and matrix dispersion were facilitated by using supercritical CO₂, which further enhanced the impregnation of PMMA on SWCNTs.

3.5. PFC adsorption onto carbon nanotubes

The increasing application of CNTs as adsorbents for organic pollutant removal is continuously evolving, owing to the specific properties such as large surface areas and pore volumes, which are characteristic of CNTs. Functionalization of CNTs to introduce various functional groups, which will serve as adsorption sites, is easy and can be tailored to have properties for PFAA removal. These make them extremely important for use as adsorbents. Although, not much research has been performed in this area, a review of previous studies onto CNTs is presented to understand the mechanism and interactions involved in the removal process.

3.5.1. Effect of solution pH

The removal of PFAAs onto different adsorbents is greatly influenced by the pH of the solution. The surface charges on the adsorbent, as well as the speciation of the adsorbate molecules, may change depending on the pH of the solution (Oyetade *et al.*, 2015). The removal efficiency of PFOS and PFOA onto CNTs usually decreases with increasing pH; hence, adsorption of PFAA is favoured at acidic pH conditions (Yu *et al.*, 2009; Deng *et al.*, 2012; Kwadijk *et al.*, 2013; Li *et al.*, 2015). This is possible since PFAA molecules exist as anions in water (Deng *et al.*, 2012) and their pK_a values are lower than 1, and not greater than 3.5 (Higgins and Luthy, 2006; Arvaniti *et al.*, 2012). Also, removal onto CNTs at basic conditions is generally low, due to electrostatic repulsion between the negatively charged adsorbent and anionic PFAA species (Deng *et al.*, 2012; Li *et al.*, 2013; Li *et al.*, 2015). However, at acidic pH conditions, the adsorbent surface is positively charged, thus, enhancing ionic interaction between PFAA anions and adsorbents (Chen *et al.*, 2011; Deng *et al.*, 2012). A similar trend is reported for the sorption of PFOS and PFOA, with the highest removal efficiency taking place within a pH range of 2 to 5 (Li *et al.*, 2011; Zhou *et al.*, 2012; Kwadijk *et al.*, 2013; Yao *et al.*, 2014; Li *et al.*, 2015). The sorption of PFAAs onto adsorbents has also been reported to be enhanced in the presence of divalent cations such as Ca^{2+} and Mg^{2+} (Kwadijk *et al.*, 2013; Du *et al.*, 2014). Du *et al.* (2014) attributed this effect to the formation of more basic sites on the surface of adsorbents due to the presence of these cations, therefore enhancing removal through the formation of a divalent cation bridging effect (Du *et al.*, 2014). Similarly, decreasing PFOS removal was obtained for increasing Cl^- concentration, due to increased competition for positive sites on the adsorbent between PFOS anions and Cl^- in solution as demonstrated by Li *et al.*, (2015). Hence, solution pH plays a significant role in the removal of PFAAs from aqueous solution.

3.5.2. Adsorption kinetics

The adsorption kinetics provide information on the dynamics and rate-determining step of the process. Equilibrium data obtained for removal is often fitted into adsorption models such as the pseudo-first order (Ho, 2003; Ho, 2004; Lin and Wang, 2009), pseudo-second order (Ho and McKay, 1999; Ho, 2003; Lin and Wang, 2009), Elovich (Chien and Clayton, 1980) and intraparticle diffusion models (Demirbas *et al.*, 2004). Table 3.2 gives the equations of the commonest kinetics models used for adsorption. In general, sorption of PFAAs onto adsorbents increases with an increase in contact time until a state where adsorption is limited is reached. At this stage, adsorption is said to reach a state of equilibrium.

Table 3.2: Kinetics models usually investigated for adsorption studies

Models	Equations*	Parameters	References
Pseudo-first order	$q_t = q_{eq}(1 - e^{-k_1 t})$	q_{eq}, k_1	(Ho, 2003; Ho, 2004; Lin and Wang, 2009)
Pseudo-second order	$q_t = \frac{k_2 q_{eq}^2 t}{1 + k_2 q_{eq} t}$	k_2, q_{eq}	(Ho and McKay, 1999; Ho, 2003; Lin and Wang, 2009)
Elovich	$q_t = \frac{1}{\beta} \ln(\alpha\beta) + \frac{1}{\beta} \ln t$	α, β	(Chien and Clayton, 1980)
Intraparticle diffusion	$q_t = k_{id} \sqrt{t} + l$	k_{id}, l	(Demirbas <i>et al.</i> , 2004)

* q_t , quantity of adsorbate adsorbed at time t (mg g^{-1}); q_{eq} , quantity of adsorbate adsorbed at equilibrium (mg g^{-1}); α , adsorption rate constant ($\text{mg g}^{-1} \text{min}^{-1}$); β , desorption rate constant (g mg^{-1}); k_1 , pseudo-first order rate constant (min^{-1}); k_2 , pseudo-second order rate constant ($\text{g mg}^{-1} \text{min}^{-1}$); k_{id} , intraparticle diffusion rate constant ($\text{mg g}^{-1} \text{min}^{0.5}$), l , is a constant related to the boundary layer thickness (mg g^{-1}).

The sorption kinetics of six PFAAs (PFOA, PFHxA, PFHxS, PFBS, PFBA and PFOS) on SWCNTs and MWCNTs were studied by Deng *et al.*, (2012). Sorption equilibrium was achieved on all adsorbents within 15 h, with faster sorption achieved for PFOS, PFOA and PFHxS than other contaminants. PFOS and PFOA achieved about 95% removal after 5 h, while 7.5% of PFBA was removed after 48 h. Chen *et al.*, (2011) reported that sorption equilibrium on CNTs for the removal of PFOS was achieved after 2 h. Similarly, equilibrium was achieved after 2 h for the adsorption of PFOS and PFOA on CNTs in a study conducted by Yao *et al.*, (2014). A faster equilibrium was achieved for the sorption of PFOA and PFOS on CNTs than on granulated activated carbon (GAC) wherein equilibrium was achieved after 24 h (Yao *et al.*, 2014; Deng *et al.*, 2015). In fact Yao *et al.*, (2014) reported that equilibrium was achieved on GAC after 168 h. These results were consistent with data reported by Dai *et al.*, (2013) for PFOS removal on carbon nanotube-filled electrospun membranes, wherein equilibrium was also achieved after 5 h. Also, sorption was fastest on modified CNTs than it was on pure membranes. This indicates that the sorption properties of pure membranes were better enhanced to favour removal of PFOS in aqueous solution (Dai *et al.*, 2013). Li *et al.*, (2011) also reported faster sorption of PFOS onto MWCNTs than other adsorbents such as activated carbon, resin, zeolite and sludge. This suggests that CNTs provides faster sorption for the removal of PFOS and PFOA than conventional adsorbents such as activated carbon. This could be because CNTs possess good pore volume/sizes and dimensions/surface area when compared to most conventional adsorbents. In a study by Li *et al.*, (2013), the sorption efficiency of PFOS on SWCNTs was predicted by using molecular dynamics simulation (MD). The results indicate that the outer diameters and inner surfaces had considerable influence on the extent of adsorption of PFOS onto nanotubes (Li *et al.*, 2013). Adsorption on mesoporous materials is assumed to be faster than macroporous porous adsorbents, hence the porosity and surface area

of adsorbents play an important role in determining the extent of sorption on adsorbents (Punyapalukul *et al.*, 2013).

Chen *et al.*, (2011) demonstrated that the equilibrium data was better described by the pseudo-second order model, indicating that sorption was controlled by chemical reaction involving an exchange or sharing of electrons between active sites of adsorbents and the adsorbates (Oyetade *et al.*, 2015). This further indicates that adsorption is dependent on the number of active sites present on the adsorbents. Sorption on porous materials is usually controlled by external diffusion, boundary layer diffusion and the intraparticle diffusion. The rate-controlling step was determined by use of the intraparticle diffusion model, but intraparticle diffusion was not the only sorption-controlling step (Du *et al.*, 2015). Similar results were reported for carbon nanotube-filled electrospun membrane (Dai *et al.*, 2013), MWCNTs (Li *et al.*, 2011; Yao *et al.*, 2014), activated carbon (Yu *et al.*, 2009), clay (Zhao *et al.*, 2014), resin (Yu *et al.*, 2009) and porous silica (Punyapalukul *et al.*, 2013).

3.3.3. Adsorption Isotherms

An estimate of the adsorption capacity of adsorbents for pollutant removal from aqueous solution is given by isotherms. The equilibrium data obtained for adsorption is usually tested against various sorption models involving two-parameter and three-parameter models. Some of the models used for adsorption are the Langmuir (Langmuir, 1918), Freundlich (Freundlich, 1906), Temkin (Temkin and Pyzhev, 1940), Dubinin-Radushkevich (Dubinin and Radushkevich, 1947), Redlich-Peterson (Redlich and Peterson, 1959), Toth (Toth, 1971), Sips (Sips, 1948) and Khan (Khan *et al.*, 1996) isotherms. Of these ones, the frequently used models are the Langmuir and Freundlich isotherms. The Langmuir isotherm assumes that adsorption occurs on a monolayer surface; and all adsorption sites are equivalent with no interaction between adjacent adsorbate molecules (Langmuir, 1918). The maximum monolayer adsorption capacity (q_m) takes place when the adsorption sites are occupied (i.e. when the sites are saturated). The heat of adsorption is assumed to be the same for all sites. The Freundlich isotherm is suitable for heterogeneous surfaces and assumes that adsorption occurs on a multilayer surface (Freundlich, 1906). The Langmuir and Freundlich equations for both models are given in equations 3.1 and 3.2, respectively.

$$q_{eq} = \frac{q_m b C_{eq}}{1 + b C_{eq}} \quad (3.1)$$

$$q_{eq} = K_F C_{eq}^{1/n} \quad (3.2)$$

where q_{eq} is the adsorption capacity (mg g^{-1}); C_{eq} is the equilibrium concentration of adsorbate in solution (mg dm^{-3}); q_m is the maximum monolayer capacity (mg g^{-1}); b is the Langmuir isotherm constant ($\text{dm}^3 \text{mg}^{-1}$); K_F is the Freundlich isotherm constant ($\text{mg g}^{-1}(\text{dm}^3 \text{mg}^{-1})^n$); and n is the adsorption intensity.

Chen *et al.*, (2011) reported that the sorption processes of PFOS on various MWCNTs were better described by the Langmuir and Freundlich isotherms. Sorption of PFOS on SWCNTs was better described by the Freundlich model. It was reported that the sorption of PFOS onto CNTs was 3 to 8 times higher than on other adsorbents such as chars and ash. Deng *et al.*, (2012) also reported the Freundlich model as the best isotherm suited for the description of data obtained for PFOA sorption on various CNTs. The sorption of PFOS onto MWCNTs showed similar trends as reported by Dai *et al.*, (2013), Kwadijk *et al.*, (2013) and Li *et al.*, (2011). This indicates that adsorption of PFCs occurs *via* multilayer adsorption of the adsorbates onto the surfaces of CNTs. The adsorption capacity of CNTs was also noticed to increase with increasing surface area (Chen *et al.*, 2011; Deng *et al.*, 2012; Dai *et al.*, 2013). This further elucidates that surface area and pore volumes play a major role in adsorption. Table 3.3 summarizes the adsorption capacity of commonly used adsorbents for the removal of PFOS and PFOA from aqueous solution. The adsorption capacity (q_m) of CNTs was observed to compare favourably with other adsorbents, indicating the possible use of CNTs for PFC removal. It is noticeable that higher adsorption capacities (q_m) were reported for the removal of PFOS than PFOA on most adsorbents. Perfluorinated sulfonates (PFSA) are more hydrophobic, possessing lower pK_a values, than the corresponding perfluorinated carboxylates (PFCAs) (Higgins and Luthy, 2006; Arvaniti *et al.*, 2012) containing the same number of carbon atoms. Reports have indicated that this property induces better removal of PFSA onto oxide surfaces of adsorbents, thereby resulting in higher adsorption capacities (q_m) (Du *et al.*, 2014).

Table 3.3: Comparison of Langmuir monolayer adsorption capacities (q_m) for the removal of PFOS and PFOA using various adsorbents

Adsorbents	Conditions	$q_m/\text{mg g}^{-1}$		References
		PFOS	PFOA	
Powdered activated carbon	pH 5.0, 250 mg dm ⁻³ , 12 h, 298 K, 100 mg	520.13	277.43	(Yu <i>et al.</i> , 2009)
	100 mg dm ⁻³ , pH 7, 3 h, 298 K, 67 mg	714.3	434.8	(Punyapalakul <i>et al.</i> , 2013)
Granulated activated carbon	pH 7.2, 283 K, 150 mg dm ⁻³ , 48 h	196.2-236.4	112.1	(Ochoa-Herrera and Sierra-Alvarez, 2008)
	50 mg dm ⁻³ , pH 5.0, 24 h, 20 mg, 294 K	22.1	22.7	(Yao <i>et al.</i> , 2014)
	pH 5.0, 250 mg dm ⁻³ , 168 h, 298 K, 100 mg	185.04	161.49	(Yu <i>et al.</i> , 2009)
Zeolite	pH 7.2, 283 K, 150 mg dm ⁻³ , 48 h	12-114.7	-	(Ochoa-Herrera and Sierra-Alvarez, 2008)
	100 mg dm ⁻³ , pH 7, 3 h, 298 K, 67 mg	50.9-75.7	15.5-17.9	(Punyapalakul <i>et al.</i> , 2013)
Maize-straw chars	pH 7.0, 500 mg dm ⁻³ , 298 K, 384 h	164	-	(Chen <i>et al.</i> , 2011)
Willow-derived chars	pH 7.0, 500 mg dm ⁻³ , 298 K, 384 h	91.6	-	(Chen <i>et al.</i> , 2011)
Maize-straw origin ash	pH 7.0, 500 mg dm ⁻³ , 298 K, 48 h	811	-	(Chen <i>et al.</i> , 2011)
SWCNT	pH 7.0, 100 mg dm ⁻³ , 298 K, 2 h	712	-	(Chen <i>et al.</i> , 2011)
MWCNT	pH 5.0, 50 mg dm ⁻³ , 2 h, 20 mg, 294 K	21.3	12.4	(Yao <i>et al.</i> , 2014)
MWCNT	pH 7.0, 500 mg dm ⁻³ , 298 K, 2 h	656	-	(Chen <i>et al.</i> , 2011)
MWCNT	pH 7.0, 500 mg dm ⁻³ , 298 K, 2 h	514	-	(Chen <i>et al.</i> , 2011)
MWCNT	pH 7.0, 10 mg, 24 h, 298 K, 50 mg dm ⁻³	-	95.24	(Deng <i>et al.</i> , 2012)

3.6. Adsorption mechanisms of PFAAs

The mechanism for the sorption of PFAA onto CNTs may not be straightforward due to the properties of the compounds. They contain a hydrophilic functional head, and both hydrophobic and oleophobic C-F chains, which makes their mechanism complicated. Several mechanisms, such as electrostatic, hydrophobic, π - π and hydrogen bonding interactions, have been proposed for PFAA removal from aqueous solution. This is due to variations in the surface properties of the adsorbents which may be used for adsorption. Reports have shown that PFAAs exist as anions in an aquatic environment, possessing very low pK_a values (Higgins and Luthy, 2006; Arvaniti *et al.*, 2012; Du *et al.*, 2014). This property may induce electrostatic interactions between the PFC anions and positively charged surfaces of the adsorbents. This is one of the commonest reported interactions for the removal of PFAAs onto various adsorbents (Zhang *et al.*, 2009; Gao and Chorover, 2012; Zareitalabad *et al.*, 2013; Yao *et al.*, 2014; Du *et al.*, 2015; Li *et al.*, 2015). Oxidized CNTs usually possess a point of zero charge (pH_{PZC}) between 3 and 5 (Chen *et al.*, 2011; Hamza *et al.*, 2013; Oyetade *et al.*, 2015). This implies that the surface of CNTs is negatively charged at a solution pH greater than pH_{PZC} . An electrostatic repulsion between anionic PFCs and negatively charged surfaces is induced at this stage (Li *et al.*, 2015). However, the surfaces of CNTs are positively charged at lower pH values, enhancing electrostatic attraction between PFC anions and adsorbents (Du *et al.*, 2015; Li *et al.*, 2015).

Furthermore, the kinetics data is mostly described by the pseudo-second order model (Yu *et al.*, 2009; Chen *et al.*, 2011; Deng *et al.*, 2015; Du *et al.*, 2015), indicating that the mechanism for the process is determined by the bimolecular interaction between the adsorbent and adsorbate, through the formation of a chemical bond by the sharing or exchange of electrons (Hamza *et al.*, 2013; Oyetade *et al.*, 2015). This therefore elucidates that the mechanism for PFAA sorption may be explained *via* electrostatic interaction.

However, some researchers have proposed that hydrogen bonding may be responsible for the adsorption of PFAA anions onto oxygen-containing adsorbents. Xu *et al.*, (2013) associated PFOS removal to hydrogen interactions between the sulfo-group on PFOS and –OH groups on adsorbents. They suggested that interactions were enhanced between the oxygen atoms contained in PFAA anions, which act as acceptors to initiate hydrogen bonding, and functional groups such as –COOH and –OH contained in the adsorbents. Hydrogen bonding could also occur through interactions between fluorine atoms on PFAAs and –OH groups on the adsorbents (Deng *et al.*, 2012). This theory was further supported by Gao and Chorover, (2012) wherein PFOA and PFOS were also sorbed *via* hydrogen bonding onto oxygen-containing adsorbents. However, in a study by Zhang *et al.*, (2009) they reported that an increase in the number of oxygen groups on MWCNTs may reduce the

sorption of organic compounds. Pristine MWCNTs were observed to have better sorption of organic compounds than oxidized MWCNTs due to the formation of water clusters on the surface of the tubes. This was supported by Deng *et al.*, (2012), wherein they noted that hydrogen bonding may be impossible with pristine CNTs, since they do not contain hydrogen atoms. In a similar study by Li *et al.*, (2011), PFOA, PFOS and PFOSA were adsorbed by using MWCNTs containing different oxygen contents. They reported a higher adsorption capacity for MWCNTs with lower oxygen contents, inferring that hydrogen bonding interactions between –OH containing functional groups on the adsorbents and PFAA anions do not play a major role in adsorption. Hence, the mechanisms involved for PFAA removal onto oxygen-containing adsorbents is not well understood, and more studies need to be carried out for a better understanding of the interactions involved.

Due to the absence of π - π electrons in PFAAs, interactions through π - π bonding are minimal (Deng *et al.*, 2012; Du *et al.*, 2014). However, studies have also shown that PFAA anions can adsorb on negatively charged adsorbents *via* hydrophobic interactions. Studies have shown that CNTs possess strong affinity for removal of organic compounds due to strong π - π electrons in their structure (Li *et al.*, 2011). PFAAs possess hydrophobic properties due to inherent strong C-F bonds; which facilitate interactions between hydrophobic surfaces of adsorbents and its molecule (Punyapalukul *et al.*, 2013). This phenomenon was supported by Deng *et al.*, (2012), wherein PFAA anions were adsorbed onto the negatively charged surfaces of CNTs, hence supporting hydrophobic interactions. They reported a decreased adsorption uptake of PFAAs with a decrease in the chain length of molecules (i.e. highest adsorption was obtained for adsorbates with higher C-F chain lengths). This trend was also supported by Chen *et al.*, (2011), Du *et al.*, (2015), Li *et al.*, (2011), Milinovic *et al.*, (2015) and Yu *et al.*, (2009). Also, Deng *et al.*, (2012) reported that PFAAs containing sulfonic groups were better adsorbed than the corresponding carboxylates with the same chain length due to higher hydrophobicity experienced with sulfonic-containing PFAAs. This hypothesis was justified by the studies of Deng *et al.*, (2015), Li *et al.*, (2011), Du *et al.*, (2015), Ahrens *et al.*, (2011), and Milinovic *et al.*, (2015), wherein reported adsorption capacities of PFOS were higher than PFOA.

The formation of hemi-micelles and micelles on adsorbent surfaces has also been reported to affect the extent of PFAA removal (Deng *et al.*, 2012; Du *et al.*, 2014). More hydrophobic PFAAs, such as PFOS and PFOA, form hemi-micelles and micelles by the aggregation of C-F chains in water molecules. The critical micelle concentration (CMC) of PFOA and PFOS are 15696 and 4573 mg dm⁻³ respectively (Chen *et al.*, 2011; Du *et al.*, 2014). The formation of hemi-micelles and micelles through hydrophobic interactions onto the surface of adsorbents may hinder the sorption of PFAAs when the adsorbed anion concentration reaches the range of 0.01 to 0.001 of their CMC values (Du *et al.*, 2014; Deng *et al.*, 2015).

This result in the blocking of the inner pores of the adsorbent and may translate into obtaining a lower adsorption uptake of PFAA anions (Deng *et al.*, 2015). Deng *et al.*, (2015) obtained lower Langmuir monolayer adsorption capacities for the sorption of PFOS onto activated carbon than the expected equilibrium concentrations. Similar trends was reported by Yu *et al.*, (2009) and they attributed this effect to the higher hydrophobicity of PFOS, which may enhance the formation of micelles on the surface of adsorbents, hence resulting in lower adsorption capacities.

The formation of hemi-micelles and micelles on the surfaces of adsorbents was also reported to enhance the removal of long-chain PFAAs, such as PFOA and PFOS, by Du *et al.*, (2015). Increasing adsorption capacities for the sorption of PFOS onto positively charged adsorbents were reported by Chen *et al.*, (2011), and attributed to the formation of micelles on the surface. They postulated that aggregation of micelles onto the adsorbent surface enhanced the bilayer coverage of micelles with continued increase in PFOS concentration, resulting in an increased removal of PFOS by the adsorbent. Bilayer formation of PFOS onto positively charged surfaces of adsorbents therefore enhanced the Langmuir adsorption capacities. Similar results have also been reported by Zhang *et al.*, (2011), Karoyo and Wilson, (2013) and Du *et al.*, (2014).

Hence, the mechanism of PFAA adsorption onto the surfaces of adsorbents can proceed *via* any of the discussed processes depending on the surface of the adsorbent. However, more studies need to be carried out in order to sufficiently understand these processes.

3.7. Conclusions

From the assessed reports, evidence exists that PFAAs are emerging pollutants in various environmental media. This is largely attributed to the indiscriminate discharge of untreated effluents into various environmental media, with water bodies being the major recipient. This poses a serious environmental risk to man and its environs due to the persistence and toxicity of these contaminants. Removal of PFAAs through adsorption was assessed and found to have proved very effective.

The use of CNTs as adsorbents for PFAA removal showed better efficiencies than other conventional adsorbents due to their inherent properties such as large surface areas and moderate porosity available for adsorption. Although, some conventional adsorbents possess higher surface areas than CNTs, the ease of functionalization of CNTs to introduce new adsorption sites makes them more effective than conventional adsorbents. The removal of PFAAs by CNTs achieved good adsorption efficiencies, obtaining equilibrium faster than

most conventional adsorbents. The morphology and the ease with which CNTs can be modified to possess hydrophobic, hydrophilic or amphiphilic properties further enhances their potential as adsorbents for PFAAs. This demonstrates the effective application of CNTs for PFAA removal, with a possibility of regenerating the adsorbent for reuse. Various studies demonstrated that adsorption of PFAAs onto CNTs was *via* electrostatic, hydrophobic, π - π , and hydrogen bonding interactions, hence revealing that the adsorption mechanism of PFAAs onto CNTs is quite complicated.

It is clear that more studies need to be carried out for a better understanding of the adsorption mechanisms of PFAAs onto CNTS. Also, further development of novel and innovative CNT-based adsorbents for the effective removal of PFAAs from wastewater before its disposal into water bodies is required.

References

- Ahmad, A.L., W.A. Harris and B.S. Ooi, 2012. Removal of dye from wastewater of textile industry using membrane technology. *Jurnal Teknologi*, 36: 31–44.
- Ahrens, L., 2011. Polyfluoroalkyl compounds in the aquatic environment: A review of their occurrence and fate. *J. Environ. Monit.*, 13: 20-31.
- Ahrens, L., L.W.Y. Yeung, S. Taniyasu, P.K.S. Lam and N. Yamashita, 2011. Partitioning of perfluorooctanoate (PFOA), perfluorooctane sulfonate (PFOS) and perfluorooctane sulfonamide (PFOSA) between water and sediment. *Chemosphere*, 85: 731-737.
- Altmann, J., F. Zietzschmann, E.-L. Geiling, A.S. Ruhl, A. Sperlich and M. Jekel, 2015. Impacts of coagulation on the adsorption of organic micropollutants onto powdered activated carbon in treated domestic wastewater. *Chemosphere*, 125: 198-204.
- Arias, V.A., M. Mallavarapu and R. Naidu, 2015. Identification of the source of PFOS and PFOA contamination at a military air base site. *Environ. Monit. Assess.*, 187: 1-8.
- Arora, N. and N.N. Sharma, 2014. Arc discharge synthesis of carbon nanotubes: Comprehensive review. *Diam. Relat. Mater.*, 50: 135-150.
- Arvaniti, O.S., Y. Hwang, H.R. Andersen, A.S. Stasinakis, N.S. Thomaidis and M. Aloupi, 2015. Reductive degradation of perfluorinated compounds in water using Mg-aminoclay coated nanoscale zero valent iron. *Chem. Eng. J.*, 262: 133-139.
- Arvaniti, O.S., E.I. Ventouri, A.S. Stasinakis and N.S. Thomaidis, 2012. Occurrence of different classes of perfluorinated compounds in greek wastewater treatment plants and determination of their solid–water distribution coefficients. *J. Hazard. Mater.*, 239-240: 24-31.
- Balasubramanian, K. and M. Burghard, 2005. Chemically functionalized carbon nanotubes. *Small*, 1: 180-192.
- Bamoharram, F.F., A. Ahmadpour and M.M. Heravi, 2011. Synthesis of carbon nanotubes via catalytic chemical vapor deposition method and their modification with preyssler anion, $[\text{NaP}_5\text{W}_{30}\text{O}_{110}]_{14}$. *Nano*, 6: 349-355.
- Brillas, E. and C.A. Martínez-Huitle, 2015. Decontamination of wastewaters containing synthetic organic dyes by electrochemical methods. An updated review. *Appl. Catal., B*, 166: 603-643.
- Cambré, S., J. Campo, C. Beirnaert, C. Verlackt, P. Cool and W. Wenseleers, 2015. Asymmetric dyes align inside carbon nanotubes to yield a large nonlinear optical response. *Nature Nanotech.*, 10: 248-252.
- Carrion, F.J., C. Espejo, J. Sanes and M.D. Bermudez, 2010. Single-walled carbon nanotubes modified by ionic liquid as antiwear additives of thermoplastics. *Compos. Sci. Technol*, 70: 2160-2167.

- Chen, X., X. Xia, X. Wang, J. Qiao and H. Chen, 2011. A comparative study on sorption of perfluorooctane sulfonate (PFOS) by chars, ash and carbon nanotubes. *Chemosphere*, 83: 1313-1319.
- Chien, S.H. and W.R. Clayton, 1980. Application of elovich equation to the kinetics of phosphate release and sorption in soils. *Soil Sci. Soc. Am. J.*, 44: 265-268.
- Chularueangaksorn, P., S. Tanaka, S. Fujii and C. Kunacheva, 2013. Adsorption of perfluorooctanoic acid (PFOA) onto anion exchange resin, non-ion exchange resin, and granular-activated carbon by batch and column. *Desalin. Water Treat.*, 52: 6542-6548.
- Dachipally, P. and S.B. Jonnalagadda, 2011. Kinetics of ozone-initiated oxidation of textile dye, amaranth in aqueous systems. *J. Environ. Sci. Health. Part A*, 46: 887-897.
- Dai, Y., J. Niu, L. Yin, J. Xu and K. Sun, 2013. Enhanced sorption of perfluorooctane sulfonate (PFOS) on carbon nanotube-filled electrospun nanofibrous membranes. *Chemosphere*, 93: 1593-1599.
- Datsyuk, V., M. Kalyva, K. Papagelis, J. Parthenios, D. Tasis, A. Siokou, I. Kallitsis and C. Galiotis, 2008. Chemical oxidation of multiwalled carbon nanotubes. *Carbon*, 46: 833-840.
- Dauchy, X., V. Boiteux, C. Rosin and J.-F. Munoz, 2012. Relationship between industrial discharges and contamination of raw water resources by perfluorinated compounds. Part I: Case study of a fluoropolymer manufacturing plant. *Bull. Environ. Contam. Toxicol.*, 89: 525-530.
- Davis, K.L., M.D. Aucoin, B.S. Larsen, M.A. Kaiser and A.S. Hartten, 2007. Transport of ammonium perfluorooctanoate in environmental media near a fluoropolymer manufacturing facility. *Chemosphere*, 67: 2011-2019.
- De Voogt, P. and M. Saez, 2006. Analytical chemistry of perfluoroalkylated substances. *Trends Anal. Chem.*, 25: 326-342.
- Demirbas, E., M. Kobyas, E. Senturk and T. Ozkan, 2004. Adsorption kinetics for the removal of chromium(VI) from aqueous solutions on the activated carbons prepared from agricultural wastes. *Water SA*, 30: 533-539.
- Deng, S., Y. Nie, Z. Du, Q. Huang, P. Meng, B. Wang, J. Huang and G. Yu, 2015. Enhanced adsorption of perfluorooctane sulfonate and perfluorooctanoate by bamboo-derived granular activated carbon. *J. Hazard. Mater.*, 282: 150-157.
- Deng, S., L. Niu, Y. Bei, B. Wang, J. Huang and G. Yu, 2013. Adsorption of perfluorinated compounds on aminated rice husk prepared by atom transfer radical polymerization. *Chemosphere*, 91: 124-130.
- Deng, S., Q. Yu, J. Huang and G. Yu, 2010. Removal of perfluorooctane sulfonate from wastewater by anion exchange resins: Effects of resin properties and solution chemistry. *Water Res.*, 44: 5188-5195.

- Deng, S., Q. Zhang, Y. Nie, H. Wei, B. Wang, J. Huang, G. Yu and B. Xing, 2012. Sorption mechanisms of perfluorinated compounds on carbon nanotubes. *Environ. Pollut.*, 168: 138-144.
- Domingo, J.L., I.E. Jogsten, U. Eriksson, I. Martorell, G. Perelló, M. Nadal and B. Van Bavel, 2012. Human dietary exposure to perfluoroalkyl substances in catalonia, spain. Temporal trend. *Food Chem.*, 135: 1575-1582.
- Du, Z., S. Deng, Y. Bei, Q. Huang, B. Wang, J. Huang and G. Yu, 2014. Adsorption behavior and mechanism of perfluorinated compounds on various adsorbents—a review. *J. Hazard. Mater.*, 274: 443-454.
- Du, Z., S. Deng, Y. Chen, B. Wang, J. Huang, Y. Wang and G. Yu, 2015. Removal of perfluorinated carboxylates from washing wastewater of perfluorooctanesulfonyl fluoride using activated carbons and resins. *J. Hazard. Mater.*, 286: 136-143.
- Dubinin, M.M. and L.V. Radushkevich, 1947. The equation of the characteristic curve of activated charcoal. *Proc. Acad. Sci, U.S.S.R, Phys. Chem. Sect.*, 55: 327-329.
- Freundlich, H., 1906. Adsorption in solids. *Z. Phys. Chem.*, 57: 385-470.
- Fujii, S., C. Polprasert, S. Tanaka, N.P.H. Lien and Y. Qiu, 2007. New pops in the water environment: Distribution, bioaccumulation and treatment of perfluorinated compounds – a review paper. *J. Water Supply Res. T.*, 56: 313-325.
- Gao, X. and J. Chorover, 2012. Adsorption of perfluorooctanoic acid and perfluorooctanesulfonic acid to iron oxide surfaces as studied by flow-through ATR-FTIR spectroscopy. *Environ. Chem.*, 9: 148-157.
- Giesy, J.P. and K. Kurunthachalam, 2001. Global distribution of perfluorooctane sulfonate in wildlife. *Environ. Sci. Technol.*, 35: 1339-1342.
- Hamza, I.A.A., B.S. Martincigh, J.C. Ngila and V.O. Nyamori, 2013. Adsorption studies of aqueous Pb(II) onto a sugarcane bagasse/multi-walled carbon nanotube composite. *Phys. Chem. Earth*, 66: 157-166.
- Hansen, K.J., H.O. Johnson, J.S. Eldridge, J.L. Butenhoff and L.A. Dick, 2002. Quantitative characterization of trace levels of PFOS and PFOA in the Tennessee river. *Environ. Sci. Technol.*, 36: 1681-1685.
- Hanssen, L., H. Röllin, J.Ø. Odland, M.K. Moe and T.M. Sandanger, 2010. Perfluorinated compounds in maternal serum and cord blood from selected areas of South Africa: Results of a pilot study. *J. Environ. Monit.*, 12: 1355-1361.
- Harada, K., N. Saito, K. Sasaki, K. Inoue and A. Koizumi, 2003. Perfluorooctane sulfonate contamination of drinking water in the Tama River, Japan: Estimated effects on resident serum levels. *Bull. Environ. Contam. Toxicol.*, 71: 31-36.
- Harada, K.H., H.-R. Yang, C.-S. Moon, N.-N. Hung, T. Hitomi, K. Inoue, N. T., T. Watanabe, S. Kamiyama, K. Takenaka, M.-Y. Kim, T. Watanabe, T. Takasuga and A. Koizumi, 2010. Levels of perfluorooctane sulfonate and perfluorooctanoic acid

- in female serum samples from Japan in 2008, Korea in 1994–2008 and vietnam in 2007–2008. *Chemosphere*, 79: 314-319.
- Herrero-Latorre, C., J. Álvarez-Méndez, J. Barciela-García, S. García-Martín and R.M. Peña-Crecente, 2015. Characterization of carbon nanotubes and analytical methods for their determination in environmental and biological samples: A review. *Anal. Chim. Acta* 853: 77-94.
- Higgins, C.P. and R.G. Luthy, 2006. Sorption of perfluorinated surfactants on sediments. *Environ. Sci. Technol.*, 40: 7251-7256.
- Ho, Y.-S., 2003. Removal of copper ions from aqueous solution by tree fern. *Water Res.*, 37: 2323-2330.
- Ho, Y.S., 2004. Comment on "cadmium removal from aqueous solutions by chitin: Kinetic and equilibrium studies". *Water Res.*, 38: 2962-2964
- Ho, Y.S. and G. McKay, 1999. Pseudo-second order model for sorption processes. *Process Biochem.*, 34: 451-465.
- Jenkins, C., M. Cruz, J. Depalma, M. Conroy, B. Benardo, M. Horbachuk, T. Sadowski, C. Broadbridge and T.C. Schwendemann, 2014. Characterization of carbon nanotube growth *via* CVD synthesis from a liquid precursor. *Int. J. High Speed Electron Syst.*, 23: 14200010-14200018.
- Jogsten, I.E., M. Nadal, B. Van Bavel, G. Lindström and J.L. Domingo, 2012. Per- and polyfluorinated compounds (PFCs) in house dust and indoor air in Catalonia, Spain: Implications for human exposure. *Environ. Int.*, 39: 172-180.
- Jonnalagadda, S.B. and S. Nadupalli, 2004. Effluent treatment using electrochemically bleached seawater—oxidative degradation of pollutants. *Talanta*, 64: 18 - 22.
- Jonnalagadda, S.B. and M.N. Shezi, 2009. Kinetics and mechanism of the oxidation of methylene violet by bromate at acidic pH and the dual role of bromide ion. *J. Phys. Chem.*, 113: 5540 - 5549.
- Kanoun, O., C. Müller, A. Benchirouf, A. Sanli, T.N. Dinh, A. Al-Hamry, L. Bu, C. Gerlach and A. Bouhamed, 2014. Flexible carbon nanotube films for high performance strain sensors. *Sensors*, 14: 10042-10071.
- Karoyo, A.H. and L.D. Wilson, 2013. Tunable macromolecular-based materials for the adsorption of perfluorooctanoic and octanoic acid anions. *J. Colloid Interface Sci.*, 402: 196-203.
- Keru, G., P.G. Ndungu and V.O. Nyamori, 2014. A review on carbon nanotube/polymer composites for organic solar cells. *Int. J. Energy Res.*, 38: 1635-1653.
- Khan, A., T. Al-Bahri and A. Al-Haddad, 1997. Adsorption of phenol based organic pollutants on activated carbon from multi-component dilute aqueous solutions. *Water Res.*, 31: 2102-2112.

- Khan, A.R., I.R. Al-Waheab and A. Al-Haddad, 1996. A generalized equation for adsorption isotherms for multi-component organic pollutants in dilute aqueous solution. *Environ. Technol.*, 17: 13-23.
- Kim, J.-W., N.M. Tue, T. Isobe, K. Misaki, S. Takahashi, P.H. Viet and S. Tanabe, 2013. Contamination by perfluorinated compounds in water near waste recycling and disposal sites in Vietnam. *Environ. Monit. Assess.*, 185: 2909-2919.
- Kwadijk, C.J., I. Velzeboer and A.A. Koelmans, 2013. Sorption of perfluorooctane sulfonate to carbon nanotubes in aquatic sediments. *Chemosphere*, 90: 1631-1636.
- Langmuir, I., 1918. The adsorption of gases on plane surfaces of glass, mica and platinum. *J. Am. Chem. Soc.*, 40: 1361-1402.
- Lau, C., K. Anitole, C. Hodes, D. Lai, A. Pfahles-Hutchens and J. Seed, 2007. Perfluoroalkyl acids: A review of monitoring and toxicological findings. *Toxicol. Sci.*, 99: 366-394.
- Lee, Y.J., M.-K. Kim, J. Bae and J.-H. Yang, 2013. Concentrations of perfluoroalkyl compounds in maternal and umbilical cord sera and birth outcomes in Korea. *Chemosphere*, 90: 1603-1609.
- Li, K., Z. Zeng, J. Xiong, L. Yan, H. Guo, S. Liu, Y. Dai and T. Chen, 2015. Fabrication of mesoporous Fe₃O₄@ SiO₂@CTAB-SiO₂ magnetic microspheres with a core/shell structure and their efficient adsorption performance for the removal of trace PFOS from water. *Colloids Surf. A Physicochem. Eng. Asp.*, 465: 113-123.
- Li, X., H. Zhao, X. Quan, S. Chen, Y. Zhang and H. Yu, 2011. Adsorption of ionizable organic contaminants on multi-walled carbon nanotubes with different oxygen contents. *J. Hazard. Mater.*, 186: 407-415.
- Li, Y., J. Niu, Z. Shen and C. Feng, 2013. Size effect of single-walled carbon nanotube on adsorption of perfluorooctanesulfonate. *Chemosphere*, 91: 784-790.
- Lin, J. and L. Wang, 2009. Comparison between linear and non-linear forms of pseudo-first-order and pseudo-second-order adsorption kinetic models for the removal of methylene blue by activated carbon. *Front. Environ. Sci. Eng.*, 3: 320-324.
- Lindh, C.H., L. Rylander, G. Toft, A. Axmon, A. Rignell-Hydbom, A. Giwercman, H.S. P., K. Góalczyk, J.K. Ludwicki, V. Zvezday, R. Vermeulen, V. Lenters, D. Heederik, J.P. Bonde and A.G.J. Bo, 2012. Blood serum concentrations of perfluorinated compounds in men from greenlandic Inuit and European populations. *Chemosphere* 88: 1269-1275.
- Ma, H., C. Burger, B.S. Hsiao and B. Chu, 2012. Highly permeable polymer membranes containing directed channels for water purification. *ACS Macro Lett.*, 1(6): 723-726.
- Madsen, H.T., N. Bajraktari, C. Hélix-Nielsen, B. Van der Bruggen and E.G. Søgaaard, 2015. Use of biomimetic forward osmosis membrane for trace organics removal. *J. Membr. Sci.*, 476: 469-474.
- Maes, J., B. De Meulenaer, P. Van Heerswynghels, W. De Greyt, G. Eppe, E. De Pauw and A. Huyghebaert, 2005. Removal of dioxins and PCB from fish oil by activated

- carbon and its influence on the nutritional quality of the oil. *J. Am. Oil Chem. Soc.*, 82: 593-597.
- Martin, J.W., D.C.G. Muir, C.A. Moody, D.A. Ellis, W.C. Kwan, K.R. Solomon and S.A. Mabury, 2002. Collection of airborne fluorinated organics and analysis by gas chromatography/chemical ionization mass spectrometry. *Anal. Chem.*, 74: 584-590.
- Martinez-Moral, M.P. and M.T. Tena, 2012. Determination of perfluorocompounds in popcorn packaging by pressurised liquid extraction and ultra-performance liquid chromatography–tandem mass spectrometry. *Talanta*, 101: 104-109.
- McCarthy, D.W., L.A. Bass, P.D. Cutler, R.E. Shefer, R.E. Klinkowstein, P. Herrero, J.S. Lewis, C.S. Cutler, C.J. Anderson and M.J. Welch, 1999. High purity production and potential applications of copper-60 and copper-61. *Nucl. Med. Biol*, 26: 351-358.
- McDonough, K., J.L. Fairey and G.V. Lowry, 2008. Adsorption of polychlorinated biphenyls to activated carbon: Equilibrium isotherms and a preliminary assessment of the effect of dissolved organic matter and biofilm loadings. *Water Res.*, 42: 575-584.
- Milinic, J., S. Lacorte, M. Vidal and A. Rigol, 2015. Sorption behaviour of perfluoroalkyl substances in soils. *Sci. Total Environ.*, 511: 63-71.
- Monroy, R., K. Morrison, K. Teo, S. Atkinson, C. Kubwabo, B. Stewart and W.G. Foster, 2008. Serum levels of perfluoroalkyl compounds in human maternal and umbilical cord blood samples. *Environ. Res.*, 108: 56-62.
- Moody, C.A. and J.A. Field, 1999. Determination of perfluorocarboxylates in groundwater impacted by fire-fighting activity. *Environ. Sci. Technol.*, 33: 2800-2806.
- Müller, C.E., A.C. Gerecke, C. Bogdal, Z. Wang, M. Scheringer and K. Hungerbühler, 2012. Atmospheric fate of poly- and perfluorinated alkyl substances (PFASs): I. Day–night patterns of air concentrations in summer in Zurich, Switzerland. *Environ. Pollut.*, 169: 196-203.
- Munsch, C., P. Marchand, A. Venisseau, B. Veyrand and Z. Zeng, 2013. Levels and trends of the emerging contaminants HBCDs (hexabromocyclododecanes) and PFCs (perfluorinated compounds) in marine shellfish along french coasts. *Chemosphere*, 91: 233-240.
- Naile, J.E., J.S. Khim, S. Hong, J. Park, B.-O. Kwon, J.S. Ryu, J.H. Hwang, P.D. Jones and J.P. Giesy, 2013. Distributions and bioconcentration characteristics of perfluorinated compounds in environmental samples collected from the west coast of Korea. *Chemosphere*, 90: 387-394.
- Namasivayam, C. and D. Kavitha, 2002. Removal of congo red from water by adsorption onto activated carbon prepared from coir pith, an agricultural solid waste. *Dyes Pigments*, 54: 47-58.

- Ochoa-Herrera, V. and R. Sierra-Alvarez, 2008. Removal of perfluorinated surfactants by sorption onto granular activated carbon, zeolite and sludge. *Chemosphere*, 72: 1588-1593.
- Ombaka, L.M., P.G. Ndungu and V.O. Nyamori, 2014. Pyrrolic nitrogen-doped carbon nanotubes: Physicochemical properties, interactions with Pd and their role in the selective hydrogenation of nitrobenzophenone. *RSC Adv.*, 5: 109-122.
- Oyetade, O.A., V.O. Nyamori, B.S. Martincigh and S.B. Jonnalagadda, 2015. Effectiveness of carbon nanotube-cobalt ferrite nanocomposites for the adsorption of rhodamine B from aqueous solutions. *RSC Adv.*, 5: 22724-22739.
- Pare, B., B. Bhawna Sarwan and S. Jonnalagadda, 2011. Photocatalytic mineralization study of malachite green on the surface of Mn-doped BiOCl activated by visible light under ambient condition. *Appl. Surf. Sci.*, 258: 247 - 253.
- Punyapalakul, P., K. Suksomboon, P. Prarat and S. Khaodhiar, 2013. Effects of surface functional groups and porous structures on adsorption and recovery of perfluorinated compounds by inorganic porous silicas. *Sep. Sci. Technol.*, 48: 775-788.
- Qiu, Y., S. Fujii, S. Tanaka, A. Koizumi and P.H.L. Nguyen, 2005. Removal characteristics of perfluorooctane sulfonate and perfluorooctanoic acid by granular activated carbon adsorption. *Proceedings of 14th KAIST-KU-NTU-NUS Symposium on Environmental Engineering, Korea*, 14: 89-97.
- Redlich, O. and D.L. Peterson, 1959. A useful adsorption isotherm. *J. Phys. Chem.*, 63: 1024.
- Rostkowski, P., N. Yamashita, I.M.K. So and S. Taniyasu, 2006. Perfluorinated compounds in streams of the Shihwa industrial zone and Lake Shihwa, South Korea. *Environ. Toxicol. Chem.*, 25: 2374-2380.
- Rueda-Márquez, J., M. Sillanpää, P. Pocostales, A. Acevedo and M. Manzano, 2015. Post-treatment of biologically treated wastewater containing organic contaminants using a sequence of H₂O₂ based advanced oxidation processes: Photolysis and catalytic wet oxidation. *Water Res.*, 71: 85-96.
- Rylander, C., D.T. Phi, J.O. Odland and T.M. Sandanger, 2009. Perfluorinated compounds in delivering women from south central Vietnam. *J. Environ. Monit.*, 11: 2002-2008.
- Santangelo, S., G. Messina, G. Faggio, S.H. Abdul Rahim and C. Milone, 2012. Effect of sulphuric-nitric acid mixture composition on surface chemistry and structural evolution of liquid-phase oxidised carbon nanotubes. *J. Raman Spectrosc.*, 43: 1432-1442.
- Shang, S., W. Zeng and X.-M. Tao, 2011. High stretchable MWNTs/polyurethane conductive nanocomposites. *J. Mater. Chem.*, 21: 7274-7280.
- Sinclair, E., D.T. Mayack, K. Roblee, N. Yamashita and K. Kannan, 2006. Occurrence of perfluoroalkyl surfactants in water, fish, and birds from new york state. *Arch. Environ. Contam. Toxicol.*, 50: 398-410.

- Sips, R., 1948. Combined form of langmuir and freundlich equations. *J. Chem. Phys.*, 16: 490-495.
- Temkin, M.I. and V. Pyzhev, 1940. Kinetics of ammonia synthesis on promoted iron catalysts. *Acta Phys. Chim.*, 12: 327-356.
- Toth, J., 1971. State equations of the solid-gas interface layers. *Acta Chim. Acad. Sci. Hung.*, 69: 311-328.
- Valsecchi, S., M. Rusconi and S. Polesello, 2013. Determination of perfluorinated compounds in aquatic organisms: A review. *Anal. Bioanal. Chem.*, 405: 143-157.
- Walters, R.W. and R.G. Luthy, 1984. Equilibrium adsorption of polycyclic aromatic hydrocarbons from water onto activated carbon. *Environ. Sci. Technol.*, 18: 395-403.
- Wang, J., H. Li, C. Shuang, A. Li, C. Wang and Y. Huang, 2015. Effect of pore structure on adsorption behavior of ibuprofen by magnetic anion exchange resins. *Microporous Mesoporous Mater.*, 210: 94-100.
- Wang, S. and Y. Peng, 2010. Natural zeolites as effective adsorbents in water and wastewater treatment. *Chem. Eng. J.*, 156: 11-24.
- Wepasnick, K.A., B.A. Smith, K.E. Schrote, H.K. Wilson, S.R. Diegelmann and D.H. Fairbrother, 2011. Surface and structural characterization of multi-walled carbon nanotubes following different oxidative treatments. *Carbon*, 49: 24-36.
- Xu, J., J. Niu and S. Zhang, 2013. Sorption of perfluorooctane sulfonate (PFOS) on electrospun fiber membranes. *Procedia Environ. Sci.*, 18: 472-477.
- Xu, Z., S. Fiedler, G. Pfister, B. Henkelmann, C. Mosch, W. Völkel, H. Fromme and K.-W. Schramm, 2013. Human exposure to fluorotelomer alcohols, perfluorooctane sulfonate and perfluorooctanoate via house dust in Bavaria, Germany. *Sci. Total Environ.*, 443: 485-490.
- Yao, Y., K. Volchek, C.E. Brown, A. Robinson and T. Obal, 2014. Comparative study on adsorption of perfluorooctane sulfonate (PFOS) and perfluorooctanoate (PFOA) by different adsorbents in water. *Water Sci. Technol.*, 70: 1983-1991.
- Yu, J.-G., X.-H. Zhao, H. Yang, X.-H. Chen, Q. Yang, L.-Y. Yu, J.-H. Jiang and X.-Q. Chen, 2014. Aqueous adsorption and removal of organic contaminants by carbon nanotubes. *Sci. Total Environ.*, 482-483: 241-251.
- Yu, Q., R. Zhang, S. Deng, J. Huang and G. Yu, 2009. Sorption of perfluorooctane sulfonate and perfluorooctanoate on activated carbons and resin: Kinetic and isotherm study. *Water Res.*, 43: 1150-1158.
- Yue, B., Y. Wang, C.Y. Huang, R. Pfeffer and Z. Iqbal, 2007. Polymeric nanocomposites of functionalized carbon nanotubes synthesized in supercritical CO₂. *J. Nanosci. Nanotechnol.*, 7: 994-1000.
- Yuge, R., S. Bandow, K. Nakahara, M. Yudasaka, K. Toyama, T. Yamaguchi, S. Iijima and T. Manako, 2014. Structure and electronic states of single-wall carbon nanohorns prepared under nitrogen atmosphere. *Carbon*, 75: 322-326.

- Zareitalabad, P., J. Siemens, M. Hamer and W. Amelung, 2013. Perfluorooctanoic acid (PFOA) and perfluorooctanesulfonic acid (PFOS) in surface waters, sediments, soils and wastewater - a review on concentrations and distribution coefficients. *Chemosphere*, 91: 725-732.
- Zhang, M., G.-H. Liu, K. Song, Z. Wang, Q. Zhao, S. Li and Z. Ye, 2015. Biological treatment of 2, 4, 6-trinitrotoluene (TNT) red water by immobilized anaerobic-aerobic microbial filters. *Chem. Eng. J.*, 259: 876-884.
- Zhang, Q., S. Deng, G. Yu and J. Huang, 2011. Removal of perfluorooctane sulfonate from aqueous solution by crosslinked chitosan beads: Sorption kinetics and uptake mechanism. *Bioresour. Technol.*, 102: 2265-2271.
- Zhang, S., T. Shao, S.S. Bekaroglu and T. Karanfil, 2009. The impacts of aggregation and surface chemistry of carbon nanotubes on the adsorption of synthetic organic compounds. *Environ. Sci. Technol.*, 43: 5719-5725.
- Zhang, Y., W. Meng, C. Guo, J. Xu, T. Yu, W. Fan and L. Li, 2012. Determination and partitioning behavior of perfluoroalkyl carboxylic acids and perfluorooctanesulfonate in water and sediment from Dianchi lake, China. *Chemosphere*, 88: 1292-1299.
- Zhao, L., J. Bian, Y. Zhang, L. Zhu and Z. Liu, 2014. Comparison of the sorption behaviors and mechanisms of perfluorosulfonates and perfluorocarboxylic acids on three kinds of clay minerals. *Chemosphere*, 114: 51-58.
- Zhao, L., Y. Li, X. Cao, Y. J. and W. Dong, 2012. Multifunctional role of an ionic liquid in melt-blended poly(methylmethacrylate)/multi-walled carbon nanotube nanocomposites. *Nanotech.*, 23: 255702-255709.
- Zhou, Y., B. Wen, Z. Pei, G. Chen, J. Lv, J. Fang, X. Shan and S. Zhang, 2012. Coadsorption of copper and perfluorooctane sulfonate onto multi-walled carbon nanotubes. *Chem. Eng. J.*, 203: 148-157.
- Zhou, Z., Y. Shi, W. Li, L. Xu and Y. Cai, 2012. Perfluorinated compounds in surface water and organisms from Baiyangdian Lake in North China: Source profiles, bioaccumulation and potential risk. *Bull. Environ. Contam. Toxicol.*, 89: 519-524.

Chapter 4

Nitrogen-functionalised carbon nanotubes as a novel adsorbent for the removal of Cu(II) from aqueous solution

Oluwaseun A. Oyetade, Vincent O. Nyamori,* Bice S. Martincigh and Sreekantha B. Jonnalagadda

School of Chemistry and Physics, University of KwaZulu-Natal, Westville Campus,
Private Bag X54001, Durban 4000, South Africa

*Corresponding author: Tel: +27 31 260 8256; Fax: +27 31 2603091; E-mail:
nyamori@ukzn.ac.za

Abstract

This study investigated the introduction of 4'-(4-hydroxyphenyl)-2,2':6',2''-terpyridine (HO-Phttpy) onto the surface of multiwalled carbon nanotubes (MWCNTs) to obtain nitrogen-functionalized MWCNTs (MWCNT-ttpty). This novel material was characterised and tested for its possible use in the remediation of wastewater contaminated with heavy metal ions. Its efficacy was compared with that of acid-functionalized MWCNTs (MWCNT-COOH) for the removal of the heavy metal ion Cu^{2+} through adsorption. The synthesis of HO-Phttpy was first synthesized, followed by the functionalization of MWCNT-COOH to afford MWCNT-ttpty. MWCNT-ttpty showed significant textural enhancement, demonstrating an increase in surface area and pore volume. Its application for Cu^{2+} removal showed a marked increase in uptake (q_e), i.e. 19.44 to 31.65 mg g^{-1} , compared with MWCNT-COOH. This is attributed to the introduction of more active/chelating sites for adsorption. The kinetics of adsorption was best described by the pseudo-second order model and among the isotherms tested, the Langmuir isotherm provided the best fit for the equilibrium data. Thermodynamic studies revealed that the adsorption process was spontaneous and endothermic. Desorption studies demonstrated a better removal efficiency of Cu^{2+} from MWCNT-ttpty, indicating its possible regeneration and the recovery of the Cu^{2+} adsorbate for reuse. Thus, MWCNT-ttpty shows superior properties for wastewater remediation.

Keywords: multiwalled carbon nanotubes, adsorption, isotherm, kinetics, thermodynamics, copper

4.1. Introduction

Carbon nanotubes (CNTs) are tubular shaped carbon nanomaterials, possessing excellent electrical, mechanical and optical properties and thermal stability.¹⁻³ This has led to a growing interest for their application in various fields. They are made up of a hexagonal lattice of carbon atoms, consisting of hollow graphite, rolled at specific angles into cylinders.⁴ CNTs are classified into single-walled carbon nanotubes (SWCNTs), double-walled carbon nanotubes (DWCNTs) and multiwalled carbon nanotubes (MWCNTs), depending on the number of concentric sheets contained in the tubes.^{4,5} They form large aggregates with low dispersability in aqueous and organic solutions due to strong van der Waals interactions between them. This necessitates the need for the development of both covalent and non-covalent strategies⁵ for CNT functionalization, in order to introduce functional groups which will enhance their application for other purposes. Covalent functionalization is often carried out through the oxidation of CNTs with acids such as HNO₃ and H₂SO₄, to introduce oxygen-containing groups such as –OH and –COOH onto the walls of the tubes.^{6,7} This approach improves the wettability of CNTs, thereby increasing their dispersability in aqueous/organic solutions. New functional groups, such as –NR, –F, –Cl and –SR, can also be incorporated onto the walls/sides of the tubes through solution chemistry.⁶

In recent times, the application of CNTs in various fields such as medicine,^{8,9} engineering,¹⁰ environmental science,⁷ energy,¹¹ catalysis and catalyst supports,⁵ amongst many others, has been reported by several authors. This is largely attributed to their inherent properties such as large surface area, pore volume and the ease in introducing new functional groups onto their walls. In spite of these studies, functionalization of CNTs to contain multiple functional groups which will further enhance chemical reactions with other molecules is still under-researched.¹

The tridentate chelating ligand, 4'-(4-hydroxyphenyl)-2,2':6',2''-terpyridine (HO-Phttpy), containing three nitrogen atoms is a good contender for the functionalization of MWCNTs, in order to introduce nitrogen-containing atoms to the structure of CNTs. HO-Phttpy has profound flexibility to form bridged metal centres by using two or more moieties, construction of supramolecular structures and formation of macrocyclic ligands.¹² Due to the strong affinity of this ligand for transition metal ions, the chelates produced have been used in luminescence and chemical sensing devices.¹³ In spite of the vast amount of work on CNTs, to the best of our knowledge, no study has investigated the effect of functionalization of oxidized MWCNTs (MWCNT-COOH) with HO-Phttpy for their increased activity as adsorbents.

One possible area of application of CNTs functionalized with nitrogen-donor ligands is the remediation of wastewater contaminated with heavy metal ions. The influx of toxic pollutants, through anthropogenic activities such as industrial and commercial applications, into the environment is a major challenge globally. Among these pollutants are heavy metals, which have generated global attention because of their toxicity, bio-accumulation in the food chain, inability to degrade to less harmful substances and ability to persist in the environment for long periods of time.¹⁴ In addition, the speciation of metals may change to more toxic forms with time and depending on environmental conditions such as pH.

In this work, the synthesized material was applied for the removal of Cu^{2+} as an example of a typical heavy metal ion discharged into the environment. The choice of copper was based on the fact that copper and its compounds are regularly used in agriculture for fertilizer production,¹⁵ electronics,¹⁶ textiles,¹⁷ medicine⁹ and metal cleaning purposes.¹⁸ The discharge of copper-contaminated effluents into aquatic environments introduces humans to necrotic changes in the liver and kidney, gastrointestinal irritations such as diarrhoea and melena, and including a number of capillary diseases; resulting in severe deleterious health effects.^{19,20} Although copper is a known essential metal at low concentrations, an excessive amount is considered harmful to both aquatic and human life.^{21,22} In fact, cases of accidental or suicidal poisoning have been reported in India and some western countries as a result of the intake of copper compounds.^{20,22} As a result of the numerous health consequences, a variety of techniques such as chemical precipitation,²³ ion exchange,²⁴ ultrafiltration,²⁵ reverse osmosis²⁶ and adsorption²⁷ have been used for Cu^{2+} removal from municipal wastewaters and industrial effluents. Of these methods, adsorption is considered most reliable for its removal from wastewater.²⁷ This approach is simple, efficient, and cost-effective, with a high potential for recycling the metal ion and the adsorbent. Thus, the removal of Cu^{2+} from aqueous solution by adsorption has been reported through the use of tree fern,²⁸ bagasse,^{29,30} peanut hull,³¹ rice husk,³² magnetite,^{33,34} peat³⁵ and activated carbon.³⁶⁻³⁸ Reports have shown that these adsorbents possess good potential for Cu^{2+} removal; however, drawbacks such as slow sorption and regeneration of adsorbents limits their usage.^{28,30,35} Pristine and functionalized CNTs have also been applied as adsorbents for Cu^{2+} removal.^{19,27,39,40} However, increased removal efficiency can be achieved by using CNT-based nanocomposites as adsorbents. Composites such as CNT/bagasse,⁴¹ CNT/magnetite,^{42,43} and CNT/chitosan⁴⁴ have demonstrated good sorption ability for Cu^{2+} removal. To further improve the efficiency of CNT-based nanomaterials, nitrogen-containing ligands can be used as modifiers for CNTs, hence, increasing the number of chelating sites available for adsorption on the adsorbent.⁴⁵

In this communication, we report the synthesis of nitrogen-functionalized MWCNTs (MWCNT-ttpy) through the functionalization of acid-functionalized MWCNTs (MWCNT-

COOH) by incorporating 4'-(4-hydroxyphenyl)-2,2':6',2''-terpyridine (HO-Phttpy) onto their structure. The effectiveness of this material in the adsorption of Cu^{2+} from aqueous solution was examined through a series of batch adsorption processes and compared with that of MWCNT-COOH. The effects of pH, contact time, adsorbent dose, temperature and initial Cu^{2+} concentration were investigated to determine the optimum conditions for the effective remediation of Cu^{2+} -polluted wastewater. In addition, desorption studies were undertaken to investigate the potential reuse of the adsorbent and recovery of the adsorbate.

4.2. Experimental

4.2.1. Materials

Copper metal powder was obtained from Johnson Matthey Chemicals (Pty) Ltd (Gauteng, South Africa) while sodium hydroxide (NaOH, 98%) and sodium bicarbonate (NaHCO_3 , 99%) were purchased from Merck Chemicals (Pty) Ltd (Gauteng, South Africa). Sodium carbonate (Na_2CO_3 , 99%) was purchased from Associated Chemical Enterprises (Johannesburg, South Africa). Chemicals such as 4-hydroxybenzaldehyde (99%), 2-acetylpyridine (99%), indium bromide (InBr_3 , 99%) and solvents such as absolute ethanol, N,N'-dimethylformamide (DMF, 99%), dimethyl sulfoxide- d_6 (DMSO- d_6 , 99%) and triethylsilane (Et_3SiH , 97%) were purchased from Sigma-Aldrich (St Louis, USA). Tetrahydrofuran (THF, 99%), chloroform (99%) and thionyl chloride (SOCl_2 , 99%) were purchased from Merck Chemicals (Pty) Ltd (Gauteng, South Africa) while aqueous ammonia (25%) was purchased from Associated Chemical Enterprises (Johannesburg, South Africa). Nitric (55%), sulfuric (98%) and hydrochloric acids (32%) were obtained from C C Imelmann Ltd (Robertsham, South Africa). All materials and chemicals were of analytical grade and used as received from suppliers without further purification. MWCNTs (purity > 95%) (P-MWCNTs), synthesized by chemical vapour deposition (CVD), were obtained from Cheap Tubes Incorporation (Brattleboro, USA).

4.2.2. Characterization

The ligand, 4'-(4-hydroxyphenyl)-2,2':6',2''-terpyridine, was characterized by using Fourier transform infrared (FTIR) spectroscopy, nuclear magnetic resonance (NMR) and mass spectrometry, and melting point measurements. The FTIR spectra were recorded on a Perkin Elmer RX 1 spectrophotometer and the melting point was determined by using a Bibby Stuart Scientific model SMP3 apparatus. ^1H and ^{13}C NMR spectra were obtained from a 400-MHz Bruker Avance III spectrometer and mass spectra were obtained on a Waters Synapt G2 mass spectrometer in electrospray positive mode.

Structural characterization of the adsorbents was carried out with a transmission electron microscope (TEM) (JEOL, TEM 1010) and a scanning electron microscope (SEM) (JEOL, TSM 6100) to visualize the morphology, structure, shape and size distribution of the nanomaterials. Images were captured by means of a Megaview 3 camera and analysed on iTEM software. The surface area of the adsorbents was determined with nitrogen as the flow gas by means of a Micromeritics Tristar II 3020 surface area and porosity analyser. Data were captured and analysed by using Tristar II 3020 version 2 software. Fourier transform infrared (FTIR) spectra of the synthesized materials were obtained when the samples were embedded into KBr pellets and were recorded on a Perkin Elmer Spectrum RX 1 spectrophotometer, in order to identify the surface functional groups present on the materials. Raman spectroscopy (DeltaNu Advantage 532TM) measurements were also performed to provide information on the purity and crystallinity of the adsorbents. Thermogravimetric (TGA) analysis (Q SeriesTM Thermal Analyzer DSC/TGA Q600) was performed to determine the thermal stability and fraction of volatile components in the samples while the Boehm titration was applied to quantitatively estimate the amount of acidic and basic groups present on the adsorbents. Elemental analysis (ThermoScientific Flash 2000) of adsorbents was also carried out to investigate the percentage composition of carbon, hydrogen, oxygen and nitrogen present in the samples.

4.2.2.1. Determination of point of zero charge (pH_{PZC})

Aliquots of 50 cm³ of 0.01 mol dm⁻³ NaCl solutions were placed into bottles and adjusted with the addition of appropriate amounts of 0.1 mol dm⁻³ HCl or NaOH to obtain an initial pH in the range of 1-10. A mass of 100 mg of adsorbent was added into each bottle and the suspension left to equilibrate on an orbital shaker for 48 h at room temperature. The solutions were filtered and the final pH of the filtrate determined. A plot of pH_{initial} – pH_{final} vs. pH_{initial} was obtained and the point of intersection of the curves gave the pH_{PZC} of the adsorbent.⁴⁶

4.2.2.2. Boehm titration

The basic and acidic properties of the adsorbents were quantitatively determined by the Boehm titration. This analysis method gives quantitative information on the amount of total basic and acidic groups on the adsorbents.⁴⁷⁻⁴⁹ As reported by Boehm *et al.*,⁵⁰ the determination of acidic groups (carboxyl, lactonic, phenolic) on the adsorbents was performed by weighing 100 mg of each sorbent into a 50 cm³ polypropylene bottle and mixed with 20 cm³ of either 0.05 mol dm⁻³ NaHCO₃, NaOH or 0.1 mol dm⁻³ Na₂CO₃ solutions. The suspensions were agitated in a thermostated water bath at room temperature for 24 h. The resulting solutions were filtered by gravity, and the amount of excess base determined quantitatively by back-titration against 0.05 mol dm⁻³ HCl solution. For the

determination of the basic groups, 100 mg of adsorbents were mixed with 0.05 mol dm⁻³ HCl solution and agitated on a thermostated water bath at room temperature for 24 h. After agitation, the suspension was filtered by gravity and the amount of basic groups in the adsorbent was determined by titrating the filtrate against 0.05 mol dm⁻³ NaOH solution. The Boehm titration is based on the assumption that NaOH gives information on the amount of carboxylic, lactonic and phenolic groups, Na₂CO₃, on the carboxylic and lactonic groups, NaHCO₃, on the carboxylic groups on each adsorbent and HCl gives the amount of basic groups on the adsorbent.⁵⁰ Results were expressed as H⁺/OH⁻ millimoles per gram of adsorbent.

4.2.3. Procedure for the synthesis of 4'-(4-hydroxyphenyl)-2,2':6',2''-terpyridine (HO-Phtppy)

The ligand was synthesized as reported by Patel *et al.*^{51,52} with some modifications. 2-Acetylpyridine (2.423 g, 20.0 mmol) was added to 15 cm³ of a 2:1 (v/v) mixture of ethanol and water containing 4-hydroxybenzaldehyde (1.221 g, 10.0 mmol). To the suspension, NaOH pellets (1.458 g, 26.0 mmol) and 30 cm³ aqueous NH₃ were added and stirred continuously at room temperature for 8 h to yield a cream-coloured precipitate. The resulting mixture was filtered, the solid obtained was washed with deionised water (5 × 10 cm³), followed by absolute ethanol (3 × 5 cm³) to obtain the crude white product (508.8 mg, 42%). m.p. 199-201 °C; IR (ATR, cm⁻¹) 3375, 1614, 1588, 1565; ¹H NMR (400 MHz, DMSO-d₆) δ: 6.92 (d, 2H, J=8.6 Hz), 7.49-7.52 (m, 2H), 7.75 (d, 2H J=8.68 Hz), 7.99-8.04 (m, 2H), 8.67-8.74 (m, 6H); ¹³C NMR (400 MHz, DMSO-d₆) δ: 160.2, 155.4, 155.1, 149.4, 149.2, 137.3, 128.0, 126.8, 124.3, 120.8, 116.8, 116.4; HR-MS [C₂₁H₁₅N₃O] ES:[M + H⁺] *m/z* Calcd 326.1215, found 326.1293. Additional spectral information is shown in Appendix I (Figs A-1.1 - A-1.3).

4.2.4. Preparation of MWCNT-COOH

Oxidation of MWCNTs was carried out as reported by Oyetade *et al.*⁷ and Santangelo *et al.*⁵³ In brief, pristine MWCNTs (1.5 g) were placed in a round-bottomed flask containing 100 cm³ of concentrated hydrochloric acid, and stirred for 4 h to remove residual metal impurities from the tubes. The resulting solution was filtered, and the solid washed with deionised water until a neutral pH was obtained. The sample obtained was dried in a vacuum oven at 80 °C overnight and stored in a desiccator for future analysis. The purified MWCNTs were then oxidized by using a mixture of sulfuric and nitric acids in a volume ratio of 1:3, and refluxed at 80 °C for 12 h. The resulting solution was diluted with deionised water, filtered, and the residue obtained was washed continuously with deionised water until a neutral pH was obtained.

4.2.5. Preparation of MWCNT-COCl

MWCNT-COOH (150 mg) were placed in a solution containing 30 cm³ of a 20:1 (v/v) mixture of SOCl₂ and dry DMF, and then refluxed at 70 °C for 24 h. The resulting mixture was filtered and the solid washed with anhydrous THF (5 × 5 cm³).⁵⁴ The solid was dried in a vacuum oven at 80 °C, and stored under an inert atmosphere of argon for further analysis.

4.2.6. Preparation of MWCNT-COOtpty

MWCNT-COCl (100 mg) were added to HO-Phttpty (100 mg) in a round-bottomed flask containing 20 cm³ of dry THF and 2-3 drops of glacial acetic acid. The mixture was refluxed at 64 °C for 24 h under an inert atmosphere of argon. After cooling to room temperature, the resulting suspension was filtered and the product obtained was washed with THF and dried in a vacuum oven at 80 °C overnight.

4.2.7. Functionalization of MWCNT-tpty

The reduction of MWCNT-COOtpty to obtain an ether was carried out as reported by Sakai *et al.*⁵⁵ MWCNT-COOtpty (100 mg), InBr₃ (10.6 mg, 0.03 mmol) and Et₃SiH (380 μL, 2.4 mmol) were added to a 30 cm³ solution of freshly distilled chloroform, and refluxed at 60 °C for 1 h under an inert atmosphere of argon. The suspension was filtered and the solid obtained was washed with chloroform, followed by water until a neutral pH was obtained. The resulting solid was dried in a vacuum oven at 80 °C overnight and stored in a desiccator for future analysis.

4.2.8. Adsorbate preparation

A standard stock solution of Cu²⁺ was prepared by dissolving approximately 1.0 g of pure copper metal into 50 cm³ of 5 mol dm⁻³ nitric acid. The solution was made up to 1000 dm³ with deionized water. From this solution, working solutions were prepared by diluting the stock solution in accurate proportions to obtain required concentrations.

4.2.9. Sorption experiments

The adsorption of Cu²⁺ on prepared adsorbents was investigated by using batch adsorption experiments. All adsorption experiments were conducted in duplicate by using 50 cm³ polypropylene plastic vials. Freshly prepared working solutions of 100 mg dm⁻³ Cu²⁺ were prepared from the stock solution daily. Adsorption experiments were performed by agitating 20 cm³ of a known Cu²⁺ concentration (100 mg dm⁻³) in a thermostated water bath at a fixed

temperature (20 °C) for 24 h with an adsorbent dose of 50 mg. The pH of the solution was adjusted by adding appropriate amounts of 0.1 mol dm⁻³ NaOH or HNO₃ to obtain the desired pH. After the required time interval, the mixtures were filtered and the final concentration of Cu²⁺ in the filtrate was determined by inductively coupled plasma-optical emission spectroscopy (ICP-OES) (PerkinElmer Optima 5300 DV). The operating conditions for ICP-OES are given in Appendix I (Table A-1.1). The effect of pH, amount of adsorbent, initial Cu²⁺ concentration, contact time and temperature was studied in order to determine the optimum conditions necessary for Cu²⁺ removal from aqueous solution. The adsorption efficiency (% adsorbed) and adsorption capacity (q_e) were calculated by using equations 4.1 and 4.2, respectively.

$$\% \text{ Adsorbed} = \left(\frac{C_i - C_{eq}}{C_i} \right) \times 100 \quad (4.1)$$

$$q_{eq} = \left(\frac{C_i - C_{eq}}{m} \right) \times V \quad (4.2)$$

C_i is the initial Cu²⁺ concentration (mg dm⁻³), C_{eq} is the equilibrium concentration of Cu²⁺ (mg dm⁻³), q_{eq} is the adsorption capacity (mg g⁻¹), m is the mass of the adsorbent (mg) and V is the volume (dm³) of the adsorbate solution used.

4.2.9.1. Kinetics, isotherm and thermodynamic studies

Kinetics studies were performed by agitating 20 cm³ aliquots of 100 mg dm⁻³ Cu²⁺ solution with an adsorbent dose of 50 mg. The mixture was placed in a thermostated water bath at 20 °C and agitated for different time intervals in the range of 5 to 1440 min. The pH of the solution was conditioned to 5 by using 0.1 mol dm⁻³ NaOH/HNO₃. After the pre-determined time intervals, the samples were filtered by gravity and the equilibrium concentration of Cu²⁺ determined by ICP-OES. The experimental data obtained were applied to the pseudo-first order, pseudo-second order, intraparticle diffusion and Elovich kinetics models given in Table 4.1.

Table 4.1: Kinetics models investigated for the adsorption of Cu²⁺

Model	Equation ^a	Parameters	References
Pseudo-first order	$q_t = q_{eq}(1 - e^{-k_1 t})$	q_{eq}, k_1	28,56,57
Pseudo-second order	$q_t = \frac{k_2 q_{eq}^2 t}{1 + k_2 q_{eq} t}$	k_2, q_{eq}	28,35,56-58
Elovich	$q_t = \frac{1}{\beta} \ln(\alpha\beta) + \frac{1}{\beta} \ln t$	α, β	59
Intraparticle diffusion	$q_t = k_{id} \sqrt{t} + l$	k_{id}, l	60

^a q_t , quantity of adsorbate adsorbed at time t (mg g⁻¹); q_{eq} , quantity of adsorbate adsorbed at equilibrium (mg g⁻¹); α , adsorption rate constant (mg g⁻¹ min⁻¹); β , desorption rate constant (g mg⁻¹); k_1 , pseudo-first order rate

constant (min^{-1}); k_2 , pseudo-second order rate constant ($\text{g mg}^{-1} \text{min}^{-1}$); k_{id} , intraparticle diffusion rate constant ($\text{mg g}^{-1} \text{min}^{0.5}$), l , is a constant related to the boundary layer thickness (mg g^{-1}).

Adsorption isotherms were investigated by using varying Cu^{2+} concentrations, ranging from 10–100 mg dm^{-3} , at a constant pH of 5. Aliquots of 20 cm^3 were mixed with 50 mg of the adsorbents and agitated on a thermostated shaking water bath under varying temperatures of 293, 303, 313 and 318 K for 24 h. The solutions were filtered by gravity and the concentrations of Cu^{2+} in the filtrates determined by ICP-OES. The experimental adsorption equilibrium data were analysed by the adsorption isotherm models given in Table 4.2. Thermodynamic parameters such as change in Gibbs energy (ΔG°), change in enthalpy (ΔH°), and change in entropy (ΔS°) were also calculated over the studied temperature range.

Table 4.2: Isotherm models investigated for the adsorption of Cu^{2+}

Isotherm model	Equation ^a	Parameters	References
Langmuir	$q_{eq} = \frac{q_m C_{eq} b}{1 + b C_{eq}}$	q_m, b	61
Freundlich	$q_{eq} = K_F C_{eq}^{1/n}$	K_F, n	62
Temkin	$q_{eq} = \frac{RT}{b_T} \ln(A_T C_{eq})$	b_T, A_T	63
Dubinin-Radushkevich	$q_{eq} = q_m e^{-\beta \varepsilon^2}$ $\varepsilon = RT \ln \left(1 + \frac{1}{C_{eq}} \right)$	q_m, β	64
Sips	$q_{eq} = \frac{b q_m C_{eq}^{1/n}}{1 + b C_{eq}^{1/n}}$	q_m, b, n	65
Toth	$q_{eq} = \frac{q_m C_{eq}}{\left(\frac{1}{K_T} + C_{eq}^{n_T} \right)^{1/n_T}}$	q_m, K_T, n_T	66
Redlich-Peterson	$q_{eq} = \frac{K_{RP} C_{eq}}{1 + \alpha_{RP} C_{eq}^g}$	K_{RP}, α_{RP}, g	67
Khan	$q_{eq} = \frac{q_m b_K C_{eq}}{(1 + b_K C_{eq})^{a_K}}$	q_m, a_K, b_K	68

^a q_{eq} , adsorption capacity (mg g^{-1}); C_{eq} , equilibrium concentration of adsorbate in solution (mg dm^{-3}); q_m , maximum monolayer capacity (mg g^{-1}); b , Langmuir isotherm constant ($\text{dm}^3 \text{mg}^{-1}$); K_F , Freundlich isotherm constant ($\text{mg g}^{-1}(\text{dm}^3 \text{mg}^{-1})^n$); n , adsorption intensity; b_T , Temkin isotherm constant; A_T , Temkin isotherm equilibrium binding constant ($\text{dm}^3 \text{g}^{-1}$); β , Dubinin-Radushkevich isotherm constant ($\text{mol}^2 \text{kJ}^{-2}$); K_T , Toth isotherm constant (mg g^{-1}); n_T , Toth isotherm constant; K_{RP} , Redlich-Peterson isotherm constant ($\text{dm}^3 \text{g}^{-1}$); α_{RP} , Redlich-Peterson isotherm constant; g , Redlich-Peterson isotherm exponent; a_k , Khan isotherm exponent; b_k , Khan isotherm constant.

4.2.9.2. Desorption experiments

Desorption studies were carried out by first contacting aliquots of 20 cm^3 of Cu^{2+} solution with a concentration of 100 mg dm^{-3} and an adsorbent dose of 50 mg for 24 h. The solution

was filtered and the loaded-adsorbent obtained was dried in a vacuum oven at 80 °C. The remaining Cu²⁺ in the filtrate was determined. A 50 mg mass of the loaded-adsorbent was added to a 10 cm³ aliquot of 0.1 mol dm⁻³ HCl and agitated for 30 min in a thermostated water bath at 20 °C. The concentration of Cu²⁺ desorbed was then determined by using ICP-OES.

4.2.10. Data analysis

The data obtained were fitted to the isotherm and kinetics models by means of the nls nonlinear regression routine in the R statistical computing environment.⁶⁹ The R statistical software takes into account the minimization of the sum of squared residuals (SSR) and the residual square errors (RSE). A comparison of all SSR and RSE values was done in order to assess the adequacy of the models. The model chosen was that with the lowest SSR.

4.3. Results and discussion

The ligand and nanomaterials synthesised were characterized by a series of techniques to ascertain the authenticity and properties of the adsorbents for Cu²⁺ removal. Subsequently, the efficiency of the novel material to adsorb Cu²⁺ was assessed and compared with that of acid-functionalized MWCNTs by means of batch adsorption processes.

4.3.1. Synthesis of 4'-(4-hydroxyphenyl)-2,2':6',2''-terpyridine (HO-Phttpy)

The synthesis of 4'-(4-hydroxyphenyl)-2,2':6',2''-terpyridine was carried out by using a “greener” synthetic approach as illustrated in Fig 4.1. The use of green solvents such as ethanol and water at room temperature affords an opportunity of obtaining products in moderate yields. Upon reacting 4-hydroxybenzaldehyde and 2-acetylpyridine in an ethanolic solution, a cream-coloured precipitate was formed. The completion of the reaction was monitored by thin layer chromatography (TLC) and FTIR and NMR spectroscopy. The formation of the product was confirmed by the disappearance of the carbonyl absorption band at ≈ 1700 cm⁻¹ and the appearance of sharp peaks at 1634 cm⁻¹ (C=N str), 1250-1335 cm⁻¹ (C-N str), 712 cm⁻¹ and 634 cm⁻¹ (indicating γ and δ Py-ring in-plane and out-of-plane deformation vibrations respectively) in the FTIR spectra (Fig 4.4c).⁷⁰⁻⁷² ¹H NMR spectrometry further confirmed the formation of the product by the disappearance of the methyl proton resonance peak (≈ 2.10 ppm) and the appearance of aromatic proton resonance peaks (≈ 7.5 -8.0 ppm) (see Fig A-1.1, Appendix I). Further verification of the product was done by ¹³C NMR and mass spectroscopy (see Fig A-1.3, Appendix I).

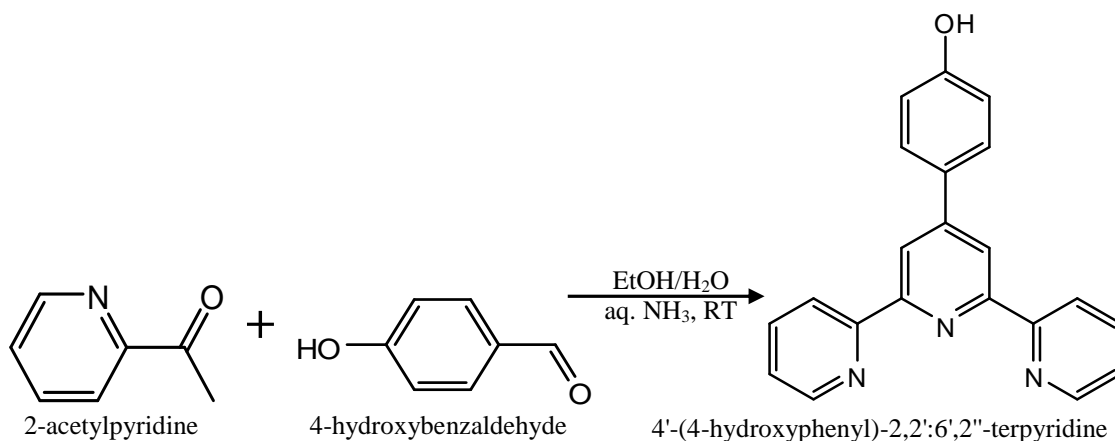


Fig 4.1: Synthesis of 4'-(4-hydroxyphenyl)-2,2':6',2''-terpyridine (HO-Phttpy).

4.3.2. Synthesis of MWCNT-ttpty

The synthesis of the novel nanomaterial was carried out first by the acylation of MWCNT-COOH with a mixture of SOCl_2 and DMF in a volume ratio of 20:1 as illustrated in Fig 4.2.

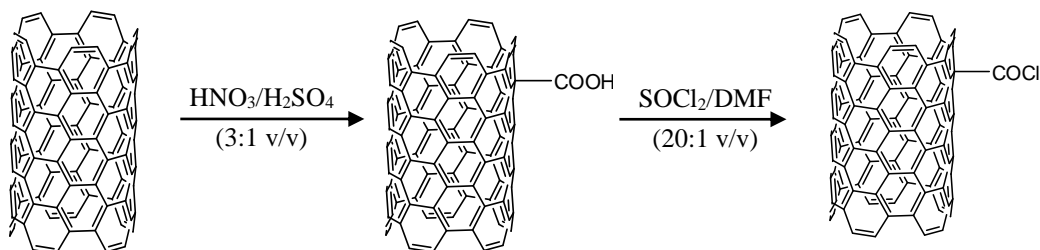


Fig 4.2: Acylation of pristine MWCNTs.

Acylated nanotubes (MWCNT-COCl) were further reacted in a mass ratio of 1:1 with HO-Phttpy to afford esterified MWCNTs (MWCNT-COOphtpy). Reduction of MWCNT-COOphtpy was carried out in distilled CHCl_3 , by using Et_3SiH as a reducing agent and InBr_3 as a catalyst, to afford ether-functionalized CNTs (MWCNT-ttpty). The route to the synthesis of MWCNT-ttpty is shown in Fig 4.3.

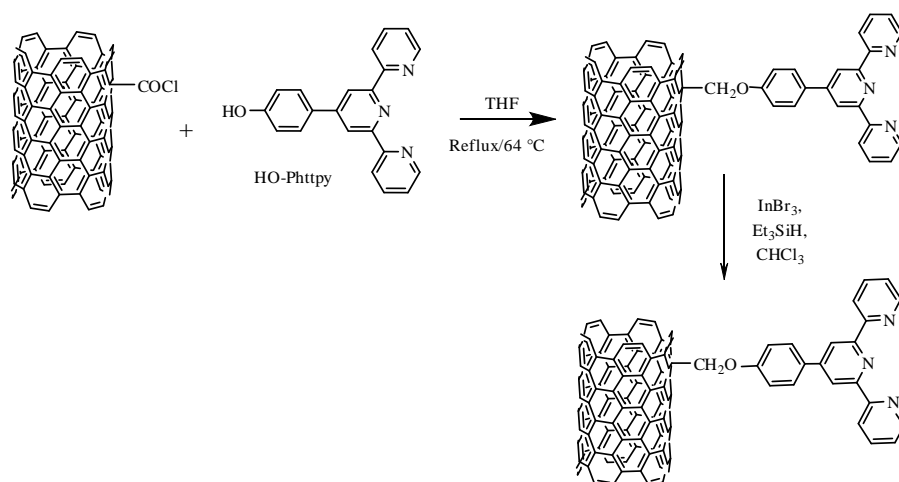


Fig 4.3: Route to the synthesis of MWCNT-ttpty.

4.3.3. Characterization of adsorbents

The synthesized products were characterized by FTIR spectroscopy. Fig 4.4 shows the FTIR spectra of (a) P-MWCNT, (b) MWCNT-COOH, (c) HO-Phttpty and (d) MWCNT-ttpty. For pristine MWCNTs (P-MWCNTs), the peaks observed at $\approx 1498\text{ cm}^{-1}$ are assigned to C=C stretching vibrations (Fig 4.4a) which are representative of graphitic structures characteristic of CNTs.¹ The peaks observed around ≈ 3500 and $\approx 2700\text{ cm}^{-1}$ are attributed to the presence of water molecules and carbon dioxide, respectively. Acidic functional groups such as carboxylic groups were introduced onto the walls of tubes after oxidation, hence a new peak at $\approx 1750\text{ cm}^{-1}$, assigned to C=O stretching, was noticeable (Fig 4.4b), indicating the presence of new groups after oxidation was carried out.³⁹ For HO-Phttpty (Fig 4.4c), peaks at 3050 cm^{-1} (aromatic C-H str), $1475\text{-}1585\text{ cm}^{-1}$ (aromatic C=C str), 1634 cm^{-1} (C=N str), $2890\text{-}2970\text{ cm}^{-1}$ (CH₂ and CH groups), 3500 cm^{-1} (O-H str), $1250\text{-}1335\text{ cm}^{-1}$ (C-N str), 712 cm^{-1} and 634 cm^{-1} (indicating γ and δ Py-ring in-plane and out-of-plane deformation vibrations respectively) were obtained.⁷⁰⁻⁷² Of importance to note is that MWCNT-ttpty (Fig 4.4d) showed a similar profile to that of the ligand (Fig 4.4c). This therefore confirms that the successful functionalization of MWCNT-COOH with HO-Phttpty was achieved, since functional groups characteristic to the ligand were present for MWCNT-ttpty.

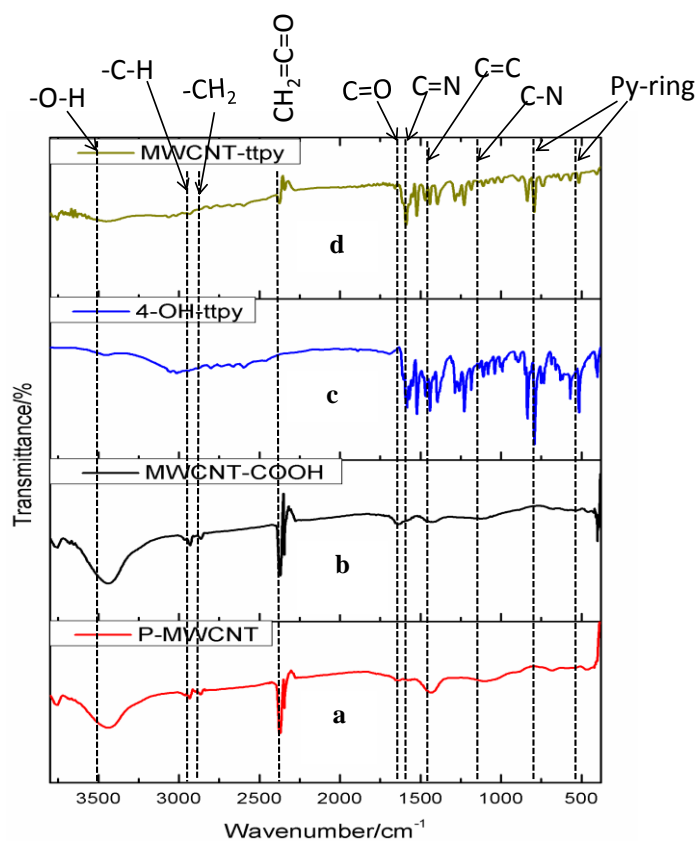


Fig 4.4: FTIR spectra of (a) P-MWCNT, (b) MWCNT-COOH, (c) HO-Phttpy and (d) MWCNT-ttpty.

To confirm the shape and structure, and determine the morphology of the synthesized adsorbents, images were collected from transmission electron microscopy (TEM) and scanning electron microscopy (SEM). The micrographs shown in Fig 4.5 represent the SEM images of (a) P-MWCNT, (b) MWCNT-COOH and (c) MWCNT-ttpty while Fig 4.6 shows the TEM images of (a) P-MWCNT, (b) MWCNT-COOH and (c) MWCNT-ttpty. As shown in Figs 4.5a and Fig 4.6a, a large entanglement of tubes was observed for P-MWCNT demonstrating a high presence of metal catalyst (shown with arrows) and amorphous carbon on the surface of the tubes. More alignment and less agglomeration was observed for MWCNT-COOH (*i.e.* tubes purified and functionalized with acids) (Fig 4.5b). This is in agreement with the study of Rosca *et al.*² Oxidation of CNTs accounts for the shortening of tubes, thereby introducing new functional groups, such as carboxylate groups, onto open ends of CNTs. Purification of CNTs removes the metal catalyst and amorphous carbon present on the surface of the tubes.¹ Also, Fig 4.6c further demonstrates that the tubular structure characteristic of MWCNTs was preserved after functionalization with the nitrogen ligand was carried out. A higher interspaced region was also noticed between tubes when compared with MWCNT-COOH (Fig 4.5b *vs.* 4.5c). The images shown in Fig 6a-b demonstrate the straight morphology for P-MWCNTs and MWCNT-COOH, while a

curved/bent morphology was obtained for MWCNT-ttpy (Fig 4.6c) due to the introduction of the ligand. Evidence of functionalization was also noted as long strands of CNTs were cut to obtain short and open-ended tubes.

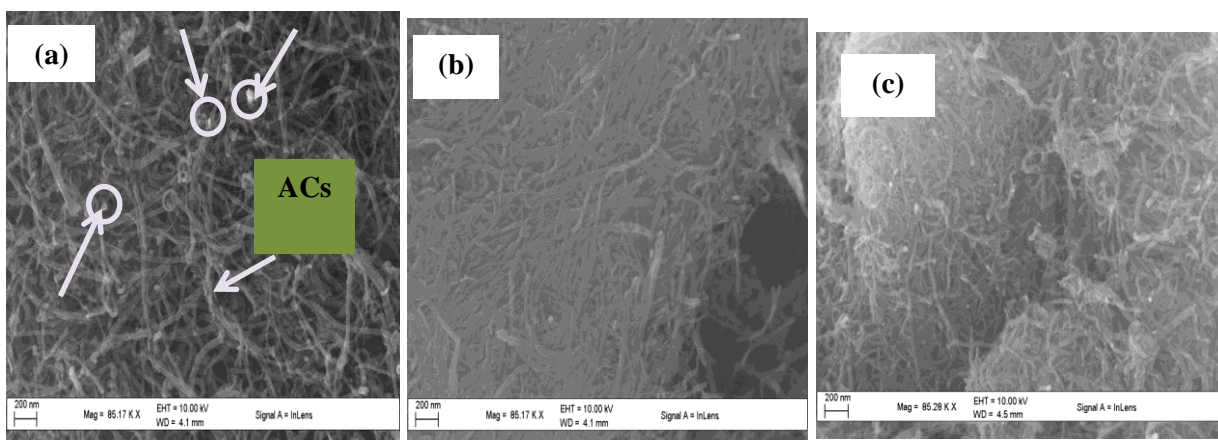


Fig 4.5: SEM images of (a) P-MWCNT, (b) MWCNT-COOH and (c) MWCNT-ttpy.

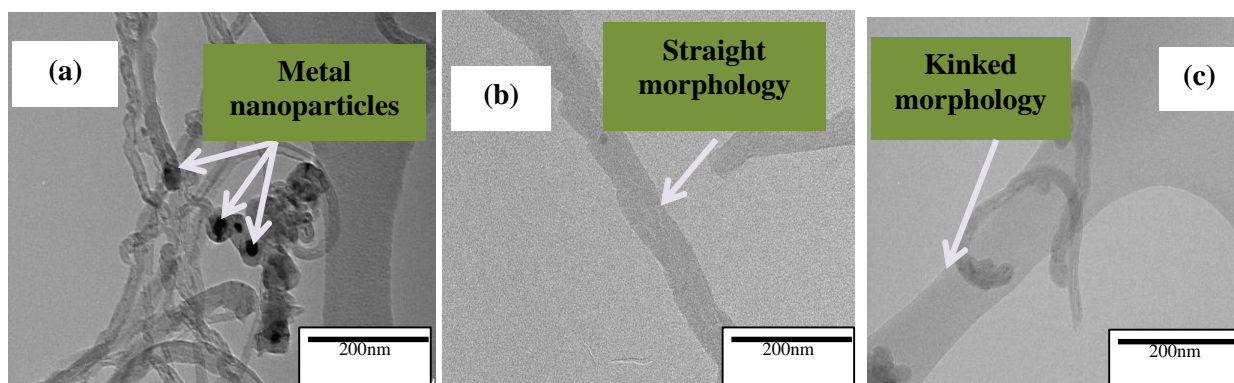


Fig 4.6: TEM images of (a) P-MWCNT, (b) MWCNT-COOH and (c) MWCNT-tpy.

In order to establish the thermal stability, purity and amount of volatile components in the synthesized adsorbents, thermogravimetric analysis (TGA) was carried out. Fig 4.7 represents the (a) thermograms (TGA) and (b) derivative thermograms (DTG) of P-MWCNT, MWCNT-COOH and MWCNT-ttpy. As observed from Fig 4.7a, both P-MWCNTs and MWCNT-COOH were more thermally stable than MWCNT-ttpy. A lower decomposition temperature was obtained for MWCNT-ttpy than for P-MWCNTs and MWCNT-COOH (Fig 4.7a). This could be attributed to the increase in defects induced by the functionalization of MWCNT-COOH. This result is consistent with data obtained from Raman spectroscopy (Table 4.4), which demonstrates that MWCNT-ttpy had a higher I_D/I_G

ratio than either P-MWCNTs or MWCNT-COOH. A higher ratio was also obtained for MWCNT-COOH when compared with P-MWCNTs. Hence, decreasing crystallinity in MWCNT-COOH and MWCNT-ttpy was associated with increasing functionalization, which thereby induces an increase in defects on P-MWCNTs, resulting in a larger I_D/I_G ratio. An increase in defective sites also accounts for a decrease in the decomposition temperature of MWCNT-COOH and MWCNT-ttpy obtained from TGA. The thermal stability of MWCNTs therefore increased in the order MWCNT-ttpy < MWCNT-COOH < P-MWCNTs. These results are consistent with recently published studies by Zhao *et al.*,¹ Ombaka *et al.*,⁷³ and Chizari *et al.*,⁷⁴ indicating that increasing functionalization results in a reduced decomposition temperature and larger I_D/I_G ratio. Purification of P-MWCNTs also resulted in the decrease of metal catalyst present in MWCNT-COOH (Fig 4.7a) as indicated by the residual mass remaining after 620 °C. Three thermal decomposition stages were obtained for MWCNT-ttpy. The first stage (in circle) showed a mass loss ($\Delta m = 9.88\%$) in the interval of 282-412 °C, suggesting the release of CH_4O (9.85%, calcd). The second decomposition step (shown with arrow) demonstrates a mass loss ($\Delta m = 35.84\%$) in the temperature range of 434-555 °C, suggesting the release of C_9H_6 (35.08%, calcd). The third decomposition step was observed for all three types of CNTs (*i.e.* P-MWCNTs, MWCNT-COOH and MWCNT-ttpy), representing the total decomposition of the graphitic structure of CNTs.

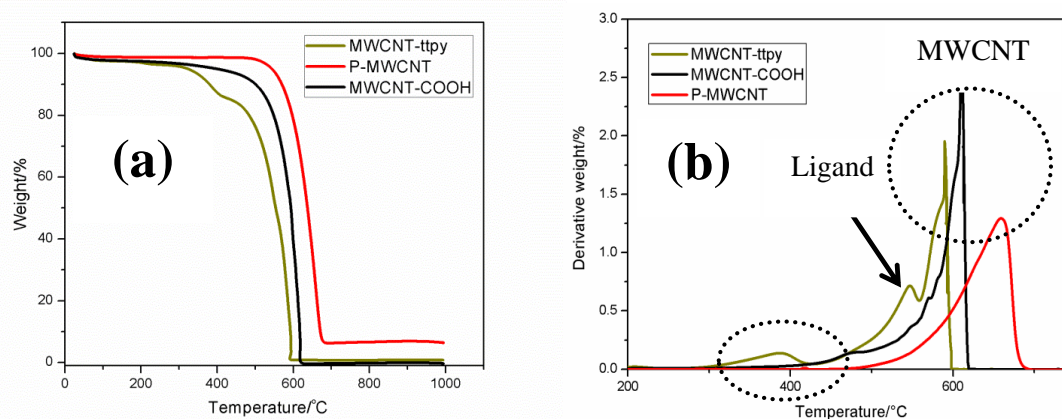


Fig 4.7: (a) Thermograms and (b) derivative thermograms of P-MWCNT, MWCNT-COOH and MWCNT-ttpy.

Elemental analysis of the adsorbents confirmed the presence of nitrogen atoms attached to the ligand on the MWCNT-ttpy. However, as expected, nitrogen atoms were absent in P-MWCNTs and MWCNT-COOH (Table 4.3). Thus, the presence of nitrogen atoms in MWCNT-ttpy confirms the successful functionalization of MWCNT-COOH with HO-Phttpy. The elemental analysis also showed an increase in the amount of oxygen in the order P-MWCNTs < MWCNT-COOH < MWCNT-ttpy. Acidic functionalization of P-MWCNTs

accounts for the increase in the oxygen content of MWCNT-COOH due to the incorporation of oxygen-containing functional groups onto the walls of tubes.⁷ An increase in the oxygen content of MWCNT-ttpy is accounted for by the functionalization of MWCNT-COOH, which introduces nitrogen and more oxygen atoms onto the tubes. This result is consistent with data obtained from the Boehm titration (Table 4.5) which demonstrates an increase in the surface acidic groups of the MWCNTs as the extent of functionalization increases.

Table 4.3: Elemental analysis of P-MWCNT, MWCNT-COOH and MWCNT-ttpy

Adsorbents	%C	%H	%O	%N	Relative ratio				General formula C _a H _b O _c N _d
					C	H	O	N	
P-MWCNT	97.34	-	2.656	-	1.000	-	0.021	-	(C ₄₈ O) _n
MWCNT-COOH	94.20	-	5.880	-	1.000	-	0.047	-	(C ₂₁ O) _n
MWCNT-ttpy	77.40	2.573	13.98	6.053	1.000	0.396	0.136	0.067	(C ₁₅ H ₆ O ₂ N) _n

The surface area of the adsorbents was noticed to increase in the order P-MWCNTs < MWCNT-COOH < MWCNT-ttpy (Table 4.4). The results obtained indicated an increase in surface area and pore volume of MWCNT-COOH when compared with P-MWCNT (Table 4.4, Entry 2 vs. 1). This is attributed to the treatment of P-MWCNT, which results in cutting of large entanglements of tubes (Fig 4.6a), thereby causing an increase in surface area and pore volume as observed in MWCNT-COOH.⁷³ Furthermore, an increase in surface area and pore volume of MWCNT-ttpy (Table 4.4, Entry 3 vs. 2) was obtained, due to increasing functionalization of MWCNT-COOH. This result confirms that surface area/pore volume of nanomaterials can be increased based on the extent of functionalization. All adsorbents were mesoporous in nature since the pore diameters were less than 50 nm. Hence, MWCNT-COOH and MWCNT-ttpy possess moderately large surface areas and increased pore volume, which might enhance faster and better sorption ability of the adsorbents for the removal of Cu²⁺ from aqueous solutions.

Table 4.4: Textural characterization of synthesized nanomaterials

Entry	Adsorbents	Surface area/m ² g ⁻¹	Pore volume/cm ³ g ⁻¹	Pore diameter/nm	I _D /I _G
1	P-MWCNT	108.8	0.494	18.44	1.17
2	MWCNT-COOH	126.8	0.692	22.95	1.19
3	MWCNT-ttpy	189.2	1.252	27.26	1.31

The nature of the acidic and basic functional groups on the adsorbents was determined by the Boehm titration method.^{48,50} Functionalization of P-MWCNT with acids markedly increased the concentration of carboxyl, phenolic and lactonic groups on MWCNT-COOH (Table 4.5). This was consistent with the FTIR spectra (Fig 4.4b) obtained, which revealed the appearance of a new peak at ≈ 1750 cm⁻¹ corresponding to the formation of carboxylic groups. This result conforms with data reported by Biniak *et al.*,⁴⁹ wherein an increase in

acidic properties was attributed to oxidation of adsorbents with acids. However, further functionalization with the nitrogen ligand decreased the concentration of the carboxyl groups but increased the concentrations of phenolic and lactonic groups. It is also worthy of note that an increase in the total number of basic groups of the adsorbents was observed as the extent of functionalization increased. MWCNT-ttpty contained the largest amount of basic groups justifying the presence of nitrogen-containing groups on the adsorbent.

Table 4.5: Surface chemistry of P-MWCNTs, MWCNT-COOH and MWCNT-ttpty determined by the Boehm titration method

Adsorbents	Carboxyl/ mmol g ⁻¹	Lactonic/ mmol g ⁻¹	Phenolic/ mmol g ⁻¹	Total acidic groups/mmol g ⁻¹	Total basic groups/mmol g ⁻¹	pH _{PZC}
P-MWCNTs	0.136	0.014	0.114	0.264	0.145	5.04
MWCNT-COOH	0.719	0.104	0.401	1.224	0.226	4.02
MWCNT-ttpty	0.613	0.165	0.544	1.322	0.752	4.48

4.4. Batch adsorption processes

Sorption processes were carried out to examine the effectiveness and efficiency of MWCNT-COOH and MWCNT-ttpty for the removal of Cu²⁺ from a simulated wastewater. The role of various parameters that influence adsorption such as pH, contact time, adsorbent dose, temperature and initial adsorbate concentration were investigated to ascertain the ideal conditions suited for Cu²⁺ removal. Kinetics, isotherm and thermodynamic studies were also carried out by using the data obtained.

4.4.1. Effect of pH

The extent of adsorption of Cu²⁺ onto the studied adsorbents was investigated at different pH values ranging from 1.0 to 10.0. Removal of Cu²⁺ from aqueous solution is usually influenced by the initial pH of the solution, since it influences the surface charges present on the adsorbent and the speciation of the metal ion in solution.⁷⁵ Fig 4.8b shows the speciation of Cu²⁺ as a function of pH in aqueous solution. Free Cu²⁺ exist only at pH values ≤ 5. Precipitation of Cu²⁺ as hydroxy species occurs when the pH of the solution is further increased.

A significant increase is noticed for the removal of Cu²⁺ from aqueous solution as the pH of the solution is increased (Fig 4.8a). The surface charge of the adsorbents is positive at pH values less than their pH_{PZC} (Table 4.5), resulting in a low removal of the adsorbate due to strong competitive activity between Cu²⁺ and H⁺ ions for active sites on the adsorbent.

Increasing the pH of the solution led to a decrease in H^+ , which enabled electrostatic attraction of Cu^{2+} onto the active sites of the adsorbents. Cationic adsorption is favourable at pH values higher than pH_{PZC} ;⁷⁶ hence, sorption of Cu^{2+} was propitious at pH conditions greater than 4.5. Higher removal efficiencies of Cu^{2+} were noticeable from pH 3 to 7 when MWCNT-ttpty was used as adsorbent. This is attributed to an increase in the number of chelating sites on the adsorbent, which permits strong binding between the nitrogen-donor atoms in the adsorbent and Cu^{2+} . Modification of MWCNT-COOH with HO-Phttpty significantly improved the textural properties of MWCNT-COOH, resulting in an increase in surface area, pore volume (Table 4.4) and active sites on MWCNT-ttpty (Table 4.5), hence, enabling better sorption ability for Cu^{2+} removal. Although the data suggest that pH 7 is optimal for the removal of Cu^{2+} , further adsorption studies were carried out at a pH value of 5, in order to limit the effect of precipitation on Cu^{2+} removal.

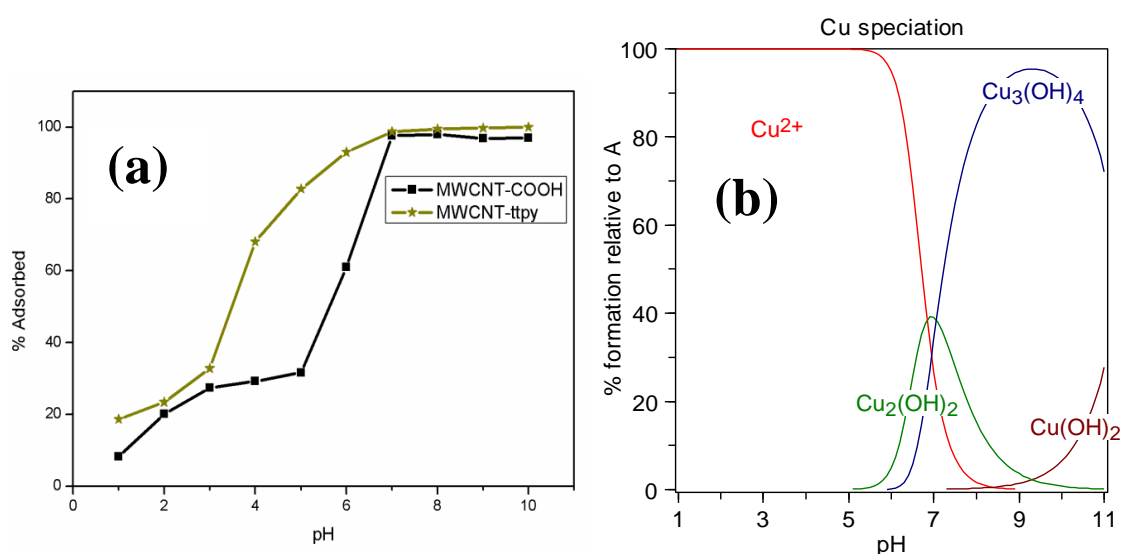


Fig 4.8: (a) Effect of pH on sorption of Cu^{2+} onto MWCNT-COOH and MWCNT-ttpty, [conditions: 20 cm^3 of 100 mg dm^{-3} Cu^{2+} , 24 h equilibration time, 50 mg adsorbent dose, agitation speed 150 rpm, temperature $20\text{ }^\circ\text{C}$] and (b) speciation of Cu^{2+} as a function of pH in aqueous solution (as calculated by HySS speciation software).⁷⁷

4.4.2. Effect of contact time

The effect of contact time for the adsorption of Cu^{2+} was examined at varying time intervals, between 5 and 1440 min, while keeping the initial Cu^{2+} concentration (100 mg dm^{-3}), pH (5.0) and adsorbent dose (50 mg) constant. The percentage removal of Cu^{2+} onto the studied adsorbents was noticeably increased with time, attaining equilibrium for MWCNT-COOH and MWCNT-ttpty at 180 min and 360 min, respectively (Fig 4.9). After this stage, the percent adsorption was observed to remain steady with little or no further increase. Initially, more active sites are available for adsorption, hence, enabling faster removal. As the binding

sites on the surface of the adsorbents were occupied, further removal of Cu^{2+} was observed to be minimal. Though adsorption was rapid in both adsorbents, MWCNT-ttpy exhibited higher removal efficiency at each time than MWCNT-COOH. This could be attributed to the greater number of chelating sites on MWCNT-ttpy, induced through the functionalization of MWCNT-COOH with a nitrogen-containing compound. In this study, the maximum time for agitation was fixed at 24 h to ascertain the complete removal of Cu^{2+} from aqueous solutions under all conditions.

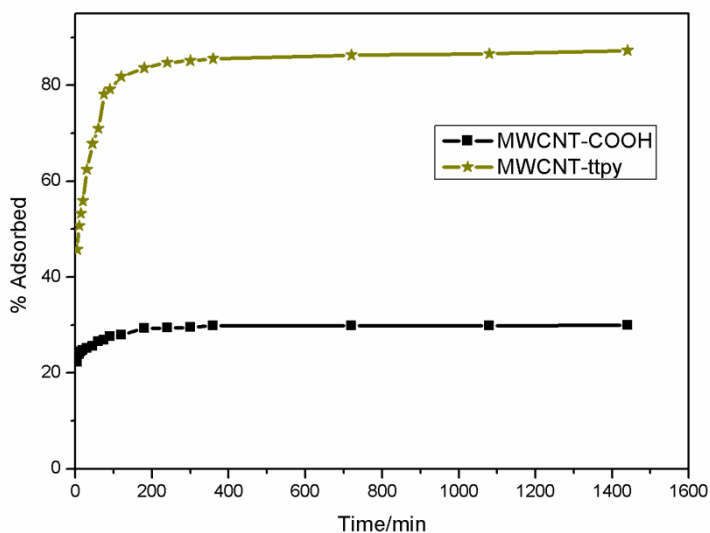


Fig 4.9: Effect of contact time for the adsorption of Cu^{2+} onto MWCNT-COOH and MWCNT-ttpy [conditions: 20 cm^3 of $100 \text{ mg dm}^{-3} \text{ Cu}^{2+}$, 50 mg adsorbent dose, pH 5.0, agitation speed 150 rpm, temperature $20 \text{ }^\circ\text{C}$].

4.4.3. Kinetics studies

Four kinetics models, namely, the pseudo-first order, pseudo-second order, Elovich and intraparticle diffusion models were applied to the experimental data in order to determine the dynamics and rate-determining step of the adsorption process. Table 4.1 gives the equations of the models used in this study in a non-linear form. The obtained experimental data were fitted into kinetics models by non-linear least square (NLLS) analysis. Previous studies have shown that to eliminate error distributions associated with models in linearized forms, NLLS analysis^{57,78,79} is a preferred choice. The curves showing a comparison of all the kinetics models fitted for the adsorption of Cu^{2+} onto MWCNT-COOH and MWCNT-ttpy are shown in Appendix I (Fig A-1.4). Data illustrating the comparison of all models with their associated sum of squared residuals (SSR) and residual square errors (RSE) is given in Table 4.6. It was observed that the data for MWCNT-ttpy best fit the pseudo-second order model, while that for MWCNT-COOH fit the Elovich model better as reflected by the lowest SSR values (Table 4.6). The pseudo-second order model assumes that the rate-limiting step for Cu^{2+} adsorption may be due to interaction through sharing or exchange

of electrons between hydroxyl/nitrogen groups and Cu^{2+} .^{28,44,58,80} Hence, this indicates that the rate of removal of Cu^{2+} from aqueous solution was determined by a bimolecular interaction between the adsorbate and active sites on the adsorbents. Similar results have been reported by Ho and McKay,⁸⁰ Popuri *et al.*,⁴⁴ Mobasherpour *et al.*,¹⁹ and Yu *et al.*,⁸¹ for removal of Cu^{2+} from aqueous solutions. The Elovich model is also based on the concept of chemisorption⁵⁸ (*i.e.* the interaction through sharing or exchange of electrons). This further elucidates that the adsorption of Cu^{2+} onto both adsorbents proceeds *via* chemical interactions between the active groups on adsorbents and cationic Cu^{2+} .

Adsorption proceeds *via* one/more of these four stages: (i) The transfer of solute from the solution to the surface of the adsorbent, (ii) solute transfer from the bulk solution to the boundary film which surrounds the adsorbent surface (film diffusion), (iii) solute transfer through the internal pores of the adsorbent (intraparticle diffusion), and (iv) interaction between adsorbate molecules with the active sites on the external surface of the adsorbent. One of these processes usually determines the rate at which the adsorbate is removed from aqueous solutions. To further elucidate on the diffusion mechanism involved in adsorption, experimental data were modelled with the intraparticle diffusion model. A plot of q_t against \sqrt{t} was plotted to obtain a straight line which did not pass through the origin. This indicates that adsorption proceeded through the intraparticle diffusion of Cu^{2+} to the pores of the adsorbent; however, it was not the only rate-controlling step.⁸²⁻⁸⁴ Adsorption therefore occurred *via* a multi-step process involving an initial rapid stage, followed by the intraparticle diffusion of adsorbates to the pores of adsorbents and then to a slower phase which proceeds towards saturation due to low adsorbate concentration.⁷⁸ Higher k_{id} and l values were obtained for MWCNT-ttpy than MWCNT-COOH, showing that adsorption was boundary-controlled and indicates better Cu^{2+} removal for MWCNT-ttpy.

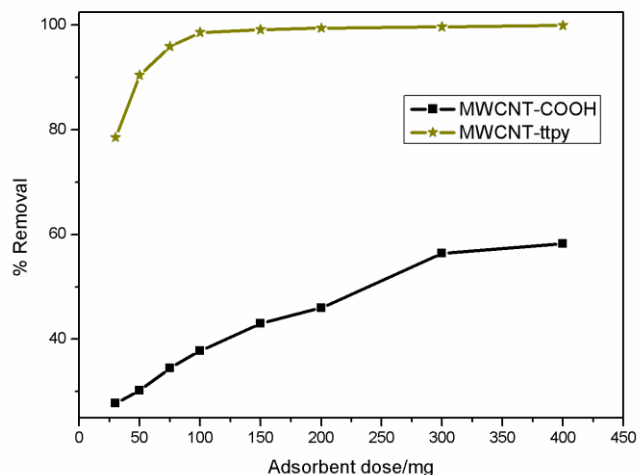


Fig 4.10: Effect of adsorbent dose for the adsorption of Cu^{2+} onto MWCNT-COOH and MWCNT-ttpy [conditions: 20 cm^3 of $100 \text{ mg dm}^{-3} \text{ Cu}^{2+}$, 24 h equilibration time, pH 5.0, agitation speed 150 rpm, temperature $20 \text{ }^\circ\text{C}$].

4.4.5. Effect of initial adsorbate concentration

The influence of increasing the adsorbate concentration was examined for different Cu^{2+} concentrations, ranging from 10-100 mg dm^{-3} , on MWCNT-COOH and MWCNT-ttpy. A decrease in the percentage removal of Cu^{2+} from 98.2% to 47.6% and 100.0% to 78.9% was obtained for MWCNT-COOH and MWCNT-ttpy, respectively. This could be attributed to the greater number of active sites available at lower Cu^{2+} concentrations, resulting in higher removal efficiencies. However, saturation of active sites occurred at higher concentrations, resulting in lower removal efficiencies. Also, an increase in the amount of Cu^{2+} removed per unit mass from 3.87 to 19.01 mg g^{-1} and 3.94 to 31.89 mg g^{-1} was obtained for MWCNT-COOH and MWCNT-ttpy, respectively. Higher initial concentrations of Cu^{2+} enhanced the adsorption process, due to an increase in the driving force by overcoming mass transfer resistance between the solid-solution interface.⁷⁵ Similar trends for the removal of Cu^{2+} from aqueous solution as concentration is varied have been reported by Tong *et al.*,⁷⁵ Ekmekyapar *et al.*,⁸⁵ and Yu *et al.*⁸¹

4.4.6. Effect of temperature

Increasing the adsorbate temperature results in an increase in the rate of diffusion across the external boundary layer, decreases the viscosity of the solution and increases the internal pores of the adsorbents.⁸⁶ The extent of adsorption was investigated over the temperature range of 293-318 K. An increase in the adsorption capacity (q_{eq}) with an increase in temperature was obtained for MWCNT-ttpy (Fig 4.11b), whereas a decrease in q_{eq} was obtained with increasing temperature for MWCNT-COOH (Fig 4.11a). An increase in

temperature favours faster mobility of Cu^{2+} , as was the case of MWCNT-ttpty, hence resulting in higher q_{eq} values. Also, higher Cu^{2+} uptake by MWCNT-ttpty at higher temperatures may be attributed to an increase in the porosity and pore volumes of adsorbents, hence, enabling the pores for better uptake of adsorbate.⁷ However, increasing the adsorbate temperature also results in a decrease of the physical adsorptive forces responsible for adsorption. This phenomenon was observed for MWCNT-COOH (Fig 4.11a), and resulted in a decrease in q_{eq} values as the temperature of the adsorbate increased. Fig 4.11a also showed a significant change in q_{eq} with temperature variation for MWCNT-COOH, whereas very little effect was observed for MWCNT-ttpty with change in temperature (Fig 4.11b). This illustrates that MWCNT-ttpty will be effective for Cu^{2+} removal, and could prove advantageous regardless of change in temperature. Also, the application of MWCNT-ttpty will be sufficient for the removal of Cu^{2+} at point source, as effluents are normally discharged at above ambient temperatures. It is also worthy of note that the amount adsorbed (q_{eq}) by MWCNT-ttpty was also greater than for MWCNT-COOH at all temperatures.

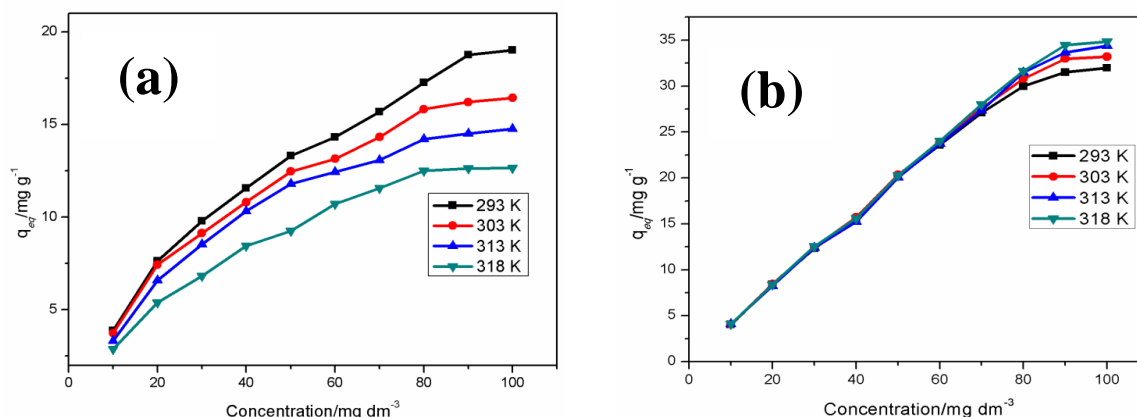


Fig 4.11: Effect of varying temperature on the adsorption of Cu^{2+} by (a) MWCNT-COOH and (b) MWCNT-ttpty.

4.4.7. Adsorption isotherms

Adsorption isotherms are usually used to describe how adsorbate molecules/ions interact with the active sites on the surface of the adsorbent and to optimize adsorbent use for large-scale removal.⁷ Eight isotherms, including two- and three- parameter models, namely, Langmuir, Freundlich, Temkin, Dubinin-Radushevick (D-R), Sips, Toth, Redlich-Peterson (R-P) and Khan, were applied to the equilibrium data obtained in this study. The equations for the isotherms are given in Table 4.2. NLLS analysis was used to fit the data and the lowest sum of squared residuals (SSR) gave an indication of the best fit for the equilibrium data obtained. The parameters obtained for the adsorption of Cu^{2+} onto MWCNT-COOH and MWCNT-ttpty are presented in Table 4.7.

Table 4.7 demonstrates that the Freundlich isotherm best describes the experimental data obtained for MWCNT-COOH, while the Langmuir isotherm best described the data obtained for MWCNT-ttpy. The curves for the best-fit isotherms for MWCNT-COOH and MWCNT-ttpy are shown in Appendix I (Fig A-1.5 – A-1.6). The Langmuir maximum adsorption capacity (q_m) varied from 15.50 to 19.44 mg g⁻¹ and 31.65 to 34.13 mg g⁻¹ for MWCNT-COOH and MWCNT-ttpy, respectively over the studied temperature range. Table 4.7 further indicates a decrease in q_m as the temperature of the adsorbate solution was increased for MWCNT-COOH, whereas an increase in q_m was obtained with increasing temperature for MWCNT-ttpy. The Langmuir adsorption constant, b (Table 4.7), indicating the high adsorptive binding power obtained for MWCNT-ttpy, is indicative of good adsorptive forces resulting in the enhancement of the binding strength as the temperature is increased.

Table 4.7: Isotherm parameters for the adsorption of Cu²⁺ onto MWCNT-COOH and MWCNT-ttpy

Isotherm	Parameter	MWCNT-COOH				MWCNT-ttpy			
		293 K	303 K	313 K	318 K	293 K	303 K	313 K	318 K
Langmuir	$q_m/\text{mg g}^{-1}$	19.44	16.87	16.35	15.59	31.65	33.04	34.13	33.97
	$b/\text{dm}^3 \text{mg}^{-1}$	0.169	0.184	0.123	0.068	3.243	5.494	9.065	17.25
	RSE ^a	1.887	1.386	0.510	0.478	1.966	3.302	3.176	5.670
	SSR ^b	28.48	15.37	2.077	1.828	30.91	87.25	80.71	257.2
Freundlich	K_F	5.244	4.756	3.876	2.533	20.40	23.88	26.05	28.54
	n	3.056	3.188	2.964	2.507	5.344	6.641	7.006	8.991
	RSE	0.604	0.575	0.701	0.585	3.425	4.295	4.589	5.951
	SSR	2.922	2.644	3.926	2.740	93.84	147.6	168.5	283.3

^aRSE - residual square error

^bSSR - sum of squared residuals

The amount of area on the adsorbent covered by Cu²⁺ can be established by dividing the theoretical specific surface area (S) into the BET surface area. The theoretical surface area was calculated by using equation (4.3) as described by Ho *et al.*⁸⁷

$$S = \frac{q_m N_A A}{M} \quad (4.3)$$

S is the area covered by the adsorbed Cu²⁺, N_A is Avogadro's constant, A is the cross-sectional area of Cu²⁺ ($1.58 \times 10^{-20} \text{ m}^2$)⁸⁷ and M is the molar mass of Cu²⁺. The values obtained for S at 20 °C for MWCNT-COOH and MWCNT-ttpy were calculated as 2.91 and 4.74 m² g⁻¹, respectively. As given by Table 4.4, the BET surface area of MWCNT-COOH and MWCNT-ttpy was 126.8 and 189.2 m² g⁻¹, respectively. Hence, the percentage of adsorbent surface covered by Cu²⁺ was calculated as 2.30% and 2.51%, respectively. Equally, q_m values at 20 °C were compared with the total number of acidic and basic groups

in MWCNT-COOH and MWCNT-ttpe determined by the Boehm titration (Table 4.5). The values obtained indicated that 25.0% of acidic groups on MWCNT-COOH and 66.2% of basic groups on MWCNT-ttpe were primarily involved in adsorption of Cu^{2+} onto active sites of adsorbents. These results indicate that chelation of Cu^{2+} with nitrogen-donor atoms in MWCNT-ttpe and electrostatic interactions with oxygen atoms in MWCNT-COOH were primarily responsible for interaction in this study. Hence, adsorption of Cu^{2+} could be said to be enhanced significantly due to the presence of N donor atoms on MWCNT-ttpe.

Also, as suggested by Hamza *et al.*⁸⁸ and Soon-An *et al.*,⁸⁹ the nature of the adsorption process can be estimated depending on the values of the separation factor (R_L) as expressed in equation (4.4). Adsorption is assumed to be favourable if $0 < R_L < 1$, unfavourable if $R_L > 1$, irreversible if $R_L = 0$ and linear if $R_L = 1$.⁸⁸⁻⁹⁰

$$R_L = \frac{1}{1+bC_i} \quad (4.4)$$

C_i is the initial Cu^{2+} concentration (mg dm^{-3}) and b is the Langmuir constant obtained from Table 4.7 ($\text{dm}^3 \text{mg}^{-1}$). All R_L values obtained in this study were found to fall between $0 < R_L < 1$, hence adsorption of Cu^{2+} onto MWCNT-COOH and MWCNT-ttpe indicates a favourable adsorption.

The Langmuir isotherm assumes monolayer coverage of adsorbates onto the surface of the adsorbent, while the Freundlich isotherm assumes that the surface of adsorbents is heterogeneous in nature.⁷ Since MWCNT-ttpe fits the Langmuir isotherm, it can be inferred that the active sites on this adsorbent are equivalent with a uniform surface, hence, the adsorbed Cu^{2+} ions on this adsorbent do not interact with each other, achieving monolayer coverage of the adsorbate. In the case of MWCNT-COOH, the values of the Freundlich constant n indicate a favourable adsorption process since values were ≤ 10 (see Table 4.7).⁷⁵

Table 4.8 shows the results of some previously published studies investigating the sorption process of Cu^{2+} from aqueous solutions onto carbon-structured materials. These results were compared with those obtained in this study. A significant increase in sorption uptake of Cu^{2+} was obtained by using MWCNT-ttpe in comparison with 8-hydroxyquinoline-functionalized MWCNTs (8-HQ-MWCNT), also functionalized with a N-donor ligand but of lower density. Table 4.8 further demonstrates better uptake of Cu^{2+} on MWCNT-ttpe in comparison with composite adsorbents such as MWCNT/bagasse and MWCNT/ Fe_2O_4 . Thus, the results reported in this study compare very favourably with data obtained from other studies.

Table 4.8: Comparison of Langmuir maximum capacity (q_m) for Cu^{2+} adsorbed onto various carbon-structured materials

Adsorbents	Conditions	$q_m/\text{mg g}^{-1}$	References
P-MWCNTs	pH 7.0, C_i 1.0 mg dm^{-3} , 250 mg dose, 120 min, 298 K	0.080	91
P-MWCNTs	pH 7.0, C_i 0.5 mg dm^{-3} , 125 mg dose, 120 min, 298 K	0.398	27
MWCNT-COOH	pH 7.0, C_i 20 mg dm^{-3} , 30 mg dose, 120 min, 293 K	12.34	19
8-HQ-MWCNT	pH 7.0, C_i 1.0 mg dm^{-3} , 250 mg dose, 120 min, 298 K	0.080	91
MWCNT/bagasse	pH 5.5, 100 mg dm^{-3} , 50 mg dose, 360 min, 301 K	15.60	41
MWCNT/ Fe_2O_4	pH 5.50, 10 mg dm^{-3} , 40 h, 353 K	8.920	43
MWCNT-COOH	pH 5.0, C_i 100 mg dm^{-3} , 50 mg dose, 24 h, 293 K	19.44	This study
MWCNT-ttpty	pH 5.0, C_i 100 mg dm^{-3} , 50 mg dose, 24 h, 293 K	31.65	This study

4.4.8. Thermodynamic parameters of adsorption

Thermodynamic parameters such as change in enthalpy (ΔH°), change in entropy (ΔS°) and change in Gibbs energy (ΔG°), were studied in order to examine the spontaneity of the adsorption process at varying temperatures. An adsorption process is considered feasible and spontaneous if negative values for ΔG° are obtained. The process is endothermic if the adsorption capacity (q_{eq}) increased with an increase in temperature and the reverse yields an exothermic process.

The change in Gibbs energy of adsorption (ΔG°) is calculated thus (equation 4.5):²⁸

$$\Delta G^\circ = -RT \ln K \quad (4.5)$$

where ΔG° is the standard Gibbs energy change (J mol^{-1}), R is the universal gas constant ($8.314 \text{ J K}^{-1} \text{ mol}^{-1}$), and T is the absolute temperature in Kelvin. The value of K was obtained from the product of q_m and b obtained from the Langmuir plot (Table 4.5).^{88,92} The value of K was corrected to be dimensionless by multiplying by 1000.⁹³

A plot of $\ln K$ against $1/T$ was found to be linear, and the values of ΔH° and ΔS° were obtained from the slope and intercept of the plot, respectively, according to the Van't Hoff equation (Eq. 4.6):

$$\ln K = -\frac{\Delta H^\circ}{RT} + \frac{\Delta S^\circ}{R} \quad (4.6)$$

Table 4.9 presents the thermodynamic parameters for the adsorption of Cu^{2+} onto MWCNT-COOH and MWCNT-ttpty. Negative values were obtained for ΔG° , indicating that the process was spontaneous and feasible for both adsorbents. An increase in negative values for ΔG° was obtained as the temperature of the adsorbate solution was increased for

MWCNT-ttpty. This confirms that increasing the temperature of the adsorbate solution resulted in better sorption for the adsorbent. In contrast, a decrease in the negative values of ΔG° was obtained as temperature is increased when MWCNT-COOH was used as adsorbent. An exothermic process of adsorption was obtained with MWCNT-COOH, indicated by the negative ΔH° value obtained. On the other hand, the application of MWCNT-ttpty as adsorbent yielded an endothermic process, which is confirmed by the positive ΔH° value obtained.

Table 4.9 further shows a positive ΔS° value for MWCNT-ttpty, which indicates an increase in the disorderliness at the solid/solution interface resulting in a favourable adsorption process. However, a negative ΔS° was obtained for MWCNT-COOH indicating a decrease in disorderliness as the adsorbent interacts with the adsorbate. Hence, the adsorption process for MWCNT-ttpty is entropy-driven, while the process is enthalpy-driven for MWCNT-COOH. The values of ΔH° obtained show that the heat evolved/absorbed was greater than for physisorption (2.1-20.9 kJ mol⁻¹), but lower than for chemisorption processes (80-200 kJ mol⁻¹).^{7,94} This indicates that the process for the removal of Cu²⁺ from aqueous solutions by using MWCNT-COOH and MWCNT-ttpty was a physico-chemical process,⁹⁴ indicating that adsorption was facilitated by both processes.

Thermodynamic parameters therefore suggest that the application of MWCNT-ttpty will be effective for remediating metal-polluted effluents discharged directly from industries.

Table 4.9: Thermodynamic parameters for the adsorption of Cu²⁺ onto MWCNT-COOH and MWCNT-ttpty

Adsorbent	T/K	$\Delta G^\circ/\text{kJ mol}^{-1}$	$\Delta H^\circ/\text{kJ mol}^{-1}$	$\Delta S^\circ/\text{J K}^{-1} \text{mol}^{-1}$
MWCNT-COOH	293	-19.72		
	303	-20.26		
	313	-19.79	-32.36	-99.19
	318	-18.42		
MWCNT-ttpty	293	-28.11		
	303	-30.50		
	313	-32.90	50.97	211.9
	318	-35.11		

4.4.9. Desorption studies

The process of desorption regenerates an adsorbent for reuse, thereby reducing the cost and availability of sorbents for adsorption. This process also limits the introduction of spent adsorbents into the environment, thereby limiting the disposal of secondary pollutants. Desorption experiments were carried out by agitating a Cu²⁺-loaded adsorbent with 10 cm³

of 0.1 mol dm^{-3} HCl in a thermostated water bath at $20 \text{ }^{\circ}\text{C}$ for 30 min. The mixture was filtered and the final concentration of Cu^{2+} determined. Results obtained showed good removal capacities of 62% and 73% for MWCNT-COOH and MWCNT-ttpty respectively, indicating that these adsorbents can be regenerated and Cu^{2+} can be recovered for reuse. Again, in this respect MWCNT-ttpty performed better, showing better desorption of Cu^{2+} than MWCNT-COOH.

4.5. Conclusions

A novel nanomaterial, synthesized by the use of 4'-(4-hydroxyphenyl)-2,2':6,2''-terpyridine as a modifier for acid-functionalized multiwalled carbon nanotubes (MWCNT-COOH), to produce nitrogen-functionalized MWCNTs (MWCNT-ttpty), was successfully synthesized. The adsorbent proved effective and efficient for the removal of Cu^{2+} from aqueous solutions, obtaining a higher Langmuir monolayer adsorption capacity (q_m) of 31.65 mg g^{-1} than the 19.44 mg g^{-1} obtained for MWCNT-COOH. Also, a higher sorption uptake of Cu^{2+} was exhibited by MWCNT-ttpty when compared with other MWCNT-containing sorbents from other studies.

This study revealed that MWCNT-ttpty can be used as an alternative adsorbent for the removal of heavy metal ions from municipal wastewater and industrial effluents, due to the high efficiency exhibited towards Cu^{2+} removal from aqueous solution. The recyclability and regeneration of this adsorbent was successful, suggesting that the spent adsorbent and Cu^{2+} can be recovered and made available for reuse.

References

1. Z. Zhao, Z. Yang, Y. Huc, J. Li and X. Fan, *Appl. Surf. Sci.*, 2013, **276**, 476-481.
2. I. D. Rosca, F. Watari, M. Uo and T. Akasaka, *Carbon*, 2005, **43**, 3124-3131.
3. N. Arora and N. N. Sharma, *Diam. Relat. Mater.*, 2014, **50**, 135-150.
4. K. Balasubramanian and M. Burghard, *Small*, 2005, **1**, 180-192.
5. L. M. Ombaka, P. Ndungu and V. O. Nyamori, *Catal. Today*, 2013, **217**, 65-75.
6. B. Pan and B. Xing, *Environ. Sci. Technol.*, 2008, **42**, 9005-9013.
7. O. A. Oyetade, V. O. Nyamori, B. S. Martincigh and S. B. Jonnalagadda, *RSC Adv.*, 2015, **5**, 22724-22739.
8. A. Bianco, K. Kostarelos and M. Prato, *Curr. Opin. Chem. Biol.*, 2005, **9**, 674-679.
9. M. Chua and C.-K. Chui, *J. Mech. Behav. Biomed. Mater.*, 2015, **44**, 164-172.
10. O. Kanoun, C. Müller, A. Benchirouf, A. Sanli, T. N. Dinh, A. Al-Hamry, L. Bu, C. Gerlach and A. Bouhamed, *Sensors*, 2014, **14**, 10042-10071.
11. G. Keru, P. G. Ndungu and V. O. Nyamori, *Int. J. Energy Res.*, 2014, **38**, 1635-1653.
12. A. M. W. Cargill Thompson, *Coord. Chem. Rev.*, 1997, **160**, 1-52.
13. L. Hou and D. Li, *Inorg. Chem. Commun.*, 2005, **8**, 190-193.
14. M. B. Ogundiran, O. A. Oyetade, J. O. Babayemi and O. Osibanjo, *Int. J. Environ. Waste Manag.*, 2014, **13**, 115-130.
15. J. W. Gartell, *Anim. Prod. Sci.*, 1980, **20**, 370-376.
16. R. Rosenberg, D. Edelstein, C.-K. Hu and K. Rodbell, *Annu. Rev. Mater. Sci.*, 2000, **30**, 229-262.
17. J. Gabbay, G. Borkow, J. Mishal, E. Magen, R. Zatzoff and Y. Shemer-A., *J. Ind. Tex.*, 2006, **35**, 323-335.
18. D. W. McCarthy, L. A. Bass, P. D. Cutler, R. E. Shefer, R. E. Klinkowstein, P. Herrero, J. S. Lewis, C. S. Cutler, C. J. Anderson and M. J. Welch, *Nucl. Med. Biol.*, 1999, **26**, 351-358.
19. I. Mobasherpour, E. Salahi and M. Ebrahimi, *J. Saudi Chem. Soc.*, 2014, **18**, 792-801.
20. B. N. Agarwal, S. Bray, P. Bercz, R. Plotzker and E. Labovitz, *Nephron*, 1975, **15**, 74-77.
21. C. M. A. Iwegbue, *Vet. Arhiv.*, 2008, **78**, 401-410.
22. A. Sinkovič, A. Strdin and F. Svenšek, *Arh Hig Rada Toksikol.*, 2008, **59**, 31-35.
23. I. Giannopoulou and D. Papias, *Hydrometallurgy*, 2008, **90**, 137-146.
24. S. Rengaraj, Y. Kim, C. K. Joo, K. Choi and J. Yi, *Korean J. Chem. Eng.*, 2004, **21**, 187-194.
25. C.-C. Tung, Y.-M. Yang, C.-H. Chang and J.-R. Maa, *Waste Manage.*, 2002, **22**, 695-701.

26. L. Feini, Z. Guoliang, M. Qin and Z. Hongzi *Chin. J. Chem. Eng.*, 2008, **16**, 441-445.
27. M. Abdel Salam, *Int. J. Env. Sci. Technol.*, 2013, **10**, 677-688.
28. Y.-S. Ho, *Water Res.*, 2003, **37**, 2323-2330.
29. P. L. Homagai, K. N. Ghimire and K. Inoue, *Bioresour. Technol.*, 2010, **101**, 2067-2069.
30. Y. Jiang, H. Pang and B. Liao, *J. Hazard. Mater.*, 2009, **164**, 1-9.
31. H. D. Özsoy, H. Kumbur and Z. Özer, *Int. J. Environ. Pollut.*, 2007, **31**, 125-134.
32. M. G. A. Vieira, A. F. De Almeida Neto, M. G. C. Da Silva, C. N. Carneiro and A. A. Melo Filho, *Braz. J. Chem. Eng.*, 2014, **31**, 519-529.
33. Y. Kim, B. Lee and J. Yi, *Sep. Sci. Technol.*, 2007, **38**, 2533-2548.
34. S. Sai Bhargav and I. Prabha, *Int. J. Chem. Chemical Eng.*, 2013, **3**, 107-112.
35. Y. S. Ho and G. McKay, *Water Air Soil Pollut.*, 2004, **158**, 77-97.
36. F. Bouhamed, Z. Elouear and J. Bouzid, *J. Taiwan Inst. Chem. Eng.*, 2012, **43**, 741-749.
37. P. N. Dave, N. Subrahmanyam and S. Sharma, *Indian J. Chem. Technol*, 2009, **16**, 234-239.
38. H. Liu, S. Feng, N. Zhang, S. Du and Y. Liu, *Front. Environ. Sci. Eng.*, 2014, **8**, 329-336.
39. M. S. Tehrani, P. A. Azar, P. Ehsani Namin and S. M. Dehaghi, *J. Appl. Environ. Biol. Sci.*, 2014, **4**, 316-326.
40. C. Lu and H. Chiu, *Chem. Eng. Sci.*, 2006, **61**, 1138-1145.
41. I. A. A. Hamza, *PhD Thesis*, 2013, **University of KwaZulu-Natal, Durban, South Africa**.
42. X. Peng, Z. Luan, Z. Di, Z. Zhang and C. Zhu, *Carbon*, 2005, **43**, 855-894.
43. J. Hu, D. Zhao and X. Wang, *Water Sci. Technol.*, 2011, **63**, 917-923.
44. S. R. Popuri, R. Frederick, C.-Y. Chang, S.-S. Fang, C.-C. Wang and L.-C. Lee, *Desalin. Water Treat.*, 2013, **52**, 691-701.
45. M. Abdel Salam, G. Al-Zhrani and S. A. Kosa, *J. Ind. Eng. Chem.*, 2014, **20**, 572-580.
46. T. A. Khan, M. Nazir and E. A. Khan, *Toxicol. Environ. Chem.*, 2013, **95**, 919-931.
47. D. J. Malika, V. Strelko, A. M. Streata and A. M. Puziyb, *Water Res.*, 2002, **36**, 1527-1538.
48. Z. Wang, M. D. Shirley, S. T. Meikle, R. L. D. Whitby and S. V. Mikhalovsky, *Carbon*, 2009, **47**, 73-79.
49. S. Biniak, G. Szymanski, J. Siedlewski and A. Swiatkowski, *Carbon* 1997, **35**, 1799-1810.
50. H. P. Boehm, *Carbon*, 2002, **40**, 145-149.
51. M. N. Patel, P. A. Dosi and B. S. Bhatt, *Med. Chem. Res.*, 2012, **21**, 2723-2733.

52. M. N. Patel, H. N. Joshi and C. R. I. Patel, *Polyhedron*, 2012, **40**, 159-167.
53. S. Santangelo, G. Messina, G. Faggio, S. H. Abdul Rahim and C. Milone, *J. Raman Spectrosc.*, 2012, **43**, 1432-1442.
54. J. Shen, W. Huang, L. Wu, Y. Hu and M. Ye, *Mater. Sci. Eng. Part A* 2007, **464**, 151-156.
55. N. Sakai, T. Moriya and T. Konakahara, *J. Org. Chem.*, 2007, **72**, 5920-5922.
56. Y. S. Ho, *Water Res.*, 2004, **38**, 2962-2964
57. J. Lin and L. Wang, *Front. Environ. Sci. Eng.*, 2009, **3**, 320-324.
58. Y.-S. Ho, *J. Hazard. Mater.*, 2006, **136**, 681-689.
59. S. H. Chien and W. R. Clayton, *Soil Sci. Soc. Am. J.*, 1980, **44**, 265-268.
60. E. Demirbas, M. Kobya, E. Senturk and T. Ozkan, *Water SA*, 2004, **30**, 533-539.
61. I. Langmuir, *J. Am. Chem. Soc.*, 1918, **40**, 1361-1402.
62. H. Freundlich, *Z. Phys. Chem.*, 1906, **57**, 385-470.
63. M. I. Temkin and V. Pyzhev, *Acta Phys. Chim.*, 1940, **12**, 327-356.
64. M. M. Dubinin and L. V. Radushkevich, *Proc. Acad. Sci, U.S.S.R, Phys. Chem. Sect.*, 1947, **55**, 327-329.
65. R. Sips, *J. Chem. Phys.*, 1948, **16**, 490-495.
66. J. Toth, *Acta Chim. Acad. Sci. Hung.*, 1971, **69**, 311-328.
67. O. Redlich and D. L. Peterson, *J. Phys. Chem.*, 1959, **63**, 1024.
68. A. R. Khan, I. R. Al-Waheab and A. Al-Haddad, *Environ. Technol.*, 1996, **17**, 13-23.
69. The R Development Core Team, *The R foundation for statistical Computing, R version 3.0.2* 2013.
70. S. Narimany and S. Ghammamy, *Global J. Pharma.*, 2013, **7**, 187-191.
71. T. L. Yang, W. W. Qin, Z. F. Xiao and W. S. Liu, *Chem. Pap.*, 2005, **59**, 17-20.
72. W. Huang, C. Li, J. Wang and L. Zhu, *Spectrosc. Lett.*, 1998, **31**, 1793-1809.
73. L. M. Ombaka, P. G. Ndungu and V. O. Nyamori, *RSC Adv.*, 2014, **5**, 109-122.
74. K. Chizari, A. Vena, L. Laurentius and U. Sundararaj, *Carbon*, 2014, **68**, 369-379.
75. K. S. Tong, M. J. Kassim and A. Azraa, *Chem. Eng. J.*, 2011, **170**, 145-153.
76. M. A. Salleh, D. K. Mahmoud, W. A. Abdul Karim and A. Idris, *Desalination*, 2011, **280**, 1-13.
77. P. Gans, *HySS, version 4.0.31*, 2009.
78. K. V. Kumar, *J. Hazard. Mater.*, 2006, **137**, 1538-1544.
79. Y. S. Ho and C. C. Wang, *Process Biochem.*, 2004, **39**, 759-763.
80. Y. S. Ho and G. McKay, *Process Biochem.*, 1999, **34**, 451-465.
81. B. Yu, Y. Zhang, A. Shukla, S. S. Shukla and K. L. Dorris, *J. Hazard. Mater.*, 2000, **B80**, 33-42.
82. S. G. Muntean, M. E. Radulescu-Grad and P. Sfarloaga, *RSC Adv.*, 2014, **4**, 27354-27362.

83. C. H. Wu, *J. Hazard. Mater.*, 2007, **144**, 93-100.
84. Y. Yao, F. Xu, M. Chen, Z. Xu and Z. Zhu, *Bioresour. Technol.*, 2010, **101**, 3040-3046.
85. F. Ekmekyapar, A. Aslan, Y. K. Bayhan and A. Cakici, *J. Hazard. Mater.*, 2006, **137**, 293-298.
86. T. A. Khan, S. Dahiya and I. Ali, *Appl. Clay Sci.*, 2012, **69**, 58-66.
87. Y.-S. Ho, *Scientometrics*, 2004, **59**, 171-177.
88. I. A. A. Hamza, B. S. Martincigh, J. C. Ngila and V. O. Nyamori, *Phys. Chem. Earth*, 2013, **66**, 157-166.
89. O. Soon-An, S. Chye-Eng and L. Poh-Eng, *Electronic J. Environ. Agric. Food Chem.*, 2007, **6**, 764-1774.
90. T. K. Sen and D. Gomez, *Desalination*, 2011, **267**, 286-294.
91. S. A. Kosa, G. Al-Zhrani and M. Abdel Salam, *Chem. Eng. J.*, 2012, **181-182**, 159-168.
92. R. Djeribi and Q. Hamdaoui, *Desalination*, 2008, **225**, 95-112.
93. S. K. Milonjić, *J. Serb. Chem. Soc.*, 2007, **72**, 1363-1367.
94. Y. Liu and Y.-J. Liu, *Sep. Purif. Technol.*, 2008, **61**, 229-242.

Chapter 5

Adsorption of Pb^{2+} and Zn^{2+} from aqueous solution onto functionalized multiwalled carbon nanotubes

Oluwaseun A. Oyetade, Vincent O. Nyamori, Bice S. Martincigh* and Sreekantha B. Jonnalagadda

School of Chemistry and Physics, University of KwaZulu-Natal, Westville Campus,
Private Bag X54001, Durban 4000, South Africa

*Corresponding author: Tel: +27 31 2601394; Fax: +27 31 2603091;
E-mail: martinci@ukzn.ac.za

Abstract

In this study, 4'-(4-hydroxyphenyl)-2,2':6',2''-terpyridine was applied as a modifier to functionalize multiwalled carbon nanotubes to afford nitrogen-functionalized carbon nanotubes (MWCNT-ttpy). The nanomaterial was characterized and their application for the removal of Pb^{2+} and Zn^{2+} from aqueous solution was investigated through batch adsorption processes. The adsorption efficiency of an acid-functionalized multiwalled carbon nanotube (MWCNT-COOH) and MWCNT-ttpy was compared to determine the sorbent with the best removal efficiency towards metal ion sorption.

The adsorption capacities (q_e) of the adsorbents increased with increasing pH, contact time and adsorbent dose. For both metal ions, better removal was observed with MWCNT-ttpy than MWCNT-COOH. In the case of Pb^{2+} , the Langmuir maximum adsorption capacity (q_m) increased from 20.60 mg g^{-1} to 36.23 mg g^{-1} , and for Zn^{2+} , q_m increased from 18.51 mg g^{-1} to 32.60 mg g^{-1} , going from MWCNT-COOH to MWCNT-ttpy, respectively. For both adsorbents, q_m for Pb^{2+} was larger than for Zn^{2+} . The pseudo-second order kinetics model fitted both systems well, indicating a bimolecular interaction between the adsorbate cations and sorbents. The adsorption processes were endothermic in nature and spontaneous. Desorption studies showed high desorption efficiencies, demonstrating the suitability of the adsorbents for reuse.

Thus, nitrogen-functionalized carbon nanotubes show promise as a good re-useable adsorbent for the removal of Pb^{2+} and Zn^{2+} from industrial effluents and wastewaters.

Keywords: Lead, zinc, adsorption, kinetics, isotherm, carbon nanotube

5.1. Introduction

Contamination of water resources with heavy metal ions is increasingly attributed to industrial and anthropogenic activities. Wastewater generated from industries, such as mining and metallurgy, and chemical manufacturing, contains one or more toxic metal ions in high concentrations, requiring further treatment before its disposal [1-3]. If this effluent is indiscriminately discharged into water bodies with little or no treatment, it poses a serious environmental risk to man and its environs [1,2,4]. Since metal ions persist in the environment for long periods of time the treatment of metal-polluted wastewater becomes an increasingly difficult task [2,3,5].

Human exposure to metal ions such as lead, cadmium, copper, nickel, mercury and zinc can result in health issues such as dysfunction of the kidney, liver, bones, muscles, central nervous system, and in extreme cases may lead to death [1,4,6]. Lead is one of the most hazardous metal pollutants and is regarded as poisonous to both man and animals [6]. In 2010, in the Northern part of Nigeria, 163 people, including 111 children, died as a result of exposure to dust contaminated with lead from mining activities [7,8]. Zinc may be considered essential, but can give rise to various health complications with increased exposure at high concentrations [9,10]. The introduction of zinc to humans through food supplements, antiseptics and deodorant formulations is of major concern to nutritionists due to various health risks associated with increased exposure to this substance [10]. Studies have also shown increased concentrations of Pb^{2+} and Zn^{2+} in various media such as water [11,12], sediments [13], landfills [14], and electronic waste [15], amongst many others.

Due to these negative effects, the treatment of metal-contaminated wastewater becomes imperative through the development of effective and innovative adsorbents. Adsorption has been identified as a fast and easy method of treatment because of its simplicity, cost-effectiveness, and the ease of regeneration and reutilization of adsorbents [3]. The removal of Pb^{2+} and Zn^{2+} have been explored by various authors by using sorbents such as rice husk [16,17], sugarcane bagasse [3], green seaweed [18], sawdust [19], marine green microalgae [20], maize tassels [21], chitosan [22], mesoporous silica [23], activated carbon [24], kaolinite [25], calcium alginate beads [26], and SBA-15 [27], amongst many others. In spite of these studies, limitations such as slow sorption and regeneration of adsorbents for reuse still pose a challenge. Thus, the development of effective adsorbents continues to grow with a view of treating wastewater contaminated with metal ions and regenerating adsorbents for the purpose of reutilization.

The use of carbon nanotubes (CNTs) for pollutant removal has generated great interest in recent years and this is due to their inherent properties such as large surface area [4], high

thermal and chemical stability [28], ease of introduction of new functional groups, and their hollow and porous structures [28]. Due to the hydrophobic nature of CNTs, dispersion in aqueous solution is difficult; hence, oxidation of CNTs by wet-chemical methods [1], oxygen plasma [29], and photo-oxidation [30] is usually carried out to increase their chemical reactivity. Chemical modification of CNTs with acids reduces their hydrophobicity and introduces new groups onto the walls of tubes [4]. The introduction of the functional groups onto CNTs increases the selectivity and sensitivity of nanotubes to organic [31,32] or inorganic [3,5] pollutants, thus enhancing the removal of adsorbates from solution.

The effectiveness of multiwalled carbon nanotubes (MWCNTs) for metal ion removal can be improved through surface modification by using various chemical agents [33]. Studies have been tailored toward removal of metal ions by the functionalization of MWCNTs to increase the number of chelating sites on the sorbent [1-4,33-37]. However, limited studies have shown the influence of nitrogen-containing compounds as a modifier on MWCNTs and investigated their capacity toward Pb^{2+} and Zn^{2+} removal from aqueous solution.

In this study, we report a comparison of the removal of Pb^{2+} and Zn^{2+} from simulated wastewater by acid-functionalized multiwalled carbon nanotubes (MWCNT-COOH) and 4-phenyl-2,2':6',2''-terpyridine-functionalized multiwalled carbon nanotubes (MWCNT-ttpy). Batch adsorption processes were carried out to investigate the influence of time, pH, adsorbent dose, initial metal ion concentration and temperature on the adsorption of Pb^{2+} and Zn^{2+} from wastewater. The data obtained were fitted to various isotherm and kinetics models in order to elucidate the adsorption mechanisms involved.

5.2 Experimental

5.2.1. Materials and chemicals

All chemicals used were of analytical grade and used without further purification. The as-prepared MWCNTs were purchased from Cheap Tubes Inc. (Brattleboro, USA), and had been synthesized through chemical vapour deposition (CVD) with a purity of 95%. Lead and zinc metal powders, tetrahydrofuran, thionyl chloride and sodium hydroxide were purchased from Merck (Pty) Ltd (Gauteng, South Africa). Aqueous ammonia (25%) was purchased from Associated Chemical Enterprises (Johannesburg, South Africa) while nitric acid (55%), sulfuric acid (98%) and hydrochloric acid (32%), were purchased from C C Imelmann Ltd (Robertsham, South Africa). Other chemicals such as 4-hydroxybenzaldehyde (99%), 2-acetylpyridine (99%), triethylsilane (Et_3SiH , 97%), indium

bromide (InBr_3 , 99%), absolute ethanol and N,N'-dimethylformamide (DMF, 99%), were purchased from Sigma-Aldrich (New Germany, South Africa).

5.2.2. Preparation of adsorbents

MWCNTs which had been oxidized in a 3:1 (v/v) concentrated nitric acid-sulfuric acid mixture (MWCNT-COOH) were dispersed in a solution containing a 20:1 (v/v) mixture of thionyl chloride and DMF, and refluxed at 70 °C for 24 h [38]. The resulting mixture was filtered, and the solid obtained was washed with deionised water until a neutral pH was achieved. These acylated MWCNTs (100 mg) were added to 100 mg of 4-phenyl-2,2':6',2''-terpyridine (HO-Phttpy) in 20 cm³ of dry tetrahydrofuran (THF) with the addition of 2-5 drops of glacial acetic acid. The suspension was refluxed at 64 °C for 24 h under an inert atmosphere of argon. The suspension was filtered and the solid obtained was washed with THF and dried in a vacuum oven. To the obtained sample (100 mg) was added freshly distilled chloroform (30 cm³), InBr_3 (10.6 mg, 0.03 mmol) and Et_3SiH (380 μL , 2.4 mmol). The suspension was stirred and refluxed at 60 °C for 1 h under an inert atmosphere of argon. The resulting mixture was filtered and the solid was washed with chloroform ($3 \times 20 \text{ cm}^3$), followed by deionised water until a neutral pH was obtained. The synthesis of 4-phenyl-2,2':6',2''-terpyridine (HO-Phttpy) and the characterization of the adsorbents have been reported in our previous work [39]. Oxidized MWCNTs (MWCNT-COOH) and 4-phenyl-2,2':6',2''-terpyridine-functionalized MWCNTs (MWCNT-ttpy) were stored and prepared for use as adsorbents in the treatment of metal-contaminated wastewater.

5.2.3. Metal analysis procedure

5.2.3.1. Equipment

A PerkinElmer Optima 5300 DV inductively coupled plasma-optical emission spectrophotometer (ICP-OES) was used to measure the initial and final concentrations of Pb^{2+} and Zn^{2+} in solution. The operating conditions used are presented in Appendix II (Table A-II.1 – A-II.2).

5.2.3.2. Preparation of adsorbate solution

Stock solutions were prepared by weighing approximately 1 g of Pb or Zn metal powder into 50 cm³ of 2 mol dm⁻³ nitric acid. The solution was made up to mark in a 1000 dm³ volumetric flask with deionised water. Working solutions of Pb^{2+} and Zn^{2+} were prepared daily from the stock solutions to obtain the desired concentrations.

5.2.4. Adsorption experiments

The optimization of adsorption parameters such as pH, contact time, adsorbent dose, initial metal ion concentration and temperature were investigated through batch adsorption experiments. To investigate the influence of pH, 20 cm³ aliquots of 100 mg dm⁻³ adsorbate solution were measured into plastic vials with the addition of 50 mg of adsorbent to each. The solutions were then equilibrated for 24 h in a thermostated water-bath at 20 °C. Solutions were conditioned to the required pH by the addition of appropriate amounts of 0.1 mol dm⁻³ NaOH or HNO₃. After agitation, the solutions were filtered, and the final concentrations of Pb²⁺ or Zn²⁺ determined by using inductively coupled plasma-optical emission spectroscopy (ICP-OES) (Perkin Elmer Optima 5300 DV). The amount of metal ion adsorbed on the adsorbents was determined from the difference between the initial and final metal ion concentrations. The removal efficiency and sorption capacity (q_e) of Pb²⁺ and Zn²⁺ were calculated according to equations 5.1 and 5.2, respectively.

$$\% \text{ adsorbed} = \left(\frac{C_i - C_{eq}}{C_i} \right) \times 100 \quad (5.1)$$

$$q_e = \left(\frac{C_i - C_{eq}}{m} \right) \times V \quad (5.2)$$

where C_i is the initial adsorbate concentration (mg dm⁻³), C_{eq} is the equilibrium concentration of adsorbate (mg dm⁻³), q_e is the adsorption capacity (mg g⁻¹), m is the mass of adsorbent (mg) and V is the volume (dm³) of the adsorbate solution used.

Kinetic studies were investigated by adding 50 mg of adsorbent into a 20 cm³ aliquot of 100 mg dm⁻³ adsorbate solution. Solutions were conditioned to the desired pH with the addition of appropriate amounts of 0.1 mol dm⁻³ NaOH or HNO₃. The suspensions were agitated in a thermostated water-bath at 20 °C for varying time intervals over the range of 5 to 1440 min. After the pre-determined time intervals, the solutions were filtered and the final concentrations of Pb²⁺ or Zn²⁺ determined by using ICP-OES. Four kinetic models, namely, the pseudo-first order [40-42], pseudo-second order [41-43], Elovich [44] and intraparticle diffusion models [45], were used to describe the equilibrium data obtained. The equations of all models used in this study are illustrated in Table 5.1.

Table 5.1: Kinetics models investigated for the adsorption of Pb²⁺ and Zn²⁺

Model	Equation*	Parameters	References
Pseudo-first order	$q_t = q_{eq}(1 - e^{-k_1 t})$	q_{eq}, k_1	[40-42]
Pseudo-second order	$q_t = \frac{k_2 q_{eq}^2 t}{1 + k_2 q_{eq} t}$	k_2, q_{eq}	[41-43]
Elovich	$q_t = \frac{1}{\beta} \ln(\alpha\beta) + \frac{1}{\beta} \ln t$	α, β	[44]
Intraparticle diffusion	$q_t = k_{id} \sqrt{t} + l$	k_{id}, l	[45]

* q_t , quantity of adsorbate adsorbed at time t (mg g^{-1}); q_{eq} , quantity of adsorbate adsorbed at equilibrium (mg g^{-1}); α , adsorption rate constant ($\text{mg g}^{-1} \text{min}^{-1}$); β , desorption rate constant (g mg^{-1}); k_1 , pseudo-first order rate constant (min^{-1}); k_2 , pseudo-second order rate constant ($\text{g mg}^{-1} \text{min}^{-1}$); k_{id} , intraparticle diffusion rate constant ($\text{mg g}^{-1} \text{min}^{0.5}$), l , is a constant related to the boundary layer thickness.

Isotherm experiments were conducted with a 20 cm³ aliquot of adsorbate solution over a concentration range of 10-100 mg dm⁻³ and an adsorbent dose of 50 mg. Solutions were conditioned to the appropriate pH and agitated in a thermostated water-bath at 20 °C for 24 h. The solutions were filtered and the final concentration of metal ion in the filtrates determined by using ICP-OES. The equilibrium data obtained were fitted into various two- and three-parameter isotherms. All isotherm equations used in this study are given in Table 5.2. Thermodynamic studies were also investigated over a temperature range of 293-318 K and calculations were performed to obtain parameters such as the standard Gibbs energy change (ΔG°), standard enthalpy change (ΔH°), and standard entropy change (ΔS°) for the adsorption process.

Table 5.2: Isotherm models investigated for the adsorption of Pb²⁺ and Zn²⁺

Isotherm model	Equation*	Parameters	References
Langmuir	$q_{eq} = \frac{q_m b C_{eq}}{1 + b C_{eq}}$	q_m, b	[46]
Freundlich	$q_{eq} = K_F C_{eq}^{1/n}$	K_F, n	[47]
Temkin	$q_{eq} = \frac{RT}{b_T} \ln(A_T C_{eq})$	b_T, A_T	[48]
Dubinin-Radushkevich	$q_{eq} = q_m e^{-\beta \varepsilon^2}$ $\varepsilon = RT \ln \left(1 + \frac{1}{C_{eq}} \right)$	q_m, β	[49]
Sips	$q_{eq} = \frac{b q_m C_{eq}^{1/n}}{1 + b C_{eq}^{1/n}}$	q_m, b, n	[50]
Toth	$q_{eq} = \frac{q_m C_{eq}}{\left(\frac{1}{K_T} + C_{eq}^{n_T} \right)^{1/n_T}}$	q_m, K_T, n_T	[51]
Redlich-Peterson	$q_{eq} = \frac{K_{RP} C_{eq}}{1 + a_{RP} C_{eq}^g}$	K_{RP}, a_{RP}, g	[52]
Khan	$q_{eq} = \frac{q_m b_K C_{eq}}{(1 + b_K C_{eq})^{a_K}}$	q_m, a_K, b_K	[53]

* q_{eq} , adsorption capacity (mg g⁻¹); C_{eq} , equilibrium concentration of adsorbate in solution (mg dm⁻³); q_m , maximum monolayer capacity (mg g⁻¹); b , Langmuir isotherm constant (dm³ mg⁻¹); K_F , Freundlich isotherm constant (mg g⁻¹)(dm³ mg⁻¹)ⁿ; n , adsorption intensity; b_T , Temkin isotherm constant; A_T , Temkin isotherm equilibrium binding constant (dm³ g⁻¹); β , Dubinin-Radushkevich isotherm constant (mol² kJ⁻²); K_T , Toth isotherm constant (mg g⁻¹); n_T , Toth isotherm constant; K_{RP} , Redlich-Peterson isotherm constant (dm³ g⁻¹); a_{RP} , Redlich-Peterson isotherm constant; g , Redlich-Peterson isotherm exponent; a_k , Khan isotherm exponent; b_k , Khan isotherm constant.

5.2.5 Desorption studies

To reduce the cost of adsorbents, such that reutilization of sorbent and adsorbate is possible, desorption studies were conducted. To evaluate the desorption of Pb²⁺ and Zn²⁺ from the adsorbents, the equilibrium concentration was determined from the filtrate collected after the adsorption process. Then 50 mg of metal ion loaded adsorbent was agitated in a 10 cm³ aliquot of 0.1 mol dm⁻³ HCl for 1 h. The suspension was filtered and the adsorbent collected were washed with deionised water and dried in a vacuum oven at 80 °C overnight. The final concentrations of Pb²⁺ or Zn²⁺ were determined in the collected filtrate by using ICP-OES.

5.2.6. Data analysis

Isotherm and kinetic models were used to fit the data by means of the nls nonlinear regression routine in the R statistical computing environment [54]. The sum of squared residuals was used to evaluate the model with the best fit.

5.3. Results and Discussion

5.3.1. Characterization of adsorbents

The synthesized adsorbents (MWCNT-COOH and MWCNT-ttpy) were characterized and have been reported in our previous work [39]. Of notable mention is the increase in the surface area of MWCNT-ttpy from 126.8 to 189.2 m² g⁻¹, relative to MWCNT-COOH. This was attributed to the increase in the introduction of nitrogen-donor atoms onto the surface of MWCNT-COOH [39]. An increase in the surface area of MWCNT-COOH was also noticeable from 108.8 m² g⁻¹, as a result in increase in tube cutting due to oxidation. Similarly, an increase in their pore volumes after functionalization is an indication that the adsorbents should be suitable for the removal of pollutants from wastewater, since this is one of the factors on which adsorption depends.

5.3.2. Batch adsorption experiments

Experiments demonstrating the influence of pH, time, adsorbent dose, initial metal ion concentration and temperature were carried out to examine the best conditions necessary for Pb²⁺ and Zn²⁺ removal. The sorption abilities of the two types of MWCNTs, namely, acid-functionalized MWCNTs (MWCNT-COOH) and nitrogen-functionalized MWCNT (MWCNT-ttpy), for Pb²⁺ and Zn²⁺ removal were compared. The data were modelled with various kinetic and isotherm models in order to characterise the nature of the adsorption process involved.

5.3.2.1. Effect of pH

The influence of pH on the adsorption of Pb²⁺ and Zn²⁺ were investigated over a pH range of 1-10 by using MWCNT-COOH and MWCNT-ttpy. Fig. 5.1 shows that the change in pH of the adsorbate solution greatly influenced the extent of removal of Pb²⁺ and Zn²⁺ from aqueous solution. Fig. 5.1(A) and (B) shows the influence of pH on the adsorption of Pb²⁺ and Zn²⁺, respectively. The uptake of Pb²⁺ and Zn²⁺ by MWCNT-COOH and MWCNT-ttpy was low at acidic conditions, however, increased removal efficiencies were obtained as the solution pH increased (Fig. 5.1). A change in solution pH influences the chemical behaviour of the adsorbates, the charges on the adsorbents and the speciation of the metal ion in solution [35,55].

At low pH, competition between cationic metal ions and hydrogen ions for the adsorption sites increases, due to the increase in hydrogen ions contained in the solution at acidic conditions. The surface of the adsorbents becomes positively charged at this stage, resulting in electrostatic repulsion between the metal ions and active sites on the adsorbent. This phenomenon explains why decreased removal efficiencies were obtained for Pb²⁺ and Zn²⁺ at acidic conditions. However, increased pH results in a decrease of hydrogen ions, inducing

a negatively charged surface onto the adsorbents. Increased removal of Pb^{2+} and Zn^{2+} was obtained at basic conditions owing to electrostatic interaction between the cationic metal ions and negatively charged surface of the adsorbents. Similar observations were reported for the adsorption of Pb^{2+} and Zn^{2+} by Hamza *et al.* [3], Elham *et al.* [17], Rao *et al.* [35] and Goyal *et al.* [56].

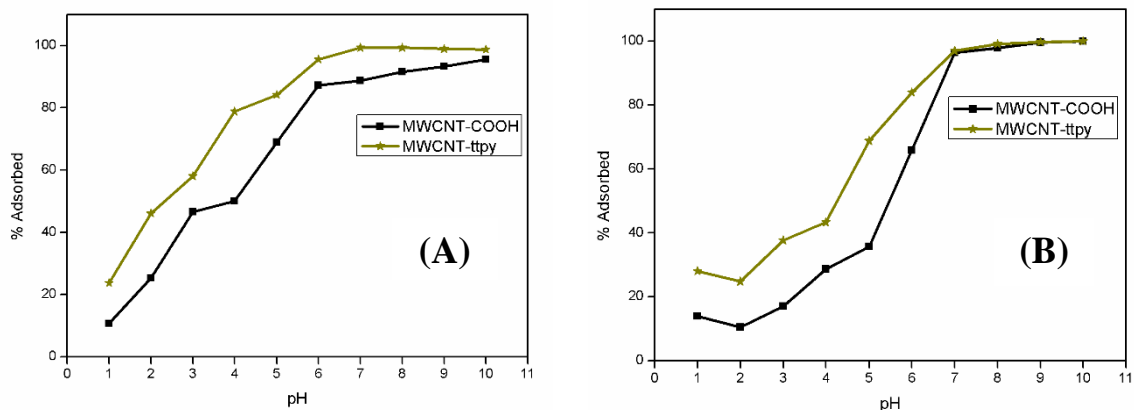


Fig. 5.1: Effect of pH on the adsorption of (A) Pb^{2+} and (B) Zn^{2+} by using MWCNT-COOH and MWCNT-tpy [conditions: 20 cm^3 of 100 mg dm^{-3} $\text{Pb}^{2+}/\text{Zn}^{2+}$, 24 h equilibration time, 50 mg adsorbent dose, agitation speed 150 rpm, temperature 20 $^\circ\text{C}$].

However, a change in pH also affects the speciation of the metal ions in solution. Fig. 5.2(A) and (B) shows the different species for Pb^{2+} and Zn^{2+} , respectively, that form under different pH conditions at a concentration of 100 mg dm^{-3} . The removal of metal ions is facilitated at basic conditions due to precipitation of metal ions in solution as hydroxo species [3]. This leads to increased removal efficiencies noticed at basic pH conditions. Hence, to effectively confirm the removal of Pb^{2+} and Zn^{2+} by adsorption only, further experiments were conducted at pH 4.5 and 5.5, respectively, where only divalent metal ions were prevalent in solution.

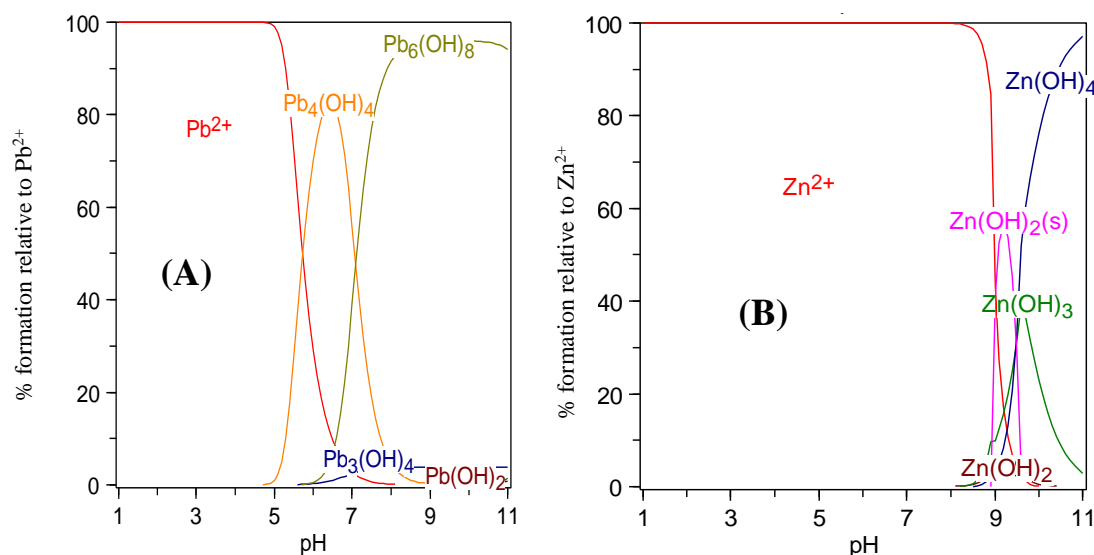


Fig. 5.2: Speciation of (A) Pb^{2+} and (B) Zn^{2+} as a function of pH in aqueous solution. Numerical values of $\log \beta$ for the metal hydroxides used in the calculation of the speciation curves were obtained from Critical Stability Constants compiled by Smith and Martell [57], and plots obtained with the aid of HySS software [58].

It is also worthy of note that increased removal efficiencies were obtained for both adsorbates with MWCNT-ttpty than with MWCNT-COOH at each pH condition (Fig. 5.1). This proves that the modification of MWCNT-COOH to introduce nitrogen-donor atoms increases the number of chelating sites on MWCNT-ttpty, thereby resulting in an increase in metal ion removal. The application of MWCNT-ttpty, therefore, proved efficient and could serve as a good alternative for metal ion sorption in wastewater.

The experimental data for the adsorption of Pb^{2+} and Zn^{2+} onto acid- and nitrogen-functionalized MWCNTs as a function of pH can be found in Appendix II.

5.3.2.2. Effect of contact time

Fig. 5.3 (A) and (B) shows the influence of varying the contact times on the adsorption of Pb^{2+} and Zn^{2+} , respectively. The effect of contact time was investigated over a period of 5-1440 min with the conditions described in Fig. 5.3 by using MWCNT-COOH and MWCNT-ttpty. The experiments demonstrate an increase in the removal of Pb^{2+} and Zn^{2+} with increasing contact time between adsorbents and adsorbates. A steady increase in removal efficiency was obtained for both processes due to the availability of more active sites at the initial stage. As the process continues, adsorption sites become saturated, hence, a state of equilibrium where little or no further increase in removal is reached. Fig. 5.3A shows that equilibrium was achieved at 90 min for both adsorbents for the removal of Pb^{2+} . The

adsorption of Pb^{2+} revealed an efficiency of 56.11% and 86.34% for MWCNT-COOH and MWCNT-ttpy, respectively, after an agitation time of 24 h (Fig. 5.3A). In the case of Zn^{2+} , equilibrium was achieved at 300 min and 360 min by using MWCNT-COOH and MWCNT-ttpy, respectively. Removal efficiencies of 47.81% and 73.01% for MWCNT-COOH and MWCNT-ttpy, respectively, were obtained after 24 h for the adsorption of Zn^{2+} (Fig. 5.3B). Experiments further showed that higher removal efficiencies were obtained for MWCNT-ttpy than MWCNT-COOH for each period in both adsorption processes. The efficiency of MWCNT-ttpy could be attributed to the increased surface area from 126.8 to 189.2 $\text{m}^2 \text{g}^{-1}$ obtained after modification was done, which creates room for more active sites available for metal ion adsorption. Also, modification of MWCNT-COOH with the ligand enabled complexation of Pb^{2+} and Zn^{2+} with nitrogen-donor groups, thereby, inducing better sorption of metal ions onto the active sites of the adsorbent. Further experiments were allowed to equilibrate for 24 h to ensure complete removal of Pb^{2+} and Zn^{2+} in solution.

The experimental data for the adsorption of Pb^{2+} and Zn^{2+} onto acid- and nitrogen-functionalized MWCNTs as a function of contact time can be found in Appendix II.

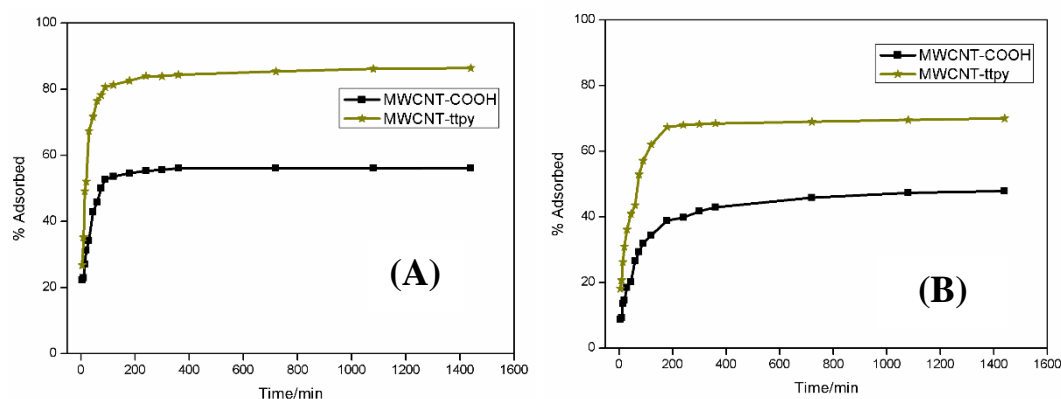


Fig. 5.3: Effect of contact time on the adsorption of (A) Pb^{2+} and (B) Zn^{2+} by using MWCNT-COOH and MWCNT-ttpy [conditions: 20 cm^3 of 100 mg dm^{-3} $\text{Pb}^{2+}/\text{Zn}^{2+}$, pH = 4.5 (Pb^{2+}) and pH = 5.5 (Zn^{2+}), 50 mg adsorbent dose, agitation speed 150 rpm, temperature 20 °C].

To investigate the kinetics of Pb^{2+} and Zn^{2+} adsorption onto MWCNT-COOH and MWCNT-ttpy, the equilibrium data obtained were fitted into the pseudo-first order, pseudo-second order, Elovich and intraparticle models. The equations for the models are given in Table 5.1. The calculated kinetic parameters obtained from these models are given in Table 5.3. The results indicated that the kinetics data obtained for the removal of Pb^{2+} and Zn^{2+} were better described by the pseudo-second order model. This inference is based on the fact that this model has the lowest sum of squared residuals (SSR) and residual standard error (RSE)

values. The mechanism for the adsorption of Pb^{2+} and Zn^{2+} onto MWCNT-COOH and MWCNT-ttpy indicates that sorption proceeds through a bimolecular interaction between the cationic metal ions and the active sites of the adsorbents.

Table 5.3: Kinetic parameters for the adsorption of Pb^{2+} and Zn^{2+} on MWCNT-COOH and MWCNT-ttpy [conditions: 20 cm^3 of 100 mg dm^{-3} $\text{Pb}^{2+}/\text{Zn}^{2+}$, pH = 4.5 (Pb^{2+}) and pH = 5.5 (Zn^{2+}), 50 mg adsorbent dose, agitation speed 150 rpm, temperature 20 °C]

Model	Parameter	Pb^{2+}		Zn^{2+}	
		MWCNT-COOH	MWCNT-ttpy	MWCNT-COOH	MWCNT-ttpy
Experimental	$q_{meas}/\text{mg g}^{-1}$	21.62	35.29	18.55	28.93
Pseudo-first order	$k_1/10^{-2}/\text{min}$	4.150	5.398	1.554	2.369
	$q_{eq}/\text{mg g}^{-1}$	20.87	34.00	17.17	26.95
	RSE*	1.516	1.326	1.132	2.025
	SSR†	34.48	26.39	19.23	61.49
	$k_2/10^{-3}/\text{g mg}^{-1} \text{ min}^{-1}$				
Pseudo-second order	¹	2.956	2.274	1.081	1.178
	$q_{eq}/\text{mg g}^{-1}$	22.26	36.25	19.06	29.28
	RSE	1.004	0.938	0.595	1.134
	SSR	15.12	13.19	5.310	19.29
Intraparticle diffusion	$k_{id}/\text{mg g}^{-1} \text{ min}^{-0.5}$	0.945	1.560	0.719	1.179
	$l/\text{mg g}^{-1}$	3.982	3.702	0.717	2.539
	RSE	8.802	15.35	4.575	9.017
	SSR	1240	3769	334.8	1300
Elovich	$\alpha/\text{mg g}^{-1} \text{ min}^{-1}$	16.54	46.00	1.335	4.559
	$\beta/\text{g mg}^{-1}$	0.366	0.239	0.314	0.226
	RSE	1.985	3.639	1.092	2.029
	SSR	59.08	198.6	17.89	61.75

*RSE - residual standard error, †SSR – sum of squared residuals

To further explain the diffusion mechanism of the adsorption processes, the kinetic results were analysed by the intraparticle diffusion model. Adsorption onto porous materials generally proceeds by a multi-step process. These steps involve four processes, namely, the transfer of solute from the solution to the surface of the adsorbent, followed by the solute transfer from the bulk solution to the boundary film that surrounds the adsorbent surface (film diffusion), then the solute transfer through the internal pores of the adsorbent (intraparticle diffusion), and subsequently the interaction between adsorbate molecules with the active sites on the external surface of the adsorbent. In order to determine the processes which best explain Pb^{2+} and Zn^{2+} sorption; a plot of q_e versus \sqrt{t} was obtained. Since all plots obtained in this study were linear, and do not pass through the origin, it is indicative

that the adsorption process was controlled by two or more steps [59,60]. These plots reveal that adsorption was initially controlled by transportation of Pb^{2+} and Zn^{2+} to the external surface of the adsorbents through film diffusion, followed by intraparticle diffusion of adsorbates to the internal pores of the adsorbents and a stage where intraparticle diffusion slows down due to low adsorbate concentration [61]. These processes explain that the rate-controlling steps for the adsorption of Pb^{2+} and Zn^{2+} were multi-step since plots obtained do not pass through the origin. An increase in the intraparticle diffusion constant (k_{id}) and the boundary layer constant (l) was also noticed with MWCNT-ttpy for both cations, indicating that the adsorption of Pb^{2+} and Zn^{2+} onto MWCNT-COOH and MWCNT-ttpy was boundary-controlled.

5.3.2.3. Effect of adsorbent dose

The influence of varying adsorbent dose on the adsorption of Pb^{2+} and Zn^{2+} is shown in Fig. 5.4 (A) and (B) respectively. The dose of adsorbent was varied over a range of 30-400 mg and equilibrated for 24 h. The figures show that the concentrations of metal ions in solution decrease with increasing amounts of adsorbent. At a fixed metal ion concentration, increase in the adsorbent dose provides increased surface area, resulting in the availability of more active sites. This explains why higher removal efficiencies were obtained for both adsorption processes with increasing dosage of MWCNT-COOH and MWCNT-ttpy. Again, the removal efficiency of MWCNT-ttpy was higher than that of MWCNT-COOH in both adsorption processes, demonstrating the effectiveness of MWCNT-ttpy for divalent metal ion removal.

The experimental data for the adsorption of Pb^{2+} and Zn^{2+} onto acid- and nitrogen-functionalized MWCNTs as a function of adsorbent dose can be found in Appendix II.

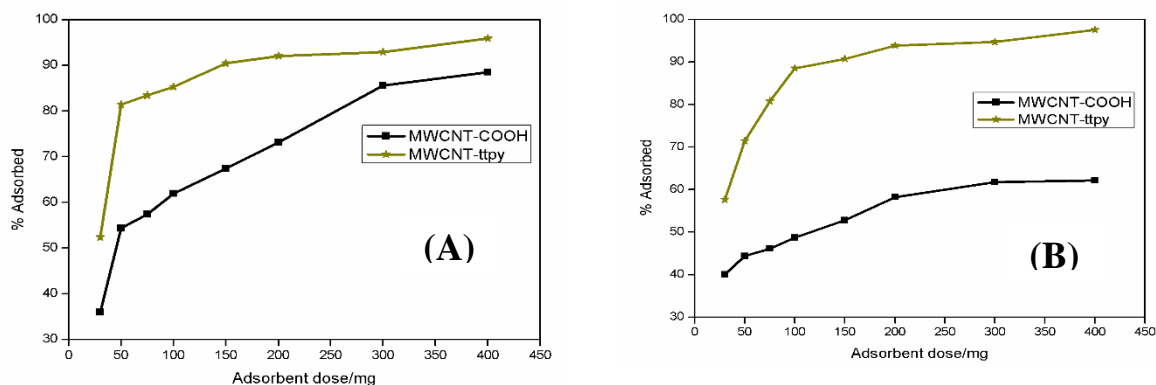


Fig. 5.4: Effect of adsorbent dose on the adsorption of (A) Pb²⁺ and (B) Zn²⁺ by using MWCNT-COOH and MWCNT-ttpy [conditions: 20 cm³ of 100 mg dm⁻³ Pb²⁺/Zn²⁺, 24 h equilibration time, pH = 4.5 (Pb²⁺) and pH = 5.5 (Zn²⁺), agitation speed 150 rpm, temperature 20 °C].

5.3.2.4. Effect of temperature

The influence of the change in adsorbate temperature was examined over the range of 293-318 K at varying concentrations of 10-100 mg dm⁻³. Figs. 5.5 and 5.6 show this effect for the adsorption of Pb²⁺ and Zn²⁺ respectively. The uptake of Pb²⁺ and Zn²⁺ onto MWCNT-COOH and MWCNT-ttpy increases with an increase in adsorbate temperature. An increase in adsorbate temperature may result in decreased solution viscosity and a rise in diffusion rate and kinetic energy of the metal ions onto the active sites of the adsorbent [35]. These factors also accounts for the activation of the pores/sites of MWCNT-COOH and MWCNT-ttpy for metal ion removal and therefore induces increased uptake of Pb²⁺ and Zn²⁺ at higher temperatures. This trend indicates an endothermic process of adsorption for both metal ions. The experiment further reveals the potential application of these adsorbents for the treatment of metal-contaminated effluents directly discharged from industries, since effluents are normally discharged at temperatures higher than 298 K.

Fig. 5.5 and 5.6 further explain the influence of varying adsorbate concentration of Pb²⁺ and Zn²⁺, respectively, onto both adsorbents. Similar trends were noticed for both adsorbate solutions with MWCNT-COOH and MWCNT-ttpy. The figures show an increase in adsorption capacity (q_e) as the adsorbate concentration increases from 10-100 mg dm⁻³. An increase in the amount of Pb²⁺ removed per unit mass (q_e) of adsorbent from 3.900 to 20.34 mg g⁻¹ and from 4.024 to 33.78 mg g⁻¹ was obtained for MWCNT-COOH and MWCNT-ttpy, respectively, at 293 K (Figs. 5.5A and 5.5B). Consequently, an increase in Zn²⁺ uptake (q_e) from 1.874 to 12.90 mg g⁻¹ and 3.779 to 28.35 mg g⁻¹ was also noticed for MWCNT-COOH and MWCNT-ttpy, respectively, at 293 K (Figs. 5.6A and 5.6B). Similar trends were noticeable over the same concentration range for other temperatures of 303 K, 313 K

and 318 K (Figs 5.5-5.6). This could be associated to the increase in the driving force required to overcome the resistance for the active sites on the adsorbents at high metal ions concentration. This in turn produces better uptake of metal ions (q_e) onto the adsorbents at higher metal ion concentrations. Hence, increasing metal ion concentration results into better sorption onto the adsorbents. The application of these sorbents could therefore be said to be effective even at high metal ion concentrations. However, MWCNT-tpy showed a better removal efficiency over MWCNT-COOH for both metal ions. For both adsorbents, the removal efficiency of Pb^{2+} was greater than for Pb^{2+} .

The experimental data for the adsorption of Pb^{2+} and Zn^{2+} onto acid- and nitrogen-functionalized MWCNTs as a function of temperature can be found in Appendix II.

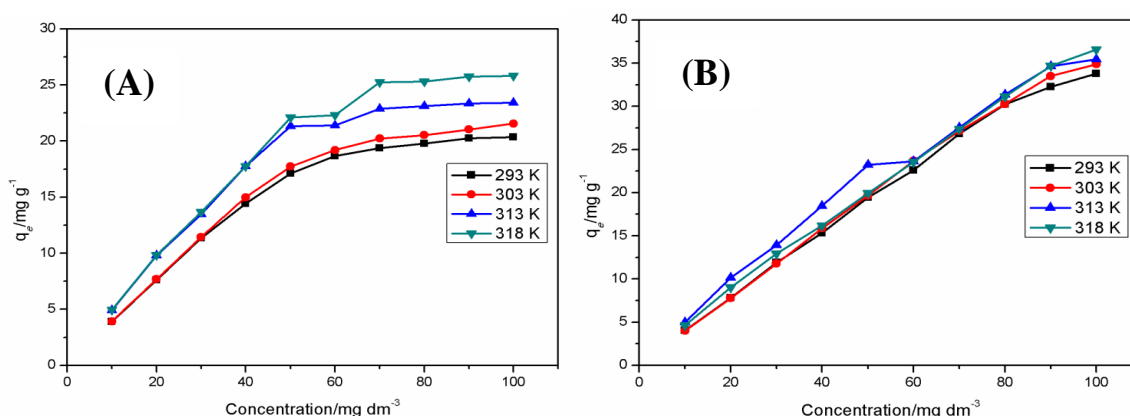


Fig. 5.5: Effect of varying temperature on the adsorption of Pb^{2+} (A) MWCNT-COOH and (B) MWCNT-tpy [conditions: $20\ cm^3$ of $10\text{-}100\ mg\ dm^{-3}$ Pb^{2+} , 24 h equilibration time, pH = 4.5, agitation speed 150 rpm, temperature 20-45 °C].

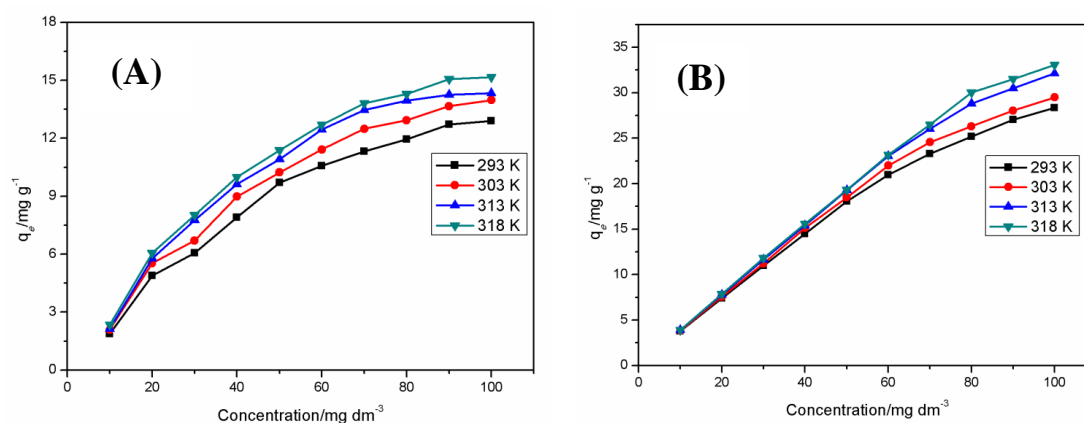


Fig. 5.6: Effect of varying temperature on the adsorption of Zn^{2+} (A) MWCNT-COOH and (B) MWCNT-tpy [conditions: $20\ cm^3$ of $10\text{-}100\ mg\ dm^{-3}$ Zn^{2+} , 24 h equilibration time, pH = 5.5 (Zn^{2+}), agitation speed 150 rpm, temperature 20-45 °C].

5.3.2.5. Isotherm studies

Isotherms provide information on the effectiveness of adsorbents, the mechanisms/interactions involved in adsorption, and the distribution of adsorbate molecules/ions in solid and liquid phases. Two-and three-parameter isotherm models consisting of the Freundlich, Langmuir, Temkin, Dubinin-Radushkevich (D-R), Sips, Redlich-Peterson (R-P), Khan and Toth models were applied to the experimental data obtained for the adsorption of Pb^{2+} and Zn^{2+} . The equations of all eight isotherms are given in Table 5.3. Isotherm parameters were obtained by fitting the equilibrium data to the models described, and are given in Tables 5.4 and 5.5 for the adsorption of Pb^{2+} and Zn^{2+} , respectively.

Table 5.4: Isotherm parameters for the adsorption of Pb^{2+} onto MWCNT-COOH and MWCNT-ttpy

Isotherms	Parameters	MWCNT-COOH				MWCNT-ttpy			
		293 K	303 K	313 K	318 K	293 K	303 K	313 K	318 K
Langmuir	q_m	20.69	21.49	23.89	26.03	36.23	34.46	34.68	36.31
	b	0.740	0.921	1.648	1.979	0.907	1.538	6.441	5.809
	RSE*	0.579	0.420	0.807	1.253	1.637	1.703	4.352	3.837
	SSR†	2.680	1.411	5.212	12.56	21.43	23.20	151.5	117.8
Freundlich	K_F	9.801	10.61	13.98	15.47				
	n	4.740	4.880	5.888	5.660				
	RSE	1.983	2.163	2.822	2.580				
	SSR	31.46	37.42	63.70	53.24				
Sips	q_m	21.40	21.98	24.34	27.88				
	b	0.726	0.889	1.542	1.505				
	n	1.167	1.121	1.125	1.434				
	RSE	0.511	0.349	0.804	0.953				
	SSR	1.826	0.854	4.519	6.354				
R-P	K_{RP}	17.45	22.40	38.91	62.72				
	α_{RP}	0.936	1.146	1.617	2.658				
	β	0.970	0.972	1.002	0.966				
	RSE	0.562	0.353	0.862	1.266				
	SSR	2.211	0.870	5.206	11.22				

*RSE residual standard error, †SSR – sum of squared residuals

Table 5.5: Isotherm parameters for the adsorption of Zn²⁺ onto MWCNT-COOH and MWCNT-ttpy

Isotherms	Parameters	MWCNT-COOH				MWCNT-ttpy			
		293 K	303 K	313 K	318 K	293 K	303 K	313 K	318 K
Langmuir	q_m	18.51	18.42	18.14	18.55	32.60	31.99	34.46	34.45
	b	0.037	0.051	0.069	0.077	0.226	0.406	0.685	1.157
	RSE*	0.275	0.293	0.385	0.340	0.504	0.627	0.707	1.166
	SSR†	0.604	0.689	1.183	0.927	2.030	3.144	3.996	10.89
Freundlich	K_F	1.681	2.227	2.835	3.117	8.559	11.04	14.26	16.87
	n	1.991	2.188	2.418	2.479	2.628	3.054	3.260	3.520
	RSE	0.636	0.636	0.980	0.746	2.151	2.808	3.402	3.466
	SSR	3.202	3.239	7.689	4.456	37.03	63.07	92.58	96.08
Sips	q_m	18.52	20.45	17.73	21.00	31.60	30.51	32.99	36.08
	b	0.037	0.058	0.066	0.090	0.222	0.406	0.729	1.020
	n	1.000	1.131	0.962	1.191	0.938	0.875	0.872	1.128
	RSE	0.294	0.276	0.408	0.278	0.505	0.498	0.536	1.115
	SSR	0.604	0.533	1.163	0.541	1.786	1.734	2.007	8.707

*RSE – residual standard error, †SSR – sum of squared residuals

The results indicate that the equilibrium data obtained for Pb²⁺ removal by using MWCNT-COOH and MWCNT-ttpy were best described by the Langmuir model (Table 5.4). This inference is made based on the lowest sum of squared residuals (SSR) and the residual standard errors (RSE), both of which are an indication of the model which best fits the experimental data. Of the three-parameter isotherms tested, the Redlich-Peterson and Sips models described the equilibrium data for MWCNT-COOH. The isotherm parameters obtained for the adsorption of Zn²⁺ by using MWCNT-COOH and MWCNT-ttpy are presented in Table 5.5. For the two-parameter models, the Langmuir isotherm best described the data for both adsorbents, while for the three-parameter models, the Sips model, which is a generalization of the Langmuir and Freundlich isotherms, was best suited for modelling the data (Table 5.5).

An increase in the Langmuir maximum adsorption capacity (q_m) ranging from 20.69 to 26.03 mg g⁻¹ for MWCNT-COOH and 36.23 to 36.31 mg g⁻¹ for MWCNT-ttpy was obtained for the adsorption of Pb²⁺ over the studied temperature range. Similarly, q_m values increased from 18.51 to 18.55 mg g⁻¹ for MWCNT-COOH and 32.60 to 34.45 mg g⁻¹ for MWCNT-ttpy for the adsorption of Zn²⁺. The binding strength between Pb²⁺ or Zn²⁺ and the adsorbents can also be estimated from the Langmuir isotherm constant (b). An increase in its value over the temperature range was obtained for both metal ions with MWCNT-COOH and MWCNT-ttpy, indicating great binding strength between the adsorbates and the adsorbents [3]. Larger values were obtained with MWCNT-ttpy, showing better interaction between adsorbates and adsorbents.

The Langmuir isotherm was primarily considered best for describing data obtained for the adsorption of Pb^{2+} and Zn^{2+} onto MWCNT-COOH and MWCNT-tpy. This study therefore infers that adsorption proceeded through a monolayer coverage of adsorbates on adsorbents; possessing identical sites with uniform energy and no interaction between adjacent species. The values of q_m obtained from this study were compared with those previously reported for the removal of Pb^{2+} and Zn^{2+} by using multiwalled carbon nanotubes. Table 5.6 indicates that our results compare favourably with those obtained by other workers. An increase in the uptake of metal ions was noticed with functionalized MWCNTs, which generally agree with results obtained in this study.

Table 5.6: Comparison of Langmuir maximum capacity (q_m) for the adsorption of Pb^{2+} and Zn^{2+} onto CNT-containing adsorbents

Adsorbents	Conditions	Adsorbate	$q_m/mg\ g^{-1}$	References
Pristine MWCNT	pH 6.2, C_i 5-100 $mg\ dm^{-3}$, 200 min, 298 K	Pb^{2+}	2.940	[4]
Pristine MWCNT	pH 5.7, C_i 2-80 $mg\ dm^{-3}$, 10 mg, 60 min, 298 K	Pb^{2+}	6.710	[62]
Oxidized MWCNT	pH 6.2, C_i 5-100 $mg\ dm^{-3}$, 200 min, 298 K	Pb^{2+}	37.36	[4]
Oxidized MWCNT	pH 5.7, C_i 2-80 $mg\ dm^{-3}$, 10 mg, 60 min, 298 K	Pb^{2+}	27.80	[62]
SWCNT	pH 7.0, C_i 10-80 $mg\ dm^{-3}$, 12 h, 298 K	Zn^{2+}	28.22	[37]
Purified CNT	pH 7.0, C_i 10-80 $mg\ dm^{-3}$, 12 h, 298 K	Zn^{2+}	22.58	[37]
MWCNT-COOH	pH 4.5, C_i 10-100 $mg\ dm^{-3}$, 50 mg dose, 24 h, 293 K	Pb^{2+}	20.69	This study
MWCNT-ttpty	pH 4.5, C_i 10-100 $mg\ dm^{-3}$, 50 mg dose, 24 h, 293 K	Pb^{2+}	36.23	This study
MWCNT-COOH	pH 5.5, C_i 10-100 $mg\ dm^{-3}$, 50 mg dose, 24 h, 293 K	Zn^{2+}	18.51	This study
MWCNT-ttpty	pH 5.5, C_i 10-100 $mg\ dm^{-3}$, 50 mg dose, 24 h, 293 K	Zn^{2+}	32.60	This study

5.3.2.6. Thermodynamic studies

To determine the spontaneity and feasibility of the adsorption processes, thermodynamic parameters such as enthalpy change (ΔH°), entropy change (ΔS°) and Gibbs energy change (ΔG°) were calculated from equations 5.3 and 5.4 [63]:

$$\Delta G^\circ = -RT \ln K \quad (5.3)$$

$$\ln K = -\frac{\Delta H^\circ}{RT} + \frac{\Delta S^\circ}{R} \quad (5.4)$$

where K is the distribution adsorption coefficient, calculated from the product of q_m and b , obtained from the Langmuir plot (Table 5.4-5.5). The calculated K value was made dimensionless by multiplying by 1000 [3,64,65], R is the universal gas constant ($8.314 \text{ J K}^{-1} \text{ mol}^{-1}$) and T is the absolute temperature in Kelvin. A plot of $\ln K$ against $1/T$ was obtained and the thermodynamic parameters, ΔH° and ΔS° , were calculated from the slope and intercept, respectively [3,64,65].

Table 5.7 and 5.8 list the thermodynamic parameters obtained for the adsorption of Pb^{2+} and Zn^{2+} , respectively. Both adsorption processes show negative ΔG° values, which increase as the temperature of solution increases. This trend indicates a spontaneous process which is more favourable at high temperatures for removal of Pb^{2+} and Zn^{2+} . The ions in solution desolvate faster at higher temperatures, inducing faster diffusion of ions to the pores of adsorbent, and may be responsible for the more favourable process at higher temperatures [4]. Positive ΔH° and ΔS° values were also obtained for both processes with MWCNT-COOH and MWCNT-ttpty. ΔH° values indicate that the adsorption process was endothermic in nature while positive ΔS° shows an increase in the randomness at the solid-solution interface. It was, however, noticed that larger ΔG° , ΔH° and ΔS° values were obtained for MWCNT-ttpty, indicating better sorption of Pb^{2+} and Zn^{2+} to active sites of this adsorbent. In turn, the adsorption of Pb^{2+} was greater than for Zn^{2+} for both adsorbents.

Thermodynamic parameters also provide insights into the mechanism involved in adsorption. An adsorption process is considered physisorption if ΔG° values are between -20 and 0 kJ mol^{-1} [4], or ΔH° values are between 2.1 and 20.9 kJ mol^{-1} [3,66]. The process is considered chemisorption if ΔG° values are between -80 to -400 kJ mol^{-1} [4] and ΔH° values are between 80 to 200 kJ mol^{-1} [3]. The calculated ΔG° and ΔH° values indicate that the values obtained were higher than the predicted values for physisorption, but lower than for chemisorption. This shows that the adsorption of Pb^{2+} and Zn^{2+} onto MWCNT-COOH and MWCNT-ttpty was a physico-chemical process. In all cases, the adsorption processes were entropy-driven.

Table 5.7: Thermodynamic parameters for the adsorption of Pb²⁺ onto MWCNT-COOH and MWCNT-ttpy

Adsorbent	T/K	$\Delta G^\circ/\text{kJ mol}^{-1}$	$\Delta H^\circ/\text{kJ mol}^{-1}$	$\Delta S^\circ/\text{J K}^{-1} \text{mol}^{-1}$
MWCNT-COOH	293	-23.47		
	303	-24.92		
	313	-27.53	38.87	212.0
	318	-28.68		
MWCNT-ttpy	293	-25.33		
	303	-27.40		
	313	-32.05	65.22	308.1
	318	-32.41		

Table 5.8: Thermodynamic parameters for the adsorption of Zn²⁺ onto MWCNT-COOH and MWCNT-ttpy

Adsorbent	T/K	$\Delta G^\circ/\text{kJ mol}^{-1}$	$\Delta H^\circ/\text{kJ mol}^{-1}$	$\Delta S^\circ/\text{J K}^{-1} \text{mol}^{-1}$
MWCNT-COOH	293	-15.91		
	303	-17.24		
	313	-18.56	22.80	132.1
	318	-19.21		
MWCNT-ttpy	293	-21.69		
	303	-23.86		
	313	-26.20	50.57	246.1
	318	-28.01		

5.3.2.7. Desorption

To avoid the disposal of metal-contaminated adsorbents into the environment, and thereby generating secondary wastes, desorption studies were carried out in order to regenerate the adsorbents and isolate metal ions for other industrial applications. The used adsorbents (50 mg) were weighed and agitated in a 10 cm³ aliquot of 0.1 mol dm⁻³ HCl for 30 min. The suspensions were filtered after agitation and the concentrations of the desorbed metal ions were determined by using ICP-OES.

The percentage desorption from Pb-loaded MWCNT-COOH was found to be 82% and a value of 77% was obtained for Pb-loaded MWCNT-ttpy. Desorption percentages of 72% and 76% were obtained for Zn-loaded MWCNT-COOH and MWCNT-ttpy respectively. These results indicate that recovery of Pb²⁺ and Zn²⁺ from the loaded adsorbent is possible and that adsorbents can be recycled.

5.4. Conclusions

The removal of Pb^{2+} and Zn^{2+} from aqueous solution was investigated by using acid-functionalized MWCNT (MWCNT-COOH) and nitrogen-functionalized MWCNT (MWCNT-ttpy) through batch adsorption experiments. The extent of adsorption was influenced by changes in the solution pH, adsorbent dose and contact time between the adsorbents with the adsorbates. Adsorption experiments were conducted at a pH of 4.5 and 5.5 for Pb^{2+} and Zn^{2+} , respectively.

The study of the kinetics of adsorption revealed that the data for both metal ions was best described by the pseudo-second order model, involving a bimolecular interaction between the active sites on the adsorbents and the cationic metal ions. Isotherm studies revealed that the Langmuir model best describes the equilibrium data obtained for both processes, suggesting monolayer coverage of adsorbates onto the active sites of the adsorbents. All adsorption processes proved to be spontaneous, feasible and endothermic. Also, the removal of Pb^{2+} and Zn^{2+} from aqueous solution was found to be entropy-driven.

A better sorption ability for Pb^{2+} and Zn^{2+} was achieved with MWCNT-ttpy, owing to the increase in surface area and the nature of the complexation sites on the ligand attached to the MWCNT adsorbent. This suggests that the modification of MWCNTs with a nitrogen-donor ligand such as HO-Phttpy afforded an adsorbent that is both effective and efficient for the removal of heavy metal ions from polluted wastewaters.

References

- [1] Ş.S. Bayazit, İ. İnci, Adsorption of Pb(II) ions from aqueous solutions by carbon nanotubes oxidized different methods, *J. Ind. Eng. Chem.*, 19 (2013) 2064-2071.
- [2] G. Mamba, X.Y. Mbianda, P.P. Govender, B.B. Mamba, R.W. Krause, Application of multiwalled carbon nanotube-cyclodextrin polymers in the removal of heavy metals from water, *J. Appl. Sci.*, 10 (2010) 940-949.
- [3] I.A.A. Hamza, B.S. Martincigh, J.C. Ngila, V.O. Nyamori, Adsorption studies of aqueous Pb(II) onto a sugarcane bagasse/multi-walled carbon nanotube composite, *Phys. Chem. Earth*, 66 (2013) 157-166.
- [4] G.D. Vuković, A.D. Marinković, S.D. Škapin, M.Đ. Ristić, R. Aleksić, A.A. Perić-Grujić, P.S. Uskoković, Removal of lead from water by amino modified multi-walled carbon nanotubes, *Chem. Eng. J.*, 173 (2011) 855-865.
- [5] A. Stafiej, K. Pyrzynska, Adsorption of heavy metal ions with carbon nanotubes, *Sep. Purif. Technol.*, 58 (2007) 49-52.
- [6] N.M. Mubarak, J.N. Sahu, E.C. Abdullah, N.S. Jayakumar, Removal of heavy metals from wastewater using carbon nanotubes, *Sep. Purif. Rev.*, 43 (2013) 311-338.
- [7] C.A. Dooyema, A. Neri, Y.-C. Lo, J. Durant, P.I. Dargan, T. Swarthout, O. Biya, S.O. Gidado, S. Haladu, N. Sani-Gwarzo, P.M. Nguku, H. Akpan, S. Idris, A.M. Bashir, M.J. Brown, Outbreak of fatal childhood lead poisoning related to artisanal gold mining in northwestern Nigeria, 2010, *Environ. Health Perspect.*, 120 (2012) 601-607.
- [8] L. Yi-Chun, C.A. Dooyema, A. Neri, J. Durant, T. Jefferies, M.-M. A., L. de Ravello, D. Thoroughman, L. Davis, R.S. Dankoli, M.Y. Samson, L.M. Ibrahim, O. Okechukwu, N.T. Umar-Tsafe, A.H. Dama, M. Jean Brown, Childhood lead poisoning associated with gold ore processing: a village-level investigation-Zamfara State, Nigeria, October-November 2010, *Environ. Health Perspect.*, 120 (2012) 1450-1455.
- [9] G.J. Fosmire, Zinc toxicity, *Am. J. Clin. Nutr.*, 51 (1990) 225-227.
- [10] L.M. Plum, L. Rink, H. Haase, The essential toxin: Impact of zinc on human health, *Int. J. Environ. Res. Public Health*, 7 (2010) 1342-1365.
- [11] J. Chen, S. Xiao, X. Wu, K. Fang, W. Liu, Determination of lead in water samples by graphite furnace atomic absorption spectrometry after cloud point extraction, *Talanta*, 67 (2005) 992-996.
- [12] J. Chen, K.C. Teo, Determination of cadmium, copper, lead and zinc in water samples by flame atomic absorption spectrometry after cloud point extraction, *Anal. Chim. Acta*, 450 (2001) 215-222.
- [13] K.I. Mahan, T.A. Foderaro, T.L. Garza, R.M. Martinez, G.A. Maroney, M.R. Trivisonno, E.M. Willging, Microwave digestion techniques in the sequential extraction of calcium, iron, chromium, manganese, lead, and zinc in sediments, *Anal. Chem.*, 59 (1987) 938-945.

- [14] A. Adeniyi, Determination of cadmium, copper, iron, lead, manganese, and zinc in water leaf (*Talinum triangulare*) in dumpsites, *Environ. Int.*, 22 (1996) 259-262.
- [15] M.B. Ogundiran, O.A. Oyetade, J.O. Babayemi, O. Osibanjo, Potential environmental hazards of non-rechargeable electric torch wastes in Nigeria *Int. J. Environ. Waste Manag.*, 13 (2014) 115-130.
- [16] M.G.A. Vieira, A.F. De Almeida Neto, M.G.C. Da Silva, C.N. Carneiro, A.A. Melo Filho, Adsorption of lead and copper ions from aqueous effluents on rice husk ash in a dynamic system *Braz. J. Chem. Eng.*, 31 (2014) 519-529.
- [17] A. Elham, T. Hossein, H. Mahnoosh, Removal of Zn(II) and Pb(II) ions Using Rice Husk in Food Industrial Wastewater, *J. Appl. Sci. Environ. Manag.*, 14 (2010) 159-162.
- [18] I.W. Mwangi, J.C. Ngila, Removal of heavy metals from contaminated water using ethylenediamine-modified green seaweed (*caulerpa serrulata*), *Phys. Chem. Earth*, 50-52 (2012) 111-120.
- [19] B. Yasemin, T. Zeki, Removal of heavy metals from aqueous solution by sawdust adsorption, *J. Environ. Sci.*, 19 (2007) 160-166.
- [20] P. Pavasant, R. Apiratikul, V. Sungkhum, P. Suthiparinyanont, S. Wattanachira, T.F. Marhaba, Biosorption of Cu^{2+} , Cd^{2+} , Pb^{2+} , and Zn^{2+} using dried marine green macroalga *Caulerpa lentillifera*, *Bioresour. Technol.*, 97 (2006) 2321-2329.
- [21] I.W. Mwangi, J.C. Ngila, J.O. Okonkwo, A comparative study of modified and unmodified maize tassels for removal of selected trace metals in contaminated water, *Toxicol. Environ. Chem.*, 94 (2012) 20-39.
- [22] Y. Zhou, B. Gao, A.R. Zimmerman, J. Fang, Y. Sun, X. Cao, Sorption of heavy metals on chitosan-modified biochars and its biological effects, *Chem. Eng. J.*, 231 (2013) 512-518.
- [23] Y. Kim, B. Lee, J. Yi, Preparation of functionalized mesostructured silica containing magnetite (MSM) for the removal of copper ions in aqueous solutions and its magnetic separation, *Sep. Sci. Technol.*, 38 (2007) 2533-2548.
- [24] M. Kobya, E. Demirbas, E. Senturk, M. Ince, Adsorption of heavy metals from aqueous solution by activated carbon prepared from apricot stone, *Bioresour. Technol.*, 96 (2005) 1511521.
- [25] M.M. Kamel, M.A. Ibrahim, A.M. Ismael, M.A. El-Motaleeb, Adsorption of some heavy metal ions from aqueous solutions by using kaolinite clay, *Ass. Univ. Bull. Environ. Res.*, 7 (2004) 101-110.
- [26] Y.-L. Lai, M. Thirumavalavan, J.-F. Lee, Effective adsorption of heavy metal ions (Cu^{2+} , Pb^{2+} , Zn^{2+}) from aqueous solution by immobilization of adsorbents on *Ca*-alginate beads, *Toxicol. Environ. Chem.*, 92 (2010) 697-705.
- [27] L. Giraldo, J.C. Moreno-Piraján, Study on the adsorption of heavy metal ions from aqueous solution on modified SBA-15, *Mater. Res.*, 16 (2013) 745-754.

- [28] J.-P. Tessonnier, D. Rosenthal, T.W. Hansen, C. Hess, M.E. Schuster, R. Blume, F. Girgsdies, N. Pfänder, O. Timpe, D.S. Su, R. Schlögl, Analysis of the structure and chemical properties of some commercial carbon nanostructures, *Carbon*, 47 (2009) 1779-1798.
- [29] C. Chen, B. Liang, A. Ogino, X. Wang, M. Nagatsu, Oxygen functionalization of multiwall carbon nanotubes by microwave-excited surface-wave plasma treatment, *J. Phys. Chem. C*, 113 (2009) 7659-7665.
- [30] B. Parekh, T. Debies, P. Knight, K. Santhanam, G. Takacs, Surface functionalization of multiwalled carbon nanotubes with UV and vacuum UV photo-oxidation, *J. Adhes. Sci. Technol.*, 20 (2006) 1833-1846.
- [31] K. Yang, W. Wu, Q. Jing, L. Zhu, Aqueous adsorption of aniline, phenol, and their substitutes by multi-walled carbon nanotubes, *Environ. Sci. Technol.*, 42 (2008) 7931-7936.
- [32] R.Q. Long, R.T. Yang, Carbon nanotubes as superior sorbent for dioxin removal, *J. Am. Chem. Soc.*, 123 (2001) 2058-2059.
- [33] S.A. Kosa, G. Al-Zhrani, M. Abdel Salam, Removal of heavy metals from aqueous solutions by multi-walled carbon nanotubes modified with 8-hydroxyquinoline, *Chem. Eng. J.*, 181-182 (2012) 159-168.
- [34] S.R. Popuri, R. Frederick, C.-Y. Chang, S.-S. Fang, C.-C. Wang, L.-C. Lee, Removal of copper(II) ions from aqueous solutions onto chitosan/carbon nanotubes composite sorbent, *Desalin. Water Treat.*, 52 (2013) 691-701.
- [35] G. Rao, C. Lu, F. Su, Sorption of divalent metal ions from aqueous solution by carbon nanotubes: A review, *Sep. Purif. Technol.*, 58 (2007) 224-231.
- [36] S. Srivastava, Sorption of divalent metal ions from aqueous solution by oxidized carbon nanotubes and nanocages: A review, *Adv. Mat. Lett.*, 4 (2013) 2-8.
- [37] C. Lu, H. Chiu, Adsorption of zinc(II) from water with purified carbon nanotubes, *Chem. Eng. Sci.*, 61 (2006) 1138-1145.
- [38] S. Santangelo, G. Messina, G. Faggio, S.H. Abdul Rahim, C. Milone, Effect of sulphuric-nitric acid mixture composition on surface chemistry and structural evolution of liquid-phase oxidised carbon nanotubes, *J. Raman Spectrosc.*, 43 (2012) 1432-1442.
- [39] O.A. Oyetade, V.O. Nyamori, B.S. Martincigh, S.B. Jonnalagadda, Nitrogen-functionalised carbon nanotubes as a novel adsorbent for the removal of Cu(II) from aqueous solution, (unpublished results).
- [40] Y.S. Ho, Comment on "Cadmium removal from aqueous solutions by chitin: kinetic and equilibrium studies", *Water Res.*, 38 (2004) 2962-2964
- [41] J. Lin, L. Wang, Comparison between linear and non-linear forms of pseudo-first-order and pseudo-second-order adsorption kinetic models for the removal of methylene blue by activated carbon, *Front. Environ. Sci. Eng.*, 3 (2009) 320-324.

- [42] Y.-S. Ho, Removal of copper ions from aqueous solution by tree fern, *Water Res.*, 37 (2003) 2323-2330.
- [43] Y.S. Ho, G. McKay, Pseudo-second order model for sorption processes, *Process Biochem.*, 34 (1999) 451-465.
- [44] S.H. Chien, W.R. Clayton, Application of Elovich equation to the kinetics of phosphate release and sorption in soils, *Soil Sci. Soc. Am. J.*, 44 (1980) 265-268.
- [45] E. Demirbas, M. Kobya, E. Senturk, T. Ozkan, Adsorption kinetics for the removal of chromium(VI) from aqueous solutions on the activated carbons prepared from agricultural wastes, *Water SA*, 30 (2004) 533-539.
- [46] I. Langmuir, The adsorption of gases on plane surfaces of glass, mica and platinum, *J. Am. Chem. Soc.*, 40 (1918) 1361-1402.
- [47] H. Freundlich, Adsorption in solids, *Z. Phys. Chem.*, 57 (1906) 385-470.
- [48] M.I. Temkin, V. Pyzhev, Kinetics of ammonia synthesis on promoted iron catalysts, *Acta Phys. Chim.*, 12 (1940) 327-356.
- [49] M.M. Dubinin, L.V. Radushkevich, The equation of the characteristic curve of activated charcoal, *Proc. Acad. Sci, U.S.S.R, Phys. Chem. Sect.*, 55 (1947) 327-329.
- [50] R. Sips, Combined form of Langmuir and Freundlich equations, *J. Chem. Phys.*, 16 (1948) 490-495.
- [51] J. Toth, State equations of the solid-gas interface layers, *Acta Chim. Acad. Sci. Hung.*, 69 (1971) 311-328.
- [52] O. Redlich, D.L. Peterson, A useful adsorption isotherm, *J. Phys. Chem.*, 63 (1959) 1024.
- [53] A.R. Khan, I.R. Al-Waheab, A. Al-Haddad, A generalized equation for adsorption isotherms for multi-component organic pollutants in dilute aqueous solution, *Environ. Technol.*, 17 (1996) 13-23.
- [54] The R Development Core Team, The R foundation for statistical Computing, R version 3.0.2 (2013).
- [55] O.A. Oyetade, V.O. Nyamori, B.S. Martincigh, S.B. Jonnalagadda, Effectiveness of carbon nanotube-cobalt ferrite nanocomposites for the adsorption of rhodamine B from aqueous solutions, *RSC Adv.*, 5 (2015) 22724-22739.
- [56] M. Goyal, V.K. Rattan, D. Aggarwal, R.C. Bansal, Removal of copper from aqueous solutions by adsorption on activated carbons, *Colloids Surf. A Physicochem. Eng. Asp.*, 190 (2001) 229-238.
- [57] R.M. Smith, A.E. Martell, *Critical Stability Constants*, 6 (1976) Plenum Press, New York.
- [58] P. Gans, Hyperquad simulation and speciation: , HySS, version 4.0.31, (2009).
- [59] S.G. Muntean, M.E. Radulescu-Grad, P. Sfarloaga, Dye adsorbed on copolymer, possible specific sorbent for metal ions removal, *RSC Adv.*, 4 (2014) 27354-27362.

- [60] C.H. Wu, Adsorption of reactive dye onto carbon nanotubes: equilibrium, kinetics and thermodynamics, *J. Hazard. Mater.*, 144 (2007) 93-100.
- [61] K.S. Tong, M.J. Kassim, A. Azraa, Adsorption of copper ion from its aqueous solution by a novel biosorbent *Uncaria gambir*: Equilibrium, kinetics, and thermodynamic studies, *Chem. Eng. J.*, 170 (2011) 145-153.
- [62] M.S. Tehrani, P.A. Azar, P. Ehsani Namin, S.M. Dehaghi, Removal of lead ions from aqueous solution using multi-walled carbon nanotubes: The effect of functionalization, *J. Appl. Environ. Biol. Sci.*, 4 (2014) 316-326.
- [63] K.M. Doke, E.M. Khan, Adsorption thermodynamics to clean up wastewater;critical review, *Rev. Environ. Sci. Bio.*, 12 (2013) 25-44.
- [64] S.K. Milonjić, A consideration of the correct calculation of thermodynamic parameters of adsorption, *J. Serb. Chem. Soc.*, 72 (2007) 1363-1367.
- [65] R. Djeribi, Q. Hamdaoui, Sorption of copper(II) from aqueous solutions by cedar sawdust and crushed brick, *Desalination*, 225 (2008) 95-112.
- [66] Y. Liu, Y.-J. Liu, Biosorption isotherms, kinetics and thermodynamics, *Sep. Purif. Technol.*, 61 (2008) 229-242.

Chapter 6

Removal of Cd²⁺ and Hg²⁺ onto nitrogen-functionalized carbon nanotube from aqueous solutions

Oluwaseun A. Oyetade, Vincent O. Nyamori, Bice S. Martincigh* and Sreekantha B. Jonnalagadda

School of Chemistry and Physics, University of KwaZulu-Natal, Westville Campus,
Private Bag X54001, Durban 4000, South Africa

*Corresponding author: Tel: +27 31 2601394; Fax: +27 31 2603091; E-mail:
martinci@ukzn.ac.za

Abstract

The efficiency of nitrogen-functionalized multiwalled carbon nanotubes (MWCNT-tty) for the removal of Cd^{2+} and Hg^{2+} from aqueous solutions was investigated and compared with their uptake on acid-functionalized multiwalled carbon nanotubes (MWCNT-COOH). Batch adsorption experiments investigating the influence of pH, contact time, adsorbent dose, metal ion concentration and adsorbate temperature were performed to determine the best sorption conditions for removal.

The experimental data obtained for both adsorbates were best described by the pseudo-second order model, indicating a bimolecular chemical interaction between active sites on the adsorbents and the metal ion species. The Langmuir and Sips models best described the equilibrium data obtained for both sorbates. For Cd^{2+} , an uptake (q_m) of 10.41 mg g^{-1} for MWCNT-COOH was achieved and 41.51 mg g^{-1} for MWCNT-tty. An increase in Hg^{2+} uptake was also obtained for MWCNT-tty of 36.13 mg g^{-1} compared with 33.89 mg g^{-1} for MWCNT-COOH. Hence, MWCNT-tty proved to be more effective towards the removal of both adsorbates, relative to MWCNT-COOH.

Desorption experiments conducted by using HCl as eluent afforded excellent recovery of sorbates and regeneration of sorbents, thus, increasing the chances of reutilization of sorbents. Hence, the application of MWCNT-tty as a potential sorbent for effluent and wastewater treatment is feasible and should be further explored for water pollution control.

Keywords: nitrogen-functionalized multiwalled carbon nanotubes, kinetics, isotherm, cadmium, mercury

6.1. Introduction

The increase in the contamination of water supplies with toxins, such as heavy metals, has intensified in recent times due to the proliferation of urbanization and industrialization [1,2]. Industrial activities from battery manufacturing, electroplating, tanning and mining, produce effluents containing a variety of pollutants, especially metal ions in large amounts. Therefore, metal ions are largely distributed into natural waters through the indiscriminate discharge of industrial effluents into these water bodies [3,4].

Heavy metal contamination is one of the most significant environmental challenges and this is due to their solubility in water, mobility, accumulation and persistence in the environment [4]. Cadmium and mercury are regarded as one of the most poisonous pollutants [4,5], whose intake, even at low concentrations, results in several long-term health effects in man, wildlife and aquatic life [6]. The pathway through which Cd^{2+} enters into the environment is *via* the discharge of wastes generated from smelting, alloy production, electroplating, batteries, mining and refinery operations [3,7]. An intake of Cd^{2+} can result in damage of the lungs, kidneys, and pancreas, and may also lead to various cardiovascular diseases [3,4,8]. Due to its ability to bio-accumulate in man, Cd^{2+} may persist in the human system for a period of 10 years [6,9]. Based on these consequences, 0.005 mg dm^{-3} and 0.003 mg dm^{-3} were recommended by the United States Environmental Protection Agency (US EPA) and the World Health Organization (WHO), respectively, as the maximum permissible limits of Cd^{2+} in drinking water [7,9-11].

Additionally, the intake of mercury and its associated compounds can lead to several developmental and neurological changes in living organisms [12]. Exposure to mercury is considered toxic to man, resulting in blood vessel congestion, kidney and lung dysfunction, cancerous, teratogenic and mutagenic diseases and, in extreme cases, may lead to death [12-14]. The release of Hg^{2+} into the environment is associated with vapours produced from volcanic eruptions and weathering of rocks [5], and emissions from coal-burning power plants and waste incinerators [15-17]. The most common discharge route of Hg^{2+} into aqueous solutions is the release of wastewater produced from paint, pulp, paper, fertilizer, and chlor-alkali manufacturing industries into receiving water streams [5,13]. The mercury poisoning reported in Minamata, Japan, was initiated by the release of methylmercury-contaminated wastewater, produced from an industrial factory into water bodies in 1956 [5,13,14]. This resulted in the bioaccumulation of mercury in aquatic life. Its subsequent ingestion by man, resulted in acute aftermaths such as coma and death. To this end, 0.006 mg dm^{-3} was recommended by WHO as the maximum permissible limit of Hg^{2+} in drinking water [10,11].

In spite of the restraints on the use of Cd^{2+} and Hg^{2+} by the Restriction of Hazardous Substance Directives (RoHS) [18], these toxic metals are still employed for applications such as electrical and lightening equipment in industries [18] and often used in thermometers and manometers in the laboratory. Hence, the generation of contaminated wastewater polluted by these toxins still exists. The treatment of wastewater is therefore of utmost importance before it is discharged into receiving streams. Several techniques such as chemical precipitation [19], electrodeposition [20,21], reverse osmosis [22], coagulation [23], ion-exchange [24] and adsorption [1,5] have been employed for heavy metal removal from wastewater. The efficacy of some of these techniques for metal ion removal have been poor [3,4,13]. However, adsorption is a promising method for metal ion removal from wastewater due to its simplicity, cost-effectiveness and the ability to regenerate spent adsorbents for reuse [3,7,9]. Adsorbents are easily handled [25]; hence, the usage of sorbents such as activated carbon [26], resins [27], biochars [4], bagasse [28], rice husk [29] and clay [8,30], amongst many others has been employed for Cd^{2+} and Hg^{2+} removal. Slow sorption processes, low adsorption capacity and inability to regenerate sorbents for reuse are some drawbacks attributed to the use of some conventional sorbents [31]. Hence, there is a need for the development of a fast, effective and efficient sorbent for the remediation of wastewater contaminated with Cd^{2+} or Hg^{2+} .

A growing research interest in the utilization of shaped carbon nanostructured materials as adsorbents has led to the application of multiwalled carbon nanotubes (MWCNTs) for pollutant removal in environmental sciences. MWCNTs possess remarkable physical and chemical properties with extraordinary thermal stability, and high porosities and surface areas available for adsorption [32,33]. Although MWCNTs are highly hydrophobic in nature, their surfaces are easily functionalized to contain a number of functional groups which serve as active sites for the removal of targeted pollutants from aqueous solutions. MWCNTs have been successfully applied for the removal of a variety of pollutants such as perfluorinated compounds [34], polyaromatic compounds [35], dyes [31,36], and phenol [37], amongst many. Metal ions, such as Cd^{2+} and Hg^{2+} , have also been removed from wastewater by using MWCNT-containing adsorbents [2,7,9]. For increased application in a practical sense, the adsorption efficiency of MWCNTs needs to be improved to favour the effective and efficient removal of Cd^{2+} and Hg^{2+} from wastewater.

To overcome this hurdle, 4'-(4-hydroxyphenyl)-2,2':6',2''-terpyridine (HO-Phttpy) was employed as a modifier for further functionalization of acid-functionalized MWCNTs (MWCNT-COOH). This process aims to improve the surface area and pore volume of the adsorbent, and hence increasing the number of chelating sites available for adsorption. In this work, the effectiveness of 4'-(4-hydroxyphenyl)-2,2':6',2''-terpyridinyl-functionalized MWCNT (MWCNT-ttpy) was tested for the removal of Cd^{2+} and Hg^{2+} from aqueous

solutions through a series of batch experiments. The uptake of the two adsorbates onto MWCNT-ttpy was compared with the adsorption capacity of MWCNT-COOH. Also, the kinetics and equilibrium isotherms were investigated.

6.2 Experimental

6.2.1. Materials and chemicals

Cadmium metal powder (99.9%) was obtained from Thomas Baker Chemicals (Pvt) Ltd. (Mumbai, India), while mercury(II)nitrate-mono-hydrate ($\text{Hg}(\text{NO}_3)_2 \cdot \text{H}_2\text{O}$) and potassium chloride (KCl, 99.8%) were obtained from BDH Laboratory Supplies (Poole, England). Diphenyl carbazone was purchased from The British Drug Houses Ltd (London, England). Sodium hydroxide (NaOH, 98%) was purchased from Merck Chemicals (Pty) Ltd (Gauteng, South Africa) while chemicals such as sodium borohydride (99%), 4-hydroxybenzaldehyde (99%), 2-acetylpyridine (99%), indium bromide (InBr_3 , 99%) and solvents such as absolute ethanol, *N,N'*-dimethylformamide (DMF, 99%), dimethyl sulfoxide- d_6 (DMSO-d_6 , 99%) and triethylsilane (Et_3SiH , 97%) were purchased from Sigma-Aldrich (St Louis, USA). Tetrahydrofuran (THF, 99%), chloroform (99%) and thionyl chloride (SOCl_2 , 99%) were purchased from Merck Chemicals (Pty) Ltd (Gauteng, South Africa) while aqueous ammonia (25%) was purchased from Associated Chemical Enterprises (Johannesburg, South Africa). Nitric (55%), sulfuric (98%) and hydrochloric acids (32%) were obtained from C C Imelmann Ltd (Robertsham, South Africa). All materials and chemicals were of analytical grade and used as received from suppliers without further purification. Pristine-MWCNTs (P-MWCNTs) (purity > 95%), synthesized by chemical vapour deposition (CVD), were obtained from Cheap Tubes Incorporation (Brattleboro, USA).

6.2.2. Adsorbent preparation

6.2.2.1. Preparation of oxidized MWCNTs (MWCNT-COOH)

Oxidation of MWCNTs was carried out as reported by Santangelo *et al.* [38]. Pristine-MWCNTs (1.5 g) were placed in a round-bottomed flask containing 100 cm^3 of concentrated hydrochloric acid, and stirred for 4 h to remove residual metal impurities from the tubes. The resulting solution was filtered, and the solid washed with deionised water until a neutral pH was obtained. The sample obtained was dried in a vacuum oven at 80 °C overnight and stored in a desiccator for future analysis. The purified MWCNTs were then oxidized by using a mixture of sulfuric and nitric acids in a volume ratio of 1:3, and refluxed at 80 °C for 12 h. The resulting solution was diluted with deionised water, filtered, and the residue obtained was washed continuously with deionised water until a neutral pH was obtained.

6.2.2.2. Synthesis of 4'-(4-hydroxyphenyl)-2,2':6',2''-terpyridine (HO-Phttpy)

The ligand was synthesized as reported by Patel *et al.* [39,40] with some modifications. 2-Acetylpyridine (2.423 g, 20.0 mmol) was added to 15 cm³ of a 2:1 (v/v) mixture of ethanol and water containing 4-hydroxybenzaldehyde (1.221 g, 10.0 mmol). To the suspension, NaOH pellets (1.458 g, 26.0 mmol) and 30 cm³ aqueous NH₃ were added and stirred continuously at room temperature for 8 h to yield a cream-coloured precipitate. The resulting mixture was filtered, the solid obtained was washed with deionised water (5 × 10 cm³), followed by absolute ethanol (3 × 5 cm³) to obtain the crude white product (508.8 mg, 42%). m.p. 199-201 °C; IR (ATR, cm⁻¹) 3375, 1614, 1588, 1565; ¹H NMR (400 MHz, DMSO-d₆) δ: 6.92 (d, 2H, J=8.6 Hz), 7.49-7.52 (m, 2H), 7.75 (d, 2H J=8.68 Hz), 7.99-8.04 (m, 2H), 8.67-8.74 (m, 6H); ¹³C NMR (400 MHz, DMSO-d₆) δ: 160.2, 155.4, 155.1, 149.4, 149.2, 137.3, 128.0, 126.8, 124.3, 120.8, 116.8, 116.4; HR-MS [C₂₁H₁₅N₃O] ES:[M + H⁺] *m/z* Calcd 326.1215, found 326.1293.

6.2.2.3. Preparation of nitrogen-functionalized MWCNTs (MWCNT-ttpty)

Oxidized MWCNTs (150 mg) were dispersed in 30 cm³ of a solution containing a 20:1 (v/v) mixture of SOCl₂ and DMF, and then refluxed at 70 °C for 24 h [41]. The resulting mixture was filtered, and the solid obtained was washed with deionised water until a neutral pH was achieved. Acylated MWCNTs (100 mg) were added to 100 mg of HO-Phttpy in 20 cm³ of dry tetrahydrofuran (THF) with the addition of 2-5 drops of glacial acetic acid. The suspension was refluxed at 64 °C for 24 h under an inert atmosphere of argon. The suspension was filtered, and the solid obtained was washed with THF and dried in a vacuum oven.

The sample obtained (100 mg) was added to freshly distilled chloroform (30 cm³), InBr₃ (10.6 mg 0.03 mmol) and Et₃SiH (380 μL, 2.4 mmol). The suspension was stirred and refluxed at 60 °C for 1 h under an inert atmosphere of argon. The resulting mixture was filtered and the solid washed with chloroform, followed by water until a neutral pH was obtained. Evidence of the successful preparation of MWCNT-COOH and MWCNT-ttpty was obtained by various characterization techniques such as electron microscopy (scanning and transmission), Fourier transform infrared (FTIR) and Raman spectroscopy, thermogravimetric analysis, elemental analysis and BET surface area analysis.

6.2.3. Metal analysis procedure

6.2.3.1. Equipment

A PerkinElmer Optima 5300 DV inductively coupled plasma-optical emission spectrophotometer (ICP-OES) was used to measure the initial and final concentrations of Cd^{2+} in solution. The operating conditions used are presented in Appendix III (Table A-III.1). A PerkinElmer AAnalyst 200 atomic absorption spectrometer, equipped with a PerkinElmer mercury hydride system (MHS 15) was used for Hg^{2+} determination by using sodium borohydride (NaBH_4) as reductant. The operating conditions for cold vapour atomic absorption spectrometer (CVAAS) are listed in Appendix III (Table A-III.2).

6.3.2.2. Preparation of adsorbate solution

A stock solution of Cd^{2+} was prepared by dissolving 1 g of cadmium metal in 20 cm^3 of concentrated HCl acid and 3-5 drops of HNO_3 acid. The solution was then made up to the mark in a 1000 cm^3 volumetric flask with deionised water. Working solutions of desired concentrations were made by dilution of this stock solution.

A 1.713 g mass of $\text{Hg}(\text{NO}_3)_2 \cdot \text{H}_2\text{O}$ was dissolved in 10 cm^3 of nitric acid and diluted to the mark in a 500 cm^3 volumetric flask with deionised water. This solution was standardized against potassium chloride by using diphenylcarbazone indicator [42]. A solution of Hg^{2+} with a concentration of 1000 mg dm^{-3} was prepared by measuring the required volume of the $\text{Hg}(\text{NO}_3)_2 \cdot \text{H}_2\text{O}$ stock solution and diluting to the mark, in a 1000 cm^3 volumetric flask with deionised water. Working solutions of Hg^{2+} were prepared from the 1000 mg dm^{-3} $\text{Hg}(\text{NO}_3)_2 \cdot \text{H}_2\text{O}$ solution by dilution to obtain the desired concentration.

6.2.3.3. Calibration of spectrophotometers

The inductive coupled plasma-optical emission spectrometer (ICP-OES) and cold vapour atomic absorption spectrophotometer (CVAAS) were calibrated for Cd^{2+} and Hg^{2+} analysis, respectively, by preparing standard solutions of $\text{Cd}^{2+}/\text{Hg}^{2+}$ with concentrations within the range of 0-100 mg dm^{-3} at each time of analysis. Calibration plots were obtained in these ranges and the initial and final concentrations of $\text{Cd}^{2+}/\text{Hg}^{2+}$ in the samples were estimated from these plots.

6.2.4. Batch adsorption studies

The influence of adsorption parameters, such as pH, contact time, adsorbent dose, initial ion concentration and temperature, were investigated through batch adsorption experiments of the sorption of Cd^{2+} and Hg^{2+} onto MWCNT-COOH and MWCNT-tpy. Experiments were conducted sequentially to obtain the best experimental conditions for the adsorption of Cd^{2+}

and Hg^{2+} from aqueous solutions. Working solutions of Cd^{2+} and Hg^{2+} with concentrations of 100 mg dm^{-3} and 50 mg dm^{-3} , respectively, were prepared from the respective stock solutions.

Adsorption experiments were conducted by measuring 25 cm^3 aliquots of Cd^{2+} or Hg^{2+} solution into 100 cm^3 polypropylene plastic vials, and conditioned to obtain the desired pH with the addition of appropriate amounts of 0.1 mol dm^{-3} NaOH or HNO_3 solution. A mass of 50 mg of each adsorbent was added into the solution and agitated in a thermostated water bath pre-set at $20 \text{ }^\circ\text{C}$ for 24 h . After agitation, the solutions were filtered, and the final concentrations of Cd^{2+} or Hg^{2+} determined by ICP-OES and CVAAS, respectively. The amount of metal ion adsorbed on each sorbent was estimated from the difference between the initial and equilibrium metal ion concentrations. The adsorption capacity (q_e) of Cd^{2+} and Hg^{2+} was calculated from Eq. 6.1.

$$q_e = \left(\frac{C_i - C_{eq}}{m} \right) \times V \quad (6.1)$$

where C_i is the initial adsorbate concentration (mg dm^{-3}), C_{eq} is the equilibrium concentration of adsorbate (mg dm^{-3}), q_e is the adsorption capacity (mg g^{-1}), m is the mass of adsorbent (mg) and V is the volume (dm^3) of the adsorbate solution used. The percentage removal (% adsorbed) of Cd^{2+} and Hg^{2+} was calculated according to Eq. 6.2.

$$\% \text{ adsorbed} = \left(\frac{C_i - C_{eq}}{C_i} \right) \times 100 \quad (6.2)$$

6.2.4.1. Kinetics, isotherm and thermodynamic studies

The equilibration time of the adsorption process for each metal ion was determined by means of kinetic experiments. This was carried out by weighing about 50 mg of each sorbent into 100 cm^3 polypropylene bottles, containing 25 cm^3 aliquots of Cd^{2+} or Hg^{2+} solution. The solutions were conditioned to obtain the desired pH by adding appropriate amounts of 0.1 mol dm^{-3} NaOH or HNO_3 solution, and thereafter the bottles were placed in a thermostated water bath at $20 \text{ }^\circ\text{C}$. These samples were agitated over a time interval in the range of 5 to 1440 min . After the pre-determined time intervals, the samples were filtered by gravity and the concentration of Cd^{2+} or Hg^{2+} determined by ICP-OES or CVAAS, respectively. The experimental adsorption data obtained were applied to the pseudo-first order, pseudo-second order, intraparticle diffusion and Elovich kinetics models as given in Table 6.1.

Table 6.1: Kinetics models used for the adsorption of Cd²⁺ and Hg²⁺

Model	Equation*	Parameters	References
Pseudo-first order	$q_t = q_{eq}(1 - e^{-k_1 t})$	q_{eq}, k_1	[43-45]
Pseudo-second order	$q_t = \frac{k_2 q_{eq}^2 t}{1 + k_2 q_{eq} t}$	k_2, q_{eq}	[43,45,46]
Elovich	$q_t = \frac{1}{\beta} \ln(\alpha\beta) + \frac{1}{\beta} \ln t$	α, β	[47]
Intraparticle diffusion	$q_t = k_{id} \sqrt{t} + l$	k_{id}, l	[48]

* q_t , quantity of adsorbate adsorbed at time t (mg g^{-1}); q_{eq} , quantity of adsorbate adsorbed at equilibrium (mg g^{-1}); α , adsorption rate constant ($\text{mg g}^{-1} \text{min}^{-1}$); β , desorption rate constant (g mg^{-1}); k_1 , pseudo-first order rate constant (min^{-1}); k_2 , pseudo-second order rate constant ($\text{g mg}^{-1} \text{min}^{-1}$); k_{id} , intraparticle diffusion rate constant ($\text{mg g}^{-1} \text{min}^{0.5}$), l , is a constant related to the boundary layer thickness.

Adsorption isotherms were obtained by using varying concentrations of Cd²⁺ or Hg²⁺, concentrations, ranging from 10–100 mg dm^{-3} , at a constant pH of 5.5 and 6.0, respectively. Aliquots of 25 cm^3 were mixed with 50 mg of each adsorbent and agitated in a thermostated shaking water bath for 24 h. The effect of temperature on the adsorption of Cd²⁺ were only conducted at varying temperatures of 293, 303, 313 and 318 K, while adsorption experiments for Hg²⁺ investigating the influence of temperature was conducted at 293 and 303 K, due to the volatility of Hg²⁺. The experimental adsorption equilibrium data were analysed by various two- or three-parameter isotherm models, such as the Langmuir, Freundlich, Temkin, Dubinin-Radushkevich, Sips, Toth, Redlich-Peterson and Khan models as given in Table 6.2. Thermodynamic parameters such as change in Gibbs energy (ΔG°), change in enthalpy (ΔH°), and change in entropy (ΔS°) were also calculated over the studied temperature ranges.

Table 6.2: Isotherm models used for the adsorption of Cd²⁺ and Hg²⁺

Isotherm	Equation*	Parameters	References
Langmuir	$q_{eq} = \frac{q_m b C_{eq}}{1 + b C_{eq}}$	q_m, b	[49]
Freundlich	$q_{eq} = K_F C_{eq}^{1/n}$	K_F, n	[50]
Temkin	$q_{eq} = \frac{RT}{b_T} \ln(A_T C_{eq})$	b_T, A_T	[51]
Dubinin-Radushkevich	$q_{eq} = q_m e^{-\beta \varepsilon^2}$ $\varepsilon = RT \ln \left(1 + \frac{1}{C_{eq}} \right)$	q_m, β	[52]
Sips	$q_{eq} = \frac{b q_m C_{eq}^{1/n}}{1 + b C_{eq}^{1/n}}$	q_m, b, n	[53]
Toth	$q_{eq} = \frac{q_m C_{eq}}{\left(\frac{1}{K_T} + C_{eq}^{n_T} \right)^{1/n_T}}$	q_m, K_T, n_T	[54]
Redlich-Peterson	$q_{eq} = \frac{K_{RP} C_{eq}}{1 + a_{RP} C_{eq}^g}$	K_{RP}, a_{RP}, g	[55]
Khan	$q_{eq} = \frac{q_m b_K C_{eq}}{(1 + b_K C_{eq})^{a_K}}$	q_m, a_K, b_K	[56]

* q_{eq} , adsorption capacity (mg g⁻¹); C_{eq} , equilibrium concentration of adsorbate in solution (mg dm⁻³); q_m , maximum monolayer capacity (mg g⁻¹); b , Langmuir isotherm constant (dm³ mg⁻¹); K_F , Freundlich isotherm constant (mg g⁻¹)(dm³ mg⁻¹)ⁿ; n , adsorption intensity; b_T , Temkin isotherm constant; A_T , Temkin isotherm equilibrium binding constant (dm³ g⁻¹); β , Dubinin-Radushkevich isotherm constant (mol² kJ⁻²); K_T , Toth isotherm constant (mg g⁻¹); n_T , Toth isotherm constant; K_{RP} , Redlich-Peterson isotherm constant (dm³ g⁻¹); a_{RP} , Redlich-Peterson isotherm constant; g , Redlich-Peterson isotherm exponent; a_K , Khan isotherm exponent; b_K , Khan isotherm constant.

6.2.5. Desorption experiments

After conducting adsorption experiments with a 50 mg dm⁻³ solution of Cd²⁺ or Hg²⁺ by using a 50 mg dose of each adsorbent, the loaded adsorbents were separated from the suspensions by filtration and the metal ion concentration in the filtrates was determined by using the appropriate previously described techniques. The collected sorbents were washed with deionised water to remove unadsorbed metal ions and dried in a vacuum oven at 80 °C. Desorption experiments were then conducted by agitating 50 mg of the metal loaded-adsorbent with 25 cm³ of 0.1 mol dm⁻³ HCl for 30 min. The mixture was then filtered and the concentration of the desorbed metal ions in the filtrates was determined as described before.

6.2.6. Data analysis

The data obtained were fitted to the isotherm and kinetics models by means of the nonlinear regression routine (*nls*) in the R statistical computing environment [57]. The R statistical software takes into account the minimization of the sum of squared residuals (SSR) and the residual square errors (RSE). A comparison of all SSR and RSE values was done and the adequacy of the models was assessed from the value with the lowest SSR.

6.3. Results and discussion

6.3.1. Characterization of adsorbents

The characterization of the two adsorbents, MWCNT-COOH and MWCNT-ttpy has been previously reported by Oyetade *et al* [58]. Some pertinent characteristics of the adsorbents are presented in Table 6.3 and 6.4. As can be seen in Table 6.3, the surface area and pore volume of MWCNT-ttpy are larger than those obtained for MWCNT-COOH. Also, MWCNT-ttpy contains a larger number of functional groups per unit mass than MWCNT-COOH (Table 6.4). These properties demonstrates that both adsorbents may be suitable for metal ion sorption from aqueous solutions.

Table 6.3: Textural characterization of synthesized nanomaterials

Entry	Adsorbents	Surface area/m ² g ⁻¹	Pore volume/cm ³ g ⁻¹	Pore diameter/nm
1	P-MWCNT	108.8	0.494	18.44
2	MWCNT-COOH	126.8	0.692	22.95
3	MWCNT-ttpy	189.2	1.252	27.26

Table 6.4: Surface chemistry of P-MWCNTs, MWCNT-COOH and MWCNT-ttpy determined by the Boehm titration method

Adsorbents	Carboxyl/ mmol g ⁻¹	Lactonic/ mmol g ⁻¹	Phenolic/ mmol g ⁻¹	Total acidic groups/mmol g ⁻¹	Total basic groups/mmol g ⁻¹
P-MWCNTs	0.136	0.014	0.114	0.264	0.145
MWCNT-COOH	0.719	0.104	0.401	1.224	0.226
MWCNT-ttpy	0.613	0.165	0.544	1.322	0.752

6.3.2. Batch adsorption experiments

Batch adsorption experiments were conducted to investigate the optimum conditions for Cd²⁺ and Hg²⁺ removal from aqueous solutions. In this section, the influence of pH, contact time, adsorbent dose, initial metal ion concentration and adsorbate temperature were investigated and their results presented. Kinetics, isotherm and thermodynamic studies were

also investigated to understand the mechanisms involved in the removal of the targeted metal ions from aqueous solutions.

6.3.2.1. Effect of pH

Metal ion adsorption is significantly influenced by the solution pH, since it controls the distribution of species, surface charges and also the degree of ionization of the sorbent [5]. The influence of pH on the sorption of Cd^{2+} and Hg^{2+} onto MWCNT-COOH and MWCNT-ttpy from aqueous solutions was studied over a pH range of 1-10. Fig 6.1 shows that the percent adsorbed for Cd^{2+} and Hg^{2+} by both adsorbents increases as the solution pH becomes more basic. The extent of Cd^{2+} removal by MWCNT-COOH increased steadily from 9.5% to 59.0%, while higher removal efficiencies of 22.0% to 99.2% were obtained with MWCNT-ttpy over the same pH range (Fig 6.1a). Similarly, an increase in Hg^{2+} removal onto MWCNT-COOH from 55.8% to 85.9%, and from 83.0% to 88.0% by MWCNT-ttpy, was observed with increasing solution pH as shown in Fig 6.1b.

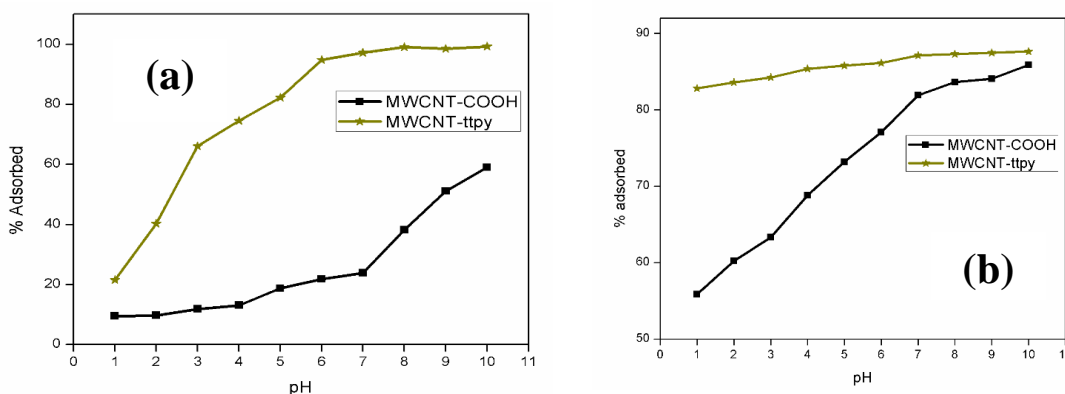


Fig 6.1: Effect of pH on the adsorption of (a) Cd^{2+} and (b) Hg^{2+} by using MWCNT-COOH and MWCNT-ttpy [conditions: 25 cm³ of $\text{Cd}^{2+}/\text{Hg}^{2+}$ solution, 24 h equilibration time, 50 mg adsorbent dose, agitation speed 150 rpm, temperature 20 °C].

These observations signify that the sorption of Cd^{2+} and Hg^{2+} was greatly enhanced by the change in solution pH. A lower removal of adsorbates under acidic conditions can be attributed to increasing competition between hydrogen ions and metal cations in solution. Also, this phenomenon induces an electrostatic repulsion between the metal cations and positive charges on the adsorbent, resulting in a lower removal under acidic conditions. An increase in solution pH reduces the amount of hydrogen ions and increases the number of hydroxyl ions in solution. This process facilitates the sorption of both adsorbates *via* electrostatic attraction between cations and negative charges on the adsorbent. Similar trends were reported by Kadirvelu *et al.* [5], Shadbad *et al.* [59], Hadavifar *et al.* [60], Liang *et al.* [9] and Li *et al.* [7] involving the sorption of Cd^{2+} and Hg^{2+} onto MWCNT-containing

sorbents. It is also worthy of note that the sorption of Cd^{2+} and Hg^{2+} onto MWCNT-ttpy was more pronounced than MWCNT-COOH. This could be due to the affinity of nitrogen-donor atoms in MWCNT-ttpy preferentially binding to soft metal ions such as Cd^{2+} , and an increase in the number of coordination sites available for chelation on the adsorbent. These results are in agreement with the study reported by Hadavifar *et al.* [60], where amino and thiol-functionalized MWCNTs proved more effective for Hg^{2+} removal than MWCNTs.

The experimental data for the adsorption of Cd^{2+} and Hg^{2+} as a function of pH can be found in Appendix III.

As shown in Fig 6.2, various species of cadmium such as $\text{Cd}(\text{OH})^+$, $\text{Cd}(\text{OH})_2$, $\text{Cd}(\text{OH})_3$, $\text{Cd}(\text{OH})_4$ and $\text{Cd}_4(\text{OH})_4$ can be formed with increasing alkalinity of the solution. Similarly, species such as $\text{Hg}(\text{OH})_2$, $\text{Hg}(\text{OH})_3^-$ and $\text{Hg}(\text{OH})^+$ may be formed under alkaline conditions. Hence, subsequent experiments were conducted at pH 5.5 and 6.0 for Cd^{2+} and Hg^{2+} , respectively, in order to avoid precipitation of metal ions accompanying adsorption in solution. At both of these pH values, the metal ions exist as free metal ions available for adsorption and do not exist as hydrolysed or protonated species.

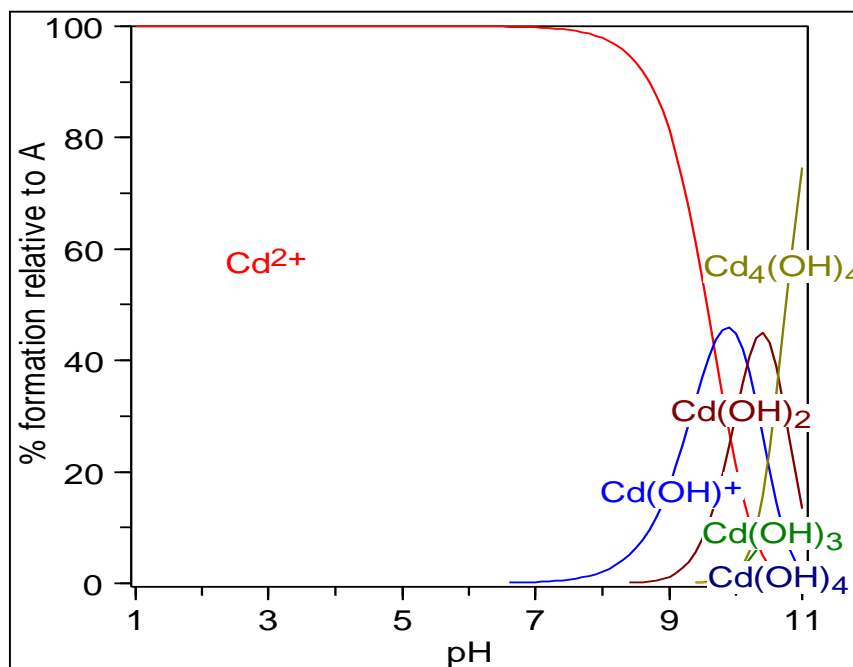


Fig 6.2: Speciation of Cd^{2+} as a function of pH in aqueous solutions. Numerical values of $\log \beta$ for the metal hydroxides used in the calculation of the speciation curves were obtained from Critical Stability Constants compiled by Smith and Martell [61], and plots obtained with the aid of HySS software [62].

6.3.2.2. Effect of contact time

To investigate the effect of contact time on the adsorption of Cd^{2+} and Hg^{2+} onto MWCNT-COOH and MWCNT-ttpy, adsorption experiments were agitated over a period of 5-1440 min. Fig 6.3 shows the percentage removal of Cd^{2+} and Hg^{2+} onto MWCNT-COOH and MWCNT-ttpy as a function of time. The figures reveals that the removal of both adsorbates increases with an increase in agitation time. Fig 6.3a shows that equilibrium for the removal of Cd^{2+} was reached within 360 min by using MWCNT-COOH and within 360 min by MWCNT-ttpy. However, the percentage adsorbed was four times greater for MWCNT-ttpy than MWCNT-COOH. This signifies that MWCNT-ttpy is a better adsorbent for Cd^{2+} removal than MWCNT-COOH. This could be as a result of the introduction of nitrogen-donor atoms onto the adsorbent, which possess strong affinity towards cadmium metal ions. The soft Cd^{2+} ions will bind preferentially with the borderline pyridinyl-nitrogen donors in MWCNT-ttpy than the harder oxygen donors in MWCNT-COOH.

Similar trends were observed for the removal of Hg^{2+} onto MWCNT-COOH and MWCNT-ttpy (Fig 6.3b). Fig 6.3b shows that equilibrium was achieved at 240 min and 120 min by using MWCNT-COOH and MWCNT-ttpy, respectively. However, the difference in the percentage adsorbed by the two adsorbents was not as marked for Hg^{2+} as it was for Cd^{2+} (Fig 6.3b vs a).

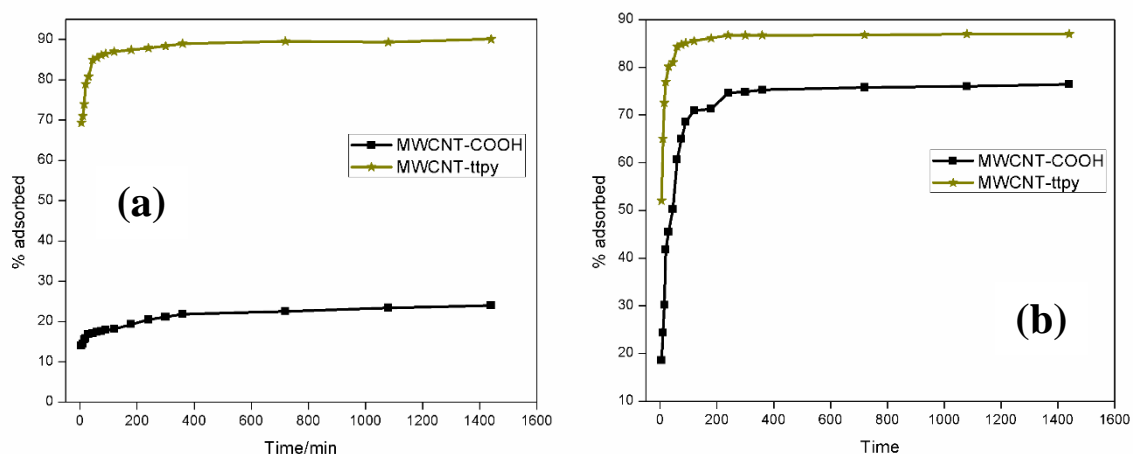


Fig 6.3: Effect of contact time on the adsorption of (a) Cd^{2+} and (b) Hg^{2+} by using MWCNT-COOH and MWCNT-ttpy [conditions: 25 cm³ of 100 mg dm⁻³ Cd^{2+} , or 50 mg dm⁻³ Hg^{2+} , 50 mg adsorbent dose, pH = 5.5 (Cd^{2+}) and pH = 6.0 (Hg^{2+}), agitation speed 150 rpm, temperature 20 °C].

The rate of adsorption was rapid for the removal of Cd^{2+} and Hg^{2+} onto MWCNT-ttpy, attaining a percent removal efficiency of 70% and 50%, respectively, after 5 min. The removal of adsorbates onto both sorbents, however, begins to slow down after the equilibrium time, due to saturation of the active sites on the adsorbents. Hence, the initial

fast removal can be attributed to the availability of active sites which decreases with increase in time. In this study, in order to ensure effective removal of adsorbates for higher concentrations, all experiments were equilibrated for 24 h.

The experimental data for the adsorption of Cd^{2+} and Hg^{2+} as a function of contact time can be found in Appendix III.

6.3.2.2.1. Kinetic studies

The mechanism of adsorption was investigated by modelling the kinetic data, to determine the rate-controlling step of the process. These experiments were conducted at fixed initial metal ion concentration, pH value, adsorbent dose, adsorbate volume and temperature. The experimental data collected at varying contact time, between 5-1440 min were analysed through the kinetics models given in Table 6.3. A comparison of the stated models was done by using the non-linear regression (*nls*) routine in the R statistical computing software [57]. Table 6.5 presents the kinetics parameters obtained for both adsorption processes by using MWCNT-COOH and MWCNT-ttpty. The adequacy of the model which best describes the adsorption process was chosen based on the lowest values obtained for the sum of squared residuals (SSR).

The adsorption of Cd^{2+} onto MWCNT-COOH and MWCNT-ttpty was better described by the Elovich and pseudo-second order models, respectively (Table 6.5). On the other hand, the adsorption of Hg^{2+} onto both adsorbents was best described by the pseudo-second order model. The pseudo-second order models assumes that adsorption proceeds through a bimolecular chemical interaction between the adsorbate ions and the active sites on the adsorbents [63]. The adsorption of Hg^{2+} onto both adsorbents, and the removal of Cd^{2+} to MWCNT-ttpty proceeded through this process. Hence, these adsorption processes were facilitated *via* bimolecular interactions between nitrogen- or oxygen- donor atoms and the metal cations. The Elovich model, on the other hand, is used to describe chemical sorption of gases onto solid surfaces. The mechanism of Cd^{2+} removal onto MWCNT-COOH therefore proceeded through the diffusion of adsorbate ions from the bulk solution to the surface of the adsorbent. Tofighy *et al.* [64], Liang *et al.* [64] and Vukovic *et al.* [65] also reported that Cd^{2+} removal by CNT-containing sorbents were better described by the pseudo-second order model. However, they did not attempt to use the Elovich model. Also, the removal of Hg^{2+} produced similar trends as reported by Chen *et al.* [63], Shadbad *et al.* [59] and Kabbashi *et al.* [15]. The figures showing the fit of the experimental data for each model are shown in Appendix III (Fig A-III.1).

Table 6.5: Kinetic parameters for the adsorption of Cd²⁺ and Hg²⁺ on MWCNT-COOH and MWCNT-ttpy [conditions: 25 cm³ of 100 mg dm⁻³ Cd²⁺ at pH 5.5, or 50 mg dm⁻³ Hg²⁺ at pH 6.0, 50 mg adsorbent dose, agitation speed 150 rpm, temperature 20 °C]

Model	Parameter	Cd ²⁺		Hg ²⁺	
		MWCNT-COOH	MWCNT-ttpy	MWCNT-COOH	MWCNT-ttpy
Experimental	q _{meas} /mg g ⁻¹	9.734	36.72	18.55	22.41
Pseudo-first order	k _f /10 ⁻² /min	0.150	0.178	0.033	0.156
	q _{eq} /mg g ⁻¹	7.999	38.38	15.21	21.90
	RSE *	1.071	2.581	0.722	0.729
	SSR †	17.22	99.94	7.811	7.968
Pseudo second order	k ₂ /10 ⁻³ /g mg ⁻¹ min ⁻¹	0.025	0.009	0.003	0.014
	q _{eq} /mg g ⁻¹	8.478	39.73	16.41	22.65
	RSE	0.781	1.294	0.550	0.292
	SSR	9.151	25.10	4.539	1.280
Intraparticle diffusion	k _{id} /mg g ⁻¹ min ^{-0.5}	0.401	1.830	0.677	1.032
	l/mg g ⁻¹	5.603	26.63	1.470	11.30
	RSE	3.878	21.48	5.949	12.23
	SSR	240.6	7382	566.3	2394
Elovich	α/mg g ⁻¹ min ⁻¹	4.169	27.460	4.599	4.534
	β/g mg ⁻¹	0.756	2.074	0.434	8.343
	RSE	0.190	2.036	1.608	1.514
	SSR	0.541	62.20	38.80	34.38

*- residual squared error; †- sum of squared residuals

The mechanism of adsorption can proceed *via* one or more of the following steps: (i) the transfer of solute from the bulk solution to the surface of the adsorbent, (ii) transfer of the solute from the bulk solution to the boundary film which surrounds the adsorbent surface (film diffusion), (iii) solute transfer through the internal pores of the adsorbent (intraparticle diffusion), and (iv) interaction between adsorbate molecules with the active sites on the external surface of the adsorbent. A plot of q_e versus \sqrt{t} gives an explanation into the processes controlling the adsorption processes. It is assumed that the process is multi-step controlled if a linear plot is obtained which does not pass through the origin [66,67]. When a linear plot which passes through the origin is obtained, adsorption is assumed to proceed only by the intraparticle diffusion of adsorbates onto sites of the adsorbent [66]. All linear plots obtained in this study did not pass through the origin, indicative that the adsorption of Cd²⁺ and Hg²⁺ was controlled by a series of steps. Hence, it could be inferred that the removal of Cd²⁺ and Hg²⁺ onto MWCNT-COOH and MWCNT-ttpy proceeded through intraparticle diffusion, and a number of other steps accompanying adsorption. Table 6.5

further demonstrates higher intraparticle diffusion constants (k_{id}) and boundary layer (l) values for MWCNT-ttpy than MWCNT-COOH for both adsorption processes. These results are indicative that adsorption was boundary-controlled, hence, an increase in the uptake of adsorbates was noticed with increase in l values. Similarly, Table 6.5 shows that higher l values were obtained for Cd^{2+} sorption by using both sorbents, compared with their corresponding values for Hg^{2+} sorption. This implied that both adsorbents had better affinity for the removal of Cd^{2+} than Hg^{2+} .

6.3.2.3. Effect of adsorbent dose

The influence of increasing adsorbent dose for the adsorption of Cd^{2+} and Hg^{2+} onto MWCNT-COOH and MWCNT-ttpy from aqueous solutions was investigated over a dosage range of 30-400 mg. Fig 6.4 shows an increase in the removal efficiency of Cd^{2+} and Hg^{2+} onto MWCNT-COOH and MWCNT-ttpy as the adsorbent mass is increased. An increase in the removal of adsorbates can be attributed to the increase in the surface area and the number of active sites on the adsorbent, as a result of increasing the adsorbent dose [60]. The improved efficiency of MWCNT-ttpy over MWCNT-COOH is seen in Fig 6.4, where sorption was greatly enhanced for Cd^{2+} and Hg^{2+} removal. As before, in the case of Cd^{2+} , MWCNT-ttpy exhibits a large improvement over MWCNT-COOH. This can be attributed to the fact that both metal ions are soft acids and are expected to form strong covalent bonds with borderline bases such as nitrogen.

The experimental data for the adsorption of Cd^{2+} and Hg^{2+} as a function of adsorbent dose can be found in Appendix III.

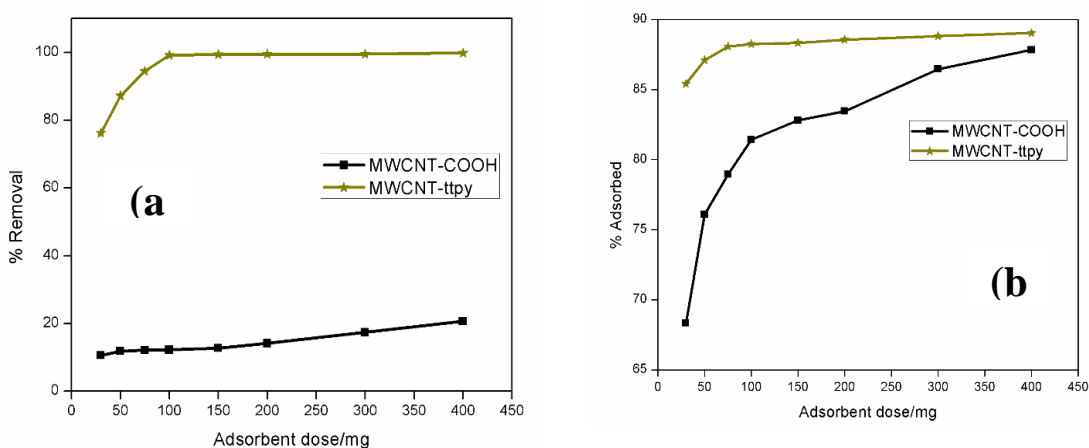


Fig 6.4: Effect of adsorbent dose on the adsorption of (a) Cd^{2+} and (b) Hg^{2+} by using MWCNT-COOH and MWCNT-ttpy [conditions: 25 cm³ of 100 mg dm⁻³ Cd^{2+} , or 50 mg dm⁻³ Hg^{2+} , 24 h equilibration time, pH = 5.5 (Cd^{2+}) and pH = 6.0 (Hg^{2+}), agitation speed 150 rpm, temperature 20 °C].

6.3.2.4. Effect of initial metal ion concentration

The influence of the initial metal ion concentration on the adsorption of Cd^{2+} and Hg^{2+} onto MWCNT-COOH and MWCNT-tpy was examined over a concentration range of 10-100 mg dm^{-3} . As observed in both cases, an increase in the metal ion concentration, resulted in a decrease in the percentage removal from 38.2 to 16.8% and 97.7 to 88.0% for Cd^{2+} , and 90.0 to 62.9% and 98.8 to 81.9% for Hg^{2+} , onto MWCNT-COOH and MWCNT-tpy, respectively. The observed decrease is due to the presence of more metal ions in solution, which limits the number of available adsorption sites [13]. This trend, however, yielded an increase in metal ion uptake per unit mass of adsorbent (q_e) with increase in concentration as shown in Figs 6.5 and 6.6. This can be attributed to an increasing number of collisions between the metal ions and active sorbent sites, resulting in higher occupation of the sites at high initial concentrations, and thus high adsorption capacities [13]. As the initial metal ion concentration is increased, the uptake of adsorbates is noticed to reach a plateau where no further increase takes place. This plateau is as a result of the complete occupation of the active sites at a particular concentration, and little or no further increase can occur.

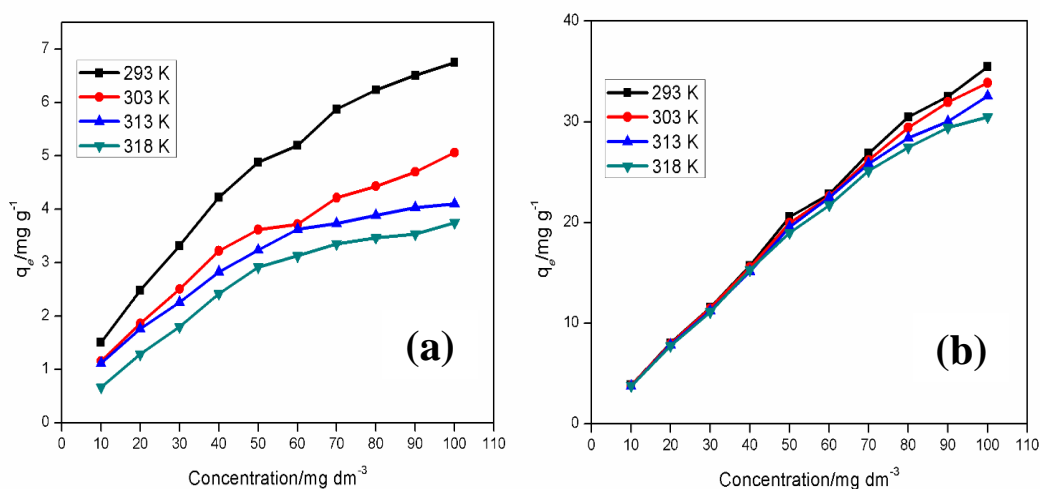


Fig 6.5: Effect of temperature on the adsorption of Cd^{2+} onto (a) MWCNT-COOH and (b) MWCNT-tpy [conditions: 25 cm^3 of Cd^{2+} solution, 24 h equilibration time, 50 mg adsorbent dose, pH = 5.5, agitation speed 150 rpm].

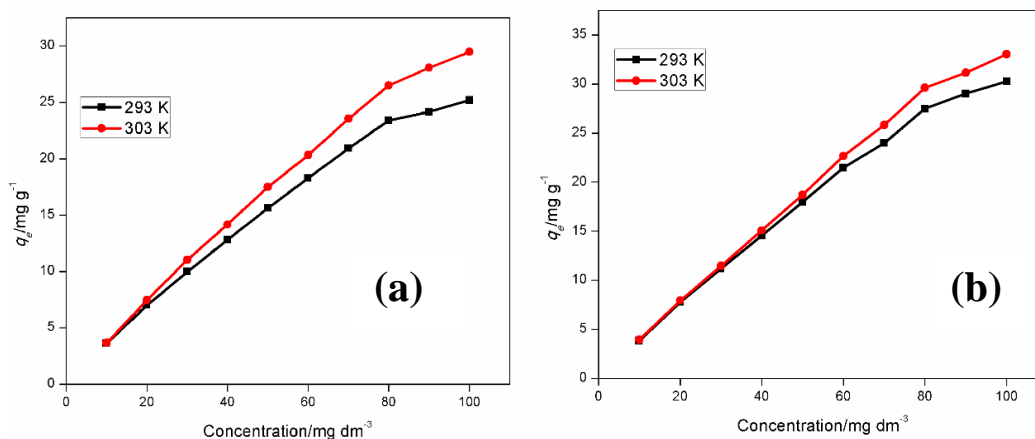


Fig 6.6: Effect of temperature on the adsorption of Hg^{2+} onto (a) MWCNT-COOH and (b) MWCNT-tty [conditions: 25 cm^3 of Hg^{2+} solution, 24 h equilibration time, 50 mg adsorbent dose, $\text{pH} = 6.0$, agitation speed 150 rpm].

Fig 6.5a shows that the sorption of Cd^{2+} onto MWCNT-COOH was low compared with MWCNT-tty (Fig 6.5b). This could be as a result of the low affinity of hard oxygen-donor atoms towards soft metals such as cadmium. The much enhanced uptake of Cd^{2+} by MWCNT-tty could be as a result of the presence of nitrogen-donor atoms on the adsorbent, which act as chelating sites for the adsorbate. Fig 6.6 demonstrates that both adsorbents had good efficiency towards the removal of Hg^{2+} over the concentration range studied. Hence, the sorption of Hg^{2+} could be said to be effective by using either oxygen-or nitrogen-containing MWCNTs.

The experimental data for the sorption of Cd^{2+} and Hg^{2+} onto MWCNT-COOH and MWCNT-tty as a function of varying initial metal ion concentration can be found in Appendix III.

6.3.2.5. Effect of temperature

The influence of temperature on the adsorption of Cd^{2+} was studied over a temperature range of $20 \text{ }^\circ\text{C}$ to $45 \text{ }^\circ\text{C}$. However, due to volatility losses which could result in environmental hazards associated with Hg^{2+} at increased temperatures, its temperature effects were examined only at $20 \text{ }^\circ\text{C}$ and $30 \text{ }^\circ\text{C}$. The sorption of Cd^{2+} onto both adsorbents was noticed to decrease with an increase in temperature (Fig 6.5). This is attributed to a decrease in the physical adsorptive forces (van der Waals) between the metal ion and active sites on the adsorbent [13], hence, resulting in a sorption decrease as temperature is increased. The adsorption of Cd^{2+} onto the adsorbents was therefore exothermic in nature. In contrast, Fig 6.6 shows an increase in the removal of Hg^{2+} as the adsorbate temperature is increased from $20 \text{ }^\circ\text{C}$ to $30 \text{ }^\circ\text{C}$. This could be due to volatility losses of Hg^{2+} at increased temperatures, an

increase in the mobility of Hg^{2+} towards the adsorbent sites and an increase in the size of the adsorbent pores [13]. These results are in agreement with inferences drawn by Hadi *et al.* [13], demonstrating the endothermic nature of adsorption for the removal of Hg^{2+} from aqueous solutions. The thermodynamic parameters, such as enthalpy change, entropy change and change in Gibbs energy for the adsorption of Cd^{2+} were calculated and are presented in Section 6.3.7. However, thermodynamic parameters for Hg^{2+} sorption could not be calculated due to environmental exposure, which could be associated with increased adsorbate temperature, hence, experiments were performed at only two temperatures from which inferences cannot be drawn.

6.3.2.6. Isotherm studies

Equilibrium adsorption isotherms are mathematical expressions used to estimate the capacity of an adsorbent towards the removal of a targeted pollutant and describe the distribution of species in the solid-liquid phases [6]. Adsorption experiments were performed by adding specific amounts of the adsorbents into different aliquots of $\text{Cd}^{2+}/\text{Hg}^{2+}$ solutions of varying metal ion concentrations ranging from 10-100 mg dm^{-3} over a temperature range of 293-318 K for Cd^{2+} and 293-303 K for Hg^{2+} . The equilibrium data obtained were fitted into various two- and three-parameter isotherms listed in Table 6.4 and the fit of the models to the experimental data were compared to obtain the isotherms that best describe the adsorption process. The adequacy of a model was decided based on the lowest values for the sum of squared residuals (SSR) and the residual squared errors (RSE) obtained.

Tables 6.6 and 6.7 give the isotherm parameters for models which fit the equilibrium data most appropriately for the adsorption of Cd^{2+} and Hg^{2+} , respectively. The figures showing the fit for these isotherms are presented in Appendix III (Figs A-III.2 – A-III.5). The Langmuir isotherm was the best two-parameter model that could describe the adsorption of Cd^{2+} onto both sorbents (Table 6.6). The equilibrium data obtained for MWCNT-COOH could not be described by any of the three-parameter isotherm models, however, data obtained for MWCNT-ttpy were best described by the Redlich-Peterson (R-P) and Sips models.

Table 6.6: Isotherm parameters for the adsorption of Cd²⁺ onto MWCNT-COOH and MWCNT-ttpy

Isotherms	Parameter	MWCNT-COOH				MWCNT-ttpy			
		293 K	303 K	313 K	318 K	293 K	303 K	313 K	318 K
Langmuir	q_m	10.41	7.503	5.804	6.3026	41.51	39.71	38.89	36.94
	b	0.022	0.022	0.029	0.017	0.558	0.426	0.288	0.250
	RSE*	0.121	0.120	0.102	0.138	1.110	0.452	1.080	0.618
	SSR[‡]	0.117	0.114	0.084	0.151	9.864	1.631	9.331	3.052
Freundlich	K_F	0.631	0.451	0.507	0.280	-	-	-	-
	n	1.833	1.845	2.091	1.697	-	-	-	-
	RSE	0.200	0.137	0.187	0.450	-	-	-	-
	SSR	0.319	0.150	0.279	0.237	-	-	-	-
Sips	q_m	-	-	-	-	37.36	37.97	34.62	34.31
	b	-	-	-	-	0.635	0.439	0.2745	0.242
	n	-	-	-	-	0.781	0.914	0.7739	0.8627
	RSE	-	-	-	-	0.632	0.315	0.700	0.404
	SSR	-	-	-	-	2.792	0.694	3.429	1.140
R-P	K	-	-	-	-	19.01	15.02	8.932	7.671
	α	-	-	-	-	0.316	0.306	0.1292	0.1323
	β	-	-	-	-	1.154	1.0777	1.194	1.144
	RSE	-	-	-	-	0.804	0.224	0.780	0.255
	SSR	-	-	-	-	4.524	0.3503	4.256	0.4549

*-residual squared errors, [‡]- sum of squared residuals

The data obtained for the sorption of Hg²⁺ onto both adsorbents over a temperature range of 293 K to 303 K, were best described by the Langmuir and Freundlich models for the two-parameter isotherms, and the Sips model for the three-parameter isotherms (Table 6.7).

Table 6.7: Isotherm parameters for the adsorption of Hg^{2+} onto MWCNT-COOH and MWCNT-ttpy

Isotherms	Parameter	MWCNT-COOH		MWCNT-ttpy	
		293 K	303 K	293 K	303 K
Langmuir	q_m	33.89	37.67	36.13	38.86
	b	0.085	0.146	0.217	0.348
	RSE*	0.769	0.545	1.234	2.019
	SSR[‡]	4.733	2.376	12.18	32.62
Freundlich	K_F	4.965	7.155	9.263	12.82
	n	2.118	2.162	2.524	2.811
	RSE	1.384	1.564	1.598	2.702
	SSR	15.33	19.57	20.44	58.39
Sips	q_m	37.00	40.47	46.04	42.14
	b	0.090	0.147	0.205	0.341
	n	1.106	1.090	1.37	1.16
	RSE	0.785	0.521	0.919	2.106
	SSR	4.312	1.903	5.912	31.05

*-residual squared errors, [‡]- sum of squared residuals

The Langmuir model is used to describe systems with homogeneous adsorbent surfaces where it is assumed that the adsorbent surfaces contain a finite number of identical sites with uniform energies of adsorption, hence no interactions exist between adjacent adsorbed species [6,68]. The Freundlich isotherm, however, describes a system where adsorption occurs on multilayer surfaces, containing heterogeneous adsorbent sites. Hence, since the sorption of Cd^{2+} and Hg^{2+} onto MWCNT-COOH and MWCNT-ttpy fit better to the Langmuir model than the Freundlich model, it could be assumed that all sites were equivalent, holding one adsorbate molecule without interactions with adjacent sites [68]. This model has been chosen as an isotherm of choice by other authors such as Wu *et al.* [6], Perez-Aquilar *et al.* [2], Kabbashi *et al.* [15] and Chen *et al.* [63] for the sorption of Cd^{2+} and Hg^{2+} from aqueous solutions. Of the three-parameter isotherms, the Sips model which is a combination of the Langmuir and Freundlich model was chosen to best describe both systems. A comparison of the maximum Langmuir adsorption capacity (q_m) of MWCNT-COOH and MWCNT-ttpy demonstrates that both sorbents compare favourably with other adsorbents from previous studies (see Table 6.8). The capacity of MWCNT-ttpy was far greater than all other sorbents compared for the removal of Cd^{2+} , while the sorbent also shows a favourable uptake of Hg^{2+} when compared with other related sorbents (Table 6.8). This therefore shows that the application of MWCNT-ttpy is suitable, obtaining excellent uptakes of Cd^{2+} and Hg^{2+} from aqueous solutions. It is also interesting to note that a better

adsorption ability for Cd^{2+} was obtained in this work for MWCNTs functionalized with a N-donor ligand (HO-Phttpy) than when nitrogen was doped into MWCNTs [2]. However, only slight improvement was noticed when MWCNT-ttpy was applied for Hg^{2+} removal compared with MWCNT-COOH.

Table 6.8: Comparison of the adsorption capacity of Cd^{2+} and Hg^{2+} onto MWCNT-COOH and MWCNT-ttpy with that of other sorbents

Adsorbent	Cd^{2+}	Hg^{2+}	References
MWCNT	5.40	-	[69]
MWCNT(H_2SO_4)*	8.60	-	[69]
MWCNT($\text{H}_2\text{SO}_4/\text{KMnO}_4$)	46.3	-	[69]
MWCNT	1.10	-	[7]
MWCNT(H_2O_2)	2.60	-	[7]
MWCNT(KMnO_4)	11.0	-	[7]
MWCNT(HNO_3)	5.10	-	[7]
N-doped MWCNT	9.33	-	[2]
MWCNT	5.62	-	[70]
MWCNT(H_2SO_4)	20.2	-	[70]
MWCNT(HNO_3)	10.9	-	[71]
MWCNT-EDA	25.7	-	[65]
MWCNT	-	84.0	[59]
MWCNT-SH	-	16.9	[60]
MWCNT- SiO_2	-	13.3	[72]
MWCNT	-	25.6	[73]
MWCNT(HNO_3)	-	27.3	[74]
MWCNT	-	5.47	[74]
MWCNT	-	0.36	[63]
MWCNT(HNO_3)	-	0.41	[63]
MWCNT($\text{H}_2\text{SO}_4/\text{KMnO}_4$)	-	0.42	[63]
MWCNT($\text{H}_2\text{SO}_4/\text{HNO}_3$)	10.4	33.4	This study
N-functionalized MWCNT	41.5	36.1	This study

*Modifying agents in brackets

Additionally, the parameters obtained from the Langmuir model can be used to estimate the favourability of the adsorption process. The constant, separation factor (R_L), can be calculated as given in Eq. 6.3 [75,76]:

$$R_L = \frac{1}{1+bC_i} \quad (6.3)$$

where C_i is the initial $\text{Cd}^{2+}/\text{Hg}^{2+}$ concentration (mg dm^{-3}) and b is the Langmuir constant obtained from Table 6.6 and 6.7 ($\text{dm}^3 \text{mg}^{-1}$). The favourability of the adsorption process can be estimated depending on the values of R_L . Adsorption is assumed to be favourable if $0 <$

$R_L < 1$, unfavourable if $R_L > 1$, irreversible if $R_L = 0$ and linear if $R_L = 1$ [75]. All R_L values obtained in this study were found to fall between $0 < R_L < 1$, hence adsorption of Cd^{2+} and Hg^{2+} onto MWCNT-COOH and MWCNT-ttpe indicated a favourable adsorption. The smaller the R_L values, the more favourable the process is. The calculated values of R_L obtained for Hg^{2+} produced lower values compared with those obtained for Cd^{2+} , onto both adsorbents. This may be indicative that the sorption of Hg^{2+} was more favourable than Cd^{2+} sorption. The calculated R_L values obtained at varying temperatures for the sorption of Cd^{2+} and Hg^{2+} from aqueous solutions are presented in Appendix III.

6.3.2.7. Thermodynamic parameters of adsorption

The thermodynamics parameters of adsorption such as the change in entropy (ΔS°), change in enthalpy (ΔH°) and change in Gibbs energy (ΔG°) were calculated for the removal of Cd^{2+} from aqueous solutions. The calculations could not be done for the adsorption of Hg^{2+} from aqueous solutions due to limitations of performing experiments at only two temperatures, hence, there was insufficient data to draw inferences. Thermodynamic parameters are calculated to understand the feasibility and spontaneity of the adsorption process. The process is feasible and spontaneous when ΔG° values are negative. A positive ΔH° value signifies the process is endothermic and the reverse is an exothermic process.

The change in Gibbs energy is calculated from the expression in Eq. (6.4) [45]:

$$\Delta G^\circ = -RT \ln K \quad (6.4)$$

where ΔG° is the standard Gibbs energy change (J mol^{-1}), R is the universal gas constant ($8.314 \text{ J K}^{-1} \text{ mol}^{-1}$), and T is the absolute temperature in Kelvin. The value of K was obtained from the product of q_m and b obtained from the Langmuir plot (Table 6.6) [77,78]. The value of K was corrected to be dimensionless by multiplying by 1000 [79].

In order to obtain ΔH° and ΔS° values, a linear plot of $\ln K$ against $1/T$ by using the Van't Hoff expression given in Eq. 6.5, was used. Estimated values of ΔH° and ΔS° were calculated from the slope and intercept of the line, respectively.

$$\ln K = -\frac{\Delta H^\circ}{RT} + \frac{\Delta S^\circ}{R} \quad (6.5)$$

The values obtained, as given in Table 6.9, demonstrate that the sorption of Cd^{2+} onto MWCNT-COOH and MWCNT-ttpe was both feasible and spontaneous, as indicated by the negative ΔG° values. Similarly, negative ΔH° and ΔS° values were obtained for both sorbents (Table 6.9), indicating that the sorption of Cd^{2+} onto MWCNT-COOH and

MWCNT-ttpy is exothermic in nature and favourable at lower temperatures. The values of ΔH° obtained show that the heat evolved/absorbed was in the range for a physisorption (2.1-20.9 kJ mol⁻¹) process [31,80]. This indicates that the process for the removal of Cd²⁺ from aqueous solutions by using MWCNT-COOH was primarily physisorption. The sorption of Cd²⁺ onto MWCNT-ttpy can be assumed to be physico-chemical process, since ΔH° values were higher than the predicted values for a physisorption process [31,80]. Previous studies by Hamza *et al.* [28], Al Othman *et al.* [25] and Kumar *et al.* [29] demonstrated that Cd²⁺ sorption was more favourable at low adsorbate temperature.

Table 6.9: Thermodynamic parameters for the adsorption of Cd²⁺ onto MWCNT-COOH and MWCNT-ttpy

Adsorbent	T/K	$\Delta G^\circ/\text{kJ mol}^{-1}$	$\Delta H^\circ/\text{kJ mol}^{-1}$	$\Delta S^\circ/\text{J K}^{-1} \text{mol}^{-1}$
MWCNT-COOH	293	-13.28		
	303	-12.82		
	313	-13.32	-19.56	-78.96
	318	-12.39		
MWCNT-ttpy	293	-24.48		
	303	-24.53		
	313	-24.26	-28.74	-71.72
	318	-24.14		

6.3.3. Desorption studies

To investigate the regeneration of adsorbents for reuse, desorption experiments were performed on Cd²⁺/Hg²⁺-loaded sorbents. In this study, 0.1 mol dm⁻³ HCl was used to desorb the metal ions from the adsorbents. Prior to desorption, the concentration of metal ions on the loaded adsorbents was obtained, and subsequently agitated for 30 min in contact with 25 cm³ of eluent. The removal of Cd²⁺ from the adsorbents was effective achieving a percentage removal of 74% and 82% from MWCNT-COOH and MWCNT-ttpy, respectively. The removal of Hg²⁺ from sorbents produced a percentage removal of 92% and 81% from MWCNT-COOH and MWCNT-ttpy, respectively. The choice of eluent was based on previous reports by Hamza *et al.* [28,77], Vukovic *et al.* [65], Saber-Samandari *et al.* [81], Perez-Aquilar *et al.* and Srivastava *et al.* [82] justifying the removal of metal ions by using acidic solutions. The removal of Cd²⁺ and Hg²⁺ from MWCNT-COOH and MWCNT-ttpy proved efficient by using HCl, hence, isolation of the adsorbate and reutilization of the sorbents is a viable option. The application of the sorbents for the removal of metal ions in solution should be economical, preventing the discharge of spent-sorbents and thereby avoiding the discharge of secondary pollutants into the environment.

6.4. Conclusions

In this study, nitrogen-functionalized multiwalled carbon nanotubes (MWCNT-ttpe) were applied for the removal of Cd^{2+} and Hg^{2+} from aqueous solutions. Their efficiency for metal ion removal was compared with that of acid-functionalized multiwalled carbon nanotubes (MWCNT-COOH), in order to determine which of the two sorbents was more effective.

The results obtained showed that MWCNT-ttpe was much more effective towards Cd^{2+} and marginally more effective for Hg^{2+} than MWCNT-COOH. For Cd^{2+} , four-fold increase in removal (*i.e.* 10.41 mg g^{-1} to 41.51 mg g^{-1}) was achieved by MWCNT-ttpe over MWCNT-COOH. Although, the removal efficiencies of both sorbents towards Hg^{2+} removal were similar, an increase in its uptake was obtained for MWCNT-ttpe. This demonstrates the effectiveness of CNTs functionalized with a nitrogen-donor ligand towards the removal of divalent metal ions in solution. The pseudo-second order model described the kinetics data most appropriately, indicating a bimolecular chemical interaction between metal cations and the active surface of the adsorbents. Hence, the sorption of Cd^{2+} and Hg^{2+} primarily interacted with the active sites on the adsorbents *via* coordinating (dative covalent) bonding.

Of the two-parameter isotherms tested, the Langmuir model best described the sorption of both adsorbates, while the Sips model was the best of the three-parameter isotherms for the sorption of Cd^{2+} by MWCNT-ttpe and for Hg^{2+} with both adsorbents. An increase in temperature resulted in a decrease in the uptake of Cd^{2+} , indicating that adsorption is best at low temperatures. However, the sorption of Hg^{2+} showed an increase in removal with an increase in temperature. This is indicative that the sorbents are effective for Hg^{2+} removal at high temperatures, and can be applied to effluents discharged at above ambient temperatures. Desorption of both adsorbents from the sorbents also produced good efficiencies, indicating that the sorbates and sorbents can be recovered and recycled for reuse. This study therefore demonstrated that MWCNT-ttpe is a good adsorbent for the removal of metal ions from solution and its application in industry could be further explored.

References

- [1] M. Rahman, S. Gul, M. Ajmal, A. Iqbal, A. Achakzai, Removal of cadmium from aqueous solutions using excised leaves of quetta pine (*pinus halepensis mill.*), Bangladesh J. Bot., 42 (2014) 277-281.
- [2] N.V. Perez-Aguilar, E. Muñoz-Sandoval, P.E. Diaz-Flores, J.R. Rangel-Mendez, Adsorption of cadmium and lead onto oxidized nitrogen-doped multiwall carbon nanotubes in aqueous solution: equilibrium and kinetics, J. Nanopart. Res., 12 (2010) 467-480.
- [3] M. Mohammadi, A. Ghaemi, M. Torab-Mostaedi, M. Asadollahzadeh, A. Hemmati, Adsorption of cadmium(II) and nickel(II) on dolomite powder, Desalin. Water Treat., 53 (2013) 149-157.
- [4] T. Chen, Z. Zhou, R. Han, R. Meng, H. Wang, W. Lu, Adsorption of cadmium by biochar derived from municipal sewage sludge: Impact factors and adsorption mechanism, Chemosphere, 134 (2015) 286-293.
- [5] K. Kadirvelu, M. Kavipriya, C. Karthika, N. Vennilamani, S. Pattabhi, Mercury(II) adsorption by activated carbon made from sago waste, Carbon, 42 (2004) 745-752.
- [6] S. Wu, K. Zhang, X. Wang, Y. Jia, B. Sun, T. Luo, F. Meng, Z. Jin, D. Lin, W. Shen, L. Kong, J. Liu, Enhanced adsorption of cadmium ions by 3D sulfonated reduced graphene oxide, Chem. Eng. J., 262 (2015) 1292-1302.
- [7] Y.-H. Li, S. Wang, Z. Luan, J. Ding, C. Xu, D. Wu, Adsorption of cadmium(II) from aqueous solution by surface oxidized carbon nanotubes, Carbon, 41 (2003) 1057-1062.
- [8] B.B. Johnson, Effect of pH, temperature, and concentration on the adsorption of cadmium on goethite, Environ. Sci. Technol., 24 (1990) 112-118.
- [9] J. Liang, J. Liu, X. Yuan, H. Dong, G. Zeng, H. Wu, H. Wang, J. Liu, S. Hua, S. Zhang, Z. Yu, X. He, Y. He, Facile synthesis of alumina-decorated multi-walled carbon nanotubes for simultaneous adsorption of cadmium ion and trichloroethylene, Chem. Eng. J., 273 (2015) 101-110.
- [10] World Health Organization (WHO), Guidelines for Drinking-water Quality, Geneva, (2008).
- [11] World Health Organization (WHO), Guidelines for Drinking-water Quality, Geneva, (2011).
- [12] E. Kopysc, K. Pyrzynska, S. Garbos, E. Bulska, Determination of mercury by cold-vapor atomic absorption spectrometry with preconcentration on a gold-trap, Anal. Sci., 16 (2000) 1309-1312.
- [13] P. Hadi, M.H. To, C.W. Hui, C.S. Lin, G. McKay, Aqueous mercury adsorption by activated carbons, Water Res., 73 (2015) 37-55.

- [14] D. Mohan, V.K. Gupta, S.K. Srivastava, S. Chander, Kinetics of mercury adsorption from wastewater using activated carbon derived from fertilizer waste, *Colloids and Surfaces A: Physicochem. Eng. Aspects*, 177 (2009) 169-181.
- [15] N.A. Kabbashi, M. Elwathig, A. AbuSam, I.N. Bt Jamil, Kinetic study on Hg(II) removal by CNT, *Prog. Nanotech. Nanomater.*, 4 (2015) 1-6.
- [16] Y. Zhang, L. Zhao, R. Guo, N. Song, J. Wang, Y. Cao, W. Orndorff, W.-P. Pan, Mercury adsorption characteristics of HBr-modified fly ash in an entrained-flow reactor, *J. Environ. Sci.*, 33 (2015) 156-162.
- [17] Q. Zhou, Y. Duan, C. Zhu, J. Zhang, M. She, H. Wei, Y. Hong, Adsorption equilibrium, kinetics and mechanism studies of mercury on coal-fired fly ash, *Korean J. Chem. Eng.*, 32 (2015) 1405-1413.
- [18] The European Parliament and the Council of the European Union, Directive 2011/65/EU of the European Parliament and of the Council of 8 June 2011 on the restriction of the use of certain hazardous substances in electrical and electronic equipment, *Official Journal of the European Union*, 174 (2011) 88-110.
- [19] L.Y. Blue, P. Jana, D.A. Atwood, Aqueous mercury precipitation with the synthetic dithiolate, BDTH₂, *Fuel*, 89 (2010) 1326-1330.
- [20] N. Ratner, D. Mandler, Electrochemical detection of low concentrations of mercury in water using gold nanoparticles, *Anal. Chem.*, 87 (2015) 5148-5155.
- [21] A. Elsherief, Removal of cadmium from simulated wastewaters by electrodeposition on spiral wound steel electrode, *Electrochim Acta*, 48 (2003) 2667-2673.
- [22] C.S. Slater, A. Ferrari, P. Wisniewski, Removal of cadmium from metal processing wastewaters by reverse osmosis, *J. Environ. Sci. Health Part A: Tox. Hazard Subst. Environ. Eng.*, 22 (1987) 707-728.
- [23] Y.K. Henneberry, T.E.C. Kraus, J.A. Fleck, D.P. Krabbenhoft, P.M. Bachand, W.R. Horwath, Removal of inorganic mercury and methylmercury from surface waters following coagulation of dissolved organic matter with metal-based salts, *Sci. Total Environ.*, 409 (2011) 631-637.
- [24] T.S. Anirudhan, L. Divya, M. Ramachandran, Mercury(II) removal from aqueous solutions and wastewaters using a novel cation exchanger derived from coconut coir pith and its recovery, *J. Hazard. Mater.*, 157 (2008) 620-627.
- [25] Z.A. Al Othman, A. Hashem, M.A. Habila, Kinetic, equilibrium and thermodynamic studies of cadmium(II) adsorption by modified agricultural wastes, *Molecules*, 16 (2011) 10443-10456.
- [26] D. Mohan, K.P. Singh, Single-and multi-component adsorption of cadmium and zinc using activated carbon derived from bagasse—an agricultural waste, *Water Res.*, 36 (2002) 2304-2318.
- [27] C. Xiong, C. Yao, Study on the adsorption of cadmium (II) from aqueous solution by D152 resin, *J. Hazard. Mater.*, 166 (2009) 815-820.

- [28] I.A.A. Hamza, Preparation and evaluation of a sugarcane bagasse multi-walled carbon nanotube composite for the adsorption of heavy metals from aqueous solutions, PhD Thesis, University of KwaZulu-Natal, Durban, South Africa (2013).
- [29] P.S. Kumar, K. Ramakrishnan, S.D. Kirupha, S. Sivanesan, Thermodynamic and kinetic studies of cadmium adsorption from aqueous solution onto rice husk, *Brazilian J. Chem. Eng.*, 27 (2010) 347-355.
- [30] M. Ahmed, I. Elmuntasir, Selective adsorption of cadmium species onto organic clay using experimental and geochemical speciation modeling data, *Int. J. Eng. Sci. Technol.*, 8 (2016) 128.
- [31] O.A. Oyetade, V.O. Nyamori, B.S. Martincigh, S.B. Jonnalagadda, Effectiveness of carbon nanotube-cobalt ferrite nanocomposites for the adsorption of rhodamine B from aqueous solutions, *RSC Adv.*, 5 (2015) 22724-22739.
- [32] A. Dourani, M. Hamadani, M. Haghgoo, Morphology and electrical properties of multi-walled carbon nanotube/carbon aerogel prepared by using Polyacrylonitrile as precursor, *RSC Adv.*, 5 (2015) 49944-49952.
- [33] Y. Li, J. Niu, Z. Shen, C. Feng, Size effect of single-walled carbon nanotube on adsorption of perfluorooctanesulfonate, *Chemosphere*, 91 (2013) 784-790.
- [34] Y. Zhou, B. Wen, Z. Pei, G. Chen, J. Lv, J. Fang, X. Shan, S. Zhang, Coadsorption of copper and perfluorooctane sulfonate onto multi-walled carbon nanotubes, *Chem. Eng. J.*, 203 (2012) 148-157.
- [35] Z. Wang, J. Zhao, L. Song, H. Mashayekhi, B. Chefetz, B. Xing, Adsorption and desorption of phenanthrene on carbon nanotubes in simulated gastrointestinal fluids, *Environ. Sci. Technol.*, 45 (2011) 6018-6024.
- [36] J.-L. Gong, B. Wang, G.-M. Zeng, C.-P. Yang, C.-G. Niu, Q.-Y. Niu, W.-J. Zhoua, Y. Liang, Removal of cationic dyes from aqueous solution using magnetic multi-wall carbon nanotube nanocomposite as adsorbent, *J. Hazard. Mater.*, 164 (2009) 1517-1522.
- [37] G.-C. Chen, X.-Q. Shan, Y.-S. Wang, B. Wen, Z.-G. Pei, Y.-N. Xie, T. Liu, J.J. Pignatello, Adsorption of 2,4,6-trichlorophenol by multi-walled carbon nanotubes as affected by Cu(II), *Water Res.*, 43 (2009) 2409-2418.
- [38] S. Santangelo, G. Messina, G. Faggio, S.H. Abdul Rahim, C. Milone, Effect of sulphuric-nitric acid mixture composition on surface chemistry and structural evolution of liquid-phase oxidised carbon nanotubes, *J. Raman Spectrosc.*, 43 (2012) 1432-1442.
- [39] M.N. Patel, P.A. Dosi, B.S. Bhatt, Synthesis, characterization, antibacterial activity and DNA interaction studies of drug-based mixed ligand copper(II) complexes with terpyridines, *Med. Chem. Res.*, 21 (2012) 2723-2733.

- [40] M.N. Patel, H.N. Joshi, C.R.I. Patel, Copper(II) complexes with norfloxacin and neutral terpyridines: Cytotoxic, antibacterial, superoxide dismutase and DNA-interaction approach, *Polyhedron*, 40 (2012) 159-167.
- [41] J. Shen, W. Huang, L. Wu, Y. Hu, M. Ye, Study on amino-functionalized multiwalled carbon nanotubes, *Mater. Sci. Eng. Part A*, 464 (2007) 151-156.
- [42] A.I. Vogel, *A textbook of quantitative inorganic analysis including elementary instrumental analysis*, 3rd Ed. (1961).
- [43] J. Lin, L. Wang, Comparison between linear and non-linear forms of pseudo-first-order and pseudo-second-order adsorption kinetic models for the removal of methylene blue by activated carbon, *Front. Environ. Sci. Eng.*, 3 (2009) 320-324.
- [44] Y.S. Ho, Comment on "Cadmium removal from aqueous solutions by chitin: kinetic and equilibrium studies", *Water Res.*, 38 (2004) 2962-2964
- [45] Y.-S. Ho, Removal of copper ions from aqueous solution by tree fern, *Water Res.*, 37 (2003) 2323-2330.
- [46] Y.S. Ho, G. McKay, Pseudo-second order model for sorption processes, *Process Biochem.*, 34 (1999) 451-465.
- [47] S.H. Chien, W.R. Clayton, Application of Elovich equation to the kinetics of phosphate release and sorption in soils, *Soil Sci. Soc. Am. J.*, 44 (1980) 265-268.
- [48] E. Demirbas, M. Kobyas, E. Senturk, T. Ozkan, Adsorption kinetics for the removal of chromium(VI) from aqueous solutions on the activated carbons prepared from agricultural wastes, *Water SA*, 30 (2004) 533-539.
- [49] I. Langmuir, The adsorption of gases on plane surfaces of glass, mica and platinum, *J. Am. Chem. Soc.*, 40 (1918) 1361-1402.
- [50] H. Freundlich, Adsorption in solids, *Z. Phys. Chem.*, 57 (1906) 385-470.
- [51] M.I. Temkin, V. Pyzhev, Kinetics of ammonia synthesis on promoted iron catalysts, *Acta Phys. Chim.*, 12 (1940) 327-356.
- [52] M.M. Dubinin, L.V. Radushkevich, The equation of the characteristic curve of activated charcoal, *Proc. Acad. Sci, U.S.S.R, Phys. Chem. Sect.*, 55 (1947) 327-329.
- [53] R. Sips, Combined form of Langmuir and Freundlich equations, *J. Chem. Phys.*, 16 (1948) 490-495.
- [54] J. Toth, State equations of the solid-gas interface layers, *Acta Chim. Acad. Sci. Hung.*, 69 (1971) 311-328.
- [55] O. Redlich, D.L. Peterson, A useful adsorption isotherm, *J. Phys. Chem.*, 63 (1959) 1024.
- [56] A.R. Khan, I.R. Al-Waheab, A. Al-Haddad, A generalized equation for adsorption isotherms for multi-component organic pollutants in dilute aqueous solution, *Environ. Technol.*, 17 (1996) 13-23.
- [57] The R Development Core Team, *The R foundation for statistical Computing*, R version 3.0.2 (2013).

- [58] O.A. Oyetade, V.O. Nyamori, B.S. Martincigh, S.B. Jonnalagadda, Nitrogen-functionalised carbon nanotubes as a novel adsorbent for the removal of Cu(II) from aqueous solution, (unpublished results).
- [59] M.J. Shadbad, A. Mohebbi, A. Soltani, Mercury(II) removal from aqueous solutions by adsorption on multi-walled carbon nanotubes, *Korean J. Chem. Eng.*, 28 (2011) 1029-1034.
- [60] M. Hadavifar, N. Bahramifar, H. Younesi, Q. Li, Adsorption of mercury ions from synthetic and real wastewater aqueous solution by functionalized multi-walled carbon nanotube with both amino and thiolated groups, *Chem. Eng. J.*, 237 (2014) 217-228.
- [61] R.M. Smith, A.E. Martell, *Critical Stability Constants*, 6 (1976) Plenum Press, New York.
- [62] P. Gans, Hyperquad simulation and speciation: , HySS, version 4.0.31, (2009).
- [63] P.A. Chen, C.-F. Hsu, D.-W. Tsai, Y.-M. Lu, W.-J. Huang, Adsorption of mercury from water by modified multiwalled carbon nanotubes: Adsorption behaviour and interference resistance by coexisting anions, *Environ. Technol.*, 35 (2014) 1935-1944.
- [64] M.A. Tofighy, T. Mohammadi, Adsorption of divalent heavy metal ions from water using carbon nanotube sheets, *J. Hazard. Mater.*, 185 (2011) 140-147.
- [65] G.D. Vukovic, A.D. Marinkovic, M. Coli, M.D. Ristic, R. Aleksic, A.A. Peric-Gruji, P.S. Uskokovic, Removal of cadmium from aqueous solutions by oxidized and ethylenediamine-functionalized multi-walled carbon nanotubes, *Chem. Eng. J.*, 157 (2010) 238-248.
- [66] S.G. Muntean, M.E. Radulescu-Grad, P. Sfarloaga, Dye adsorbed on copolymer, possible specific sorbent for metal ions removal, *RSC Adv.*, 4 (2014) 27354-27362.
- [67] C.H. Wu, Adsorption of reactive dye onto carbon nanotubes: equilibrium, kinetics and thermodynamics, *J. Hazard. Mater.*, 144 (2007) 93-100.
- [68] B. Yu, Y. Zhang, A. Shukla, S.S. Shukla, K.L. Dorris, The removal of heavy metal from aqueous solutions by sawdust adsorption — removal of copper, *J. Hazard. Mater.*, B80 (2000) 33-42.
- [69] C.-Y. Kuo, H.-Y. Lin, Adsorption of aqueous cadmium (II) onto modified multi-walled carbon nanotubes following microwave/chemical treatment, *Desalination*, 249 (2009) 792-796.
- [70] H.-H. Cho, K. Wepasnick, B.A. Smith, F.K. Bangash, D.H. Fairbrother, W.P. Ball, Sorption of aqueous Zn[II] and Cd[II] by multiwall carbon nanotubes: The relative roles of oxygen-containing functional groups and graphenic carbon, *Langmuir*, 26 (2009) 967-981.
- [71] Y.-H. Li, J. Ding, Z. Luan, Z. Di, Y. Zhu, C. Xu, D. Wu, B. Wei, Competitive adsorption of Pb²⁺, Cu²⁺ and Cd²⁺ ions from aqueous solutions by multiwalled carbon nanotubes, *Carbon*, 41 (2003) 2787-2792.

- [72] T.A. Saleh, Isotherm, kinetic, and thermodynamic studies on Hg(II) adsorption from aqueous solution by silica-multiwalled carbon nanotubes, *Environ. Sci. Pollut. Res.*, (2015) 1-11.
- [73] K. Yaghmaeian, R.K. Mashizi, S. Nasser, A.H. Mahvi, M. Alimohammadi, S. Nazmara, Removal of inorganic mercury from aquatic environments by multi-walled carbon nanotubes, *J. Environ. Health Sci. Eng.*, 13 (2015) 1-9.
- [74] A. Gupta, S. Vidyarthi, N. Sankararamakrishnan, Enhanced sorption of mercury from compact fluorescent bulbs and contaminated water streams using functionalized multiwalled carbon nanotubes, *J. Hazard. Mater.*, 274 (2014) 132-144.
- [75] O. Soon-An, S. Chye-Eng, L. Poh-Eng, Kinetics of adsorption of Cu(II) and Cd(II) from aqueous solution on rice husk and modified rice husk, *Electronic J. Environ. Agric. Food Chem.*, 6 (2007) 764-1774.
- [76] F. Krika, N. Azzouz, M.C. Ncibi, Adsorptive removal of cadmium from aqueous solution by cork biomass: Equilibrium, dynamic and thermodynamic studies, *Arabian J. Chem.*, (2011) In press.
- [77] I.A.A. Hamza, B.S. Martincigh, J.C. Ngila, V.O. Nyamori, Adsorption studies of aqueous Pb(II) onto a sugarcane bagasse/multi-walled carbon nanotube composite, *Phys. Chem. Earth*, 66 (2013) 157-166.
- [78] R. Djeribi, Q. Hamdaoui, Sorption of copper(II) from aqueous solutions by cedar sawdust and crushed brick, *Desalination*, 225 (2008) 95-112.
- [79] S.K. Milonjić, A consideration of the correct calculation of thermodynamic parameters of adsorption, *J. Serb. Chem. Soc.*, 72 (2007) 1363-1367.
- [80] Y. Liu, Y.-J. Liu, Biosorption isotherms, kinetics and thermodynamics, *Sep. Purif. Technol.*, 61 (2008) 229-242.
- [81] S. Saber-Samandari, M. Gazi, Removal of mercury(II) from aqueous solution using chitosan-graft-polyacrylamide semi-IPN hydrogels, *Sep. Sci. Tech.*, 48 (2013) 1382-1390.
- [82] S. Srivastava, Sorption of divalent metal ions from aqueous solution by oxidized carbon nanotubes and nanocages: A review, *Adv. Mat. Lett.*, 4 (2013) 2-8.

Chapter 7

Adsorption of Pb^{2+} , Zn^{2+} , Cd^{2+} and Cu^{2+} onto nitrogen-functionalized multiwalled carbon nanotubes: Single- and multi- component adsorption study

Oluwaseun A. Oyetade, Vincent O. Nyamori, Bice S. Martincigh* and Sreekantha B. Jonnalagadda

School of Chemistry and Physics, University of KwaZulu-Natal, Westville Campus,
Private Bag X54001, Durban 4000, South Africa

*Corresponding author: Tel: +27 31 2601394; Fax: +27 31 2603091; E-mail:
martinci@ukzn.ac.za

Abstract

The adsorption behaviour of nitrogen-functionalized multiwalled carbon nanotubes (MWCNT-ttpy) for the removal of the divalent heavy metals Pb^{2+} , Zn^{2+} , Cd^{2+} and Cu^{2+} was investigated in single- and multi-component adsorption systems. Batch experiments investigating the effect of pH and initial metal ion concentration were undertaken and equilibrium data modelled by using the Langmuir isotherm.

This study revealed that metal ion sorption in a competitive system depends largely on affinity towards nitrogen, pH and initial concentration of other competitors in solution. The Langmuir maximum adsorption capacities (q_m) in a single-solute system were significantly higher than those obtained for a competitive system. The sorption of metal ions followed the sequence, $\text{Cd} > \text{Pb} > \text{Cu} > \text{Zn}$, in a single-component system. This order was attributed to the preferential attraction of soft metals onto nitrogen-donor atoms in the adsorbent. The results also demonstrated a sequence, $\text{Pb} > \text{Cu} > \text{Cd} > \text{Zn}$, in a multi-component adsorption systems, as a result of increasing hydrated ionic radii. Hence, the removal of these pollutants from real water samples demonstrated good sorptive ability by using MWCNT-ttpy, indicating its potential application in real-life scenarios.

Keywords: multiwalled carbon nanotubes, adsorption, heavy metals, isotherm, wastewater

7.1. Introduction

The release of metal-containing substances into natural environments, primarily associated with increased industrialization, is of great concern to researchers and control agencies, due to their elevated concentrations in the ecosystem [1-4]. Effluents containing metal ions are sometimes discharged indiscriminately at high concentrations and are accumulated in soil and water systems [2,5,6]. Heavy metals are highly soluble in water, and hence can be easily transported in water systems, undergoing various chemical transformations and resulting in their accumulation in aquatic life, man and the environment [7]. Contaminated effluents and wastewater usually contain a variety of toxic metal ions [7-9]. The adsorption behaviour of a metal specie may be significantly influenced as a result of the presence of another in solution [10]. This significantly translates into a decrease in the removal of each metal ion in solution, due to increased competition of ions to occupy active sites on the adsorbent [8,10,11]. Heavy metals such as lead, zinc, cadmium and copper ions are predominantly present at high concentrations in discharged effluents [11]; hence, the effect of a metal ion in a multicomponent system is of paramount significance in order to understand their adsorption behaviour in competitive systems.

Various techniques such as ion-exchange, electrodeposition, coagulation, co-precipitation, oxidation, ultrafiltration, reverse osmosis and electro-dialysis have been investigated for the removal of heavy metal ions from aqueous solutions [6,12-14], however, their application in real-life situations have been limited, due to factors such as high cost and sludge generation, and low removal efficiency, amongst many others [5,12]. Adsorption offers an easy and simple removal approach to yield excellent efficiencies for high or low adsorbate concentrations [6,15], and provides an opportunity for sorbent and sorbate recovery for the process of reuse [16,17]. This technique is therefore a preferred choice for metal ion removal in aqueous systems [18]. Adsorbents such as bentonite [1,5], peat [9,19], hydroxyapatite [10], kaolinite [11], bagasse [7], and activated carbon [8] have been examined for metal ion removal in both single- and multi-component ion adsorption systems. In a multicomponent system, the activity of such adsorbents for metal ion removal are surprisingly low and this due to reduced active/chelating sites on adsorbents, resulting in minimal uptake of metal ions and increased difficulty in sorbent regeneration. The development of sorbents that contain more metal chelators for increased active sites, to enhance better sorption of metal ions in multicomponent systems, therefore, continues to be explored.

Multiwalled carbon nanotubes (MWCNTs) are promising nanomaterials explored for pollutant removal in environmental sciences, as a result of their excellent physical and chemical properties [6,18] and ease in introducing functional groups onto the surface of tubes [16]. Functionalization of MWCNTs significantly increases their textural properties,

dispersability in aqueous solutions [20,21], while introducing defects to the surface of tubes [20]. The presence of defects allows easy design of CNTs to contain functional groups of interest, hence, resulting in increasing activity of CNTs for the removal of metal ion pollutants. The introduction of nitrogen-containing functional groups to the side walls of CNTs, increases the chelating/active sites on the adsorbent, and may result in enhanced uptake of metal ion from aqueous solutions, especially in a multicomponent system.

In this chapter, a nitrogen-tridentate ligand (4'-(4-hydroxyphenyl)-2,2':6',2''-terpyridine) was used as a modifier to obtain nitrogen-functionalized MWCNTs (MWCNT-ttpe), and their effectiveness for the simultaneous removal of divalent metal ions, such as lead, zinc, cadmium and copper, in a single- and multi-component system was examined through batch experiments. The removal of the said metal ions under optimized conditions was also investigated in real water samples by using MWCNT-ttpe, to examine their efficacy in real-life scenarios.

7.2. Experimental

7.2.1. Materials and chemicals

All chemicals used were of analytical grade and used without further purification. The as-prepared MWCNTs were purchased from Cheap Tubes Inc. (Brattleboro, USA), synthesized by chemical vapour deposition (CVD) with a purity of 95%. Sodium hydroxide pellets (98%), and lead and zinc metal powders were purchased from Merck (Pty) Ltd (Gauteng, South Africa) while nitric acid (55%), sulfuric acid (98%) and hydrochloric acid (32%), were purchased from C C Imelmann Ltd (Robertsham, South Africa). Copper metal powder was obtained from Johnson Matthey Chemicals Ltd, (Gauteng, South Africa), while cadmium metal powder (99.9%) was purchased from Thomas Baker Chemicals (Pvt) Ltd, (Mumbai, India).

7.2.2. Adsorbent preparation

7.2.2.1. Preparation of MWCNT-COOH

Oxidation of MWCNTs was carried out as reported by Oyetade *et al.* [16] and Santangelo *et al.* [22]. Pristine MWCNTs (1.5 g) were placed in a round-bottomed flask containing 100 cm³ of concentrated hydrochloric acid, and stirred for 4 h to remove residual metal impurities from the tubes. The resulting mixture was filtered, and the solid washed with deionised water until a neutral pH was obtained. The sample obtained was dried in a vacuum oven at 80 °C overnight and stored in a desiccator for future analysis. The purified MWCNTs were then oxidized by using a mixture of sulfuric and nitric acids in a volume ratio of 1:3, and

refluxed at 80 °C for 12 h. The resulting mixture was diluted with deionised water, filtered, and the residue obtained was washed continuously with deionised water until a neutral pH was obtained.

7.2.2.2. Synthesis of 4'-(4-hydroxyphenyl)-2,2':6',2''-terpyridine (HO-Phttpy)

The ligand was synthesized as reported by Patel *et al.* [23,24] with some modifications. 2-Acetylpyridine (2.423 g, 20.0 mmol) was added to 15 cm³ of a 2:1 (v/v) mixture of ethanol and water containing 4-hydroxybenzaldehyde (1.221 g, 10.0 mmol). To the solution, NaOH pellets (1.458 g, 26.0 mmol) and aqueous NH₃ (30 cm³) were added and stirred continuously at room temperature for 8 h to yield a cream-coloured precipitate. The resulting mixture was filtered, the solid obtained was washed with deionised water (5 × 10 cm³), followed by absolute ethanol (3 × 5 cm³) to obtain the crude white product (508.8 mg, 42%). m.p. 199-201 °C; IR (ATR, cm⁻¹) 3375, 1614, 1588, 1565; ¹H NMR (400 MHz, DMSO-d₆) δ: 6.92 (d, 2H, J=8.6 Hz), 7.49-7.52 (m, 2H), 7.75 (d, 2H J=8.68 Hz), 7.99-8.04 (m, 2H), 8.67-8.74 (m, 6H); ¹³C NMR (400 MHz, DMSO-d₆) δ: 160.2, 155.4, 155.1, 149.4, 149.2, 137.3, 128.0, 126.8, 124.3, 120.8, 116.8, 116.4; HR-MS [C₂₁H₁₅N₃O] ES:[M + H⁺] m/z Calcd 326.1215, found 326.1293.

7.2.2.3. Preparation of MWCNT-ttpy

Oxidized MWCNTs (150 mg) were dispersed in 30 cm³ of a solution containing 20:1 (v/v) mixture of thionyl chloride and N,N'-dimethyl formamide (DMF) and refluxed at 70 °C for 24 h [25]. The resulting mixture was filtered, and the solid obtained was washed with deionised water until a neutral pH was obtained. Acylated MWCNTs (100 mg) were added to 100 mg of HO-Phttpy in 20 cm³ of dry tetrahydrofuran (THF) with the addition of 2-5 drops of glacial acetic acid. The suspension was refluxed at 64 °C for 24 h under an inert atmosphere of argon. The suspension was filtered, the solid obtained was washed with THF and dried in a vacuum oven.

To the obtained sample (100 mg), 30 cm³ of freshly distilled chloroform was added into a round-bottomed flask with the addition of InBr₃ (10.6 mg 0.03 mmol) and Et₃SiH (380 μL, 2.4 mmol). The suspension was stirred and refluxed at 60 °C for 1 h under an inert atmosphere of argon. The resulting mixture was filtered and the solid washed with chloroform, followed by water until a neutral pH was obtained. Evidence of the successful preparation of MWCNT-COOH and MWCNT-ttpy were confirmed by various characterization techniques such as electron microscopy (scanning and transmission), Fourier transform infrared (FTIR) and Raman spectroscopy, thermogravimetric analysis, elemental analysis and BET surface area analysis.

7.2.3. Metal analysis procedure

7.2.3.1. Equipment

A PerkinElmer Optima 5300 DV inductively coupled plasma-optical emission spectrometer (ICP-OES) was used to measure the initial and final concentrations of the metal ions in solution. The operating conditions used are presented in Table 7.1.

Table 7.1: Operating conditions for ICP-OES used for metal ion determination

Wavelength (Pb ²⁺)	220.353 nm
Wavelength (Zn ²⁺)	213.857 nm
Wavelength (Cd ²⁺)	267.716 nm
Wavelength (Cu ²⁺)	224.700 nm
RF power	1300 W
Plasma gas flow rate	15 dm ³ min ⁻¹
Pump	1.5 cm ³ min ⁻¹
Auxiliary gas flow rate	0.2 dm ³ min ⁻¹
Nebulizer gas flow rate	0.8 dm ³ min ⁻¹
Nebulizer pressure	2 bars
Analyzer type	Axial
Replicates	3
Sample read delay	60 s

7.2.3.2. Preparation of adsorbate solution

Separately stock solutions of each of the following, Pb²⁺, Zn²⁺, Cd²⁺ and Cu²⁺ were prepared by weighing an exact known amount of approximately 1 g of each pure metal powder into 150 cm³ of 2 mol dm⁻³ nitric acid. The solutions were made up to mark in 1000 dm³ volumetric flasks with deionised water. Working solutions were prepared daily from the stock solutions to obtain the desired concentrations.

7.2.3.3. Calibration of ICP-OES spectrometer

The spectrometer was calibrated by using a mixed standard containing Pb²⁺, Zn²⁺, Cd²⁺ and Cu²⁺ within the concentration range of 0-100 mg dm⁻³. Calibration plots were obtained each time the instrument was used for the determination of metal ions present in samples.

7.2.4. Batch adsorption studies

Single ion adsorption experiments were conducted within a metal ion concentration range of 10-100 mg dm⁻³ in 50 cm³ polyethylene bottles, containing 25 cm³ aliquots of Pb²⁺, Zn²⁺, Cd²⁺ and Cu²⁺ and 50 mg dose of adsorbent. The pH of the suspensions was adjusted to be

5.0 by the addition of appropriate amounts of 0.1 mol dm⁻³ NaOH or HNO₃. The suspensions were equilibrated for metal ion adsorption in a thermostated water bath at 20 °C for 24 h. After agitation, the suspensions were filtered, and the final concentrations of each metal ion determined by using ICP-OES.

The influence of pH on a multicomponent adsorption system was investigated over a pH range of 1-10. About 25 cm³ aliquots of a mixed adsorbate solution containing 50 mg dm⁻³ metal ion concentration was conditioned to obtain the desired pH by the addition of appropriate amounts of 0.1 mol dm⁻³ NaOH or HNO₃. The suspensions were equilibrated after the addition of 200 mg adsorbent in a thermostated water bath at 20 °C for 24 h. After agitation, the suspensions were filtered, and the final concentrations of each metal ion determined by using ICP-OES.

Competitive adsorption experiments were conducted at 20 °C for both equal and varied initial metal ion concentrations ranging from 10-50 mg dm⁻³. To achieve this, 25 cm³ of a solution containing equal or varying concentrations of Pb²⁺, Zn²⁺, Cd²⁺ and Cu²⁺ was conditioned to pH 5.5 with the addition of appropriate amounts of 0.1 mol dm⁻³ NaOH or HNO₃. An adsorbent dose of 200 mg was added to the solution and thereafter the mixture was agitated in a thermostated water bath at 20 °C for 24 h. The suspensions were filtered and the final concentrations of the metal ion in the filtrates were determined by using ICP-OES.

The amount of each metal ion adsorbed on the adsorbent was determined from the difference between the initial and equilibrium metal ion concentrations. The removal efficiency and sorption capacity (q_e) of metal ions were calculated according to equations 7.1 and 7.2, respectively.

$$\% \text{ adsorbed} = \left(\frac{C_i - C_{eq}}{C_i} \right) \times 100 \quad (7.1)$$

$$q_e = \left(\frac{C_i - C_{eq}}{m} \right) \times V \quad (7.2)$$

where C_i is the initial adsorbate concentration (mg dm⁻³), C_{eq} is the equilibrium concentration of adsorbate (mg dm⁻³), q_e is the adsorption capacity (mg g⁻¹), m is the mass of adsorbent (mg) and V is the volume (dm³) of the adsorbate solution used.

7.2.4.1. Isotherms

The Langmuir adsorption isotherm is used to describe the monolayer adsorption of sorbates onto homogeneous sites. This model was used to describe the equilibrium data obtained for the removal of adsorbates in both single- and multi-component systems. The Langmuir isotherm equation is represented in Eq. 7.3 [26].

$$q_{eq} = \frac{q_m b C_{eq}}{1 + b C_{eq}} \quad (7.3)$$

where q_{eq} is the amount adsorbed per unit mass of adsorbent at equilibrium (mg g^{-1}), C_{eq} is the equilibrium concentration of adsorbate in solution after adsorption (mg dm^{-3}), q_m represents the maximum adsorption capacity (mg g^{-1}), and b is the empirical Langmuir adsorption constant ($\text{dm}^3 \text{mg}^{-1}$).

7.2.4.2. Data analysis

The data obtained were fitted to the isotherm and kinetics models by means of the nonlinear regression routine (*nls*) in the R statistical computing environment [27]. The R statistical software takes into account the minimization of the sum of squared residuals (SSR) and the residual square errors (RSE). A comparison of all SSR and RSE values was done and the adequacy of the models was assessed from the value with the lowest SSR.

7.2.4.3. Distribution coefficient

The distribution coefficient (K_d) is applied in order to estimate the affinity of a sorbent towards a solute [28-30]. The higher the value, the better is the affinity of the metal ion for the sorbent. The coefficient was calculated as indicated in Eq. 7.4.

$$K_d = \frac{C_i - C_{eq}}{C_{eq}} \times \frac{V}{m} \quad (7.4)$$

where C_i is the initial concentration (mg dm^{-3}), C_{eq} is the equilibrium concentration (mg dm^{-3}), m is the adsorbent mass (g), and V is the volume of the solution (dm^3).

7.2.5. Analysis of real water samples

Three water samples were collected from three sites on the Umgeni river: (i) the tributary on the confluence of the Umgeni and Msunduzi rivers, (ii) the outflow from the EThekweni wastewater treatment plant and (iii) the Blue Lagoon (mouth of Umgeni river). The initial concentrations of Pb^{2+} , Zn^{2+} and Cu^{2+} in the sample was determined by using ICP-OES. An aliquot of 25 cm^3 of each of the water sample was measured into 50 cm^3 polypropylene

bottles, conditioned to pH 5, and 50 mg of the adsorbent was added. The suspensions were agitated in a thermostated water bath at 20 °C for 1 h. After agitation, the suspensions were filtered and their supernatants analysed for the final concentrations of metal ions in solution. The removal efficiency and adsorption capacity for each metal ion were evaluated according to equations 7.1 and 7.2, respectively.

7.3. Results and discussion

The MWCNT-ttpy adsorbent was successfully synthesized and characterized by using various techniques. As reported in our previous work [31], an increase in the textural characteristics (surface area and pore volume) of the adsorbent was noticed, due to increase in the extent of functionalization, by the incorporation of nitrogen-donor atoms to the surface of the tubes. This process significantly increased the functional groups attached onto MWCNTs [31], hence resulting in increased metal sorption.

As a result of the increased activity of nitrogen-functionalized MWCNTs (MWCNT-ttpy) towards divalent metal ion removal as observed from our previous studies (Chapters 4, 5 and 6), the efficiency of the sorbent was examined for metal ion removal in a multi-component system. This was done to investigate the behaviour of MWCNT-ttpy in real-life scenarios where wastewaters contain a variety of metal ions simultaneously in solution. This section therefore presents results obtained for the sorption of metal ions in a competitive multi-component adsorption system. These results are compared with those obtained in a single-component system.

7.3.1. Adsorption of metal ions in single-solute systems

Adsorption experiments were conducted at pH 5.0 in single-component systems within a concentration range of 10-100 mg dm⁻³. As described in Fig 7.1, the uptake of metal ions (q_e) by MWCNT-ttpy increases gradually as the initial concentration of each metal ion increases. This is in accordance with the assumption that an increase in the initial metal ion concentration of an adsorbate significantly enhances the driving force required to overcome the sorbent-sorbate resistance; consequently resulting in higher q_e values [17].

Pearson, in 1968, established a principle underlying the preferential complexation of Lewis acids (metal ions) with Lewis bases (nitrogen or oxygen-containing ligands). Borderline (Pb²⁺, Cu²⁺ and Zn²⁺) and soft (Cd²⁺) metals were reported to be preferentially attracted towards oxygen- and nitrogen-containing ligands, respectively [32]. This principle justified

the favourable uptake of Cd^{2+} onto MWCNT-ttpy (Fig 7.1). Hence, the adsorption of metal ions onto MWCNT-ttpy was in the order of $\text{Cd} > \text{Pb} > \text{Cu} > \text{Zn}$ (Fig 7.1).

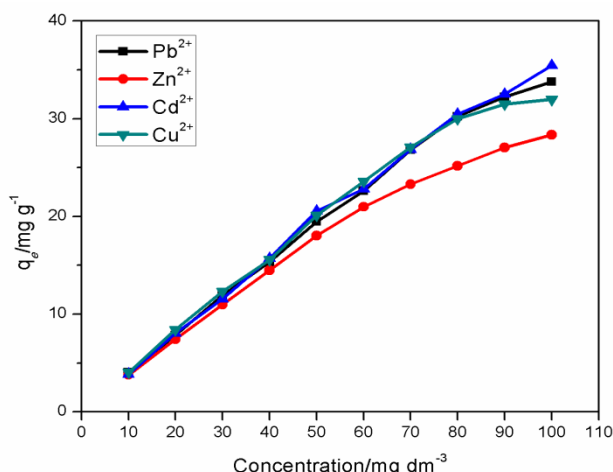


Fig 7.1: Amounts adsorbed of Pb^{2+} , Zn^{2+} , Cd^{2+} and Cu^{2+} onto MWCNT-ttpy in a single adsorption system [conditions: 20 cm^3 of adsorbate solution, 24 h equilibration time, pH 5.0, adsorbent dose 50 mg, agitation speed 150 rpm, temperature $20 \text{ }^\circ\text{C}$].

7.3.2. Adsorption of metal ions in multicomponent systems

7.3.2.1. Effect of pH

To investigate the influence of pH on the removal of Pb^{2+} , Zn^{2+} , Cd^{2+} and Cu^{2+} from aqueous solution in a multicomponent system, a 25 cm^3 aliquot containing 50 mg dm^{-3} solution of each of the four metal ions was measured into 50 cm^3 polyethylene bottles and its pH adjusted within the range of 1-10 by adding appropriate amounts of either 0.1 mol dm^{-3} NaOH or HNO_3 to obtain the desired pH. A mass of 0.2 g of MWCNT-ttpy was added to each solution and agitated in a thermostated water bath at $20 \text{ }^\circ\text{C}$ for 24 h. After agitation, the suspensions were filtered and the equilibrium concentrations of the remaining metal ions in the filtrates was determined by ICP-OES.

As shown in Fig 7.2, the percentage removal of metal ions significantly increased as the solutions became more alkaline. Low removal of adsorbates was noticeable at acidic conditions (*i.e.* pH 1-3) and this is due to competition between hydrogen and metal ions in solution. This significantly reduced the sorption of metal ions onto MWCNT-ttpy. Significant removal of Pb^{2+} and Cu^{2+} was noticeable between pH 3-7, attaining a percentage removal above 90%. The removal of Cd^{2+} became noticeable around pH 5-8, while Zn^{2+} removal was only pronounced between pH 7-10. Hence, the sorption of metal ions onto MWCNT-ttpy was enhanced as the solution tends to basic, owing to their chelation with the negative charged surface of the adsorbent (Fig 7.2). A continued increase in solution pH to 10, resulted in an increase in removal of all metal ions to a maximum of 98%. This could

be due to increasing precipitation accompanying the sorption of metal ions in solution. Hence, the removal of the studied metal ions in a competitive system was in the order $Pb^{2+} > Cu^{2+} > Cd^{2+} > Zn^{2+}$. The observed trend was in agreement with previously reported studies by Hamza *et al.* [7], Chen *et al.* [10], Srivastava *et al.* [11] and Sdiri *et al.* [33]. Hence, in order to avoid the precipitation of metal ions, the competitive adsorption of Pb^{2+} , Zn^{2+} , Cd^{2+} and Cu^{2+} was investigated at a pH of 5.5 in this study.

The experimental data for the competitive adsorption of a multicomponent metal ion solution onto MWCNT-ttpy as a function of pH can be found in Appendix IV (Table A-IV.1 – Table A-IV.4).

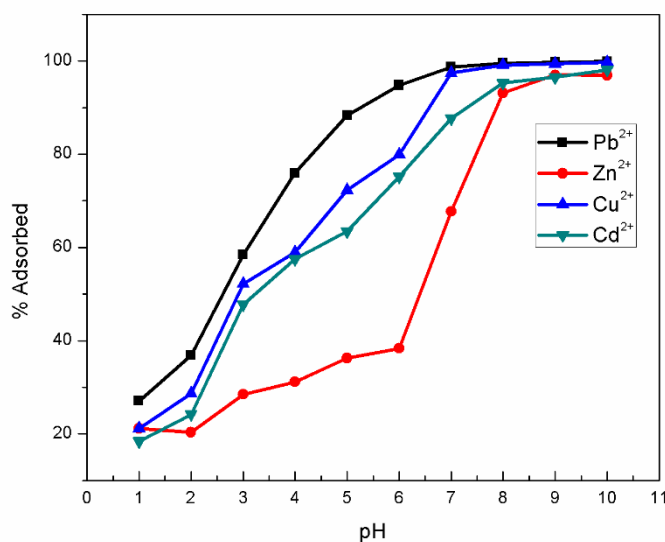


Fig 7.2: Effect of pH on the competitive adsorption of metal ions on MWCNT-ttpy [conditions: 25 cm³ of 50 mg dm⁻³ of each adsorbate, 24 h equilibration time, adsorbent dose 200 mg, agitation speed 150 rpm, temperature 20 °C].

7.3.2.2. Effect of equal initial metal ion concentration

The influence of the same initial metal ion concentration in a multicomponent adsorption system was examined and the results are presented in Fig 7.3. In general, the percentage removal of adsorbates was noticed to decrease with an increase in the initial concentration of the metal ions (Fig 7.3a). The figure also showed that the sorption of Pb^{2+} from a multicomponent system was highest at all concentrations, and lowest for Zn^{2+} . Across the metal ion concentrations of 10 to 60 mg dm⁻³, the percentage removal of adsorbates was in the order of Pb^{2+} (76.3% to 89.0%); Cu^{2+} (71.5% to 84.4%); Cd^{2+} (63.5% to 78.8%) and Zn^{2+} (18.1% to 40.1%) (Fig 7.3a). However, Fig 7.3b showed an increase in the uptake of the corresponding metal ion with increase in concentration. The low uptake (q_e) of Zn^{2+} in a multicomponent system (Fig 7.3b) could be due to the presence of other competitors, which have occupied the active sites of the adsorbent due to their smaller hydrated ionic

radii. As proposed by Chen *et al.* [10], the removal of divalent metal ions is inversely proportional to the hydrated ionic radii of the metal species in solution. The ionic radii of the studied metal ion species is in the order of Pb^{2+} (4.01 Å) < Cu^{2+} (4.19 Å) < Cd^{2+} (4.26 Å) < Zn^{2+} (4.30 Å) [7,10]. Also, considering that the pore diameter of MWCNT-tpy (272.6 Å) is far greater than the radii of all the metal ions studied, their sorption could be decided upon by the size of the metal ion species. Hence, metal ions with smaller ionic radii might have greater access to adsorbent sites, hence accounting for the observed sorption in the sequence of $\text{Pb} > \text{Cu} > \text{Cd} > \text{Zn}$. Therefore, it could be said that the sorption of these metal ions obeyed this principle, since their removal was in the same order.

The selectivity of metal ions obtained in this study was mostly in accordance with previously reported studies. A study investigating the competitive sorption of metal ions onto graphene oxide by Sitko *et al.* [34] gave the same trend as that reported in this study. Chen *et al.* [10] and Li *et al.* [6] reported the same sequence of $\text{Pb} > \text{Cu} > \text{Cd}$ from a multicomponent system onto nano-hydroxyapatite and MWCNTs, respectively. However, a sequence of $\text{Pb} > \text{Cu} > \text{Zn} > \text{Cd}$ was reported by Srivastava *et al.* [11] and Sdiri *et al.* [35] from a multicomponent system onto kaolinite and clay, respectively. This order was slightly different to that reported in this study. The removal of metal ions from wastewater will therefore principally depend on the textural characteristics of the sorbent used.

The experimental data for the competitive adsorption of Pb^{2+} , Zn^{2+} , Cd^{2+} and Cu^{2+} in a multicomponent system as a function of equal initial metal ion concentration can be found in Appendix IV (Table A-IV.5 – Table A-IV.8).

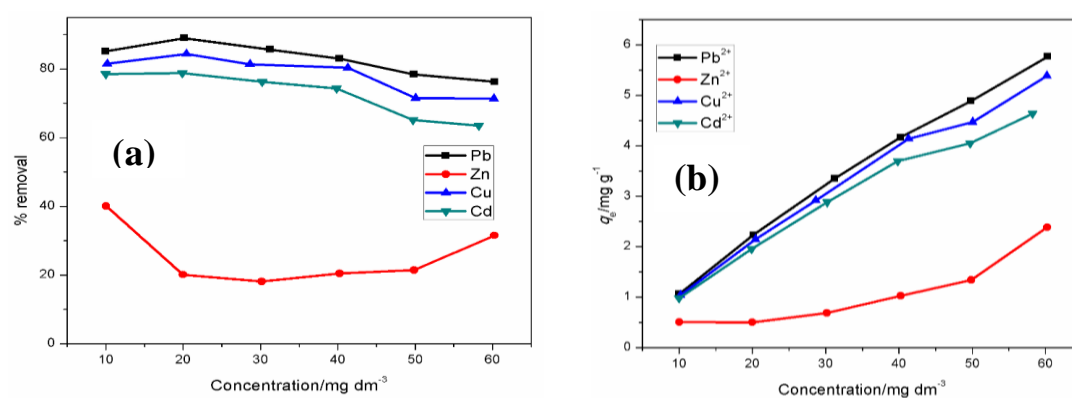


Fig 7.3: The effect of the same initial metal ion concentration in a multicomponent system for the adsorption of Pb^{2+} , Zn^{2+} , Cd^{2+} and Cu^{2+} . (a) Percentage uptake (%) and (b) amount adsorbed per unit mass (mg g^{-1}) [conditions: 25 cm³ of adsorbate solution, pH 5.5, 24 h equilibration time, adsorbent dose 50 mg, agitation speed 150 rpm, temperature 20 °C].

7.3.2.3 Effect of varying metal ion concentration

In a multicomponent adsorption system, the presence of a particular metal ion might induce/dissuade the removal of other metal ions in solution. The preferential removal of metal ions depends largely on the properties of the sorbent and the nature of the metal ions in solution. In this section, the influence of the initial concentration of other metal ions on the removal of a particular metal in a competitive system was investigated by keeping the concentration of a metal ion constant at 20 mg dm^{-3} , while others were varied simultaneously between $10\text{-}50 \text{ mg dm}^{-3}$.

7.3.2.3.1 Effect of the presence of Cu^{2+} , Cd^{2+} and Zn^{2+} on Pb^{2+} sorption

The influence of the presence of other metal ions on the sorption of Pb^{2+} was investigated by keeping its concentration at 20 mg dm^{-3} , while the concentration of other species was varied within $10\text{-}50 \text{ mg dm}^{-3}$.

In general, the sorption of all metal ions, except Cd^{2+} , gradually decreased with an increase in the initial metal ion concentration of other competitors. As shown in Fig 7.4, the percentage Pb^{2+} adsorbed onto MWCNT-tpy steadily decreased from 78.5% to 47.4% as the concentrations of the other species were increased from $10\text{-}50 \text{ mg dm}^{-3}$. Also, the percentage removal of Pb^{2+} was never the highest of the four metal ions considered. This could be associated with the increase in competition for active sites by other competitors, hence, resulting in a gradual decrease in Pb^{2+} removal as the concentrations of the other metal species increased. This trend was also noticeable for the removal of Cu^{2+} and Zn^{2+} , decreasing from 89.6% to 57.15% and 39.11% to 21.43%, respectively. Interestingly, Cu^{2+} showed the greatest removal percentage at 10 mg dm^{-3} when Pb^{2+} was present at 20 mg dm^{-3} . However, the presence of Pb^{2+} in solution had no significant influence on the sorption of Cd^{2+} . This could be attributed to the preferential complexation of Cd^{2+} to MWCNT-tpy active sites, since soft metals such as Cd^{2+} have a high affinity for N-containing compounds [32]. This preferential adsorption exhibited by Cd^{2+} , is not affected by the presence of other competitor ions. However, the other ions compete for the remaining N- and O-donor sites. The sequence and metal ion affinity were in the order of $\text{Cd}^{2+} > \text{Pb}^{2+} > \text{Cu}^{2+} > \text{Zn}^{2+}$ according to the K_d values for this sorption (Appendix IV). This order, according to the K_d values, also indicates the affinity of metal ions towards MWCNT active sites [29]. The experimental data for this sorption can be seen in Appendix IV (Table A-IV.9 –Table A-IV.12).

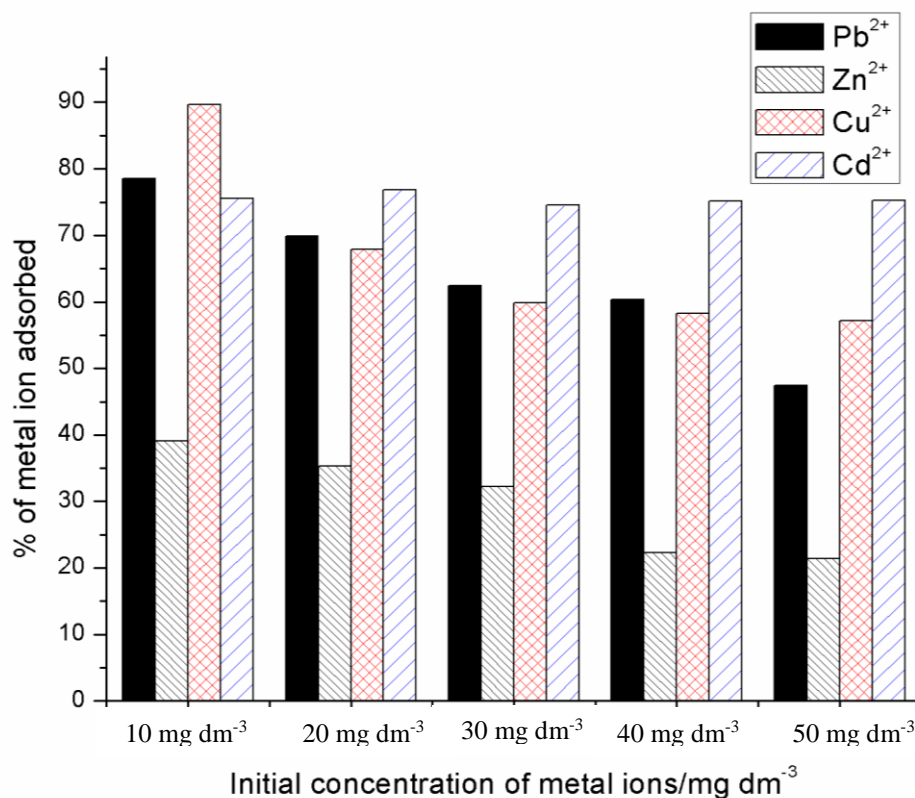


Fig 7.4: Competitive removal of Pb²⁺ at a fixed concentration of 20 mg dm⁻³ in a mixed metal ion solution with concentrations ranging from 10 to 50 mg dm⁻³. [conditions: adsorbent dose of 200 mg, pH 5.5, agitation time of 24 h, agitation speed of 150 rpm and temperature at 20 °C].

7.3.2.3.2. Effect of the presence of Pb²⁺, Cd²⁺ and Zn²⁺ on Cu²⁺ sorption

The influence of other competitors on the sorption of Cu²⁺ was investigated by keeping its concentration constant at 20 mg dm⁻³, while other metal ion competitors were simultaneously varied between 10-50 mg dm⁻³.

The adsorption of Cu²⁺ in a competitive system steadily decreased from 91.2% to 42.9% as the initial metal ion concentration of other competitors increased from 10-50 mg dm⁻³ (Fig 7.5). This could also be associated with the increase in competition with other metal ion species at increased concentrations, resulting in its decreased adsorption. However, a higher Cu²⁺ percentage was obtained for all concentrations other than 50 mg dm⁻³. Similar decreasing removal efficiencies were observed for Cd²⁺ and Zn²⁺ from 48.3% to 37.9% and 33.4% to 13.3%, respectively (Fig 7.5). However, the sorption of Pb²⁺ was not significantly influenced across the concentration range. It remained within the range of 50-58%, hence,

the affinity of metal ions for complexation with MWCNT-ttpe when keeping the concentration of Cu^{2+} constant was in the order $\text{Cu} > \text{Pb} > \text{Cd} > \text{Zn}$, based on obtained K_d values (Appendix IV) [30]. The experimental data for this sorption is presented in Appendix IV (Table A-IV-13 – Table A-IV.16).

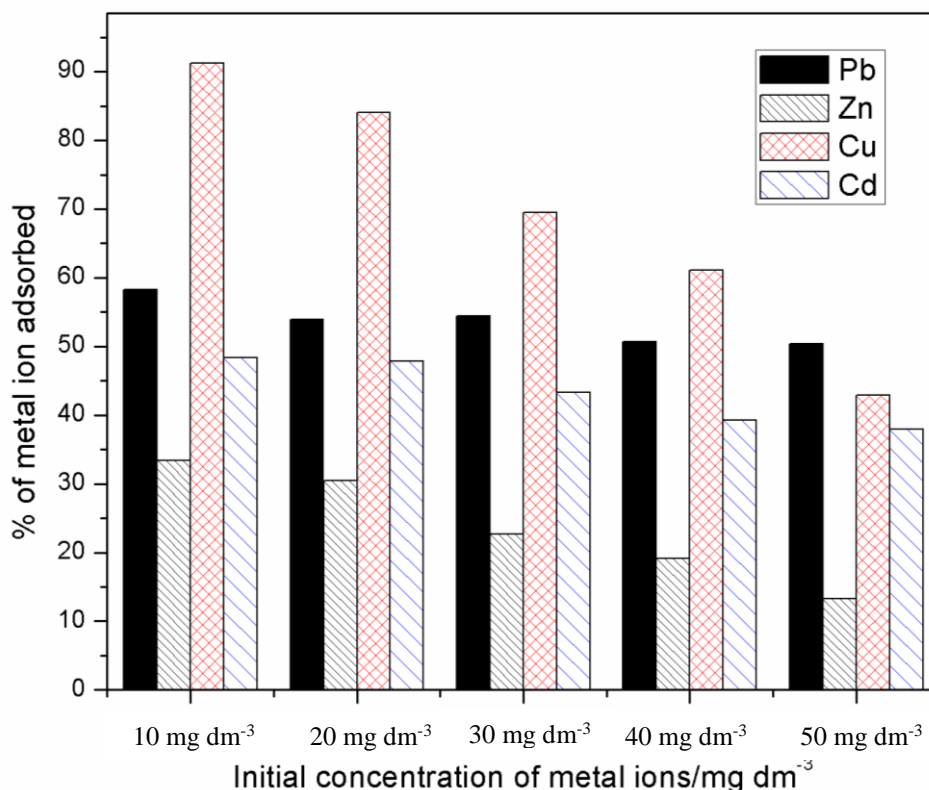


Fig 7.5: Competitive removal of Cu^{2+} at a fixed concentration of 20 mg dm^{-3} in a mixed metal ion solution with concentrations ranging from 10 to 50 mg dm^{-3} . [conditions: adsorbent dose of 200 mg, pH 5.5, agitation time of 24 h, agitation speed of 150 rpm and temperature at $20 \text{ }^\circ\text{C}$].

7.3.2.3.3. Effect of the presence of Pb^{2+} , Cu^{2+} and Zn^{2+} on Cd^{2+} sorption

The sorption of Cd^{2+} in a competitive system was investigated by keeping its concentration constant at 20 mg dm^{-3} , while varying the concentrations of the other metal ions between 10- 50 mg dm^{-3} . The affinity of Cd^{2+} onto MWCNT-ttpe was noticeable, even at higher concentrations of other competitors, although a decrease in percentage removal was obtained at increasing concentrations of the competitors (Fig 7.6). The percentage removal of Cd^{2+} was highest for all five concentrations. This was followed by Cu^{2+} , then Pb^{2+} and the lowest removal in all cases was for Zn^{2+} . This adsorption behaviour of Cd^{2+} and Cu^{2+} could be attributed to the preferential uptake of both adsorbates by N-donor atoms, hence, forming strong chelates between them. Based on the K_d values obtained, the maximum adsorption

capacity of MWCNT-tpy follows the sequence $Cd > Cu > Pb > Zn$ (see Table A-IV.17 – Table A-IV.20, Appendix IV).

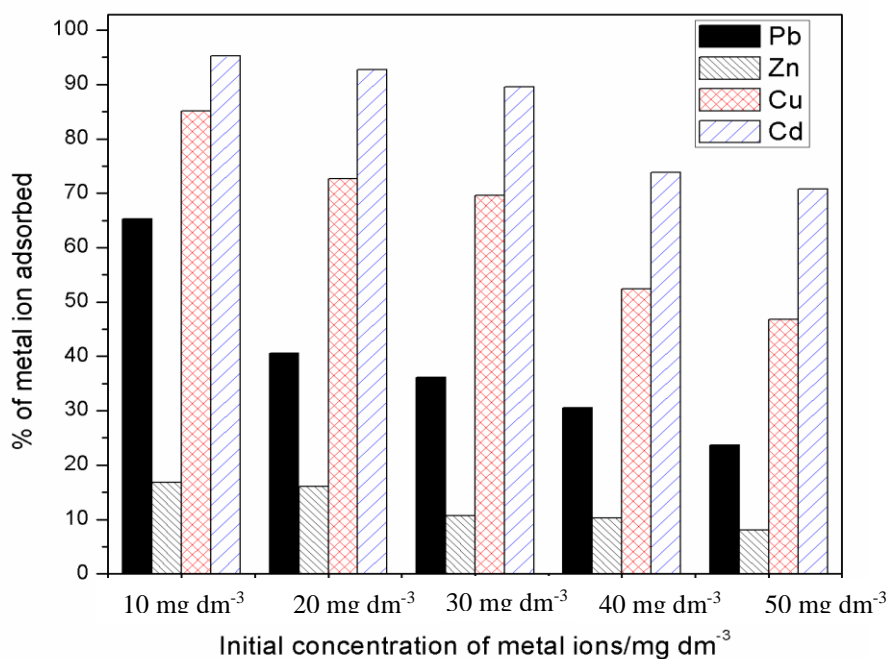


Fig 7.6: Competitive removal of Cd^{2+} at a fixed concentration of 20 mg dm^{-3} in a mixed metal ion solution with concentrations ranging from 10 to 50 mg dm^{-3} . [conditions: adsorbent dose of 200 mg, pH 5.5, agitation time of 24 h, agitation speed of 150 rpm and temperature at $20 \text{ }^\circ\text{C}$].

7.3.2.3.4. Effect of the presence of Cu^{2+} , Cd^{2+} and Pb^{2+} on Zn^{2+} sorption

The influence of varying concentrations of other competitors on the sorption of Zn^{2+} in a multicomponent system was investigated by maintaining its concentration at 20 mg dm^{-3} , while others were varied between $10\text{-}50 \text{ mg dm}^{-3}$ simultaneously. Interestingly, the sorption of Zn^{2+} onto MWCNT-tpy was lowest at all concentrations, obtaining a maximum percentage removal of 19.9% at an initial concentration of 10 mg dm^{-3} for the competitor ions (Fig 7.7). Further increases in the concentrations of the competitors decreased its removal to 4.85%, indicating poor removal of Zn^{2+} in a multicomponent system (Fig 7.7). The sorption of Cd^{2+} remained highest at all concentrations followed by Pb^{2+} and Cu^{2+} . Hence, the sequence of $Cd^{2+} > Pb^{2+} > Cu^{2+} > Zn^{2+}$ was obtained as a function of K_d values (see Table A-IV.21 – Table A-IV.24, Appendix IV).

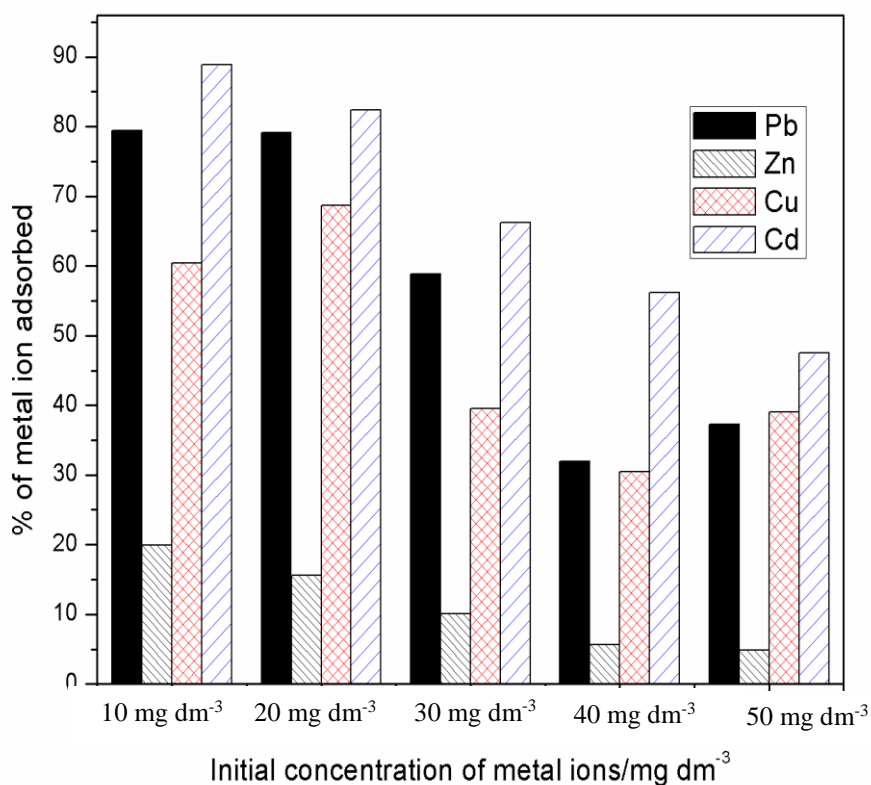


Fig 7.7: Competitive removal of Zn²⁺ at a fixed concentration of 20 mg dm⁻³ in a mixed metal ion solution with concentrations ranging from 10 to 50 mg dm⁻³. [conditions: adsorbent dose of 200 mg, pH 5.5, agitation time of 24 h, agitation speed of 150 rpm and temperature at 20 °C].

7.3.3. Adsorption isotherms

In order to understand the adsorption mechanism in a multi-component competitive system, the equilibrium data for the adsorption of Pb²⁺, Cd²⁺, Cu²⁺ and Zn²⁺ onto MWCNT-tty on single- and multi-component systems were both analysed by using the Langmuir model given in Eq. 7.3. The Langmuir parameters are given in Table 7.2, and plots of the Langmuir adsorption isotherms for single- and multi-component systems can be found in Appendix IV (Fig A-IV.1). Table 7.2 indicates a significant decrease in the uptake (q_m) of each metal in a competitive system when compared with values obtained for single adsorption systems. This decrease can be associated to the competition for active sites among the metal cations in solution, hence, resulting in a decrease of q_m values. From the q_m values obtained, the affinity of MWCNT-tty for metal ions follows the sequence Cd > Pb > Cu > Zn in a single sorption system and Pb > Cu > Cd > Zn in a multicomponent adsorption system (Table 7.2). As discussed earlier, the sequence obtained corresponds to those previously reported by

Sitko *et al.* [34], Li *et al.* [6], Chen *et al.* [10], and Fei *et al.* [36] in single- and multi-component adsorption systems.

The adsorption behaviour of a particular metal ion can be influenced by the presence of other metal ions in solution for a multicomponent system. This effect was assessed by Zhu *et al.* [37] to ascertain if the sorption capacity of a metal depends on others in solution. The ratio of the maximum adsorption capacity in a single- and a multi-component system (q_m'/q_m) was calculated to estimate the interfering effects of metal ions present in solution. They proposed that the adsorption process is synergistic if $q_m'/q_m > 1$, antagonistic if $q_m'/q_m < 1$ and no net interaction when $q_m'/q_m = 1$ [37]. Table 7.2 indicates that all q_m'/q_m values obtained in this study were less than 1, indicating that the sorption of Pb^{2+} , Cd^{2+} , Cu^{2+} and Zn^{2+} were all influenced by the presence of other competitors in solution. Therefore, this antagonistic approach further justifies the reduced q_m values obtained in a multicomponent system.

Table 7.2: The Langmuir parameters for the adsorption of Pb^{2+} , Cd^{2+} , Cu^{2+} and Zn^{2+} on MWCNT-ttpty in a single- and multi-component system

Metals	Single metal adsorption				Competitive adsorption				
	q_m/mg^{-1}	$b/\text{dm}^3 \text{g}^{-1}$	SSR ^a	RSE ^b	q_m'/mg^{-1}	$b/\text{dm}^3 \text{g}^{-1}$	SSR ^a	RSE ^b	q_m'/q_m
Pb^{2+}	36.46	0.889	25.52	1.786	8.574	0.136	0.268	0.259	0.235
Cd^{2+}	41.51	0.558	9.864	1.110	6.744	0.100	0.188	0.217	0.162
Cu^{2+}	31.58	3.407	34.06	2.063	7.977	0.109	0.452	0.336	0.253
Zn^{2+}	28.74	0.224	1.989	0.497	4.398	0.018	0.033	0.091	0.153

^a- Sum of squared residuals, ^b- residual squared errors

7.3.4. Analysis of real samples

In order to affirm the selectivity of MWCNT-ttpty and test its efficacy for metal ion removal in a real life scenario, water samples were collected from three different points on the Umgeni river. The initial metal ion concentrations found in the water samples is given in Table 7.3. Interestingly, a removal efficiency greater than 95% was obtained for all three metal ions in the three water samples (Table 7.3). Although the initial concentrations of Pb^{2+} , Cu^{2+} and Zn^{2+} in samples were in measureable amounts ($\geq 10 \text{ mg dm}^{-3}$), MWCNT-ttpty successfully sequestered these toxic heavy metal ions from the environmental samples. This further authenticates that MWCNT-ttpty and the method of adsorption presented are effective and efficient when applied to real samples. Hence, the application of MWCNT-ttpty should be further explored for the remediation of wastewater or effluents discharged from industries.

Table 7.3: Analysis of real water samples

Sample Name	C_i Pb	C_i Zn	C_i Cu	C_{eq} Pb	C_{eq} Zn	C_{eq} Cu	% Pb	% Zn	% Cu
Tributary	8.137	12.36	3.442	0.058	0.134	0.000	99.29	98.92	100.0
Blue Lagoon	5.087	6.112	6.114	0.216	0.000	0.005	95.75	100.0	99.92
Ethwekini	10.34	4.332	8.114	0.123	0.100	0.127	98.81	97.69	98.43

C_i : initial concentration, C_{eq} : equilibrium concentrations

7.4. Conclusions

The sorption of Pb^{2+} , Cd^{2+} , Cu^{2+} and Zn^{2+} onto nitrogen-functionalized multiwalled carbon nanotubes (MWCNT-ttpy) was investigated in single- and multi-component adsorption systems. Batch experiments investigating the effect of pH and initial metal ion concentration were studied on both types of adsorption systems. The equilibrium adsorption data was modelled by the Langmuir isotherm to understand the mechanism involved for each process.

The study revealed that the Langmuir isotherm model describes the experimental data well for in both systems, however, lower metal ion uptake (q_m) was observed in a competitive system compared with a single-solute system. The sorption of all metal ions onto MWCNT-ttpy was antagonistic, thereby increasing competition for active sites and lower uptake of some metal ions over others. Hence, the sorption of a particular metal ion was greatly influenced by the presence of other competing ions in solution, regardless of their initial concentration. In single-solute systems, the sequence and affinity of MWCNT-ttpy for metal ions was in the order of $Cd > Pb > Cu > Zn$. However, an order of $Pb > Cu > Cd > Zn$ was obtained for multicomponent adsorption. The sorption of Zn^{2+} onto the sorbent was lowest in both systems, unlike Cd^{2+} whose affinity was always the greatest, except in the presence of constant Cu^{2+} . Thus, MWCNT-ttpy demonstrated good selectivity for Cd^{2+} , Pb^{2+} and Cu^{2+} , and the removal of Zn^{2+} was fair in a multicomponent system.

Therefore, this study highlights the potential application of MWCNT-ttpy in wastewater treatment especially at high pollutant concentrations, owing to its selectivity towards the removal of divalent metal such as Cd^{2+} , Pb^{2+} , Cu^{2+} and Zn^{2+} from aquatic environments.

References

- [1] T.K. Sen, D. Gomez, Adsorption of zinc (Zn^{2+}) from aqueous solution on natural bentonite, *Desalination* 267 (2011) 286-294.
- [2] A.J. Ahamed, A.S. Begum, Adsorption of copper from aqueous solution using low cost adsorbent, *Arch. Appl. Sci. Res.* 4 (2012) 1532-1539.
- [3] K.S. Tong, M.J. Kassim, A. Azraa, Adsorption of copper ion from its aqueous solution by a novel biosorbent *Uncaria gambir*: Equilibrium, kinetics, and thermodynamic studies, *Chem. Eng. J.* 170 (2011) 145-153.
- [4] M.A. Tofighy, T. Mohammadi, Adsorption of divalent heavy metal ions from water using carbon nanotube sheets, *J. Hazard. Mater.* 185 (2011) 140-147.
- [5] Z. Melichova, L. Hromada, Adsorption of Pb^{2+} and Cu^{2+} ions from aqueous solutions on natural bentonite, *Pol. J. Environ. Stud.* 22 (2013) 457-464.
- [6] Y.-H. Li, J. Ding, Z. Luan, Z. Di, Y. Zhu, C. Xu, D. Wu, B. Wei, Competitive adsorption of Pb^{2+} , Cu^{2+} and Cd^{2+} ions from aqueous solutions by multiwalled carbon nanotubes, *Carbon* 41 (2003) 2787-2792.
- [7] I.A.A. Hamza, Preparation and evaluation of a sugarcane bagasse multi-walled carbon nanotube composite for the adsorption of heavy metals from aqueous solutions, PhD Thesis University of KwaZulu-Natal, Durban, South Africa (2013).
- [8] R. Mihalache, I. Peleanu, I. Meghea, A. Tudorache, Competitive adsorption models of organic pollutants from bi- and tri-solute systems on activated carbon, *J. Radioanal. Nucl. Chem.* 229 (1998) 133-137.
- [9] Y.S. Ho, G. McKay, Competitive sorption of copper and nickel ions from aqueous solution using peat, *Adsorption* 5 (1999) 409-417.
- [10] S.B. Chen, Y.B. Ma, L. Chen, K. Xian, Adsorption of aqueous Cd^{2+} , Pb^{2+} , Cu^{2+} ions by nano-hydroxyapatite: Single- and multi-metal competitive adsorption study, *Geochem. J.* 44 (2010) 233-239.
- [11] P. Srivastava, B. Singh, M. Angove, Competitive adsorption behavior of heavy metals on kaolinite, *J. Colloid Interface Sci.* 290 (2005) 28-38.
- [12] M.E. Argun, S. Dursun, C. Ozdemir, M. Karatas, Heavy metal adsorption by modified oak sawdust: thermodynamics and kinetics, *J. Hazard. Mater.* 141 (2007) 77-85.
- [13] C. Ozdemir, M. Karatas, S. Dursun, M. Argun, S. Dogan, Effect of $MnSO_4$ on the chromium removal from the leather industry wastewater, *Environ. Technol.* 26 (2005) 397-400.
- [14] N. Meunier, P. Drogui, C. Montané, R. Hausler, G. Mercier, J.-F. Blais, Comparison between electrocoagulation and chemical precipitation for metals removal from acidic soil leachate, *J. Hazard. Mater.* 137 (2006) 581-590.
- [15] W. Pranata Putra, A. Kamari, S. Najiah Mohd Yusoff, C. Fauziah Ishak, A. Mohamed, N. Hashim, I. Md Isa, Biosorption of $Cu(II)$, $Pb(II)$ and $Zn(II)$ Ions from Aqueous

- Solutions Using Selected Waste Materials: Adsorption and Characterisation Studies, *J. Encap. Adsorption Sci.* 4 (2014) 25-35.
- [16] O.A. Oyetade, V.O. Nyamori, B.S. Martincigh, S.B. Jonnalagadda, Effectiveness of carbon nanotube-cobalt ferrite nanocomposites for the adsorption of rhodamine B from aqueous solutions, *RSC Adv.* 5 (2015) 22724-22739.
- [17] I.A.A. Hamza, B.S. Martincigh, J.C. Ngila, V.O. Nyamori, Adsorption studies of aqueous Pb(II) onto a sugarcane bagasse/multi-walled carbon nanotube composite, *Phys. Chem. Earth* 66 (2013) 157-166.
- [18] G. Rao, C. Lu, F. Su, Sorption of divalent metal ions from aqueous solution by carbon nanotubes: A review, *Sep. Purif. Technol.* 58 (2007) 224-231.
- [19] Y.S. Ho, D.A.J. Wase, C.F. Forster, Kinetic Studies of Competitive Heavy Metal Adsorption by Sphagnum Moss Peat, *Environ. Technol.* 17 (1996) 71-77.
- [20] S. Hussain, R. Amade, E. Jover, E. Bertran, Nitrogen plasma functionalization of carbon nanotubes for supercapacitor applications, *J. Mater. Sci.* 48 (2013) 7620-7628.
- [21] G. Kalita, S. Adhikari, H.R. Aryal, R. Afre, T. Soga, M. Sharon, M. Umeno, Functionalization of multi-walled carbon nanotubes (MWCNTs) with nitrogen plasma for photovoltaic device application, *Curr. Appl. Phys.* 9 (2009) 346-351.
- [22] S. Santangelo, G. Messina, G. Faggio, S.H. Abdul Rahim, C. Milone, Effect of sulphuric-nitric acid mixture composition on surface chemistry and structural evolution of liquid-phase oxidised carbon nanotubes, *J. Raman Spectrosc.* 43 (2012) 1432-1442.
- [23] M.N. Patel, P.A. Dosi, B.S. Bhatt, Synthesis, characterization, antibacterial activity and DNA interaction studies of drug-based mixed ligand copper(II) complexes with terpyridines, *Med. Chem. Res.* 21 (2012) 2723-2733.
- [24] M.N. Patel, H.N. Joshi, C.R.I. Patel, Copper(II) complexes with norfloxacin and neutral terpyridines: Cytotoxic, antibacterial, superoxide dismutase and DNA-interaction approach, *Polyhedron* 40 (2012) 159-167.
- [25] J. Shen, W. Huang, L. Wu, Y. Hu, M. Ye, Study on amino-functionalized multiwalled carbon nanotubes, *Mater. Sci. Eng. Part A* 464 (2007) 151-156.
- [26] I. Langmuir, The adsorption of gases on plane surfaces of glass, mica and platinum, *J. Am. Chem. Soc.* 40 (1918) 1361-1402.
- [27] The R Development Core Team, The R foundation for statistical Computing, R version 3.0.2 (2013).
- [28] S.A. Khan, M.A. Khan, Adsorption of chromium (III), chromium (VI) and silver (I) on bentonite, *Waste Manage.* 15 (1995) 271-282.
- [29] T.K. Naiya, A.K. Bhattacharya, S. Mandal, S.K. Das, The sorption of lead (II) ions on rice husk ash, *J. Hazard. Mater.* 163 (2009) 1254-1264.

- [30] K.K. Choy, J.F. Porter, G. McKay, Langmuir isotherm models applied to the multicomponent sorption of acid dyes from effluent onto activated carbon, *J. Chem. Eng. Data* 45 (2000) 575-584.
- [31] O.A. Oyetade, V.O. Nyamori, B.S. Martincigh, S.B. Jonnalagadda, Nitrogen-functionalised carbon nanotubes as a novel adsorbent for the removal of Cu(II) from aqueous solution, (unpublished results).
- [32] R.G. Pearson, Hard and soft acids and bases, HSAB, Part 1: Fundamental principles, *J. Chem. Educ.* 45 (1968) 581.
- [33] A. Sdiri, T. Higashi, F. Jamoussi, S. Bouaziz, Effects of impurities on the removal of heavy metals by natural limestones in aqueous systems, *J. Environ. Manage.* 93 (2012) 245-253.
- [34] R. Sitko, E. Turek, B. Zawisza, E. Malicka, E. Talik, J. Heimann, A. Gagor, B. Feist, R. Wrzalik, Adsorption of divalent metal ions from aqueous solutions using graphene oxide, *Dalton Trans.* 42 (2013) 5682-5689.
- [35] A. Sdiri, T. Higashi, R. Chaabouni, F. Jamoussi, Competitive removal of heavy metals from aqueous solutions by montmorillonitic and calcareous clays, *Water Air Soil Pollut.* 223 (2011) 1191-1204.
- [36] F. Qin, B. Wen, X.-Q. Shan, Y.-N. Xie, T. Liu, S.-Z. Zhang, S.U. Khan, Mechanisms of competitive adsorption of Pb, Cu, and Cd on peat, *Environ. Pol.* 144 (2006) 669-680.
- [37] Y. Zhu, J. Hu, J. Wang, Competitive adsorption of Pb (II), Cu (II) and Zn (II) onto xanthate-modified magnetic chitosan, *J. Hazard. Mater.* 221 (2012) 155-161.

Chapter 8

Kinetics, isotherm and thermodynamic studies for the removal of bisphenol A and ibuprofen from aqueous solution by using nitrogen-functionalized multiwalled carbon nanotubes

Oluwaseun A. Oyetade, Vincent O. Nyamori, Sreekantha B. Jonnalagadda and Bice S. Martincigh*

School of Chemistry and Physics, University of KwaZulu-Natal, Westville Campus,
Private Bag X54001, Durban 4000, South Africa

*Corresponding author: Tel: +27 31 2601394; Fax: +27 31 2603091; E-mail:
martinci@ukzn.ac.za

Abstract

This study aims at investigating the efficiency of chemically functionalized multiwalled carbon nanotubes (MWCNTs) for the removal of bisphenol A (BPA) and ibuprofen (IBP) from aqueous solution by adsorption. Acid-functionalized MWCNTs (MWCNT-COOH) and nitrogen-functionalized MWCNTs (MWCNT-ttpe) were used as adsorbents and their adsorption capacities compared for the removal of BPA and IBP.

The results indicate that the kinetics data was better described by the pseudo-second order model, indicating a bimolecular interaction between the adsorbates and adsorbents. Adsorption of BPA was investigated at pH 7 with equilibrium achieved within 240 min and 360 min for MWCNT-COOH and MWCNT-ttpe, respectively. Optimum conditions for the adsorption of IBP were obtained at pH 2 and equilibrium for both adsorbents was attained within 360 min. Isotherm studies show that data obtained for both substances best fit the Langmuir model except for MWCNT-ttpe, which was better described by the Freundlich model for IBP removal. An increase in the Langmuir monolayer adsorption capacity (q_m) was obtained for MWCNT-ttpe, indicating improved sorption after functionalization of MWCNT-COOH with 4'-(4-hydroxyphenyl)-2,2':6',2''-terpyridine.

Thermodynamic studies reveal that the removal of BPA and IBP with both adsorbents was spontaneous. The removal of BPA was endothermic whereas that of IBP was an exothermic process. Desorption of the loaded adsorbents showed good removal efficiencies for both processes indicating that the sorbents can be regenerated for reuse. This study confirms the potential application of MWCNT-COOH and MWCNT-ttpe as possible alternatives for the treatment of wastewater polluted with EDCs.

Keywords: Bisphenol A, ibuprofen, adsorption, multiwalled carbon nanotube, isotherm, kinetics

8.1 Introduction

Endocrine disrupting chemicals (EDCs) are substances that imitate naturally occurring hormones, by occupying hormone receptors in the body to generate overstimulation in humans and animals [1]. Intake of these substances into the human body can alter developmental, neurological and reproductive systems in man, resulting in several deleterious diseases [2,3]. The potential use of these compounds in food production and other related applications is of concern to environmentalists due to the toxicity of these compounds [3,4]. This work investigates bisphenol A and ibuprofen as two common EDCs typically found in wastewaters.

Bisphenol A (BPA) has wide application in the manufacture of plastics, household appliances, flame retardants and other commercial products. The determination of BPA has been reported in various environmental media such as in water ($>10 \text{ mg dm}^{-3}$) [5] and landfill leachates ($>17 \text{ mg dm}^{-3}$) [3]. The release of BPA into water stems from leaching of plastics, manufacturing processes and disposal of BPA-containing products on landfills after their end-of-life. The intake of this substance result in adverse effects on man, aquatic organisms and the environment [6]. Potential effects of BPA on human health include cancer, birth defects, brain damage, infertility, obesity, diabetes and immunodeficiency, amongst other serious disorders [2,7].

Ibuprofen (IBP) is one of the most consumed medicines in the world [8] because of its use as an analgesic, antipyretic, and non-steroidal anti-inflammatory drug (NSAID) [9,10]. The discharge of pharmaceutical toxins into the environment is usually from residues from pharmaceutical manufacturing, and human and veterinary waste. Evidence of IBP has been reported in some environmental media such as in water [11,12], soil [13] and landfill leachates [12]. The presence of this contaminant is perceived to have a negative influence, such as infertility and reproductive disorders [14], on human health if an adequate disposal route is not taken.

Unfortunately, typical wastewater treatment facilities are not designed to remove EDCs from water, and the concentrations of these compounds build-up in water bodies [15]. Adsorption has been shown to be an effective means of removing EDCs [2,15], but, the need exists to develop new adsorbents for their effective removal.

Surface functionalization of adsorbents plays a vital role in the removal of EDCs from aqueous solutions. This has resulted in the study of a number of adsorbents with different functional groups, with the aim to improve the removal of such organic contaminants from aqueous solution. Adsorption of EDCs, such as BPA and IBP, have been conducted by using

activated carbon [9,10], fly ash [16], bio-chars [14], zeolite [15], bio-sorbent [4], and sediment [17], amongst many others. The regeneration of these sorbents and low sorption capacities creates a huge challenge in achieving efficient removal of these pollutants [4,15]. Thus, more investigation is needed to improve the removal efficiencies of the adsorbents and to understand the mechanisms which control adsorption.

Multiwalled carbon nanotubes (MWCNTs) have gained wide application for various purposes, such as catalyst supports [18], and energy storage devices [19], amongst many others. MWCNTs have emerged as one of the most investigated shaped carbon nanomaterials (SCNMs) for the removal of organic contaminants from aqueous solution. The ease with which new functional groups are incorporated onto the walls of MWCNTs allows their increased use for many applications. MWCNTs consist of two or more layers of graphene sheets rolled into a cylinder, containing carbon atoms interlinked by π - π bonds [20]. The presence of these bonds creates possible interaction with organic contaminants *via* π - π interactions. The removal of organic pollutants such as trichlorophenol [21], polychlorinated biphenyls (PCBs) [22], trichlorobenzene [23,24], nitroaromatics [24], hexane [24], benzene [24], and polyaromatic hydrocarbons (PAHs) [1], amongst many, have been investigated by using CNT-containing nanomaterials. Reports have demonstrated good sorption ability for pollutant removal with a high possibility of regenerating CNTs for reuse.

Functionalization of MWCNTs can be achieved by incorporating π - π containing compounds onto the walls of tubes, thereby increasing the active sites available for adsorption. Recently published studies revealed further functionalization of MWCNTs with 8- hydroxyquinoline [25], 3-aminopropyl [26], dodecylamine [26], triethoxysilane [26], and organic hydrazines [27], amongst many others, in order to introduce multiple functional groups onto the walls of tubes. Due to the increase in hydrophobicity of CNTs through modification with organic compounds, removal of organic contaminants through π - π interactions can be achieved. Adsorption occurs mainly *via* mechanisms such as electrostatic, hydrophobic, ion-exchange and π - π interactions. Functionalized MWCNTs can interact with pollutant molecules through any of these processes, hence making them suitable materials for adsorption.

In our previous work, 4'-(4-hydroxyphenyl)-2,2':6',2''-terpyridine (HO-Phttpy) was synthesized and used for the functionalization of acid-oxidized multiwalled carbon nanotubes (MWCNT-COOH) to obtain a nitrogen-functionalized MWCNTs (MWCNT-ttpy). Herein, we report the use of MWCNT-COOH and MWCNT-ttpy for the removal of BPA and IBP as models of common EDC pollutants for the remediation of polluted wastewater. Batch adsorption studies were investigated by varying conditions, such as pH,

contact time, adsorbent dose, initial adsorbate concentration and temperature, to examine best conditions necessary for effective removal.

8.2. Experimental

8.2.1. Materials and chemicals

All chemicals and solvents used were of analytical grade and used as received except when stated otherwise. Pristine MWCNTs (>95%) were purchased from Cheap Tubes Incorporation (Brattleboro, USA). Orthophosphoric acid (85%) was purchased from BDH Chemicals (Poole, England) while sulfuric (98%), nitric (55%) and hydrochloric acids (32%) were obtained from C C Imelmann Ltd (Robertsham, South Africa). Solvents such as thionyl chloride (SOCl_2 , 99%) and N,N'-dimethylformamide (DMF, 98%) were purchased from Merck Chemicals (Pty) Ltd (Gauteng, South Africa) and Sigma-Aldrich (New Germany, South Africa), respectively. High performance liquid chromatography (HPLC) grade methanol and acetonitrile were purchased from Sigma-Aldrich (New Germany, South Africa). Chemicals such as bisphenol A (97%), and ibuprofen sodium salt (99%) were purchased from Sigma-Aldrich (New Germany, South Africa), while sodium hydroxide pellets (98%) were purchased from Merck Chemicals (Pty) Ltd (Gauteng, South Africa).

8.2.2 Synthesis and characterization of adsorbents

The synthesis of 4'-(4-hydroxyphenyl)-2,2':6',2''-terpyridine was carried out *via* the method described by Patel *et al.* [28]. Pristine multiwalled carbon nanotubes (P-MWCNTs) were purified with hydrochloric acid and later oxidized with a mixture of nitric and sulphuric acid in a volume ratio of 3:1. Purification and oxidation were carried out as described by Santangelo *et al.* [29] and Oyetade *et al.* [30]. The acid-functionalized MWCNTs (MWCNT-COOH) were acylated with a mixture of SOCl_2 and DMF in a volume ratio of 20:1 respectively, and further functionalized with 4'-(4-hydroxyphenyl)-2,2':6',2''-terpyridine (HO-Phttpy) to obtain nitrogen-functionalized MWCNTs (MWCNT-ttpy). The synthesized adsorbents and ligand were characterized through various techniques. Characterization of 4'-(4-hydroxyphenyl)-2,2':6',2''-terpyridine and the synthesized adsorbents has been reported in our previous work [31].

8.2.3. Instrumentation

The concentrations of BPA and IBP were determined with a UFLC-XR Shimadzu Prominence LC chromatographic system (LC-20AD XR) equipped with a vacuum degasser (DGU-20A₃), autosampler (SIL-20A XR), thermostated column oven (CTO-20A), fraction collector (FRC-10A), communications bus module (LBM-20A) and a diode array detector

(SPD-M20A). Separation of analytes was achieved on a Brownlee C18 column of 5 μm particle size with dimensions of 150×4.6 mm (PerkinElmer, Norwalk, USA).

8.2.3.1 Chromatographic conditions

The mobile phase for elution of BPA consisted of a mixture of 30:70 (v/v) acetonitrile and ultrapure water. Chromatograms were collected at 230 nm by using a PDA detector, with an injection volume of 20 μL at a column temperature of 30 $^{\circ}\text{C}$ and an eluant flow rate of 1.2 ml min^{-1} . For IBP, the mobile phase was a mixture of 80:20 (v/v) methanol and 5 mM phosphoric acid made in ultrapure water. Chromatograms were recorded at a wavelength of 220 nm, with an injection volume of 50 μL at a column temperature of 30 $^{\circ}\text{C}$ and an eluant flow rate of 1.0 ml min^{-1} .

8.2.4. Sorbate preparation

The standards used in this study were of analytical grade and used without further purification. Stock solutions of BPA and IBP were prepared separately by accurately weighing 1 g of the pure powders to make a concentration of 1 g dm^{-3} in methanol. Working solutions of BPA/IBP were prepared daily from the stock solutions in deionised water to obtain the desired concentrations. For quantification purposes, a calibration plot was prepared within the range of experimental concentrations used under the same instrumental conditions.

8.2.5. Sorption Experiments and detection of BPA and IBP

All adsorption experiments were performed in duplicate in a thermostated water bath in 50 cm^3 glass bottles. Single batch experiments were conducted to investigate the effects of pH, contact time, adsorbent dose, initial adsorbate concentration and temperature of adsorbate solution in order to determine the best experimental conditions for adsorbate removal. To investigate the effect of pH, 25 cm^3 aliquots of 50 mg dm^{-3} adsorbate solutions were measured into glass bottles with the addition of 50 mg doses of adsorbent. The pH of the solutions was adjusted by adding the required amount of 0.1 mol dm^{-3} NaOH or HNO₃ to obtain the desired pH. The solutions were then agitated in a thermostated water bath at 25 $^{\circ}\text{C}$ for 24 h. After agitation, the resulting solutions were filtered and the filtrates transferred into 1.5 cm^3 amber vials. The initial and final concentration of BPA/IBP were determined by using HPLC-UV. The adsorption efficiency and adsorption capacity (q_e) were calculated from equations 8.1 and 8.2 respectively.

$$\% \text{ Adsorbed} = \left(\frac{C_i - C_{eq}}{C_i} \right) \times 100 \quad (8.1)$$

$$q_e = \left(\frac{C_i - C_{eq}}{m} \right) \times V \quad (8.2)$$

where C_i is the initial BPA/IBP concentration (mg dm^{-3}), C_{eq} is the equilibrium concentration of BPA/IBP (mg dm^{-3}), q_e is the adsorption capacity (mg g^{-1}), m is the mass of adsorbent (mg) and V is the volume (dm^3) of the adsorbate solution used.

Kinetic studies were investigated by agitating 25 cm^3 aliquots of 50 mg dm^{-3} adsorbate solutions with a 50 mg dose of adsorbent at varying time intervals between 5-1440 min. Solutions were conditioned to the desired pH value and agitated in a thermostated water bath at $25 \text{ }^\circ\text{C}$. After the pre-determined time intervals, the solutions were filtered, the filtrates collected into vials and the final concentrations of BPA/IBP were determined by using HPLC-UV. The kinetics data obtained were fitted into the pseudo-first order, pseudo-second order, Elovich and intraparticle diffusion models. The equations of all models are given in Table 8.1.

Table 8.1: Kinetics models investigated for the adsorption of BPA and IBP

Model	Equation [†]	Parameters	References
Pseudo-first order	$q_t = q_{eq}(1 - e^{-k_1 t})$	q_{eq}, k_1	[32-34]
Pseudo-second order	$q_t = \frac{k_2 q_{eq}^2 t}{1 + k_2 q_{eq} t}$	k_2, q_{eq}	[32,33,35]
Elovich	$q_t = \frac{1}{\beta} \ln(\alpha\beta) + \frac{1}{\beta} \ln t$	α, β	[36]
Intraparticle diffusion	$q_t = k_{id} \sqrt{t} + l$	k_{id}, l	[37]

[†] q_t , quantity of adsorbate adsorbed at time t (mg g^{-1}); q_{eq} , quantity of adsorbate adsorbed at equilibrium (mg g^{-1}); α , adsorption rate constant ($\text{mg g}^{-1} \text{ min}^{-1}$); β , desorption rate constant (g mg^{-1}); k_1 , pseudo-first order rate constant (min^{-1}); k_2 , pseudo-second order rate constant ($\text{g mg}^{-1} \text{ min}^{-1}$); k_{id} , intraparticle diffusion rate constant ($\text{mg g}^{-1} \text{ min}^{0.5}$), l , is a constant related to the boundary layer thickness (mg g^{-1}).

Isotherm studies were investigated with a 25 cm^3 aliquot of adsorbate solution over a concentration range of $10\text{-}100 \text{ mg dm}^{-3}$ and an adsorbent dose of 50 mg . Solutions were conditioned to the appropriate pH and agitated in a thermostated water bath at $25 \text{ }^\circ\text{C}$ for 24 h. The solutions were filtered, the filtrates transferred into vials and the final concentrations determined. The equilibrium data obtained were fitted into various two-and three-parameter isotherms. All isotherm equations used in this study are given in Table 8.2. Thermodynamic studies was also investigated over a temperature range of $298\text{-}318 \text{ K}$ and parameters such as the standard Gibbs energy change (ΔG°), standard enthalpy change (ΔH°), and standard entropy change (ΔS°) for the adsorption processes were calculated.

Table 8.2: Isotherm models investigated for the adsorption of BPA and IBP

Isotherm model	Equation [†]	Parameters	References
Langmuir	$q_{eq} = \frac{q_m b C_{eq}}{1 + b C_{eq}}$	q_m, b	[38]
Freundlich	$q_{eq} = K_F C_{eq}^{1/n}$	K_F, n	[39]
Temkin	$q_{eq} = \frac{RT}{b_T} \ln(A_T C_{eq})$	b_T, A_T	[40]
Dubinin-Radushkevich	$q_{eq} = q_m e^{-\beta \varepsilon^2}$ $\varepsilon = RT \ln \left(1 + \frac{1}{C_{eq}} \right)$	q_m, β	[41]
Sips	$q_{eq} = \frac{b q_m C_{eq}^{1/n}}{1 + b C_{eq}^{1/n}}$	q_m, b, n	[42]
Toth	$q_{eq} = \frac{q_m C_{eq}}{\left(\frac{1}{K_T} + C_{eq}^{n_T} \right)^{1/n_T}}$	q_m, K_T, n_T	[43]
Redlich-Peterson	$q_{eq} = \frac{K_{RP} C_{eq}}{1 + a_{RP} C_{eq}^g}$	K_{RP}, a_{RP}, g	[44]
Khan	$q_{eq} = \frac{q_m b_K C_{eq}}{(1 + b_K C_{eq})^{a_K}}$	q_m, a_K, b_K	[45]

[†] q_{eq} , adsorption capacity (mg g⁻¹); C_{eq} , equilibrium concentration of adsorbate in solution (mg dm⁻³); q_m , maximum monolayer capacity (mg g⁻¹); b , Langmuir isotherm constant (dm³ mg⁻¹); K_F , Freundlich isotherm constant (mg g⁻¹)(dm³ mg⁻¹)ⁿ; n , adsorption intensity; b_T , Temkin isotherm constant; A_T , Temkin isotherm equilibrium binding constant (dm³ g⁻¹); β , Dubinin-Radushkevich isotherm constant (mol² kJ⁻²); K_T , Toth isotherm constant (mg g⁻¹); n_T , Toth isotherm constant; K_{RP} , Redlich-Peterson isotherm constant (dm³ g⁻¹); a_{RP} , Redlich-Peterson isotherm constant; g , Redlich-Peterson isotherm exponent; a_K , Khan isotherm exponent; b_K , Khan isotherm constant.

8.2.6 Desorption studies

The reutilization of spent adsorbents was investigated through desorption processes by agitating a 50 mg BPA/IBP-loaded adsorbent in a 10 cm³ mixture of ethanol and acetic acid in a volume ratio of 9:1, respectively, for 1 h [46]. After agitation, the suspensions were filtered and the final concentrations of BPA/IBP in the filtrate determined by HPLC-UV.

8.2.7. Data analysis

The adsorption data were fitted to isotherm and kinetic models by means of the *nls* nonlinear regression routine in the R statistical computing environment [47].

8.3. Results and discussion

The removal of BPA or IBP from simulated wastewater was studied by using MWCNT-COOH and MWCNT-tpy. Results investigating the batch adsorption processes varying conditions such as pH, contact time, adsorbent dose, initial adsorbate concentration and temperature are presented in the subsequent sections. The adsorption data were fitted into kinetic and isotherm models, while a thermodynamic study was also performed to understand the feasibility and spontaneity of the adsorption processes.

8.3.1 Effect of pH

The influence of pH on the adsorption of BPA and IBP was investigated over a pH range of 1.0-10.0. The change in acidity/basicity of the adsorbate solution greatly influenced the removal of BPA and IBP (Fig 8.1). Fig 8.1a shows that both adsorbents were efficient for BPA removal at acidic pH. High removal efficiencies greater than 90% were obtained for MWCNT-tpy, demonstrating better sorption than MWCNT-COOH. Virtually no change was noticed for the removal of BPA on MWCNT-tpy over a pH range of 1 to 6. This demonstrates that the binding affinity of BPA molecules onto the active sites on MWCNT-tpy was not altered under acidic pH conditions [4], revealing that the adsorbent can be effective over this pH range. For MWCNT-COOH, there was a steady drop in removal percentage with increase in pH for BPA. The adsorption of IBP from aqueous solution by using MWCNT-COOH and MWCNT-tpy also exhibited favourable removal efficiencies at more acidic pH conditions (Fig 8.1b). Again, MWCNT-tpy showed better ability than MWCNT-COOH for IBP removal (Fig 8.1b). However, for IBP, the percentage removal decreased for both sorbents as the pH increased.

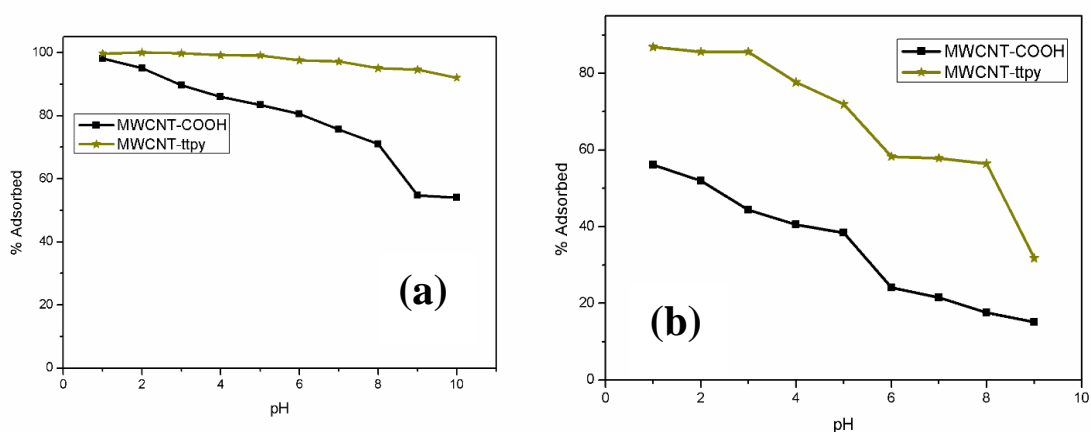


Fig 8.1: Effect of pH for the adsorption of (a) BPA and (b) IBP onto MWCNT-COOH and MWCNT-tpy [conditions: 25 cm³ of 50 mg dm⁻³ BPA/IBP, 24 h equilibration time, 50 mg adsorbent dose, agitation speed 150 rpm, temperature 25 °C].

The trend noticeable with both adsorbates can be explained based on the surface charges present on the adsorbent and the pK_a values of BPA and IBP. The charge densities on the adsorbents changes with increasing pH conditions. The point of zero charge (pH_{PZC}), as reported in our previous studies for MWCNT-COOH and MWCNT-ttPy are 4.02 and 4.48, respectively [31]. The surface of the adsorbents will thereby exhibit a positive charge in acidic solutions. The reported pK_a values of BPA and IBP are 9.6-10.2 [7,48] and 4.91 [49], respectively. De-protonation of these molecules occurs when the pH of the solution is greater than the pK_a [49,50]. This results in the formation of anions, resulting in a build-up of negative ions in solution. At basic pH conditions, electrostatic repulsion between the negatively charged surface of the adsorbent and the anionic forms of BPA and IBP occurs, resulting in a decrease of the binding affinity between adsorbent and adsorbate. Functional groups such as hydroxyl and carboxyl on BPA and IBP respectively will also not interact with π -containing aromatic rings on the adsorbents [14]. Hence, adsorption through hydrophobic interactions is also inhibited. These phenomena explain the decreased efficiency under alkaline conditions for removal of BPA and IBP. At acidic pH conditions, BPA and IBP remain non-dissociated and neutral, and the adsorbent remains positively charged. The adsorbent sites therefore becomes protonated and hydrogen bonding becomes feasible since BPA/IBP exists as neutral molecules when $pH < pK_a$ [51]. Furthermore, since the adsorbents predominantly contain π -electrons which can interact with organic pollutants containing aromatic rings, intermolecular forces between BPA/IBP and the sorbents could be established through π - π interactions. These processes explain why adsorption is facilitated under acidic conditions. Adsorption of BPA and IBP in this study was therefore attributed primarily to interactions between neutral molecules of BPA and IBP onto the active sites of adsorbents *via* hydrogen and/or π - π interactions. Similar interactions have been reported for BPA [2,3,5,50] and IBP [14,49] in other reported articles. For effective comparison, adsorption experiments were investigated at pH 7 and 2 for removal of BPA and IBP, respectively.

8.3.2 Effect of time

The influence of contact time on the adsorption of BPA and IBP was investigated over a period of 5-1440 min at conditions described in Fig 8.2. The figure shows a gradual increase in removal of BPA and IBP as time (t) was varied. The active sites available for adsorption were sufficient initially resulting in a rapid removal of adsorbates. A state of equilibrium, where little or no further increase in adsorption efficiency was reached with increasing time, due to saturation of active sites on the adsorbents. Equilibrium was achieved for BPA within 240 min and 360 min for MWCNT-COOH and MWCNT-ttPy, respectively (Fig 8.2a). Likewise, a state of equilibrium was achieved for IBP within 360 min for both adsorbents (Fig 8.2b). Higher removal efficiencies were obtained for MWCNT-ttPy indicating better

sorption of BPA/IBP onto nitrogen-functionalized tubes. Sorption on MWCNT-ttpty was rapid with a removal efficiency of 38% and 64% obtained for BPA and IBP respectively after 5 min. This demonstrates that functionalization of MWCNT-COOH with HO-Phttpty significantly improved the sorption ability of MWCNT-ttpty, showing high potential for BPA/IBP removal almost immediately on contact with the sorbent. For further adsorption experiments, an agitation time of 24 h was used for both adsorbates to ensure their complete removal from solution.

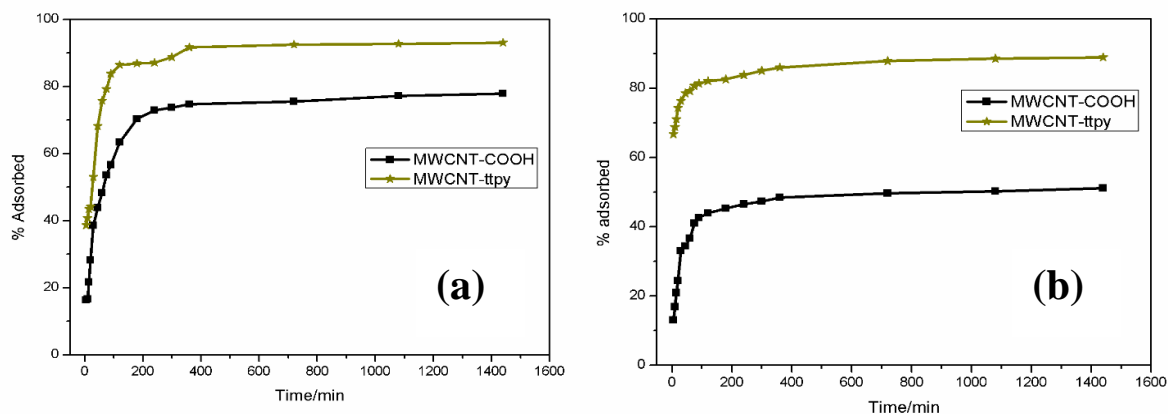


Fig 8.2: Effect of contact time for the adsorption of (a) BPA and (b) IBP onto MWCNT-COOH and MWCNT-ttpty [conditions: 25 cm³ of 50 mg dm⁻³ BPA/IBP, pH=7.0 (BPA) and pH=2.0 (IBP), 50 mg adsorbent dose, agitation speed 150 rpm, temperature 25 °C].

8.3.2.1 Kinetic studies

The rate/mechanism for the adsorption of BPA and IBP onto the studied adsorbents was determined by measuring the change in concentration of the adsorbate as time (t) was varied. The data obtained were fitted into four kinetic models, namely, the pseudo-first order, pseudo-second order, Elovich and intraparticle diffusion models. A knowledge of the dynamics is paramount to the design of large-scale adsorption technologies for BPA and IBP removal. The non-linear equations, described as a better way of obtaining kinetic parameters [4], are presented in Table 8.1. The kinetic parameters with their respective sum of squared residuals (SSR) for each model are given in Table 8.3. The dependence of the model that best fits the experimental data was decided based on the one with the lowest SSR value.

The adsorption of BPA onto both adsorbents was better described by the pseudo-second order model (Table 8.3). However, the data obtained for the adsorption of IBP onto MWCNT-COOH and MWCNT-ttpty were better represented by pseudo-second order and Elovich models, respectively (Table 8.3). This result is in agreement with Guedidi *et al.*

[52] who reported that the adsorption of IBP was better described by the Elovich model at acidic conditions. Also, recently published articles on the adsorption of BPA [3,4,50,53,54] revealed that the equilibrium data were better described by the pseudo-second order model. The pseudo second-order model is based on the assumption that the rate-limiting step for adsorption is through chemical interactions involving the sharing or exchange of electrons between the adsorbate and adsorbent [55]. The results obtained in this study further elucidate the theory, since adsorption of BPA/IBP onto studied the adsorbents could be assumed to proceed through hydrogen and/or π - π interactions. These processes involve the sharing of electrons between π -electron containing atoms in the adsorbents and aromatic-ring electrons in the adsorbates. These results, therefore, revealed that the mechanism of adsorption for removal of BPA and IBP was through a bimolecular interaction existing between the adsorbate and the active sites on the adsorbent.

The increase in the specific surface area (SSA) from $126.8 \text{ m}^2 \text{ g}^{-1}$ to $189.2 \text{ m}^2 \text{ g}^{-1}$ after functionalization of MWCNT-COOH is attributed to one of the factors responsible for an increase in adsorption capacity (q_e) of MWCNT-ttpty obtained for both adsorption processes (Table 8.3). Also, higher adsorption rate constants (h_o) obtained for MWCNT-ttpty for both processes account for the increase in active sites on the adsorbent, hence achieving higher adsorption capacities (q_e) [3,54]. The functionalization of MWCNT-COOH with HO-Phttpty accounts for an increase in SSA and the number of active sites on the adsorbent, therefore enabling better removal of BPA and IBP onto MWCNT-ttpty.

Table 8.3: Kinetic parameters for the adsorption of BPA and IBP on MWCNT-COOH and MWCNT-ttpy [conditions: 25 cm³ of 50 mg dm⁻³ BPA/IBP, pH = 7.0 (BPA) and pH = 2.0 (IBP), 50 mg adsorbent dose, agitation speed 150 rpm, temperature 25 °C]

Model	Parameter	BPA		IBP	
		MWCNT-COOH	MWCNT-ttpy	MWCNT-COOH	MWCNT-ttpy
Pseudo first-order	k_1/min	-	0.040	0.034	0.279
	$q_{eq}/\text{mg g}^{-1}$	-	18.79	10.96	18.92
	SSR ^a	-	20.03	7.162	24.89
Pseudo second-order	$k_2/10^{-3}/\text{g mg}^{-1} \text{min}^{-1}$	1.642	3.206	4.226	2.651
	$h_o/\text{mg g}^{-1} \text{min}^{-1}$	0.485	1.286	0.593	1.014
	$q_{eq}/\text{mg g}^{-1}$	17.18	20.03	11.85	19.56
	SSR	3.659	20.77	1.292	8.392
Intraparticle diffusion	$k_{id}/\text{mg g}^{-1} \text{min}^{-0.5}$	0.672	0.852	0.494	0.921
	SSR	394.8	975.2	282.3	1831
Elovich	$\alpha/\text{mg g}^{-1} \text{min}^{-1}$	1.783	14.53	3.532	4.998
	$\beta/\text{g mg}^{-1}$	0.363	0.406	0.604	1.081
	SSR	26.36	45.65	13.03	1.485

^a: Sum of squared residuals

8.3.3 Effect of adsorbent dose

The effect of increasing adsorbent dose was investigated over a mass range of 30-400 mg. Fig 8.3 shows that increasing amounts of adsorbent at the same adsorbate concentration result in a percentage increase of adsorbates removed from solution. This is in with the fact that increasing the mass of adsorbent for the same adsorbate concentration increases the number of active sites available for adsorption [30]. This translates into an increased removal of adsorbates, until a point of equilibrium where the concentration of adsorbate becomes the limiting factor. Hence, the removal of BPA and IBP were better enhanced with increasing dose, obtaining better efficiencies by using MWCNT-ttpy. In this study, a mass of 50 mg was considered appropriate for adsorption, since effective comparison can be made at this dosage.

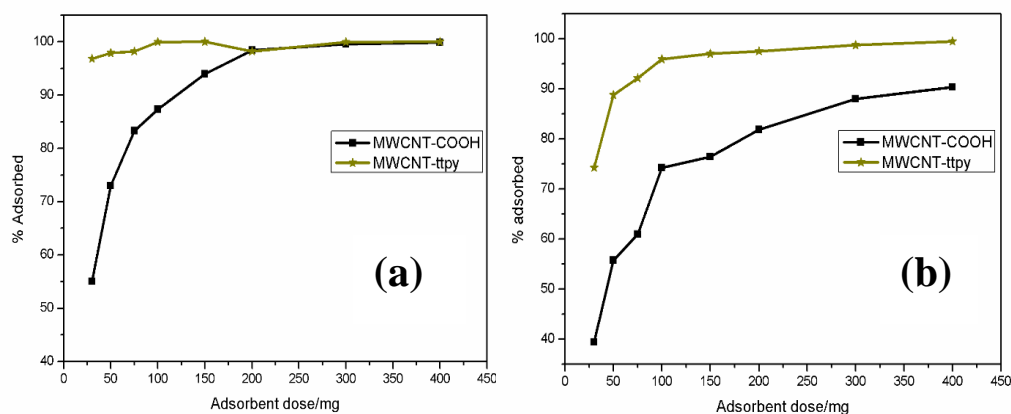


Fig 8.3: Effect of adsorbent dose for the adsorption of (a) BPA and (b) IBP onto MWCNT-COOH and MWCNT-tty [conditions: 25 cm³ of 50 mg dm⁻³ BPA/IBP, 24 h equilibration time, pH = 7.0 (BPA) and pH = 2.0 (IBP), agitation speed 150 rpm, temperature 25 °C].

8.3.4 Effect of temperature

The temperature dependency of the adsorption of BPA and IBP was investigated at 298, 303, 313 and 318 K over a concentration range of 10-100 mg dm⁻³. Figs 8.4 and 8.5 show the influence of increasing temperature on the adsorption of BPA and IBP respectively. The mass transfer and diffusion of molecules onto the active sites on the adsorbents is usually enhanced with an increase in adsorbate temperature. The mobility of BPA molecules to active sites on the adsorbent was increased with an increase in temperature. Hence, an increase in temperature resulted in an enhancement of BPA removal (Fig 8.4). Adsorption of BPA revealed a higher q_e at each sorbate concentration as the temperature was gradually increased for both adsorbents (Fig 8.4). However, this change was not very marked. This indicates an endothermic process of adsorption was favoured. The process clearly explains that MWCNT-COOH and MWCNT-tty could prove effective for the removal of BPA regardless of adsorbate temperature, therefore making them suitable for the direct treatment of BPA-polluted effluents before its discharge.

Furthermore, increasing the temperature of the adsorbates may also lead to a decrease in binding energy between molecules and adsorbent. Fig 8.5 shows a decrease in adsorption capacity (q_e) of the adsorbent as the temperature of the adsorbate was increased for IBP removal. In fact a decrease in q_e was obtained at each adsorbate concentration for both adsorbents, indicating an exothermic process of adsorption. Adsorption of IBP by using MWCNT-COOH and MWCNT-tty was therefore favoured at low adsorbate temperature as indicated in Fig 8.5.

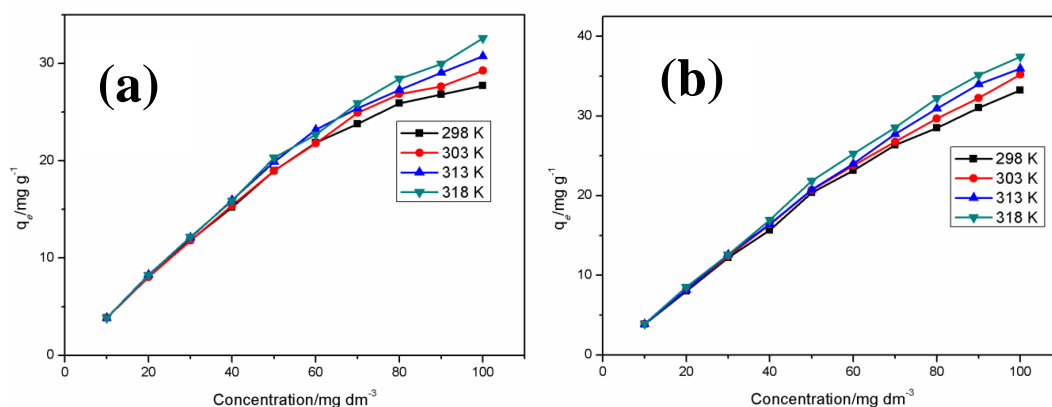


Fig 8.4: Effect of temperature for the adsorption of BPA on (a) MWCNT-COOH and (b) MWCNT-ttpy [conditions: 25 cm³ of BPA solution, 24 h equilibration time, pH = 7.0, 50 mg adsorbent dose, agitation speed 150 rpm].

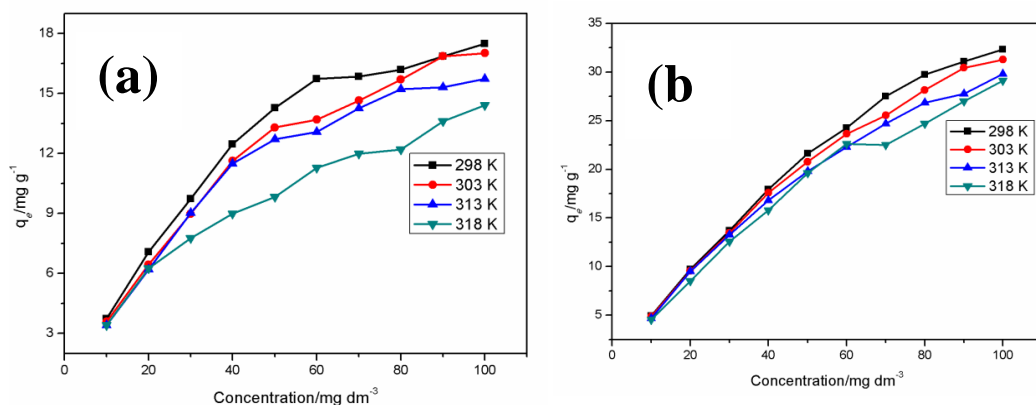


Fig 8.5: Effect of temperature for the adsorption of IBP on (a) MWCNT-COOH and (b) MWCNT-ttpy [conditions: 25 cm³ of IBP solution, 24 h equilibration time, pH = 2.0, 50 mg adsorbent dose, agitation speed 150 rpm].

8.3.5 Isotherm studies

Isotherms are needed in order to develop a design for adsorption involving removal of BPA and IBP in a large-scale scenario [2]. The equilibrium data obtained were fitted into eight models consisting of two- and three-parameter isotherms. The non-linear equations of all isotherms are given in Table 8.2. Non-linear least squares (NLLS) analysis was carried out on all models, and the choice of isotherm was based on the one with the lowest SSR value. Tables 8.4 and 8.5 give the parameters of the isotherms which best describe the equilibrium data for the adsorption of BPA and IBP respectively. Table 8.4 illustrates that the equilibrium data obtained for BPA removal by using MWCNT-COOH and MWCNT-ttpy was better described by the Langmuir model, showing the lowest SSR values when compared with other models. An increase in the Langmuir maximum adsorption capacity

(q_m) and Freundlich sorption coefficient (K_F) was obtained with increasing temperature, demonstrating the endothermic nature of BPA sorption on the studied adsorbents. The adsorptive power (b) was also noticed to increase with increasing temperature, indicating strong binding interactions between the BPA molecule and the adsorbents [56] (Table 8.4).

The equilibrium data obtained for IBP removal by using MWCNT-COOH and MWCNT-ttpe best fit the Langmuir and Freundlich isotherms, respectively. A decrease in q_m and K_F as temperature was increased indicates an exothermic process for removal (Table 8.5). The values obtained for $1/n$ were also less than 1, indicating a favourable process of adsorption was achieved by using MWCNT-ttpe for IBP removal.

The Langmuir model assumes that the interactions between the adsorbate and adsorbent occur on a homogeneous monolayer surface and no interactions occur between adjacent molecules on the adsorbent [30]. The Freundlich model assumes a heterogeneous surface, and is therefore based on a multi-layer principle of adsorption. Isotherm studies confirmed monolayer interactions for the adsorption of BPA and IBP, however, multi-layer interaction was demonstrated for IBP removal by using MWCNT-ttpe. An assessment of the adsorbents used in this study was performed by comparing the Langmuir monolayer adsorption capacities (q_m) with literature values reported for other adsorbents. Table 8.6 clearly shows that although results obtained from some previous reports were higher than those obtained in this study, the results obtained were favourably comparable with those reported. This further confirms that MWCNT-COOH and MWCNT-ttpe are promising alternatives for remediating EDC-contaminated industrial effluents and wastewater before their discharge into water bodies.

Table 8.4: Isotherm parameters for the adsorption of BPA [conditions: 25 cm³ of 10-100 mg dm⁻³ BPA at different temperatures of 298, 303, 313 and 318 K, 24 h equilibration time, pH = 7.0, 50 mg adsorbent dose, agitation speed 150 rpm]

Isotherms	Parameter	MWCNT-COOH				MWCNT-ttpe			
		298 K	303 K	313 K	318 K	298 K	303 K	313 K	318 K
Langmuir	q_m	30.88	32.58	33.53	35.60	38.40	38.82	40.95	42.25
	b	0.235	0.238	0.284	0.287	0.227	0.306	0.323	0.470
	SSR	7.719	10.24	7.026	6.224	15.01	10.77	16.28	7.996
Freundlich	K_F	8.921	9.277	10.17	10.30	9.916	11.29	12.25	14.78
	n	2.921	2.841	2.880	2.683	2.505	2.573	2.570	2.691
	SSR	22.99	24.08	25.90	24.45	19.15	17.00	29.40	57.89

SSR: Sum of squared residuals

Table 8.5: Isotherm parameters for the adsorption of IBP [conditions: 25 cm³ of 10-100 mg dm⁻³ IBP at different temperatures of 298, 303, 313 and 318 K, 24 h equilibration time, pH = 2.0, 50 mg adsorbent dose, agitation speed 150 rpm]

Isotherms	Parameter	MWCNT-COOH				MWCNT-ttpy			
		298 K	303 K	313 K	318 K	298 K	303 K	313 K	318 K
Langmuir	q_m	20.26	20.57	18.89	18.93	34.03	32.79	30.59	32.94
	b	0.098	0.070	0.076	0.031	0.301	0.256	0.242	0.120
	SSR	2.144	2.214	2.121	1.912	49.78	33.07	25.33	13.94
Freundlich	K_F	4.353	3.343	3.409	1.680	11.98	10.07	9.062	6.589
	n	2.873	2.495	2.647	2.075	3.435	3.082	3.048	2.502
	SSR	16.12	8.145	11.06	1.356	8.386	5.917	7.837	24.75

SSR: Sum of squared residuals

Table 8.6: Comparison of Langmuir maximum capacities (q_m) with data obtained from literature

Adsorbents	Conditions	Adsorbate	$q_m/\text{mg g}^{-1}$	References
Zeolite	pH 7.0, C_i 20 mg dm ⁻³ , 50 mg dose, 298 K	BPA	11.20	[57]
MWCNT	pH 6.0, C_i 10 mg dm ⁻³ , 25 mg dose, 24 h, 300 K	BPA	59.17	[58]
SWCNT	pH 8.0 C_i 50 mg dm ⁻³ , 50 mg dose, 60 min, 293 K	BPA	71.10	[2]
SWCNT	pH 8.2, C_i 50 mg dm ⁻³ , 240 min, 298 K	BPA	13.39-16.05	[59]
Activated carbon	pH 3.0, C_i 60 mg dm ⁻³ , 25 mg, 298 K	IBP	28.50	[49]
Oxidized MWCNT	pH 7.0, C_i 2 mg dm ⁻³ , 2 mg dose, 296 K	IBP	19.40	[8]
Oxidized MWCNT	pH 4.0, C_i 2 mg dm ⁻³ , 2 mg dose, 296 K	IBP	40.20	[8]
MWCNT-COOH	pH 7.0, C_i 50 mg dm ⁻³ , 50 mg dose, 24 h, 298 K	BPA	30.88	This study
MWCNT-ttpy	pH 7.0, C_i 50 mg dm ⁻³ , 50 mg dose, 24 h, 298 K	BPA	38.40	This study
MWCNT-COOH	pH 2.0, C_i 50 mg dm ⁻³ , 50 mg dose, 24 h, 298 K	IBP	20.06	This study
MWCNT-ttpy	pH 2.0, C_i 50 mg dm ⁻³ , 50 mg dose, 24 h, 298 K	IBP	34.03	This study

8.3.6 Thermodynamic studies

Thermodynamic parameters such as the standard Gibbs energy change (ΔG°), standard enthalpy change (ΔH°) and standard entropy change (ΔS°) provide in-depth information into the feasibility and the internal energy changes [50] experienced during the adsorption process. These parameters were calculated from the temperature-dependent isotherms at different temperatures of 298, 303, 313 and 318 K. The standard Gibbs energy change (ΔG°) was calculated by using equation (8.3) [32]:

$$\Delta G^\circ = -RT \ln K \quad (8.3)$$

where R is the universal gas constant ($8.314 \text{ J K}^{-1} \text{ mol}^{-1}$), T is the absolute temperature in Kelvin, K is the distribution adsorption coefficient and ΔG° is the standard Gibbs energy change (J mol^{-1}). The product of q_m and b obtained from Langmuir plot (Table 8.4-8.5) gives the calculated value of K [56,60], which was then multiplied by 1000 to obtain a dimensionless value [61].

The standard change in enthalpy (ΔH°) and standard change in entropy (ΔS°) were calculated from the intercept and slope obtained from the linear plot of $\ln K$ against $1/T$, by using the Van't Hoff equation given in eqn 8.4 [30].

$$\ln K = \frac{-\Delta H^\circ}{RT} + \frac{\Delta S^\circ}{R} \quad (8.4)$$

The calculated thermodynamic parameters obtained from equations 8.3 and 8.4 for the adsorption of BPA and IBP are presented in Table 8.7 and 8.8 respectively. The adsorption processes of BPA and IBP were spontaneous in nature, obtaining negative values of ΔG° for both processes. An increase in negative values of ΔG° for the adsorption of BPA by using MWCNT-COOH and MWCNT-ttpy indicates a spontaneous and favourable process at higher adsorbate temperature (Table 8.7). In contrast, a decrease in ΔG° values with increasing temperature for the adsorption of IBP by using MWCNT-COOH and MWCNT-ttpy indicates removal was favoured at low temperature (Table 8.8) [46]. The standard change in enthalpy (ΔH°) obtained showed positive and negative values for adsorption of BPA and IBP respectively. This suggests an endothermic and exothermic nature of removal for BPA and IBP respectively. Positive ΔS° values obtained for BPA indicate an increase in the disorder of the solid-solution interface during adsorption, while the negative value of ΔS° obtained for IBP with both adsorbents indicates a decrease in the disorder at the solid-liquid interface [46]. Adsorption of BPA onto both adsorbents was entropy-driven, but enthalpy-driven for IBP removal.

Inferences on the type of binding between the adsorbent and adsorbate can also be drawn from thermodynamic parameters. The heat evolved during physical adsorption (physisorption) is the range of 2.1-20.9 kJ mol⁻¹, while heat of a chemical process (chemisorption) is in the range of 80-200 kJ mol⁻¹ [30,56,62]. The study shows that the removal of BPA with MWCNT-ttpy was a physico-chemical process since ΔH° were less than values predicted for chemisorption but greater than values for physisorption [62].

Table 8.7: Thermodynamic parameters for the adsorption of BPA onto MWCNT-COOH and MWCNT-ttpy

Adsorbent	T/K	$\Delta G^\circ/\text{kJ mol}^{-1}$	$\Delta H^\circ/\text{kJ mol}^{-1}$	$\Delta S^\circ/\text{J K}^{-1} \text{mol}^{-1}$
MWCNT-COOH	298	-22.02		
	303	-22.56		
	313	-23.84	14.02	120.9
	318	-24.41		
MWCNT-ttpy	298	-22.48		
	303	-23.64		
	313	-24.70	27.60	168.3
	318	-26.16		

Table 8.8: Thermodynamic parameters for the adsorption of IBP onto MWCNT-COOH and MWCNT-ttpy

Adsorbent	T/K	$\Delta G^\circ/\text{kJ mol}^{-1}$	$\Delta H^\circ/\text{kJ mol}^{-1}$	$\Delta S^\circ/\text{J K}^{-1} \text{mol}^{-1}$
MWCNT-COOH	298	-18.81		
	303	-18.32		
	313	-18.92	-38.24	-64.99
	318	-16.85		
MWCNT-ttpy	298	-22.49		
	303	-22.76		
	313	-23.19	-24.96	-65.18
	318	-21.90		

8.3.7 Desorption studies

The reuse of adsorbents plays an important role in adsorption to mitigate the direct discharge of spent-adsorbents, thereby generating secondary pollutants into the environment. To protect against this, desorption of BPA/IBP on spent-adsorbents was investigated for the process of regenerating and reutilization of the adsorbents. To achieve this, 50 mg BPA/IBP-loaded adsorbent was weighed into glass bottles, containing 10 cm³ mixture of ethanol and acetic acid, in a volume ratio of 9:1, respectively, and agitated in a thermostated

water bath for 1 h [46]. The final concentrations of BPA and IBP were determined by HPLC-UV, and their desorption efficiencies were evaluated.

The results obtained indicated a fairly good desorption of BPA/IBP from the adsorbents after a cycle of agitation. The desorption percentages achieved were 72.1% and 76.5% of BPA-loaded onto MWCNT-COOH and MWCNT-ttpy respectively. Desorption of IBP-loaded onto MWCNT-COOH and MWCNT-ttpy afforded 58% and 61.2% removal efficiency respectively. This indicates that the adsorbents can be recycled after some cycles of agitation and reused, thus making them efficient for practical industrial applications.

8.4. Conclusions

This study examines the sorption behaviour of BPA and IBP from aqueous solution by using acid-functionalized multiwalled carbon nanotubes (MWCNT-COOH) and nitrogen-functionalized multiwalled carbon nanotubes (MWCNT-ttpy), under certain environmental conditions. The results showed higher adsorption capacities (q_e) were obtained for MWCNT-ttpy for both adsorption processes when compared with MWCNT-COOH. The increased capacity of MWCNT-ttpy was attributed to the functionalization of MWCNT-COOH with 4'-(4-hydroxyphenyl)-2,2':6',2''-terpyridine (HO-Phttpy), which improved the sorption of BPA and IBP onto the active sites of MWCNT-ttpy. Adsorption of BPA was investigated at pH 7 and equilibrium was achieved within 240 min and 360 min for MWCNT-COOH and MWCNT-ttpy, respectively. Removal of IBP from aqueous solution was investigated at pH 2 and equilibrium was achieved for both adsorbents within 360 min. The pseudo-second order model best describes the kinetics of adsorption. Strong hydrophobic interactions between phenyl groups in the adsorbates and π -electron containing adsorbents were primarily responsible for the removal of BPA and IBP. The equilibrium data obtained for MWCNT-COOH and MWCNT-ttpy were better described by the Langmuir model for both processes, except for MWCNT-ttpy which better fits the Freundlich model for the adsorption of IBP. All adsorption processes were feasible and spontaneous, with an endothermic nature of adsorption obtained for the removal of BPA from aqueous solution. The removal of IBP demonstrated an exothermic nature of adsorption indicating an enthalpy-driven process. Desorption of BPA/IBP-loaded adsorbents afforded good removal efficiencies, indicating possible reutilization of the adsorbents for similar processes. The adsorbents used in this study have proved effective for BPA and IBP removal, hence, their potential for the treatment of EDC-contaminated wastewater should be further explored.

References

- [1] K. Sun, K. Ro, M. Guo, J. Novak, H. Mashayekhi, B. Xing, Sorption of bisphenol A, 17 α -ethinyl estradiol and phenanthrene on thermally and hydrothermally produced biochars, *Bioresour. Technol.* 102 (2011) 5757-5763.
- [2] M.H. Dehghani, A.H. Mahvi, N. Rastkari, R. Saeedi, S. Nazmara, E. Iravani, Adsorption of bisphenol A (BPA) from aqueous solutions by carbon nanotubes: Kinetic and equilibrium studies, *Desalin. Water Treat.* 54 (2014) 84-92.
- [3] G. Liu, J. Ma, X. Li, Q. Qin, Adsorption of bisphenol A from aqueous solution onto activate d carbons with different modification treatments, *J. Hazard. Mater.* 164 (2009) 1275-1280.
- [4] Y. Zhou, P. Lu, J. Lu, Application of natural biosorbent and modified peat for bisphenol A removal from aqueous solutions, *Carbohydr. Polym.* 88 (2012) 502-508.
- [5] W.-T. Tsai, C.-W. Lai, T.-Y. Su, Adsorption of bisphenol-A from aqueous solution onto minerals and carbon adsorbents, *J. Hazard. Mater.* B134 (2006) 169-175.
- [6] M. Clara, B. Strenn, E. Saracevic, N. Kreuzinger, Adsorption of bisphenol-A, 17 β estradiole and 17 α -ethinylestradiole to sewage sludge, *Chemosphere* 56 (2004) 843-851.
- [7] R. Gong, J. Liang, J. Chen, F. Huang, Removal of bisphenol A from aqueous solution by hydrophobic sorption of hemimicelles, *Int. J. Environ. Sci. Tech.* 6 (2009) 539-544.
- [8] H.-H. Cho, H. Huang, K. Schwab, Effects of solution chemistry on the adsorption of ibuprofen and triclosan onto carbon nanotubes, *Langmuir* 27 (2011) 12960.
- [9] A.S. Mestre, J. Pires, J.M.F. Nogueira, J.B. Parra, A.P. Carvalho, C.O. Ania, Waste-derived activated carbons for removal of ibuprofen from solution: Role of surface chemistry and pore structure, *Bioresour. Technol.* 100 (2009) 1720.
- [10] A.S. Mestre, J. Pires, J.M.F. Nogueira, A.P. Carvalho, Activated carbons for the adsorption of ibuprofen, *Carbon* 45 (2007) 1979-1988.
- [11] R. Amdany, L. Chimuka, E. Cukrowska, Determination of naproxen, ibuprofen and triclosan in wastewater using the polar organic chemical integrative sampler (POCIS): A laboratory calibration and field application, *Water SA* 40 (2014) 407-413.
- [12] P. Paíga, L.H.L.M. Santos, C.G. Amorim, A.N. Araújo, M.C.B.S.M. Montenegro, A. Pena, C. Delerue-Matos, Pilot monitoring study of ibuprofen in surface waters of north of Portugal, *Environ. Sci. Pollut. Res.* 20 (2013) 2410-2420.
- [13] V. González-Naranjo, K. Boltes, M. Biel, Mobility of ibuprofen, a persistent active drug, in soils irrigated with reclaimed water, *Plant Soil Environ.* 59 (2013) 68-73.
- [14] C. Jung, J. Park, K.H. Lim, S. Park, J. Heo, N. Her, J. Oh, S. Yun, Y. Yoon, Adsorption of selected endocrine disrupting compounds and pharmaceuticals on activated biochars, *J. Hazard. Mater.* 263 (2013) 702-710.

- [15] Y. Dong, D. Wu, X. Chen, Y. Lin, Adsorption of bisphenol A from water by surfactant-modified zeolite, *J. Colloid Interface Sci.* 348 (2010) 585-590.
- [16] M. Galhetas, A.S. Mestre, M.L. Pinto, I. Gulyurtlu, H. Lopes, A.P. Carvalho, Carbon-based materials prepared from pine gasification residues for acetaminophen adsorption, *Chem. Eng. J.* 240 (2014) 344-351.
- [17] Y.-H. Fei, B. Xing, X.-Y. Li, Changes in the adsorption of bisphenol A, 17 α -ethinyl estradiol, and phenanthrene on marine sediment in Hong Kong in relation to the simulated sediment organic matter decomposition, *Environ. Pollut.* 192 (2014) 139-146.
- [18] L.M. Ombaka, P.G. Ndungu, V.O. Nyamori, Pyrrolic nitrogen-doped carbon nanotubes: Physicochemical properties, interactions with Pd and their role in the selective hydrogenation of nitrobenzophenone, *RSC Adv.* 5 (2014) 109-122.
- [19] G. Keru, P.G. Ndungu, V.O. Nyamori, A review on carbon nanotube/polymer composites for organic solar cells, *Int. J. Energy Res.* 38 (2014) 1635-1653.
- [20] L.M. Ombaka, P. Ndungu, V.O. Nyamori, Usage of carbon nanotubes as platinum and nickel catalyst support in dehydrogenation reactions, *Catal. Today* 217 (2013) 65-75.
- [21] G.-C. Chen, X.-Q. Shan, Y.-S. Wang, B. Wen, Z.-G. Pei, Y.-N. Xie, T. Liu, J.J. Pignatello, Adsorption of 2,4,6-trichlorophenol by multi-walled carbon nanotubes as affected by Cu(II), *Water Res.* 43 (2009) 2409-2418.
- [22] K. McDonough, J.L. Fairey, G.V. Lowry, Adsorption of polychlorinated biphenyls to activated carbon: Equilibrium isotherms and a preliminary assessment of the effect of dissolved organic matter and biofilm loadings, *Water Res.* 42 (2008) 575-584.
- [23] X. Ma, S. Uddin, Desorption of 1,3,5-trichlorobenzene from multi-walled carbon nanotubes: Impact of solution chemistry and surface chemistry, *Nanomaterials* 3 (2013) 289-302.
- [24] M. Kragulj, J. Trickovic, B. Dalmacija, A. Kukovecz, Z. Kónya, J. Molnar, S. Roncevic, Molecular interactions between organic compounds and functionally modified multiwalled carbon nanotubes, *Chem. Eng. J.* 225 (2013) 144-152.
- [25] M. Abdel Salam, G. Al-Zhrani, S.A. Kosa, Removal of heavy metal ions from aqueous solution by multi-walled carbon nanotubes modified with 8-hydroxyquinoline: Kinetic study, *J. Ind. Eng. Chem.* 20 (2014) 572-580.
- [26] V.T. Le, C.L. Ngo, Q.T. Le, T.T. Ngo, D.N. Nguyen, M.T. Vu, Surface modification and functionalization of carbon nanotube with some organic compounds, *Adv. Nat. Sci.:Nanosci. Nanotechnol.* 4 (2013) 35017-35022.
- [27] T. Yokoi, S. Iwamatsu, S. Komai, T. Hattori, S. Murata, Chemical modification of carbon nanotubes with organic hydrazines, *Carbon* 43 (2005) 2869-2874.

- [28] M.N. Patel, H.N. Joshi, C.R.I. Patel, Copper(II) complexes with norfloxacin and neutral terpyridines: Cytotoxic, antibacterial, superoxide dismutase and DNA-interaction approach, *Polyhedron* 40 (2012) 159-167.
- [29] S. Santangelo, G. Messina, G. Faggio, S.H. Abdul Rahim, C. Milone, Effect of sulphuric-nitric acid mixture composition on surface chemistry and structural evolution of liquid-phase oxidised carbon nanotubes, *J. Raman Spectrosc.* 43 (2012) 1432-1442.
- [30] O.A. Oyetade, V.O. Nyamori, B.S. Martincigh, S.B. Jonnalagadda, Effectiveness of carbon nanotube-cobalt ferrite nanocomposites for the adsorption of rhodamine B from aqueous solutions, *RSC Adv.* 5 (2015) 22724-22739.
- [31] O.A. Oyetade, V.O. Nyamori, B.S. Martincigh, S.B. Jonnalagadda, Nitrogen-functionalised carbon nanotubes as a novel adsorbent for the removal of Cu(II) from aqueous solution, (unpublished results).
- [32] Y.-S. Ho, Removal of copper ions from aqueous solution by tree fern, *Water Res.* 37 (2003) 2323-2330.
- [33] Y.S. Ho, Comment on "Cadmium removal from aqueous solutions by chitin: Kinetic and equilibrium studies", *Water Res.* 38 (2004) 2962-2964
- [34] J. Lin, L. Wang, Comparison between linear and non-linear forms of pseudo-first-order and pseudo-second-order adsorption kinetic models for the removal of methylene blue by activated carbon, *Front. Environ. Sci. Eng.* 3 (2009) 320-324.
- [35] Y.S. Ho, G. McKay, Sorption of copper(II) from aqueous solution by peat, *Water Air Soil Pollut.* 158 (2004) 77-97.
- [36] S.H. Chien, W.R. Clayton, Application of Elovich equation to the kinetics of phosphate release and sorption in soils, *Soil Sci. Soc. Am. J.* 44 (1980) 265-268.
- [37] E. Demirbas, M. Kobyas, E. Senturk, T. Ozkan, Adsorption kinetics for the removal of chromium(VI) from aqueous solutions on the activated carbons prepared from agricultural wastes, *Water SA* 30 (2004) 533-539.
- [38] I. Langmuir, The adsorption of gases on plane surfaces of glass, mica and platinum, *J. Am. Chem. Soc.* 40 (1918) 1361-1402.
- [39] H. Freundlich, Adsorption in solids, *Z. Phys. Chem.* 57 (1906) 385-470.
- [40] M.I. Temkin, V. Pyzhev, Kinetics of ammonia synthesis on promoted iron catalysts, *Acta Phys. Chim.* 12 (1940) 327-356.
- [41] M.M. Dubinin, L.V. Radushkevich, The equation of the characteristic curve of activated charcoal, *Proc. Acad. Sci, U.S.S.R, Phys. Chem. Sect.* 55 (1947) 327-329.
- [42] R. Sips, Combined form of Langmuir and Freundlich equations, *J. Chem. Phys.* 16 (1948) 490-495.
- [43] J. Toth, State equations of the solid-gas interface layers, *Acta Chim. Acad. Sci. Hung.* 69 (1971) 311-328.

- [44] O. Redlich, D.L. Peterson, A useful adsorption isotherm, *J. Phys. Chem.* 63 (1959) 1024.
- [45] A.R. Khan, I.R. Al-Waheab, A. Al-Haddad, A generalized equation for adsorption isotherms for multi-component organic pollutants in dilute aqueous solution, *Environ. Technol.* 17 (1996) 13-23.
- [46] F. Duan, C. Chen, L. Chen, Y. Sun, Y. Wang, Y. Yang, X. Liu, Y. Qin, Preparation and evaluation of water-compatible surface molecularly imprinted polymers for selective adsorption of bisphenol A from aqueous solution, *Ind. Eng. Chem. Res.* 53 (2014) 14291-14300.
- [47] The R Development Core Team, The R foundation for statistical Computing, R version 3.0.2 (2013).
- [48] C.A. Staples, P.B. Dome, G.M. Klecka, S.T. Oblock, L.R. Harris, A review of the environmental fate, effects, and exposures of bisphenol A, *Chemosphere* 36 (1998) 2149-2173.
- [49] S.K. Behera, S.Y. Oh, H.S. Park, Sorptive removal of ibuprofen from water using selected soil minerals and activated carbon, *Int. J. Environ. Sci. Technol.* 9 (2012) 85-94.
- [50] J. Xu, L. Wang, Y. Zhu, Decontamination of bisphenol A from aqueous solution by graphene adsorption, *Langmuir* 28 (2012) 8418-8425.
- [51] T.M.S. Attia, X.L. Hu, Y.D. Qiang, Synthesized magnetic nanoparticles coated zeolite for the adsorption of pharmaceutical compounds from aqueous solution using batch and column studies, *Chemosphere* 93 (2013) 2076-2085.
- [52] H. Guedidi, L. Reinert, Y. Soneda, N. Bellakhal, L. Duclaux, Adsorption of ibuprofen from aqueous solution on chemically surface-modified activated carbon cloths, *Arabian J. Chem.* (2014) In Press.
- [53] W. Han, L. Luo, S. Zhang, Adsorption of bisphenol A on lignin: effects of solution chemistry, *Int. J. Environ. Sci. Technol.* 9 (2012) 543-548.
- [54] S. Zheng, Z. Sun, Y. Park, G.A. Ayoko, R.L. Frost, Removal of bisphenol A from wastewater by Ca-montmorillonite modified with selected surfactants, *Chem. Eng. J.* 234 (2013) 416-422.
- [55] Y.S. Ho, G. McKay, Pseudo-second order model for sorption processes, *Process Biochem.* 34 (1999) 451-465.
- [56] I.A.A. Hamza, B.S. Martincigh, J.C. Ngila, V.O. Nyamori, Adsorption studies of aqueous Pb(II) onto a sugarcane bagasse/multi-walled carbon nanotube composite, *Phys. Chem. Earth* 66 (2013) 157-166.
- [57] W.-T. Tsai, K.-J. Hsien, H.-C. Hsu, Adsorption of organic compounds from aqueous solution onto the synthesized zeolite, *J. Hazard. Mater.* 166 (2009) 635-641.

- [58] C.-Y. Kuo, Comparison with as-grown and microwave modified carbon nanotubes to removal aqueous bisphenol A, *Desalination* 249 (2009) 976-982.
- [59] L. Joseph, J. Heo, Y.-G. Park, J.R.V. Flora, Y. Yoon, Adsorption of bisphenol A and 17 α -ethinyl estradiol on single walled carbon nanotubes from seawater and brackish water, *Desalination* 281 (2011) 68-74.
- [60] R. Djeribi, Q. Hamdaoui, Sorption of copper(II) from aqueous solutions by cedar sawdust and crushed brick, *Desalination* 225 (2008) 95-112.
- [61] S.K. Milonjić, A consideration of the correct calculation of thermodynamic parameters of adsorption, *J. Serb. Chem. Soc.* 72 (2007) 1363-1367.
- [62] Y. Liu, Y.-J. Liu, Biosorption isotherms, kinetics and thermodynamics, *Sep. Purif. Technol.* 61 (2008) 229-242.

Chapter 9

Co-adsorption of bisphenol A and ibuprofen onto functionalized multiwalled carbon nanotubes: Influence of metal ions in solution

Oluwaseun A. Oyetade, Vincent O. Nyamori, Sreekantha B. Jonnalagadda and Bice S. Martincigh*

School of Chemistry and Physics, University of KwaZulu-Natal, Westville Campus,
Private Bag X54001, Durban 4000, South Africa

*Corresponding author: Tel: +27 31 2601394; Fax: +27 31 2603091; E-mail:
martinci@ukzn.ac.za

Abstract

The ability of nitrogen-functionalized multiwalled carbon nanotubes (MWCNT-ttpe) to adsorb bisphenol A (BPA) and ibuprofen (IBP) in both single and binary pollutant systems was investigated. In addition, the influence of the presence of heavy metal ions, namely, Pb^{2+} and Cd^{2+} , was also studied in order to investigate the efficacy of MWCNT-ttpe for the simultaneous removal of metal ions and organic pollutants in a competitive system.

Adsorption of BPA and IBP was primarily based on the hydrophobic nature of the adsorbates. Hence, the sorption of IBP in both single- and binary systems was higher than BPA removal onto MWCNT-ttpe, as a result of its increased hydrophobicity. The sorption of BPA and IBP was enhanced in the presence of Cd^{2+} , however, a decrease in organic sorption was noticed in the presence of Pb^{2+} in solution. Therefore, the removal of metal ions and organic pollutants was cooperative in a competitive multi-component adsorption system. The adsorption equilibrium data was modelled by the Langmuir model, and increased uptake of BPA and IBP was obtained in single-solute systems than binary systems.

Hence, the simultaneous sorption of metal ions and organic pollutants from aqueous solution was successful by using MWCNT-ttpe, and their application for wastewater remediation should be explored.

Keywords: adsorption, multiwalled carbon nanotubes, metal ions, bisphenol A, ibuprofen

9.1. Introduction

The presence of emerging contaminants, such as endocrine disrupting chemicals (EDCs) and pharmaceuticals and personal care products (PPCPs) in aquatic environment has prompted the development of various technologies through which effluents containing them can be remediated. Bisphenol A (BPA), a typical EDC substance, is primarily used for the manufacture of plastic products and epoxy resin linings in food and beverage cans [1,2]. Ibuprofen (IBP), on the other hand, is one of the commonest non-steroidal anti-inflammatory drugs (NSAID) used to relieve pain, fever, and treat minor injuries and arthritis in humans and also for veterinary applications [3,4]. The reliance on these two substances in both manufacturing and pharmaceutical industries generates contaminated effluents which are discharged into various aquatic environments [5,6], and if untreated pose serious environmental challenges to man and its environs. An excessive intake of BPA and IBP has been associated with their interference with hormonal receptors, resulting in reproductive and neurological disorders in man [1,2]. Unfortunately, wastewater treatment facilities are not designed to eliminate such emerging pollutants, especially in trace amounts, due to their recalcitrant nature [6-8]. Solid and liquid discharges released from industries may contain various organic and/or inorganic pollutants in them, and hence, adequate/simple technologies must be formulated to ensure the complete removal of such pollutants from aqueous solutions.

The adsorption of organic pollutants such as BPA and IBP from aqueous solutions presents a colossal challenge to researchers, due to their hydrophobic nature, hence, the development of sorbents which will facilitate their removal requires careful planning. Interaction between sorbents and sorbates to ensure effective removal of organic pollutants from aqueous solutions must be methodically designed to include functional groups that will promote adsorption. Adsorbents such as activated carbon [9], lignin [10], soils [3], zeolite [11], and carbon nanotubes [12], amongst many others, have been synthesized to primarily contain hydrophilic functional groups (-OH, -COOH), which may hinder interaction between organic pollutants and the sorbent at the sorbate-sorbent interface. Therefore, the nature of an adsorbent plays an important role in deciding the extent of removal of organic pollutants from solution. Hence, the development of suitable sorbents that contain functional groups that will enhance hydrophobic and/or π - π interactions between the sorbate and sorbent in order to achieve complete removal of such pollutants remains a challenge.

The ease in introducing preferred functional groups to the ends of multiwalled carbon nanotubes (MWCNTs) [13] presents researchers with an opportunity of exploring several strategies of incorporating active groups onto their walls. Kosa *et al.* [13] investigated the efficiency of 8-hydroxyquinoline-functionalized MWCNTs towards metal ion removal.

Similarly, amine-containing compounds were used as modifiers of MWCNTs by Wang *et al.*, [14] Yang *et al.*, [15] and Vukovic *et al.*, [16] while thiol-functionalized MWCNTs were synthesized by Hadavifar *et al.* [17] and Bandaru *et al.* [18]. These modifications were undertaken to improve the efficiency of MWCNTs for the removal of targeted pollutants from aqueous solutions. This approach has been reported to enhance the removal of specific pollutants from aqueous solutions, owing to an increase in the number of active sites, surface area and pore volume of the adsorbents [19]. Although, studies have demonstrated that the removal of organic pollutants from aqueous solution is primarily influenced *via* hydrophobic and π - π interactions [12,20-22], the development of sorbents to contain hydrophobic functional heads to enhance their increased sorption is still under-researched.

Further, the development of sorbents containing amphiphilic properties, to aid the simultaneous removal of both organic and inorganic contaminants from wastewater is imperative, since typical wastewaters contain a mixture of such pollutants. Depending on the nature of the active sites on a sorbent, the presence of a contaminant can either induce or depress the sorption of another in the same solution. This necessitated an investigation of the removal of BPA and IBP, representing model of EDC and PPCP pollutants, respectively, in a competitive adsorption system. The influence of inorganic pollutants such as metal ions on the binary sorption of BPA and IBP was also investigated to understand the mechanisms involved in such an adsorption process. The particular heavy metal ions chosen for study were Pb^{2+} and Cd^{2+} , because of their well-known persistence in the environment [23].

Hence, this chapter examines the adsorption behaviour of nitrogen-functionalized MWCNTs by using (4'-(4-hydroxyphenyl)-2,2':6',2''-terpyridine) as a modifier, for the competitive removal of BPA and IBP from aqueous solutions. The capacity of the synthesized amphiphilic sorbent was also investigated for the removal of divalent metal ions such as lead and cadmium in a multicomponent system containing BPA and IBP, through batch adsorption processes.

9.2. Experimental

9.2.1. Materials and chemicals

All chemicals and solvents used were of analytical grade and used as received except when stated otherwise. Pristine MWCNTs (>95%) were purchased from Cheap Tubes Inc. (Brattleboro, USA). Orthophosphoric acid (85%) was purchased from BDH Chemicals (Poole, England) while sulfuric (98%), nitric (55%) and hydrochloric acids (32%) were

obtained from C C Imelmann Ltd (Robertsham, South Africa). Solvents such as thionyl chloride (99%) and N,N'-dimethylformamide (DMF) (98%) were purchased from Merck Chemicals (Pty) Ltd (Gauteng, South Africa) and Sigma-Aldrich (New Germany, South Africa), respectively. High performance liquid chromatography (HPLC) grade methanol and acetonitrile were purchased from Sigma-Aldrich (New Germany, South Africa). Chemicals such as bisphenol A (97%) and ibuprofen sodium salt (99%) were purchased from Sigma-Aldrich (New Germany, South Africa), while sodium hydroxide pellets (98%) and lead metal powder were obtained from Merck Chemicals (Pty) Ltd (Gauteng, South Africa). Cadmium metal powder (99%) was purchased from Thomas Baker Chemicals (Pvt) Ltd, (Mumbai, India).

9.2.2. Synthesis and characterization of adsorbents

The synthesis of 4'-(4-hydroxyphenyl)-2,2':6',2''-terpyridine (HO-Phttpy) was carried out *via* the method described by Patel *et al.* [24]. The characterization of the synthesized ligand was done by using Fourier transform infrared (FTIR), mass and nuclear magnetic resonance (NMR) spectroscopy. Pristine multiwalled carbon nanotubes (P-MWCNTs) were purified with hydrochloric acid and later oxidized with a mixture of nitric and sulfuric acids in a volume ratio of 3:1. Purification and oxidation were carried out as described by Santangelo *et al.* [25] and Oyetade *et al.* [26]. The acid-functionalized MWCNTs (MWCNT-COOH) were further acylated by using a mixture of thionyl chloride and DMF in a volume ratio of 20:1, respectively. The tubes obtained were further functionalized with HO-Phttpy to obtain nitrogen-functionalized MWCNTs (MWCNT-ttpy). The synthesized adsorbents were characterized by various techniques, including electron microscopy (scanning and transmission), FTIR and Raman spectroscopy, thermogravimetric analysis, elemental analysis and BET surface area analysis.

9.2.3. Analysis of adsorbates

9.2.3.1. Instrumentation

The concentrations of BPA and IBP were determined with a UFLC-XR Shimadzu Prominence LC chromatographic system (LC-20AD XR) equipped with a vacuum degasser (DGU-20A₃), autosampler (SIL-20A XR), thermostated column oven (CTO-20A), fraction collector (FRC-10A), communications bus module (LBM-20A) and a diode array detector (SPD-M20A). Separation of the analytes was effected on a Brownlee C18 column 5 μ m particle size and dimension of 150 \times 4.6 mm (PerkinElmer, Norwalk, USA). For metal ion analysis, a Perkin Elmer Optima 5300 DV inductively coupled plasma-optical emission

spectrometer (ICP-OES) was used to measure the initial and final concentrations of metal ions in solution.

9.2.3.2. Preparation of standard stock solutions

Individual stock solutions of 1000 mg dm^{-3} of BPA and IBP were prepared by dissolving 1 g of the pure powder in 50 cm^3 of methanol. The solution was then made up to mark in a 1000 dm^3 volumetric flask with deionised water. Working solutions of desired concentrations of BPA/IBP were prepared daily from the stock solution in deionised water. Individual stock solutions of Pb^{2+} and Cd^{2+} were prepared by dissolving 1 g of the pure metal in 2 mol dm^{-3} nitric acid. The solution was made up to mark in a 1000 dm^3 volumetric flask with deionised water. Working solutions of desired concentrations were prepared from the stock solution and the initial concentrations of metal ions determined by using ICP-OES.

9.2.3.3. Chromatographic conditions for the quantification of BPA and IBP

The mobile phase for BPA analysis consisted of a mixture of 30:70 (v/v) acetonitrile and ultrapure water. Chromatograms were collected at 230 nm by using a PDA detector. The injection volume was $20 \mu\text{L}$ at a column temperature of $30 \text{ }^\circ\text{C}$ and a mobile phase flow rate of $1.2 \text{ cm}^3 \text{ min}^{-1}$. For IBP, the mobile phase was a mixture of 80:20 (v/v) methanol and 5 mM phosphoric acid made in ultrapure water. Chromatograms were recorded at a wavelength of 220 nm. The injection volume was $50 \mu\text{L}$ at a column temperature of $30 \text{ }^\circ\text{C}$ and an eluant flow rate of $1.0 \text{ cm}^3 \text{ min}^{-1}$. For quantification purposes, a calibration plot of each analyte was prepared within the range of experimental concentrations used under the same instrumental conditions.

9.2.3.4. ICP-OES conditions for quantification of metal ions

The operating conditions for the Perkin Elmer Optima 5300 DV ICP-OES are presented in Table 9.1. The spectrometer was calibrated within the concentration ranges of $0\text{-}50 \text{ mg dm}^{-3}$ and calibration plots were obtained each time the instrument was used for metal ion detection.

Table 9.1: Operating conditions for the ICP-OES determination of metal ion concentrations

Wavelength (Pb ²⁺)	220.353 nm
Wavelength (Cd ²⁺)	267.716 nm
RF power	1300 W
Plasma gas flow rate	15 dm ³ min ⁻¹
Pump	1.5 cm ³ min ⁻¹
Auxiliary gas flow rate	0.2 dm ³ min ⁻¹
Nebulizer gas flow rate	0.8 dm ³ min ⁻¹
Nebulizer pressure	2 bars
Analyzer type	Axial
Replicates	3
Sample read delay	60 s

9.2.4. Batch adsorption studies

Adsorption experiments were conducted within a concentration range of 10-100 mg dm⁻³ in 50 cm³ glass bottles for single-solute adsorption systems. A 25 cm³ aliquot of each sorbate solution (BPA and IBP) was measured into the glass bottles and the solution adjusted to pH 2.0 with the addition of appropriate volumes of 0.1 mol dm⁻³ NaOH or HNO₃. About 50 mg of MWCNT-tpy was weighed into each bottle and the mixtures were agitated in a thermostated water bath at 25 °C for 24 h. After agitation, the suspensions were filtered and the equilibrium concentrations of the adsorbates in the filtrates were determined by using HPLC-UV.

In a binary adsorption system, the effect of pH was conducted by measuring 25 cm³ aliquots containing 15 mg dm⁻³ each of a mixed adsorbate solution of BPA and IBP into 50 cm³ glass bottles. The solutions were adjusted to have a pH over the range of 1-10 by adding appropriate volumes of 0.1 mol dm⁻³ NaOH or HNO₃. About 75 mg of the adsorbent (MWCNT-tpy) was added into each solution and the suspensions were agitated in a thermostated water bath at 25 °C for 24 h. After agitation, the resulting solutions were filtered and the filtrates transferred into 1.5 cm³ amber vials. The initial and equilibrium concentrations of BPA and IBP were determined by HPLC-UV. The percent removal of BPA and IBP and the uptake of sorbates onto sorbents (q_e) were calculated according to equations 9.1 and 9.2, respectively.

$$\% \text{ adsorbed} = \left(\frac{C_i - C_{eq}}{C_i} \right) \times 100 \quad (9.1)$$

$$q_e = \left(\frac{C_i - C_{eq}}{m} \right) \times V \quad (9.2)$$

where C_i is the initial adsorbate concentration (mg dm^{-3}), C_{eq} is the equilibrium concentration of adsorbate (mg dm^{-3}), q_e is the adsorption capacity (mg g^{-1}), m is the mass of adsorbent (mg) and V is the volume (dm^3) of the adsorbate solution used.

9.2.4.1. Isotherms

To investigate the effect of the presence of a particular adsorbate on the sorption of the other, isotherm studies were conducted in a binary system by measuring 25 cm^3 aliquots of a mixed adsorbate solution at equal concentrations between $5\text{-}60 \text{ mg dm}^{-3}$ into glass bottles, and the solutions were conditioned to obtain pH 2. About 100 mg of adsorbent was weighed into each bottle and the suspensions agitated in a thermostated water bath at $20 \text{ }^\circ\text{C}$ for 24 h. The equilibrium concentrations of each sorbate was determined from the filtrates by using HPLC-UV. A similar process was performed to investigate the sorption of a particular sorbate in the presence of the other at varying initial adsorbate concentration. Additionally, the influence of the presence of Pb^{2+} or Cd^{2+} was investigated on the adsorption of BPA and IBP at both equal and varying initial sorbates concentrations.

The equilibrium data obtained for single and binary adsorption of BPA and IBP were fitted to the Langmuir adsorption isotherm model, which describes the monolayer adsorption of sorbates onto homogeneous sites. The Langmuir isotherm equation is given in Eq. 9.3 [27].

$$q_{eq} = \frac{q_m b C_{eq}}{1 + b C_{eq}} \quad (9.3)$$

where q_{eq} is the amount adsorbed per unit mass of adsorbent at equilibrium (mg g^{-1}), C_{eq} is the equilibrium concentration of adsorbate in solution after adsorption (mg dm^{-3}), q_m represents the maximum adsorption capacity (mg g^{-1}), and b is the empirical Langmuir adsorption constant ($\text{dm}^3 \text{ mg}^{-1}$).

9.2.4.2. Data analysis

The data obtained were fitted to the isotherm and kinetics models by means of the nonlinear regression routine (*nls*) in the R statistical computing environment [28]. The R statistical software takes into account the minimization of the sum of squared residuals (SSR) and the residual square errors (RSE). A comparison of all SSR and RSE values was done and the adequacy of the models was assessed from the value with the lowest SSR.

9.2.4.3. Distribution coefficients

The distribution coefficient (K_d) was applied in order to estimate the affinity of a sorbent towards a solute [29-31]. The coefficient was calculated as indicated in Eq. 9.4. The coefficient is indicative of the sorbate affinity for active sites on the adsorbent.

$$K_d = \frac{C_i - C_{eq}}{C_{eq}} \times \frac{V}{m} \quad (9.4)$$

where C_i is the initial concentration (mg dm^{-3}), C_{eq} is the equilibrium concentration (mg dm^{-3}), m is the adsorbent mass (g), and V is the volume of the solution (dm^3).

9.3. Results and discussion

The characterization of the synthesized adsorbent (MWCNT-ttpy) has been reported in our previous work by Oyetade *et al.* [32]. The improved textural characteristics of this sorbent suggests its potential application for the removal of organic pollutants from aqueous solutions. Similarly, elemental analysis confirms the presence of nitrogen-donor atoms on the adsorbent [32]. This suggests that MWCNT-ttpy should prove effective for the removal of both metal ions and organic pollutants from an aqueous solution, containing both contaminants. Hence, this sorbent was applied for the adsorption of BPA and IBP in both single and binary adsorption systems. The influence of Pb^{2+} and Cd^{2+} , as models pollutants of heavy metals ions, was also investigated in a competitive adsorption system containing both BPA and IBP. The equilibrium adsorption data for all systems was modelled by using the Langmuir isotherm model.

9.3.1. Adsorption of BPA and IBP in single adsorption systems

In a single-solute system, adsorption experiments were conducted at pH 2 within the concentration range of 10-100 mg dm^{-3} . Fig 9.1 shows a similar profile for both the adsorption of BPA and IBP onto MWCNT-ttpy. The uptake of both adsorbates by MWCNT-ttpy increased with increasing concentration, due to an increase in the driving force required to overcome the resistance between the sorbate-sorbent interface (Fig 9.1) [33].

Although the removal of BPA and IBP onto MWCNT-ttpy were of similar magnitudes to one another at all concentrations, a higher uptake of IBP over BPA was noticed in a single-solute system (Fig 9.1). This trend can be associated with the somewhat higher partition coefficient value of IBP than BPA. The partition coefficient (P) describes the lipo- or hydro-

philicity of a substance, by estimating the concentration of a compound in two immiscible solvents [34]. Researchers rely on these values to gauge the hydro- or lipo-philicity of a molecule in an octanol-water system [34]. The higher the log P values, the greater is the hydrophobic nature of the molecule [34]. The partition coefficients of IBP and BPA in an octanol-water system are 3.50 [35] and 3.4 [36], respectively. Although, the difference is slight, this phenomenon could be a decider in determining the affinity of sorbates onto MWCNT-ttpy, hence, resulting in a somewhat increased removal of IBP than BPA [37]. This assumption was supported by Jung *et al.* [37,38], who also suggested that the removal of some EDCs and PPCPs onto MWCNTs was determined by the partition coefficient values of the molecules. The sorption of BPA and IBP onto MWCNT-ttpy may therefore be associated with hydrogen and/or hydrophobic interactions between the sorbate and sorbents.

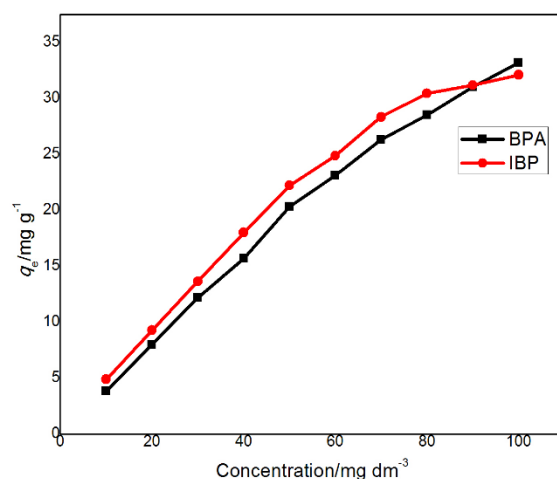


Fig 9.1: Amounts of BPA and IBP adsorbed onto MWCNT-ttpy in a single adsorption system [conditions: 25 cm³ of 10-100 mg dm⁻³ adsorbate solution, 24 h equilibration time, pH 2.0, adsorbent dose 50 mg, agitation speed 150 rpm, and temperature 25 °C].

9.3.2. Adsorption in binary systems

9.3.2.1. Effect of pH

In order to investigate the influence of pH on the adsorption of BPA and IBP onto MWCNT-ttpy in binary systems, adsorption experiments were conducted within a pH range of 1-10 by using a mixed adsorbate solution of containing 15 mg dm⁻³ of each pollutant. A 75 mg dose of MWCNT-ttpy was added into the solution and the mixture was then agitated in a thermostated water bath at 25 °C for 24 h. The sorption of both adsorbates demonstrated similar trends, showing a decrease in the percentage removal of sorbates as the solution pH is gradually increased (Fig 9.2). This trend is determined by the surface charge densities on

the adsorbent and the protonation behaviour of the adsorbates over the studied pH range [33,38]. Anions of BPA and IBP are formed when the solution pH is greater than the pK_a values of each molecule [38]. The pK_a values of BPA and IBP are 9.6-10.2 [39] and 4.91 [4], respectively. The deprotonation of these molecules into anions will therefore occur as the solution becomes more alkaline. The point of zero charge (pH_{PZC}) of MWCNT-ttpy is 4.48 [32], which will in turn be negatively charged in basic conditions, hence resulting in a reduction in π - π and electrostatic interactions between the sorbate molecules and adsorbent surfaces [38]. These phenomenon explains the reduced removal efficiencies of BPA and IBP onto MWCNT-ttpy under alkaline conditions (Fig 9.2). The removal of BPA exhibited minimal effect towards pH change within the range of 1-7, as a result of the molecule having higher pK_a value than IBP, however, its sorption was also noticed to decrease as the solution pH increased above 8.0 (Fig 9.2).

High adsorbate removal in acidic medium was attributed to the non-dissociation of BPA and IBP within the pH range of 1-4 [40], accounting for increased sorption of molecules *via* hydrogen and/or hydrophobic interaction with the adsorbent surface (Fig 9.2). Jung *et al.* [38], Tsai *et al.* [33] and Guedidi *et al.*[40], reported similar trends for the removal of BPA and IBP from aqueous solutions. Hence, pH 2.0 was chosen in this study to investigate the multicomponent sorption of BPA and IBP onto MWCNT-ttpy.

The experimental data investigating the binary adsorption of BPA and IBP onto MWCNT-ttpy in a binary system as a function of pH can be found in Appendix VI (Table A-VI.1 – Table A-VI.2).

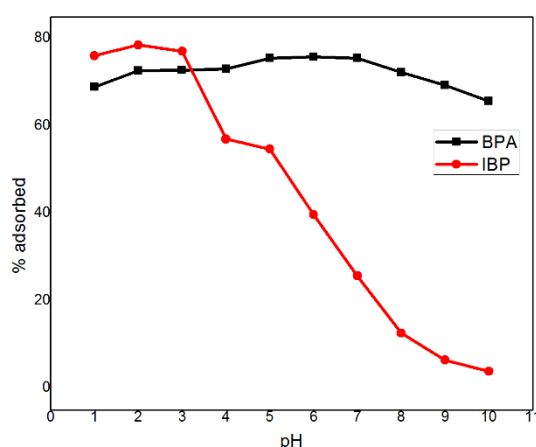


Fig 9.2: Effect of pH for the binary adsorption of BPA and IBP onto MWCNT-ttpy [conditions: 25 cm³ of 15 mg dm⁻³ adsorbate, 24 h equilibration time, adsorbent dose 75 mg, agitation speed 150 rpm and temperature 25 °C].

9.3.2.2. Effect of equal initial concentration

The influence of adsorbates at equal initial concentration in a binary system was investigated within a concentration range of 5-60 mg dm⁻³. These experiments were performed in order to understand the behaviour of MWCNT-ttpy towards the removal of BPA and IBP in synthetic wastewater, assuming both sorbates were present in equal amounts. Fig 9.3 presents (a) the percentage adsorbed and (b) the amount of adsorbate removed per unit mass (q_e) in a binary sorption process containing BPA and IBP at equal initial concentrations. It was observed that the removal of both sorbates onto MWCNT-ttpy gradually decreased over the concentration range (Fig 9.3a). Sorbates were observed to adsorb highest at low initial concentrations and decrease with increasing initial adsorbate concentrations (Fig 9.3a). This can be attributed to the availability of active sites for sorption at low adsorbate concentrations [33]. However, as the initial adsorbate concentration is increased, the active sites on adsorbent become occupied, hence limiting the removal of adsorbates from solution. This factor is responsible for the observed trends in the binary sorption of BPA and IBP onto MWCNT-ttpy. It was also noted that the removal of IBP molecules in binary systems was higher than that of BPA. The affinity of IBP for MWCNT-ttpy could be due to the increase in hydrophobic state of IBP molecules than BPA, therefore favouring its removal over BPA [37]. This observation was also confirmed from Fig 9.3b, which demonstrates a higher removal of IBP per unit mass of MWCNT-ttpy than BPA. The uptake of adsorbates per unit mass of adsorbent (q_e) was noticed to increase sharply as their concentrations were increased. The amount of IBP adsorbed increased from 1.72 mg g⁻¹ to 8.67 mg g⁻¹, while BPA sorption increased from 1.03 mg g⁻¹ to 7.06 mg g⁻¹. These experiments explicitly prove the favourability of MWCNT-ttpy towards the removal of these pollutants in a competitive system. Adsorption of organic pollutants onto MWCNT-ttpy could therefore be said to largely depend on the hydrophobic state of the sorbates involved.

The experimental data for the competitive adsorption of BPA and IBP in a binary component system as a function of equal initial adsorbate concentration can be found in Appendix VI (Table A-VI.3 – Table A-VI.4).

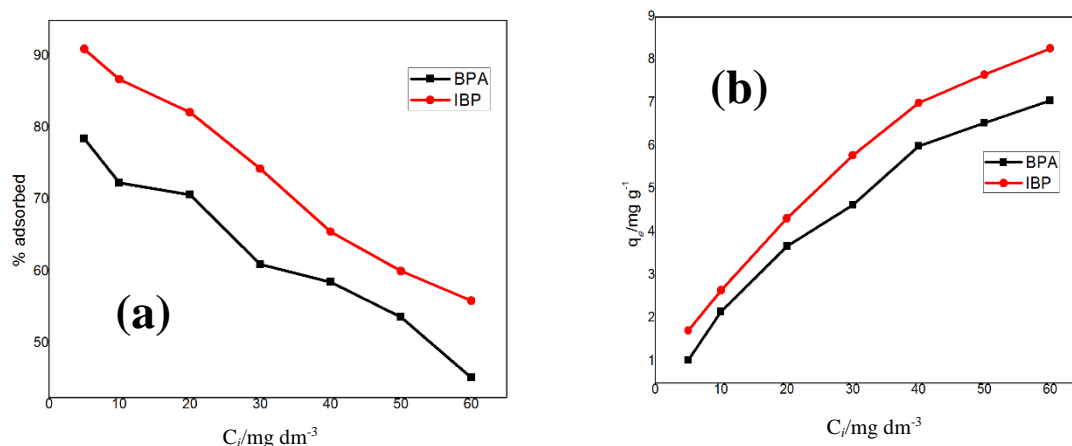


Fig 9.3: The effect of same initial metal ion concentration in a multicomponent system for the adsorption of BPA and IBP. (a) Percentage uptake (%) and (b) amount adsorbed per unit mass of adsorbent (mg g^{-1}) [conditions: 25 cm^3 of $10\text{-}60 \text{ mg dm}^{-3}$ adsorbate solution, pH 2.0, 24 h equilibration time, adsorbent dose 100 mg , agitation speed 150 rpm , temperature $25 \text{ }^\circ\text{C}$].

9.3.2.3. Effect of varying adsorbate concentration

Effluents and wastewaters contain a variety of contaminants in different concentrations, hence necessitating an investigation of the behaviour of MWCNT-tpy in a real-life scenario for the removal of organic pollutants in different concentrations. This was conducted by keeping the concentration of a particular sorbate constant at 20 mg dm^{-3} , while varying the initial concentration of the other pollutant between $5\text{-}60 \text{ mg dm}^{-3}$. The presence of metal ions such as Pb^{2+} and Cd^{2+} was also studied in order to investigate the competitive sorption of pollutants in a model sample. The following section discusses the results for these adsorption processes.

9.3.2.3.1. Effect of the presence of BPA on the adsorption of IBP

The influence of BPA in solution on the adsorption of IBP was investigated by varying the initial IBP concentration from $5\text{-}60 \text{ mg dm}^{-3}$, while keeping the initial concentration of BPA constant at 20 mg dm^{-3} . Fig 9.4 shows that the competition between both sorbates for active sites was primarily based on the initial concentration of the sorbates in solution. The percentage removal of BPA was greater than that of IBP from 5 to 30 mg dm^{-3} , but lower than that of IBP from $40\text{-}60 \text{ mg dm}^{-3}$ (Fig 9.4). However, the greatest removal of BPA was observed when IBP concentration was 60 mg dm^{-3} , the highest value studied. Since the log P values of both sorbates are quite close to one other [35,36], sorption was based on adsorbate amount and not on their hydrophobic state. These trends were also confirmed by the distribution coefficient (K_d) values (Appendix VI), that showed larger K_d values for BPA

at high IBP concentrations. Thus, the adsorption of BPA and IBP in a binary solution exhibits synergistic effects rather than competition. This may reflect that these two adsorbates bind at different sites on the surface of the adsorbent, and therefore do not compete for the same sites. The experimental data investigating the competitive sorption of BPA and IBP in a binary component system as a function of varying initial adsorbate concentration can be found in Appendix VI (Table A-VI.5 – Table A-VI.6).

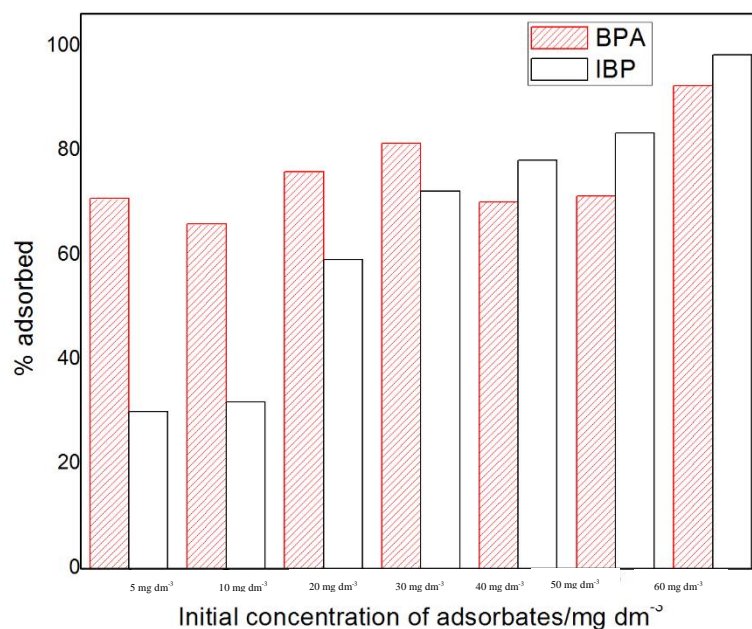


Fig 9.4: Removal of IBP at fixed 20 mg dm⁻³ BPA concentration in a mixed adsorbate solution. [conditions: adsorbent dose 100 mg, pH 2.0, agitation time, 24 h, agitation speed 150 rpm and temperature 25 °C].

9.3.2.3.2. Effect of the presence of IBP on the adsorption of BPA

The influence of IBP in solution on the sorption of BPA was investigated by varying BPA concentration from 5-60 mg dm⁻³, while keeping the initial concentration of IBP constant at 20 mg dm⁻³. Fig 9.5 shows the preferential removal of IBP over BPA as the concentration was varied from 5 to 40 mg dm⁻³. Thereafter, the percentage removal for BPA was greater than that of IBP because of its presence in greater amount. The behaviour observed here is similar to that observed when BPA was fixed and IBP was varied, indicating synergy rather than competition. This trend was determined by the initial adsorbate concentration in solution. This trend was also supported by the increase in K_d values of IBP over the values obtained for BPA. The experimental data demonstrating this sorption is presented in Appendix VI (Table A-VI.7 – Table A-VI.8).

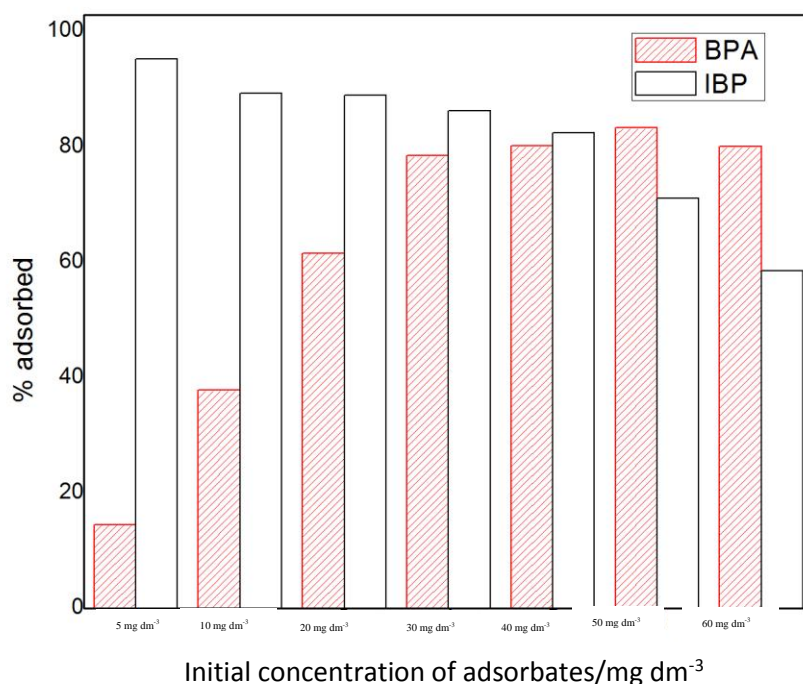


Fig 9.5: Removal of BPA at fixed 20 mg dm⁻³ IBP concentration in a mixed adsorbate solution. [conditions: adsorbent dose 100 mg, pH 2.0, agitation time, 24 h, agitation speed 150 rpm and temperature 25 °C].

9.3.2.3.3. Effect of the presence of Cd²⁺ on the adsorption of IBP and BPA

The influence of the presence of Cd²⁺ on the adsorption of BPA and IBP was studied by varying their concentrations within 5-60 mg dm⁻³, while keeping the initial Cd²⁺ concentration constant at 20 mg dm⁻³. Fig 9.6 shows that the adsorption of Cd²⁺ was not influenced by the presence of BPA and IBP. The sorption of IBP was, however, higher than BPA sorption in the presence of Cd²⁺ in solution, as was the case in the absence of Cd²⁺ (see Fig 9.3). This behaviour can be attributed to the preferential sorption of IBP over BPA *via* increased hydrophobic interactions with the surface of MWCNT-ttpty. The sorption of BPA and IBP was not influenced by the presence of Cd²⁺ in solution, as good removal efficiencies (> 70%) were obtained for BPA and IBP. In fact, they were better than in the absence of Cd²⁺ (Fig 9.6 vs 9.3). This trend could be attributed to the *in situ* formation of complexes between Cd²⁺, acting as the central metal cation, and BPA and IBP acting as the ligands during adsorption. The formation of these complexes in solution could facilitate the cooperative sorption of all pollutants in solution. This assumption was supported by Bautista-Toledo *et al.* [41], who reported a cooperative sorption between Cr³⁺ and BPA through a similar process. The metal ion Cr³⁺ acted as a metallic cation with BPA as the ligand, hence, facilitating sorption of both adsorbates from an aqueous solution [41]. Of

importance, is to note that the sorption of BPA and IBP also decreased gradually as their concentrations were increased. This could be attributed to the increase in the initial adsorbate concentration, which limits the available active sites on the adsorbent for removal. Hence, the potential application of MWCNT-ttpy as an adsorbent for the removal of pollutants such as metal ions and organic compounds in a multicomponent system is promising for wastewater remediation in industries and water treatment facilities.

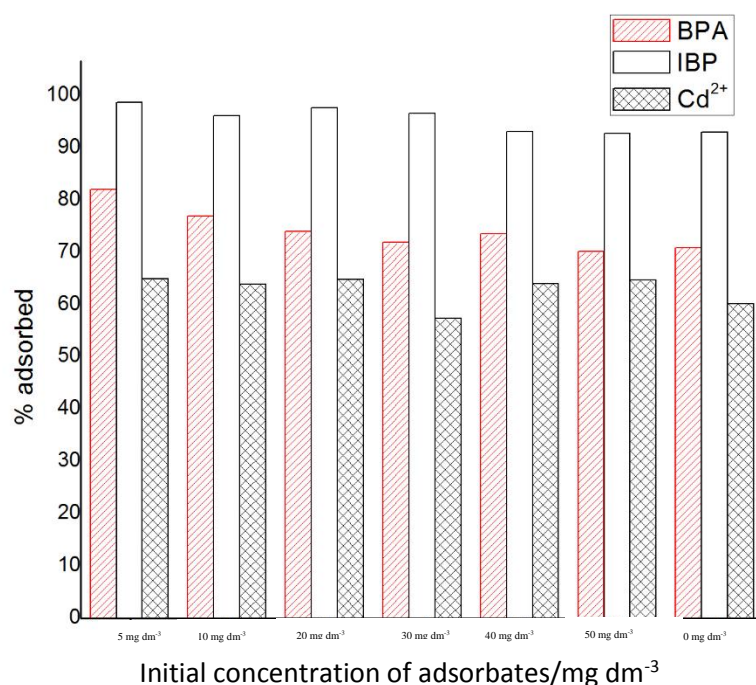


Fig 9.6: Competitive removal of BPA and IBP at fixed Cd²⁺ concentration in a mixed adsorbate solution. [conditions: Cd²⁺ 20 mg dm⁻³, BPA/IBP 5 to 60 mg dm⁻³, adsorbent dose 100 mg, pH 2.0, agitation time, 24 h, agitation speed 150 rpm and temperature 25 °C].

9.3.2.3.4. Effect of the presence of Pb²⁺ on the adsorption of IBP and BPA

The influence of Pb²⁺ on the adsorption of BPA and IBP in a multicomponent adsorption system was examined by keeping the Pb²⁺ concentration constant at 20 mg dm⁻³, while those of other competitors were varied between 5-60 mg dm⁻³. Fig 9.7 shows that the removal of Pb²⁺ increased from 93.6% to 98.6%, as the concentrations of the other competitors were increased. Hence, Pb²⁺ removal onto MWCNT-ttpy was not inhibited as a result of increases in the concentrations of BPA and IBP in aqueous solution. The affinity of MWCNT-ttpy towards the removal of Pb²⁺ even in the presence of contaminants such as BPA and IBP

could be due to the fact that the N-donor atoms on the adsorbent were still available for metal ion chelation, hence interference with organic molecules was not pronounced.

However, Fig 9.6 also demonstrates a significant influence on the sorption of BPA and IBP due to the presence of Pb^{2+} in solution. The sorption of BPA and IBP was significant attaining a percentage removal of 84.8% and 88.5%, respectively, at an initial adsorbate concentration of 5 mg dm^{-3} (Fig 9.7). At increased initial concentrations of BPA and IBP (60 mg dm^{-3}), the percentage removal reduced to 29.0% and 31.7%, respectively, and this is due to the competition between both adsorbates at increased concentration. This inference was based on the fact that the percentage removal of BPA and IBP was not particularly different from one another at every concentration. Hence, adsorption of BPA and IBP molecules was primarily based on competition for active sites on the adsorbent. On comparison with Fig 9.3, it was observed that a decrease in the removal of BPA and IBP was observed in the presence of Pb^{2+} . This behaviour justifies that the sorption of BPA and IBP was largely competitive in the presence of Pb^{2+} in solution.

It is important to note that the sorption of BPA and IBP was enhanced in the presence of Cd^{2+} (Fig 9.6), however, a decrease in their sorption was noticed in the presence of Pb^{2+} . This could be attributed to the increasing attraction of Cd^{2+} over Pb^{2+} onto nitrogen-donor atoms on MWCNT-ttpy, hence, interference with other active sites for organic removal was minimised. MWCNT-ttpy proved effective in the simultaneous removal of both metal ions and organic pollutants from aqueous solutions, and could be used for the remediation of wastewater and industrial effluents. The experimental data for this sorption is presented in Appendix VI (Table A-VI.9 – Table A-VI.11).

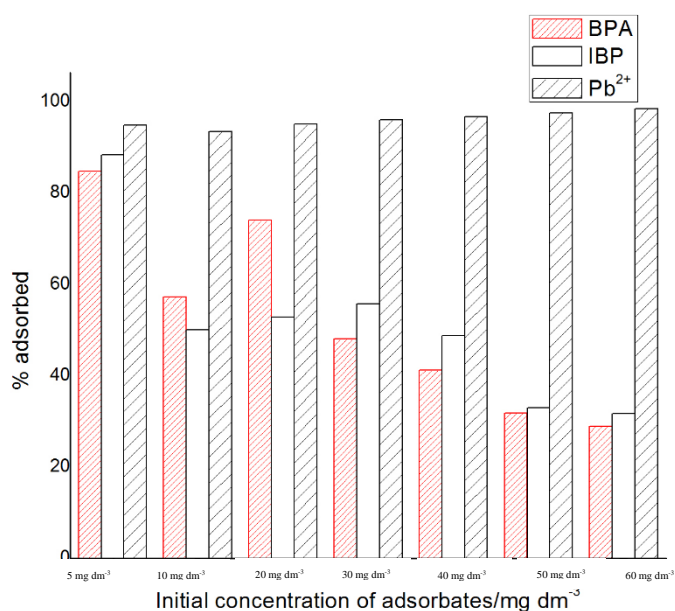


Fig 9.7: Competitive removal of BPA and IBP at fixed Pb²⁺ concentration in a mixed adsorbate solution. [conditions: Pb²⁺ 20 mg dm⁻³, BPA/IBP 5 to 60 mg dm⁻³, adsorbent dose, 100 mg, pH 2.0, agitation time, 24 h, agitation speed 150 rpm and temperature 25 °C].

9.3.3 Competitive adsorption isotherms

The equilibrium data obtained for the adsorption of BPA and IBP in single and binary adsorption systems were analysed by using the Langmuir isotherm model as given in Eq. 9.3. This model is commonly used to describe single and binary adsorption systems involving the removal of large organic compounds from aqueous solutions [42]. The model assumes that the surface of the adsorbent is homogeneous, and no interaction exists between adjacent adsorbed molecules [42]. The Langmuir parameters obtained for both processes are presented in Table 9.2, while the fit of the isotherm model is shown in Appendix VI (Fig A-VI.1). The uptake of BPA and IBP onto MWCNT-ttpe in a binary adsorption system (q_m') were four-fold less than the amount of BPA and IBP adsorbed in a single-solute system (q_m) (Table 9.2). The decrease in uptake values may be associated with the increase in competition amongst the adsorbate molecules for active sites on the surface of the adsorbent. This assumption was supported by the values obtained from the ratio of adsorption capacities in single and binary systems (q_m'/q_m). As proposed by Zhu *et al.* [43], this ratio may be used to predict the processes or the sorption pattern between adsorbates for competitive adsorption systems. Adsorbates in a multicomponent system are assumed to interact *via* the following routes: synergistic if $q_m'/q_m > 1$, antagonistic if $q_m'/q_m < 1$ and no net interaction

when $q_m'/q_m = 1$ [43]. Table 7.2 indicates that all q_m'/q_m values obtained in this study were less than 1, indicating that the sorption of BPA and IBP was antagonistic. This implies that adsorption was dependent on the competition amongst adsorbates for active sites on the adsorbent and their relative affinities for the adsorbent [42]. This effect was made obvious in the binary adsorption system wherein IBP was better adsorbed onto MWCNT-ttpy than BPA, possibly due to somewhat higher hydrophobicity (Table 9.2). The sorption of organic compounds onto MWCNT-ttpy will largely depend on the properties of the pollutants involved, and hence, how they influence each other in solution.

Table 9.2: The Langmuir parameters for the adsorption of BPA and IBP in single and binary adsorption systems onto MWCNT-ttpy.

Adsorbate	Single metal adsorption				Binary adsorption				
	q_m/mg^{-1}	$b/\text{dm}^3 \text{g}^{-1}$	SSR ^a	RSE ^b	q_m'/mg^{-1}	$b/\text{dm}^3 \text{g}^{-1}$	SSR ^a	RSE ^b	q_m'/q_m
BPA	38.31	0.229	13.77	1.312	8.900	0.096	0.267	0.2311	0.243
IBP	34.51	0.300	43.23	2.325	9.303	0.254	0.233	0.241	0.258

^a Sum of squared residuals; ^b residual squared errors

9.4. Conclusions

In this study, the efficacy of nitrogen-functionalized multiwalled carbon nanotubes (MWCNT-ttpy) towards the removal of BPA and IBP in a competitive adsorption process was investigated *via* batch experiments. The influence of Pb^{2+} and Cd^{2+} as model pollutants of heavy metals in a multicomponent system containing BPA and IBP was also studied. The equilibrium data obtained were modelled by using the Langmuir adsorption isotherm to understand the mechanism involved in the competitive removal of BPA and IBP from aqueous solutions.

The results obtained signify that adsorption was decided on by the nature of the adsorbates and adsorbent in solution. In single- and binary adsorption systems, the sorption of IBP onto MWCNT-ttpy showed greater removal efficiencies as a result of its somewhat increased hydrophobicity over BPA. The adsorption of BPA and IBP was however influenced by the presence of metal ion cations such as Pb^{2+} and Cd^{2+} . A cooperative removal process was achieved in the multicomponent systems containing metal ions and organic pollutants.

The equilibrium data obtained for the sorption of BPA and IBP in single-solute and binary adsorption systems were described by using the Langmuir model. A higher uptake of both sorbates was obtained in single-solute systems than binary adsorption systems. This was

associated with the increase in competition between adsorbate molecules for active sites on the adsorbent. The affinity of sorbate molecules for the surface of MWCNT-ttpy played a significant role in deciding their uptake. Hence, the sorption of BPA and IBP in binary systems was antagonistic.

In conclusion, the application of MWCNT-ttpy proved efficient for the removal of BPA and IBP in a competitive system. The sorbent also behaved appropriately well towards the removal of both metal ions and organic contaminants simultaneously in solution. This therefore further justifies the application of MWCNT-ttpy for the treatment of effluents and wastewater contaminated with a variety of pollutants.

References

- [1] C. Erler, J. Novak, Bisphenol A exposure: human risk and health policy, *J. Pediatr. Nurs.* 25 (2010) 400-407.
- [2] M.H. Dehghani, A.H. Mahvi, N. Rastkari, R. Saeedi, S. Nazmara, E. Iravani, Adsorption of bisphenol A (BPA) from aqueous solutions by carbon nanotubes: Kinetic and equilibrium studies, *Desalin. Water Treat.* 54 (2014) 84-92.
- [3] E. Estevez, J.M. Hernandez-Moreno, J.R. Fernandez-Vera, M.P. Palacios-Diaz, Ibuprofen adsorption in four agricultural volcanic soils, *Sci. Total Environ.* 468-469 (2014) 406-414.
- [4] S.K. Behera, S.Y. Oh, H.S. Park, Sorptive removal of ibuprofen from water using selected soil minerals and activated carbon, *Int. J. Environ. Sci. Technol.* 9 (2012) 85-94.
- [5] Y. Dong, D. Wu, X. Chen, Y. Lin, Adsorption of bisphenol A from water by surfactant-modified zeolite, *J. Colloid Interface Sci.* 348 (2010) 585-590.
- [6] R. Amdany, L. Chimuka, E. Cukrowska, Determination of naproxen, ibuprofen and triclosan in wastewater using the polar organic chemical integrative sampler (POCIS): A laboratory calibration and field application, *Water SA* 40 (2014) 407-413.
- [7] S. Yuan, N. Gou, A.N. Alshwabkeh, A.Z. Gu, Efficient degradation of contaminants of emerging concerns by a new electro-Fenton process with Ti/MMO cathode, *Chemosphere* 93 (2013) 2796-2804.
- [8] S. Zheng, Z. Sun, Y. Park, G.A. Ayoko, R.L. Frost, Removal of bisphenol A from wastewater by Ca-montmorillonite modified with selected surfactants, *Chem. Eng. J.* 234 (2013) 416-422.
- [9] A.S. Mestre, J. Pires, J.M.F. Nogueira, A.P. Carvalho, Activated carbons for the adsorption of ibuprofen, *Carbon* 45 (2007) 1979-1988.
- [10] W. Han, L. Luo, S. Zhang, Adsorption of bisphenol A on lignin: Effects of solution chemistry, *Int. J. Environ. Sci. Technol.* 9 (2012) 543-548.
- [11] W.-T. Tsai, K.-J. Hsien, H.-C. Hsu, Adsorption of organic compounds from aqueous solution onto the synthesized zeolite, *J. Hazard. Mater.* 166 (2009) 635-641.
- [12] X. Li, H. Zhao, X. Quan, S. Chen, Y. Zhang, H. Yu, Adsorption of ionizable organic contaminants on multi-walled carbon nanotubes with different oxygen contents, *J. Hazard. Mater.* 186 (2011) 407-415.
- [13] S.A. Kosa, G. Al-Zhrani, M. Abdel Salam, Removal of heavy metals from aqueous solutions by multi-walled carbon nanotubes modified with 8-hydroxyquinoline, *Chem. Eng. J.* 181-182 (2012) 159-168.
- [14] Y. Wang, Z. Iqbal, S.V. Malhotra, Functionalization of carbon nanotubes with amines and enzymes, *Chem. Phys. Lett.* 402 (2005) 96-101.

- [15] W. Yang, P. Ding, L. Zhou, J. Yu, X. Chen, F. Jiao, Preparation of diamine modified mesoporous silica on multi-walled carbon nanotubes for the adsorption of heavy metals in aqueous solution, *Appl. Surf. Sci.* 282 (2013) 38-45.
- [16] G.D. Vuković, A.D. Marinković, S.D. Škapin, M.Đ. Ristić, R. Aleksić, A.A. Perić-Grujić, P.S. Uskoković, Removal of lead from water by amino modified multi-walled carbon nanotubes, *Chem. Eng. J.* 173 (2011) 855-865.
- [17] M. Hadavifar, N. Bahramifar, H. Younesi, Q. Li, Adsorption of mercury ions from synthetic and real wastewater aqueous solution by functionalized multi-walled carbon nanotube with both amino and thiolated groups, *Chem. Eng. J.* 237 (2014) 217-228.
- [18] N.M. Bandaru, N. Reta, H. Dalal, A.V. Ellis, J. Shapter, N.H. Voelcker, Enhanced adsorption of mercury ions on thiol derivatized single wall carbon nanotubes, *J. Hazard. Mater.* 261 (2013) 534-541.
- [19] G.D. Vukovic, A.D. Marinkovic, M. Coli, M.D. Ristic, R. Aleksic, A.A. Peric-Gruji, P.S. Uskokovic, Removal of cadmium from aqueous solutions by oxidized and ethylenediamine-functionalized multi-walled carbon nanotubes, *Chem. Eng. J.* 157 (2010) 238-248.
- [20] K. Yang, L. Zhu, B. Xing, Adsorption of polycyclic aromatic hydrocarbons by carbon nanomaterials, *Environ. Sci. Technol.* 40 (2006) 1855-1861.
- [21] R.W. Walters, R.G. Luthy, Equilibrium adsorption of polycyclic aromatic hydrocarbons from water onto activated carbon, *Environ. Sci. Technol.* 18 (1984) 395-403.
- [22] X. Chen, X. Xia, X. Wang, J. Qiao, H. Chen, A comparative study on sorption of perfluorooctane sulfonate (PFOS) by chars, ash and carbon nanotubes, *Chemosphere* 83 (2011) 1313-1319.
- [23] M.B. Ogundiran, O.A. Oyetade, J.O. Babayemi, O. Osibanjo, Potential environmental hazards of non-rechargeable electric torch wastes in Nigeria *Int. J. Environ. Waste Manag.* 13 (2014) 115-130.
- [24] M.N. Patel, H.N. Joshi, C.R.I. Patel, Copper(II) complexes with norfloxacin and neutral terpyridines: Cytotoxic, antibacterial, superoxide dismutase and DNA-interaction approach, *Polyhedron* 40 (2012) 159-167.
- [25] S. Santangelo, G. Messina, G. Faggio, S.H. Abdul Rahim, C. Milone, Effect of sulphuric-nitric acid mixture composition on surface chemistry and structural evolution of liquid-phase oxidised carbon nanotubes, *J. Raman Spectrosc.* 43 (2012) 1432-1442.
- [26] O.A. Oyetade, V.O. Nyamori, B.S. Martincigh, S.B. Jonnalagadda, Effectiveness of carbon nanotube-cobalt ferrite nanocomposites for the adsorption of rhodamine B from aqueous solutions, *RSC Adv.* 5 (2015) 22724-22739.

- [27] I. Langmuir, The adsorption of gases on plane surfaces of glass, mica and platinum, *J. Am. Chem. Soc.* 40 (1918) 1361-1402.
- [28] The R Development Core Team, The R foundation for statistical Computing, R version 3.0.2 (2013).
- [29] S.A. Khan, M.A. Khan, Adsorption of chromium (III), chromium (VI) and silver (I) on bentonite, *Waste Manage.* 15 (1995) 271-282.
- [30] T.K. Naiya, A.K. Bhattacharya, S. Mandal, S.K. Das, The sorption of lead (II) ions on rice husk ash, *J. Hazard. Mater.* 163 (2009) 1254-1264.
- [31] K.K. Choy, J.F. Porter, G. McKay, Langmuir isotherm models applied to the multicomponent sorption of acid dyes from effluent onto activated carbon, *J. Chem. Eng. Data* 45 (2000) 575-584.
- [32] O.A. Oyetade, V.O. Nyamori, B.S. Martincigh, S.B. Jonnalagadda, Nitrogen-functionalised carbon nanotubes as a novel adsorbent for the removal of Cu(II) from aqueous solution, (unpublished results).
- [33] W.-T. Tsai, C.-W. Lai, T.-Y. Su, Adsorption of bisphenol-A from aqueous solution onto minerals and carbon adsorbents, *J. Hazard. Mater.* B134 (2006) 169-175.
- [34] G. Cevc, Partition coefficient vs. binding constant: How best to assess molecular lipophilicity, *Eur. J. Pharm. Biopharm.* 92 (2015) 204-215.
- [35] T. Scheytt, P. Mersmann, R. Lindstadt, T. Heberer, 1-Octanol/water partition coefficients of 5 pharmaceuticals from human medical care: Carbamazepine, clofibrac acid, diclofenac, ibuprofen, and propyphenazone, *Water Air Soil Pollut.* 165 (2005) 3-11.
- [36] S. Borrirukwisitsak, H.E. Keenan, C. Gauchotte-Lindsay, Effects of salinity, pH and temperature on the octanol-water partition coefficient of bisphenol A, *Int. J. Environ Sci. Dev.* 3 (2012) 460-464.
- [37] C. Jung, J. Park, K.H. Lim, S. Park, J. Heo, N. Her, J. Oh, S. Yun, Y. Yoon, Adsorption of selected endocrine disrupting compounds and pharmaceuticals on activated biochars, *J. Hazard. Mater.* 263 (2013) 702-710.
- [38] C. Jung, A. Son, N. Her, K.-D. Zoh, J. Cho, Y. Yoon, Removal of endocrine disrupting compounds, pharmaceuticals, and personal care products in water using carbon nanotubes: A review, *J. Ind. Eng. Chem.* 27 (2015) 1-11.
- [39] C.A. Staples, P.B. Dome, G.M. Klecka, S.T. Oblock, L.R. Harris, A review of the environmental fate, effects, and exposures of bisphenol A, *Chemosphere* 36 (1998) 2149-2173.
- [40] H. Guedidi, L. Reinert, Y. Soneda, N. Bellakhal, L. Duclaux, Adsorption of ibuprofen from aqueous solution on chemically surface-modified activated carbon cloths, *Arabian J. Chem.* (2014) In Press.

- [41] M.I. Bautista-Toledo, J. Rivera-Utrilla, R. Ocampo-Pérez, F. Carrasco-Marín, M. Sánchez-Polo, Cooperative adsorption of bisphenol-A and chromium(III) ions from water on activated carbons prepared from olive-mill waste, *Carbon* 73 (2014) 338-350.
- [42] S.J. Allen, G. McKay, J.F. Porter, Adsorption isotherm models for basic dye adsorption by peat in single and binary component systems, *J. Colloid Interface Sci.* 280 (2004) 322-333.
- [43] Y. Zhu, J. Hu, J. Wang, Competitive adsorption of Pb (II), Cu (II) and Zn (II) onto xanthate-modified magnetic chitosan, *J. Hazard. Mater.* 221 (2012) 155-161.

Chapter 10

Effectiveness of carbon nanotube/cobalt ferrite nanocomposites for the adsorption of rhodamine B from aqueous solutions

Oluwaseun A. Oyetade, Vincent O. Nyamori,* Bice S. Martincigh and Sreekantha B. Jonnalagadda

School of Chemistry and Physics, University of KwaZulu-Natal, Westville Campus,
Private Bag X54001, Durban 4000, South Africa

*Corresponding author: Tel: +27 31 260 8256; Fax: +27 31 2603091; E-mail:
nyamori@ukzn.ac.za

Abstract

The efficiency of adsorption of rhodamine B (RhB) from aqueous solution was investigated through a series of batch experiments by using cobalt ferrite nanoparticles (CoFe_2O_4), acid-functionalized multiwalled carbon nanotubes (MWCNT-COOH) and carbon nanotube-cobalt ferrite nanocomposites. The adsorption capacity was evaluated as a function of pH, contact time, adsorbent dose, dye concentration and temperature. The effect of increasing the percentage of MWCNT-COOH in the nanocomposites was also studied. The adsorption capacity was lowest in CoFe_2O_4 (5.165 mg g^{-1}) and highest with MWCNT-COOH (42.68 mg g^{-1}). For the nanocomposites, the adsorption capacity was enhanced with an increase in the amount of MWCNT-COOH. The optimum pH for adsorption was observed at 7 at which equilibrium was reached after 360 min. The kinetics of adsorption was fitted to the pseudo-first order, pseudo-second order, Elovich and intraparticle diffusion models. The results showed that the pseudo-second order model best described the data as reflected in the lowest value for the sum of squared residuals. Among the various adsorption isotherms tested, the Langmuir isotherm provided the best fit to the equilibrium data. The thermodynamic parameters, ΔH° , ΔS° and ΔG° , were obtained over a temperature range of 20-45 °C. Adsorption was spontaneous, endothermic and entropy-driven, except for one of the doped nanocomposites for which adsorption was exothermic. A good desorption of RhB from the loaded adsorbents was obtained by using either acetone or ethanol with a desorption efficiency in the range of 62-95%.

Keywords: Multiwalled carbon nanotubes, cobalt ferrite nanoparticles, nanocomposites, adsorption, wastewater, rhodamine B

10.1. Introduction

Treatment of wastewater generated from textile manufacturing, printing and dyeing is a major environmental problem due to the presence of dissolved dye materials. Rhodamine B (RhB) is a basic red cationic dye, usually used for commercial and industrial applications. The indiscriminate discharge of RhB-contaminated effluents into aqueous media introduces man, aquatic life and the environment to potentially harmful effects, ranging from minor irritations to major diseases.¹⁻³ Water, which makes up about 70% of the earth's surface, is a principal recipient of the discharge of organic and inorganic pollutants. Since freshwater is a limited resource, the remediation of wastewater before its disposal is of major importance. Several techniques, such as coagulation,^{4,5} chemical oxidation,⁶⁻⁸ photochemical,^{9,10} membrane separation and ion exchange,¹¹ irradiation,¹² decolourization by white fungi,¹³ ozonation,^{14,15} electrochemical destruction^{16,17} and aerobic/anaerobic microbial degradation,^{2,7} have been proposed for dye remediation in wastewater. In spite of the availability of these methods, steep challenges, such as sludge generation, high usage of energy, generation of dissolved oxygen, longer retention time,² release of aromatic compounds, formation of by-products, high operation costs and operation difficulty, are characteristic of these processes.¹

Adsorption has been considered ideal for the removal of pollutants from the environment because it is economically feasible and time-saving with easy operation. Also, adsorbents exhibit high pollutant removal efficiency and are easily regenerated/reused.¹⁸ Due to these facts, many studies have been tailored towards the removal of pollutants with this technique. Materials such as activated carbon,¹⁹ bagasse,²⁰ peanut hull,²¹ charcoal,³ hydrogels,²² clay,²³ organomontmorillonites,²⁴ fly ash,²⁵ red mud,²⁶ kaolinite,²⁷ leaves,²⁸ dimethyl terephthalate,²⁹ resin,³⁰ chestnut³¹ and fruit waste^{32,33} have been used for the removal of dyes from wastewater. However, limitations such as cost, loss of adsorption efficiency after regeneration, slow sorption and inconveniences encountered during separation are recognizable facts.

For these reasons, magnetic separation has been used as a preferred method for the removal of pollutants because it is easy, suitable for bulk solutions in heterogeneous systems and serves as a fast method of separation under external magnetic fields. Magnetic nanoparticles are considered potential adsorbents for aqueous pollutants due to the high surface area³⁴ possessed by these materials. Several nanoparticles, such as nickel ferrites,³⁴ maghemite,³⁵ and magnetite,³⁶ among others, have been proposed for effective removal of dyes in aqueous solution.

Since the discovery of carbon nanotubes (CNTs),³⁷ they have emerged as an adsorbent of interest for the removal of organic and/or inorganic pollutants from the environment.^{38,39} CNTs possess tubular nanostructures with unique mechanical, physical, chemical and electrical properties,³⁸ and possess large surface areas in addition to their layered structures.⁴⁰ Due to their hydrophobicity, they are usually oxidized with acids to improve dispersion in water. Modification of CNTs to attach acidic groups has been attempted through both chemical and physical methods.⁴¹ Chemical functionalization with acids causes shortening and thinning of tubes, and introduces polar functional groups such as -COOH and -OH on the tips or side-walls of CNTs.⁴² This process helps in improving electrostatic interaction for removal of organic and/or inorganic pollutants onto CNTs. The use of CNTs as adsorbents for removal of pollutants such as heavy metals,^{18,43} polychlorinated biphenyls (PCBs)⁴⁴ and trihalomethane,³⁹ among many others, has also been explored.

Magnetic nanocomposites often allow easy separation of adsorbents from an aqueous phase by means of an external magnetic field.³⁴ This process overcomes the limitation of separation often encountered when using CNTs.

In this study, we investigated the ability of cobalt ferrite nanoparticles (CoFe_2O_4) and functionalized multiwalled carbon nanotubes (MWCNT-COOH) to adsorb a representative dye, RhB, from aqueous solution. This particular dye was chosen for adsorption due to its toxic nature and wide use in industry, and the fact that its behaviour is similar to that of other dyes in its class. In addition, nanocomposites containing varying ratios of MWCNT-COOH and CoFe_2O_4 were synthesized and tested for RhB removal. The effect of increasing percentages of MWCNT-COOH in the nanocomposites was studied to determine the effect on the removal efficiency and to understand the processes/interactions involved in dye removal. To the best of our knowledge, no previous study has shown the effect of increasing concentrations of CNTs on CoFe_2O_4 for the removal of anthropogenic dyes. Batch adsorption processes involving the effect of pH, adsorbent dose, contact time, initial dye concentration and temperature were investigated to determine the optimum conditions necessary for RhB removal from aqueous solution. Studies on desorption of the dye were also performed to assess the durability, reusability and regeneration of the adsorbents.

10.2. Experimental

10.2.1. Chemicals

Pristine multiwalled carbon nanotubes (MWCNTs) (purity > 95 wt%) synthesized by chemical vapour deposition (CVD) were purchased from Cheap Tubes Inc. (Brattleboro,

USA). The length of the MWCNTs ranged from 10 to 20 μm , with an average length of 17 μm . Their outer diameters fell between 30 to 50 nm, with an average outer diameter of 39 nm. Nitric (55%), sulfuric (98%) and hydrochloric (32%) acids were purchased from C C Imelmann Ltd (Robertsham, South Africa). Rhodamine B was purchased from Coleman & Bell Co. (Norwood, USA) while $\text{Fe}(\text{NO}_3)_3 \cdot 9\text{H}_2\text{O}$, NaOH, and $\text{Co}(\text{NO}_3)_2 \cdot 6\text{H}_2\text{O}$ were purchased from Merck Chemicals Ltd (Gauteng, South Africa).

10.2.2. Preparation of cobalt ferrite nanoparticles

Cobalt ferrite nanoparticles were prepared by the co-precipitation method as reported by Maaz *et al.*⁴⁵ Solutions of $2 \text{ mol dm}^{-3} \text{Fe}(\text{NO}_3)_3 \cdot 9\text{H}_2\text{O}$ and $1 \text{ mol dm}^{-3} \text{Co}(\text{NO}_3)_2 \cdot 6\text{H}_2\text{O}$ were prepared, and 25 cm^3 of each solution were mixed and stirred under an inert atmosphere of nitrogen for 30 min. The pH of the resulting solution was then adjusted by the addition of $6 \text{ mol dm}^{-3} \text{NaOH}$ to attain the desired pH range of 10–13. The mixture was stirred further for another 1 h under inert conditions. The resulting solid was filtered, and washed first with ethanol, and then with deionised water until a neutral pH was obtained.

10.2.3. Preparation of functionalized multiwalled carbon nanotubes

Pristine MWCNTs (1.5 g) were placed in a round-bottomed flask to which 100 cm^3 of concentrated hydrochloric acid (32%) was added to remove metallic impurities from the tubes by dissolution. The suspension was stirred for 2 h; the tubes were filtered and washed with deionised water until a neutral pH was obtained. The MWCNTs were dried in a vacuum oven at $80 \text{ }^\circ\text{C}$ overnight. The purified MWCNTs were functionalized by using a mixture of concentrated sulfuric and nitric acids in a volume ratio of 1:3 and refluxed at $80 \text{ }^\circ\text{C}$ for 12 h. The resulting solution was diluted with deionised water, filtered and the tubes washed with deionised water until a neutral pH was obtained.⁴⁶

10.2.4. Preparation of composite samples (MWCNT-COOH-CoFe₂O₄)

MWCNT-COOH (1.5 g) were placed in 100 cm^3 of deionised water and stirred under an inert atmosphere of nitrogen for 30 min. Solutions of $2 \text{ mol dm}^{-3} \text{Fe}(\text{NO}_3)_3 \cdot 9\text{H}_2\text{O}$ and $1 \text{ mol dm}^{-3} \text{Co}(\text{NO}_3)_2 \cdot 6\text{H}_2\text{O}$ were prepared and an aliquot of 25 cm^3 of each solution was added to the CNT suspension. The mixture was continuously stirred at room temperature for 1 h. The suspension was then conditioned to a pH of 10 with the addition of $6 \text{ mol dm}^{-3} \text{NaOH}$ solution, and allowed to stir at room temperature for another hour. The mixture was filtered, the solid washed with ethanol and subsequently with deionised water until a neutral pH was obtained.⁴⁵ The samples were dried at $80 \text{ }^\circ\text{C}$ in a vacuum oven overnight. Nanocomposites of varying percentages were prepared and labelled as MWCNT-CoFe₂O₄-29%, MWCNT-CoFe₂O₄-50% and MWCNT-CoFe₂O₄-75%. Details of the compositions and sample identification are shown in Table 10.1.

Table 10.1: Adsorbent composition/identification

Sample Identifier	% Composition by mass	
	CoFe ₂ O ₄	MWCNT-COOH
CoFe ₂ O ₄	100	0
29%	71	29
50%	50	50
75%	25	75
MWCNT-COOH	0	100

10.2.5. Characterization of adsorbents

The specific surface area of the CNTs was determined with nitrogen as the flow gas by means of a Micromeritics Tristar II 3020 surface area and porosity analyser. Data were captured and analysed by using Tristar II 3020 version 2 software. Characterization of synthesized materials was done with a transmission electron microscope (TEM) (JEOL, TEM 1010) and a high resolution transmission electron microscope (HRTEM) (JEOL, TEM 2100) to visualize the morphology, and to determine the shape and mean particle size. Images were captured by means of a Megaview 3 camera and analysed on iTEM software. Gatan digital micrograph software was used in analysing images obtained from HRTEM. Fourier transform infrared (FTIR) spectrometry (Perkin Elmer Spectrum RX 1 spectrometer) was used to characterize the surface functionalities on adsorbents by incorporating the materials in a KBr disc. Raman spectroscopy (DeltaNu Advantage 532TM) measurements were performed to provide information on the purity and crystallinity of adsorbents.

10.2.5.1. Determination of point of zero charge (pH_{PZC})

Aliquots of 50 cm³ of 0.01 mol dm⁻³ NaCl solutions were measured into bottles and adjusted with the addition of appropriate amounts of 0.1 mol dm⁻³ HCl or NaOH to obtain an initial pH in the range of 1-10. A mass of 100 mg of adsorbent was added into each bottle and the suspension left to equilibrate on an orbital shaker for 48 h. The solutions were filtered and the final pH of the filtrates determined. A plot of pH_{initial} – pH_{final} against pH_{initial} was obtained and the point of intersection of the curves gave the pH_{PZC} of the adsorbent.³¹

10.2.6. Adsorbate preparation

The dye (RhB) used in this study was of analytical grade and used without further purification. A calibration curve was obtained from dye solutions ranging from 1 to 7 mg dm⁻³ at a wavelength of maximum absorption (λ_{\max}) of 554 nm (Fig A-VII.1, Appendix VII) by means of a UV-vis-NIR spectrophotometer (Shimadzu, UV-3600). The concentration of RhB in samples was determined by using the calibration curve prepared. A stock solution

of RhB was prepared by accurately weighing 1 g of the pure powder to make a solution containing 1 g dm^{-3} RhB in deionised water.

10.2.7. Batch adsorption procedure

Freshly prepared working solutions of RhB were prepared from the stock solution to obtain the required concentrations. The pH values of solutions were adjusted by adding an appropriate amount of 0.1 mol dm^{-3} NaOH or HNO_3 to obtain the desired pH. Adsorption studies were carried out by agitating 25 cm^3 of a known concentration of RhB solution with 50 mg of adsorbent at a fixed temperature ($20 \text{ }^\circ\text{C}$) for 24 h in stoppered glass bottles. The mixtures were filtered by gravity, and the final concentration of RhB in the filtrate was determined at 554 nm (λ_{max} of RhB) by means of ultraviolet-visible (UV-vis) spectrophotometry. The effect of pH, adsorbent dose, temperature and initial RhB concentration were studied for each adsorbent to determine the optimum conditions necessary for adsorption. The adsorption efficiency (% adsorbed) and adsorption capacity (q_e) were calculated by using equations 10.1 and 10.2 respectively.

$$\% \text{ adsorbed} = \left(\frac{C_i - C_{eq}}{C_i} \right) \times 100 \quad (10.1)$$

$$q_e = \left(\frac{C_i - C_{eq}}{m} \right) \times V \quad (10.2)$$

where C_i is the initial RhB concentration (mg dm^{-3}), C_{eq} is the equilibrium concentration of RhB (mg dm^{-3}), q_e is the adsorption capacity (mg g^{-1}), m is the mass (mg) of the adsorbent and V is the volume (dm^3) of the adsorbate solution used.

10.2.7.1. Kinetics studies

Kinetics studies were investigated by contacting 25 cm^3 of 100 mg dm^{-3} RhB solution with 50 mg of adsorbent at pH 7 in stoppered glass bottles. The solutions were agitated in a thermostated shaking water bath at $20 \text{ }^\circ\text{C}$ for different time intervals in the range of 5-1440 min. After the pre-determined time intervals, the samples were filtered and the final concentrations of RhB determined spectrophotometrically. The experimental adsorption data were applied to the pseudo-first order, pseudo-second order, intraparticle diffusion and Elovich kinetics models given in Table 10.2.

Table 10.2: Kinetics models investigated for the adsorption of RhB onto CoFe₂O₄, MWCNT-COOH, and CNT-CoFe₂O₄ composites

Model	Equation [†]	Parameters	References
Pseudo-first order	$q_t = q_{eq}(1 - e^{-k_1 t})$	q_{eq}, k_1	59, 78, 79
Pseudo-second order	$q_t = \frac{k_2 q_{eq}^2 t}{1 + k_2 q_{eq} t}$	k_2, q_{eq}	60, 78, 79
Elovich	$q_t = \frac{1}{\beta} \ln(\alpha\beta) + \frac{1}{\beta} \ln t$	α, β	62
Intraparticle diffusion	$q_t = k_{id} \sqrt{t} + l$	k_{id}, l	61

[†] q_t , quantity of adsorbate adsorbed at time t (mg g^{-1}); q_{eq} , quantity of adsorbate adsorbed at equilibrium (mg g^{-1}); α , adsorption rate constant ($\text{mg g}^{-1} \text{min}^{-1}$); β , desorption rate constant (g mg^{-1}); k_1 , pseudo-first order rate constant (min^{-1}); k_2 , pseudo-second order rate constant ($\text{g mg}^{-1} \text{min}^{-1}$); k_{id} , intraparticle diffusion rate constant ($\text{mg g}^{-1} \text{min}^{0.5}$); l , is a constant related to the boundary layer thickness (mg g^{-1}).

10.2.7.2. Adsorption isotherms

Solutions of RhB with initial concentrations ranging from 10-100 mg dm^{-3} were prepared at a constant pH of 7. Aliquots of 25 cm^3 were mixed with 50 mg of the adsorbent and agitated in a thermostated shaking water bath at 20-45 °C for 24 h in stoppered glass bottles. The solutions were filtered and the concentrations of RhB in the filtrates determined spectrophotometrically. The experimental adsorption equilibrium data were analysed by the adsorption models given in Table 10.3.

Table 10.3: Isotherm models investigated for the adsorption of RhB onto CoFe₂O₄, MWCNT-COOH, and CNT-CoFe₂O₄ composites

Isotherm model	Equation [†]	Parameters	References
Langmuir	$q_{eq} = \frac{q_m b C_{eq}}{1 + b C_{eq}}$	q_m, b	67
Freundlich	$q_{eq} = K_F C_{eq}^{1/n}$	K_F, n	66
Temkin	$q_{eq} = \frac{RT}{b_T} \ln(A_T C_{eq})$	b_T, A_T	68
Dubinin-Radushkevich	$q_{eq} = q_m e^{-\beta \varepsilon^2}$ $\varepsilon = RT \ln \left(1 + \frac{1}{C_{eq}} \right)$	q_m, β	69
Sips	$q_{eq} = \frac{b q_m C_{eq}^{1/n}}{1 + b C_{eq}^{1/n}}$	q_m, b, n	70
Toth	$q_{eq} = \frac{q_m C_{eq}}{\left(\frac{1}{K_T} + C_{eq}^{n_T} \right)^{1/n_T}}$	q_m, K_T, n_T	73
Redlich-Peterson	$q_{eq} = \frac{K_{RP} C_{eq}}{1 + a_{RP} C_{eq}^g}$	K_{RP}, a_{RP}, g	72
Khan	$q_{eq} = \frac{q_m b_K C_{eq}}{(1 + b_K C_{eq})^{a_K}}$	q_m, a_K, b_K	71

[†] q_{eq} , adsorption capacity (mg g⁻¹); C_{eq} , equilibrium concentration of adsorbate in solution (mg dm⁻³); q_m , maximum monolayer capacity (mg g⁻¹); b , Langmuir isotherm constant (dm³ mg⁻¹); K_F , Freundlich isotherm constant (mg g⁻¹)(dm³ mg⁻¹)ⁿ; n , adsorption intensity; b_T , Temkin isotherm constant; A_T , Temkin isotherm equilibrium binding constant (dm³ g⁻¹); β , Dubinin-Radushkevich isotherm constant (mol² kJ⁻²); K_t , Toth isotherm constant (mg g⁻¹); n_T , Toth isotherm constant; K_{RP} , Redlich-Peterson isotherm constant (dm³ g⁻¹); a_{RP} , Redlich-Peterson isotherm constant; g , Redlich-Peterson isotherm exponent; a_k , Khan isotherm exponent; b_k , Khan isotherm constant.

10.2.7.3. Desorption experiments

Desorption studies were investigated by first contacting aliquots of 25 cm³ of 100 mg dm⁻³ RhB solution with 50 mg of adsorbent. The solutions were agitated on a thermostated shaking water bath at 20 °C for 24 h. After agitation, the solutions were filtered and the equilibrium concentration of RhB in the filtrates was determined. The RhB-loaded adsorbent was dried in a vacuum oven at 80 °C. The 50 mg of the RhB-loaded adsorbent was weighed and subsequently agitated with either a 10 cm³ aliquot of acetone or ethanol for 30 min. The final concentration of RhB desorbed was then obtained from the filtrates collected.

10.2.8. Data Analysis

Experimental data were fitted to the kinetics and isotherm models by means of the nls nonlinear regression routine in the R statistical computing environment.⁴⁷ In the case of all

models chosen, an examination of the residuals was performed in order to assess the adequacy of the model.

10.3. Results and discussion

The adsorbents synthesized were characterized by a number of different techniques to confirm that the materials obtained would be effective for adsorption. A comparison of the efficiency of these adsorbents for RhB removal was investigated at varying conditions by means of batch adsorption experiments.

10.3.1. Characterization of adsorbents

The FTIR study of acid-functionalized CNTs (MWCNT-COOH) confirmed the presence of C=C, C=O, CH₂, C-O and O-H functional groups, demonstrating the successful introduction of O-containing groups on the tubes (Fig. 10.1). As reported by Buang *et al.*,⁴⁸ O-H and C=O functional groups are usually produced after oxidation of pristine MWCNTs. The peaks at 3200 cm⁻¹ (O-H stretching mode), 1635-1700 cm⁻¹ (C=O stretching mode), 1452-1600 cm⁻¹ (C=C stretching mode), and 2200-2500 cm⁻¹ (oxygen containing groups such as lactonic and anhydride groups), are evidence of functionalization of MWCNTs.³⁶ These peaks remained present in the spectra of the nanocomposites containing MWCNT-COOH. Fig. 10.1 further shows the FTIR spectra of the CoFe₂O₄ nanoparticles and CNT-CoFe₂O₄ nanocomposites. The spectra of the CoFe₂O₄ nanoparticles were observed to show sharp intense peaks at 560 cm⁻¹ which are usually associated with metal-oxygen (Fe(Co)-O) stretching vibrations in the ferrite lattice which is in agreement with previously published data.^{36,49,50} These peaks, at about 560 cm⁻¹, remained present in composites, although a shift in the Fe(Co)-O peaks to higher wavenumber was noticed. The shift could be attributed to interactions between the ferrites and MWCNT-COOH through O-containing functional groups.³⁶ The presence of these peaks demonstrates that nanocomposites containing MWCNT-COOH and ferrites were successfully synthesized. The intensity of the Fe(Co)-O stretching vibrations was noticed to decrease as the percentage of MWCNT-COOH increased in composites. This indicates that the percentage of the more abundant material determines the intensity of the peaks obtained in the FTIR spectra.

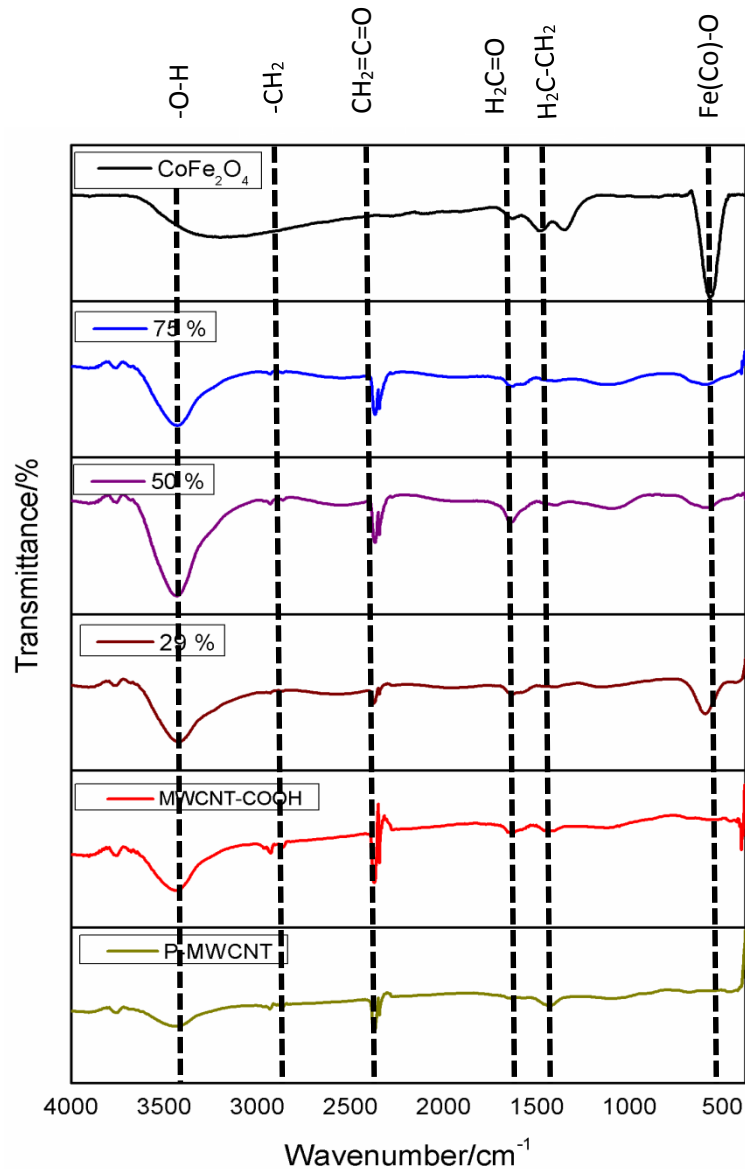


Fig. 10.1: FTIR spectra of pristine-MWCNT, MWCNT-COOH, CoFe_2O_4 and CNT- CoFe_2O_4 nanocomposites.

To observe the structure and size distribution of the nanomaterials produced, images were collected from TEM and HRTEM. Fig. 10.2 shows HRTEM images of (a) MWCNT-COOH, (b) CoFe_2O_4 nanoparticles and (c) 29% composite, while Fig. 10.3 shows TEM images of (a) 29% and (b) 75% nanocomposites at the same magnification. It was observed that the tubular-shaped structure characteristic of MWCNTs was preserved after functionalization was carried out (Fig 10.2a), however, functional groups such as $-\text{COOH}$ are not usually visible on HRTEM micrographs. Uniform cubic-shaped materials were obtained for the CoFe_2O_4 nanoparticles with a high degree of agglomeration as demonstrated with arrows in Fig. 10.2b. Similarly, a high degree of agglomeration of CoFe_2O_4 nanoparticles was noticed on the sides of tubes. The tubular structure of CNTs was also

preserved for all synthesised nanocomposites (see Fig. 10.3). It was also noticed that the amount of agglomerated CoFe_2O_4 nanoparticles reduces as the percentage of MWCNT-COOH increases in the composites (Fig 10.3a vs 10.3b). Similar trends have been reported for ferrites⁵¹ and magnetic carbon nanotubes^{49,52} in previous studies. This therefore demonstrates that nanocomposites containing MWCNTs and CoFe_2O_4 nanoparticles were successfully synthesized, since the cubic shape of ferrites and the tubular structures of MWCNTs were preserved in the nanocomposites.

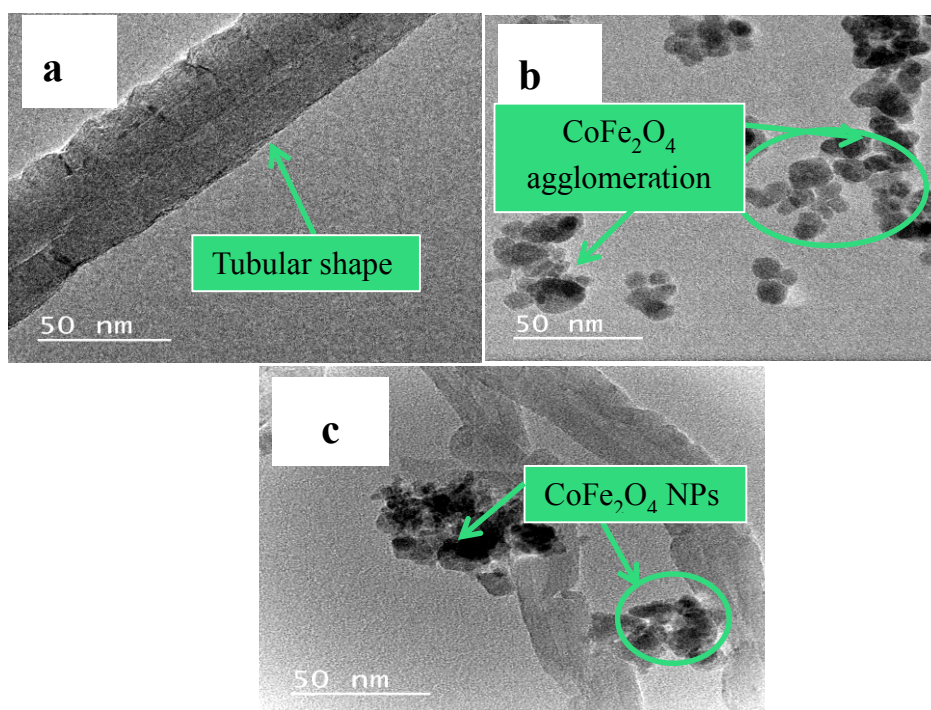


Fig. 10.2: HRTEM images of (a) MWCNT-COOH, (b) CoFe_2O_4 nanoparticles and (c) 29% MWCNT-COOH- CoFe_2O_4 nanocomposites.

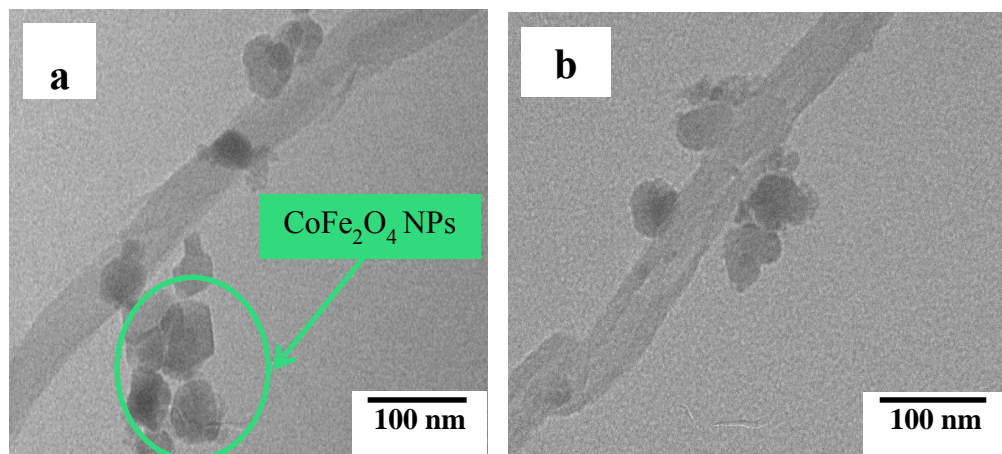


Fig. 10.3: TEM images of (a) 29% and (b) 75% MWCNT-COOH-CoFe₂O₄ nanocomposites.

The surface area and porosity of nanomaterials is usually obtained by applying the Brunauer, Emmett and Teller (BET) and the Barrett-Joyner-Halenda (BJH) theories respectively. CoFe₂O₄ nanoparticles and CNTs have been reported to have moderately large surface areas.^{34,46,53} and is confirmed in this work as demonstrated in entries 1 and 2 of Table 10.4. Oxidation of purified MWCNTs with acids introduces defects and shortening of tubes, thereby increasing the surface area of MWCNT-COOH.^{41,54} The extent of disorder/defects and crystallinity of MWCNTs was evaluated with the use of Raman spectroscopy. The most characteristic peaks usually observed are the D band (1350 cm⁻¹) and G band (1580 cm⁻¹). The D band (I_D) gives information on the disorder-induced modes and defects in the graphene sheets at the walls of the tubes, while the G band (I_G) gives information on the crystalline graphitic arrangement on the MWCNTs.⁵⁵ The relative intensity ratio of the bands (I_D/I_G) was calculated. A larger ratio indicates a greater disruption of the sp² hybridized atoms to the sp³ hybridized atoms, hence, interpreted as a high defect/deformation occurring on the walls/sides of the tubes.⁵⁴ Raman spectroscopic measurements performed on the MWCNTs indicate that the I_D/I_G ratio increased after functionalization with acids (entry 3 vs 2, Table 10.4). This could be due to the fact that oxidation of MWCNTs increases the defects and decreases the graphitic structure of the tubes resulting in a larger I_D/I_G ratio being obtained.^{41,46,54} An increase in the surface area of MWCNT-COOH to 126.8 m² g⁻¹ was measured after functionalization (entry 3 vs 2 of Table 10.4). A further increase in the surface area of the adsorbents was achieved by preparing composites containing varying percentages of CoFe₂O₄ and MWCNT-COOH. An increase in the surface area of nanocomposites synthesized from MWCNTs and iron nanoparticles was similarly reported by Gong *et al.*⁵⁶ It was further observed that the BET surface area, pore volume and pore diameter of the composites increased with an increase in the MWCNT-COOH content (entries 4-6, Table 10.4). The pore volume of these materials

was noticeably increased from 0.40 to 1.16 cm³ g⁻¹ which could further aid in the availability of more active sites. Hence, the materials produced in this study possess moderately large surface areas with reasonable pore volumes and should exhibit good adsorption properties.

Table 10.4: Textural characteristics of adsorbents.

Entry	Adsorbent	Surface area/m ² g ⁻¹	Pore volume/cm ³ g ⁻¹	Pore diameter/nm	I _D /I _G	pH _{PZC}
1	CoFe ₂ O ₄	116.4	0.158	4.568	-	7.00
2	Pristine-MWCNTs	108.8	0.494	18.44	1.17	5.04
3	MWCNT-COOH	126.8	0.692	22.95	1.19	4.02
4	29%	128.1	0.400	10.98	0.22	6.20
5	50%	140.0	0.544	14.87	0.35	6.16
6	75%	293.4	1.160	16.89	0.83	4.50

10.3.2. Batch adsorption experiments

The adsorption of RhB by CoFe₂O₄, MWCNT-COOH and CNT-CoFe₂O₄ nanocomposites was investigated for the efficient remediation of polluted wastewater. The adsorption capacity of the adsorbents was compared to determine the adsorbent with the best efficiency for RhB removal. Factors such as pH, contact time, initial RhB concentration, adsorbent dose and temperature were varied in order to attain the optimum conditions for RhB adsorption. Desorption studies for all the adsorbents were also carried out to examine the feasibility of regenerating the used adsorbents for further use.

10.3.2.1. Effect of pH

The pH of a solution can affect the surface charge on a particular adsorbent and the charge of the adsorbate.²⁷ The influence of pH on adsorbents was investigated by agitating a known concentration of RhB solution for 24 h with an adsorbent dose of 50 mg. The solutions were adjusted to obtain an initial pH value in the range of 1-10. Fig. 10.4 shows that the adsorption of RhB onto all adsorbents was greatly influenced by the pH of the solution. At low pH values, RhB is cationic and therefore adsorption onto the protonated adsorbents was minimal; however, an increase in efficiency was noticed as the solution was changed to basic. With increasing pH from 1.0 to 10.0, interactions between RhB and the negatively charged surface groups on the adsorbents increased, with optimum conditions obtained at pH 6-8 for all adsorbents (Fig 10.4). At this pH, RhB assumes the quinonoid structure (i.e. it exists in the zwitterion form).⁵⁷ As stated by Salleha et al.,¹ cationic adsorption is favoured when the pH of the solution is greater than the point of zero charge (pH_{PZC}). This statement concurs with these results since as illustrated in Table 10.4; the pH_{PZC} values measured are lower than the optimum pH condition obtained for each adsorbent. This fact supports that

electrostatic interaction between the RhB zwitterion and the negatively charged surface of the adsorbents is responsible for adsorption. However, it is also worthy of note that with increasing pH the dissociation of the aromatic carboxylic acid group in RhB will increase as will deprotonation of the nitrogen groups, thereby increasing electrostatic repulsion between RhB and the negatively charged adsorbents. Fig 10.4 demonstrates this effect that an increase in the basicity of the solution (i.e. pH > 8) results in a decrease in adsorption capacity (q_e) of the adsorbents. Similar observations were reported by Annadurai *et al.*⁵⁸ and Zhang *et al.*²⁰ for RhB removal. This therefore suggests that adsorption is primarily influenced by electrostatic interaction between the RhB zwitterion and the adsorbents; however, other factors such as the molecular structure of the adsorbate might also influence adsorption.

The experimental data for the adsorption of RhB onto CoFe₂O₄, 29%, 50% nanocomposites and MWCNT-COOH as a function of pH is presented in Appendix VII.

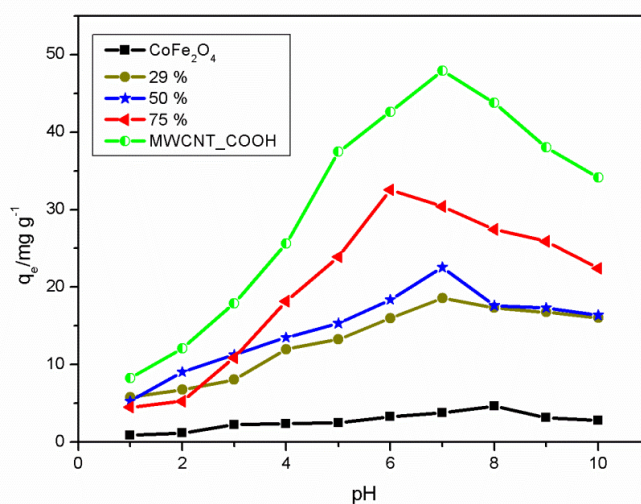


Fig. 10.4: Effect of pH on the adsorption of RhB [conditions: 25 cm³ of 100 mg dm⁻³ or 50 mg dm⁻³ RhB, 24 h equilibration time, 50 mg adsorbent dose, agitation speed 150 rpm, temperature 20 °C].

Although, the adsorption capacity was best for the MWCNT-COOH, in the case of the nanocomposites it was noticeably increased as the percentage of MWCNT-COOH increased. This could be as a result of the increase in the number of defects (as observed in the increasing I_D/I_G ratio shown in Table 10.4) and the presence of a greater number of oxygen-containing functional groups introduced by chemical oxidation of the MWCNTs. Both of these create more active sites for electrostatic interaction and hence enhance adsorption (Fig. 10.4). All further adsorption experiments were carried out at a pH value of

7, since this value falls within the optimum range for all the adsorbents considered in this work.

10.3.2.2. Effect of contact time

In order to obtain the contact time required to achieve equilibrium, the experimental investigation of the adsorption of RhB from aqueous solutions onto CoFe_2O_4 , MWCNT-COOH and CNT- CoFe_2O_4 nanocomposites was performed for different time intervals. Fig. 10.5 shows that the adsorption capacity (q_e) of RhB onto all adsorbents increases as the contact time increases. For all adsorbents, sorption was rapid in the first 360 min owing to the fact that more sites were available for adsorption on the adsorbents, creating room for fast interaction between the adsorbent and adsorbate. As the process continues, adsorption sites become limited and the rate of adsorption is influenced by the speed at which the adsorbates move from the external to the internal sites of the adsorbent particles. The faster it takes to reach equilibrium, the better an adsorbent is. It is noticed that as the time increases (beyond 360 min), adsorption reaches a state of equilibrium, hence, adsorption was seen to slow down at this time due to saturation of active sites on the adsorbents. It could therefore be said that the equilibrium time for all adsorbents in this study was achieved at 6 h. However, in this study, an equilibration time of 24 h was used to ascertain the complete removal of RhB under all conditions.¹⁸

The experimental data for the adsorption of RhB onto CoFe_2O_4 , 29%, 50% nanocomposites and MWCNT-COOH as a function of contact time is presented in Appendix VII.

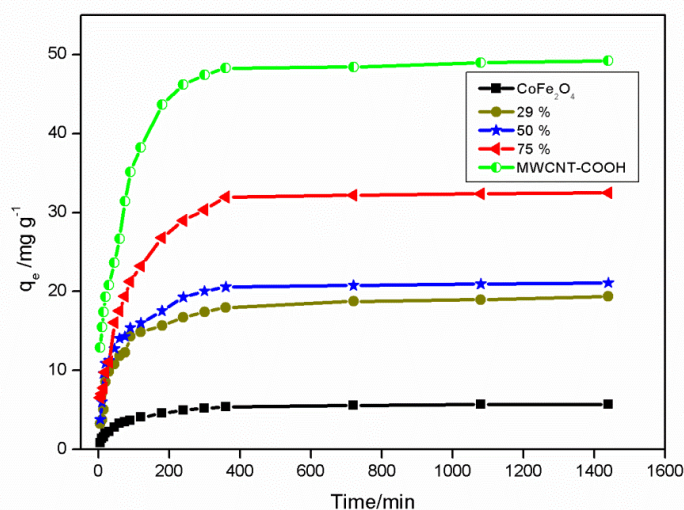


Fig. 10.5: Effect of contact time on the adsorption of RhB [conditions: 25 cm^3 of 100 mg dm^{-3} or 50 mg dm^{-3} RhB, 50 mg adsorbent dose, pH 7, agitation speed 150 rpm, temperature 20 $^\circ\text{C}$].

Fig. 10.5 further demonstrates that for the nanocomposites, the adsorption capacity was enhanced as the amount of MWCNT-COOH was increased. This is clearly explained by the fact that as the content of MWCNT-COOH in the composites increases; more negative sites are introduced, therefore favouring adsorption.

10.3.2.3. Adsorption kinetics

The mechanism and rate-determining step of adsorption of RhB onto CoFe₂O₄, CNT-CoFe₂O₄ nanocomposites and MWCNT-COOH was investigated by fitting the Lagergren pseudo-first order,⁵⁹ pseudo-second order,⁶⁰ intraparticle diffusion⁶¹ and Elovich models⁶² to the kinetics data. The equations for these models are given in Table 10.2. Adsorption usually occurs through four processes: diffusion of the adsorbate from the bulk solution onto the surface of the adsorbent, the passage of adsorbate through the liquid film attached to the surface of the adsorbent (film diffusion), diffusion of adsorbate through the pores of the adsorbent (intraparticle diffusion) and interaction of the adsorbate with the active sites on the adsorbent.¹⁸ The dependence of the model which best fits the experimental data was determined based on the model with lowest value for the sum of squared residuals (SSR) and the residual standard error (RSE). Based on these estimates, the kinetics data obtained were best described by the pseudo-second order model (Table 10.5). The model is based on the assumption that adsorption occurs through bimolecular interactions involving sharing or exchange of electrons between RhB and the adsorbent.

Considering that various mechanisms usually control adsorption kinetics, the intraparticle diffusion model was also utilized to explain the rate-limiting step of the process. A plot of q_e versus $t^{1/2}$ is usually indicative of the multistep-controlling processes of adsorption.³² Adsorption is assumed to proceed only through intraparticle diffusion if a linear plot which also passes through the origin is obtained. It is, however, assumed that the process is controlled by two or more steps if a linear plot which does not pass through the origin is obtained.⁶³⁻⁶⁵ Plots obtained from this study produced linear plots, which do not pass through the origin. Therefore, these results suggest that though adsorption proceeded *via* intraparticle diffusion, it was not the only rate-controlling step for the process. The plots further illustrate that the adsorption of RhB proceeded through transportation of RhB to the external surface of the adsorbent by film diffusion, followed by intraparticle diffusion of RhB to the pores of the adsorbent, and subsequently intraparticle diffusion slows down due to the low RhB concentration.⁶³⁻⁶⁵ Thus a multi-step process is involved. The intraparticle diffusion constant (k_{id}) and boundary layer (l) were obtained from the slope and intercept of the plots respectively. Data obtained for k_{id} and l show an increase with the addition of MWCNT-COOH to the composites (Table 10.5). These results demonstrate that adsorption was boundary-layer controlled for all adsorption processes. Increasing amounts of

MWCNT-COOH in the adsorbents resulted in an increase in the boundary thickness (l); hence resulting in higher adsorption capacities (q_e) obtained (Table 10.5).

Table 10.5: Kinetics parameters for adsorption of RhB [Conditions: 25cm³ of 100 mg dm⁻³ or 50 mg dm⁻³ RhB for CoFe₂O₄, MWCNT-COOH, 29%, 50% and 75% MWCNT-CoFe₂O₄ nanocomposites, pH 7.0, 50 mg of adsorbent, agitation speed 150 rpm, temperature 20 °C]

Model	Parameters	CoFe ₂ O ₄	29%	50%	75%	MWCNT-COOH
Experimental	$q_{meas}/\text{mg g}^{-1}$	5.673	19.40	21.08	32.49	49.19
Pseudo-first order	k_1/min^{-1}	-	-	-	0.014	0.017
	$q_{eq}/\text{mg g}^{-1}$	-	-	-	31.25	47.23
	RSE ^a	-	-	-	0.749	0.693
	SSR ^b	-	-	-	55.76	274.0
Pseudo-second order	$k_2/\text{g mg}^{-1} \text{min}^{-1}$	3.685	1.472	1.932	0.543	0.507
	$q_{eq}/\text{mg g}^{-1}$	5.877	19.43	20.86	34.61	51.26
	RSE	0.093	0.013	0.098	0.438	0.509
	SSR	0.453	6.870	14.28	25.63	146.2
Intraparticle diffusion	$k_{id}/\text{mg g}^{-1} \text{min}^{-0.5}$	0.223	0.767	0.859	1.282	1.994
	$l/\text{mg g}^{-1}$	0.659	0.719	0.893	2.804	7.086
	RSE	1.447	1.355	1.452	1.654	1.662
	SSR	33.48	473.7	703.2	1076	3213
Elovich	$\alpha/\text{mg g}^{-1} \text{min}^{-1}$	0.434	1.943	3.798	2.235	5.860
	$\beta/\text{g mg}^{-1}$	1.023	0.316	0.319	0.173	0.127
	RSE	0.287	0.926	1.038	1.432	2.033
	SSR	1.457	23.58	25.22	86.04	208.1

^aRSE - residual standard error, ^bSSR - sum of squared residuals

10.3.2.4. Effect of adsorbent dose

To evaluate the adsorption capacity for RhB, the mass of each adsorbent was varied from 30 to 400 mg. An increase in the adsorption capacity (q_e) was observed as the mass of adsorbent is increased (Fig. 10.6). In fact, it was observed that 100% removal efficiency was achieved for some adsorbents when the dose was increased to 400 mg. This is due to the fact that as the mass of adsorbent is increased, the surface area available for adsorption increases, thereby creating more active sites for adsorption. Table 10.4 demonstrates that the pore volume is lowest in CoFe₂O₄ and increases as more MWCNT-COOH content was added to the composites. The increase in the adsorption capacity (q_e) for the same mass of adsorbent (Fig. 10.6) could be as a result of the increase in pore volume which enabled greater removal of RhB as the MWCNT-COOH content is increased. Hence, surface area and pore volume of adsorbents plays a major role in enhancing the capacity of adsorbents in adsorption. However, adsorption was noticed to reach a constant value where further

adsorption becomes negligible with increase in adsorbent mass due to the limited amount of RhB available. Again, the amount of RhB adsorbed was in the same order as the percentage content of MWCNT-COOH.

The experimental data for the adsorption of RhB onto CoFe₂O₄, 29%, 50% nanocomposites and MWCNT-COOH as a function of adsorbent dose is presented in Appendix VII.

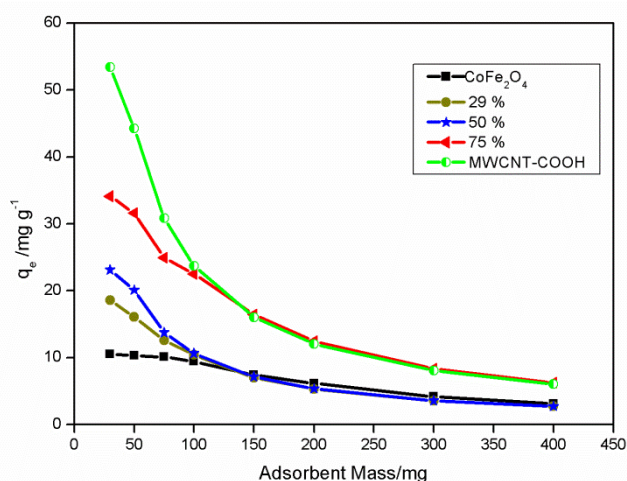


Fig. 10.6: Effect of adsorbent dose on the adsorption of RhB [conditions: 25 cm³ of 100 mg dm⁻³ or 50 mg dm⁻³ RhB, 24 h equilibration time, pH 7, agitation speed 150 rpm, temperature 20 °C].

10.3.2.5. Effect of initial RhB concentration

To effectively explain the increase in the activities (q_e) of each adsorbent, different concentration ranges with the same amount of adsorbent were used. Generally, it was observed that as the concentration of adsorbate increases, the adsorption capacity (q_e) increased for a fixed quantity of adsorbent while the percentage adsorption decreased. At low adsorbate concentrations, more active sites are available on the adsorbent; hence the removal efficiency is high. The increase in adsorption capacity with an increase in the initial concentration of adsorbate is as a result of an increase in the driving force due to the concentration gradient developed between the bulk solution and the surface of the adsorbent. However, at higher concentrations, the active sites of adsorbents become saturated with RhB molecules as the process continues. Hence, this process led to a decrease in the percentage adsorption and an increase in the uptake of the adsorbate (q_e) by the adsorbents as the concentration is increased.

10.3.2.6. Effect of temperature

The adsorption of RhB onto each adsorbent was investigated at 293, 303, 313 and 318 K. An increase in the adsorption capacity of RhB was observed with increase in temperature from 293 to 318 K for CoFe_2O_4 , and the 29% and 75% composites, and MWCNT-COOH (Fig 10.7 a-b, d-e). This indicates the endothermic nature of the adsorption process. As the temperature increases, the kinetic energy of the RhB molecules increases, resulting in enhancement of the rate of adsorption. Also, an increase in temperature could result in an increase in the pore volumes of the adsorbents, enabling an increase in the active sites available for adsorption.^{27,31} However, a marked difference was observed for the composite produced with a 50% dosage of MWCNT-COOH in CoFe_2O_4 . An exothermic adsorption process was observed for this adsorbent (see Fig. 10.7c), i.e. the extent of adsorption decreased with an increase in temperature.

The experimental data for the adsorption of RhB onto CoFe_2O_4 , 29%, 50% nanocomposites and MWCNT-COOH as a function of temperature is presented in Appendix VII.

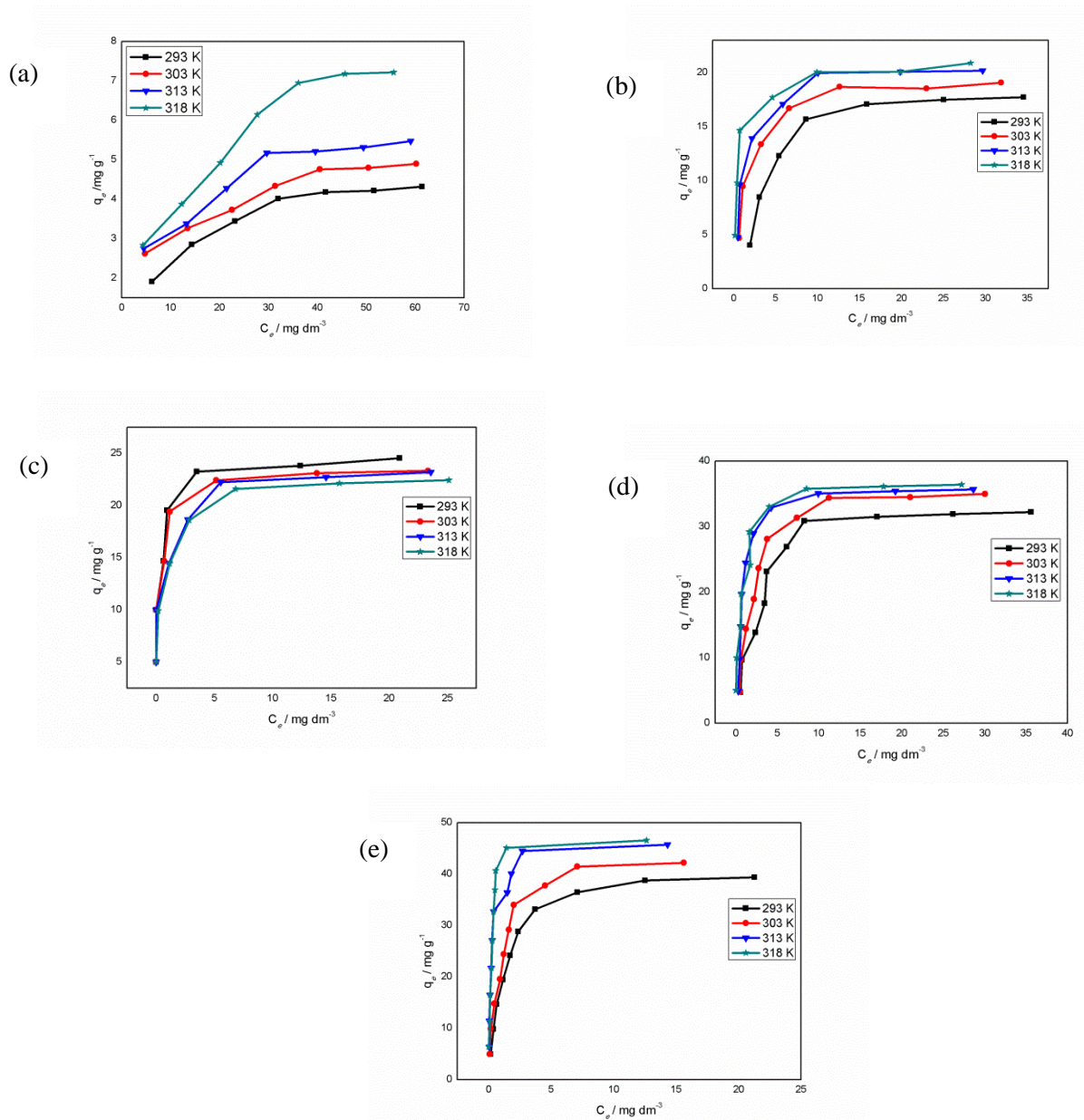


Fig 10.7: Effect of change in temperature on the adsorption of RhB (a) CoFe₂O₄, (b) 29%, (c) 50%, (d) 75% MWCNT-COOH-CoFe₂O₄ nanocomposites and (e) MWCNT-COOH [conditions: 25 cm³ of 100 mg dm⁻³ or 50 mg dm⁻³ RhB, 24 h equilibration time, pH 7, agitation speed 150 rpm, 50 mg adsorbent dose].

10.3.2.7. Adsorption isotherms

Isotherm models provide information on the capacity of adsorbents or the amount needed to remove a unit mass of pollutant under the same conditions. Eight models, including various two-parameter (Freundlich,⁶⁶ Langmuir,⁶⁷ Temkin,⁶⁸ Dubinin-Radushkevich⁶⁹) and three-parameter (Sips,⁷⁰ Khan,⁷¹ Redlich-Peterson,⁷² Toth⁷³) isotherms, were applied to the equilibrium data obtained. The equations of the tested models are given in Table 10.3. Tables 10.6-10.8 give the calculated isotherm parameters for all the models tested. The model which best describes the equilibrium data was chosen based on the lowest SSR value.

Table 10.9 summarizes the parameters of the models which best fit the equilibrium data obtained for each adsorbent. Results obtained indicated that the Langmuir isotherm, which assumes monolayer adsorption onto homogeneous surfaces with a finite number of identical adsorption sites,⁶⁷ is the best of the models considered for CoFe₂O₄, MWCNT-COOH and the 50% nanocomposite. Results further demonstrated that the Langmuir isotherm is the best of the two-parameter models considered and the Sips model, which is a combination of the Langmuir and Freundlich isotherms,⁷⁰ is the best of the three-parameter models for 29% and 75% MWCNT-CoFe₂O₄ nanocomposites. This implies that the uptake of RhB onto the active sites of the adsorbents occurs on uniform and equivalent sites, wherein there exists no interaction between adjacent adsorbate ions. The value of b (Table 10.9) gives an indication of the binding power (i.e. adsorptive strength) between adsorbent and adsorbates. An increase in adsorptive strength (b) was obtained with increasing amounts of MWCNT-COOH in the composites (Table 10.9). This further elucidates that strong interactions were formed between RhB and the adsorbents as the content of MWCNT-COOH increases.

Table 10.6: Isotherm parameters for the adsorption of RhB onto CoFe₂O₄ and 29% composite

Adsorbent	Isotherm	Parameters	Temperature/K				Adsorbent	Temperature/K			
			293 K	303 K	313 K	318 K		293 K	303 K	313 K	318 K
CoFe ₂ O ₄							29%				
	Langmuir	q_m	5.165	5.289	6.102	7.950		21.17	20.24	21.32	20.60
		b	0.092	0.154	0.134	0.103		0.222	0.652	0.846	2.401
		RSE ^a	0.738	0.909	1.004	0.746		1.464	0.849	1.116	0.923
		SSR ^b	0.053	0.454	0.642	3.602		10.71	3.608	6.230	5.111
	Freundlich	K_F	1.120	1.688	1.782	1.981		6.345	9.189	10.25	12.22
		n	3.080	3.753	3.512	3.207		3.126	4.220	4.341	5.868
		RSE	0.425	2.302	4.257	10.34		2.570	2.330	2.566	2.472
		SSR	0.278	0.122	0.436	4.462		33.03	27.15	32.93	36.65
	Temkin	b_T	2060	-	-	-		24.58	-	-	-
		A_T	1.605	-	-	-		836.9	-	-	-
		SSR	2.955	1.552	1.83	6.274		79.31	18.26	23.31	51.69
	D-R	q_m	4.909	-	-	-		17.12	-	-	-
		n	474.7	-	-	-		2005	-	-	-
		SSR	7.154	5.156	5.544	16.42		203.3	37.96	31.38	122.56
	Sips	q_m	17.87	19.61	20.85	20.16		17.87	19.61	20.85	20.16
		b	0.085	0.666	0.885	3.203		0.084	0.666	0.885	3.203
		n	0.500	0.876	0.909	0.797		0.499	0.876	0.909	0.797
		RSE	0.383	0.889	1.223	0.908		0.383	0.889	1.223	0.908

	SSR	1184	1414	1639	1679	0.586	3.163	5.987	4.119
Toth	q_m	0.299	0.2987	0.299	0.856	47.32	-	47.3	0.856
	K_T	-1.269	-1.269	-1.269	- 0.888	23.94	-	23.94	-0.888
	n_T	0.604	0.60372	0.604	0.667	1.291	-	1.291	0.667
	SSR	0.084	-	4.920	0.305	7.236	75.22	156.4	-
R-P	K_{RP}	3.080	11.88	17.11	49.98	3.08	11.88	17.11	49.98
	α_{RP}	0.039	0.519	0.759	2.444	0.039	0.520	0.760	2.444
	g	1.382	1.039	1.019	0.997	1.382	1.039	1.019	0.997
	RSE	1.402	2.062	1.869	0.859	0.923	0.902	1.236	1.011
	SSR	1062	1395	1634	1715	3.408	3.251	6.115	5.106
Khan	q_m	48.60	23.27	23.27	33.00	48.60	23.27	23.27	33.00
	α_K	1.129	1.050	0.523	0.961	1.129	1.050	1.051	0.961
	b_K	0.272	0.523	1.051	2.238	1.213	0.902	0.523	3.032
	RSE	1.231	0.902	1.992	3.032	0.148	2.479	1.103	0.208
	SSR	5209	1390	1342	8267	1308	3.255	23.11	1510

^aRSE - residual standard error, ^bSSR - sum of squared residuals.

Table 10.7: Isotherm parameters for the adsorption of RhB onto 50% and 75% nanocomposites

Adsorbent	Isotherm	Parameters	Temperature/K				Adsorbent	Temperature/K			
			293 K	303 K	313 K	318 K		293 K	303 K	313 K	318 K
50%							75%				
	Langmuir	q_m	21.79	24.13	23.90	24.63		35.91	37.67	37.51	38.10
		b	3.247	1.380	2.760	3.006		0.426	0.552	1.156	1.681
		RSE ^a	4.604	4.070	4.666	0.734		1.340	1.671	2.406	2.868
		SSR ^b	40.30	126.1	127.6	130.6		14.36	22.34	46.30	65.81
	Freundlich	K_F	14.69	15.93	17.59	18.38		13.46	15.40	18.91	22.24
		n	6.613	7.521	9.717	10.50		3.513	3.703	4.536	5.241
		RSE	4.474	4.167	4.899	0.388		3.945	4.736	5.769	3.890
		SSR	34.97	134.0	136.1	144.0		124.5	179.5	266.2	121.0
	Temkin	b_T	2060	-	-	-		2060	-	-	-
		A_T	1.605	-	-	-		1.605	-	-	-
		SSR	-	-	-	-		4643	5160	5752	-
	D-R	q_m	21.43	-	-	-		31.63	-	-	-
		β	3143	-	-	-		1782	-	-	-
		SSR	713.6	205.9	143.5	-		395.6	191.3	116.4	363.9
	Sips	q_m	27.27	19.61	20.85	20.16		34.64	36.51	35.14	40.77
		b	1.199	0.666	0.885	3.203		0.347	0.517	1.815	1.269
		n	2.128	0.876	0.909	0.797		0.847	0.803	0.595	1.463
		RSE	-	-	-	-		1.277	1.352	1.686	2.705
		SSR	153.6	487.1	-	-		40.15	13.40	13.50	69.74

Toth	q _m	0.299	-	0.299	0.856	0.299	-	0.299	0.856
	K _T	-1.269	-	-1.269	-0.888	-1.269	-	-1.269	-0.888
	n _T	0.604	-	0.604	0.667	0.604	-	0.604	0.667
	SSR	-	-	-	-	-	-	-	-
R-P	K _{RP}	183.4	11.88	17.11	49.98	12.55	160.3	17.11	49.98
	α _{RP}	11.14	0.519	0.7595	2.444	0.258	0.288	0.760	2.444
	g	0.890	1.039	1.019	0.997	1.091	1.124	1.018	0.997
	RSE	-	-	-	-	1.206	1.277	1.236	1.011
	SSR	155.9	487.4	-	-	10.18	11.42	1526	1427
Khan	q _m	11.98	22.13	22.13	33.00	48.60	56.37	56.37	33.00
	a _K	0.885	0.985	3.155	0.961	1.129	1.175	1.175	0.961
	b _K	13.17	3.156	0.985	2.238	0.272	0.305	0.305	2.238
	RSE	-	-	-	-	1.213	1.313	1.659	3.032
	SSR	156.2	132.4	-	-	10.30	12.07	321.0	544.3

^aRSE - residual standard error, ^bSSR - sum of squared residuals.

Table 10.8: Isotherm parameters for the adsorption of RhB onto MWCNT-COOH

Adsorbent	Isotherm	Parameters	Temperature/K			
			293 K	303 K	313 K	318 K
MWCNT-COOH	Langmuir	q_m	42.68	45.80	45.49	51.08
		b	0.794	1.070	5.000	4.137
		RSE ^a	0.779	1.975	2.025	3.632
		SSR ^b	4.860	31.21	32.79	105.5
	Freundlich	K_F	18.89	22.31	31.03	1.922
		n	3.525	3.531	4.891	3.183
		RSE	4.638	4.750	6.543	0.388
		SSR	172.1	180.5	342.5	269.3
	Temkin	b_T	2060	-	-	-
		A_T	1.605	-	-	-
		SSR	6547	7378	9377	-
	D-R	q_m	36.32	-	-	-
		β	3917	-	-	-
		SSR	1094	570.7	356.5	604.6
	Sips	q_m	41.63	47.24	45.40	20.16
		b	0.827	0.999	5.098	3.203
		n	0.920	1.098	0.992	0.797
		RSE	0.706	2.050	2.164	0.908
		SSR	3.487	29.41	32.77	4308
	Toth	q_m	0.299	-	306.8	0.856
			-			
		K_T	1.269	-	1286	-0.888
		n_T	0.604	-	3.251	0.667
	R-P	SSR	-	-	128.6	-
		K_{RP}	29.91	11.88	17.11	154.2
		α_{RP}	0.606	0.520	0.760	2.471
		g	1.053	1.037	1.019	1.109
		RSE	0.578	0.902	1.236	2.955
	Khan	SSR	2.337	3105	4870	61.13
		q_m	51.58	51.59	51.59	33.00
		a_K	1.075	1.045	1.045	0.961
		b_K	0.596	0.885	0.885	2.238
RSE		0.566	2.083	4.211	3.032	
	SSR	2.240	30.37	1366	1998	

^aRSE - residual standard error, ^bSSR - sum of squared residuals

Table 10.9: Summary of the best fit isotherm parameters for the adsorption of RhB onto CoFe₂O₄, MWCNT-COOH, 29%, 50% and 75% MWCNT-CoFe₂O₄ nanocomposites

Adsorbent	Isotherm	Parameters	Temperature/K			
			293 K	303 K	313 K	318 K
CoFe ₂ O ₄	Langmuir	q _m	5.165	5.289	6.102	7.950
		<i>b</i>	0.092	0.154	0.134	0.103
		RSE ^a	4.604	4.070	4.666	0.734
		SSR ^b	0.053	0.454	0.642	3.602
	Freundlich	K _F	1.120	1.688	1.782	1.981
		<i>n</i>	3.080	3.753	3.512	3.207
		RSE	0.425	2.302	4.257	10.34
		SSR	0.278	0.122	0.436	4.462
29%	Langmuir	q _m	21.17	20.24	21.32	20.60
		<i>b</i>	0.222	0.652	0.846	2.401
		RSE	1.464	0.849	1.116	0.923
		SSR	10.71	3.608	6.230	5.111
	Sips	q _m	17.87	19.61	20.85	20.16
		<i>b</i>	0.084	0.666	0.885	3.203
		<i>n</i>	0.499	0.876	0.909	0.797
		RSE	0.383	0.889	1.223	0.908
		SSR	0.586	3.163	5.987	4.119
50%	Langmuir	q _m	21.79	24.13	23.90	24.63
		<i>b</i>	3.247	1.380	2.760	3.006
		RSE	4.604	4.070	4.666	0.734
		SSR	40.30	126.1	127.6	130.6
	Freundlich	K _F	14.69	15.93	17.59	18.38
		<i>n</i>	6.613	7.521	9.717	10.50
		RSE	4.474	4.167	4.899	0.388
		SSR	34.97	134.0	136.1	144.0
75%	Langmuir	q _m	35.91	37.67	37.51	38.10
		<i>b</i>	0.426	0.552	1.156	1.681
		RSE	1.340	1.671	2.406	2.868
		SSR	14.36	22.34	46.30	65.81
	Sips	q _m	34.64	36.51	35.14	40.77
		<i>b</i>	0.347	0.517	1.815	1.269
		<i>n</i>	0.847	0.803	0.595	1.463

		RSE	1.277	1.352	1.686	2.705
		SSR	40.15	13.40	13.50	69.74
MWCNT-						
COOH	Langmuir	q_m	42.68	45.80	45.49	51.08
		b	0.794	1.070	5.000	4.137
		RSE	0.779	1.975	2.025	3.632
		SSR	4.86	31.21	32.79	105.5

^aRSE - residual standard error, ^bSSR - sum of squared residuals.

10.3.2.8. Thermodynamic parameters of adsorption

The quantity adsorbed at each temperature was examined to obtain the thermodynamic parameters of adsorption. The change in Gibbs energy, ΔG° , was calculated from equation (10.3):⁷⁴

$$\Delta G^\circ = -RT \ln K \quad (10.3)$$

where ΔG° is the standard Gibbs energy change in J mol^{-1} , R is the gas constant ($8.314 \text{ J K}^{-1} \text{ mol}^{-1}$), T is the temperature in Kelvin and K was obtained from the product of q_m and b obtained from the Langmuir plot (Table 10.9).^{18,75} The value of K was corrected to be dimensionless by multiplying by a factor of 1000.⁷⁶

A linear plot of $\ln K$ against $1/T$ was obtained from which the slope and intercept correspond to the value of the change in enthalpy, ΔH° , and change in entropy, ΔS° , respectively, according to the Van't Hoff equation (eqn 10.4):⁷⁴

$$\ln K = -\frac{\Delta H^\circ}{RT} + \frac{\Delta S^\circ}{R} \quad (10.4)$$

Negative values were obtained for ΔG° indicating the spontaneous and feasible nature of the adsorption of RhB onto the adsorbents investigated (Table 10.10). It was also noticed that the negative values increase with an increase in temperature indicating better adsorption as the temperature is increased. The ΔS° values for all adsorbents were observed to be positive indicating an increase in the degree of disorderliness of the system as temperature is increased. This result demonstrates that adsorption was entropy-driven for all adsorbents in this study since an endothermic enthalpy of adsorption was observed for most of the adsorbents. Adsorbates can interact with the surface of an adsorbent through physical interaction (physisorption) or chemical sorption (chemisorption). When the heat of adsorption is between 2.1 to 20.9 kJ mol^{-1} , a physisorption process is assumed to occur while chemisorption could be said to occur when the heat of adsorption is between 80 to 200 kJ mol^{-1} .^{18,77} However, as noticed from Table 10.10, the values of ΔH° show that for CoFe_2O_4 and the 50% nanocomposite, RhB was physisorbed to the surface of the adsorbents while for the MWCNT-COOH, 29% and 75% nanocomposites the interaction could be a physio-chemical process, since the ΔH° values were higher than for a physisorption process, but lower than for chemisorption.^{18,77} This demonstrates that adsorption of RhB onto the adsorbents studied could be as a result of interaction of the adsorbent and adsorbate *via* the formation of a strong ionic bond (chemisorption) and interaction through weaker van der Waals forces between the adsorbate and adsorbents (physisorption). It is worthy of note that

the 50% dosage nanocomposite displayed an exothermic ΔH° . This shows that though adsorption was spontaneous, the reaction was exothermic in nature and hence for this adsorbent, enthalpy was the driving factor.

Table 10.10: Thermodynamic parameters for the adsorption of RhB onto CoFe₂O₄, 29%, 50%, 75% composites and MWCNT-COOH

Adsorbent	T/K	$\Delta G^\circ/\text{kJ mol}^{-1}$	$\Delta H^\circ/\text{kJ mol}^{-1}$	$\Delta S^\circ/\text{J K}^{-1} \text{mol}^{-1}$
CoFe ₂ O ₄	293	-15.01		
	303	-16.88		
	313	-17.45	15.95	106.7
	318	-17.73		
29%	293	-20.60		
	303	-23.90		
	313	-25.50	65.02	292.3
	318	-28.58		
50%	293	-27.21		
	303	-25.42		
	313	-27.04	-5.581	70.51
	318	-29.19		
75%	293	-23.47		
	303	-25.05		
	313	-27.79	44.87	232.3
	318	-29.26		
MWCNT-COOH	293	-25.41		
	303	-27.21		
	313	-32.10	65.17	307.9
	318	-32.42		

The Langmuir adsorption capacities (q_m) of adsorbents were compared with those obtained from previously published data (Table 10.11) for the removal of RhB from simulated wastewater. The table illustrates that the uptake (q_e) of adsorbents used in this study compares favourably with previously obtained data. An increase in the efficiency of adsorbents was achieved with an increase in carbon-based materials which resulted in the increase in the adsorption capacities (q_m).

Table 10.11: Comparison of adsorption capacities of various reported adsorbents for rhodamine B with present study.

Adsorbents	Conditions	$q_m/\text{mg g}^{-1}$	References
Pristine MWCNT	pH 7.0, C_i 10 mg dm^{-3} , 10 min, 100 mg dose	3.533	80
$\text{Fe}_3\text{O}_4/\text{MWCNT-COOH}$	pH 6.0, C_i 15 mg dm^{-3} , 80 min, 3 mg dose, 298 K	11.44	81
Activated carbon	pH 2.3, C_i 40 mg dm^{-3} , 60 min, 8 mg dose, 313 K	4.93	82
Fe_3O_4 -activated carbon	pH 4.0, C_i 20 mg dm^{-3} , 45 min, 30 mg dose, 298 K	47.62	83
$\text{Fe}_3\text{O}_4/\text{humic acid}$	pH 6.0, C_i 50 mg dm^{-3} , 15 min, 50 mg dose	161.8	84
CoFe_2O_4	pH 7.0, C_i 50 mg dm^{-3} , 360 min, 50 mg dose, 293 K	5.17	This Study
MWCNT- CoFe_2O_4 (29%)	pH 7.0, C_i 50 mg dm^{-3} , 360 min, 50 mg dose, 293 K	21.17	This Study
MWCNT- CoFe_2O_4 (50%)	pH 7.0, C_i 50 mg dm^{-3} , 360 min, 50 mg dose, 293 K	21.79	This Study
MWCNT- CoFe_2O_4 (75%)	pH 7.0, C_i 100 mg dm^{-3} , 360 min, 50 mg dose, 293 K	35.91	This Study
MWCNT-COOH	pH 7.0, C_i 100 mg dm^{-3} , 360 min, 50 mg dose, 293 K	42.68	This Study

10.3.3. Desorption Studies

Desorption studies were carried out to determine the reusability of the adsorbents tested, by agitating 50 mg of the RhB-loaded sample with either 10 cm³ of ethanol or acetone. It is important to ascertain whether used adsorbents can be regenerated and made effective for reuse. In this way the discharge of secondary pollutants into the environment is hindered in that the spent adsorbents are recycled for reuse and not disposed directly after usage. The adsorbate (in this case the RhB dye) can also be recovered for reuse. The experimental results (Table 10.12) show a good desorption efficiency of RhB by using either ethanol or acetone. Acetone was found to better desorb the dye with efficiencies between 80 and 95%. Characterization of the regenerated adsorbents was carried out and the results were found to be similar to those obtained with freshly prepared unused adsorbents, therefore confirming the reusability. Hence, all adsorbents used in this study can be regenerated for reuse.

Table 10.12: Percentage desorption of RhB by using acetone or ethanol [Conditions: 10 cm³ of either acetone or ethanol, 50 mg of RhB-loaded adsorbent, agitation speed 150 rpm, equilibration time 30 min, and temperature 20 °C]

Adsorbents	Desorption/%	
	Acetone	Ethanol
CoFe ₂ O ₄	90.60	88.61
29%	93.20	64.23
50%	82.46	62.45
75%	80.41	74.50
MWCNT-COOH	94.63	82.52

10.4. Conclusions

Adsorption of RhB from aqueous solution was successfully carried out by using CoFe₂O₄ nanoparticles, MWCNT-COOH, and CNT-CoFe₂O₄ nanocomposites. Characterization of the adsorbents confirmed the presence of functional groups available for interaction with RhB. Based on the experimental results obtained, it was observed that the adsorption capacity of adsorbents to remove RhB significantly increased from 5.165 to 42.68 mg g⁻¹ with increasing MWCNT-COOH content. The highest adsorption capacity was obtained with MWCNT-COOH as adsorbent, however, CNT-based nanocomposites showed better capacities than CoFe₂O₄ nanoparticles. This study therefore demonstrates that the incorporation of carbon-based nanomaterials, such as MWCNTs, can improve the textural characteristics and adsorption capacity of CoFe₂O₄, thereby, making them suitable adsorbents for wastewater remediation.

The maximum removal of RhB from a simulated wastewater was achieved at an optimum pH of 7, and equilibrium was reached after 360 min. The kinetics of adsorption followed the pseudo-second order model indicating a bimolecular rate-determining step. The equilibrium data was better described by the Langmuir isotherm model indicating monolayer coverage of RhB onto the homogeneous sites of the adsorbents. An increase in the adsorption capacity was achieved as the temperature of the solution was increased except for the 50% nanocomposite. This factor makes these adsorbents useful in the treatment of effluents discharged directly from industries since these are typically above ambient temperatures. The adsorption process was thermodynamically spontaneous and entropy-driven for the adsorbents except for the 50 % nanocomposite. The adsorbed RhB was efficiently desorbed with either ethanol or acetone, but the latter showed the highest desorption capacity. Thus, these adsorbents show potential for reuse and do not create a secondary pollutant problem.

We therefore infer that electrostatic interaction between RhB and the adsorbents was primarily responsible for adsorption in this study. The interactions between the adsorbate and adsorbents were strong, indicating both physisorption and chemisorption processes. It is worthy of note that though MWCNT-COOH showed the best adsorption capacity, the nanocomposites provide an advantage of magnetic separation, which limits problems associated with removal of adsorbents from aqueous media. This study, therefore, demonstrates that cobalt ferrite nanoparticles, multiwalled carbon nanotubes, and CNT-based nanocomposites provide potential applications for the removal of pollutants from the environment through adsorption. Furthermore, the synthesized nanocomposites were found to be stable, durable and hence reusable for RhB adsorption.

References

1. M. A. M. Salleha, D. K. Mahmoud, W. A. A. Karim and A. Idris, *Desalination*, 2011, **280**, 1-13.
2. T. Robinson, G. McMullan, R. Marchant and P. Nigam, *Bioresour. Technol.*, 2001, **77**, 247-255.
3. T. P. S. Sumanjit, I. K. Walia and I. Kansal, *J.Surf. Sci. Technol.*, 2008, **24**, 179-193.
4. A. Y. Zahrim and N. Hilal, *Water Res. Ind.*, 2013, **3**, 23-34.
5. V. P. Kasperchik, A. L. Yaskevich and A. V. Bilyukevich, *Petrol. Chem.*, 2012, **52**, 545-556.
6. S. Nadupalli, N. Koorbanally and S. B. Jonnalagadda, *J. Phys. Chem. A*, 2011, **115**, 11682-11688.
7. O. Türgay, G. Ersöz, S. Atalay, J. Forss and U. Welander, *Sep. Purif. Technol*, 2011, **79**, 26-33.
8. S. Nadupalli, N. Koorbanally and S. B. Jonnalagadda, *J. Phys. Chem A*, 2011, **115**, 7948-7954.
9. A. Rezaee, M. T. Ghaneian, A. Khavanin, S. J. Hashemian, G. Moussan, G. Ghanizadeh and E. Hajizadeh, *Iranian J. Environ. Health Sci. Eng.*, 2008, **5**, 95-100.
10. B. Pare, B. Bhawna Sarwan and S. Jonnalagadda, *Appl. Surf. Sci.*, 2011, **258**, 247 - 253.
11. A. Ahmad, W. Harris and B. S. Ooi, *Jurnal Teknologi*, 2002, **36**, 31-44.
12. L. Wojnarovits and E. Takacs, *Radiat. Phys. Chem.*, 2008, **77**, 225-244.
13. K. Murugesan and P. T. Kalaichelvan, *Indian J. Exp Biol*, 2003, **41**, 1076-1087.
14. M. A. García-Morales, G. Roa-Morales, C. Barrera-Díaz, V. Martínez Miranda, P. Balderas Hernández and T. B. Pavón Silva, *Int. J. Electrochem Sci.*, 2013, **8**, 8752-8763.
15. P. Dachipally and S. B. Jonnalagadda, *J. Environ. Sci. Health., Part A*, 2011, **46**, 887-897.
16. Y. Yan, M. Zhang, K. Gong, L. Su, Z. Guo and L. Mao, *Chem. Mater.*, 2005, **17**, 3457-3462.
17. S. B. Jonnalagadda and S. Nadupalli, *Talanta*, 2004, **64**, 18 - 22.
18. I. A. A. Hamza, B. S. Martincigh, J. C. Ngila and V. O. Nyamori, *Phys. Chem. Earth*, 2013, **66**, 157-166.
19. Y. Li, Q. Du, T. Liu, X. Peng, J. Wang, J. Sun, Y. Wang, S. Wu, Z. Wang, Y. Xia and L. Xia, *Chem. Eng. Res. Des.*, 2013, **91**, 361-368.
20. Z. Zhang, I. M. O'Hara, G. A. Kent and W. O. S. Doherty, *Ind. Crop Prod.*, 2013, **42**, 41-49.
21. R. Gong, Y. Sun, J. Chen, H. Liu and C. Yang, *Dyes Pigments*, 2005, **67**, 175-181.

22. M. C. Akkaya, S. Emik, G. Guclu, B. T. Iyim and S. Ozgumus, *J. Appl. Polym. Sci.*, 2009, **114**, 1150-1159.
23. S. H. Kareem and E. Abd-Al-Hussien, *J. Baghdad Sci.*, 2012, **9**, 680-688.
24. C. C. Wang, L. C. Juang, T. C. Hsu, C. K. Lee, J. F. Lee and F. C. Huang, *J. Colloid Interface Sci.*, 2004, **273**, 80-86.
25. O. S. Bello, O. A. Olusegun and V. O. Njoku, *B. Chem Soc. Ethiopia*, 2013, **27**, 191-204.
26. S. Wang, Y. Boyjoo, A. Choueib and Z. H. Zhu, *Water Res.*, 2005, **39**, 129-138.
27. T. A. Khan, S. Dahiya and I. Ali, *Appl. Clay Sci.*, 2012, **69**, 58-66.
28. Mundhe K. S., Gaikwad A. B., Torane R. C., Deshpande N. R. and Kashalkar R. V., *J. Chem. Pharm. Res.*, 2012, **4**, 423-463.
29. G. Guclu, *Desalination*, 2010, **259**, 53-58.
30. T. B. Iyim, I. Acar and S. Ozgumus, *J. Appl. Polym. Sci.*, 2008, **109**, 2774-2780.
31. T. A. Khan, M. Nazir and E. A. Khan, *Toxicol. Environ. Chem.*, 2013, **95**, 919-931.
32. P. Parimaladevi and V. Venkateswaran, *J. Appl. Technol. Environ. Sanit.*, 2011, **1**, 285-293.
33. C. Namasivayam, N. Muniasamy, K. Gayatri, M. Rani and K. Ranganathan, *Bioresour. Technol.*, 1996, **57**, 37-43.
34. L. Wang, J. Li, Y. Wang, L. Zhao and Q. Jiang, *Chem. Eng. J.*, 2010, **181-182**, 72-79.
35. R. Jiang, Y. Q. Fu, H. Y. Zhu, J. Yao and L. Xiao, *J. Appl. Polym. Sci.*, 2012, **125**, E540-E549.
36. L. Ai, C. Zhang, F. Liao, Y. Wanga, M. Li, L. Meng and J. Jiang, *J. Hazard. Mater.*, 2011, **198**, 282-290.
37. S. Iijima, *Nature*, 1991, **354**, 56-58.
38. B. Pan and B. Xing, *Environ. Sci. Technol.*, 2008, **42**, 9005-9013.
39. C. Lu, Y.-L. Chung and K.-F. Chang, *Water Res.*, 2005, **39**, 1183-1189.
40. K. Balasubramanian and M. Burghard, *Small*, 2005, **1**, 180-192.
41. V. Datsyuk, M. Kalyva, K. Papagelis, J. Parthenios, D. Tasis, A. Siokou, I. Kallitsis and C. Galiotis, *Carbon*, 2008, **46**, 833-840.
42. J. Shen, W. Huang, L. Wu, Y. Hu and M. Ye, *Mater. Sci. Eng., A* 2007, **464**, 151-156.
43. C. Lu and H. Chiu, *Chem. Eng. Sci.*, 2006, **61**, 1138-1145.
44. K. McDonough, J. L. Fairey and G. V. Lowry, *Water Res.*, 2008, **42**, 575-584.
45. K. Maaz, A. Mumtaz, S. K. Hasanain and A. Ceylan, *J. Magn. Magn Mater.*, 2007, **308**, 289-295.
46. S. Santangelo, G. Messina, G. Faggio, S. H. Abdul Rahim and C. Milone, *J. Raman Spectrosc.*, 2012, **43**, 1432-1442.
47. The R development core team, *R version 3.0.2* 2013.

48. N. A. Buang, F. Fadil, A. Abdul Majid and S. Shahir, *Dig. J. Nanomater. Bios.*, 2012, **7**, 33-39.
49. A. K. Mishra and S. Ramaprabhu, *J. Phys. Chem. C*, 2010, **114**, 2583-2590.
50. L. Kong, X. Lu and W. Wanjin Zhang, *J. Solid State Chem.*, 2008, **181**, 628-636.
51. Y.-Y. Xu, M. Zhou, H.-J. Genga, J.-J. Haoa, Q.-Q. Oua, S.-D. Qia, H.-L. Chen and X.-G. Chen, *Appl. Surf. Sci.*, 2012, **258**, 3897-3902.
52. B. Jia and L. Gao, *J. Phys. Chem. B*, 2007, **111**, 5337-5343.
53. A. Afkhami and R. Moosavi, *J. Hazard. Mater.*, 2010, **174**, 398 - 403.
54. Z. Zhao, Z. Yang, H. Yu., J. Li and X. Fan, *Appl. Surf. Sci.*, 2013, **276**, 476-481.
55. Y. Zhang, H. He, C. Gao and J. Wu, *Langmuir* 2009, **25**, 5814-5824.
56. J.-L. Gong, B. Wang, G.-M. Zeng, C.-P. Yang, C.-G. Niu, Q.-Y. Niu, W.-J. Zhoua and Y. Liang, *J. Hazard. Mater.*, 2009, **164**, 1517-1522.
57. Canadian Environmental Protection Agency, *Chemical Abstracts Service Registry Number*, 2010, **509-34-2**.
58. G. Annadurai, R.-S. Juang and D.-J. Lee, *J. Hazard. Mater.*, 2002, **B92**, 263-274.
59. Y. S. Ho, *Water Res.*, 2004, **38**, 2962-2964
60. Y. S. Ho and G. McKay, *Process Saf. Environ. Prot.*, 1998, **76**, 183-191.
61. E. Demirbas, M. Kobya, E. Senturk and T. Ozkan, *Water S.A.*, 2004, **30**, 533-539.
62. S. H. Chien and W. R. Clayton, *Soil Sci. Soc. of Am. J.*, 1980, **44**, 265-268.
63. Y. Yao, F. Xu, M. Chen, Z. Xu and Z. Zhu, *Bioresour. Technol.*, 2010, **101**, 3040-3046.
64. C. H. Wu, *J. Hazard. Mater.*, 2007, **144**, 93-100.
65. S. G. Muntean, M. E. Radulescu-Grad and P. Sfarloaga, *RSC Adv.*, 2014, **4**, 27354-27362.
66. H. Freundlich, *Z Phys. Chem.*, 1906, **57**, 385-470.
67. I. Langmuir, *J. Am. Chem. Soc.*, 1918, **40**, 1361-1402.
68. M. I. Temkin and V. Pyzhev, *Acta Phys. Chim*, 1940, **12**, 327-356.
69. M. M. Dubinin and L. V. Radushkevich, *Proc. Natl. Acad. Sci.*, 1947, **55**, 327-329.
70. R. Sips, *J. Chem. Phys*, 1948, **16**, 490-495.
71. A. R. Khan, I. R. Al-Waheab and A. Al-Haddad, *Environ. Technol.*, 1996, **17**, 13-23.
72. O. Redlich and D. L. Peterson, *J. Phys. Chem*, 1959, **63**, 1024.
73. J. Toth, *Acta Chim. Acad. Sci. Hung.*, 1971, **69**, 311-328.
74. K. M. Doke and E. M. Khan, *Rev. Environ. Sci. Bio.*, 2013, **12**, 25-44.
75. R. Djeribi and Q. Hamdaoui, *Desalination*, 2008, **225**, 95-112.
76. S. K. Milonjić, *J. Serb. Chem. Soc.*, 2007, **72**, 1363-1367.
77. Y. Liu and Y.-J. Liu, *Sep. Purif. Technol.*, 2008, **61**, 229-242.
78. Y.-S. Ho, *Water Res.*, 2003, **37**, 2323-2330.
79. J. Lin and L. Wang, *Front. Environ. Sci. En.*, 2009, **3**, 320-324.

80. S. Kumar, G. Bhanjana, K. Jangra, N. Dilbaghi and A. Umar, *J. Nanosci. Nanotechno.*, 2014, **14**, 4331-4336.
81. K. Kerkez and S. S. Bayazit, *J. Nanopart. Res.*, 2014, **16**, 2431-2441.
82. V. K. Gupta, R. Jain, M. N. Siddiqui, T. A. Saleh, S. Agarwal, S. Malati and D. Pathak, *J. Chem. Eng. Data*, 2010, **55**, 5225-5229.
83. T. Madrakian, A. Afkhami, H. Mahmood-Kashani and M. Ahmad, *Iran Chem. Soc.*, 2013, **10**, 481-189.
84. L. Peng, P. Qina, M. Lei, Q. Zeng, H. Song, J. Yang, J. Shao, B. Liao and J. Gua, *J. Hazard. Mater.*, 2012, **209-210**, 193-198.

Chapter 11

General conclusions and recommendations

The declining level of freshwater on the planet requires immediate need for prudent management of water resources. One of many ways through which this can be achieved is to ensure adequate water recycling. For water reclamation, the removal of toxic pollutants from wastewater and industrial effluents is a crucial step to achieving a clean water supply. Also, in order to avert deleterious health complications associated with the intake of contaminated water, there is an urgent need for the remediation of wastewater before it is discharged into water streams. In spite of the availability of techniques which have been applied towards achieving effective and efficient removal of pollutants from wastewater, adsorption has been considered best due to its simplicity and the possibility of reutilization of sorbents. In view of this, carbon nanomaterials, containing multiwalled carbon nanotubes (MWCNTs), were synthesized and employed for the removal of pollutants such as heavy metal ions (Pb^{2+} , Cu^{2+} , Cd^{2+} , Hg^{2+} and Zn^{2+}), organic substances (bisphenol A and ibuprofen) and organic dyes (rhodamine B) from simulated aqueous solutions.

Nitrogen-functionalized multiwalled carbon nanotubes (MWCNT-ttpy) were synthesized by attaching a nitrogen donor ligand (4-phenyl-2, 2':6', 2''-terpyridine) to the surface of MWCNTs. This nanomaterial was applied for the removal of the stated heavy metal ions, bisphenol A and ibuprofen from aqueous solutions. The sorption capacity of this novel sorbent was compared with that of oxygen-functionalized multiwalled carbon nanotubes (MWCNT-COOH), to evaluate the sorbent with the highest removal efficiency. The removal of rhodamine B dye from aqueous solution was investigated by using cobalt ferrite nanoparticles, MWCNT-COOH and composites made from both nanomaterials in percentages of 29%, 50% and 75%. The characterization of all adsorbents synthesized was performed by using techniques such as TEM, SEM, TGA, BET, FTIR and Raman spectroscopy.

The application of MWCNT-COOH and MWCNT-ttpy for the removal of Pb^{2+} , Cd^{2+} , Hg^{2+} , Cu^{2+} , Zn^{2+} , bisphenol A and ibuprofen was examined *via* batch adsorption experiments. The effects of pH, contact time, adsorbent dose, initial adsorbate concentration and temperature was investigated for each adsorption process. Similarly, these parameters were examined for the adsorption of rhodamine B dye onto cobalt-ferrite nanoparticles (CoFe_2O_4),

MWCNT-COOH and carbon nanotube-cobalt ferrite nanocomposites in percentages of 29%, 50% and 75%.

Based on the results obtained from this study, the following conclusions can be drawn:

1. The synthesis of 4-phenyl-2, 2':6', 2''-terpyridine was successful and confirmed by using techniques such as FTIR, NMR and mass spectrometry.
2. The synthesis and characterization of MWCNT-COOH and MWCNT-ttpty was successful. An increase in the surface area of MWCNT-ttpty from $126.8 \text{ m}^2 \text{ g}^{-1}$ for MWCNT-COOH to $189.2 \text{ m}^2 \text{ g}^{-1}$ for MWCNT-ttpty was associated with the increase in the extent of functionalization of MWCNTs. An increase in the pore volume of MWCNT-ttpty was also noticeable and both adsorbents were mesoporous in nature. The presence of nitrogen in MWCNT-ttpty was verified *via* elemental analysis, thereby confirming the successful introduction of 4-phenyl-2, 2':6', 2''-terpyridine to the backbone of MWCNT. The morphology of MWCNT-COOH and MWCNT-ttpty showed straight and curved structures, respectively. Raman analysis indicated that MWCNT-ttpty was more defective, accounting for its reduced thermal stability obtained from thermogravimetric analysis. FTIR spectra confirmed the introduction of oxygen- and nitrogen functional groups onto the walls of MWCNT-COOH and MWCNT-ttpty, respectively. These properties suggests that both sorbents could be suitable for the removal of metal ions and organic pollutants from wastewater.
3. Carbon nanotube-cobalt ferrite nanocomposites were successfully synthesized in varying percentages of 29%, 50% and 75%. The textural characterization revealed an increase in surface area and pore volume with an increase in the amount of MWCNT-COOH in each composite. Raman analysis also demonstrated an increase in the I_D/I_G ratio, signaling an increase in the amount of defects with an increase in MWCNT. FTIR spectra confirmed the synthesis of the nanomaterials, revealing the presence of functional groups which would aid the removal of rhodamine B dye from aqueous solutions.
4. The removal of Cu^{2+} from aqueous solution by using MWCNT-COOH and MWCNT-ttpty was investigated at pH 5.0. The application of MWCNT-ttpty for Cu^{2+} removal demonstrated a marked increase in the Langmuir adsorption capacity (q_m) from 19.44 to 31.65 mg g^{-1} compared with MWCNT-COOH. The higher uptake of Cu^{2+} by MWCNT-ttpty was associated with the increase in the number of active sites, created by the possible chelation of the metal ion to the nitrogen-donor atoms contained in the adsorbent. The kinetics of adsorption was described by the pseudo-second order model, while the equilibrium data were best fitted by the Langmuir isotherm. Adsorption was spontaneous for both sorbents, exhibiting an endothermic nature. This implied that Cu^{2+} uptake onto MWCNT-COOH and MWCNT-ttpty

increased with an increase in temperature. Hence, these sorbents can be applied directly for the treatment of industrial effluents at point source, since they are usually discharged at above ambient temperatures.

5. The removal of Pb^{2+} from aqueous solutions by using MWCNT-COOH and MWCNT-ttpty was carried out at pH 4.5. The uptake of Pb^{2+} increased from 20.60 mg g^{-1} to 36.23 mg g^{-1} with higher sorption capacity noticed for MWCNT-ttpty. The kinetics of adsorption for both sorbents was best described by the pseudo-second order model. The Langmuir model provided the best fit for the equilibrium data obtained, while the Redlich-Peterson and Sips model were the best suited of the three-parameter isotherms tested. Adsorption was also spontaneous, feasible and endothermic by using both sorbents.
6. The application of MWCNT-ttpty showed increased potential for the removal of Zn^{2+} compared with MWCNT-COOH. Equilibrium was reached after 300 min and 360 min for Zn^{2+} removal onto MWCNT-COOH and MWCNT-ttpty, respectively. The data was best described by the pseudo-second order kinetics model, while the Langmuir and Sips models provided a good fit for the isotherm studies. Adsorption was favourable at high temperatures and spontaneous for the removal of Zn^{2+} from aqueous solutions.
7. A four-fold increase from 10.41 mg g^{-1} to 41.51 mg g^{-1} was obtained for the removal of Cd^{2+} onto MWCNT-ttpty, compared with MWCNT-COOH. The interaction of Cd^{2+} onto active sites proceeded *via* a chemical interaction involving the sharing or exchange of electrons between the active sites on the adsorbents and the metal cation. Hence, adsorption was bimolecular, as supported by the pseudo-second order kinetic model. Of the two-parameter isotherms tested, the Langmuir model best fits the equilibrium data, while the Sips model gave a good representation of the three-parameter isotherms used. However, better Cd^{2+} uptake was achieved at low temperatures, signifying an exothermic nature of adsorption.
8. Due to high toxicity associated with Hg^{2+} inhalation at higher temperatures, its removal was only investigated at 20 °C and 30 °C. Nonetheless, increasing adsorbate temperature resulted in an increase in the removal of Hg^{2+} from aqueous solutions. The kinetics of adsorption onto MWCNT-COOH and MWCNT-ttpty was best described by the pseudo-second order model. Both sorbents showed great potential for Hg^{2+} , obtaining an adsorption capacity (q_m) of 33.89 mg g^{-1} for MWCNT-COOH and 36.13 mg g^{-1} for MWCNT-ttpty at 20 °C. These results implied that both sorbents are suitable for the treatment of Hg^{2+} -contaminated wastewater or industrial effluents.
9. The application of MWCNT-COOH and MWCNT-ttpty was also explored for the removal of two endocrine disruptors (i.e. bisphenol A and ibuprofen) from aqueous

solutions. Adsorption was conducted at an optimum pH of 7.0 and 2.0 for the removal of bisphenol A and ibuprofen, respectively. The kinetics data obtained for both sorbates were better described by the pseudo-second order kinetics model. Isotherm studies showed that data obtained for both substances best fits the Langmuir model. This implied that the sorption of both substances onto MWCNT-COOH and MWCNT-ttpy occurred on a monolayer surface. Additionally, the application of MWCNT-ttpy for bisphenol A and ibuprofen removal, showed increased uptake compared with MWCNT-COOH. This was attributed to the increase in the hydrophobic nature of MWCNT-ttpy, demonstrating π - π interaction between the adsorbates and the adsorbents. Adsorption was spontaneous for all processes. However, an endothermic and exothermic nature of adsorption was obtained for the removal of bisphenol A and ibuprofen, respectively, from aqueous solution.

10. For both the single-solute and multicomponent adsorption systems, the equilibrium data was well described by the Langmuir adsorption isotherm. However, the Langmuir maximum adsorption capacities (q_m) in a single-solute system were significantly higher than those obtained in a competitive system. This trend was attributed to an increase in competition between metal cations for active sites on the MWCNT-ttpy adsorbent. The sorption of metal ions onto MWCNT-ttpy followed the sequence $Cd > Pb > Cu > Zn$ and $Pb > Cu > Cd > Zn$ in a single- and multi-component adsorption systems, respectively. In multi-metal systems, the removal of a particular metal ion was primarily based on the initial concentration of other competitors in solution. Although, the sorption of metal ions was higher in a single-solute system, MWCNT-ttpy showed great selectivity for metal ion removal in multicomponent adsorption systems. The effectiveness of MWCNT-ttpy for the removal of metal ions was confirmed by using real samples, wherein removal efficiencies reached 95%. These results therefore justifies the potential application of MWCNT-ttpy for the treatment of metal-contaminated wastewater or industrial effluents.
11. The co-adsorption of bisphenol A and ibuprofen onto MWCNT-ttpy was investigated at an optimum pH 2.0. The equilibrium data in single-solute and binary adsorption systems were described by the Langmuir isotherm model. The removal of both sorbates was primarily based on their hydrophobic nature, hence, the sorption of ibuprofen onto MWCNT-ttpy in both systems was higher than that obtained for bisphenol A. The influence of the presence of metal ions such as Cd^{2+} and Pb^{2+} was investigated on the competitive sorption of bisphenol A and ibuprofen. Adsorption in this system was cooperative, largely depending on the initial concentration of competitors, hydrophobic state and affinity of adsorbates for active sites on the adsorbent. Similarly, lower adsorption capacities were obtained in a

multicomponent system due to increased competition between sorbates in solution. The application of MWCNT-ttpy therefore proved efficient in multicomponent systems containing a mixture of different classes of pollutants.

12. The removal of rhodamine B from aqueous solution was investigated by using cobalt ferrite nanoparticles, acid-functionalized multiwalled carbon nanotubes (MWCNT-COOH) and carbon nanotube-cobalt ferrite nanocomposites. The optimum pH for adsorption was observed at 7 at which equilibrium was reached after 360 min. The adsorption capacity was lowest in CoFe_2O_4 (5.165 mg g^{-1}) and highest with MWCNT-COOH (42.68 mg g^{-1}). Increasing the content of MWCNT-COOH from 29% to 75% in composites enhanced the sorption capacity from 21.17 mg g^{-1} to 35.91 mg g^{-1} . The kinetics data obtained for all sorbents were best described by the pseudo-second order kinetic model. The Langmuir isotherm provided the best fit to the equilibrium data obtained. The adsorption of rhodamine B was spontaneous, endothermic and entropy-driven, except for one of the doped nanocomposites for which adsorption was exothermic.
13. Desorption of all sorbents used in the study exhibited effective removal of sorbates from the surface of adsorbents. This process attempts to regenerate spent-adsorbents for reutilization, thereby preventing the discharge of secondary pollutants into the environment. Thus, all sorbents were regenerated by washing with conventional solvents and/or acids, and produced good desorption yields between the ranges of 60% to 94%.

Thus, it can be concluded that nanomaterials based on MWCNTs are effective and sufficiently robust for the removal of different classes of pollutant and should be further explored.

Based on these results, the following are recommended for future work.

- An investigation of the effect of varying denticity of the ligand attached to MWCNTs for the removal of targeted pollutants from aqueous solutions.
- An investigation of the application of nitrogen-functionalized multiwalled carbon nanotubes in wastewater treatment facilities for the removal of various classes of pollutants.

Appendix I

Data for Copper(II)

Table A-I.1: Operating conditions for the PerkinElmer Optima 5300 DV inductively coupled plasma-optical emission spectrometer (ICP-OES) for Cu²⁺ analysis

Wavelength	224.700 nm
RF power	1300 W
Plasma gas flow rate	15 dm ³ min ⁻¹
Pump	1.5 cm ³ min ⁻¹
Auxiliary gas flow rate	0.2 dm ³ min ⁻¹
Nebulizer gas flow rate	0.8 dm ³ min ⁻¹
Nebulizer pressure	2 bars
Analyzer type	Axial
Replicates	3
Sample read delay	60 s

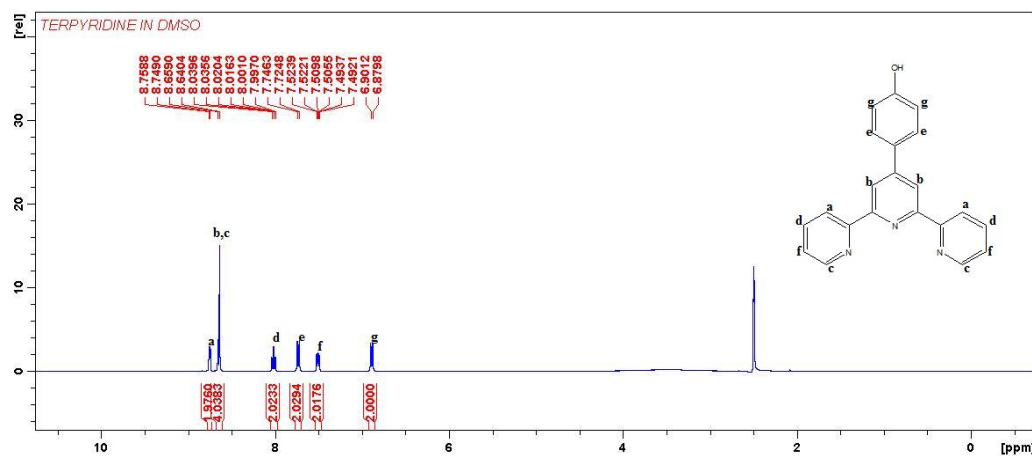


Fig A-I.1: ¹H NMR spectrum of HO-Phttpy.

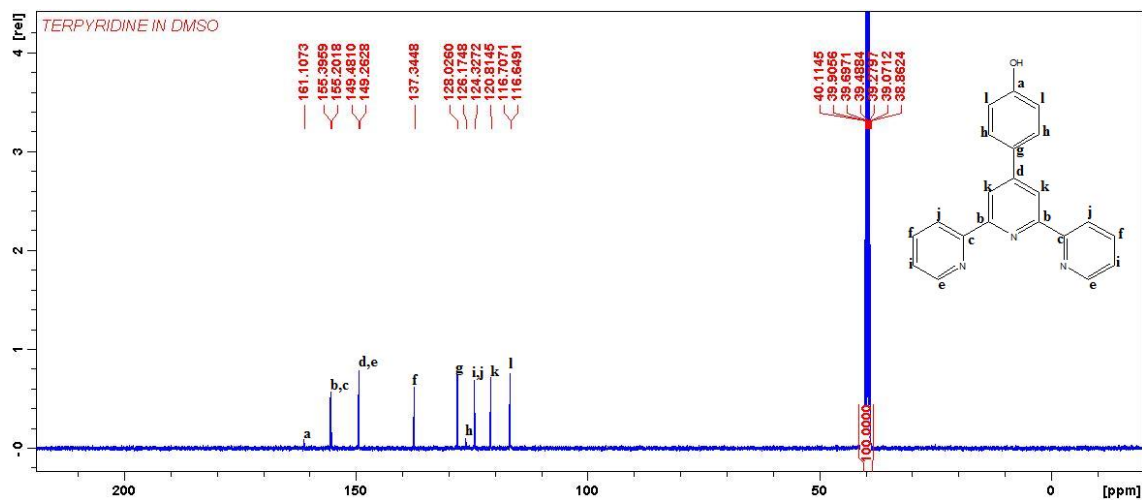


Fig A-I.2: ^{13}C NMR spectrum of HO-Phttpy.

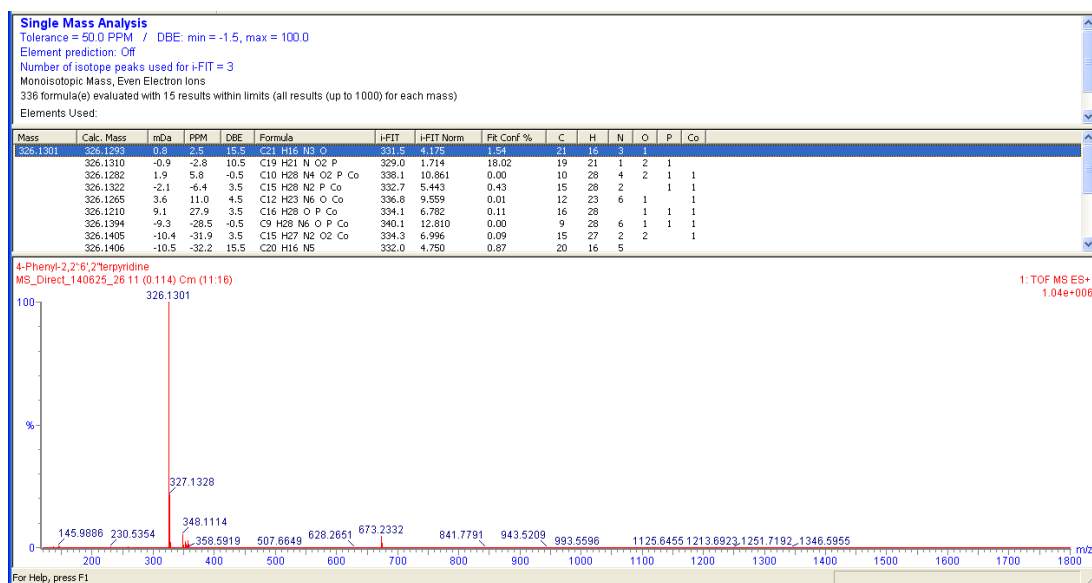


Fig A-I.3: Mass spectrum of HO-Phttpy.

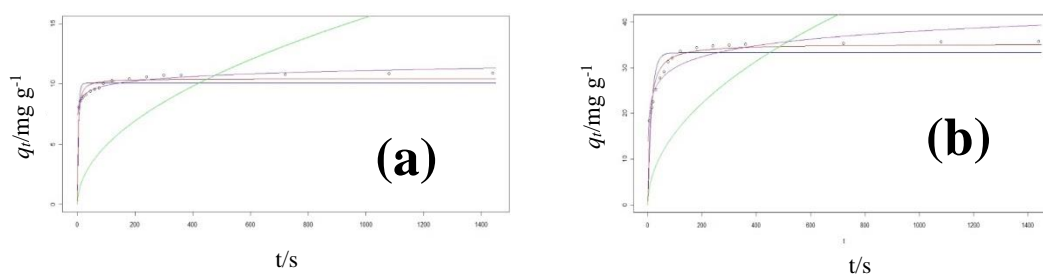


Fig A-I.4: Comparison of kinetics models fitted to the experimental data for the adsorption of Cu^{2+} onto (a) MWCNT-COOH and (b) MWCNT-tpy (pseudo-first order —, pseudo-second order —, intraparticle diffusion — and Elovich model —).

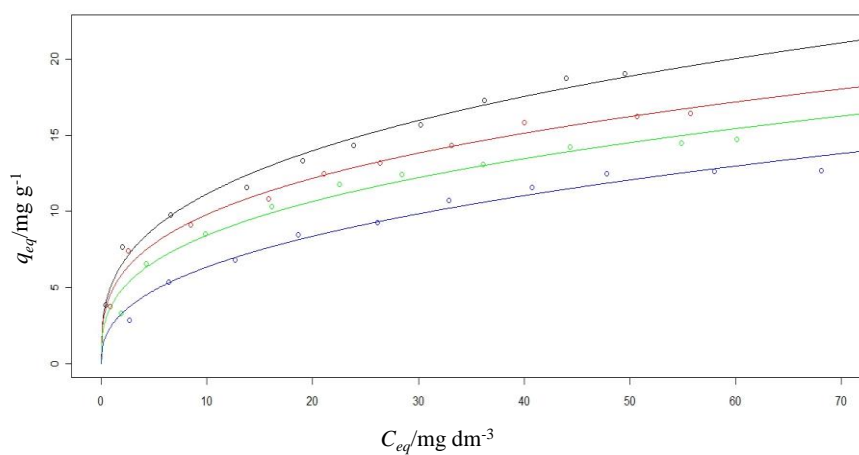


Fig A-I.5: The Freundlich adsorption isotherm fitted to the experimental data for the adsorption of Cu^{2+} onto MWCNT-COOH at various temperatures (293 K —, 303 K —, 313 K — and 318 K —).

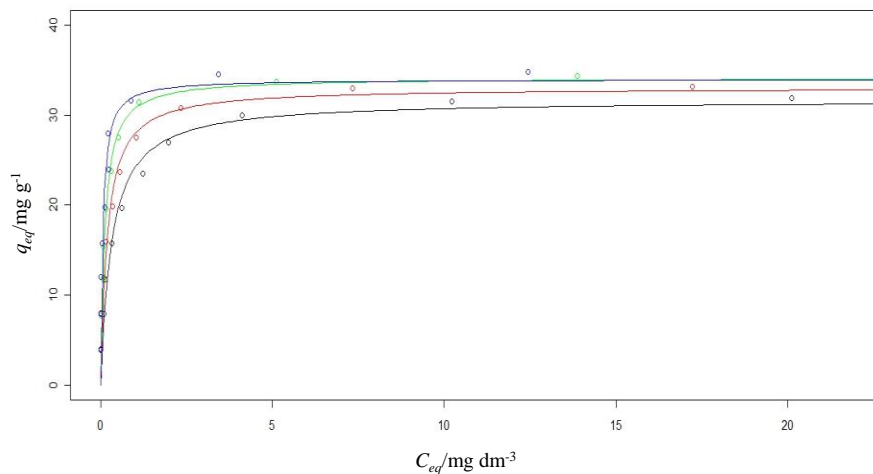


Fig A-I.6: The Langmuir adsorption isotherm fitted to the experimental data for the adsorption of Cu^{2+} onto MWCNT-tpy at various temperatures (293 K —, 303 K —, 313 K — and 318 K —).

Table A-I.2: Experimental data for the adsorption of Cu^{2+} onto MWCNT-COOH as a function of pH [conditions: contact time 24 h, agitation speed 150 rpm, temperature 20 °C]

pH	$C_i/\text{mg dm}^{-3}$	$C_{eq}/\text{mg dm}^{-3}$	Mass/g	Volume/ dm^3	% adsorbed	$q_e/\text{mg g}^{-1}$
1	101.9	94.41	0.0512	0.020	7.350	2.926
2	101.9	81.58	0.0517	0.020	19.94	7.861
3	101.9	75.65	0.0512	0.020	25.76	10.25
4	101.9	69.56	0.0513	0.020	31.74	12.61
5	101.9	68.19	0.0506	0.020	33.08	13.32
6	101.9	57.81	0.0508	0.020	43.27	17.36
7	101.9	1.914	0.0503	0.020	98.12	39.76
8	101.9	1.832	0.0501	0.020	98.20	39.95
9	101.9	4.144	0.0514	0.020	95.93	38.04
10	101.9	2.071	0.0501	0.020	97.97	39.85

Table A-I.3: Experimental data for the adsorption of Cu²⁺ onto MWCNT-COOH as a function of time [conditions: pH 5.0, agitation speed 150 rpm, temperature 20 °C]

Time/min	$C_i/\text{mg dm}^{-3}$	$C_{eq}/\text{mg dm}^{-3}$	Mass/g	Volume/dm ³	% adsorbed	$q_e/\text{mg g}^{-1}$
5	92.36	71.78	0.0511	0.020	22.28	8.055
10	92.36	70.30	0.0515	0.020	23.88	8.567
15	92.36	69.77	0.0515	0.020	24.46	8.773
20	92.36	69.55	0.0509	0.020	24.70	8.963
30	92.36	69.14	0.0509	0.020	25.14	9.124
45	92.36	68.74	0.0503	0.020	25.57	9.392
60	92.36	67.79	0.0513	0.020	26.60	9.579
75	92.36	67.52	0.0514	0.020	26.89	9.665
90	92.36	66.85	0.0508	0.020	27.62	10.04
120	92.36	66.55	0.0502	0.020	27.94	10.28
180	92.36	65.30	0.0520	0.020	29.30	10.41
240	92.36	65.20	0.0513	0.020	29.41	10.59
300	92.36	65.10	0.0509	0.020	29.51	10.71
360	92.36	64.82	0.0513	0.020	29.82	10.74
720	92.36	64.78	0.0511	0.020	29.86	10.79
1080	92.36	64.74	0.0509	0.020	29.90	10.85
1440	92.36	64.71	0.0508	0.020	29.94	10.89

Table A-I.4: Experimental data for the adsorption of Cu²⁺ onto MWCNT-COOH as a function of adsorbent dose [conditions: pH 5.0, contact time 24 h, agitation speed 150 rpm, temperature 20 °C]

$C_i/\text{mg dm}^{-3}$	$C_{eq}/\text{mg dm}^{-3}$	Mass/g	Volume/dm ³	% adsorbed	$q_e/\text{mg g}^{-1}$
103.4	74.69	0.030	0.020	27.77	18.11
103.4	72.14	0.050	0.020	30.23	12.33
103.4	67.75	0.075	0.020	34.48	9.494
103.4	64.30	0.100	0.020	37.81	7.563
103.4	58.91	0.150	0.020	43.03	5.912
103.4	55.83	0.200	0.020	46.01	4.684
103.4	45.05	0.300	0.020	56.43	3.858
103.4	43.22	0.400	0.020	58.20	2.996

Table A-I.5: Experimental data for the adsorption of Cu²⁺ onto MWCNT-COOH as a function of temperature
[conditions: pH 5.0, contact time 24 h, agitation speed 150 rpm]

T/K	C _i /mg dm ⁻³	C _{eq} /mg dm ⁻³	Mass/g	Volume/dm ³	% adsorbed	q _e /mg g ⁻¹
298 K	10.24	0.419	0.0507	0.020	98.21	3.874
	21.12	1.980	0.0501	0.020	95.70	7.641
	31.36	6.543	0.0507	0.020	82.72	9.790
	42.92	13.77	0.0504	0.020	72.88	11.57
	52.50	19.03	0.0503	0.020	66.94	13.31
	59.74	23.87	0.0501	0.020	59.78	14.32
	69.73	30.22	0.0504	0.020	56.44	15.68
	79.98	36.22	0.0507	0.020	54.70	17.26
	91.42	43.99	0.0506	0.020	52.70	18.75
97.16	49.53	0.0501	0.020	47.63	19.01	
303 K	10.24	0.846	0.0503	0.020	91.74	3.735
	21.12	2.543	0.0500	0.020	87.96	7.431
	31.36	8.442	0.0502	0.020	73.08	9.131
	42.92	15.84	0.0501	0.020	63.09	10.81
	52.50	21.05	0.0505	0.020	59.90	12.46
	59.74	26.35	0.0508	0.020	55.89	13.15
	69.73	33.14	0.0511	0.020	52.47	14.32
	79.98	40.02	0.0505	0.020	49.96	15.83
	91.42	50.66	0.0503	0.020	44.59	16.21
97.16	55.74	0.0504	0.020	42.63	16.44	
313 K	10.24	1.890	0.0502	0.020	81.54	3.327
	21.12	4.223	0.0514	0.020	80.00	6.575
	31.36	9.854	0.0505	0.020	68.58	8.517
	42.92	16.14	0.0519	0.020	62.40	10.32
	52.50	22.50	0.0509	0.020	57.14	11.79
	59.74	28.46	0.0503	0.020	52.36	12.44
	69.73	36.12	0.0505	0.020	47.75	13.07
	79.98	44.31	0.0502	0.020	44.60	14.21
	91.42	54.87	0.0504	0.020	39.98	14.50
97.16	60.13	0.0502	0.020	38.11	14.75	
318 K	10.24	2.640	0.0512	0.020	74.22	2.969
	21.12	6.408	0.0505	0.020	69.66	5.827
	31.36	12.66	0.0509	0.020	59.63	7.348
	39.55	18.63	0.0506	0.020	48.74	8.269
	51.20	26.13	0.0516	0.020	47.75	9.717
	60.30	32.89	0.0506	0.020	45.88	10.83
	70.22	40.77	0.0506	0.020	42.60	11.64
	80.11	47.84	0.0515	0.020	40.35	12.53
	89.94	57.99	0.0507	0.020	34.95	12.60

100.2 68.11 0.0504 0.020 33.03 12.73

Table A-I.6: Experimental data for the adsorption of Cu²⁺ onto MWCNT-tty as a function of pH [conditions: contact time 24 h, agitation speed 150 rpm, temperature 20 °C]

pH	C _i /mg dm ⁻³	C _{eq} /mg dm ⁻³	Mass/g	Volume/dm ³	% adsorbed	q _e /mg g ⁻¹
1	103	83.44	0.0500	0.020	18.99	7.824
2	103	79.22	0.0500	0.020	23.09	9.512
3	103	70.22	0.0502	0.020	31.83	13.06
4	103	31.44	0.0505	0.020	69.48	28.34
5	103	17.22	0.0496	0.020	83.28	34.59
6	103	6.88	0.0495	0.020	93.32	38.84
7	103	0.998	0.0494	0.020	99.03	41.30
8	103	0.482	0.0508	0.020	99.53	40.36
9	103	0.221	0.0498	0.020	99.79	41.28
10	103	0.000	0.0506	0.020	100.0	40.71

Table A-I.7: Experimental data for the adsorption of Cu²⁺ onto MWCNT-tty as a function of time [conditions: pH 5.0, agitation speed 150 rpm, temperature 20 °C]

Time/min	C _i /mg dm ⁻³	C _{eq} /mg dm ⁻³	Mass/g	Volume/dm ³	% adsorbed	q _e /mg g ⁻¹
5	103.0	55.88	0.0511	0.020	45.75	18.44
10	103.0	50.77	0.0515	0.020	50.71	20.28
15	103.0	48.12	0.0515	0.020	53.28	21.31
20	103.0	45.44	0.0509	0.020	55.88	22.62
30	103.0	38.71	0.0509	0.020	62.42	25.26
45	103.0	33.14	0.0503	0.020	67.83	27.78
60	103.0	29.88	0.0502	0.020	70.99	29.13
75	103.0	22.54	0.0514	0.020	78.12	31.31
90	103.0	21.44	0.0508	0.020	79.18	32.11
120	103.0	18.72	0.0502	0.020	81.83	33.58
180	103.0	16.84	0.0501	0.020	83.65	34.40
240	103.0	15.72	0.0502	0.020	84.74	34.77
300	103.0	15.33	0.0501	0.020	85.12	35.00
360	103.0	14.88	0.0501	0.020	85.55	35.18
720	103.0	14.11	0.0503	0.020	86.30	35.34
1080	103.0	13.84	0.050	0.020	86.56	35.66
1440	103.0	13.11	0.0502	0.020	87.27	35.81

Table A-I.8: Experimental data for the adsorption of Cu²⁺ onto MWCNT-ttpy as a function of adsorbent dose
[conditions: pH 5.0, contact time 24 h, agitation speed 150 rpm, temperature 20 °C]

C _i /mg dm ⁻³	C _{eq} /mg dm ⁻³	Mass/g	Volume/dm ³	% adsorbed	q _e /mg g ⁻¹
103.0	22.11	0.031	0.020	78.53	52.02
103.0	9.854	0.050	0.020	90.43	37.11
103.0	4.211	0.075	0.020	95.91	26.20
103.0	1.410	0.100	0.020	98.63	20.26
103.0	0.877	0.151	0.020	99.15	13.57
103.0	0.543	0.200	0.020	99.47	10.27
103.0	0.321	0.300	0.020	99.69	6.843
103.0	0.088	0.402	0.020	99.91	5.120

Table A-I.9: Experimental data for the adsorption of Cu²⁺ onto MWCNT-ttpy as a function of temperature
[conditions: pH 5.0, contact time 24 h, agitation speed 150 rpm, temperature 20 °C]

T/K	C _i /mg dm ⁻³	C _{eq} /mg dm ⁻³	Mass/g	Volume/dm ³	% adsorbed	q _e /mg g ⁻¹
298 K	10.24	0.000	0.0507	0.020	100.0	4.039
	21.12	0.094	0.0501	0.020	99.55	8.394
	31.36	0.121	0.0507	0.020	99.61	12.32
	39.55	0.322	0.0504	0.020	99.19	15.57
	51.20	0.611	0.0503	0.020	98.81	20.11
	60.30	1.214	0.0501	0.020	97.99	23.59
	70.22	1.977	0.0504	0.020	97.18	27.08
	80.11	4.115	0.0507	0.020	94.86	29.98
	89.94	10.22	0.0506	0.020	88.64	31.51
	100.2	20.12	0.0501	0.020	79.92	31.97
303 K	10.24	0.000	0.0503	0.020	100.0	4.072
	21.12	0.000	0.0500	0.020	100.0	8.448
	31.36	0.088	0.0502	0.020	99.72	12.46
	39.55	0.144	0.0501	0.020	99.64	15.73
	51.20	0.332	0.0500	0.020	99.35	20.35
	60.30	0.544	0.0502	0.020	99.10	23.81
	70.22	1.021	0.0502	0.020	98.55	27.57
	80.11	2.331	0.0505	0.020	97.09	30.80
	89.94	7.331	0.0501	0.020	91.85	32.98
	100.2	17.22	0.0500	0.020	82.81	33.19
313 K	10.24	0.000	0.0502	0.020	100.00	4.080
	21.12	0.000	0.0514	0.020	100.00	8.218
	31.36	0.053	0.0505	0.020	99.83	12.40
	39.55	0.082	0.0519	0.020	91.96	15.21
	51.20	0.15	0.0509	0.020	97.23	20.06
	60.30	0.611	0.0503	0.020	99.91	23.73

	70.22	1.144	0.0505	0.020	99.92	27.36
	80.11	1.112	0.0502	0.020	98.77	31.47
	89.94	5.112	0.0504	0.020	92.79	33.66
	100.2	13.88	0.0502	0.020	88.84	34.39
318 K	10.24	0.000	0.0498	0.020	100.0	4.112
	21.12	0.000	0.0505	0.020	100.0	8.364
	31.36	0.000	0.0500	0.020	100.0	12.54
	39.55	0.032	0.0506	0.020	99.92	15.62
	51.20	0.114	0.0504	0.020	99.78	20.27
	60.30	0.221	0.0500	0.020	99.63	24.03
	70.22	0.206	0.0500	0.020	99.71	28.01
	80.11	0.877	0.0501	0.020	98.91	31.63
	89.94	3.422	0.0502	0.020	96.20	34.47
	100.2	12.44	0.0504	0.020	87.58	34.83

Table A-I.10: Separation factor values (R_L) for the adsorption of Cu^{2+} onto MWCNT-COOH at different temperatures

$C_i/\text{mg dm}^{-3}$	298 K	303 K	313 K	318 K
10.24	0.366	0.347	0.443	0.590
21.12	0.219	0.205	0.278	0.410
31.36	0.159	0.148	0.206	0.319
42.92	0.121	0.112	0.159	0.255
52.50	0.101	0.094	0.134	0.219
59.74	0.090	0.083	0.120	0.198
69.73	0.078	0.072	0.104	0.174
79.98	0.069	0.064	0.092	0.155
91.42	0.061	0.056	0.082	0.139
97.16	0.057	0.053	0.077	0.131

Table A-I.11: Separation factor values (R_L) for the adsorption of Cu^{2+} onto MWCNT-ttph at different temperatures

$C_i/\text{mg dm}^{-3}$	298 K	303 K	313 K	318 K
10.24	0.0292	0.0175	0.0107	0.0056
21.12	0.0144	0.0085	0.0052	0.0027
31.36	0.0097	0.0058	0.0035	0.0018
39.55	0.0077	0.0046	0.0028	0.0015
51.20	0.0060	0.0035	0.0021	0.0011
60.30	0.0051	0.0030	0.0018	0.0010
70.22	0.0044	0.0026	0.0016	0.0008
80.11	0.0038	0.0023	0.0014	0.0007
89.94	0.0034	0.0020	0.0012	0.0006
100.2	0.0031	0.0018	0.0011	0.0006

Appendix II

Data for Lead(II) and Zinc(II)

Table A-II.1: Operating conditions for the ICP-OES spectrometer used for Pb²⁺ and Zn²⁺ determination

Wavelength (Pb ²⁺)	220.353 nm
Wavelength (Zn ²⁺)	213.857 nm
RF power	1300 W
Plasma gas flow rate	15 dm ³ min ⁻¹
Pump	1.5 cm ³ min ⁻¹
Auxiliary gas flow rate	0.2 dm ³ min ⁻¹
Nebulizer gas flow rate	0.8 dm ³ min ⁻¹
Nebulizer pressure	2 bars
Analyzer type	Axial
Replicates	3
Sample read delay	60 s

Table A-II.2: Experimental data for the adsorption of Pb²⁺ onto MWCNT-COOH as a function of pH [conditions: contact time 24 h, agitation speed 150 rpm, temperature 20 °C]

pH	C _i /mg dm ⁻³	C _{eq} /mg dm ⁻³	Mass/g	Volume/dm ³	%adsorbed	q _e /mg g ⁻¹
1	97.63	86.10	0.0511	0.020	11.81	4.513
2	97.63	73.97	0.0512	0.020	24.23	9.242
3	97.63	50.15	0.0503	0.020	48.63	18.88
4	97.63	47.88	0.0506	0.020	50.96	19.66
5	97.63	30.42	0.0505	0.020	68.84	26.62
6	97.63	11.85	0.0501	0.020	87.86	34.24
7	97.63	11.14	0.0500	0.020	88.59	34.60
8	97.63	8.730	0.0507	0.020	91.06	35.07
9	97.63	6.130	0.0502	0.020	93.72	36.45
10	97.63	3.970	0.0508	0.020	95.93	36.87

Table A-II.3: Experimental data for the adsorption of Pb²⁺ onto MWCNT-COOH as a function of time [conditions: pH 4.5, agitation speed 150 rpm, temperature 20 °C]

Time/min	C _i /mg dm ⁻³	C _{eq} /mg dm ⁻³	Mass/g	Volume/dm ³	% adsorbed	q _e /mg g ⁻¹
5	96.70	75.20	0.0509	0.020	22.23	8.448
10	96.70	74.60	0.0504	0.020	22.85	8.770
15	96.70	70.51	0.0508	0.020	27.08	10.31
20	96.70	66.54	0.0504	0.020	31.19	11.97
30	96.70	63.72	0.0505	0.020	34.11	13.06
45	96.70	55.32	0.0506	0.020	42.79	16.36
60	96.70	52.40	0.0506	0.020	45.81	17.51
75	96.70	48.31	0.0508	0.020	50.04	19.05
90	96.70	45.74	0.0509	0.020	52.70	20.02
120	96.70	44.88	0.0504	0.020	53.59	20.56
180	96.70	43.88	0.0506	0.020	54.62	20.88
240	96.70	43.32	0.0505	0.020	55.20	21.14
300	96.70	42.98	0.0507	0.020	55.55	21.19
360	96.70	42.51	0.0506	0.020	56.04	21.42
720	96.70	42.49	0.0502	0.020	56.06	21.60
1080	96.70	42.47	0.0502	0.020	56.08	21.61
1440	96.70	42.44	0.0502	0.020	56.11	21.62

Table A-II.4: Experimental data for the adsorption of Pb²⁺ onto MWCNT-COOH as a function of adsorbent dose [conditions: pH 4.5, contact time 24 h, agitation speed 150 rpm, temperature 20 °C]

C _i /mg dm ⁻³	C _{eq} /mg dm ⁻³	Mass/g	Volume/dm ³	% adsorbed	q _e /mg g ⁻¹
96.70	61.96	0.030	0.02	35.93	23.16
96.70	44.11	0.050	0.02	54.38	21.04
96.70	41.13	0.075	0.02	57.47	14.82
96.70	36.80	0.100	0.02	61.94	11.98
96.70	31.48	0.150	0.02	67.45	8.696
96.70	25.93	0.200	0.02	73.19	7.077
96.70	13.97	0.300	0.02	85.55	5.515
96.70	11.09	0.400	0.02	88.53	4.281

Table A-II.5: Experimental data for the adsorption of Pb²⁺ onto MWCNT-COOH as a function of temperature
[conditions: pH 4.5, contact time 24 h, agitation speed 150 rpm]

T/K	$C_i/\text{mg dm}^{-3}$	$C_{eq}/\text{mg dm}^{-3}$	Mass/g	Volume/ dm^3	% adsorbed	$q_e/\text{mg g}^{-1}$
298 K	10.55	0.211	0.0502	0.020	98.00	4.119
	21.11	0.922	0.0501	0.020	95.63	8.059
	30.23	1.434	0.0503	0.020	95.26	11.45
	38.52	3.442	0.0507	0.020	91.06	13.84
	49.82	6.991	0.0503	0.020	85.97	17.03
	60.11	13.05	0.0503	0.020	78.29	18.71
	70.24	20.86	0.0507	0.020	70.30	19.48
	80.22	29.44	0.0511	0.020	63.30	19.87
	90.33	39.11	0.0503	0.020	56.70	20.37
	100.4	48.33	0.0508	0.020	51.87	20.50
303 K	10.55	0.188	0.0500	0.020	98.22	4.145
	21.11	0.612	0.0504	0.020	97.10	8.134
	30.23	1.322	0.0501	0.020	95.63	11.54
	38.52	2.337	0.0503	0.020	93.93	14.39
	49.82	5.662	0.0500	0.020	88.64	17.66
	60.11	11.23	0.0508	0.020	81.32	19.24
	70.24	18.44	0.051	0.020	73.75	20.31
	80.22	27.88	0.0508	0.020	65.25	20.61
	90.33	36.77	0.0506	0.020	59.29	21.17
	100.4	45.77	0.0503	0.020	54.42	21.73
313 K	12.43	0.088	0.0502	0.020	99.29	4.917
	25.44	0.501	0.0509	0.020	98.03	9.799
	35.04	0.844	0.0507	0.020	97.59	13.49
	46.24	1.544	0.0503	0.020	96.66	17.77
	58.46	4.788	0.0503	0.020	91.81	21.34
	59.66	5.210	0.0509	0.020	91.27	21.39
	70.00	11.45	0.0512	0.020	83.64	22.87
	80.20	20.44	0.0517	0.020	74.51	23.12
	90.00	30.14	0.0513	0.020	66.51	23.34
	99.19	39.44	0.0510	0.020	60.24	23.43
318 K	12.43	0.033	0.0501	0.020	99.73	4.949
	25.44	0.311	0.0511	0.020	98.78	9.835
	35.04	0.622	0.0503	0.020	98.22	13.685
	46.24	1.022	0.0509	0.020	97.79	17.77
	58.46	3.215	0.0500	0.020	94.50	22.10
	59.66	3.744	0.0501	0.020	93.72	22.32
	75.20	11.86	0.0502	0.020	84.23	25.24
	80.40	15.84	0.0510	0.020	80.30	25.32
	90.10	22.77	0.0523	0.020	74.73	25.75

99.19 32.44 0.0517 0.020 67.30 25.82

Table A-II.6: Experimental data for the adsorption of Pb²⁺ onto MWCNT-ttpy as a function of pH [conditions: contact time 24 h, agitation speed 150 rpm, temperature 20 °C]

pH	C _i /mg dm ⁻³	C _{eq} /mg dm ⁻³	Mass/g	Volume/dm ³	% adsorbed	q _e /mg g ⁻¹
1	102.6	78.33	0.0500	0.020	23.65	9.708
2	102.6	54.88	0.0498	0.020	46.51	19.16
3	102.6	44.12	0.0502	0.020	57.00	23.30
4	102.6	21.44	0.0500	0.020	79.10	32.46
5	102.6	15.22	0.0502	0.020	85.17	34.81
6	102.6	4.906	0.0500	0.020	95.22	39.08
7	102.6	0.802	0.0500	0.020	99.22	40.72
8	102.6	0.717	0.0500	0.020	99.30	40.75
9	102.6	0.823	0.0500	0.020	99.20	40.71
10	102.6	1.314	0.0501	0.020	98.72	40.43

Table A-II.7: Experimental data for the adsorption of Pb²⁺ onto MWCNT-ttpy as a function of time [conditions: pH 4.5, agitation speed 150 rpm, temperature 20 °C]

Time/min	C _i /mg dm ⁻³	C _{eq} /mg dm ⁻³	Mass/g	Volume/dm ³	% adsorbed	q _e /mg g ⁻¹
5	102.6	75.22	0.0501	0.020	26.69	10.930
10	102.6	66.55	0.0503	0.020	35.14	14.33
15	102.6	52.22	0.0500	0.020	49.10	20.15
20	102.6	49.22	0.0505	0.020	52.03	21.14
30	102.6	33.55	0.0503	0.020	67.30	27.46
45	102.6	29.12	0.0502	0.020	71.62	29.27
60	102.6	24.21	0.0501	0.020	76.40	31.29
75	102.6	22.44	0.0502	0.020	78.13	31.94
90	102.6	19.88	0.0508	0.020	80.62	32.57
120	102.6	19.22	0.0502	0.020	81.27	33.22
180	102.6	17.92	0.0501	0.020	82.53	33.80
240	102.6	16.46	0.0500	0.020	83.96	34.46
300	102.6	16.55	0.0498	0.020	83.87	34.56
360	102.6	16.11	0.0496	0.020	84.30	34.88
720	102.6	15.02	0.0500	0.020	85.36	35.03
1080	102.6	14.22	0.0501	0.020	86.14	35.28
1440	102.6	14.02	0.0502	0.020	86.34	35.29

Table A-II.8: Experimental data for the adsorption of Pb²⁺ onto MWCNT-tpy as a function of adsorbent dose
[conditions: pH 4.5, contact time 24 h, agitation speed 150 rpm, temperature 20 °C]

$C_i/\text{mg dm}^{-3}$	$C_{eq}/\text{mg dm}^{-3}$	Mass/g	Volume/ dm^3	% adsorbed	$q_e/\text{mg g}^{-1}$
103.4	49.25	0.0312	0.020	52.37	34.71
103.4	19.22	0.0497	0.020	81.41	33.88
103.4	17.12	0.0746	0.020	83.45	23.13
103.4	15.21	0.1005	0.020	85.29	17.55
103.4	9.887	0.1503	0.020	90.44	12.44
103.4	8.221	0.2001	0.020	92.05	9.513
103.4	7.322	0.3001	0.020	92.92	6.403
103.4	4.221	0.4005	0.020	95.92	4.953

Table A-II.9: Experimental data for the adsorption of Pb²⁺ onto MWCNT-tpy as a function of temperature
[conditions: pH 4.5, contact time 24 h, agitation speed 150 rpm, temperature 20 °C]

T/K	$C_i/\text{mg dm}^{-3}$	$C_{eq}/\text{mg dm}^{-3}$	Mass/g	Volume/ dm^3	% adsorbed	$q_e/\text{mg g}^{-1}$
298 K	10.55	0.000	0.0497	0.020	100.00	4.245
	21.11	0.228	0.0505	0.020	98.92	8.270
	30.23	0.522	0.0495	0.020	98.27	12.00
	38.52	0.821	0.0511	0.020	97.87	14.75
	49.82	1.336	0.050	0.020	97.32	19.39
	60.11	2.112	0.0512	0.020	96.49	22.66
	70.24	3.271	0.0498	0.020	95.34	26.90
	80.22	4.722	0.0498	0.020	94.11	30.32
	90.33	8.114	0.0508	0.020	91.02	32.37
100.4	15.88	0.0498	0.020	84.18	33.95	
303 K	10.55	0.000	0.0499	0.020	100.0	4.228
	21.11	0.113	0.0511	0.020	99.46	8.218
	30.23	0.332	0.0504	0.020	98.90	11.86
	38.52	0.493	0.0498	0.020	98.72	15.27
	49.82	0.772	0.0501	0.020	98.45	19.58
	60.11	1.277	0.0496	0.020	97.88	23.72
	70.24	2.118	0.0500	0.020	96.98	27.25
	80.22	3.115	0.0508	0.020	96.12	30.36
	90.33	6.224	0.0500	0.020	93.11	33.64
100.4	12.44	0.0502	0.020	87.61	35.05	
313 K	12.43	0.000	0.0499	0.020	100.0	4.982
	25.44	0.000	0.0502	0.020	100.0	10.14
	35.04	0.088	0.0502	0.020	99.75	13.93
	46.24	0.133	0.0500	0.020	99.71	18.44
	58.46	0.422	0.0500	0.020	99.28	23.22
	59.66	0.434	0.0501	0.020	99.27	23.64

	70.00	0.877	0.0502	0.020	98.75	27.54
	80.20	1.344	0.0503	0.020	98.32	31.35
	90.00	3.221	0.0501	0.020	96.42	34.64
	99.19	10.22	0.0502	0.020	89.70	35.45
318 K	11.40	0.000	0.0494	0.020	100.00	4.615
	22.40	0.000	0.0496	0.020	100.00	9.032
	32.50	0.088	0.0501	0.020	99.73	12.94
	40.50	0.104	0.0500	0.020	99.74	16.16
	49.79	0.226	0.0497	0.020	99.55	19.95
	59.88	0.422	0.0505	0.020	99.30	23.55
	69.40	0.621	0.0503	0.020	99.11	27.35
	79.88	1.055	0.0506	0.020	98.68	31.16
	89.77	2.144	0.0505	0.020	97.61	34.70
	105.4	13.44	0.0503	0.020	87.25	36.56

Table A-II.10: Separation factor values (R_L) for the adsorption of Pb^{2+} onto MWCNT-COOH at different temperatures

$C_i/mg\ dm^{-3}$	298 K	303 K	313 K	318 K
10.55	0.114	0.093	0.054	0.046
21.11	0.060	0.049	0.028	0.023
30.23	0.043	0.035	0.020	0.016
38.52	0.034	0.027	0.016	0.013
49.82	0.026	0.021	0.012	0.010
60.11	0.022	0.018	0.010	0.008
70.24	0.019	0.015	0.009	0.007
80.22	0.017	0.013	0.008	0.006
90.33	0.015	0.012	0.007	0.006
100.4	0.013	0.011	0.006	0.005

Table A-II.11: Separation factor values (R_L) for the adsorption of Pb^{2+} onto MWCNT-ttpy at different temperatures

$C_i/mg\ dm^{-3}$	298 K	303 K	313 K	318 K
10.55	0.095	0.058	0.015	0.016
21.11	0.050	0.030	0.007	0.008
30.23	0.035	0.021	0.005	0.006
38.52	0.028	0.017	0.004	0.004
49.82	0.022	0.013	0.003	0.003
60.11	0.018	0.011	0.003	0.003
70.24	0.015	0.009	0.002	0.002
80.22	0.014	0.008	0.002	0.002
90.33	0.012	0.007	0.002	0.002
100.4	0.011	0.006	0.002	0.002

Table A-II.12: Experimental data for the adsorption of Zn²⁺ onto MWCNT-COOH as a function of pH
[conditions: contact time 24 h, agitation speed 150 rpm, temperature 20 °C]

pH	C _i /mg dm ⁻³	C _{eq} /mg dm ⁻³	Mass/g	Volume/dm ³	%adsorbed	q _e /mg g ⁻¹
1	99.43	81.94	0.0507	0.020	17.59	6.899
2	99.43	87.27	0.0509	0.020	12.23	4.778
3	99.43	82.37	0.0503	0.020	17.16	6.783
4	99.43	70.09	0.0501	0.020	29.51	11.71
5	99.43	64.88	0.0508	0.020	34.75	13.60
6	99.43	30.77	0.0505	0.020	69.05	27.19
7	99.43	3.807	0.0511	0.020	96.17	37.43
8	99.43	2.430	0.0506	0.020	97.56	38.34
9	99.43	0.884	0.0503	0.020	99.11	39.18
10	99.43	0.000	0.0502	0.020	100.00	39.61

Table A-II.13: Experimental data for the adsorption of Zn²⁺ onto MWCNT-COOH as a function of time
[conditions: pH 5.5, agitation speed 150 rpm, temperature 20 °C]

Time/min	C _i /mg dm ⁻³	C _{eq} /mg dm ⁻³	Mass/g	Volume/dm ³	% adsorbed	q _e /mg g ⁻¹
5	98.35	89.78	0.0503	0.020	8.714	3.408
10	98.35	89.34	0.0505	0.020	9.161	3.568
15	98.35	84.97	0.0501	0.020	13.60	5.341
20	98.35	84.16	0.0500	0.020	14.43	5.676
30	98.35	80.23	0.0502	0.020	18.42	7.219
45	98.35	78.52	0.0503	0.020	20.16	7.885
60	98.35	72.14	0.0503	0.020	26.65	10.42
75	98.35	69.52	0.0500	0.020	29.31	11.53
90	98.35	66.95	0.0504	0.020	31.93	12.46
120	98.35	64.55	0.0502	0.020	34.37	13.47
180	98.35	60.11	0.0502	0.020	38.88	15.24
240	98.35	59.22	0.0501	0.020	39.79	15.62
300	98.35	57.41	0.0501	0.020	41.63	16.34
360	98.35	56.14	0.0501	0.020	42.92	16.85
720	98.35	53.33	0.0501	0.020	45.78	17.97
1080	98.35	51.88	0.0506	0.020	47.25	18.37
1440	98.35	51.33	0.0507	0.020	47.81	18.55

Table A-II.14: Experimental data for the adsorption of Zn²⁺ onto MWCNT-COOH as a function of adsorbent dose [conditions: pH 5.5, contact time 24 h, agitation speed 150 rpm, temperature 20 °C]

$C_i/\text{mg dm}^{-3}$	$C_{eq}/\text{mg dm}^{-3}$	Mass/g	Volume/ dm^3	% adsorbed	$q_e/\text{mg g}^{-1}$
98.35	58.94	0.0302	0.020	40.07	26.10
98.35	54.74	0.0504	0.020	44.34	17.31
98.35	52.98	0.0757	0.020	46.13	11.99
98.35	50.49	0.1004	0.020	48.66	9.534
98.35	46.41	0.1500	0.020	52.81	6.925
98.35	41.08	0.2005	0.020	58.23	5.713
98.35	37.59	0.3009	0.020	61.78	4.039
98.35	37.22	0.4001	0.020	62.16	3.056

Table A-II.15: Experimental data for the adsorption of Zn²⁺ onto MWCNT-COOH as a function of temperature [conditions: pH 5.5, contact time 24 h, agitation speed 150 rpm]

T/K	$C_i/\text{mg dm}^{-3}$	$C_{eq}/\text{mg dm}^{-3}$	Mass/g	Volume/ dm^3	% adsorbed	$q_e/\text{mg g}^{-1}$
298 K	7.360	2.674	0.0500	0.020	46.86	1.874
	21.45	9.221	0.0501	0.020	61.15	4.882
	29.46	14.19	0.0504	0.020	50.90	6.060
	41.62	21.77	0.0502	0.020	49.63	7.908
	52.17	27.89	0.0500	0.020	48.56	9.712
	60.10	33.63	0.0501	0.020	44.12	10.57
	70.63	42.14	0.0503	0.020	40.70	11.33
	78.13	47.88	0.0506	0.020	37.81	11.96
	88.93	56.77	0.0506	0.020	35.73	12.71
99.43	66.91	0.0504	0.020	32.52	12.90	
303 K	7.360	2.133	0.0500	0.020	71.02	2.091
	21.45	7.432	0.0507	0.020	65.35	5.530
	29.46	12.39	0.0509	0.020	57.94	6.707
	41.62	19.13	0.0501	0.020	54.04	8.978
	52.17	26.24	0.0507	0.020	49.70	10.23
	60.10	31.45	0.0502	0.020	47.67	11.41
	70.63	39.22	0.0503	0.020	44.47	12.49
	78.13	45.46	0.0505	0.020	41.81	12.94
	88.93	54.15	0.0509	0.020	39.11	13.67
99.43	64.43	0.0501	0.020	35.20	13.97	
313 K	7.360	1.995	0.0501	0.020	72.89	2.142
	21.45	6.992	0.0500	0.020	67.40	5.783
	29.46	10.02	0.0501	0.020	65.99	7.760
	41.62	17.44	0.0503	0.020	58.10	9.614
	52.17	24.88	0.0500	0.020	52.31	10.92
	60.10	28.96	0.0500	0.020	51.81	12.46
	70.63	36.78	0.0503	0.020	47.93	13.46

	78.13	43.11	0.0502	0.020	44.82	13.95
	88.93	53.15	0.0502	0.020	40.23	14.25
	99.43	63.45	0.0502	0.020	36.19	14.33
318 K	7.360	1.445	0.0505	0.020	80.37	2.343
	21.45	6.220	0.0502	0.020	71.00	6.068
	29.46	9.320	0.0502	0.020	68.36	8.024
	41.62	16.43	0.0504	0.020	60.52	10.00
	52.17	23.44	0.0505	0.020	55.07	11.38
	60.10	28.37	0.0500	0.020	52.80	12.69
	70.63	35.77	0.0505	0.020	49.36	13.81
	78.13	42.12	0.0504	0.020	46.09	14.29
	88.93	50.31	0.0513	0.020	43.43	15.06
	99.43	61.06	0.0506	0.020	38.59	15.17

Table A-II.16: Experimental data for the adsorption of Zn²⁺ onto MWCNT-tty as a function of pH [conditions: contact time 24 h, agitation speed 150 rpm, temperature 20 °C]

pH	$C_i/\text{mg dm}^{-3}$	$C_{eq}/\text{mg dm}^{-3}$	Mass/g	Volume/dm ³	%adsorbed	$q_e/\text{mg g}^{-1}$
1	100.4	72.11	0.0507	0.0200	28.21	11.18
2	100.4	74.90	0.0509	0.0200	25.43	10.04
3	100.4	60.34	0.0503	0.0200	39.92	15.94
4	100.4	58.13	0.0501	0.0200	42.12	16.89
5	100.4	30.22	0.0508	0.0200	69.91	27.65
6	100.4	17.22	0.0505	0.0200	82.86	32.96
7	100.4	2.982	0.0511	0.0200	97.03	38.14
8	100.4	1.274	0.0506	0.0200	98.73	39.20
9	100.4	0.433	0.0503	0.0200	99.57	39.76
10	100.4	0.000	0.0502	0.0200	100.0	40.02

Table A-II.17: Experimental data for the adsorption of Zn²⁺ onto MWCNT-tty as a function of time [conditions: pH 5.5, agitation speed 150 rpm, temperature 20 °C]

Time/min	$C_i/\text{mg dm}^{-3}$	$C_{eq}/\text{mg dm}^{-3}$	Mass/g	Volume/dm ³	% adsorbed	$q_e/\text{mg g}^{-1}$
5	100.4	82.33	0.0503	0.020	18.03	7.201
10	100.4	79.74	0.0505	0.020	20.61	8.198
15	100.4	74.22	0.0501	0.020	26.11	10.47
20	100.4	69.44	0.0500	0.020	30.86	12.40
30	100.4	64.21	0.0502	0.020	36.07	14.43
45	100.4	59.42	0.0503	0.020	40.84	16.31
60	100.4	56.74	0.0503	0.020	43.51	17.38
75	100.4	47.33	0.0500	0.020	52.88	21.24
90	100.4	43.14	0.0504	0.020	57.05	22.74
120	100.4	39.22	0.0502	0.020	60.95	24.39

180	100.4	37.44	0.0502	0.020	62.72	25.10
240	100.4	36.11	0.0501	0.020	64.05	25.68
300	100.4	31.92	0.0501	0.020	68.22	27.35
360	100.4	31.73	0.0501	0.020	68.41	27.43
720	100.4	29.22	0.0501	0.020	70.91	28.43
1080	100.4	28.01	0.0513	0.020	72.11	28.24
1440	100.4	27.11	0.0507	0.020	73.01	28.93

Table A-II.18: Experimental data for the adsorption of Zn²⁺ onto MWCNT-ttpy as a function of adsorbent dose [conditions: pH 5.5, contact time 24 h, agitation speed 150 rpm, temperature 20 °C]

$C_i/\text{mg dm}^{-3}$	$C_{eq}/\text{mg dm}^{-3}$	Mass/g	Volume/ dm^3	% adsorbed	$q_e/\text{mg g}^{-1}$
100.4	42.55	0.0302	0.020	57.64	38.34
100.4	28.73	0.0504	0.020	71.40	28.46
100.4	19.33	0.0757	0.020	80.75	21.43
100.4	11.52	0.1004	0.020	88.53	17.71
100.4	9.334	0.1500	0.020	90.71	12.15
100.4	6.160	0.2005	0.020	93.87	9.404
100.4	5.324	0.3009	0.020	94.70	6.322
100.4	2.441	0.4001	0.020	97.57	4.899

Table A-II.19: Experimental data for the adsorption of Zn²⁺ onto MWCNT-ttpy as a function of temperature [conditions: pH 5.5, contact time 24 h, agitation speed 150 rpm, temperature 20 °C]

T/K	$C_i/\text{mg dm}^{-3}$	$C_{eq}/\text{mg dm}^{-3}$	Mass/g	Volume/ dm^3	% adsorbed	$q_e/\text{mg g}^{-1}$
298 K	10.11	0.553	0.0500	0.020	94.53	3.823
	20.22	1.442	0.0501	0.020	92.87	7.496
	29.64	2.334	0.0504	0.020	92.13	10.84
	39.87	3.665	0.0502	0.020	90.81	14.42
	50.11	4.884	0.0500	0.020	90.25	18.09
	59.66	7.442	0.0501	0.020	87.53	20.85
	70.41	11.44	0.0503	0.020	83.75	23.45
	80.16	16.33	0.0506	0.020	79.63	25.23
	90.74	21.55	0.0506	0.020	76.25	27.35
99.68	28.55	0.0504	0.020	71.36	28.23	
303 K	10.11	0.411	0.0500	0.020	95.93	3.880
	20.22	0.830	0.0507	0.020	95.90	7.649
	29.64	1.442	0.0509	0.020	95.13	11.08
	39.87	2.113	0.0501	0.020	94.70	15.07
	50.11	3.118	0.0507	0.020	93.78	18.54
	59.66	4.772	0.0502	0.020	92.00	21.87
	70.41	8.220	0.0503	0.020	88.33	24.73
	80.16	13.55	0.0505	0.020	83.10	26.38

	90.74	18.63	0.0509	0.020	79.47	28.33
	99.68	26.11	0.0501	0.020	73.81	29.37
313 K	10.11	0.221	0.0501	0.020	97.81	3.948
	20.22	0.488	0.0500	0.020	97.59	7.893
	29.64	0.774	0.0501	0.020	97.39	11.52
	39.87	1.224	0.0503	0.020	96.93	15.37
	50.11	1.772	0.0500	0.020	96.46	19.34
	59.66	2.433	0.0500	0.020	95.92	22.89
	70.41	4.553	0.0503	0.020	93.53	26.19
	80.16	7.665	0.0502	0.020	90.44	28.88
	90.74	13.44	0.0502	0.020	85.19	30.80
	99.68	19.33	0.0502	0.020	80.61	32.01
318 K	10.11	0.131	0.0505	0.020	98.70	3.952
	20.22	0.228	0.0502	0.020	98.87	7.965
	29.64	0.331	0.0502	0.020	98.88	11.68
	39.87	0.755	0.0504	0.020	98.11	15.52
	50.11	1.221	0.0505	0.020	97.56	19.36
	59.66	2.114	0.0500	0.020	96.46	23.02
	70.41	3.153	0.0505	0.020	95.52	26.64
	80.16	4.332	0.0504	0.020	94.60	30.09
	90.74	9.223	0.0513	0.020	89.84	31.78
	99.68	16.33	0.0506	0.020	83.62	32.94

Table A-II.20: Separation factor values (R_L) for the adsorption of Zn^{2+} onto MWCNT-COOH at different temperatures

$C_i/mg\ dm^{-3}$	298 K	303 K	313 K	318 K
7.360	0.786	0.727	0.663	0.638
21.45	0.558	0.478	0.403	0.377
29.46	0.478	0.400	0.330	0.306
41.62	0.394	0.320	0.258	0.238
52.17	0.341	0.273	0.217	0.199
60.10	0.310	0.246	0.194	0.178
70.63	0.277	0.217	0.170	0.155
78.13	0.257	0.201	0.156	0.143
88.93	0.233	0.181	0.140	0.127
99.43	0.214	0.165	0.127	0.116

Table A-II.21: Separation factor values (R_L) for the adsorption of Zn^{2+} onto MWCNT-tty at different temperatures

$C_i/\text{mg dm}^{-3}$	298 K	303 K	313 K	318 K
10.11	0.304	0.196	0.126	0.079
20.22	0.180	0.109	0.067	0.041
29.64	0.130	0.077	0.047	0.028
39.87	0.100	0.058	0.035	0.021
50.11	0.081	0.047	0.028	0.017
59.66	0.069	0.040	0.024	0.014
70.41	0.059	0.034	0.020	0.012
80.16	0.052	0.030	0.018	0.011
90.74	0.046	0.026	0.016	0.009
99.68	0.043	0.024	0.014	0.009

Appendix III

Data for cadmium(II) and mercury(II)

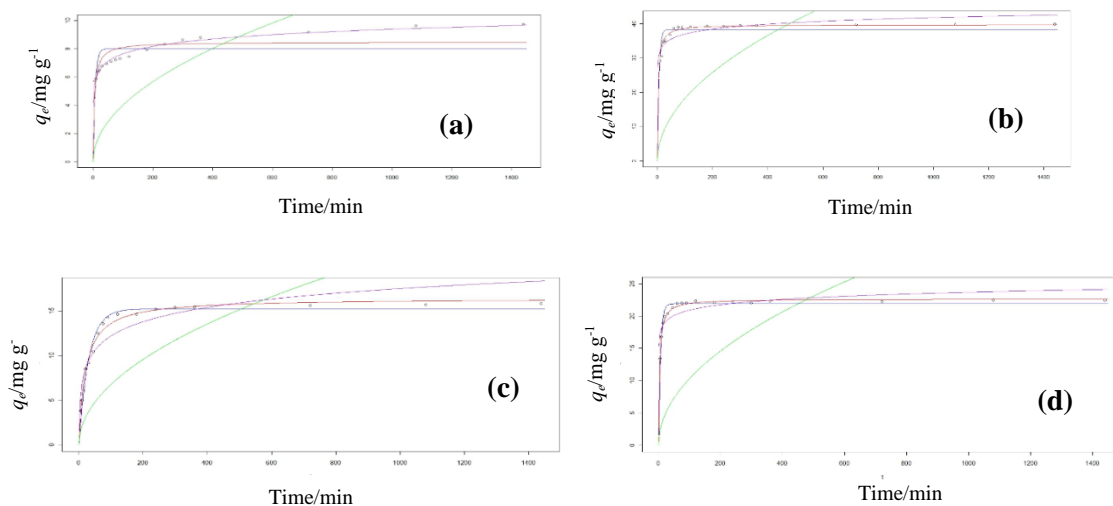


Fig A-III.1: Comparison of the various kinetic models fitted to the experimental data of Cd²⁺ (a-b) and Hg²⁺ (c-d) onto MWCNT-COOH and MWCNT-tpy, respectively (pseudo-first order —, pseudo-second order —, intraparticle diffusion —, Elovich —).

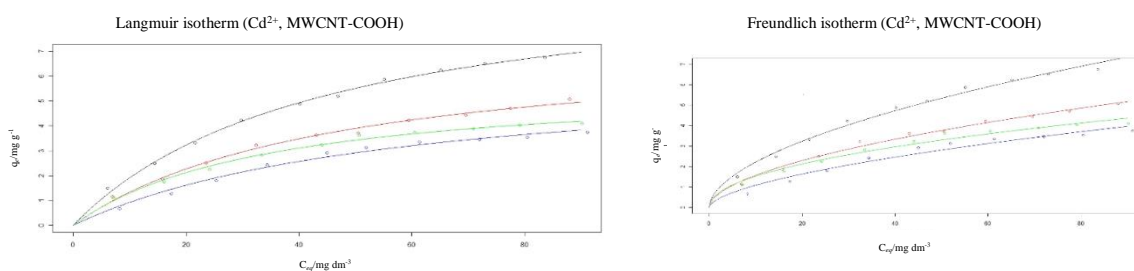


Fig A-III.2: The adsorption isotherms fitted into experimental data for the adsorption of Cd²⁺ onto MWCNT-COOH at various temperatures (293 K —, 303 K —, 313 K —, 318 K —).

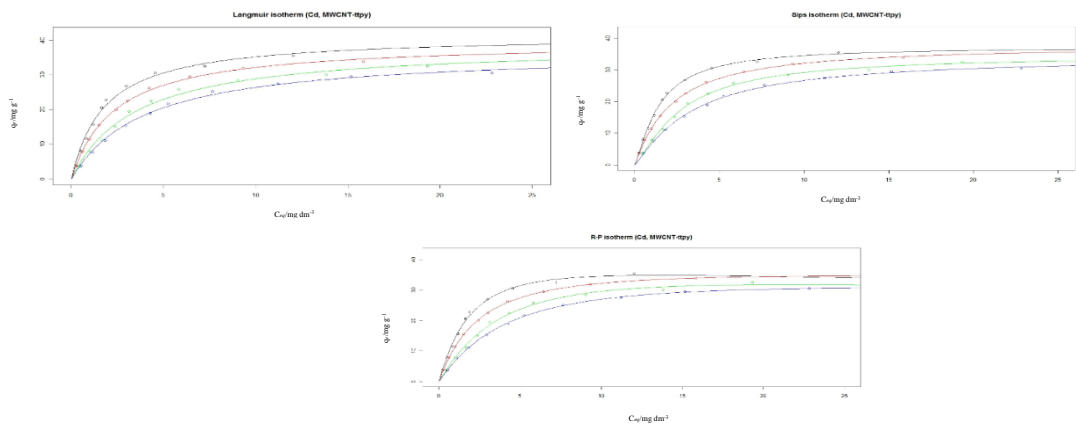


Fig A-III.3: The adsorption isotherms fitted into experimental data for the adsorption of Cd^{2+} onto MWCNT-tpty at various temperatures (293 K —, 303 K —, 313 K —, 318 K —).

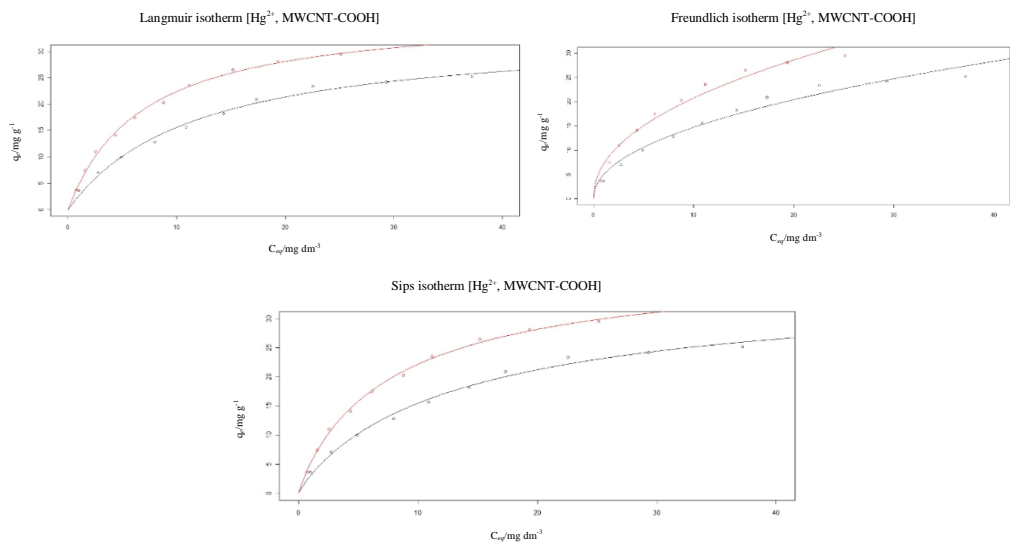


Fig A-III.4: The adsorption isotherms fitted into experimental data for the adsorption of Hg^{2+} onto MWCNT-COOH at various temperatures (293 K —, 303 K —, 313 K —, 318 K —).

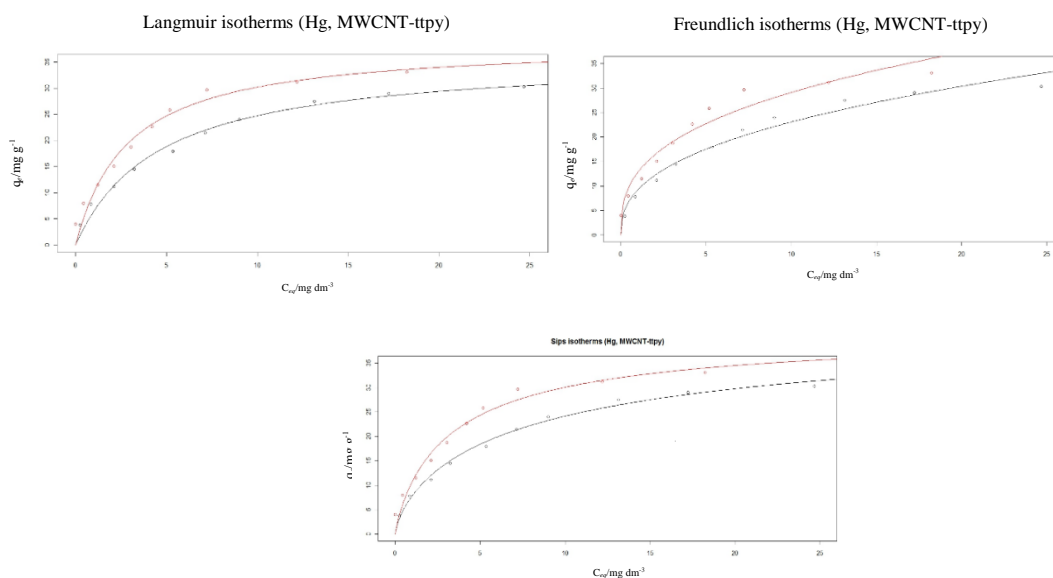


Fig A-III.5: The adsorption isotherms fitted into experimental data for the adsorption of Hg^{2+} onto MWCNT-tpy at various temperatures (293 K —, 303 K —, 313 K —, 318 K —).

Table A-III.1: Operating conditions for the ICP-OES spectrometer used for Cd^{2+} determination

Wavelength (Cd^{2+})	267.716 nm
RF power	1300 W
Plasma gas flow rate	$15 \text{ dm}^3 \text{ min}^{-1}$
Pump	$1.5 \text{ cm}^3 \text{ min}^{-1}$
Auxiliary gas flow rate	$0.2 \text{ dm}^3 \text{ min}^{-1}$
Nebulizer gas flow rate	$0.8 \text{ dm}^3 \text{ min}^{-1}$
Nebulizer pressure	2 bars
Analyzer type	Axial
Replicates	3
Sample read delay	60 s

Table A-III.2: Operating conditions for the CVAAS determination of Hg^{2+} by using NaBH_4 as reductant.

Analytical wavelength	235.6 nm
Slit width	0.7 nm
Radiation source	Hollow cathode lamp for Hg
QTA heating	No flame
Prepared measured volume	10 cm^3
Pre-reaction purge time	5 s
Post reaction purge time	50 s
Inert gas	Argon
Pressure	250-350 kPa

Table A-III.3: Experimental data for the adsorption of Cd²⁺ onto MWCNT-COOH as a function of pH
[conditions: contact time 24 h, agitation speed 150 rpm, temperature 20 °C]

pH	C _i /mg dm ⁻³	C _{eq} /mg dm ⁻³	Mass/g	Volume/dm ³	%adsorbed	q _e /mg g ⁻¹
1	102.6	9.730	0.0502	0.020	9.483	3.876
2	102.6	9.970	0.0500	0.020	9.717	3.988
3	102.6	12.14	0.0499	0.020	11.83	4.866
4	102.6	13.39	0.0499	0.020	13.05	5.37
5	102.6	19.19	0.0509	0.020	18.70	7.54
6	102.6	22.36	0.0496	0.020	21.79	9.02
7	102.6	24.47	0.0491	0.020	23.85	9.97
8	102.6	39.18	0.0494	0.020	38.19	15.86
9	102.6	52.38	0.0497	0.020	51.05	21.08
10	102.6	60.49	0.0506	0.020	58.96	23.91

Table A-III.4: Experimental data for the adsorption of Cd²⁺ onto MWCNT-COOH as a function of time
[conditions: pH 4.5, agitation speed 150 rpm, temperature 20 °C]

Time/min	C _i /mg dm ⁻³	C _{eq} /mg dm ⁻³	Mass/g	Volume/dm ³	% adsorbed	q _e /mg g ⁻¹
5	102.1	87.87	0.0497	0.02	13.94	5.726
10	102.1	87.32	0.0503	0.02	14.48	5.877
15	102.1	86.22	0.05	0.02	15.55	6.352
20	102.1	85.93	0.05	0.02	15.84	6.468
30	102.1	84.94	0.0506	0.02	16.81	6.783
45	102.1	84.64	0.0503	0.02	17.10	6.942
60	102.1	84.35	0.05	0.02	17.38	7.100
75	102.1	84.15	0.0498	0.02	17.58	7.209
90	102.1	83.88	0.0498	0.02	17.85	7.32
120	102.1	83.57	0.0498	0.02	18.15	7.44
180	102.1	82.39	0.0496	0.02	19.30	7.95
240	102.1	81.22	0.0501	0.02	20.45	8.34
300	102.1	80.55	0.0498	0.02	21.11	8.65
360	102.1	79.81	0.0506	0.02	21.83	8.81
720	102.1	79.08	0.05	0.02	22.55	9.21
1080	102.1	78.22	0.0496	0.02	23.39	9.63
1440	102.1	77.62	0.0503	0.02	23.98	9.73

Table A-III.5: Experimental data for the adsorption of Cd²⁺ onto MWCNT-COOH as a function of adsorbent dose [conditions: pH 4.5, contact time 24 h, agitation speed 150 rpm, temperature 20 °C]

$C_i/\text{mg dm}^{-3}$	$C_{eq}/\text{mg dm}^{-3}$	Mass/g	Volume/ dm^3	% adsorbed	$q_e/\text{mg g}^{-1}$
102.3	10.80	0.0298	0.02	10.56	7.25
102.3	12.08	0.0500	0.02	11.81	4.83
102.3	12.36	0.0754	0.02	12.08	3.28
102.3	12.49	0.0998	0.02	12.21	2.503
102.3	12.96	0.1496	0.02	12.67	1.733
102.3	14.47	0.2001	0.02	14.14	1.446
102.3	17.76	0.3010	0.02	17.36	1.180
102.3	21.08	0.4020	0.02	20.61	1.049

Table A-III.6: Experimental data for the adsorption of Cd²⁺ onto MWCNT-COOH as a function of temperature [conditions: pH 4.5, contact time 24 h, agitation speed 150 rpm]

T/K	$C_i/\text{mg dm}^{-3}$	$C_{eq}/\text{mg dm}^{-3}$	Mass/g	Volume/ dm^3	% adsorbed	$q_e/\text{mg g}^{-1}$
298 K	9.894	6.112	0.0503	0.020	38.23	1.504
	20.52	14.36	0.0497	0.020	30.02	2.479
	29.85	21.62	0.0496	0.020	27.57	3.319
	40.49	29.77	0.0508	0.020	26.48	4.220
	52.3	40.13	0.0499	0.020	23.27	4.878
	59.77	46.91	0.0495	0.020	21.52	5.196
	69.98	55.15	0.0505	0.020	21.19	5.873
	80.71	65.16	0.0499	0.020	19.27	6.232
	89.33	72.96	0.0503	0.020	18.33	6.509
	100.5	83.66	0.0499	0.020	16.76	6.749
303 K	9.894	6.992	0.0503	0.020	29.02	1.154
	20.52	15.84	0.0503	0.020	23.40	1.861
	29.85	23.6	0.0499	0.020	20.83	2.505
	40.49	32.44	0.0500	0.020	20.13	3.220
	52.3	43.09	0.0509	0.020	18.42	3.619
	59.77	50.53	0.0497	0.020	15.40	3.718
	69.98	59.50	0.0497	0.020	14.97	4.217
	80.71	69.65	0.0499	0.020	13.83	4.433
	89.33	77.53	0.0502	0.020	13.11	4.701
	100.5	88.00	0.0494	0.020	12.50	5.061
313 K	9.894	7.088	0.0502	0.020	28.06	1.118
	20.52	16.11	0.0501	0.020	22.05	1.760
	29.85	24.16	0.0505	0.020	18.97	2.253
	40.49	33.44	0.0499	0.020	17.63	2.826
	52.3	44.06	0.0509	0.020	16.48	3.238
	59.77	50.66	0.0503	0.020	15.18	3.622

	69.98	60.55	0.0505	0.020	13.47	3.735
	80.71	70.96	0.0502	0.020	12.19	3.884
	89.33	79.17	0.0504	0.020	11.29	4.032
	100.5	90.21	0.0502	0.020	10.29	4.100
318 K	9.894	8.224	0.0503	0.020	16.70	0.664
	20.52	17.34	0.0496	0.020	15.90	1.282
	29.85	25.37	0.0498	0.020	14.93	1.799
	40.49	34.41	0.0503	0.020	15.20	2.417
	52.3	45.03	0.0498	0.020	14.54	2.920
	59.77	51.88	0.0505	0.020	13.15	3.125
	69.98	61.43	0.0510	0.020	12.21	3.353
	80.71	72.05	0.0500	0.020	10.83	3.464
	89.33	80.53	0.0498	0.020	9.778	3.534
	100.5	91.16	0.0498	0.020	9.340	3.751

Table A-III.7: Experimental data for the adsorption of Cd²⁺ onto MWCNT-ttpty as a function of pH [conditions: contact time 24 h, agitation speed 150 rpm, temperature 20 °C]

pH	C _i /mg dm ⁻³	C _{eq} /mg dm ⁻³	Mass/g	Volume/dm ³	%adsorbed	q _e /mg g ⁻¹
1	102.6	80.51	0.0492	0.020	21.53	8.980
2	102.6	61.34	0.0500	0.020	40.21	16.50
3	102.6	34.81	0.0502	0.020	66.07	27.01
4	102.6	26.14	0.0506	0.020	74.52	30.22
5	102.6	18.22	0.0506	0.020	82.24	33.35
6	102.6	5.371	0.0497	0.020	94.77	39.13
7	102.6	2.864	0.0499	0.020	97.21	39.97
8	102.6	0.947	0.0494	0.020	99.08	41.16
9	102.6	1.545	0.0500	0.020	98.49	40.42
10	102.6	0.808	0.0501	0.020	99.21	40.64

Table A-III.8: Experimental data for the adsorption of Cd²⁺ onto MWCNT-ttpty as a function of time [conditions: pH 4.5, agitation speed 150 rpm, temperature 20 °C]

Time/min	C _i /mg dm ⁻³	C _{eq} /mg dm ⁻³	Mass/g	Volume/dm ³	% adsorbed	q _e /mg g ⁻¹
5	102.1	31.31	0.0498	0.02	69.33	28.43
10	102.1	29.55	0.0498	0.02	71.06	29.14
15	102.1	26.58	0.0495	0.02	73.97	30.51
20	102.1	21.51	0.0503	0.02	78.93	32.04
30	102.1	19.61	0.0502	0.02	80.79	32.86
45	102.1	15.33	0.0500	0.02	84.99	34.71
60	102.1	14.830	0.0499	0.02	85.48	34.98
75	102.1	14.160	0.0496	0.02	86.13	35.46
90	102.1	13.810	0.0499	0.02	86.47	35.39

120	102.1	13.260	0.0500	0.02	87.01	35.54
180	102.1	12.840	0.0499	0.02	87.42	35.78
240	102.1	12.360	0.0504	0.02	87.89	35.61
300	102.1	11.880	0.0505	0.02	88.36	35.73
360	102.1	11.220	0.0503	0.02	89.01	36.14
720	102.1	10.640	0.0502	0.02	89.58	36.44
1080	102.1	10.880	0.0501	0.02	89.34	36.42
1440	102.1	10.120	0.0501	0.02	90.09	36.72

Table A-III.9: Experimental data for the adsorption of Cd²⁺ onto MWCNT-ttpy as a function of adsorbent dose [conditions: pH 4.5, contact time 24 h, agitation speed 150 rpm, temperature 20 °C]

$C_i/\text{mg dm}^{-3}$	$C_{eq}/\text{mg dm}^{-3}$	Mass/g	Volume/ dm^3	% adsorbed	$q_e/\text{mg g}^{-1}$
102.3	24.37	0.0303	0.02	76.18	51.44
102.3	13.110	0.0496	0.02	87.18	35.96
102.3	5.68	0.0754	0.02	94.45	25.63
102.3	0.823	0.1029	0.02	99.20	19.72
102.3	0.611	0.1491	0.02	99.40	13.64
102.3	0.566	0.2032	0.02	99.45	10.01
102.3	0.543	0.3002	0.02	99.47	6.779
102.3	0.193	0.3997	0.02	99.81	5.109

Table A-III.10: Experimental data for the adsorption of Cd²⁺ onto MWCNT-ttpy as a function of temperature [conditions: pH 4.5, contact time 24 h, agitation speed 150 rpm, temperature 20 °C]

T/K	$C_i/\text{mg dm}^{-3}$	$C_{eq}/\text{mg dm}^{-3}$	Mass/g	Volume/ dm^3	% adsorbed	$q_e/\text{mg g}^{-1}$
298 K	9.894	0.226	0.0501	0.020	97.7	3.859
	20.52	0.506	0.0499	0.020	97.53	8.022
	29.85	0.814	0.0502	0.020	97.27	11.57
	40.49	1.177	0.0501	0.020	97.09	15.69
	52.30	1.622	0.0493	0.020	96.90	20.56
	59.77	1.886	0.0508	0.020	96.84	22.79
	69.98	2.966	0.0499	0.020	95.76	26.86
	80.71	4.541	0.05	0.020	94.37	30.47
	89.33	7.234	0.0505	0.020	91.90	32.51
	100.5	12.03	0.0499	0.020	88.03	35.46
303 K	9.894	0.273	0.0503	0.020	97.2	3.825
	20.52	0.614	0.0500	0.020	97.0	7.962
	29.85	1.007	0.0502	0.020	96.63	11.49
	40.49	1.512	0.0501	0.020	96.27	15.56
	52.30	2.441	0.0500	0.020	95.33	19.94
	59.77	3.044	0.0502	0.020	94.91	22.60

	69.98	4.213	0.0502	0.020	93.98	26.20
	80.71	6.442	0.0505	0.020	92.02	29.41
	89.33	9.331	0.0501	0.020	89.55	31.94
	100.5	15.84	0.0500	0.020	84.24	33.86
313 K	9.894	0.443	0.0504	0.020	94.51	3.750
	20.52	1.018	0.0497	0.020	97.51	7.848
	29.85	1.677	0.0502	0.020	93.91	11.22
	40.49	2.361	0.0504	0.020	95.32	15.13
	52.30	3.13	0.0503	0.020	98.33	19.55
	59.77	4.331	0.0493	0.020	92.40	22.49
	69.98	5.824	0.0497	0.020	91.65	25.82
	80.71	9.043	0.0505	0.020	89.58	28.38
	89.33	13.81	0.0503	0.020	83.91	30.03
	100.5	19.31	0.0499	0.020	81.19	32.54
318 K	9.894	0.511	0.0497	0.020	94.8	3.776
	20.52	1.141	0.0499	0.020	94.4	7.767
	29.85	1.831	0.0504	0.020	93.9	11.12
	40.49	2.933	0.0491	0.020	92.76	15.30
	52.30	4.288	0.0506	0.020	91.80	18.98
	59.77	5.243	0.0502	0.020	91.23	21.72
	69.98	7.663	0.0496	0.020	89.05	25.13
	80.71	11.21	0.0506	0.020	86.11	27.47
	89.33	15.16	0.0504	0.020	83.03	29.43
	100.5	22.81	0.0510	0.020	77.30	30.47

Table A-III.9: Separation factor values (R_L) for the adsorption of Cd^{2+} onto MWCNT-COOH at different temperatures

$C_i/\text{mg dm}^{-3}$	298 K	303 K	313 K	318 K
9.894	0.819	0.824	0.783	0.855
20.52	0.685	0.693	0.635	0.739
29.85	0.599	0.608	0.545	0.661
40.49	0.524	0.533	0.469	0.589
52.3	0.461	0.470	0.406	0.526
59.77	0.428	0.436	0.374	0.493
69.98	0.389	0.398	0.338	0.454
80.71	0.356	0.365	0.307	0.419
89.33	0.333	0.341	0.286	0.394
100.5	0.308	0.315	0.262	0.366

Table A-III.10: Separation factor values (R_L) for the adsorption of Cd^{2+} onto MWCNT-tty at different temperatures

$C_i/\text{mg dm}^{-3}$	298 K	303 K	313 K	318 K
9.894	0.1534	0.1918	0.2598	0.2879
20.52	0.0803	0.1027	0.1447	0.1631
29.85	0.0566	0.0729	0.1042	0.1182
40.49	0.0424	0.0548	0.0790	0.0899
52.30	0.0331	0.0430	0.0623	0.0710
59.77	0.0291	0.0378	0.0549	0.0627
69.98	0.0250	0.0325	0.0473	0.0541
80.71	0.0217	0.0283	0.0412	0.0472
89.33	0.0197	0.0256	0.0374	0.0429
100.5	0.0175	0.0228	0.0334	0.0383

Table A-III.13: Experimental data for the adsorption of Hg^{2+} onto MWCNT-COOH as a function of pH
[conditions: contact time 24 h, agitation speed 150 rpm, temperature 20 °C]

pH	$C_i/\text{mg dm}^{-3}$	$C_{eq}/\text{mg dm}^{-3}$	Mass/g	Volume/ dm^3	% adsorbed	$q_e/\text{mg g}^{-1}$
1	53.02	23.42	0.0505	0.025	55.83	14.65
2	53.02	21.11	0.0497	0.025	60.18	16.05
3	53.02	19.46	0.0508	0.025	63.30	16.52
4	53.02	16.54	0.0514	0.025	68.80	17.74
5	53.02	14.22	0.0513	0.025	73.18	18.91
6	53.02	12.16	0.0514	0.025	77.07	19.87
7	53.02	9.580	0.0515	0.025	81.93	21.09
8	53.02	8.681	0.0516	0.025	83.63	21.48
9	53.02	8.453	0.0500	0.025	84.06	22.28
10	53.02	7.493	0.0515	0.025	85.87	22.10

Table A-III.14: Experimental data for the adsorption of Hg^{2+} onto MWCNT-COOH as a function of time
[conditions: pH 6.0, agitation speed 150 rpm, temperature 20 °C]

Time/min	$C_i/\text{mg dm}^{-3}$	$C_{eq}/\text{mg dm}^{-3}$	Mass/g	Volume/ dm^3	% adsorbed	$q_e/\text{mg g}^{-1}$
5	51.83	42.23	0.0501	0.025	18.52	4.790
10	51.83	39.18	0.0506	0.025	24.41	6.250
15	51.83	36.22	0.0512	0.025	30.50	7.720
20	51.83	30.14	0.0511	0.025	41.85	10.61
30	51.83	28.24	0.0513	0.025	45.51	11.50
45	51.83	25.77	0.0499	0.025	50.28	13.06
60	51.83	20.35	0.0504	0.025	60.74	15.62
75	51.83	18.14	0.0497	0.025	65.00	16.95
90	51.83	16.29	0.0498	0.025	68.57	17.84
120	51.83	15.05	0.0502	0.025	70.96	18.32
180	51.83	14.88	0.0505	0.025	71.29	18.29

240	51.83	13.14	0.0509	0.025	74.65	19.00
300	51.83	13.03	0.0504	0.025	74.86	19.25
360	51.83	12.81	0.0505	0.025	75.28	19.32
720	51.83	12.55	0.0503	0.025	75.79	19.52
1080	51.83	12.43	0.0502	0.025	76.02	19.62
1440	51.83	12.22	0.0501	0.025	76.42	19.77

Table A-III.15: Experimental data for the adsorption of Hg^{2+} onto MWCNT-COOH as a function of adsorbent dose [conditions: pH 6.0, contact time 24 h, agitation speed 150 rpm, temperature 20 °C]

$C_i/\text{mg dm}^{-3}$	$C_{eq}/\text{mg dm}^{-3}$	Mass/g	Volume/ dm^3	% adsorbed	$q_e/\text{mg g}^{-1}$
53.02	16.80	0.2990	0.025	68.31	3.028
53.02	12.68	0.0515	0.025	76.08	19.58
53.02	11.16	0.0762	0.025	78.95	13.73
53.02	9.841	0.1009	0.025	81.44	10.70
53.02	9.116	0.1495	0.025	82.81	7.342
53.02	8.771	0.2005	0.025	83.46	5.527
53.02	7.173	0.3011	0.025	86.47	3.807
53.02	6.448	0.4050	0.025	87.84	2.875

Table A-III.16: Experimental data for the adsorption of Hg^{2+} onto MWCNT-COOH as a function of temperature [conditions: pH 6.0, contact time 24 h, agitation speed 150 rpm]

T/K	$C_i/\text{mg dm}^{-3}$	$C_{eq}/\text{mg dm}^{-3}$	Mass/g	Volume/ dm^3	% adsorbed	$q_e/\text{mg g}^{-1}$
298 K	9.884	0.988	0.0492	0.025	90.00	3.616
	20.16	2.744	0.0497	0.025	86.39	7.008
	29.84	4.889	0.0500	0.025	83.62	9.980
	40.15	7.981	0.0502	0.025	80.12	12.82
	50.18	10.84	0.0504	0.025	78.40	15.61
	60.26	14.31	0.0503	0.025	76.25	18.27
	69.52	17.33	0.0499	0.025	75.07	20.92
	81.72	22.54	0.0506	0.025	72.42	23.39
	90.19	29.31	0.0504	0.025	67.50	24.16
100.2	37.18	0.05	0.025	62.88	25.19	
303 K	9.884	0.722	0.0501	0.025	92.7	3.657
	20.16	1.558	0.0499	0.025	92.3	7.456
	29.84	2.533	0.0495	0.025	91.51	11.03
	40.15	4.334	0.0506	0.025	89.21	14.16
	50.18	6.119	0.0504	0.025	87.81	17.48
	60.26	8.772	0.0507	0.025	85.44	20.31
	69.52	11.18	0.0495	0.025	83.92	23.57
	81.72	15.18	0.0502	0.025	81.42	26.51
	90.19	19.34	0.0505	0.025	78.56	28.06
100.2	25.14	0.0509	0.025	74.90	29.48	

Table A-III.17: Experimental data for the adsorption of Hg^{2+} onto MWCNT-ttpy as a function of pH
[conditions: contact time 24 h, agitation speed 150 rpm, temperature 20 °C]

pH	$C_i/\text{mg dm}^{-3}$	$C_{eq}/\text{mg dm}^{-3}$	Mass/g	Volume/ dm^3	%adsorbed	$q_e/\text{mg g}^{-1}$
1	53.02	9.114	0.0513	0.025	82.81	21.40
2	53.02	8.696	0.0510	0.025	83.62	21.73
3	53.02	8.353	0.0500	0.025	84.25	22.33
4	53.02	7.751	0.0505	0.025	85.38	22.41
5	53.02	7.534	0.0516	0.025	85.79	22.04
6	53.02	7.368	0.0504	0.025	86.12	22.65
7	53.02	6.836	0.0503	0.025	87.13	22.96
8	53.02	6.748	0.0501	0.025	87.29	23.09
9	53.02	6.642	0.0497	0.025	87.47	23.33
10	53.02	6.551	0.0512	0.025	87.64	22.69

Table A-III.18: Experimental data for the adsorption of Hg^{2+} onto MWCNT-ttpy as a function of time
[conditions: pH 6.0, agitation speed 150 rpm, temperature 20 °C]

Time/min	$C_i/\text{mg dm}^{-3}$	$C_{eq}/\text{mg dm}^{-3}$	Mass/g	Volume/ dm^3	% adsorbed	$q_e/\text{mg g}^{-1}$
5	51.83	24.84	0.0503	0.025	52.07	13.42
10	51.83	18.13	0.0501	0.025	65.02	16.82
15	51.83	14.22	0.0498	0.025	72.56	18.88
20	51.83	11.96	0.0502	0.025	76.92	19.86
30	51.83	10.29	0.0509	0.025	80.15	20.40
45	51.83	9.811	0.0494	0.025	81.07	21.27
60	51.83	8.126	0.0497	0.025	84.34	21.99
75	51.83	7.887	0.0499	0.025	84.80	22.02
90	51.83	7.722	0.0500	0.025	85.10	22.05
120	51.83	7.493	0.0496	0.025	85.54	22.35
180	51.83	7.191	0.0505	0.025	86.13	22.10
240	51.83	6.874	0.0507	0.025	86.74	22.17
300	51.83	6.871	0.0512	0.025	86.74	21.95
360	51.83	6.862	0.0504	0.025	86.76	22.31
720	51.83	6.853	0.0505	0.025	86.78	22.27
1080	51.83	6.744	0.0501	0.025	86.99	22.50
1440	51.83	6.732	0.0503	0.025	87.01	22.41

Table A-III.19: Experimental data for the adsorption of Hg²⁺ onto MWCNT-tpy as a function of adsorbent dose [conditions: pH 6.0, contact time 24 h, agitation speed 150 rpm, temperature 20 °C]

$C_i/\text{mg dm}^{-3}$	$C_{eq}/\text{mg dm}^{-3}$	Mass/g	Volume/ dm^3	% adsorbed	$q_e/\text{mg g}^{-1}$
53.02	7.729	0.2910	0.025	85.42	3.89
53.02	6.836	0.0509	0.025	87.11	22.68
53.02	6.32	0.0751	0.025	88.08	15.55
53.02	6.22	0.1006	0.025	88.27	11.630
53.02	6.18	0.1488	0.025	88.34	7.870
53.02	6.06	0.2003	0.025	88.57	5.861
53.02	5.92	0.3000	0.025	88.83	3.925
53.02	5.81	0.4013	0.025	89.04	2.941

Table A-III.20: Experimental data for the adsorption of Hg²⁺ onto MWCNT-tpy as a function of temperature [conditions: pH 6.0, contact time 24 h, agitation speed 150 rpm, temperature 20 °C]

T/K	$C_i/\text{mg dm}^{-3}$	$C_{eq}/\text{mg dm}^{-3}$	Mass/g	Volume/ dm^3	% adsorbed	$q_e/\text{mg g}^{-1}$
298 K	9.884	0.241	0.0503	0.025	97.56	3.834
	20.16	0.84	0.0497	0.025	95.81	7.773
	29.84	2.114	0.0496	0.025	92.92	11.180
	40.15	3.228	0.0508	0.025	91.96	14.536
	50.18	5.344	0.0499	0.025	89.35	17.970
	60.26	7.134	0.0495	0.025	88.16	21.465
	69.52	8.994	0.0505	0.025	87.06	23.971
	81.72	13.14	0.0499	0.025	83.92	27.487
	90.19	17.22	0.0503	0.025	80.91	29.014
	100.16	24.67	0.0499	0.025	75.37	30.257
303 K	9.884	0	0.0501	0.025	98.84	3.946
	20.16	0.422	0.0497	0.025	98.69	7.943
	29.84	1.224	0.0499	0.025	95.39	11.469
	40.15	2.116	0.0505	0.025	95.09	15.063
	50.18	3.044	0.0504	0.025	94.27	18.705
	60.26	4.187	0.0495	0.025	93.46	22.656
	69.52	5.17	0.0498	0.025	91.92	25.842
	81.72	7.225	0.0503	0.025	93.12	29.620
	90.19	12.18	0.0501	0.025	86.68	31.142
	100.16	18.22	0.0496	0.025	81.94	33.040

Table A-III.21: Separation factor values (R_L) for the adsorption of Hg^{2+} onto MWCNT-COOH at different temperatures

$C_i/mg\ dm^{-3}$	298 K	303 K	313 K	318 K
9.894	0.0302	0.0181	0.0110	0.0058
20.52	0.0148	0.0088	0.0053	0.0028
29.85	0.0102	0.0061	0.0037	0.0019
40.49	0.0076	0.0045	0.0027	0.0014
52.30	0.0059	0.0035	0.0021	0.0011
59.77	0.0051	0.0030	0.0018	0.0010
69.98	0.0044	0.0026	0.0016	0.0008
80.71	0.0038	0.0023	0.0014	0.0007
89.33	0.0034	0.0020	0.0012	0.0006
100.5	0.0031	0.0018	0.0011	0.0006

Table A-III.22: Separation factor values (R_L) for the adsorption of Hg^{2+} onto MWCNT-ttpty at different temperatures

$C_i/mg\ dm^{-3}$	298 K	303 K	313 K	318 K
9.894	0.374	0.355	0.451	0.598
20.52	0.224	0.209	0.284	0.417
29.85	0.165	0.154	0.214	0.330
40.49	0.128	0.118	0.167	0.266
52.3	0.102	0.094	0.135	0.219
59.77	0.090	0.083	0.120	0.197
69.98	0.078	0.072	0.104	0.174
80.71	0.068	0.063	0.092	0.154
89.33	0.062	0.057	0.083	0.141
100.5	0.056	0.051	0.075	0.128

Appendix IV

Data for competitive adsorption of divalent metal ions

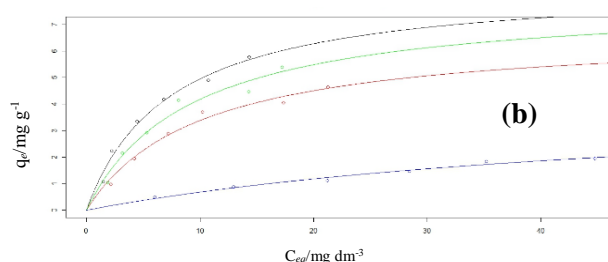


Fig A-IV.1: Langmuir adsorption isotherm models fitted for the adsorption of Pb^{2+} , Cd^{2+} , Cu^{2+} and Zn^{2+} onto MWCNT-tty in a multi-component adsorption system (Pb^{2+} ———, Cd^{2+} ———, Cu^{2+} ——— and Zn^{2+} ———).

(A) Effect of pH on multicomponent adsorption

Table A-IV.1: Experimental data for the competitive adsorption of Pb^{2+} onto MWCNT-tty as a function of pH [conditions: contact time 24 h, agitation speed 150 rpm, temperature 20 °C]

pH	Mass/g	$C_i/mg\ dm^{-3}$	$C_{eq}/mg\ dm^{-3}$	Vol./ dm^3	% adsorbed	$q_e/mg\ g^{-1}$
1	0.2005	52.69	38.45	0.025	27.03	1.776
2	0.2001	52.69	33.27	0.025	36.86	2.426
3	0.2002	52.69	21.88	0.025	58.47	3.847
4	0.2002	52.69	12.67	0.025	75.95	4.998
5	0.2004	52.69	6.140	0.025	88.35	5.807
6	0.1999	52.69	2.745	0.025	94.81	6.247
7	0.2002	52.69	0.661	0.025	98.75	6.497
8	0.2002	52.69	0.222	0.025	99.58	6.552
9	0.2000	52.69	0.134	0.025	99.75	6.570
10	0.2005	52.69	0.041	0.025	99.92	6.565

Table A-IV.2: Experimental data for the competitive adsorption of Cu^{2+} onto MWCNT-tty as a function of pH [conditions: contact time 24 h, agitation speed 150 rpm, temperature 20 °C]

pH	Mass/g	$C_i/mg\ dm^{-3}$	$C_{eq}/mg\ dm^{-3}$	Vol./ dm^3	% adsorbed	$q_e/mg\ g^{-1}$
1	0.2005	50.48	39.82	0.025	21.12	1.329
2	0.2001	50.48	36.02	0.025	28.65	1.807
3	0.2002	50.48	24.11	0.025	52.24	3.293
4	0.2002	50.48	20.72	0.025	58.95	3.716
5	0.2004	50.48	13.99	0.025	72.29	4.552
6	0.1999	50.48	10.12	0.025	79.95	5.048
7	0.2002	50.48	1.284	0.025	97.46	6.143
8	0.2002	50.48	0.431	0.025	99.15	6.250
9	0.2000	50.48	0.282	0.025	99.44	6.275
10	0.2005	50.48	0.114	0.025	99.77	6.280

Table A-IV.3: Experimental data for the competitive adsorption of Cd²⁺ onto MWCNT-ttpy as a function of pH [conditions: contact time 24 h, agitation speed 150 rpm, temperature 20 °C]

pH	Mass/g	C _i /mg dm ⁻³	C _{eq} /mg dm ⁻³	Vol./dm ³	% adsorbed	q _e /mg g ⁻¹
1	0.2005	49.96	40.76	0.025	18.41	1.147
2	0.2001	49.96	37.88	0.025	24.18	1.509
3	0.2002	49.96	26.11	0.025	47.74	2.978
4	0.2002	49.96	21.23	0.025	57.51	3.588
5	0.2004	49.96	18.24	0.025	63.49	3.957
6	0.1999	49.96	12.37	0.025	75.24	4.701
7	0.2002	49.96	6.143	0.025	87.70	5.472
8	0.2002	49.96	2.334	0.025	95.33	5.947
9	0.2000	49.96	1.716	0.025	96.57	6.031
10	0.2005	49.96	0.922	0.025	98.15	6.114

Table A-IV.4: Experimental data for the competitive adsorption of Zn²⁺ onto MWCNT-ttpy as a function of pH [conditions: contact time 24 h, agitation speed 150 rpm, temperature 20 °C]

pH	Mass/g	C _i /mg dm ⁻³	C _{eq} /mg dm ⁻³	Vol./dm ³	% adsorbed	q _e /mg g ⁻¹
1	0.2005	52.16	41.14	0.025	21.13	1.374
2	0.2001	52.16	41.57	0.025	20.30	1.323
3	0.2002	52.16	37.3	0.025	28.49	1.856
4	0.2002	52.16	35.9	0.025	31.17	2.030
5	0.2004	52.16	33.25	0.025	36.25	2.359
6	0.1999	52.16	32.16	0.025	38.34	2.501
7	0.2002	52.16	16.82	0.025	67.75	4.413
8	0.2002	52.16	3.546	0.025	93.20	6.071
9	0.2000	52.16	1.553	0.025	97.02	6.326
10	0.2005	52.16	1.598	0.025	96.94	6.304

(B) Multicomponent adsorption of metal ion species at same concentration

Table A-IV.5: Experimental data for the competitive adsorption of Pb²⁺ onto MWCNT-ttpy in a multicomponent system at the same concentration [conditions: pH 5.5, contact time 24 h, agitation speed 150 rpm, temperature 20 °C]

Mass/g	C _i /mg dm ⁻³	C _{eq} /mg dm ⁻³	Vol./dm ³	% adsorbed	q _e /mg g ⁻¹
0.2004	9.992	1.482	0.025	85.17	1.062
0.2008	20.16	2.22	0.025	88.99	2.234
0.1997	31.24	4.47	0.025	85.69	3.351
0.2003	40.22	6.824	0.025	83.03	4.168
0.2000	49.83	10.74	0.025	78.45	4.886
0.1992	60.27	14.31	0.025	76.26	5.768

Table A-IV.6: Experimental data for the competitive adsorption of Zn²⁺ onto MWCNT-tpy in a multicomponent system at the same concentration [conditions: pH 5.5, contact time 24 h, agitation speed 150 rpm, temperature 20 °C]

Mass/g	C _i /mg dm ⁻³	C _{eq} /mg dm ⁻³	Vol./dm ³	% adsorbed	q _e /mg g ⁻¹
0.2004	10.04	6.014	0.025	40.10	0.502
0.2008	19.98	15.96	0.025	20.12	0.500
0.1997	30.16	24.69	0.025	18.14	0.685
0.2003	40.22	32	0.025	20.44	1.026
0.2000	49.88	39.19	0.025	21.43	1.336
0.1992	60.24	41.24	0.025	31.54	2.385

Table A-IV.7: Experimental data for the competitive adsorption of Cu²⁺ onto MWCNT-tpy in a multicomponent system at the same concentration [conditions: pH 5.5, contact time 24 h, agitation speed 150 rpm, temperature 20 °C]

Mass/g	C _i /mg dm ⁻³	C _{eq} /mg dm ⁻³	Vol./dm ³	% adsorbed	q _e /mg g ⁻¹
0.2004	10.19	1.884	0.025	81.51	1.036
0.2008	20.42	3.184	0.025	84.41	2.146
0.1997	28.64	5.336	0.025	81.37	2.917
0.2003	41.29	8.115	0.025	80.35	4.141
0.2000	50.04	14.28	0.025	71.46	4.470
0.1992	60.18	17.24	0.025	71.35	5.389

Table A-IV.8: Experimental data for the competitive adsorption of Cd²⁺ onto MWCNT-tpy in a multicomponent system at the same concentration [conditions: pH 5.5, contact time 24 h, agitation speed 150 rpm, temperature 20 °C]

Mass/g	C _i /mg dm ⁻³	C _{eq} /mg dm ⁻³	Vol./dm ³	% adsorbed	q _e /mg g ⁻¹
0.2004	9.986	2.141	0.025	78.56	0.979
0.2008	19.88	4.211	0.025	78.82	1.951
0.1997	30.22	7.184	0.025	76.23	2.884
0.2003	39.84	10.22	0.025	74.35	3.697
0.2000	49.72	17.33	0.025	65.14	4.049
0.1992	58.21	21.26	0.025	63.48	4.637

(C) Multicomponent adsorption with one component at a fixed concentration and the others at varying initial metal ion concentrations

(a). Effect of multicomponent concentration on Pb²⁺ adsorption from aqueous solutions onto MWCNT-tpy

Table A-IV.9: Effect of initial concentration on multicomponent adsorption of Pb²⁺ onto MWCNT-tpy [conditions: conditions: pH 5.5, contact time 24 h, agitation speed 150 rpm, temperature 20 °C]

$C_i/\text{mg dm}^{-3}$	$C_{eq}/\text{mg dm}^{-3}$	Mass/g	Vol./dm ³	% ads.	$q_e/\text{mg g}^{-1}$	K_d
20.14	4.331	0.1997	0.025	78.50	1.979	0.457
20.66	6.220	0.2008	0.025	69.89	1.798	0.289
19.88	7.470	0.2011	0.025	62.42	1.543	0.207
19.74	7.824	0.2004	0.025	60.36	1.487	0.190
20.42	10.74	0.2000	0.025	47.40	1.210	0.113

Table A-IV.10: Effect of initial concentration on multicomponent adsorption of Zn²⁺ onto MWCNT-tpy [conditions: conditions: pH 5.5, contact time 24 h, agitation speed 150 rpm, temperature 20 °C]

$C_i/\text{mg dm}^{-3}$	$C_{eq}/\text{mg dm}^{-3}$	Mass/g	Vol./dm ³	% ads.	$q_e/\text{mg g}^{-1}$	K_d
9.877	6.014	0.1997	0.025	39.11	0.484	0.080
19.24	12.44	0.2008	0.025	35.34	0.847	0.068
30.15	20.44	0.2011	0.025	32.21	1.207	0.059
41.18	32.00	0.2004	0.025	22.29	1.145	0.036
49.88	39.19	0.2000	0.025	21.43	1.336	0.034

Table A-IV.11: Effect of initial concentration on multicomponent adsorption of Cu²⁺ onto MWCNT-tpy [conditions: conditions: pH 5.5, contact time 24 h, agitation speed 150 rpm, temperature 20 °C]

$C_i/\text{mg dm}^{-3}$	$C_{eq}/\text{mg dm}^{-3}$	Mass/g	Vol./dm ³	% ads.	$q_e/\text{mg g}^{-1}$	K_d
9.922	1.032	0.1997	0.025	89.60	1.113	1.078
20.17	6.471	0.2008	0.025	67.92	1.706	0.264
30.06	12.08	0.2011	0.025	59.81	2.235	0.185
39.28	16.41	0.2004	0.025	58.22	2.853	0.174
50.04	21.44	0.2000	0.025	57.15	3.575	0.167

Table A-IV.12: Effect of initial concentration on multicomponent adsorption of Cd²⁺ onto MWCNT-tpy [conditions: conditions: pH 5.5, contact time 24 h, agitation speed 150 rpm, temperature 20 °C]

$C_i/\text{mg dm}^{-3}$	$C_{eq}/\text{mg dm}^{-3}$	Mass/g	Vol./dm ³	% ads.	$q_e/\text{mg g}^{-1}$	K_d
8.766	2.141	0.1997	0.025	75.58	0.829	0.387
18.19	4.211	0.2008	0.025	76.85	1.740	0.413
28.24	7.184	0.2011	0.025	74.56	2.618	0.364
41.16	10.22	0.2004	0.025	75.17	3.860	0.378
49.72	12.33	0.2000	0.025	75.20	4.674	0.379

(b). Effect of multicomponent concentration on Cu²⁺ adsorption from aqueous solutions onto MWCNT-tpy

Table A-IV.13: Effect of initial concentration on multicomponent adsorption of Cu²⁺ onto MWCNT-tpy [conditions: conditions: pH 5.5, contact time 24 h, agitation speed 150 rpm, temperature 20 °C]

$C_i/\text{mg dm}^{-3}$	$C_{eq}/\text{mg dm}^{-3}$	Mass/g	Vol./dm ³	% ads.	$q_e/\text{mg g}^{-1}$	K_d
18.77	1.655	0.2008	0.025	91.18	2.131	1.288
19.71	3.145	0.2116	0.025	84.04	1.957	0.622
20.16	6.144	0.2004	0.025	69.52	1.749	0.285
20.28	7.886	0.2002	0.025	61.11	1.548	0.196
21.74	12.41	0.2000	0.025	42.92	1.167	0.094

Table A-IV.14: Effect of initial concentration on multicomponent adsorption of Pb²⁺ onto MWCNT-tpy [conditions: conditions: pH 5.5, contact time 24 h, agitation speed 150 rpm, temperature 20 °C]

$C_i/\text{mg dm}^{-3}$	$C_{eq}/\text{mg dm}^{-3}$	Mass/g	Vol./dm ³	% ads.	$q_e/\text{mg g}^{-1}$	K_d
8.714	3.639	0.2008	0.025	58.24	0.632	0.174
20.26	9.334	0.2116	0.025	53.93	1.291	0.138
31.22	14.22	0.2004	0.025	54.45	2.121	0.149
40.28	19.87	0.2002	0.025	50.67	2.549	0.128
48.72	24.15	0.2000	0.025	50.43	3.074	0.127

Table A-IV.15: Effect of initial concentration on multicomponent adsorption of Zn²⁺ onto MWCNT-tpy [conditions: conditions: pH 5.5, contact time 24 h, agitation speed 150 rpm, temperature 20 °C]

$C_i/\text{mg dm}^{-3}$	$C_{eq}/\text{mg dm}^{-3}$	Mass/g	Vol./dm ³	% ads.	$q_e/\text{mg g}^{-1}$	K_d
9.182	6.114	0.2008	0.025	33.41	0.382	0.062
20.44	14.22	0.2116	0.025	30.43	0.735	0.052
31.26	24.18	0.2004	0.025	22.65	0.883	0.037
40.27	32.56	0.2002	0.025	19.15	0.963	0.030
50.11	43.47	0.2000	0.025	13.25	0.831	0.019

Table A-IV.16: Effect of initial concentration on multicomponent adsorption of Cd²⁺ onto MWCNT-tpy [conditions: conditions: pH 5.5, contact time 24 h, agitation speed 150 rpm, temperature 20 °C]

$C_i/\text{mg dm}^{-3}$	$C_{eq}/\text{mg dm}^{-3}$	Mass/g	Vol./dm ³	% ads.	$q_e/\text{mg g}^{-1}$	K_d
10.04	5.188	0.2008	0.025	48.33	0.604	0.116
21.54	11.22	0.2116	0.025	47.91	1.219	0.109
30.26	17.16	0.2004	0.025	43.29	1.634	0.095
39.84	24.18	0.2002	0.025	39.31	1.956	0.081
50.29	31.22	0.2000	0.025	37.92	2.386	0.076

(c). Effect of multicomponent concentration on Cd²⁺ adsorption from aqueous solutions onto MWCNT-tpy

Table A-IV.17: Effect of initial concentration on multicomponent adsorption of Cd²⁺ onto MWCNT-tpy [conditions: conditions: pH 5.5, contact time 24 h, agitation speed 150 rpm, temperature 20 °C]

$C_i/\text{mg dm}^{-3}$	$C_{eq}/\text{mg dm}^{-3}$	Mass/g	Vol./dm ³	% ads.	$q_e/\text{mg g}^{-1}$	K_d
18.22	0.876	0.2009	0.025	95.19	2.158	2.464
19.81	1.442	0.2004	0.025	92.72	2.291	1.589
19.13	1.994	0.2022	0.025	89.58	2.119	1.063
19.76	5.174	0.2014	0.025	73.82	1.811	0.350
20.14	5.889	0.199	0.025	70.76	1.792	0.304

Table A-IV.18: Effect of initial concentration on multicomponent adsorption of Pb²⁺ onto MWCNT-tpy [conditions: conditions: pH 5.5, contact time 24 h, agitation speed 150 rpm, temperature 20 °C]

$C_i/\text{mg dm}^{-3}$	$C_{eq}/\text{mg dm}^{-3}$	Mass/g	Vol./dm ³	% ads.	$q_e/\text{mg g}^{-1}$	K_d
9.177	3.188	0.2009	0.025	65.26	0.745	0.234
20.81	12.37	0.2004	0.025	40.56	1.053	0.085
30.54	19.52	0.2022	0.025	36.08	1.363	0.070
38.14	26.47	0.2014	0.025	30.60	1.449	0.055
50.08	38.21	0.199	0.025	23.70	1.493	0.039

Table A-IV.19: Effect of initial concentration on multicomponent adsorption of Zn²⁺ onto MWCNT-tpy [conditions: conditions: pH 5.5, contact time 24 h, agitation speed 150 rpm, temperature 20 °C]

$C_i/\text{mg dm}^{-3}$	$C_{eq}/\text{mg dm}^{-3}$	Mass/g	Vol./dm ³	% ads.	$q_e/\text{mg g}^{-1}$	K_d
9.882	8.224	0.2009	0.025	16.78	0.206	0.025
19.24	16.14	0.2004	0.025	16.11	0.387	0.024
29.27	26.14	0.2022	0.025	10.69	0.387	0.015
39.26	35.22	0.2014	0.025	10.29	0.501	0.014
50.21	46.18	0.199	0.025	8.026	0.507	0.011

Table A-IV.20: Effect of initial concentration on multicomponent adsorption of Cu²⁺ onto MWCNT-tpy [conditions: conditions: pH 5.5, contact time 24 h, agitation speed 150 rpm, temperature 20 °C]

$C_i/\text{mg dm}^{-3}$	$C_{eq}/\text{mg dm}^{-3}$	Mass/g	Vol./dm ³	% ads.	$q_e/\text{mg g}^{-1}$	K_d
9.664	1.441	0.2009	0.025	85.09	1.023	0.710
20.05	5.477	0.2004	0.025	72.68	1.818	0.332
30.43	9.247	0.2022	0.025	69.61	2.619	0.283
38.29	18.25	0.2014	0.025	52.34	2.488	0.136
49.22	26.17	0.199	0.025	46.83	2.899	0.111

(d). Effect of multicomponent concentration on Zn²⁺ adsorption from aqueous solutions onto MWCNT-ttpy

Table A-IV.21: Effect of initial concentration on multicomponent adsorption of Zn²⁺ onto MWCNT-ttpy [conditions: conditions: pH 5.5, contact time 24 h, agitation speed 150 rpm, temperature 20 °C]

$C_i/\text{mg dm}^{-3}$	$C_{eq}/\text{mg dm}^{-3}$	Mass/g	Vol./dm ³	% ads.	$q_e/\text{mg g}^{-1}$	K_d
20.16	16.14	0.2006	0.025	19.94	0.501	0.031
20.44	17.26	0.2014	0.025	15.56	0.395	0.023
20.31	18.27	0.2005	0.025	10.04	0.254	0.014
19.24	18.15	0.201	0.025	5.665	0.136	0.007
19.17	18.24	0.206	0.025	4.851	0.113	0.006

Table A-IV.22: Effect of initial concentration on multicomponent adsorption of Pb²⁺ onto MWCNT-ttpy [conditions: conditions: pH 5.5, contact time 24 h, agitation speed 150 rpm, temperature 20 °C]

$C_i/\text{mg dm}^{-3}$	$C_{eq}/\text{mg dm}^{-3}$	Mass/g	Vol./dm ³	% ads.	$q_e/\text{mg g}^{-1}$	K_d
9.924	2.041	0.2006	0.025	79.43	0.982	0.481
20.18	4.221	0.2014	0.025	79.08	1.981	0.469
30.05	12.38	0.2005	0.025	58.80	2.203	0.178
40.12	27.29	0.201	0.025	31.98	1.596	0.058
49.86	31.28	0.206	0.025	37.26	2.255	0.072

Table A-IV.23: Effect of initial concentration on multicomponent adsorption of Cu²⁺ onto MWCNT-ttpy [conditions: conditions: pH 5.5, contact time 24 h, agitation speed 150 rpm, temperature 20 °C]

$C_i/\text{mg dm}^{-3}$	$C_{eq}/\text{mg dm}^{-3}$	Mass/g	Vol./dm ³	% ads.	$q_e/\text{mg g}^{-1}$	K_d
10.22	4.044	0.2006	0.025	60.43	0.770	0.190
19.64	6.148	0.2014	0.025	68.70	1.675	0.272
30.09	18.21	0.2005	0.025	39.48	1.481	0.081
41.28	28.72	0.201	0.025	30.43	1.562	0.054
51.23	31.25	0.206	0.025	39.00	2.425	0.078

Table A-IV.24: Effect of initial concentration on multicomponent adsorption of Cd²⁺ onto MWCNT-ttpy [conditions: conditions: pH 5.5, contact time 24 h, agitation speed 150 rpm, temperature 20 °C]

$C_i/\text{mg dm}^{-3}$	$C_{eq}/\text{mg dm}^{-3}$	Mass/g	Vol./dm ³	% ads.	$q_e/\text{mg g}^{-1}$	K_d
11.16	1.247	0.2006	0.025	88.83	1.235	0.991
21.28	3.745	0.2014	0.025	82.40	2.177	0.581
30.12	10.18	0.2005	0.025	66.20	2.486	0.244
42.29	18.54	0.201	0.025	56.16	2.954	0.159
51.04	26.81	0.206	0.025	47.47	2.941	0.110

Appendix V

Data for Bisphenol (BPA) and Ibuprofen (IBP)

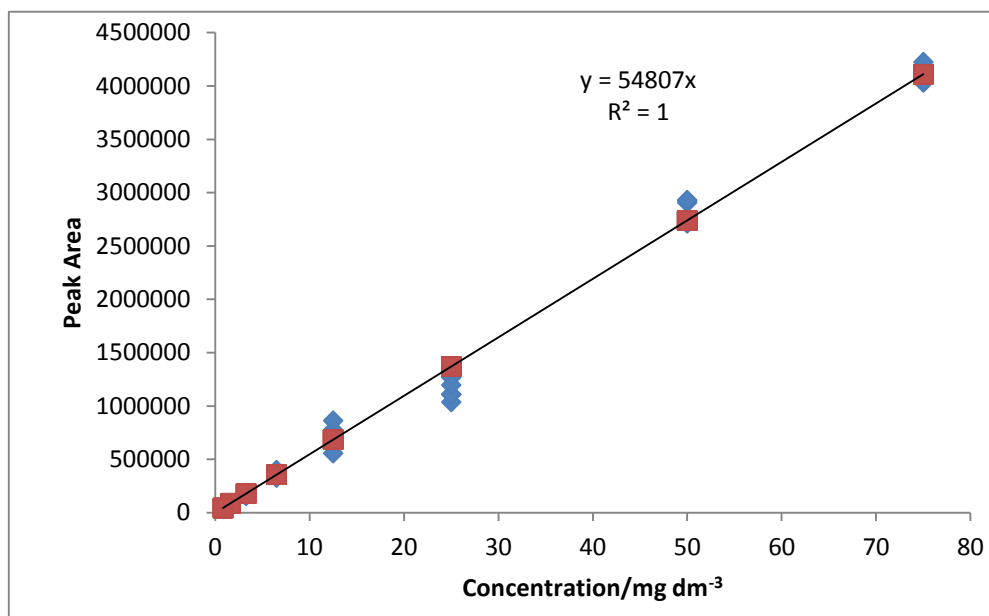


Fig A-V.1: Calibration graph of BPA

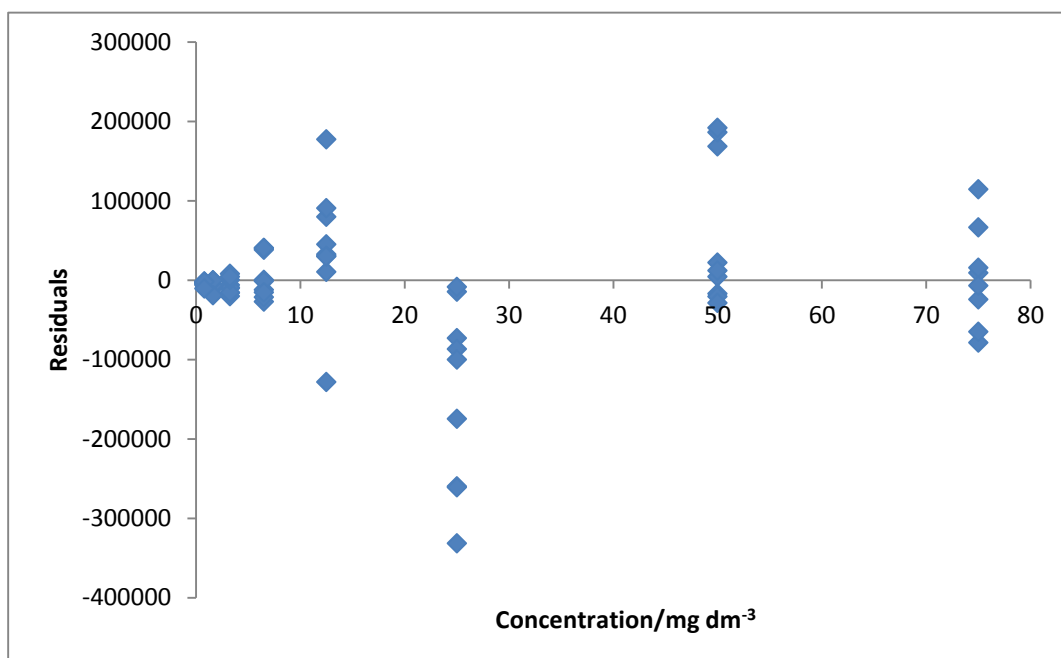


Fig A-V.2: Residual plot of BPA

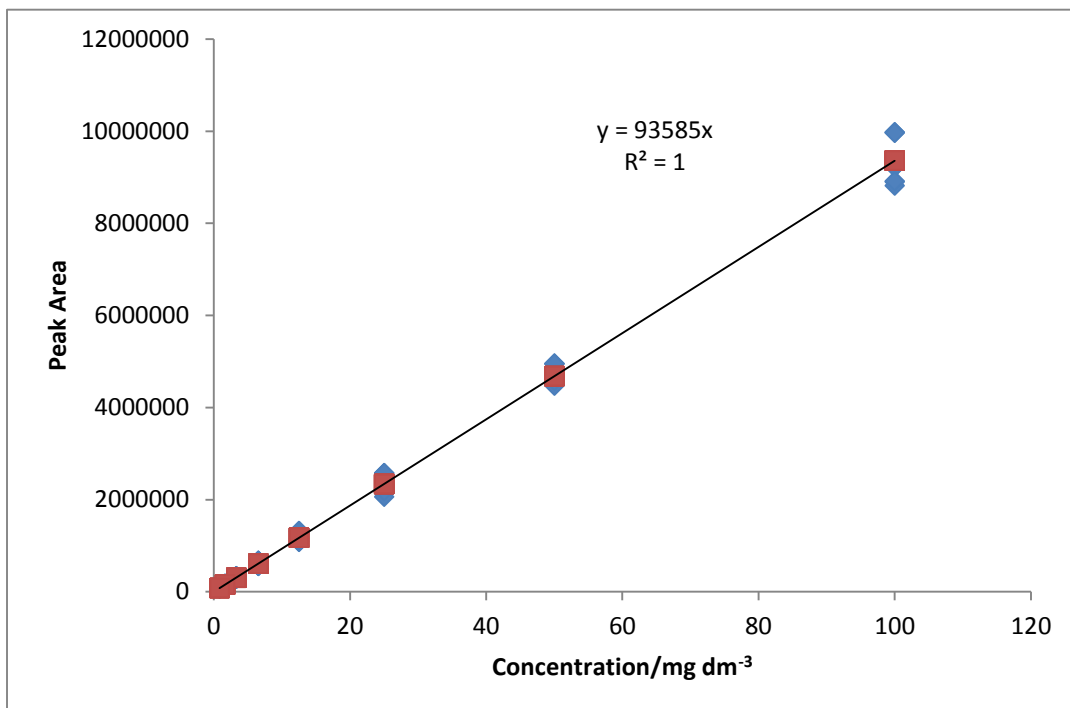


Fig A-V.3: Calibration graph of IBP

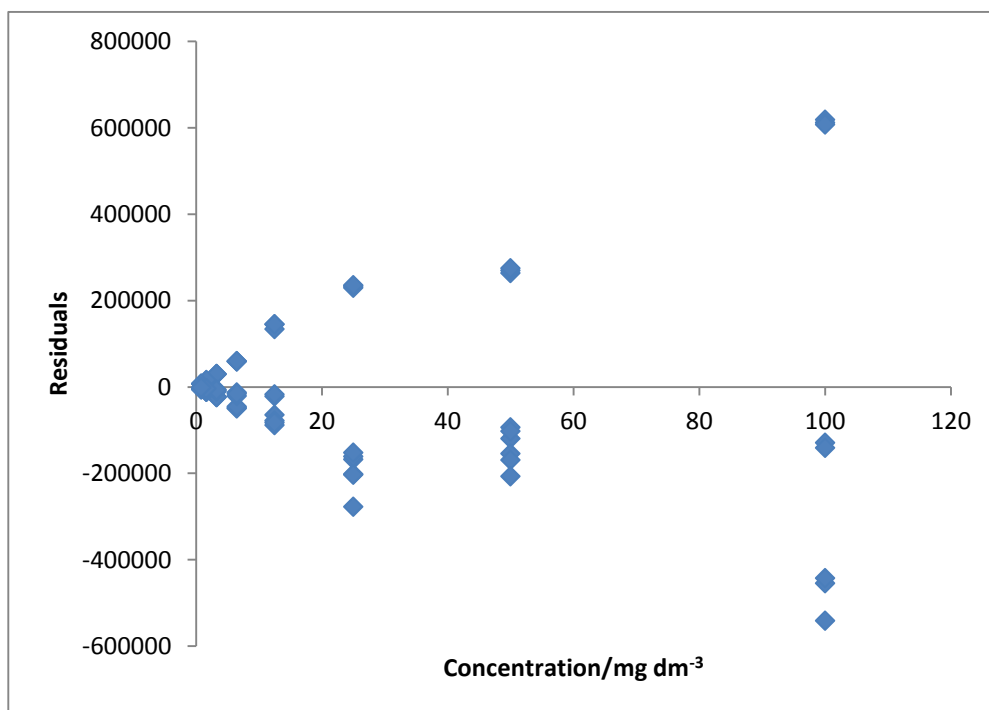


Fig A-V.4: Residual plot of IBP

The chromatograms of standards and samples for the determination of initial and final concentrations of BPA and IBP in aqueous solutions were determined by using the LC method reported.

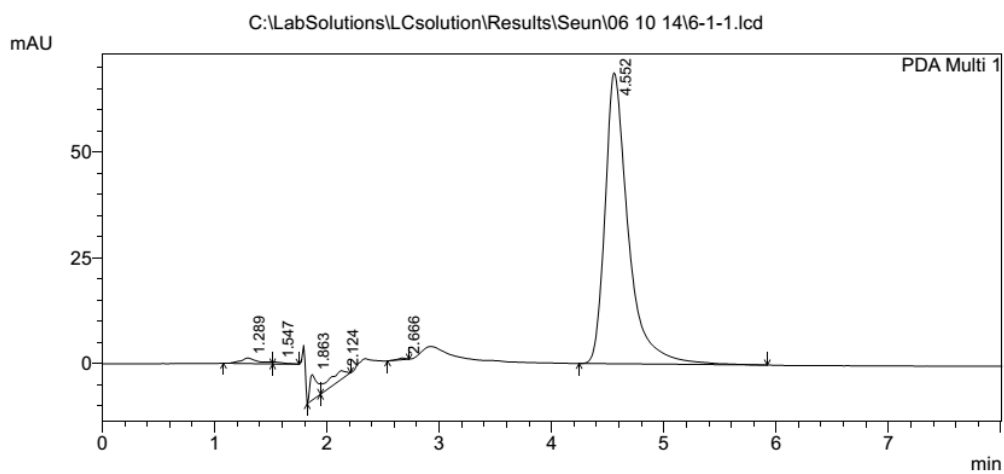


Fig A-V.5: Chromatogram for BPA standard

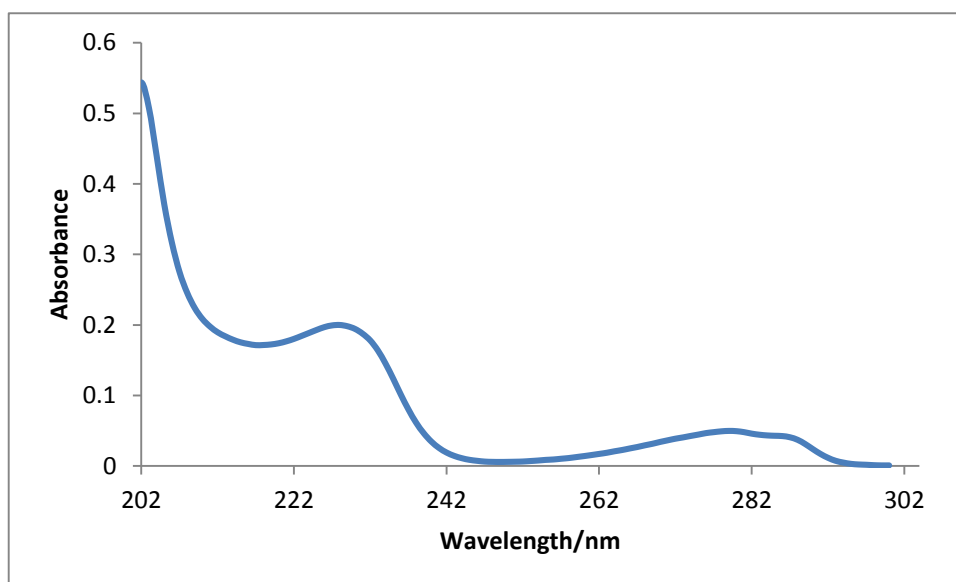


Fig A-V.6: UV spectrum of BPA

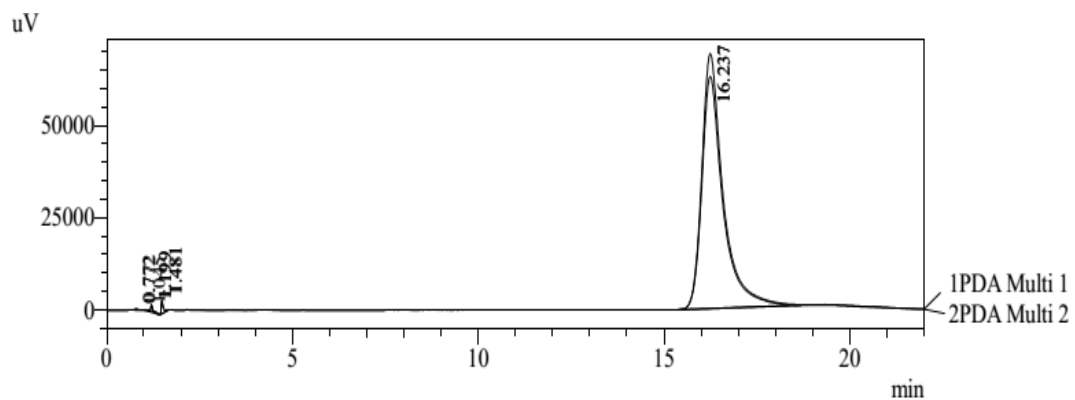


Fig A-V.7: Chromatogram of IBP standard

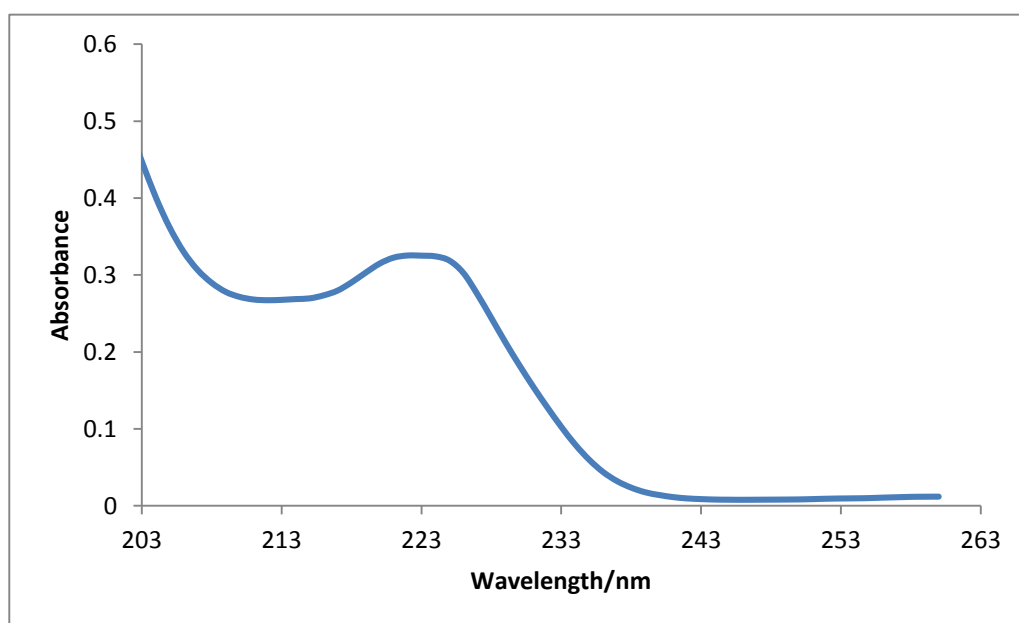


Fig A-V.8: UV spectrum of IBP

Table A-V.1: Experimental data for the adsorption of BPA onto MWCNT-COOH as a function of pH
[conditions: contact time 24 h, agitation speed 150 rpm, temperature 25 °C]

pH	$C_i/\text{mg dm}^{-3}$	$C_{eq}/\text{mg dm}^{-3}$	Mass/g	Volume/ dm^3	% adsorbed	$q_e/\text{mg g}^{-1}$
1	50.079	0.251	0.0503	0.025	99.50	24.77
2	50.079	1.618	0.0506	0.025	96.79	23.95
3	50.079	3.655	0.0504	0.025	92.72	23.03
4	50.079	6.926	0.0505	0.025	86.19	21.37
5	50.079	7.366	0.0503	0.025	85.31	21.23
6	50.079	9.602	0.0509	0.025	80.83	19.88
7	50.079	12.26	0.0501	0.025	75.51	18.87
8	50.079	14.69	0.0500	0.025	70.66	17.69
9	50.079	22.67	0.0493	0.025	54.74	13.90
10	50.079	23.19	0.0501	0.025	53.70	13.42

Table A-V.2: Experimental data for the adsorption of BPA onto MWCNT-COOH as a function of time
[conditions: pH 7.0, agitation speed 150 rpm, temperature 25 °C]

Time/min	$C_i/\text{mg dm}^{-3}$	$C_{eq}/\text{mg dm}^{-3}$	Mass/g	Volume/ dm^3	% adsorbed	$q_e/\text{mg g}^{-1}$
5	42.78	35.96	0.0500	0.025	15.95	3.411
10	42.78	35.74	0.0500	0.025	16.45	3.518
15	42.78	32.65	0.0500	0.025	23.67	5.064
20	42.78	30.83	0.0500	0.025	27.94	5.976
30	42.78	26.32	0.0495	0.025	38.47	8.312
45	42.78	24.31	0.0501	0.025	43.17	9.215
60	42.78	22.35	0.0496	0.025	47.77	10.30
75	42.78	21.23	0.0498	0.025	50.38	10.82
90	42.78	19.08	0.0508	0.025	55.40	11.66
120	42.78	17.45	0.0498	0.025	59.22	12.72
180	42.78	13.26	0.0503	0.025	69.01	14.67
240	42.78	11.78	0.0508	0.025	72.45	15.25
300	42.78	11.53	0.0506	0.025	73.04	15.44
360	42.78	10.95	0.0507	0.025	74.40	15.69
720	42.78	10.64	0.0498	0.025	75.12	16.13
1080	42.78	9.715	0.0507	0.025	77.29	16.30
1440	42.78	9.554	0.0504	0.025	77.67	16.48

Table A-V.3: Experimental data for the adsorption of BPA onto MWCNT-COOH as a function of adsorbent dose [conditions: pH 7.0, contact time 24 h, agitation speed 150 rpm, temperature 25 °C]

$C_i/\text{mg dm}^{-3}$	$C_{eq}/\text{mg dm}^{-3}$	Mass/g	Volume/ dm^3	% adsorbed	$q_e/\text{mg g}^{-1}$
45.58	20.66	0.0307	0.025	54.67	20.29
45.58	12.14	0.0515	0.025	73.37	16.23
45.58	7.504	0.0754	0.025	83.54	12.62
45.58	6.060	0.0993	0.025	86.70	9.95
45.58	2.851	0.1513	0.025	93.75	7.060
45.58	0.839	0.2009	0.025	98.16	5.567
45.58	0.205	0.2996	0.025	99.55	3.786
45.58	0.041	0.4004	0.025	99.91	2.843

Table A-V.4: Experimental data for the adsorption of BPA onto MWCNT-COOH as a function of temperature [conditions: pH 7.0, contact time 24 h, agitation speed 150 rpm]

T/K	$C_i/\text{mg dm}^{-3}$	$C_{eq}/\text{mg dm}^{-3}$	Mass/g	Volume/ dm^3	% adsorbed	$q_e/\text{mg g}^{-1}$
298 K	8.002	0.303	0.0502	0.025	76.98	3.834
	17.24	1.211	0.0493	0.025	80.12	8.126
	26.15	2.419	0.05	0.025	79.10	11.87
	35.10	4.677	0.0497	0.025	76.07	15.31
	45.58	7.729	0.0497	0.025	75.69	19.04
	53.59	10.28	0.0493	0.025	72.19	21.96
	62.45	14.15	0.0508	0.025	69.00	23.77
	70.95	18.91	0.05	0.025	65.04	26.02
	80.21	26.32	0.0501	0.025	59.88	26.89
91.44	35.64	0.0505	0.025	55.80	27.62	
303 K	8.002	0.281	0.05	0.025	77.21	3.860
	17.24	1.009	0.0503	0.025	81.13	8.065
	26.15	2.346	0.0505	0.025	79.35	11.78
	35.10	4.081	0.0504	0.025	77.56	15.39
	45.58	7.052	0.0504	0.025	77.05	19.11
	53.59	8.877	0.0511	0.025	74.52	21.87
	62.45	12.08	0.0503	0.025	71.96	25.04
	70.95	17.36	0.0498	0.025	66.99	26.90
	80.21	24.76	0.0503	0.025	61.62	27.56
91.44	32.04	0.0505	0.025	59.39	29.40	
313 K	8.002	0.263	0.0502	0.025	77.39	3.854
	17.24	0.887	0.0493	0.025	81.74	8.290
	26.15	1.891	0.0500	0.025	80.86	12.13
	35.10	3.400	0.0497	0.025	79.26	15.95
	45.58	5.959	0.0497	0.025	79.24	19.93
	53.59	7.783	0.0493	0.025	76.34	23.23
	62.45	10.70	0.0508	0.025	73.94	25.47

	70.95	16.30	0.0500	0.025	68.31	27.32
	80.21	21.63	0.0501	0.025	65.09	29.23
	91.44	29.26	0.0505	0.025	62.18	30.78
318 K	8.00	0.243	0.0501	0.025	77.59	3.872
	17.24	0.736	0.0497	0.025	82.49	8.299
	26.15	1.708	0.0503	0.025	81.47	12.148
	35.10	2.820	0.0509	0.025	80.71	15.86
	45.58	4.849	0.0500	0.025	81.45	20.36
	53.59	7.051	0.0512	0.025	77.56	22.72
	62.45	10.28	0.0503	0.025	74.54	25.93
	70.95	13.26	0.0506	0.025	72.11	28.50
	80.21	17.45	0.0511	0.025	69.74	30.71
	91.44	25.81	0.0504	0.025	65.63	32.55

Table A-V.5: Experimental data for the adsorption of BPA onto MWCNT-ttpy as a function of pH
[conditions: contact time 24 h, agitation speed 150 rpm, temperature 25 °C]

pH	$C_i/\text{mg dm}^{-3}$	$C_{eq}/\text{mg dm}^{-3}$	Mass/g	Volume/ dm^3	% adsorbed	$q_e/\text{mg g}^{-1}$
1	50.079	0.156	0.0502	0.025	99.69	24.86
2	50.079	0.000	0.0499	0.025	100.0	25.09
3	50.079	0.137	0.0501	0.025	99.73	24.92
4	50.079	0.447	0.0502	0.025	99.11	24.72
5	50.079	0.490	0.0494	0.025	99.02	25.10
6	50.079	1.293	0.0505	0.025	97.42	24.15
7	50.079	1.498	0.0499	0.025	97.01	24.34
8	50.079	2.554	0.0504	0.025	94.90	23.57
9	50.079	2.810	0.0509	0.025	94.39	23.22
10	50.079	4.069	0.0509	0.025	91.88	22.60

Table A-V.6: Experimental data for the adsorption of BPA onto MWCNT-ttpy as a function of time [conditions: pH 7.0, agitation speed 150 rpm, temperature 25 °C]

Time/min	$C_i/\text{mg dm}^{-3}$	$C_{eq}/\text{mg dm}^{-3}$	Mass/g	Volume/ dm^3	% adsorbed	$q_e/\text{mg g}^{-1}$
5	42.78	26.38	0.0500	0.025	38.34	8.104
10	42.78	25.44	0.0500	0.025	40.52	8.548
15	42.78	24.21	0.0500	0.025	43.41	9.435
20	42.78	23.82	0.0500	0.025	44.32	9.480
30	42.78	23.69	0.0495	0.025	44.62	9.487
45	42.78	16.12	0.0501	0.025	62.33	13.25
60	42.78	10.93	0.0496	0.025	74.46	15.89
75	42.78	9.661	0.0498	0.025	77.42	16.53
90	42.78	8.107	0.0508	0.025	81.05	17.34
120	42.78	5.930	0.0498	0.025	86.14	18.50
180	42.78	5.550	0.0503	0.025	87.03	18.58
240	42.78	5.486	0.0508	0.025	87.18	18.43
300	42.78	4.778	0.0506	0.025	88.83	18.93
360	42.78	3.659	0.0507	0.025	91.45	19.52
720	42.78	3.273	0.0498	0.025	92.35	19.79
1080	42.78	3.114	0.0507	0.025	92.72	19.52
1440	42.78	2.976	0.0504	0.025	93.04	19.67

Table A-V.7: Experimental data for the adsorption of BPA onto MWCNT-ttpy as a function of adsorbent dose [conditions: pH 7.0, contact time 24 h, agitation speed 150 rpm, temperature 25 °C]

$C_i/\text{mg dm}^{-3}$	$C_{eq}/\text{mg dm}^{-3}$	Mass/g	Volume/ dm^3	% adsorbed	$q_e/\text{mg g}^{-1}$
45.58	6.748	0.0304	0.025	85.19	31.93
45.58	2.691	0.0504	0.025	94.10	21.27
45.58	1.696	0.0751	0.025	96.28	14.61
45.58	1.244	0.1008	0.025	97.27	11.00
45.58	0.990	0.1508	0.025	97.83	7.392
45.58	0.792	0.2008	0.025	98.26	5.576
45.58	0.021	0.3002	0.025	99.95	3.794
45.58	0.000	0.4001	0.025	100.0	2.848

Table A-V.8: Experimental data for the adsorption of BPA onto MWCNT-ttpy as a function of temperature [conditions: pH 7.0, contact time 24 h, agitation speed 150 rpm, temperature 25 °C]

T/K	$C_i/\text{mg dm}^{-3}$	$C_{eq}/\text{mg dm}^{-3}$	Mass/g	Volume/ dm^3	% adsorbed	$q_e/\text{mg g}^{-1}$
298 K	8.002	0.205	0.0503	0.025	77.97	3.875
	17.24	0.937	0.0509	0.025	81.49	8.005
	26.15	1.692	0.0502	0.025	81.53	12.18
	35.10	3.732	0.0499	0.025	78.43	15.72
	45.58	5.054	0.0498	0.025	81.05	20.34
	53.59	7.104	0.0503	0.025	77.48	23.10

	62.45	9.38	0.0504	0.025	75.82	26.33
	70.95	13.80	0.0501	0.025	71.43	28.52
	80.21	18.08	0.0501	0.025	69.04	31.01
	91.44	23.45	0.0512	0.025	67.99	33.20
303 K	8.002	0.200	0.0504	0.025	78.02	3.870
	17.24	0.744	0.0504	0.025	82.46	8.181
	26.15	1.409	0.0497	0.025	82.47	12.45
	35.10	2.222	0.0501	0.025	82.20	16.41
	45.58	3.969	0.0505	0.025	83.22	20.60
	53.59	5.873	0.0502	0.025	79.53	23.76
	62.45	8.57	0.0503	0.025	76.97	26.78
	70.95	12.19	0.0498	0.025	73.45	29.50
	80.21	14.99	0.0505	0.025	72.47	32.29
	91.44	20.84	0.0501	0.025	70.60	35.23
313 K	8.002	0.172	0.0509	0.025	78.30	3.846
	17.24	0.606	0.0510	0.025	83.15	8.152
	26.15	1.214	0.0496	0.025	83.12	12.57
	35.10	2.063	0.0504	0.025	82.60	16.39
	45.58	3.962	0.0503	0.025	83.23	20.68
	53.59	5.161	0.0503	0.025	80.71	24.07
	62.45	6.94	0.0500	0.025	79.31	27.76
	70.95	8.87	0.0501	0.025	77.59	30.98
	80.21	12.58	0.0498	0.025	75.15	33.95
	91.44	19.81	0.0498	0.025	71.63	35.96
318 K	8.002	0.154	0.0502	0.025	78.48	3.908
	17.24	0.404	0.0493	0.025	84.16	8.535
	26.15	0.971	0.0500	0.025	83.93	12.59
	35.10	1.381	0.0497	0.025	84.31	16.96
	45.58	2.066	0.0497	0.025	87.02	21.89
	53.59	3.677	0.0493	0.025	83.19	25.31
	62.45	4.637	0.0508	0.025	82.60	28.45
	70.95	6.668	0.0500	0.025	80.35	32.14
	80.21	9.980	0.0501	0.025	78.04	35.05
	91.44	15.62	0.0505	0.025	75.81	37.53

Table A-V.9: Separation factor values (R_L) for the adsorption of BPA onto MWCNT-COOH at different temperatures

$C_i/\text{mg dm}^{-3}$	298 K	303 K	313 K	318 K
8.002	0.347	0.344	0.306	0.303
17.24	0.198	0.196	0.170	0.168
26.15	0.140	0.138	0.119	0.118
35.10	0.108	0.107	0.091	0.090
45.58	0.085	0.084	0.072	0.071
53.59	0.074	0.073	0.062	0.061
62.45	0.064	0.063	0.053	0.053
70.95	0.057	0.056	0.047	0.047
80.21	0.050	0.050	0.042	0.042
91.44	0.044	0.044	0.037	0.037

Table A-V.10: Separation factor values (R_L) for the adsorption of BPA onto MWCNT-ttpty at different temperatures

$C_i/\text{mg dm}^{-3}$	298 K	303 K	313 K	318 K
8.002	0.355	0.290	0.279	0.210
17.24	0.204	0.159	0.152	0.110
26.15	0.144	0.111	0.106	0.075
35.10	0.112	0.085	0.081	0.057
45.58	0.088	0.067	0.064	0.045
53.59	0.076	0.057	0.055	0.038
62.45	0.066	0.050	0.047	0.033
70.95	0.058	0.044	0.042	0.029
80.21	0.052	0.039	0.037	0.026
91.44	0.046	0.035	0.033	0.023

Table A-V.11: Experimental data for the adsorption of IBP onto MWCNT-COOH as a function of pH [conditions: contact time 24 h, agitation speed 150 rpm, temperature 25 °C]

pH	$C_i/\text{mg dm}^{-3}$	$C_{eq}/\text{mg dm}^{-3}$	Mass/g	Volume/ dm^3	%adsorbed	$q_e/\text{mg g}^{-1}$
1	49.08	21.53	0.0499	0.025	56.14	13.80
2	49.08	23.66	0.0503	0.025	51.79	12.63
3	49.08	27.40	0.0494	0.025	44.17	10.97
4	49.08	29.42	0.0502	0.025	40.05	9.789
5	49.08	30.12	0.0499	0.025	38.63	9.498
6	49.08	37.46	0.0502	0.025	23.67	5.785
7	49.08	38.80	0.0508	0.025	20.95	5.059
8	49.08	41.09	0.0498	0.025	16.27	4.010
9	49.08	41.72	0.0487	0.025	14.99	3.776

Table A-V.12: Experimental data for the adsorption of IBP onto MWCNT-COOH as a function of time [conditions: pH 2.0, agitation speed 150 rpm, temperature 25 °C]

Time/min	$C_i/\text{mg dm}^{-3}$	$C_{eq}/\text{mg dm}^{-3}$	Mass/g	Volume/ dm^3	% adsorbed	$q_e/\text{mg g}^{-1}$
5	46.66	40.47	0.0504	0.025	13.28	3.074
10	46.66	38.46	0.0502	0.025	17.58	4.086
15	46.66	36.56	0.0500	0.025	21.65	5.051
20	46.66	33.77	0.0497	0.025	27.63	6.485
30	46.66	31.58	0.0513	0.025	32.32	7.351
45	46.66	30.94	0.0506	0.025	33.69	7.767
60	46.66	29.59	0.0507	0.025	36.58	8.418
75	46.66	27.06	0.0499	0.025	42.02	9.824
90	46.66	26.66	0.0498	0.025	42.88	10.04
120	46.66	26.39	0.0496	0.025	43.45	10.22
180	46.66	25.79	0.0505	0.025	44.74	10.34
240	46.66	25.53	0.0498	0.025	45.28	10.61
300	46.66	25.15	0.0503	0.025	46.10	10.69
360	46.66	24.38	0.0497	0.025	47.75	11.21
720	46.66	23.74	0.0503	0.025	49.14	11.40
1080	46.66	23.36	0.0508	0.025	49.94	11.47
1440	46.66	22.95	0.0500	0.025	50.82	11.86

Table A-V.13: Experimental data for the adsorption of IBP onto MWCNT-COOH as a function of adsorbent dose [conditions: pH 2.0, contact time 24 h, agitation speed 150 rpm, temperature 25 °C]

$C_i/\text{mg dm}^{-3}$	$C_{eq}/\text{mg dm}^{-3}$	Mass/g	Volume/ dm^3	% adsorbed	$q_e/\text{mg g}^{-1}$
49.08	29.622	0.0314	0.025	39.64	15.49
49.08	22.404	0.0503	0.025	54.35	13.26
49.08	19.449	0.0754	0.025	60.37	9.82
49.08	12.603	0.1016	0.025	74.32	8.98
49.08	11.626	0.1511	0.025	76.31	6.197
49.08	9.555	0.2006	0.025	80.53	4.926
49.08	6.006	0.3012	0.025	87.76	3.575
49.08	4.850	0.3992	0.025	90.1	2.770

Table A-V.14: Experimental data for the adsorption of IBP onto MWCNT-COOH as a function of temperature
[conditions: pH 2.0, contact time 24 h, agitation speed 150 rpm]

T/K	$C_i/\text{mg dm}^{-3}$	$C_{eq}/\text{mg dm}^{-3}$	Mass/g	Volume/ dm^3	% adsorbed	$q_e/\text{mg g}^{-1}$
298 K	10.17	7.727	0.0506	0.025	75.98	3.818
	19.14	13.22	0.0497	0.025	69.09	6.651
	29.88	19.32	0.0500	0.025	64.67	9.662
	40.13	25.47	0.0508	0.025	63.46	12.53
	51.23	30.18	0.0507	0.025	58.90	14.88
	61.24	32.70	0.0500	0.025	53.39	16.35
	71.66	33.43	0.0501	0.025	46.64	16.68
	81.45	33.89	0.0501	0.025	41.61	16.91
	90.22	34.27	0.0505	0.025	37.99	16.97
99.56	34.40	0.0498	0.025	34.56	17.27	
303 K	10.17	7.426	0.0506	0.025	73.02	3.669
	19.14	11.95	0.0497	0.025	62.44	6.011
	29.88	17.84	0.0500	0.025	59.72	8.922
	40.13	23.76	0.0508	0.025	59.21	11.69
	51.23	28.21	0.0507	0.025	55.06	13.91
	61.24	28.63	0.0500	0.025	46.75	14.31
	71.66	31.01	0.0501	0.025	43.27	15.47
	81.45	32.53	0.0495	0.025	39.94	16.43
	90.22	34.27	0.0505	0.025	37.99	16.97
99.56	33.45	0.0498	0.025	33.60	16.79	
313 K	10.17	7.074	0.0506	0.025	69.55	3.495
	19.14	11.48	0.0497	0.025	59.97	5.774
	29.88	17.93	0.0500	0.025	60.01	8.965
	40.13	23.48	0.0508	0.025	58.51	11.55
	51.23	27.02	0.0507	0.025	52.74	13.32
	61.24	27.37	0.0500	0.025	44.69	13.68
	71.66	30.25	0.0501	0.025	42.21	15.09
	81.45	31.88	0.0500	0.025	39.14	15.94
	90.22	31.12	0.0505	0.025	34.50	15.41
99.56	30.90	0.0498	0.025	31.04	15.51	
318 K	10.17	3.588	0.0502	0.025	35.28	3.574
	19.14	5.427	0.0502	0.025	28.35	5.405
	29.88	7.665	0.0501	0.025	25.65	7.650
	40.13	9.165	0.0503	0.025	22.84	9.111
	51.23	11.09	0.0502	0.025	21.65	11.05
	61.24	12.63	0.0505	0.025	20.63	12.51
	71.66	13.55	0.0496	0.025	18.90	13.65
	81.45	13.60	0.0498	0.025	16.70	13.65
	90.22	13.85	0.0501	0.025	15.35	13.82

99.56 14.03 0.0502 0.025 14.09 13.97

Table A-V.15: Experimental data for the adsorption of IBP onto MWCNT-ttpy as a function of pH
[conditions: contact time 24 h, agitation speed 150 rpm, temperature 25 °C]

pH	$C_i/\text{mg dm}^{-3}$	$C_{eq}/\text{mg dm}^{-3}$	Mass/g	Volume/ dm^3	% adsorbed	$q_e/\text{mg g}^{-1}$
1	49.08	6.385	0.0497	0.025	86.99	21.48
2	49.08	7.124	0.0499	0.025	85.48	21.02
3	49.08	6.960	0.0503	0.025	85.82	20.93
4	49.08	11.05	0.0499	0.025	77.48	19.05
5	49.08	13.80	0.0505	0.025	71.88	17.46
6	49.08	20.53	0.0500	0.025	58.18	14.28
7	49.08	20.76	0.0506	0.025	57.70	13.99
8	49.08	21.42	0.0505	0.025	56.35	13.69
9	49.08	33.24	0.0508	0.025	32.27	7.794

Table A-V.16: Experimental data for the adsorption of IBP onto MWCNT-ttpy as a function of time
[conditions: pH 2.0, agitation speed 150 rpm, temperature 25 °C]

Time/min	$C_i/\text{mg dm}^{-3}$	$C_{eq}/\text{mg dm}^{-3}$	Mass/g	Volume/ dm^3	% adsorbed	$q_e/\text{mg g}^{-1}$
5	46.66	17.17	0.0498	0.025	63.20	14.80
10	46.66	15.40	0.0503	0.025	67.01	15.54
15	46.66	15.06	0.0503	0.025	67.73	15.71
20	46.66	12.91	0.0509	0.025	72.33	16.58
30	46.66	12.07	0.0505	0.025	74.14	17.13
45	46.66	10.54	0.0502	0.025	77.41	17.99
60	46.66	9.801	0.0500	0.025	79.00	18.43
75	46.66	9.116	0.0504	0.025	80.46	18.63
90	46.66	8.706	0.0507	0.025	81.34	18.72
120	46.66	8.396	0.0500	0.025	82.01	19.13
180	46.66	8.162	0.0502	0.025	82.51	19.17
240	46.66	7.744	0.0505	0.025	83.40	19.27
300	46.66	7.144	0.0501	0.025	84.69	19.72
360	46.66	6.980	0.0503	0.025	85.04	19.72
720	46.66	5.706	0.0503	0.025	87.77	20.36
1080	46.66	5.432	0.0503	0.025	88.36	20.49
1440	46.66	5.243	0.0506	0.025	88.76	20.47

Table A-V.17: Experimental data for the adsorption of IBP onto MWCNT-ttpy as a function of adsorbent dose [conditions: pH 2.0, contact time 24 h, agitation speed 150 rpm, temperature 25 °C]

$C_i/\text{mg dm}^{-3}$	$C_{eq}/\text{mg dm}^{-3}$	Mass/g	Volume/ dm^3	% adsorbed	$q_e/\text{mg g}^{-1}$
49.08	12.414	0.0310	0.025	74.71	29.57
49.08	5.618	0.0506	0.025	88.55	21.47
49.08	3.684	0.0756	0.025	92.49	15.01
49.08	1.965	0.0992	0.025	96.00	11.87
49.08	1.489	0.1490	0.025	96.97	7.985
49.08	1.235	0.2018	0.025	97.48	5.927
49.08	0.586	0.2996	0.025	98.81	4.047
49.08	0.265	0.4004	0.025	99.5	3.048

Table A-V.18: Experimental data for the adsorption of IBP onto MWCNT-ttpy as a function of temperature [conditions: pH 2.0, contact time 24 h, agitation speed 150 rpm, temperature 25 °C]

T/K	$C_i/\text{mg dm}^{-3}$	$C_{eq}/\text{mg dm}^{-3}$	Mass/g	Volume/ dm^3	% adsorbed	$q_e/\text{mg g}^{-1}$
298 K	9.887	9.857	0.0503	0.025	98.57	4.899
	19.14	18.52	0.0499	0.025	92.59	9.277
	29.88	27.75	0.0508	0.025	92.51	13.66
	40.13	35.59	0.0494	0.025	88.98	18.01
	51.23	44.90	0.0505	0.025	89.81	22.23
	61.24	50.35	0.0506	0.025	83.91	24.88
	71.66	56.57	0.0499	0.025	80.82	28.34
	81.45	61.37	0.0504	0.025	76.71	30.44
	90.22	62.98	0.0505	0.025	69.97	31.18
99.56	64.71	0.0504	0.025	64.71	32.10	
303 K	9.887	9.676	0.0503	0.025	97.87	4.809
	19.14	18.20	0.0499	0.025	95.11	9.120
	29.88	27.24	0.0508	0.025	91.16	13.40
	40.13	34.86	0.0494	0.025	86.87	17.64
	51.23	43.19	0.0505	0.025	84.31	21.38
	61.24	49.08	0.0506	0.025	80.15	24.25
	71.66	52.63	0.0499	0.025	73.45	26.37
	81.45	58.20	0.0504	0.025	71.45	28.87
	90.22	61.69	0.0505	0.025	68.37	30.54
99.56	62.62	0.0504	0.025	62.90	31.06	
313 K	9.887	9.453	0.0509	0.025	95.61	4.643
	19.14	18.07	0.0499	0.025	94.41	9.053
	29.88	26.79	0.0507	0.025	89.64	13.21
	40.13	34.25	0.0508	0.025	85.35	16.86
	51.23	41.50	0.0508	0.025	81.00	20.42
	61.24	46.58	0.0509	0.025	76.05	22.88
	71.66	51.57	0.0505	0.025	71.97	25.53

	81.45	55.89	0.0507	0.025	68.62	27.56
	90.22	56.41	0.0506	0.025	62.52	27.87
	99.56	59.42	0.0502	0.025	59.69	29.59
318 K	9.887	8.978	0.0502	0.025	89.78	4.471
	19.14	15.95	0.0493	0.025	79.74	8.087
	29.88	25.00	0.0500	0.025	83.34	12.50
	40.13	31.52	0.0497	0.025	78.80	15.85
	51.23	40.24	0.0497	0.025	80.47	20.24
	61.24	45.83	0.0493	0.025	76.38	23.24
	71.66	47.37	0.0508	0.025	67.67	23.31
	81.45	50.82	0.0500	0.025	63.53	25.41
	90.22	54.33	0.0501	0.025	60.37	27.11
	99.56	58.37	0.0505	0.025	58.37	28.90

Table A-V.19: Separation factor values (R_L) for the adsorption of IBP onto MWCNT-COOH at different temperatures

$C_i/\text{mg dm}^{-3}$	298 K	303 K	313 K	318 K
10.17	0.295	0.292	0.257	0.255
19.14	0.182	0.180	0.155	0.154
29.88	0.125	0.123	0.105	0.104
40.13	0.096	0.095	0.081	0.080
51.23	0.077	0.076	0.064	0.064
61.24	0.065	0.064	0.054	0.054
71.66	0.056	0.055	0.047	0.046
81.45	0.050	0.049	0.041	0.041
90.22	0.045	0.044	0.038	0.037
99.56	0.041	0.040	0.034	0.034

Table A-V.20: Separation factor values (R_L) for the adsorption of IBP onto MWCNT-ttph at different temperatures

$C_i/\text{mg dm}^{-3}$	298 K	303 K	313 K	318 K
9.887	0.308	0.248	0.238	0.177
19.14	0.187	0.146	0.139	0.100
29.88	0.128	0.099	0.094	0.066
40.13	0.099	0.075	0.072	0.050
51.23	0.079	0.060	0.057	0.040
61.24	0.067	0.051	0.048	0.034
71.66	0.058	0.044	0.041	0.029
81.45	0.051	0.039	0.037	0.025
90.22	0.047	0.035	0.033	0.023
99.56	0.042	0.032	0.030	0.021

Appendix VI

Data for competitive adsorption of bisphenol A and ibuprofen

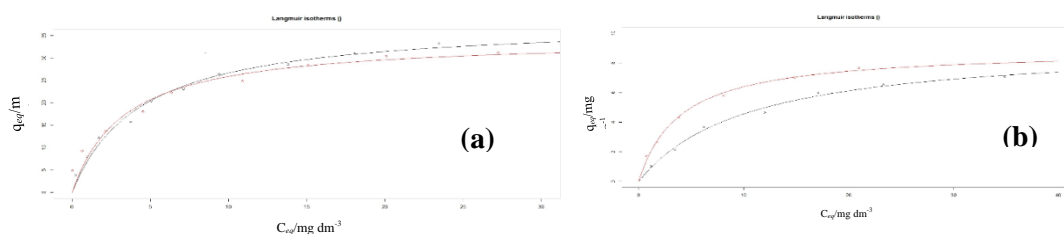


Fig A-VI.1: Langmuir adsorption isotherm models fitted for the adsorption of BPA and IBP onto MWCNT in (a) single system and (b) multicomponent competitive adsorption system (BPA — and IBP —).

(A) Effect of pH on binary adsorption systems

Table A-VI.1: Experimental data for the binary adsorption of BPA onto MWCNT-ttpy as a function of pH [conditions: contact time 24 h, agitation speed 150 rpm, temperature 25 °C]

pH	$C_i/\text{mg dm}^{-3}$	$C_{eq}/\text{mg dm}^{-3}$	Mass/g	Vol/ dm^{-3}	% ads	$q_e/\text{mg g}^{-1}$
1	15.79	10.88	0.0756	0.025	68.92	3.598
2	15.79	11.47	0.0759	0.025	72.65	3.778
3	15.79	11.49	0.0750	0.025	72.80	3.831
4	15.79	11.53	0.0750	0.025	73.04	3.844
5	15.79	11.93	0.0751	0.025	75.54	3.970
6	15.79	11.98	0.0756	0.025	75.89	3.962
7	15.79	11.93	0.0754	0.025	75.54	3.954
8	15.79	12.26	0.0758	0.025	72.33	3.766
9	15.79	12.30	0.0756	0.025	69.35	3.621
10	15.79	13.59	0.0755	0.025	65.73	3.436

Table A-VI.2: Experimental data for the binary adsorption of IBP onto MWCNT-ttpy as a function of pH [conditions: contact time 24 h, agitation speed 150 rpm, temperature 25 °C]

pH	$C_i/\text{mg dm}^{-3}$	$C_{eq}/\text{mg dm}^{-3}$	Mass/g	Vol/ dm^{-3}	% ads	$q_e/\text{mg g}^{-1}$
1	14.20	10.81	0.0756	0.025	81.52	3.573
2	14.20	11.16	0.0759	0.025	79.01	3.675
3	14.20	10.95	0.0750	0.025	76.75	3.650
4	14.20	8.098	0.0750	0.025	60.06	2.699
5	14.20	7.772	0.0751	0.025	54.02	2.587
6	14.20	5.644	0.0756	0.025	39.74	1.866
7	14.20	3.655	0.0754	0.025	25.38	1.212

8	14.20	1.795	0.0758	0.025	14.56	0.592
9	14.20	0.917	0.0756	0.025	8.507	0.303
10	14.20	0.551	0.0755	0.025	3.882	0.183

(B) Binary adsorption of BPA and IBP at same concentration

Table A-VI.3: Experimental data for the competitive adsorption of BPA onto MWCNT-ttpy in a multicomponent system at the same concentration [conditions: pH 2.0, contact time 24 h, agitation speed 150 rpm, temperature 25 °C]

$C_i/\text{mg dm}^{-3}$	$C_{eq}/\text{mg dm}^{-3}$	Mass/g	Vol./dm ³	% ads.	$q_e/\text{mg g}^{-1}$	K_d
5.306	1.139	0.1010	0.025	78.54	1.031	0.906
12.59	3.473	0.1057	0.025	72.41	2.156	0.621
21.25	6.218	0.1023	0.025	70.75	3.675	0.591
30.80	11.99	0.1014	0.025	61.06	4.636	0.387
41.29	17.12	0.1008	0.025	58.54	5.995	0.350
50.26	23.29	0.1031	0.025	53.66	6.541	0.281
63.74	34.90	0.1022	0.025	45.25	7.056	0.202

Table A-VI.4: Experimental data for the competitive adsorption of IBP onto MWCNT-ttpy in a multicomponent system at the same concentration [conditions: pH 2.0, contact time 24 h, agitation speed 150 rpm, temperature 25 °C]

$C_i/\text{mg dm}^{-3}$	$C_{eq}/\text{mg dm}^{-3}$	Mass/g	Vol./dm ³	% ads.	$q_e/\text{mg g}^{-1}$	K_d
7.632	0.687	0.1010	0.025	91.00	1.719	2.502
12.91	1.706	0.1057	0.025	86.79	2.650	1.553
21.52	3.830	0.1023	0.025	82.21	4.324	1.129
31.56	8.097	0.1014	0.025	74.34	5.785	0.714
43.06	14.82	0.1008	0.025	65.57	7.002	0.472
52.56	20.97	0.1031	0.025	60.10	7.66	0.365
60.39	26.59	0.1022	0.025	55.97	8.27	0.311

(C) Binary adsorption with one component at a fixed concentration and the other at varying initial metal ion concentrations

(a). Effect of varying IBP concentration on BPA adsorption from aqueous solutions onto MWCNT-ttpy.

Table A-VI.5: : Effect of varying initial IBP concentration on the adsorption of BPA onto MWCNT-ttpy [conditions: pH 2.0, contact time 24 h, agitation speed 150 rpm, temperature 25 °C]

$C_i/\text{mg dm}^{-3}$	$C_{eq}/\text{mg dm}^{-3}$	Mass/g	Vol./dm ³	% ads.	$q_e/\text{mg g}^{-1}$	K_d
21.90	6.386	0.1028	0.025	70.84	3.773	0.591
18.26	6.213	0.1041	0.025	65.99	2.894	0.466
20.09	4.834	0.1008	0.025	75.94	3.784	0.783
17.81	3.309	0.1022	0.025	81.42	3.55	1.072

16.63	4.952	0.1130	0.025	70.23	2.58	0.522
23.89	6.840	0.1060	0.025	71.37	4.02	0.588
16.20	1.213	0.0980	0.025	92.51	3.82	3.152

Table A-VI.6: Effect of varying initial IBP concentration on its adsorption onto MWCNT-ttpty [conditions: pH 2.0, contact time 24 h, agitation speed 150 rpm, temperature 25 °C]

$C_i/\text{mg dm}^{-3}$	$C_{eq}/\text{mg dm}^{-3}$	Mass/g	Vol./dm ³	% ads.	$q_e/\text{mg g}^{-1}$	K_d
56.93	39.82	0.1028	0.025	30.05	4.161	0.104
54.20	36.90	0.1041	0.025	31.93	4.157	0.113
40.43	16.49	0.1008	0.025	59.20	5.936	0.360
31.07	8.602	0.1022	0.025	72.31	5.495	0.639
20.13	4.401	0.1130	0.025	78.14	3.480	0.791
9.113	1.515	0.1060	0.025	83.38	1.792	1.183
8.331	0.135	0.0980	0.025	98.39	2.091	15.54

(b). Effect of varying initial BPA concentration on IBP adsorption from aqueous solutions onto MWCNT-ttpty.

Table A-VI.7: Effect of varying BPA concentration on multicomponent adsorption of IBP onto MWCNT-ttpty [conditions: pH 2.0, contact time 24 h, agitation speed 150 rpm, temperature 25 °C]

$C_i/\text{mg dm}^{-3}$	$C_{eq}/\text{mg dm}^{-3}$	Mass/g	Vol./dm ³	% ads.	$q_e/\text{mg g}^{-1}$	K_d
21.17	1.004	0.1004	0.025	95.26	5.022	5.001
19.81	2.117	0.9881	0.025	89.31	0.448	0.211
20.80	2.289	0.1016	0.025	89.00	4.554	1.990
23.38	3.202	0.1022	0.025	86.30	4.935	1.541
21.67	3.794	0.0996	0.025	82.49	4.487	1.183
21.67	6.254	0.1005	0.025	71.14	3.835	0.613
23.38	9.709	0.1008	0.025	58.47	3.390	0.349

Table A-VI.8: Effect of varying initial BPA concentration on its adsorption onto MWCNT-ttpty [conditions: pH 2.0, contact time 24 h, agitation speed 150 rpm, temperature 25 °C]

$C_i/\text{mg dm}^{-3}$	$C_{eq}/\text{mg dm}^{-3}$	Mass/g	Vol./dm ³	% ads.	$q_e/\text{mg g}^{-1}$	K_d
55.60	47.52	0.1004	0.025	14.53	2.012	0.042
47.52	29.55	0.9881	0.025	37.82	0.455	0.015
40.23	15.46	0.1016	0.025	61.57	6.095	0.394
31.90	6.864	0.1022	0.025	78.48	6.123	0.892
21.74	4.313	0.0996	0.025	80.16	4.375	1.014
8.545	1.425	0.1005	0.025	83.33	1.771	1.243
4.653	0.929	0.1008	0.025	80.04	0.924	0.994

(D) Multicomponent adsorption with metal ion at a fixed concentration and varying BPA and IBP initial concentrations

(a). Effect of multicomponent concentration on Pb²⁺ adsorption from aqueous solutions onto MWCNT-ttpy.

Table A-VI.9: Effect of same initial Pb²⁺ concentration on its adsorption onto MWCNT-ttpy [conditions: pH 2.0, contact time 24 h, agitation speed 150 rpm, temperature 25 °C]

$C_i/\text{mg dm}^{-3}$	$C_{eq}/\text{mg dm}^{-3}$	Mass/g	Vol./dm ³	% ads.	$q_e/\text{mg g}^{-1}$	K_d
19.98	0.998	0.1007	0.025	95.01	4.713	4.722
20.84	1.334	0.1018	0.025	93.60	4.790	3.591
18.22	0.884	0.0953	0.025	95.15	4.548	5.145
20.54	0.788	0.1004	0.025	96.16	4.918	6.242
19.41	0.614	0.1006	0.025	96.84	4.671	7.607
22.43	0.522	0.1001	0.025	97.67	5.472	10.48
22.34	0.318	0.1018	0.025	98.58	5.408	17.01

Table A-VI.10: Effect of initial Pb²⁺ concentration on multicomponent adsorption of BPA onto MWCNT-ttpy pH 2.0, contact time 24 h, agitation speed 150 rpm, temperature 25 °C]

$C_i/\text{mg dm}^{-3}$	$C_{eq}/\text{mg dm}^{-3}$	Mass/g	Vol./dm ³	% ads.	$q_e/\text{mg g}^{-1}$	K_d
4.221	0.640	0.1007	0.025	84.83	0.889	1.388
8.017	3.422	0.1018	0.025	57.32	1.129	0.330
23.26	6.019	0.0953	0.025	74.13	4.523	0.752
30.07	15.61	0.1004	0.025	48.10	3.602	0.231
41.07	24.14	0.1006	0.025	41.22	4.207	0.174
45.59	31.05	0.1001	0.025	31.89	3.632	0.117
57.77	41.03	0.1018	0.025	28.97	4.110	0.100

Table A-VI.11: Effect of initial Pb²⁺ concentration on multicomponent adsorption of IBP onto MWCNT-ttpy [conditions: pH 2.0, contact time 24 h, agitation speed 150 rpm, temperature 25 °C]

$C_i/\text{mg dm}^{-3}$	$C_{eq}/\text{mg dm}^{-3}$	Mass/g	Vol./dm ³	% ads.	$q_e/\text{mg g}^{-1}$	K_d
5.319	0.61	0.1007	0.025	88.51	1.169	1.912
9.807	4.90	0.1018	0.025	50.08	1.206	0.246
22.99	10.82	0.0953	0.025	52.92	3.192	0.295
32.47	14.35	0.1004	0.025	55.82	4.514	0.315
43.43	22.24	0.1006	0.025	48.79	5.266	0.237
47.20	31.62	0.1001	0.025	33.02	3.892	0.123
56.55	38.64	0.1018	0.025	31.68	4.399	0.114

(b). Effect of multicomponent concentration on Cd²⁺ adsorption from aqueous solutions onto MWCNT-ttpty.

Table A-VI.12: Effect of same initial Cd²⁺ concentration on its adsorption onto MWCNT-ttpty [conditions: pH 2.0, contact time 24 h, agitation speed 150 rpm, temperature 25 °C]

$C_i/\text{mg dm}^{-3}$	$C_{eq}/\text{mg dm}^{-3}$	Mass/g	Vol./dm ³	% ads.	$q_e/\text{mg g}^{-1}$	K_d
18.32	0.224	0.1022	0.025	98.78	4.427	19.76
17.18	0.652	0.1066	0.025	96.20	3.876	5.945
23.24	0.535	0.1006	0.025	97.70	5.642	10.55
21.44	0.721	0.1005	0.025	96.64	5.154	7.148
19.66	1.334	0.0985	0.025	93.21	4.651	3.487
19.41	1.386	0.1019	0.025	92.86	4.422	3.19
21.36	1.491	0.1003	0.025	93.02	4.952	3.32

Table A-VI.13: Effect of initial Cd²⁺ concentration on multicomponent adsorption of BPA onto MWCNT-ttpty [conditions: pH 2.0, contact time 24 h, agitation speed 150 rpm, temperature 25 °C]

$C_i/\text{mg dm}^{-3}$	$C_{eq}/\text{mg dm}^{-3}$	Mass/g	Vol./dm ³	% ads.	$q_e/\text{mg g}^{-1}$	K_d
4.314	1.510	0.1022	0.025	65.00	0.686	0.454
9.290	3.354	0.1066	0.025	63.90	1.392	0.415
19.47	6.839	0.1006	0.025	64.88	3.139	0.459
28.37	12.09	0.1005	0.025	57.37	4.048	0.335
42.04	15.09	0.0985	0.025	64.10	6.840	0.453
50.49	17.82	0.1019	0.025	64.71	8.016	0.450
60.19	23.93	0.1003	0.025	60.25	9.038	0.378

Table A-VI.14: Effect of initial Cd²⁺ concentration on multicomponent adsorption of IBP onto MWCNT-ttpty [conditions: pH 2.0, contact time 24 h, agitation speed 150 rpm, temperature 25 °C]

$C_i/\text{mg dm}^{-3}$	$C_{eq}/\text{mg dm}^{-3}$	Mass/g	Vol./dm ³	% ads.	$q_e/\text{mg g}^{-1}$	K_d
5.055	0.90	0.1022	0.025	82.17	1.016	1.127
10.16	2.33	0.1066	0.025	77.03	1.835	0.787
24.38	6.33	0.1006	0.025	74.04	4.486	0.709
28.30	7.93	0.1005	0.025	71.97	5.065	0.639
36.59	9.66	0.0985	0.025	73.61	6.835	0.708
50.74	15.11	0.1019	0.025	70.22	8.742	0.579
60.39	17.53	0.1003	0.025	70.97	10.68	0.609

Appendix VII

Data for Rhodamine B (RhB)

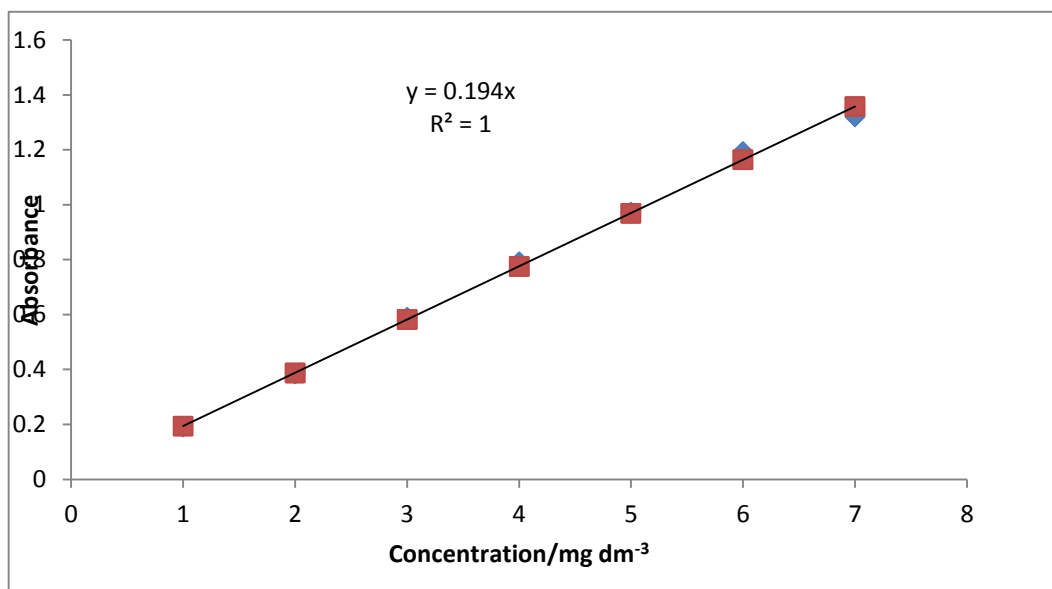


Fig A-VII.1: Calibration curve of RhB

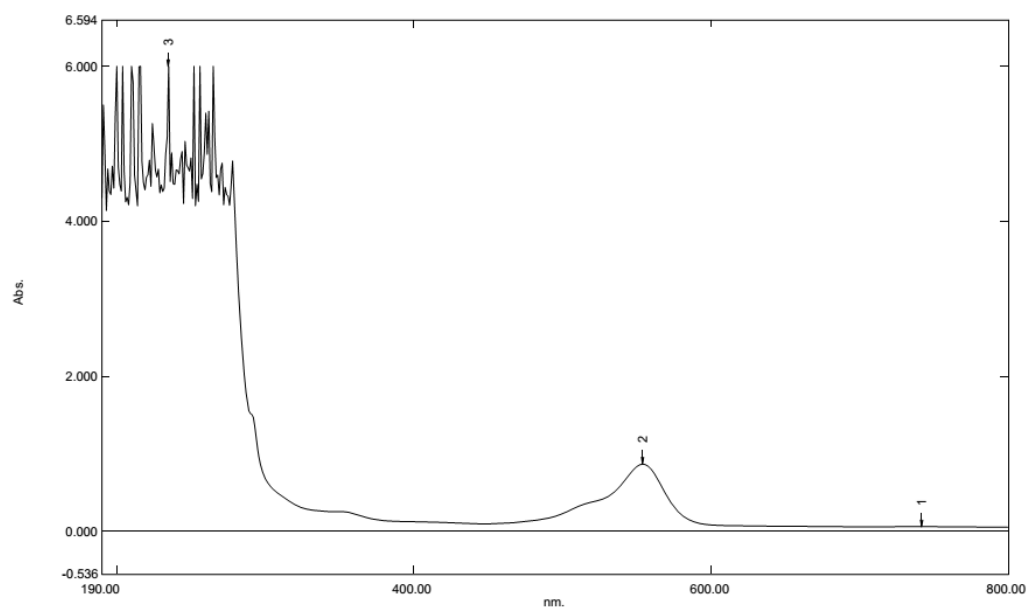


Fig A-VII.2: UV spectrum of RhB

Table A-VII.1: Experimental data for the adsorption of RhB onto CoFe₂O₄ as a function of pH [conditions: contact time 24 h, agitation speed 150 rpm, temperature 20 °C]

pH	$C_i/\text{mg dm}^{-3}$	$C_{eq}/\text{mg dm}^{-3}$	Volume/ dm^3	Mass/g	% adsorbed	$q_e/\text{mg g}^{-1}$
1.00	52.22	50.41	0.025	0.050	3.457	0.903
2.13	52.22	49.90	0.025	0.050	4.444	1.160
3.16	52.22	47.71	0.025	0.050	8.642	2.256
4.14	52.22	47.45	0.025	0.050	9.136	2.385
5.25	52.22	47.19	0.025	0.050	9.630	2.514
6.00	52.22	45.64	0.025	0.050	12.59	3.288
7.14	52.22	44.61	0.025	0.050	14.57	3.804
8.19	52.22	42.93	0.025	0.050	17.78	4.642
9.23	52.22	45.90	0.025	0.050	12.10	3.159
10.07	52.22	46.67	0.025	0.050	10.62	2.772

Table A-VII.2: Experimental data for the adsorption of RhB onto CoFe₂O₄ as a function of time [conditions: pH 7.0, agitation speed 150 rpm, temperature 20 °C]

Time/min	$C_i/\text{mg dm}^{-3}$	$C_{eq}/\text{mg dm}^{-3}$	Mass/g	Volume/ dm^3	% adsorbed	$q_e/\text{mg g}^{-1}$
5	50.67	48.99	0.050	0.025	3.308	0.838
10	50.67	47.96	0.050	0.025	5.344	1.354
15	50.67	47.58	0.050	0.025	6.107	1.547
20	50.67	46.54	0.050	0.025	8.142	2.063
30	50.67	46.16	0.050	0.025	8.906	2.256
45	50.67	45.13	0.050	0.025	10.94	2.772
60	50.67	44.09	0.050	0.025	12.98	3.288
75	50.67	43.71	0.050	0.025	13.74	3.481
90	50.67	43.32	0.050	0.025	14.50	3.675
120	50.67	42.55	0.050	0.025	16.03	4.061
180	50.67	41.52	0.050	0.025	18.07	4.577
240	50.67	40.74	0.050	0.025	19.59	4.964
300	50.67	40.23	0.050	0.025	20.61	5.222
360	50.67	39.84	0.050	0.025	21.37	5.415
720	50.67	39.58	0.050	0.025	21.88	5.544
1080	50.67	39.32	0.050	0.025	22.39	5.673
1440	50.67	39.32	0.050	0.025	22.39	5.673

Table A-VII.3: Experimental data for the adsorption of RhB onto CoFe₂O₄ as a function of adsorbent dose [conditions: pH 7.0, contact time 24 h, agitation speed 150 rpm, temperature 20 °C]

$C_i/\text{mg dm}^{-3}$	$C_{eq}/\text{mg dm}^{-3}$	Mass/g	Volume/ dm^3	% adsorbed	$q_e/\text{mg g}^{-1}$
50.67	38.04	0.030	0.025	24.94	10.53
50.67	30.04	0.050	0.025	40.71	10.31
50.67	20.37	0.075	0.025	59.80	10.10
50.67	12.89	0.100	0.025	74.55	9.444
50.67	6.271	0.150	0.025	87.62	7.400
50.67	1.233	0.200	0.025	97.57	6.180
50.67	0.624	0.300	0.025	98.77	4.171
50.67	0.505	0.400	0.025	99.00	3.135

Table A-VII.4: Experimental data for the adsorption of CoFe₂O₄ as a function of temperature [conditions: pH 7.0, contact time 24 h, agitation speed 150 rpm]

T/K	$C_{eq}/\text{mg dm}^{-3}$	Mass/g	Conc (Cf)	% adsorbed	$q_e/\text{mg g}^{-1}$
293 K	10.05	0.050	6.189	38.42	1.931
	19.88	0.050	14.30	28.09	2.792
	29.64	0.050	23.13	21.98	3.257
	40.66	0.050	31.98	21.36	4.342
	49.66	0.050	41.65	16.14	4.007
	60.11	0.050	51.57	14.20	4.269
	69.87	0.050	61.37	12.16	4.249
303 K	10.05	0.050	4.755	52.69	2.647
	19.88	0.050	13.47	32.24	3.205
	29.64	0.050	22.55	23.93	3.546
	40.66	0.050	31.33	22.94	4.665
	49.66	0.050	40.48	18.48	4.588
	60.11	0.050	50.41	16.13	4.849
	69.87	0.050	60.21	13.82	4.829
313 K	10.05	0.050	4.502	55.20	2.774
	19.88	0.050	13.24	33.38	3.318
	29.64	0.050	21.45	27.62	4.093
	40.66	0.050	29.65	27.07	5.503
	49.66	0.050	39.58	20.29	5.039
	60.11	0.050	49.38	17.85	5.364
	69.87	0.050	59.05	15.48	5.409
318 K	10.05	0.050	4.342	56.79	2.854
	19.88	0.050	12.25	38.36	3.813
	29.64	0.050	20.15	32.00	4.743
	40.66	0.050	27.72	31.82	6.470
	49.66	0.050	36.10	27.30	6.779
	60.11	0.050	45.64	24.07	7.234
	69.87	0.050	55.57	20.47	7.150

Table A-VII.5: Experimental data for the adsorption of RhB onto MWCNT-COOH-CoFe₂O₄ (29%) as a function of pH [conditions: contact time 24 h, agitation speed 150 rpm, temperature 20 °C]

pH	$C_i/\text{mg dm}^{-3}$	$C_{eq}/\text{mg dm}^{-3}$	Volume/ dm^3	Mass/g	% adsorbed	$q_e/\text{mg g}^{-1}$
1.03	50.41	11.60	0.025	0.050	23.01	5.799
2.02	50.41	13.53	0.025	0.050	26.85	6.766
3.15	50.41	16.11	0.025	0.050	31.96	8.056
4.12	50.41	23.98	0.025	0.050	47.56	11.99
5.12	50.41	26.55	0.025	0.050	52.68	13.28
6.00	50.41	31.97	0.025	0.050	63.42	15.99
7.16	50.41	37.13	0.025	0.050	73.65	18.56
8.11	50.41	34.68	0.025	0.050	68.79	17.34
9.00	50.41	33.52	0.025	0.050	66.49	16.76
10.00	50.41	32.10	0.025	0.050	63.68	16.05

Table A-VII.6: Experimental data for the adsorption of RhB onto MWCNT-COOH-CoFe₂O₄ (29%) as a function of time [conditions: pH 7.0, agitation speed 150 rpm, temperature 20 °C]

Time/min	$C_i/\text{mg/dm}^{-3}$	$C_{eq}/\text{mg dm}^{-3}$	Mass/g	Volume/ dm^3	% adsorbed	$q_e/\text{mg g}^{-1}$
5	50.41	43.84	0.050	0.025	13.03	3.285
10	50.41	42.93	0.050	0.025	14.83	3.736
15	50.41	40.36	0.050	0.025	19.94	5.026
20	50.41	33.26	0.050	0.025	34.01	8.571
30	50.41	30.69	0.050	0.025	39.12	9.861
45	50.41	28.88	0.050	0.025	42.71	10.76
60	50.41	26.69	0.050	0.025	47.05	11.86
75	50.41	25.92	0.050	0.025	48.59	12.25
90	50.41	21.79	0.050	0.025	56.77	14.31
120	50.41	20.63	0.050	0.025	59.08	14.89
180	50.41	19.08	0.050	0.025	62.14	15.66
240	50.41	17.02	0.050	0.025	66.24	16.69
300	50.41	15.60	0.050	0.025	69.05	17.40
360	50.41	14.44	0.050	0.025	71.35	17.98
720	50.41	12.89	0.050	0.025	74.42	18.76
1080	50.41	12.51	0.050	0.025	75.19	18.95
1440	50.41	11.60	0.050	0.025	76.98	19.40

Table A-VII.7: Experimental data for the adsorption of RhB onto MWCNT-COOH-CoFe₂O₄ (29%) as a function of adsorbent dose [conditions: pH 7.0, contact time 24 h, agitation speed 150 rpm, temperature 20 °C]

Mass/g	C _i /mg dm ⁻³	C _{eq} /mg dm ⁻³	% adsorbed	q _e /mg g ⁻¹
0.030	43.45	21.14	51.34	18.59
0.050	43.45	11.22	74.18	16.12
0.075	43.45	5.730	86.81	12.57
0.100	43.45	1.728	96.02	10.43
0.150	43.45	1.470	96.62	6.997
0.200	43.45	0.975	97.76	5.309
0.300	43.45	0.526	98.79	3.577
0.400	43.45	0.000	100.0	2.716

Table A-VII.8: Experimental data for the adsorption of onto MWCNT-COOH-CoFe₂O₄ (29%) as a function of temperature [conditions: pH 7.0, contact time 24 h, agitation speed 150 rpm]

T/K	C _i /mg dm ⁻³	C _f /mg dm ⁻³	Mass/g	% adsorbed	q _e /mg g ⁻¹
293 K	10.05	1.939	0.050	80.71	4.055
	19.88	3.084	0.050	0.123	8.398
	29.64	5.415	0.050	81.73	12.11
	40.66	8.638	0.050	78.75	16.01
	49.66	15.86	0.050	68.07	16.90
	60.11	25.01	0.050	58.39	17.55
	69.87	34.55	0.050	50.55	17.66
303 K	10.05	0.634	0.050	93.69	4.708
	19.88	1.078	0.050	94.58	9.401
	29.64	3.244	0.050	89.06	13.20
	40.66	6.601	0.050	83.76	17.03
	49.66	12.64	0.050	74.56	18.51
	60.11	22.95	0.050	61.82	18.58
	69.87	31.85	0.050	54.42	19.01
313 K	10.05	0.505	0.050	94.97	4.772
	19.88	0.732	0.050	96.32	9.574
	29.64	2.182	0.050	92.64	13.73
	40.66	5.859	0.050	85.59	17.40
	49.66	10.06	0.050	79.75	19.80
	60.11	19.86	0.050	66.97	20.13
	69.87	29.65	0.050	57.56	20.11
318 K	10.05	0.165	0.050	98.36	4.942
	19.88	0.402	0.050	97.98	9.739
	29.64	0.732	0.050	97.53	14.45
	40.66	4.621	0.050	88.64	18.02
	49.66	9.928	0.050	80.01	19.87
	60.11	19.86	0.050	66.97	20.13
	69.87	28.24	0.050	59.59	20.82

Table A-VII.9: Experimental data for the adsorption of RhB onto MWCNT-COOH-CoFe₂O₄ (50%) as a function of pH [conditions: contact time 24 h, agitation speed 150 rpm, temperature 20 °C]

pH	$C_i/\text{mg dm}^{-3}$	$C_{eq}/\text{mg dm}^{-3}$	Volume/ dm^3	Mass/g	%	
					adsorbed	$q_e/\text{mg g}^{-1}$
0.97	50.41	39.82	0.025	0.050	20.99	5.291
2.10	50.41	32.31	0.025	0.050	35.91	9.051
3.17	50.41	27.85	0.025	0.050	44.75	11.28
4.00	50.41	23.39	0.025	0.050	53.59	13.51
5.39	50.41	19.77	0.025	0.050	60.77	15.32
6.21	50.41	13.65	0.025	0.050	72.93	18.38
7.20	50.41	5.291	0.025	0.050	89.50	22.56
8.00	50.41	15.18	0.025	0.050	69.89	17.61
9.16	50.41	15.73	0.025	0.050	68.78	17.34
10.0	50.41	17.68	0.025	0.050	64.92	16.36

Table A-VII.10: Experimental data for the adsorption of RhB onto MWCNT-COOH-CoFe₂O₄ (50%) as a function of time [conditions: pH 7.0, agitation speed 150 rpm, temperature 20 °C]

Time/min	$C_i/\text{mg/dm}^{-3}$	$C_{eq}/\text{mg dm}^{-3}$	Mass/g	Volume/ dm^3	% adsorbed	$q_e/\text{mg g}^{-1}$
5	50.41	42.81	0.050	0.025	15.08	3.801
10	50.41	38.42	0.050	0.025	23.78	5.993
15	50.41	31.20	0.050	0.025	38.10	9.603
20	50.41	28.62	0.050	0.025	43.22	10.89
30	50.41	27.85	0.050	0.025	44.75	11.28
45	50.41	24.88	0.050	0.025	50.63	12.76
60	50.41	22.31	0.050	0.025	55.75	14.05
75	50.41	21.79	0.050	0.025	56.77	14.31
90	50.41	19.60	0.050	0.025	61.12	15.40
120	50.41	18.44	0.050	0.025	63.42	15.99
180	50.41	15.34	0.050	0.025	69.56	17.53
240	50.41	11.86	0.050	0.025	76.47	19.27
300	50.41	10.31	0.050	0.025	79.54	20.05
360	50.41	9.283	0.050	0.025	81.58	20.56
720	50.41	8.896	0.050	0.025	82.35	20.76
1080	50.41	8.510	0.050	0.025	83.12	20.95
1440	50.41	8.252	0.050	0.025	83.63	21.08

Table A-VII.11: Experimental data for the adsorption of RhB onto MWCNT-COOH-CoFe₂O₄ (50%) as a function of adsorbent dose [conditions: pH 7.0, contact time 24 h, agitation speed 150 rpm, temperature 20 °C]

Mass/g	C _i /mg dm ⁻³	C _{eq} /mg dm ⁻³	% adsorbed	q _e /mg g ⁻¹
0.030	43.45	15.73	63.80	23.10
0.050	43.45	3.22	92.58	20.11
0.075	43.45	2.176	94.99	13.76
0.100	43.45	0.866	98.01	10.65
0.150	43.45	0.655	98.49	7.133
0.200	43.45	0.526	98.79	5.366
0.300	43.45	0.449	98.97	3.583
0.400	43.45	0.000	100.0	2.716

Table A-VII.12: Experimental data for the adsorption of onto MWCNT-COOH-CoFe₂O₄ (50%) as a function of temperature [conditions: pH 7.0, contact time 24 h, agitation speed 150 rpm]

T/K	C _i /mg dm ⁻³	C _f /mg dm ⁻³	Mass/g	% adsorbed	q _e /mg g ⁻¹
293 K	9.996	0.000	0.050	100.0	4.998
	20.18	0.170	0.050	99.16	10.00
	30.88	1.145	0.050	96.29	14.87
	40.11	2.837	0.050	92.93	18.64
	49.74	6.833	0.050	86.26	21.45
	60.21	15.73	0.050	73.88	22.24
	69.88	25.14	0.050	64.02	22.37
303 K	9.996	0.000	0.050	100.0	4.998
	20.18	0.000	0.050	100.0	10.09
	30.88	1.088	0.050	96.48	14.90
	40.11	2.718	0.050	93.22	18.70
	49.74	5.544	0.050	88.85	22.10
	60.21	14.57	0.050	75.80	22.82
	69.88	23.59	0.050	66.24	23.14
313 K	9.996	0.000	0.050	100.0	4.998
	20.18	0.000	0.050	100.0	10.09
	30.88	0.686	0.050	97.78	15.10
	40.11	1.155	0.050	97.12	19.48
	49.74	5.157	0.050	89.63	22.29
	60.21	13.80	0.050	77.09	23.21
	69.88	23.34	0.050	66.60	23.27
318 K	9.996	0.000	0.050	100.0	4.998
	20.18	0.000	0.050	100.0	10.09
	30.88	0.629	0.050	97.96	15.13
	40.11	0.928	0.050	97.69	19.59
	49.74	3.481	0.050	93.00	23.13
	60.21	12.38	0.050	79.44	23.92
	69.88	20.89	0.050	70.11	24.50

Table A-VII.13: Experimental data for the adsorption of RhB onto MWCNT-COOH-CoFe₂O₄ (75%) as a function of pH [conditions: contact time 24 h, agitation speed 150 rpm, temperature 20 °C]

pH	$C_i/\text{mg dm}^{-3}$	$C_{eq}/\text{mg dm}^{-3}$	Volume/ dm^3	Mass/g	% adsorbed	$q_e/\text{mg g}^{-1}$
1	103.66	94.64	0.025	0.050	8.71	4.513
2	103.66	93.09	0.025	0.050	10.20	5.286
3	103.66	81.87	0.025	0.050	21.02	10.89
4	103.66	67.30	0.025	0.050	35.07	18.18
5	103.66	55.83	0.025	0.050	46.14	23.92
6	103.66	38.55	0.025	0.050	62.81	32.56
7	103.66	42.806	0.025	0.050	58.71	30.43
8	103.66	48.74	0.025	0.050	52.99	27.46
9	103.66	51.83	0.025	0.050	50.00	25.92
10	103.66	58.79	0.025	0.050	43.28	22.43

Table A-VII.14: Experimental data for the adsorption of RhB onto MWCNT-COOH-CoFe₂O₄ (75%) as a function of time [conditions: pH 7.0, agitation speed 150 rpm, temperature 20 °C]

Time/min	$C_i/\text{mg/dm}^{-3}$	$C_{eq}/\text{mg dm}^{-3}$	Mass/g	Volume/ dm^3	% adsorbed	$q_e/\text{mg g}^{-1}$
5	103.66	90.51	0.050	0.025	12.69	6.576
10	103.66	89.61	0.050	0.025	13.56	7.027
15	103.66	88.06	0.050	0.025	15.05	7.800
20	103.66	84.06	0.050	0.025	18.91	9.80
30	103.66	81.49	0.050	0.025	21.39	11.09
45	103.66	71.56	0.050	0.025	30.97	16.05
60	103.66	68.59	0.050	0.025	33.83	17.53
75	103.66	64.85	0.050	0.025	37.44	19.40
90	103.66	61.11	0.050	0.025	41.04	21.27
120	103.66	57.25	0.050	0.025	44.78	23.21
180	103.66	50.03	0.050	0.025	51.74	26.82
240	103.66	45.64	0.050	0.025	55.97	29.01
300	103.66	42.93	0.050	0.025	58.58	30.36
360	103.66	39.711	0.050	0.025	61.69	31.98
720	103.66	39.324	0.050	0.025	62.06	32.17
1080	103.66	38.938	0.050	0.025	62.44	32.36
1440	103.66	38.680	0.050	0.025	62.69	32.49

Table A-VII.15: Experimental data for the adsorption of RhB onto MWCNT-COOH-CoFe₂O₄ (75%) as a function of adsorbent dose [conditions: pH 7.0, contact time 24 h, agitation speed 150 rpm, temperature 20 °C]

Mass/g	$C_i/\text{mg dm}^{-3}$	$C_{eq}/\text{mg dm}^{-3}$	% adsorbed	$q_e/\text{mg g}^{-1}$
0.030	43.45	64.21	38.06	34.13
0.050	43.45	40.48	60.95	31.59
0.075	43.45	28.881	72.14	24.93
0.100	43.45	13.538	86.94	22.53
0.150	43.45	5.090	95.09	16.429
0.200	43.45	4.033	96.11	12.454
0.300	43.45	3.471	96.65	8.349
0.400	43.45	3.363	96.8	6.269

Table A-VII.16: Experimental data for the adsorption of RhB onto MWCNT-COOH-CoFe₂O₄ (75%) as a function of temperature [conditions: pH 7.0, contact time 24 h, agitation speed 150 rpm]

T/K	$C_i/\text{mg dm}^{-3}$	$C_f/\text{mg dm}^{-3}$	Mass/g	% adsorbed	$q_e/\text{mg g}^{-1}$
293 K	9.996	0.557	0.050	94.43	4.720
	20.18	0.707	0.050	96.50	9.737
	30.88	2.372	0.050	92.32	14.25
	40.11	3.445	0.050	91.41	18.33
	49.74	3.718	0.050	92.52	23.01
	60.21	6.137	0.050	89.81	27.04
	69.88	8.252	0.050	88.19	30.81
	80.11	17.02	0.050	78.76	31.55
	90.04	26.17	0.050	70.93	31.93
	100.1	35.59	0.050	64.44	32.24
303 K	9.996	0.444	0.050	95.56	4.776
	20.18	0.588	0.050	97.09	9.796
	30.88	1.217	0.050	96.06	14.83
	40.11	2.171	0.050	94.59	18.97
	49.74	2.739	0.050	94.49	23.50
	60.21	3.770	0.050	93.74	28.22
	69.88	7.349	0.050	89.48	31.27
	80.11	11.22	0.050	86.00	34.45
	90.04	21.02	0.050	76.66	34.51
	100.1	30.04	0.050	69.98	35.01
313 K	9.996	0.263	0.050	97.37	4.87
	20.18	0.454	0.050	97.75	9.863
	30.88	0.572	0.050	98.15	15.15
	40.11	0.676	0.050	98.32	19.72
	49.74	1.155	0.050	97.68	24.29
	60.21	2.120	0.050	96.48	29.05
	69.88	4.255	0.050	93.91	32.81
	80.11	9.928	0.050	87.61	35.09

	90.04	19.21	0.050	78.66	35.41
	100.1	28.62	0.050	71.39	35.72
318 K	9.996	0.000	0.050	100	4.998
	20.18	0.077	0.050	99.62	10.05
	30.88	0.552	0.050	98.21	15.16
	40.11	0.629	0.050	98.43	19.74
	49.74	1.712	0.050	96.56	24.01
	60.21	1.604	0.050	97.34	29.30
	69.88	3.997	0.050	94.28	32.94
	80.11	8.510	0.050	89.38	35.80
	90.04	17.79	0.050	80.24	36.12
	100.1	27.20	0.050	72.81	36.43

Table A-VII.17: Experimental data for the adsorption of RhB onto MWCNT-COOH as a function of pH [conditions: contact time 24 h, agitation speed 150 rpm, temperature 20 °C]

pH	$C_i/\text{mg dm}^{-3}$	$C_{eq}/\text{mg dm}^{-3}$	Volume/ dm^3	Mass/g	% adsorbed	$q_e/\text{mg g}^{-1}$
1	105.72	89.22	0.025	0.050	15.61	8.249
2	105.72	81.49	0.025	0.050	22.92	12.117
3	105.72	69.88	0.025	0.050	33.90	17.92
4	105.72	54.54	0.025	0.050	48.41	25.59
5	105.72	30.81	0.025	0.050	70.85	37.45
6	105.72	20.50	0.025	0.050	80.61	42.61
7	105.72	9.881	0.025	0.050	90.65	47.92
8	105.72	18.18	0.025	0.050	82.80	43.77
9	105.72	29.65	0.025	0.050	71.95	38.03
10	105.72	37.42	0.025	0.050	64.60	34.15

Table A-VII.18: Experimental data for the adsorption of RhB onto MWCNT-COOH as a function of time [conditions: pH 7.0, agitation speed 150 rpm, temperature 20 °C]

Time/min	$C_i/\text{mg/dm}^{-3}$	$C_{eq}/\text{mg dm}^{-3}$	Mass/g	Volume/ dm^3	% adsorbed	$q_e/\text{mg g}^{-1}$
5	105.72	79.94	0.050	0.025	24.39	12.891
10	105.72	74.78	0.050	0.025	29.27	15.470
15	105.72	70.91	0.050	0.025	32.92	17.404
20	105.72	67.04	0.050	0.025	36.58	19.34
30	105.72	64.08	0.050	0.025	39.39	20.82
45	105.72	58.41	0.050	0.025	44.75	23.66
60	105.72	52.35	0.050	0.025	50.49	26.69
75	105.72	42.93	0.050	0.025	59.39	31.39
90	105.72	35.46	0.050	0.025	66.46	35.13
120	105.72	29.27	0.050	0.025	72.32	38.23
180	105.72	18.44	0.050	0.025	82.56	43.64
240	105.72	13.41	0.050	0.025	87.32	46.16
300	105.72	10.83	0.050	0.025	89.76	47.44
360	105.72	9.154	0.050	0.025	91.34	48.28

720	105.72	8.896	0.050	0.025	91.58	48.41
1080	105.72	7.736	0.050	0.025	92.68	48.99
1440	105.72	7.349	0.050	0.025	93.05	49.19

Table A-VII.19: Experimental data for the adsorption of RhB onto MWCNT-COOH as a function of adsorbent dose [conditions: pH 7.0, contact time 24 h, agitation speed 150 rpm, temperature 20 °C]

Mass/g	$C_i/\text{mg dm}^{-3}$	$C_{eq}/\text{mg dm}^{-3}$	% adsorbed	$q_e/\text{mg g}^{-1}$
0.030	96.7	32.62	66.27	53.40
0.050	96.7	8.25	91.47	44.22
0.075	96.7	4.255	95.60	30.82
0.100	96.7	1.872	98.06	23.71
0.150	96.7	0.464	99.52	16.039
0.200	96.7	0.258	99.73	12.055
0.300	96.7	0.222	99.77	8.040
0.400	96.7	0.000	100.0	6.044

Table A-VII.20: Experimental data for the adsorption of RhB onto MWCNT-COOH as a function of temperature [conditions: pH 7.0, contact time 24 h, agitation speed 150 rpm]

T/K	$C_i/\text{mg dm}^{-3}$	$C_f/\text{mg dm}^{-3}$	Mass/g	% adsorbed	$q_e/\text{mg g}^{-1}$
293 K	9.996	0.170	0.050	98.30	4.913
	20.18	0.397	0.050	98.03	9.891
	30.88	0.650	0.050	97.90	15.12
	40.11	1.155	0.050	97.12	19.48
	49.74	1.717	0.050	96.55	24.01
	60.21	2.372	0.050	96.06	28.92
	69.88	3.713	0.050	94.69	33.08
	80.11	7.091	0.050	91.15	36.51
	90.04	12.51	0.050	86.11	38.77
	100.1	21.27	0.050	78.74	39.39
303 K	9.996	0.072	0.050	99.28	4.962
	20.18	0.175	0.050	99.13	10.00
	30.88	0.454	0.050	98.53	15.21
	40.11	0.908	0.050	97.74	19.60
	49.74	1.212	0.050	97.56	24.26
	60.21	1.609	0.050	97.33	29.30
	69.88	2.001	0.050	97.14	33.94
	80.11	4.513	0.050	94.37	37.80
	90.04	7.091	0.050	92.12	41.47
	100.1	15.60	0.050	84.41	42.23
313 K	12.76	0.046	0.050	99.64	6.36
	22.82	0.057	0.050	99.75	11.38
	33.01	0.113	0.050	99.66	16.45
	43.58	0.196	0.050	99.55	21.69
	54.41	0.284	0.050	99.48	27.06

	65.76	0.397	0.050	99.40	32.68
	74.27	1.485	0.050	98.00	36.39
	81.87	1.815	0.050	97.78	40.03
	91.67	2.708	0.050	97.05	44.48
	105.7	14.31	0.050	86.46	45.71
318 K	12.76	0.000	0.050	100.0	6.382
	22.82	0.093	0.050	99.59	11.36
	33.01	0.124	0.050	99.63	16.44
	43.58	0.232	0.050	99.47	21.67
	54.41	0.294	0.050	99.46	27.06
	65.76	0.397	0.050	99.40	32.68
	74.27	0.505	0.050	99.32	36.88
	81.87	0.572	0.050	99.30	40.65
	91.67	1.418	0.050	98.45	45.13
	105.7	12.64	0.050	88.05	46.54